Mesoscale Hydrological Model Validation and Verification using Stable Water Isotopes: The isoWATFLOOD Model

by

Tricia A. Stadnyk-Falcone

A thesis
presented to the University of Waterloo
in fulfillment of the
thesis requirement for the degree of
Doctor of Philosophy
in
Civil Engineering

Waterloo, Ontario, Canada, 2008

Author's Declaration

I hereby declare that I am the sole author of this thesis. This is a true copy of the thesis, including any required final revisions, as accepted by my examiners.

I understand that my thesis may be made electronically available to the public.

Abstract

This thesis develops a methodology for mesoscale model verification and validation that is founded on the rigorous constraint imposed by the need to conserve both water mass and isotopes simultaneously. The isoWATFLOOD model simulates $\delta^{18}O$ in streamflow, which effectively reduces and constrains errors associated with equifinality in streamflow generation by improving internal parameterizations.

The WATFLOOD model is a conceptually-based distributed hydrological model used for simulating streamflow on mesoscale watersheds. Given the model's intended application to mesoscale hydrology, it remains crucial to ensure conceptualizations are physically representative of the hydrologic cycle and the natural environment. Stable water isotopes because of their natural abundance and systematic fractionation have the ability to preserve information on water cycling across large domains. Several coordinated research projects have recently focused on integrating stable water isotopes into global and regional circulation models, which now provides the opportunity to isotopically force land-surface and hydrological models. Where traditionally streamflows are the primary validation criteria in hydrological modelling, problems arise in remote and ungauged basins, or large watersheds where streamflows may not be well monitored. By streamflow validation alone, no insight is obtained on the internal apportioning and physical representation of sub-processes contributing to streamflow. The primary goal of this research is to develop alternative measures to parameterize mesoscale hydrological models in a physically-based manner, and to validate such models over large domains.

This research develops improved model parameterizations that facilitate realistic runoff generation process contributions. The examination of runoff generation processes and the subsequent $\delta^{18}O$ of these processes are performed for two mesoscale watersheds: Fort Simpson, NWT and the Grand River Basin, ON. The isoWATFLOOD model is shown to reliably predict streamflow and $\delta^{18}O$ of streamflow, and simulates mesoscale isotopic fractionation associated with evaporation. In doing so, a more physically meaningful, robust modelling tool is developed that is practical for operational use. This research also contributes the first continuous record of $\delta^{18}O$ in streamflow that enables the visualization of spatial and temporal variability and dominant hydrologic controls within mesoscale watersheds.

Acknowledgements

I would first like to thank my supervisors, Dr. Nicholas Kouwen and Dr. Thomas Edwards for their guidance and life lessons. Your individual talents have led to the development of this research; and your insights have continually challenged me. Moreover, your friendships have made this journey a memorable one. Special thanks go to Tom for finding me a husband!

This research was funded by graduate scholarships from the Natural Sciences and Engineering Research Council (NSERC), by a Northern Scientific Training Program grant, the University of Waterloo and Faculty of Engineering, and by research assistantships from Dr. Kouwen. Special thanks go to my supervisors who provided additional funds to send me to conferences around the world to present this research: those experiences have truly enriched my life and have afforded several stimulating collaborations.

I would like to thank Dr. John Gibson for his support and guidance with this research, and for the Grand River Isotope data he provide. Thanks go to Al Pietroniro and the Water Survey of Canada for supplying the Fort Simpson data set. I would also like to thank the GRCA for streamflow data and their contributions to this work, particularly Dwight Boyd and Samuel Bellamy. Thank you to my committee and Dr. Eric Wood for their critique of this thesis.

To my office mates: thank you for the fun times, the office potlucks, and for just being there on "those days". To all my fellow graduate students: keep the faith – it always gets done (somehow)! Phil: thanks for always saying the wrong thing and making me laugh. Chrissy: day in and day out, you were the one beside me, as you always have been. Time is precious and I will always remember these days. And to everyone else: yes, I am finally done!

I would like to acknowledge the unbounded love, support and encouragement provided by my mom and dad over the past decade (yes, that long) of my education. When I did not believe in myself, you believed in me. When I struggled, you listened and somehow you always made it seem better. We finally did it!

Finally, to my husband: thank you for being there through thick and thin, for being a great listener, and for loving me through it all. Thank you for the long nights of doing dishes, cooking, and weekends spent cleaning the house (told you I'd get even!). It's not the destination, but the journey that is living: here's to the start of a brand new life together.

Table of Contents

List of Tables

List of Figures

Chapter 1

Introduction

There is a need to improve the understanding of hydrological flowpaths, sources and cycling within natural environments not only to determine the potential impacts of contaminants on water supplies, but to also understand and predict potential impacts of climate change on current water resources world-wide (IAEA, 2003; Kendall *et al.*, 1995). Integral to the systematic understanding of the water cycle and desegregation of flowpaths is the ability to accurately and precisely model regional hydrologic cycling. The focus has traditionally been on improving this understanding through detailed studies of small-scale catchments and localized hydrology. Although this more detailed understanding of small-scale process then provides the foundation for development of appropriate conceptualizations for mesoscale (i.e., thousands of square kilometres) watershed models, hydrology however is not linear. There is a risk in assuming small-scale processes and interactions are scalable to the larger domain, and therefore there is a risk in focusing all efforts on small catchments when in practice, it is at the larger scale that policy and management decisions are made (Soulsby *et al.*, 2006). Day-to-day operational needs necessitate the design of practical mesoscale watershed models capable of facilitating the study of hydrological behaviour and variability on watershed and regional scales.

There are a multitude of mesoscale hydrological models (Singh & Frevert, 2002; Singh & Frevert, 2006) that simulate water movement through watersheds using a varying degree of complexity. Model complexity may increase the physical-basis of a simulation, but at an increased cost for data collection, excess model parameterizations, computational expense, and simulation uncertainty. It is not necessarily the case that increased complexity leads to increased

model accuracy (Arora *et al.*, 2001; Kazezyilmaz-Alhan & Medina, 2007), and more often than not models yield highly contrasting end results (Chiang *et al.*, 2007; Henderson-Sellers, 2006; McBean & Motiee, 2008). It therefore becomes necessary to ascertain which simulations are the most representative of observed environmental and physical flow systems being modelled, and to understand the uncertainties inherent to the simulation (Joerin *et al.*, 2002; Kennedy *et al.*, 1986; Uhlenbrook & Hoeg, 2003; VanderKwaak & Loague, 2001). Validation of the sub-processes contributing to streamflow can help to reduce and constrain simulation uncertainty by determining if sub-process flow contributions are physically-representative and correctly apportioned by the model. There is therefore a need to develop practices that allow modellers to quantify runoff generation processes with greater certainty, and moreover to find feasible and efficient methods to validate the accuracy of hydrological predictions across large domains. Kirchner (2006) outlined a method to improve the estimation uncertainty of the existing suite of hydrological models by 1) making use of the extensive data networks and field observations available, 2) replacing 'black-box' approaches to modelling with 'grey box' approaches that better capture the non-linear characteristics of hydrology, 3) developing more physically-based representations of hydrologic behaviour at catchment scales, 4) decreasing the amount of parameterization in hydrologic models to ensure they are feasibly run at larger scales, and 5) developing new methods to incisively and comprehensively test these large-scale models. The ability to efficiently model mesoscale hydrology within defined limits of certainty affords increased opportunities to utilize models operationally for hydrological forecasting.

In the interests of reducing modelling uncertainties by increasing the physical representativeness of models, hydrological tracers are utilized to validate individual flowpath contributions to streamflow. Over the past few decades water isotopes (i.e., deuterium and oxygen-18) have become increasingly popular tracers used in hydrological research to improve the understanding of water cycling in watersheds (Kendall *et al.*, 2001; Laudon *et al.*, 2004; Sklash & Farvolden, 1982; Vandenschrick *et al.*, 2002). Oxygen and hydrogen stable isotopes (^{18}O and ^{2}H) are ideal tracers of water sources because they are naturally occurring constituents of water ($^{1}H^{1}H^{18}O$ and $^{1}H^{2}H^{16}O$), they are stable, they preserve hydrological information, and they characterize basin-scale hydrological responses. Water undergoes highly systematic and well defined changes in isotopic composition within the hydrological cycle resulting from fractionation accompanying phase changes and diffusive processes (IAEA, 1981). Sources

contributing to streamflow can be quantifiably segregated based on measured isotopic signatures, knowledge of the significant components (end-members) contributing to streamflow, and a distinct isotopic signature for each end-member (Dunn *et al.*, 2006; Jones *et al.*, 2006; Kendall *et al.*, 1995; Rodgers *et al.*, 2005; Soulsby *et al.*, 2003), thereby offering the opportunity to validate modelled flowpath contributions.

Global and regional circulation models currently use the systematic behaviour of stable water isotopes to ground-truth model predictions, and utilize regional isotopic differences to assess climate variability, sources and cycling of moisture (Sturm *et al.*, 2006; Sturm *et al.*, 2005). On a smaller-scale, land surface parameterization schemes are incorporating stable water isotope simulations to verify the correctness of modelled processes; validating models in the present-day to increase the certainty in forwards and backwards projections of land surface-atmospheric interactions (Henderson-Sellers, 2006; Henderson-Sellers *et al.*, 1996). At the catchment scale, stable water isotopes have been successfully utilized to identify dominant end-members contributing to streamflow in an attempt to develop physically-based representations of hydrological processes and variability (Carey & Quinton, 2005; Genereux, 2004; Laudon *et al.*, 2007; Rodgers *et al.*, 2005). Stable water isotopes have also been recently recognized for their ability to validate streamflow and hydrological process prediction in statistically-based parameterized models (Iorgulescu *et al.*, 2007), and in continental scale hydrological prediction of streamflow (Fekete *et al.*, 2006). Extending this research to mesoscale hydrological modelling will improve the prediction of streamflow and constrain model parameterizations. Particularly in ungauged basins where model calibration requires the verification of internal model dynamics and validation cannot rely on streamflow, isotope-enabled hydrological models can be isotopically validated (Weerakoon & Smakhtin, 2008; Yadav *et al.*, 2007). For such basins, parameter characterizations are crucial in ensuring the correctness of process and flow simulation.

In this thesis, the two-fold isotope and streamflow validation approach is incorporated into the WATFLOOD model; a mesoscale, partially physically-based hydrological modelling system. The isoWATFLOOD model simulates the $\delta^{18}O$ of hydrological storages and flowpaths generated by the WATFLOOD model. Modelling extremely small variations in isotope mass relative to changes in streamflow (three orders of magnitude smaller) are advantageous in

constraining internal model dynamics and contributions from isotopically distinct sub-processes. By constraining both water and isotopes, equifinality in streamflow simulation (i.e., generating the streamflows from different internal parameterizations) is restrained because of fewer correct parameterizations that align both streamflow and $\delta^{18}O$ of streamflow with measured data. The end result is a more physically representative streamflow simulation produced from physically-based, calibrated internal model dynamics: the right result for the right reasons.

1.1 Objectives

Kirchner (2006) supported the notion that mesoscale hydrological models require a rigorous approach to validation to ensure they utilize the correct theories to generate correct answers for all the right reasons. Beven (2002; 2006) popularized the use of the term 'equifinality' (von Bertalanffy, 1968) in reference to the possibility that multiple ways may exist to generate the same streamflow simulation.

The primary goal of this research is to reduce the uncertainties seemingly inherent to mesoscale hydrological modelling by developing a methodology that allows for rigorous model validation and internal verification across large domains. Using the WATFLOOD model, this research therefore seeks to

1) Perform hydrograph separation (HS) within a mesoscale hydrological model to anlayse sub-component contributions to streamflow;
2) Validate simulated mesoscale streamflow runoff generation pathways;
3) Simulate $\delta^{18}O$ simultaneously with streamflow;
4) Investigate whether simulating $\delta^{18}O$ in streamflow can be used to assess runoff generation pathways; and,
5) Evaluate $\delta^{18}O$ in streamflow and hydrological storage to observe spatial and temporal variability at the mesoscale.

Mesoscale hydrological models, despite their uncertainties, are required for operational hydrology and sustainable watershed management and practice policy design. Decisions and policy-making occur from an in-depth understanding of watershed-scale hydrological variability

and long-term susceptibility to change. The science of isotope hydrology, although well established, has not yet been widely adopted and relied upon for operational use. Significant reductions in modelling uncertainties however can result from the development of more mesoscale isotope sampling programs, which when compared to other field methods are a cost-effective and feasible means of validating models.

1.2 Long-Term Goals

This research is designed to establish a proven methodology for mesoscale hydrological model calibration and validation using stable water isotopes. In a present-day context, this thesis represents the first effort to develop a physically-based, efficient hydrological modelling system capable of continuously simulating $\delta^{18}O$ across large domains. The isoWATFLOOD model demonstrates that the simulation of both streamflow and $\delta^{18}O$ in fact leads to a more credible and physically representative model parameter set that significantly reduces the likelihood of equifinality in streamflow simulation. The model has been designed to be practical and introduces a new, feasible method for performing mesoscale model calibration and validation.

A future application of this research targets the broad-scope climate change assessment initiatives that seek to define the longer-term impacts to hydrological resources and water cycling. The efficiency of the WATFLOOD model enables both forecasting and paleo-simulations that make use of statistically generated climate scenarios. The isoWATFLOOD model may facilitate the validation of paleo-hydrological predictions through the use of, and calibration to paleo-isotope records obtained from lake sediments and glacial ice cores. Such records are typically much longer than traditional hydrometric records. The ability to validate and constrain paleo-hydrological simulations over long time sequences would increase the predictive capability of the model. The long-term goal of this research is to provide a reliable, informative, and readily accessible tool that advances the current knowledge-base of hydrological cycling and water resource sustainability.

1.3 Thesis Organization

The following presents the organizational structure of this thesis in the form of chapter briefs that are designed to assist readers in locating pertinent information contained within this document. The specific aspects of this research that have been published by the author in scientific literature, or presented at conferences have been indicated.

Chapter 1: Introduction

This chapter establishes the need for this research, outlines the objectives of this research, and describes the long-term goals and intended applications of this work.

Chapter 2: Mesoscale Hydrological and Stable Water Isotope Modelling

This chapter reviews the supporting theories and literature describing hydrological models and modelling principles, and application of stable water isotopes to hydrological research. Discussion includes a review of hydrological models suitable for this research, methods to improve model validation and calibration, fundamental theories on stable water isotopes as hydrological tracers, and current modelling initiatives utilizing isotope tracers. The section concludes with an identification of future research needs.

Chapter 3: Site Descriptions

This chapter describes the hydroclimate, geologic setting, ecology, hydrology and available data sources in the Grand River Basin, ON and the Fort Simpson Region, NWT.

Chapter 4: The WATFLOOD Hydrological Model

The framework of the WATFLOOD modelling system is presented. This chapter discusses components of the model, statistics used to evaluate the models performance, and the model set-up for each study site.

Chapter 5: WATFLOOD Hydrograph Separation

(Grand River baseflow study presented at the Conference on Stormwater and Urban Water Systems Modeling, 19 February to 20 February 2004, Toronto, ON; Fort Simpson baseflow study paper presented at the 4th International Conference on Applications of Stable Isotope Techniques to Ecological Studies, 19 April to 23 April 2004, Wellington, New Zealand, *Isotopes in Environmental and Health Studies, 41:1, 49-68*)

This chapter presents the WATFLOOD tracer module developed as part of this research to enable hydrograph separation in WATFLOOD. Two case studies are presented that quantify WATFLOOD simulated baseflow in the Grand River, ON and Fort Simpson, NWT. The first study shows highly contrasting estimations of baseflow exist among accepted models used in practice, and the second study shows how stable water isotopes assist in the verification of simulated baseflow contributions to streamflow.

Chapter 6: The Development of isoWATFLOOD

(Presented isoWATFLOOD conceptual design at the International Workshop on the Isotope Effects in Evaporation, 3 May to 6 May 2006, Pisa, Italy; Invited seminar at the Universitá di Brescia, Department of Civil Engineering, Brescia, Italy)

The framework of the isoWATFLOOD model is presented. The methodology of incorporating $\delta^{18}O$ simulation into the WATFLOOD modelling system is described in detail for each component of the model, including rationalization of the simplifying assumptions made in the model.

Chapter 7: isoWATFLOOD Diagnostics and Performance Metrics

In this chapter, isoWATFLOOD is subjected to a series of designed diagnostic and performance metric tests that evaluate the model's characteristic behaviour. The model's ability to simulate $\delta^{18}O$ in evaporation, response to precipitation, wetland hydrology and lake routing are assessed and the model is found to respond in a physically realistic manner.

Chapter 8: Validation and Verification of isoWATFLOOD

(Presented calibration results at CMOS/CGU/SGU Congress, 28 May to 1 June 2007, St. John's, Newfoundland)

This chapter presents isoWATFLOOD hydrologic and $\delta^{18}O$ simulations in the Fort Simpson, NWT region. A discussion of model calibration, including a demonstration of the equifinality concept is discussed and followed by two validations of the isoWATFLOOD model. Detailed verifications of internally modelled processes are performed that conclude the model reproduces flows and $\delta^{18}O$ in a physically representative manner in the Fort Simpson region.

Chapter 9: Stable Water Isotopes in Mesoscale Hydrological Studies

This chapter validates the isoWATFLOOD model on the largely urban and agricultural Grand River Basin, ON without re-calibration of WATFLOOD-derived parameters. It is demonstrated that the isoWATFLOOD model is capable of mesoscale hydrological and $\delta^{18}O$ simulation using a computationally efficient modelling framework. The model's application to hydrological studies of watershed variability and spatial/temporal analyses is presented.

Chapter 10: Conclusions and Recommendations

This chapter summarises the most salient findings from Chapters 5 through 9, identifying the significance of this research and proposed key objectives for future work.

Chapter 2

A Review: Hydrological and Stable Water Isotope Modelling

This chapter presents a review of concepts and literature pertinent to mesoscale hydrological modelling and the utility of stable water isotopes in model validation and hydrological verification. Many hydrological models exist and are derived from a multitude of assumptions for both very specific to generalized hydrologic scenarios (Section 2.1). Each model varies in whether it is lumped or distributed; physically-based or conceptual; intended for mesoscale or hillslope scales, capable of long time series analyses or short-term analyses; and a host of other features programmers might choose to include for various reasons. The use of hydrological models for watershed resource planning and management demands their application across large domains and with quantifiable uncertainty in modelled simulations. It is no longer acceptable to validate a model on its ability to reproduce streamflow discharge alone because frequently models are arriving at the right answer for the wrong reasons (Kirchner, 2006). Therefore research seeking to verify correct internal process representation has become necessary to further improve uncertainty estimation in hydrological modelling (Bingeman *et al.*, 2006). Hydrograph separation techniques using various forms of tracers have become a main source of diagnosing internal model behaviour (Section 2.3). Stable water isotopes are emerging as promising tools for model validation and verification studies, namely ^{18}O and ^{2}H because they are naturally occurring, conservative, and systematically change through the hydrologic cycle.

This chapter introduces the background information and relevant literature on stable water isotopes and their use in hydrological studies (Section 2.4) and for flowpath tracing (Section 2.5). The chapter reviews the latest developments occurring in the simulation of stable water isotope transport, atmospheric modelling, land-surface schemes and parametric modelling (Section 2.6). The chapter concludes with a review of the potential future research needs in hydrological and isotopic modelling.

2.1 A Review of Hydrological Modelling

Hydrological modelling is the simulation of the distribution and movement of water through the hydrologic cycle. Hydrological models attempt to simulate physical processes using mathematical equations, which may or may not be physically-based in order to predict water quantity and sometimes quality. Hydrological models are typically used in the prediction of streamflow discharge and estimation of catchment water balances. The Stanford Watershed Model (Crawford & Linsley, 1966), created in 1966 was one of the first of its kind; its inception coinciding with the advent of digital computers. Crawford and Linsley (1966) developed the model with the intention of performing quantitative analyses of hydrologic regimes using continuous simulation of mathematical relationships that describe hydrologic interaction. Their first attempt to apply mathematical equations to describe physically-based hydrological relationships has continued and evolved into a large array of numerical models used to simulate hydrological processes. Improvements in computational power and efficiency, as well as data accessibility have produced a new generation of models suitable for water resource management studies across large-domains and long-time sequences. The following section first describes common classifications of hydrological models, and the differences among models sutiable for this research. With a multitude of models to choose from for hydrological research studies, several of the most popular modelling systems, specifically hydrological models and atmosphere land-surface models will be described with reference to their applicability to mesoscale hydrological research.

Singh (2002) outlined several well-known, frequently utilized watershed models; each model having unique characteristics driven by the intended use for which the model was developed.

To better understand the historical development of hydrological modelling, a description of how various models can be classified based on process description, spatial and temporal scales and solution technique is presented. There are four classical types of models identified by Singh (2006):

1. Full physically-based (e.g., Integrated Hydrological Model (InHM): VanderKwaak, 1999; MIKE-SHE model: Abbott *et al.*, 1986a; Abbott *et al.*, 1986b);
2. Mixed conceptual (e.g., VIC: Wood *et al.*, 1992; WATFLOOD: Kouwen *et al.*, 1993; SWAT: Srinivasin & Arnold, 1994; TOPMODEL: Beven, 1997; SLURP: Kite, 2002);
3. Unit hydrograph (e.g., Instantaneous Unit Hydrograph (IUH): Clark, 1945; Nash, 1957); and,
4. Stochastic models (e.g., Akintug & Rasmussen, 2005; Burns, 2002; Krzysztofowicz, 2001).

Recent advances in computational hydrology and data processing have led to the development of full physically-based models that incorporate physical properties into mathematical equations in order to simulate water and energy movement. These models are desirable for their accurate and complete representation of physical processes, but typically require large amounts of input data and tend to be computationally intensive. The advantages of physically-based models lie in their ability to verify and examine internal model dynamics at any point in the model run. Many of these models run simultaneous water-energy balances that allow for the careful examination and more accurate prediction of hydrological processes; for example, evaporation and snowmelt. In order to simulate hydrological processes in a physical sense, such models rely on a multitude of inputs that often times come from copious amounts of measured field data that are often not accessible or feasibly measured across large domains. The models can also be computationally demanding and therefore are often restricted to use on smaller, well-instrumented study areas for research purposes and are rarely, if ever, used operationally. Full physically-based models are required to describe detailed, small-domain groundwater-surface water interactions, catchment processes, or atmosphere land-surface interactions that require accurate simulations of both energy and water balances.

Mixed conceptual models (i.e., WATFLOOD) evolved from the desire to simulate large domains using physically-based equations. Realizing that mesoscale modelling requires

computationally efficient numerical schemes and feasibly measured parameterizations of physical processes, this classification of models utilizes a large amount of logic in their structure. The logical component of such models allows for a better representation of discontinuous processes (i.e., surface runoff, interflow, recharge, dry channels, regulated flows, overbank flow) while maintaining higher computational efficiencies and minimizing sub-process parameterizations. These partially physically-based models have become increasingly more popular because of their applicability to large domains and ease in simulating long-time sequences. They are preferred in simulations where shortages of measured data exist for model parameterization and calibration, or where there are no observed data available rendering the unit hydrograph or stochastic models infeasible (i.e., hydrological forecasting).

The unit hydrograph model uses observed streamflow data and conventional unit hydrograph methods to transform runoff volume into streamflow estimation. Runoff is either measured directly or can be derived from empirical models (Viessman & Lewis, 1996); the most common empirical model being the Soil Conservation Service (SCS) method (Mockus, 1957). Unit hydrograph modelling is often the only feasible way of routing storm flows in practice. Generally reasonable estimations of runoff can be derived despite specific watershed characteristics and hydrologic processes that are not directly incorporated. The downfall to this approach is the use of linearly-based estimations representing non-linear hydrological processes (e.g., runoff), and that the model fails to represent large scale variations in antecedent conditions and temporal variability of contributing areas and water movement.

Stochastic or parametric models are statistically-based models that represent current or future hydrological processes based on observed data. They form estimations of runoff today based on past experiences, and are often used for regression-based predictions of current hydrology or future predictions of floods and severe weather events. Stochastic models are not applicable when only short-term hydrometric records are available, or when field data are scarce, as parameterization of the model becomes difficult. They are limited in their ability to perform short-term predictions of streamflow due to their reliance on longer term historical patterns, and often have difficulties reproducing short-term extreme variations of streamflow. They are most commonly used for long-term predictions of climate and hydrological variability and in determining the historical limits of natural watershed variation.

The above classifications of models can be sub-classified as either lumped or distributed modelling systems. The earliest versions of hydrological models are typically considered to be lumped models that generate an aggregated watershed response from a defined watershed area and averaged watershed parameters. The development of high resolution, distributed forcing data for precipitation and landcover have introduced the capability to consider unique physiographic regions, enabling the segregation of hydrological responses that instead are summed to derive a total watershed response (Beven, 1997; Danish Hydraulic Institute (DHI), 1993; Kouwen, 1988). Researchers have debated whether distributed models have significantly improved streamflow estimation. Tao & Kouwen (1989) showed that the use of a grouped response unit (GRU) yielded 10% improvement in simulated streamflows over the use of a lumped model. However, Refsgaard & Knudsen (1996) compared three different types of models and concluded that all models performed equally well once sufficiently calibrated, and that distributed models performed only marginally better with minimal calibration. Dibike and Coulibaly (2007) recently compared the distributed WATFLOOD model with the lumped-conceptual HBV-96 modelling system. Both models were calibrated to the same data; however, HBV-96 was calibrated for each watershed whereas WATFLOOD parameters are applied to the entire study area. They found that both models performed satisfactorily when simulating streamflow when historic records of precipitation and temperature were provided, and that the performance of both models decreased with downscaling of model forcing data.

Where it was once necessary to only estimate streamflow discharge however, the focus of modelling has shifted to include quantification of spatial variability resulting from the increasing urgency to develop sustainable watershed planning and management strategies (Singh & Frevert, 2002). There has consequentially been a greater emphasis toward using distributed modelling approaches that have integrated GIS and remote sensing inputs to describe, for example, precipitation amounts, landcover and topography. The development of distributed, physically-based models has enhanced the ability to research mesoscale variability attributed to small-scale hydrological processes contributing to runoff generation. This has contributed to the shift from lumped, conceptually-based modelling approaches to more sophisticated, fully and partially physically-based, distributed modelling approaches beginning in the late 1990s (Beven, 1997; Refsgaard & Knudsen, 1996).

The scale or resolution of a modelling system is an important discriminating factor when selecting a model. With significant advances in technology, the opportunity to simulate physically-based processes in high resolution across larger domains has emerged. Soulsby *et al.* (2006) suggest that there is a need to lessen focus on small-domain prediction and instead focus on developing and improving models that operate on watershed domains; where policy and management decisions are being made. Watershed models represent physical processes in a more conceptual manner to reduce computational requirements and required parameterizations and therefore can be used to successfully capture mesoscale variation and regional sensitivities in water budgets. Spatial resolution and temporal scaling issues are therefore often at the heart of hydrologic problems, dictating model choice and suitability (Blöschl, 2001). Temporal scales can vary substantially and are often times determined by limitations in data availability and numerical stability criteria associated with the solution technique.

The spatial and temporal scale that a modelling system operates on largely dictate the solution methods chosen for the hydrological simulation by determining whether hydrodynamic or hydrologic routing are used. Hydrodynamic routing solves the Saint-Venant equations that describe continuity between water balance and momentum, which in practice, is often (but not always) too complex for watershed modelling because it requires data that are difficult to obtain over larger domains. Most often hydrologic routing (i.e., the continuity equation based on the Saint-Venant formulation that uses empirical relationships to replace the momentum equation) is used in hydrologic and General Circulation Models (GCM's) that focus on modelling large domains. Arora *et al.* (2001) performed a detailed comparison of routing schemes for the Mackenzie Basin (1,700,000 km^2) and concluded that the results "support the use of large-scale flow routing". Models applying hydrologic routing principles often have limitations associated with basin size and discretization, and simulation of flow regime extremes.

2.2 Modelling Systems

As the previous section highlighted, the appropriateness of a modelling system to describe a hydrologic problem depends on the information required from the simulation (i.e., streamflow or internal sub-component flows), the type of data available for model forcing (i.e., lumped

parameterizations or distributed inputs), and the required spatial and temporal resolution of the simulation (i.e., catchment-scale or mesoscale). With a multitude of modelling systems to choose from it is important to understand the key differences between several of the most well-known and frequently used models. Singh (2000) presents a detailed description recounted by each model creator of the various hydrological modelling systems available to hydrological modellers. Each model has its own inherent strengths and weaknesses, and it is up to the user to determine which model is most applicable to the problem being solved. In any modelling study, the choice of model and a detailed understanding of the models assumptions and limitations are key to the success of the modelling study and the reliability of the outcome.

For hydrological investigations seeking to utilize stable water isotopes land-surface models are most representative of physical changes to isotope mass balances as they incorporate both water and energy balances (Section 2.2.1). Land-surface models are however limited in their physical-representiveness across large domains where parameterizations to describe flow processes must be estimated (not measured) due to feasibility and cost effectiveness. Therefore several partially physically-based, distributed hydrological models (Section 2.2.2) seem equally as appropriate in their potential to accurately describe mesoscale hydrological and isotopic variations. Both types of models, when applied to mesoscale watersheds, require rigorous internal calibration and verification with minimal amounts of measured data.

2.2.1 Hydrology-Land-Surface Schemes (HLSS)

Land-surface models (LSMs) perform coupled water and energy balances. They are typically preferred in hydrological research because they more accurately partition hydrological flows contributing to streamflow (Hurkmans *et al.*, 2008). Hydrology land surface schemes (HLSS) are models that interface land-surface energy and water balances with hydrological modelling in order to produce simulations of streamflow and other land surface processes. Their disadvantage tends to be their conceptualized approach to surface runoff and routing mechanisms. In keeping with a physically-based and efficient approach to hydrological simulation, the Variable Infiltration Capacity (VIC) model is one such land-surface model (LSM) used to simulate hydrological partitioning between the subsurface and runoff generation (Liang

& Lettenmaier, 1994; Liang *et al.*, 1996; Wood *et al.*, 1992). The VIC model is classified as a variable-layer soil-vegetation-atmosphere transfer (SVAT) scheme, which was developed for use in general and regional circulation and weather prediction models. Routing of surface runoff generated within the VIC model is performed by an algorithm coupled with the VIC model that generates an impulse response function based on the linearized St. Venant equation (Hurkmans *et al.*, 2008; Lohmann *et al.*, 1994a; Lohmann, *et al.*, 1994b). One distinct disadvantage of using the VIC model for hydrological routing is the models more conceptualized approach to runoff generation and the absence of a surface storage mechanism that is fundamental when modelling low-gradient land surfaces.

There are also on-going initiatives to further interface climate models with surface hydrology models, or HLSSs for the purposes of improving both flow simulations and climate predictions (Pietroniro *et al.*, 2007). Several climate models have been coupled with soil-vegetation atmospheric transfer (SVAT) schemes to improve atmospheric feedback from the land surface (both water and energy), but their operational use has been limited (Kunstmann *et al.*, 2004; Rosenzweig & Abramopoulos, 1997; Sturm, 2005). Yet there have been only a few attempts to interface atmospheric models with HLSS's to design a fully coupled system suitable for operational forecasting as well as research (Schmidt *et al.*, 2006; Seuffert *et al.*, 2002). The distinct advantage of coupling atmospheric and hydrologic interactions is the ability to validate both climate predictions using land surface hydrology, and the ability to improve hydrological parameterizations using climate drivers. Environment Canada recently announced the development of the MEC environmental modelling system that enables the coupling of different land surface schemes to atmospheric models (Pietroniro *et al.*, 2007). The MESH model (evolved from WATCLASS) is an on-going initiative to integrate surface and hydrology into the MEC modelling system.

Formerly derived from a coordinated development effort between hydrologists and atmospheric scientists, WATCLASS was developed from coupling the Canadian Land Surface Scheme (CLASS) (Verseghy, 1991; Verseghy *et al.*, 1993) and the WATFLOOD hydrological modelling system (Kouwen, 1988; Kouwen *et al.*, 1993). CLASS represents a land parameterization model that was first developed for the purposes of simulating the lower boundary of the Canadian General Circulation Model (GCM). It uses physically-based representations of land surface

processes that, as most land surface models do, require the exchange of heat flux, moisture, and momentum with the atmosphere. It does not simulate runoff from the land surface on its own, but instead is coupled with the WATROUTE routing scheme from WATFLOOD. The ability to simulate ground hydrology and atmospheric water-energy balances is the basis for the development of the MESH regional hydrological modelling system (Pietroniro *et al.*, 2007).

MESH performs detailed energy balances from the LSMs in MEC, land-surface parameterizations and sub-grid variability in landscape from CLASS, and hydrologic routing from WATFLOOD. The benefit of using WATFLOOD routing for water balance simulation is that the grouped-response unit approach enables model calibration over the entire basin simultaneously for distinct land classifications (Kouwen *et al.*, 1993). MESH streamflow simulations require long- and short-wave radiation, humidity, temperature and wind speed measured from the same reference height, and surface pressure inputs in addition to precipitation and temperature inputs required for hydrologic routing. However the integration of the two models permits runoff induced changes to influence the thermal heat capacity of surface and subsurface layers.

While MESH performs detailed water and energy balances that increase the accuracy and physical representation of hydrological processes, it is unfortunately limited by computational complexity and the multitude of input parameters required for coupled water-energy balance simulation. Classical mesoscale hydrological models however, such as WATFLOOD, are computationally less expensive and have been shown to perform better than WATCLASS for large watershed-scale streamflow simulations where streamflow discharge estimation is the main objective (MacKay *et al.*, 2003). Land-surface schemes and atmospheric-land-surface modelling systems are still in their infancy, and even though they are no doubt the future of hydrological simulation, there remains considerable testing and model evaluation that needs to be conducted before the models are ready for predictive forecasting and operational use. The integration of stable water isotopes into HLSSs and atmospheric-land-surface models is useful for model calibration and error diagnosis, but currently seems premature for reliably simulating $\delta^{18}O$ in runoff and streamflow responses.

2.2.2 Hydrological Models

The integration of stable water isotopes into a hydrological model seems to be a logical first step in resolving the ability to simulate isotopes in streamflow. With the development of the MEC modelling system for example, an isotope-enabled hydrological framework once tested can be feasibly integrated into the MESH modelling system such that atmospheric-land-surface isotopic and hydrologic interactions can be concurrently simulated. Such a coupling involves numerous logistical and computational complexities, and first requires the independent validation of each model component individually. Therefore the intent is to select a hydrological model that can be interfaced in the future with coarser-resolution atmospheric models (i.e., regional scale), and which is computationally efficient such that additional complexity from isotope mass simulation will not prohibit mesoscale simulation. With a multitude of models to choose from however, it is necessary to understand and describe the differences between the model frameworks and their practicality for this research study.

The development of InHM (VanderKwaak, 1999) introduced a modern distributed, fully-coupled, physically-based hydrological model capable of producing not just streamflow discharge, but fully coupled surface water-groundwater interaction and solute transport functionality. Making use of the multitude of hydrologic and geomorphologic studies in current research, InHM was designed to include relevant hillslope hydrology laws and catchment-specific parameters. Models such as InHM have played a crucial role in advancing the understanding of hydrological process representation, physical hydrology, and hydrogeology by fully simulating and segregating individual flowpaths. Due to the computational complexity and degree of parameterization however, the model's practical application is limited to very small watersheds and hillslope studies (Ebel *et al.*, 2007; VanderKwaak & Loague, 2001). InHM is therefore of little to no practical use for mesoscale research studies, and would not feasibly operate with additional computational complexity introduced by isotope mass transport simulation.

The Soil and Water Assessment Tool (SWAT) hydrologic model was among one of the first basin-scale models performing water quality simulations and to be fully integrated with a Graphical Information System (GIS) (Srinivasin & Arnold, 1994). It is classified as a physically-

based, semi-distributed watershed model that performs continuous simulations of watershed responses, although it does incorporate some conceptualizations of hydrological processes. Although physically-based, it is commonly applied to larger domains for the purposes of land management studies and water quality assessment modelling. The SWAT model uses a water balance approach to model surface hydrology, where surface runoff is derived using the SCS curve number procedure or Green and Ampt infiltration method (Migliaccio & Chaubey, 2008). SCS-derived runoff is known however to have difficulties reproducing measured runoff from storm events since the time distribution of rainfall is not considered, and because antecedent moisture conditions are not explicitly accounted for. Runoff generation mechanisms are required to be separable and well defined for isotopic simulation.

Another commonly used conceptually-based hydrologic model is the SLURP model developed by the National Hydrology Research Institute (NHRI). SLURP is an efficient basin-scale model that has been successfully applied to a number of watershed-scale studies (Kite, 2002), and has been proven successful for use in mountainous catchments (Thorne & Woo, 2006). SLURP also incorporates the use of digital data such as landcover maps and digital elevation data. It is limited in its application to watershed variability and land-use management studies however because it is a lumped parametric model that relies on parameterizations and simplified conceptualizations to simulate hydrologic processes. The addition of isotope simulation would therefore require additional parameterizations that may not be feasible to define in remote, ungauged basins.

TOPMODEL (Beven, 1997) was developed to introduce a model that was simplistic yet still mostly physically-based and that enabled spatial visualization of model predictions. TOPMODEL is classified as a semi-distributed, mixed conceptual model. TOPMODEL physically represents some processes, but utilizes empirical relationships for others. One such feature is the deviation from the typical square grid representation of a watershed. TOPMODEL instead characterizes topography using a distributed topographic index to determine runoff generation and simulate variable source areas of a catchment (Yang *et al.*, 2000). The model was developed for application to watershed-scale hydrological prediction and has had a number of studies validate its ability reproduce streamflow discharge (Cameron *et al.*, 2000; Choi & Beven, 2007; Nourani & Mano, 2007) and internal hydrological processes

driving streamflow estimation (Gallart *et al.*, 2007; Seibert *et al.*, 1997). TOPMODEL surface hydrology has been integrated with a land-surface scheme in the development of TOPLATS (i.e., TOPMODEL-based Land-surface-Atmosphere Transfer Scheme) (Famiglietti & Wood, 1994). The TOPLATS model has more recently been coupled with an atmospheric model (i.e., Lokal Modell) to create a coupled land-surface-atmosphere modelling system (LM-TOPLATS) (Seuffert *et al.*, 2002). The integration of isotope simulation into TOPMODEL could facilitate a future coupling of atmosphere-land-surface and hydrological isotopic simulations.

The WATFLOOD model is also a partially physically-based, distributed hydrological model that uses conceptualizations of some physical processes in order to maintain high computational efficiencies. It operates using a grouped-response unit (GRU) that enables unique hydrological responses from distinct land classifications and facilitates basin calibration on a watershed-scale (Kouwen *et al.*, 1993). The WATFLOOD model allows for the incorporation of remotely-sensed topographical, landcover and meteorological forcing data to derive more physically-representative and distributed watershed responses. The WATFLOOD routing scheme, WATROUTE has been integrated into the WATCLASS and MESH land-surface schemes to route runoff contributions to streamflow (Kouwen *et al.*, 2003; Pietroniro *et al.*, 2007). The model has been subjected to rigorous internal validation to test the physical basis of its runoff generation processes which are partially conceptualized to reduce reliance on field measurements for parameterizations of flowpaths. The model's extensive validation studies, ease of calibration and reduced parameterizations, ability to incorporate external forcing data and segregated routing processes make it another good candidate for isotopic simulation.

The choice of model for this study should ideally enable future coupling with atmospheric modelling systems for the purposes of advancing climate change prediction. Therefore the model should be comprehensive in its representation of surface hydrology and operational on large-domains over long-time periods. The model also needs to have internal flowpaths that are separable, verifiable, and reliant on as few parameterizations as possible such that model calibration is made feasible for mesoscale watersheds and remote, ungauged basins.

2.3 Hydrograph Separation (HS) Studies: Reducing Equifinality

Due to the advances made over the past few decades in hydrological modelling systems, current research focus has shifted from accurate prediction of streamflow to the accurate prediction of processes generating streamflow. To reduce uncertainty and increase the reliability of hydrological models, internal model dynamics and flow sub-processes are being verified to generate physically-based model calibrations. It is no longer adequate to simply quantify total streamflow contribution and storm flow runoff in a catchment. Instead, scientists and engineers are questioning how these values are produced within the hydrological models and realizing that there are multiple paths to the same solution: the issue of equifinality (Beven, 2002; 2006). The concept of equifinality expresses that representative modelled streamflow can be determined by a multitude of contributing fractions from various hydrological compartments. Even though there are infinite contributing fractions, in theory for a particular modelled scenario only one is correct. So the question arises: can flows be accurately partitioned into their respective hydrological compartments, and how can these individual flowpaths be validated?

HS techniques have been developed over the past few decades in order to quantify and measure the flow arriving to the stream from these multiple flow pathways. Many HS models have been essentially 'black-box' models (Kendall *et al.*, 2001) that use an abundance of external information and generally quantify only total catchment response. There have been many such scientific studies undertaken since about the early 1970s to quantify groundwater (or other source water) contributions to peak stormflow (Dincer & Davis, 1984; Fritz *et al.*, 1976; Martinec *et al.*, 1974; Pinder & Jones, 1969; Sklash & Farvolden, 1979). These studies have been successful in reproducing measured groundwater, soilwater, and overland flow contributions to total streamflow hydrographs, but only for idealized and controlled situations (Brown *et al.*, 1999; Jones *et al.*, 2006; Wagnon *et al.*, 1998); namely, smaller catchments with single input and output streams, which are monitored by intense field study programs that quantify many geological and hydrological parameters within these catchments. These studies, although valuable in their contributions to catchment-scale hydrology and hydrological processes, are concerned primarily with prediction of runoff timing and volume (Kendall *et al.*, 1995). In more recent years several more detailed studies have been conducted that seek to also verify the simulated hydrological processes contributing to runoff generation (Brassard *et al.*, 2000;

Guntner *et al.*, 1999; Kienzler & Naef, 2008; Soulsby *et al.*, 2003; Uhlenbrook & Leibundgut, 2000). Such studies have focused on understanding hydrological processes at the hillslope and catchment scale for the purposes of advancing scientific understanding of these processes and to improve the physical-basis of model calibration. Now after more than a decade of catchment-scale research, a need exists to introduce such studies on larger watersheds to gain insight on the variability of source areas, runoff generation and watershed sensitivity.

Tracer studies (chemical, physiochemical, geochemical and isotopic) have been implemented in the field to assess overland, soilwater and groundwater contributions to the total streamflow hydrograph (Brown *et al.*, 1999; Gremillion *et al.*, 2000; Hoeg *et al.*, 2000; Laudon & Slaymaker, 1997; Reddy *et al.*, 2006). The ability to individually quantify flowpaths has enabled hydrological modellers to compare modelled internal streamflow contributions to measured tracer data for the purposes of verifying the simulation of these processes and improving model calibrations. The ability to internally calibrate and verify individual hydrological processes has helped to significantly reduce modelling uncertainty associated with the equifinality of flow simulation.

It has been reported that chemical, physiochemical and geochemical HS can be prone to interpretation errors since each of these tracers are subject to change along flowpathways (i.e., they tend to be non-conservative) (Kendall *et al.*, 2001; Laudon & Slaymaker, 1997). Changes in tracer concentration along flowpaths are often what is measured and used to classify input source(s); however this requires detailed knowledge of each contributing input and their chemical, physiochemical or geochemical properties. In the cases where tracers are used to segregate pre-event and event waters ("old" versus "new" water), difficulties arise due to the displacement of soil moisture during storm events (Sklash & Farvolden, 1979). Namely, the water appearing in the stream after a storm event is not necessarily event water, but rather a mixture of previous storm waters that were stored in the soil matrix for some time and may not have been initially accounted for (in terms of both volume and concentration of tracer).

Chemical tracers are limited to short-term use so that tracer concentrations are not significantly altered, diluted or decayed. Unless used to assess surface water and runoff contributions, short-term assessments are rarely desirable because of longer-term baseflow components contributing

to streamflow (Sklash & Farvolden, 1979). Dissolved constituents (i.e., solutes and silica) are often used as chemical tracers but also do not behave conservatively at the catchment scale due to channel erosion, solute settling, and water movement through small, tortuous pore spaces that tend to trap solutes (Kendall *et al.*, 2001). Physiochemical properties (i.e., electrical conductivity and suspended solids), and geochemical tracers (i.e., silica) are also used in conjunction with other chemical tracers in order to help identify distinct end-members (i.e., source waters sustaining streamflow) (Kendall *et al.*, 2001; Laudon & Slaymaker, 1997; Wagnon *et al.*, 1998). Particularly over large scales however, physiochemical properties and geochemical tracers are often non-conservative and require detailed knowledge of hydrologic controls and end-members in order to use for the purposes of flowpath segregation and identification.

Mesoscale (continental and regional) modelling studies have been performed but are primarily restricted to climatology (Kunstmann *et al.*, 2004; Sikka & Sanjeeva, 2008). In hydrology the emphasis has been on understanding catchment-scale behaviour and less so on understanding mesoscale watershed variability and hydrologic cycling. Mesoscale watershed or regional hydrologic studies have traditionally required extensive field study programs and have relied on measured parameters, or dense meteorological coverage to obtain model input parameterizations (Chen *et al.*, 2008; Dankers *et al.*, 2007). Although ideal for modelling, such field studies and required parameterizations are not always feasible in remote or mesoscale regions. Other studies have successfully modelled regional water balances without such inputs, but have stopped short of producing streamflow discharge (Zeng *et al.*, 2008), or have simulated streamflow and used traditional statistical correlation to measured streamflows for model calibration and validation (Gotzinger & Bardossy, 2007). By traditional methods, model calibration in ungauged basins becomes problematic, with no means of quantifying modelled sub-processes contributing to streamflow. To date, mesoscale HS studies have been restricted to catchment sizes of 1,000 km^2 or less (Gotzinger & Bardossy, 2007; IAEA, 1981; Johnson *et al.*, 2005; Yang *et al.*, 2000). There is a definite need however to test the validity of hydrological models being used on watershed- and regional-scales, and to develop HS techniques that can prove to be useful in tracking individual flowpaths across large domains. One possible solution to this challenge is the use of stable water isotopes as conservative environmental tracers to identify and quantifiably segregate flowpaths.

2.4 A Review of Stable Water Isotope Hydrology

A relatively new tool being utilized to understand changes within the hydrologic cycles is stable isotopes of water. There are three stable isotopes of oxygen: ^{16}O (99.63%), ^{17}O (0.0375%), and ^{18}O (0.1995%); and two stable isotopes of hydrogen: ^{1}H (99.985%) and ^{2}H (0.015%). As a result, there are nine possible 'isotopologues' of the water molecule: $H_2{}^{16}O$ (99.6%), $H_2{}^{17}O$ (0.037%), $H_2{}^{18}O$ (0.2036%), $HD^{16}O$ (0.031%), $HD^{17}O$, $HD^{18}O$, $D_2{}^{16}O$, $D_2{}^{17}O$, and $D_2{}^{18}O$ (IAEA, 1981). Each of these species occurs naturally in the water cycle, but some (i.e., $H_2{}^{16}O$, $HD^{16}O$, $H_2{}^{18}O$ and $H_2{}^{17}O$) are more abundant than others and undergo predictable changes that can be measured with high degrees of accuracy. Oxygen and hydrogen isotopes of particular interest in the hydrological cycle are ^{18}O and ^{2}H (deuterium, D) because they are naturally occurring constituents of the water molecule, they are stable (i.e., non-decaying), and they exhibit systematic variation within the hydrological cycle resulting from phase changes and isotopic fractionation during evaporation (IAEA, 2003). Isotopic fractionation is represented by the change in (δ) ratio (R) of the less abundant isotope (^{18}O) to the more abundant isotope (^{16}O), or the mole fraction of the two species, in the local sample as compared with the world standard (Vienna Standard Mean Ocean Water, V-SMOW) $R=^{18}O/^{16}O=(1993.4\pm2.5)10^{-6}$ (Craig, 1961). Stable water isotope ratios are therefore expressed as

$$\delta = \frac{R_{sample} - R_{reference}}{R_{reference}} \qquad (2.1)$$

where R represents the mole fractions of the isotopic species, or $^{18}O/^{16}O$. As the differences between the sample and reference standard are generally quite small, delta-values are expressed in per mille (‰) differences by multiplying the above ratio by 1000.

Since water isotopes are naturally occurring and stable, anything that has utilized water as part of its structure will preserve the isotopic "signature" of the water cycle at that particular point in time. Systematic isotopic labelling or fractionation of water within the hydrological cycle occurs as a result of changes in isotope composition that accompany water cycle phase changes and diffusive transport (Edwards *et al.*, 2004; Gibson *et al.*, 1996; Gibson & Edwards, 2002), owing mainly to slight differences in molecular behaviour of the rare, heavy isotopic species. These differences in molecular behaviour are governed by the physical (e.g., mass-dependent properties such as specific gravity and diffusivity) and chemical (e.g., exchange reaction rate differences

between hydrogen and oxygen) properties of the various isotopologues of water. Due to these physical and chemical differences, the isotopologues of water have different rates of transport. Based on mass differences alone, gas kinetic theory derives a range of diffusivities for each isotopologue of water. A basic rule of thumb is that lighter isotopes diffuse more rapidly because they volatilize quickly due to higher volatilization rates (i.e., lower molar masses increase kinetic transport); and similarly, isotopically heavier molecules condense more easily (Glasstone *et al.*, 1941). The distribution of mass in the gas phase and differences in intermolecular binding forces between the heavy and light isotope species contribute to differences in isotopologue behaviour (IAEA, 1981).

The changes in relative abundance of ^{2}H and ^{18}O in natural waters is the result of isotopic fractionation resulting from evaporation and condensation or freezing of water. At thermodynamic equilibrium, forward and backward exchange reaction rates between phases are identical and reversible, following the same laws of thermodynamics as for chemical reactions. The resulting isotopic fractionation or unit separation from non-fractionated water is equal to the thermodynamic equilibrium constant, α^{*} (i.e., the exchange reaction constant), which is equal to the vapour pressure ratio of natural to isotopic water molecules (Rozanski *et al.*, 2001). Isotopic enrichment resulting from equilibrium exchange is referred to as equilibrium enrichment, ε^{*} and is defined by α^{*}-1 (for liquid to vapour exchange). Physical processes that lead to equilibrium fractionation, or enrichment are vapour exchange, freezing (if gradual), and condensation (IAEA, 1981).

Under natural environmental conditions, thermodynamic equilibrium is not always established or continually maintained. In cases such as the evaporation of a water body into an unsaturated atmosphere, additional separation (beyond equilibrium separation) between heavy and light isotopic species can occur due to kinetic fractionation effects. Kinetic enrichment, ε_{k} occurs when there are differences in reaction rates of isotopic molecules resulting from differences in molecular diffusivities of the isotopic species (Rozanski *et al.*, 2001). Reaction rates may be unidirectional and are dependent on the ratios of masses of the isotopes and their vibrational energies and are quantitatively expressed using 'absolute reaction rate theory' (Glasstone *et al.*, 1941). The rate constant for isotopic fractionation is therefore a function of the equilibrium

rate constant, but is also modified to account for dissociation rate of a molecule undergoing a phase change (IAEA, 1981). Generally speaking kinetic fractionation effects are much larger than equilibrium effects, but decrease at higher temperatures and humidities where equilibrium effects begin to dominate. The amount of kinetic isotopic enrichment is controlled by humidity deficit (1-h), surface temperature, and wind speed.

The isotopic labelling of source waters is the result of isotopic fractionation occurring both in the atmosphere (i.e., the composition of precipitation) and on the land surface (i.e., fractionation resulting from phase change).

2.4.1 Isotopes in Precipitation

The isotopic composition of precipitation formed from condensing atmospheric vapour is most commonly described by equilibrium fractionation, or Rayleigh distillation (Dansgaard, 1964):

$$R = R_0 f^{\alpha-1} \tag{2.2}$$

where R_o is the original mole fraction of vapour, f is the fraction of sample remaining=V/V_o, and α is the equilibrium fractionation factor (vapour to liquid), which is temperature dependent (IAEA, 1981). Equation 2.2 describes an enrichment of vapour or condensate in the atmosphere with increasing temperature at a rate of approximately 0.5‰ per degree Celsius for oxygen (SAHRA, 2005). The offset between vapour and condensate at high temperatures is approximately 9‰, versus 11‰ at low (<0°C) temperatures where kinetic effects are higher.

The δ^2H and $\delta^{18}O$ of world-wide precipitation are correlated and behave predictably, forming what is referred to as the Global Meteoric Water Line (GMWL). If δ^2H is plotted against $\delta^{18}O$, meteoric waters cluster along a straight line defined by $\delta^2H=8\delta^{18}O+10$ (Rozanski *et al.*, 1993). A long-term, flux-weighted average of local precipitation samples from a watershed can be used to form a Local Meteoric Water Line (LMWL), which in comparison with the GMWL will exhibit an offset arising from differences in local air masses, precipitation types and temperatures, and vapour recycling. When changes in both the hydrogen and oxygen isotopes are plotted against each other as on Figure 2.1, then the offset of the LMWL from the GMWL is clearly visible, and a unique equation describing local conditions can also be regressed.

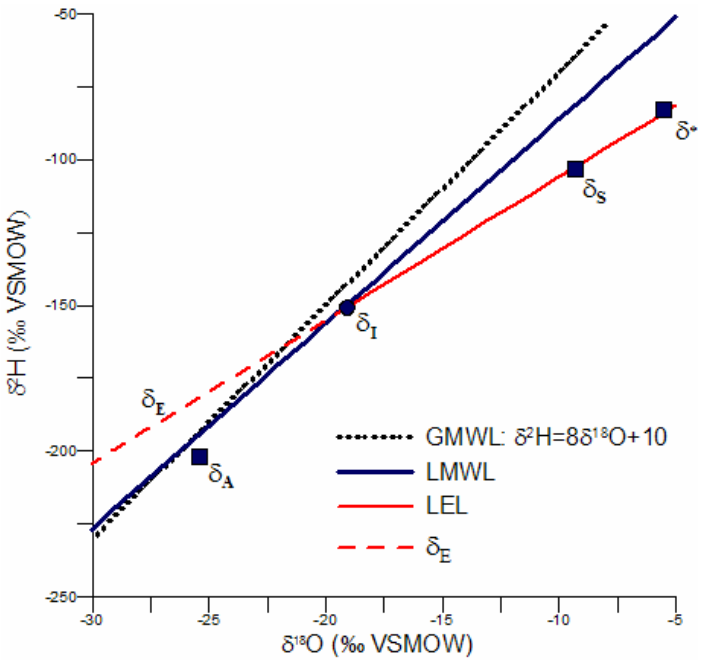

Figure 2.1 –δ^2H-$\delta^{18}O$ isotopic framework: a) GMWL representing the long-term, flux-weighted average of global precipitation approximated by $\delta^2H=8\delta^{18}O+10$ (Craig, 1961; Dansgaard, 1964); b) LMWL representing the flux-weighted average of local precipitation; c) LEL representing the regression slope of evaporating surface waters, joining the LMWL at the average, flux-weighted composition of input sources, δ_I.

There are three dominant effects controlling the signature of local precipitation: continental, temperature, and altitude effects. Figure 2.2 schematically describes the evolution of continental precipitation as ocean vapours are carried inland, lifted upward and cooled, and progressively rained out.

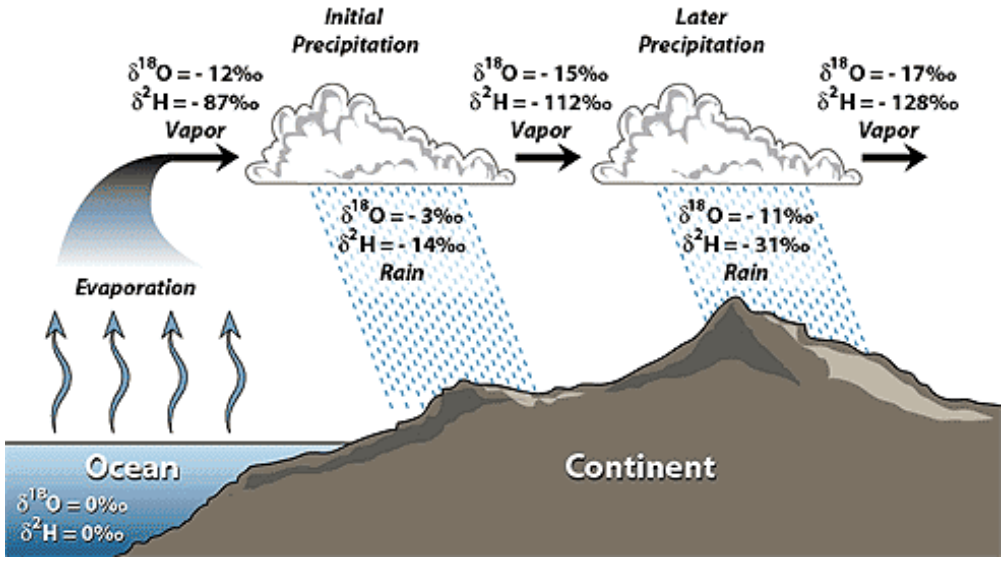

Figure 2.2 – Continental, altitudinal and fractionation effects on isotopes in precipitation (SAHRA, 2005).

Major sources of continental precipitation are the tropical oceans where the ocean water is evaporated and condensed into clouds. The water is transported pole-ward resulting in a gradual rainout and resultant depletion of the rare, heavier isotopes in the remaining cloud vapour and moisture. Mountain chains are known to deplete precipitation since rainout induced by orographic uplifting and cooler temperatures causes a loss of the heavier isotopes; generally leading to additional fractionations of 0.15 to 0.30‰ for each 100m of altitude gain (Schotterer *et al.*, 1996). The distribution of isotopes in precipitation however is most notably affected by temperature (i.e., seasonality) and amount of rainfall. Rayleigh distillation (Equation 2.2) shows that precipitable moisture becomes more depleted (i.e., in heavy isotopes) at lower temperatures. It has also been found that isotopes in precipitation in mid- to high-latitudes are directly correlated with seasonally changing temperatures. However, in low-latitudes the isotopic composition of precipitation is correlated with precipitation amount (i.e., the heavier the rainfall, the more depleted the isotopic signature) (Schotterer *et al.*, 1996).

Within the water cycle systematic labelling of precipitation begins with the source of atmospheric moisture, which is both spatially and temporally variable. For this reason, networks have been established to measure the isotopic composition of precipitation and to store and disseminate these data free to the public. The Canadian Network for Isotopes in Precipitation (CNIP), which is part of the Global Network for Isotopes in Precipitation (GNIP) (IAEA & WMO, 2006), catalogues precipitation samples within Canada. Researchers studying isotopes in precipitation and atmospheric sciences have developed maps that spatially interpolate measured isotope data accounting for equilibrium and kinetic fractionation effects, as well as temperature, continental and altitude effects Figure 2.3.

The isotopes ^{18}O and ^{2}H demonstrate great appropriateness in terms of characterizing atmospheric sources of moisture and specific climate drivers (Sturm *et al.*, 2007b). Since precipitation is used to force surface hydrology, quantifying changes in the isotopic composition of precipitation and atmospheric vapour is the first step in simulating isotopes on the land surface. One fundamental conclusion drawn from previous studies in Canada is that combined use of $\delta^{18}O$ and $\delta^{2}H$ enables the distinction of precipitation variability from varying evaporative enrichment, which offers significant advantages over use of the individual tracers alone (Gibson & Edwards, 2002; Yi *et al.*, 2008).

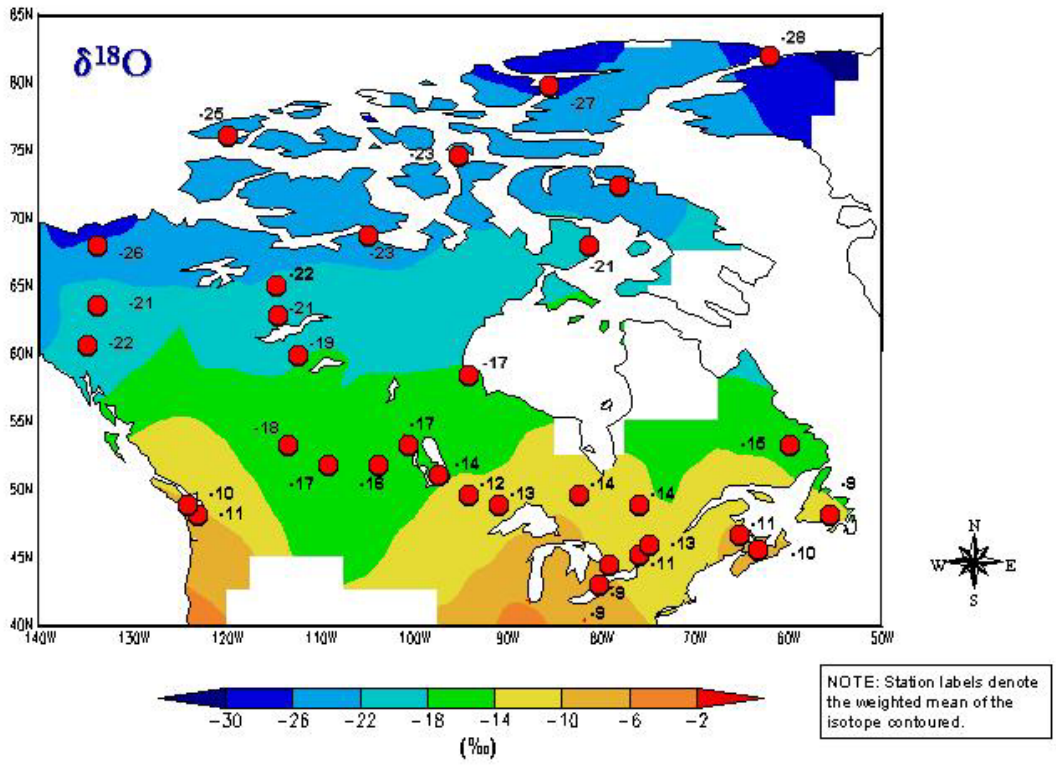

Figure 2.3 – Regional map representing a first approximation of the average distribution of oxygen-18 in mean annual precipitation in Canada, based on data from different sampling periods (Birks et al., 2004).

2.4.2 Isotopes in Evaporation

Local surface waters having undergone evaporation tend to plot below the LMWL because they become additionally enriched (i.e., above equilibrium enrichment) in heavy isotopes. Because of differences in molecular diffusivities between oxygen and hydrogen, fractionation of the hydrogen isotope is proportionally greater than that of oxygen and therefore the two isotope species do not fractionate equally. When data from evaporating surface waters are plotted in δ^2H-$\delta^{18}O$ space, the linear regression of points defines the Local Evaporation Line (LEL) (Figure 2.1) (Diefendorf & Patterson, 2005; Leng & Anderson, 2003). The LEL represents the average isotopic fractionation or enrichment surface waters will undergo across a variety of atmospheric conditions (i.e., temperature and relative humidity) in a local region. It extends from the average, flux-weighted value of surface water inputs (δ_I) to the maximum amount of enrichment a water body can undergo before desiccating (δ^*) under current atmospheric

conditions (Figure 2.1). The LEL typically has a slope between 4 and 6 in Canada. Differences in equilibrium and kinetic fractionation of isotopes of hydrogen similarly lead to a defined and predictable vertical offset from the LMWL called the *d-excess*, which can provide information on the sources of atmospheric moisture.

In contrast to isotopic enrichment in evaporating surface waters, vapour becomes more isotopically depleted because of the preferential removal of light isotope species into the vapour phase. The isotopic composition of evaporate (δ_E) is shown on Figure 2.1 as being more depleted in heavy isotopes relative to the composition of the input waters (δ_I) and lake water (δ_L). In fact, each surface water body has its own specific evaporative enrichment trend, or rate of isotopic fractionation due to catchment specific characteristics (i.e., volume of water, foliage cover, temperature, etc.). In nature thermodynamic equilibrium between the liquid and vapour phase is not typically preserved, and the result is the formation of a viscous boundary layer at the air-water interface through which moisture is transferred at a differential rate. The additional kinetic fractionation is controlled by the molecular diffusion of the isotopic species through the air phase, and by the moisture deficit (1-h) over the evaporating surface (Rozanski *et al.*, 2001). Craig & Gordon (1965) were among the first to develop a model to describe the non-equilibrium fractionation, or the gain in heavy isotopes in an evaporating, open water body as water is transported across the boundary layer via diffusion from the liquid to vapour phase. Using the classical Rideal-Langmuir linear resistance model (Rideal, 1925; Langmuir & Langmuir, 1927), water evaporating from a saturated sub-layer at the water surface is diffused through a water-vapour interface into an open, unsaturated and fully turbulent atmosphere (IAEA, 1981). Craig & Gordon related fluxes to concentrations of isotopes at the boundaries by the resistance to transport across the layer (Figure 2.4).

The change in isotopic composition of an evaporating liquid, δ_E is proportional to the transport flux of water (E) and "heavy" water (E_i). The transport flux of the common water species ($H_2{}^{16}O$) is defined by the relative humidity deficit (1-h), or driving gradient divided by the total atmospheric transport resistance, ρ:

$$E = -\frac{dN}{dt} = \frac{(1-h)}{\rho} \qquad (2.3)$$

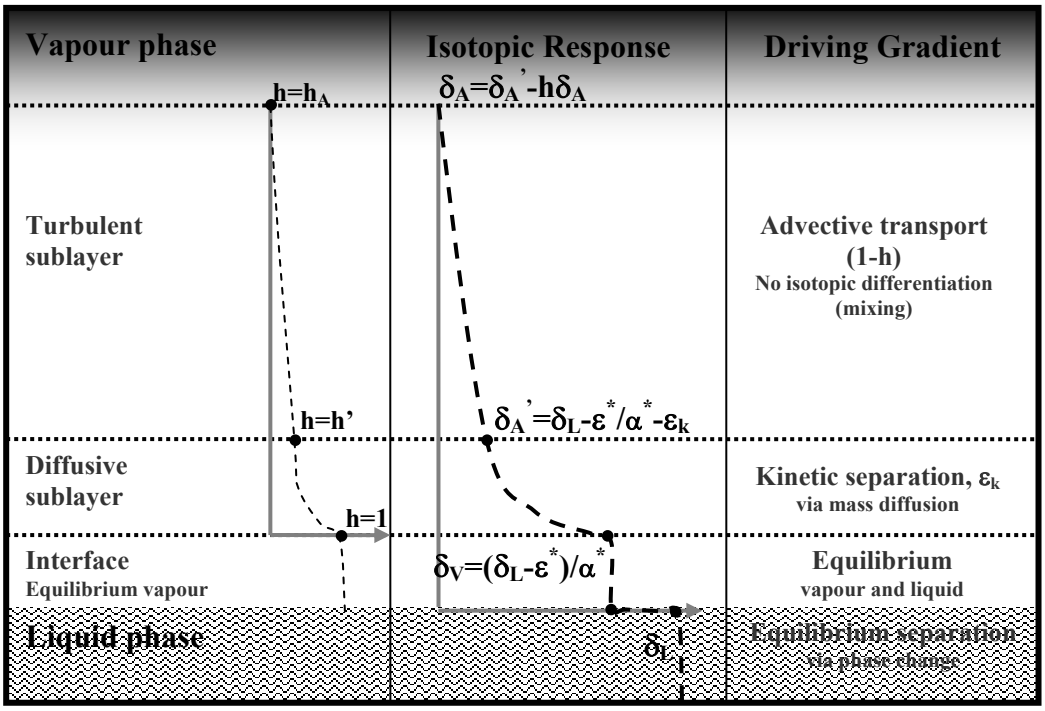

Figure 2.4 – Conceptualization of isotopic fractionation during evaporation (modified from Craig & Gordon, 1965).

The transport flux of the heavy isotope species ($H_2{}^{18}O$) is similarly defined, but instead is driven by the concentration gradient (δ_L-δ_A) relative to the specific transport resistance of the heavier isotope, ρ_i:

$$E_i = -\frac{dN_i}{dt} = \frac{(\alpha^* \delta_L - h\delta_A)}{\rho_i} \qquad (2.4)$$

where α^*, the equilibrium liquid-vapour isotopic fractionation, drives the rate of fractionation of δ_L; and the relative humidity h, drives the change in atmospheric composition, δ_A.

Craig and Gordon's conceptual model represented on Figure 2.4 illustrates that the change in isotopic composition of the evaporating flux from the boundary layer to the free atmosphere is equal to the difference between the isotope transport fluxes (E_i/E). By defining $\varepsilon=(1-h)(\rho_i/\rho-1)=\varepsilon^*/\alpha^*+\varepsilon_k$, the mean isotopic composition of evaporating moisture (δ_E) is described by (Craig & Gordon, 1965; Gonfiantini, 1986):

$$\delta_E = \frac{\left(\frac{\delta_L - \varepsilon^*}{\alpha^*}\right) - h\delta_A - \varepsilon_k}{(1-h) + \varepsilon_k} \qquad (2.5)$$

where δ_L is the lake or storage reservoir composition; ε^* is the equilibrium enrichment; α^* is the equilibrium fractionation; h is the relative humidity; δ_A is the composition of atmospheric vapour; and ε_K is the kinetic enrichment. Equation 2.5 is formulated for decimal notation as it was adapted by Gonfiantini (1986).

Equilibrium fractionation for the oxygen-18 isotope, $\alpha^*(^{18}O)_{l\text{-}v}$ is estimated using an empirical approximation developed by Horita and Wesolowski (1994):

$$1000 \ln \alpha^*(^{18}O)_{l-v} = 7.685 + 6.7123(10^3/T) - 1.6664(10^6/T^2) + 0.35041(10^9/T^3) \qquad (2.6)$$

where the equilibrium enrichment, ε^* is equal to α^*-1. The isotopic composition of atmospheric vapour, δ_A can be described by assuming that it is in equilibrium with meteoric water, δ_P; or that the displacement between δ_P and δ_A is equal to ε^*/α^* (Gibson *et al.*, 2008). The isotopic composition of atmospheric moisture (δ_A) is therefore commonly defined as:

$$\delta_A = \frac{\delta_P - \varepsilon^*}{\alpha^*} \qquad (2.7)$$

However if an evaporating water body is large enough that it contributes excess water vapour to the atmosphere (e.g., the Great Lakes in Canada), or in seasonal climates then δ_A cannot necessarily be assumed to be in equilibrium with local precipitation and instead will be better representated by an evaporation-flux-weighted δ_A (Gibson *et al.*, 2008; Yi *et al.*, 2008), where possible.

The kinetic enrichment, ε_k, describes the transport resistance associated with non-equilibrium conditions (i.e., h<1) and the ratio of the diffusivities of the two isotopic species (Craig & Gordon, 1965; Gonfiantini, 1986):

$$\varepsilon_k = (1-h)\left(\frac{\rho_i}{\rho} - 1\right) \qquad (2.8)$$

Gibson *et al.* (2008) have resolved Equation 2.8 for use on global and continental scales:

$$\varepsilon_K = n\Theta C_\kappa^0 (1-h) \qquad (2.9)$$

In Equation 2.9, η represents a turbulence parameter (0.5 for turbulent open-water bodies, 0.6 for laminar wetlands, and 1 for static soilwater); $\Theta = (1-h')/(1-h)$ is an advection term to account for the potential influence of humidity build-up over the evaporating surface and h' is the adjusted downstream humidity following the mixing of evaporated moisture (~1 for small water bodies; 0.88 for large lakes where there is significant build-up of downstream ambient moisture); and C_K^0 is 28.6‰ for oxygen as found by experiment (Gat, 1996; Vogt, 1976). The turbulence parameter η represents the amount of resistance acting to increase kinetic fractionation. High values of η correspond with higher kinetic fractionation due to differences in mass transport or diffusivity. Similarly the advection term Θ acts to reduce kinetic fractionation when there is downwind transport of ambient vapours that lower the local humidity deficit and effectively decrease diffusive mass transport.

As shown on Figure 2.1, surface waters under-going evaporation will progressively enrich towards hydrologic steady-state (i.e., inflow equal to outflow) under constant atmospheric conditions, tending toward a steady-state isotopic composition (δ_S) as f⟶0 and t⟶∞ (Gonfiantini, 1986):

$$\delta_S = \frac{\delta_L + mx\delta^*}{1+mx} \qquad (2.10)$$

where x is the evaporation to inflow ratio (E/I) representing the amount of water lost to fractionating processes; and m is the enrichment slope or rate of heavy isotope build-up originally defined by (Allison & Leaney, 1982; Welhan & Fritz, 1977) and later modified by (Gonfiantini, 1986):

$$m = \frac{h - \varepsilon_k - \varepsilon^*/\alpha^*}{1-h-\varepsilon_k} \qquad (2.11)$$

If surface water continues to evaporate and outflow exceeds inflow (i.e., the lake begins to desiccate), the isotopic composition will approach the limiting composition (δ^*) or maximum attainable enrichment of the evaporating water body under local meteorological conditions (Gat & Levy, 1978; Gat, 1981; Gonfiantini, 1986):

$$\delta^* = \frac{h\delta_A + \varepsilon_k + \varepsilon^* / \alpha^*}{h - \varepsilon_k - \varepsilon^* / \alpha^*} \qquad (2.12)$$

Both the steady-state isotopic composition (Equation 2.10) and the limiting steady-state isotopic composition (Equation 2.12) are functions of local atmospheric conditions (h, T); but unlike δ_S, δ^* is independent of lake hydrological conditions (δ_L) and dependent only on atmospheric conditions.

The applicability of Equation 2.5 to describe the isotopic composition of evaporating soilwater is not clearly established, but it is generally accepted that the modification of the ε_k term (η=1; Θ =1) can account for the lower LEL slope attributed to increased diffusive transport through the stagnant soil matrix (Gibson *et al.*, Submitted). Zimmerman *et al.* (1967) were the first to describe the change in isotopic composition of water evaporating from the pores of a saturated sand column where soil prevented pore water from being well-mixed. The change in isotopic composition through that soil column exponentially increased with depth and can be described by (Barnes & Allison, 1988):

$$\delta = \delta_{res} + (\delta_o - \delta_{res})e^{\frac{-z}{z_1}} \qquad (2.13)$$

where δ_{res} is the isotopic composition of water entering the column from below; δ_o is the surface isotopic composition; z is the depth of the column; and z_1 is a characteristic length describing evaporative resistance by effective diffusivity, evaporation rate, and tortuosity of the pore space (Barnes & Allison, 1988). Equation 2.13 implies that in order to have a steady-state concentration gradient near the soil surface at equilibrium, both diffusive (i.e., molecular transport) and convective (i.e., mechanical transport) fluxes must be in balance (Barnes & Allison, 1988). Barnes & Allison (1983) recognized that soilwater evaporation occurs from a narrow, near-surface horizontal band in wet soils, and that soil profiles can be divided into two parts: an upper zone where water moves primarily by diffusion and a lower zone where water is mechanically transported (Allison *et al.*, 1983). The isotopic composition of soilwater outside of the narrow band at the soil surface therefore becomes relatively constant with depth as infiltration is mechanically transported downward. Figure 2.5 illustrates the soilwater isotopic profile that develops as evaporation occurs from the upper zone and water is infiltrated into a lower soil zone.

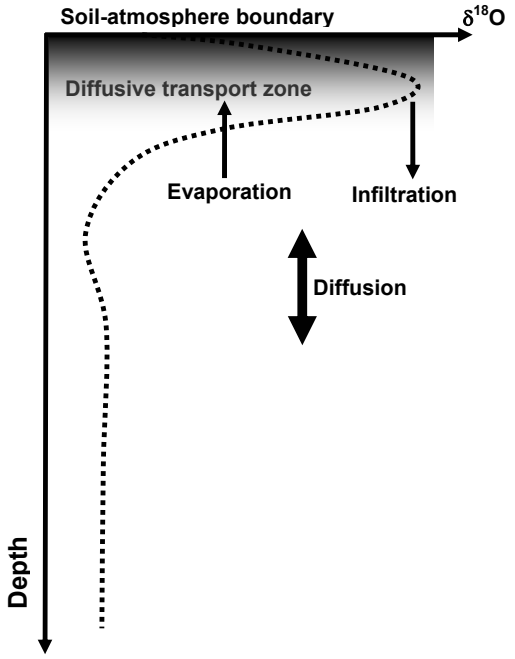

Figure 2.5 – Soilwater isotopic enrichment profile during evaporation (modified from Barnes & Turner, 1998)

Transpiration, unlike evaporation, typically does not result in significant amounts of isotopic fractionation since the plant acts more as a conduit, wicking water vapour into the atmosphere. A slight fractionation of heavy and light isotopes is observed from soilwater to the transpired vapour because plant stomata preferentially volatilize the lighter isotopes, leaving a backward flux of heavier isotopes into the leaf veins (Gat *et al.*, 2007; Ogée *et al.*, 2007). This fractionation is small in comparison to evaporation-induced fractionation and therefore transpiration-induced fractionation is generally assumed to be negligable (Dawson & Ehleringer, 1998).

Since surface, soil or plant water undergoing evaporative enrichment is distinctly altered from its original atmospheric input composition (isotopic composition of precipitation), it becomes systematically labelled and is distinct from non-evaporated (groundwater), or less-evaporated (soilwater) waters. Isotope tracers have the ability therefore to quantify dominate sources contributing to runoff, and to help assess the regional variability of runoff generation processes in mesoscale catchments (Falcone, 2007). Particularly in complex and remote hydrologic systems, isotopes have proven to be effective and feasible tools for studying mesoscale hydrologic variability (Edwards *et al.*, 2004; Gibson *et al.*, 1996; Gibson, 2002a; Gibson *et al.*, 1996; Gibson & Edwards, 2002; Gibson, 2002b; Gibson *et al.*, 2005).

2.5 Isotope Hydrograph Separation (IHS)

Stable water isotope tracers (^{18}O and ^{2}H) are useful in the study of hydrological processes contributing to streamflow generation, which is a critical component of watershed planning and management strategies. In comparison with other more traditional chemical and physiochemical tracers, water isotopes have proven to be among the most effective tools for HS studies and uniquely offer a watershed-signal linked to flowpathways enroute to the stream (Genereux & Hooper, 1998). Many of the problems associated with other chemical tracers elude stable isotope tracers: for one, they are stable (e.g., resistant to change due to interaction with a substrate); they exhibit systematic variation within the hydrological cycle; they occur naturally in all environments; and they are uniquely and indefinitely preserved in anything that has utilized, or is utilizing water. Isotope tracers have the ability to distinguish unique end-members (or sources) so long as each end-member is known and is isotopically distinguishable from the others (i.e., groundwater is generally more isotopically depleted than surface water having undergone evaporation). Isotopes of water are transported via fluxes between defined water compartments. With each flux having an assigned, distinct isotope signature or "concentration" (mole fraction or ratio of heavy to light isotope), then the internal mixing of compartments can be idealized using simplified two- and three-component mixing models. For example, a two-component mixing model to separate pre-event (Q_p, δ_p) water (e.g., soil and groundwater) from event (Q_e, δ_e) water (e.g., rainfall) contributions to total streamflow (Q_T, δ_T) is written as:

$$Q_T = Q_p + Q_e$$
$$\delta_T Q_T = \delta_p Q_p + \delta_e Q_e \ \ and \qquad (2.14)$$
$$X = \frac{\delta_T - \delta_e}{\delta_p - \delta_e}$$

Where Q represents each contributing volumetric flowrate; δ (in ‰), the concentration of heavy isotope associated with that particular end-member of the mixing model; and X the pre-event fraction of total streamflow.

According to Kendall & Coplen (2001), there are some key assumptions that must be satisfied when using mixing models for IHS:

1. Instantaneous and complete mixing of all components;
2. Identification of two or three distinctive end-members;

3. Negligible contributions to streamflow from other hydrologic end-members such that the isotopic signature of streamflow is not altered;
4. Isotopically distinct end-members;
5. Constant composition of end-members (in time and space); and
6. Conservation of the tracer.

The validity of these assumptions has been questioned by many researchers (Buttle, 1998; Harris *et al.*, 1995; Kennedy *et al.*, 1986; McDonnell, Stewart, & Owens, 1991; VanderHoven *et al.*, 2002), where debates focus on the uncertainty arising from spatial and temporal variability of isotopic composition within individual compartments or end-members. The validity of each individual assumption relies to some extent on local hydrological conditions (e.g., dominant end-members) and the extent of the spatial domain to which the assumptions are applied. It is evident that hydrologic reservoirs would vary in isotopic composition, particularly over large temporal and spatial scales; however, what is unclear is whether these variations are significant when modelling large-scale catchments. Namely, these variations are likely small when considering regional groundwater systems as opposed to local-scale groundwater variations induced by storm flow infiltration. On the larger scale, it is generally accepted and assumed that the assumptions of IHS modelling can be realistically met (Blasch & Bryson, 2007; Rodgers *et al.*, 2005; Rodgers *et al.*, 2005; Tetzlaff *et al.*, 2007; Uhlenbrook *et al.*, 2002).

Individual isotopic compositions of end-members, or water sources, can be separated from completely mixed streamflow by means of simplified mixing models (Equation 2.14). For studies predominately concerned with the separation of event ("new") from pre-event ("old") water, two-component mixing models are adequate in identifying rain, snowmelt, and groundwater end-members (Laudon *et al.*, 2002; Laudon *et al.*, 2004; Unnikrishna *et al.*, 2002; Wagnon *et al.*, 1998). A two-component mixing model can be used to compute contributions to streamflow from more than two end-members by making generalized assumptions about when various end-members are contributing significantly more than others. For example, St. Amour *et al.* (2005) used a two-component mixing model for the Fort Simpson, NWT basin to quantify the contributions of direct snowmelt, groundwater, surface water runoff, and direct channel precipitation to streamflow. Four end-members were reduced to only two by assuming that contributions by direct precipitation recharge groundwater or become direct surface runoff (for long time sequences and smaller basins); and that snowmelt occurrs only when seasonally

appropriate (Carey & Quinton, 2005; St Amour *et al.*, 2005). So long as soilwater and groundwater can be lumped isotopically a two-component mixing model is usually adequate. This is generally the case given that soilwater consists mainly of water from previous storm events that has undergone mostly transpiration (i.e., a non-fractionating process) (Kendall *et al.*, 1995). In cases where there is a significant difference isotopically between groundwater and soilwater composition (i.e., significant fractionation of soilwater by evaporation, or if the groundwater is entirely isolated from event water by a confined aquifer), then a more complicated three-component mixing model must be used (Carey & Quinton, 2005; Kendall *et al.*, 1995; Ribolzi *et al.*, 2000).

In IHS studies mixing models have been used to quantify end-member concentration or, more commonly, the end-member volume contributing to streamflow to assess the relative contribution of that source, and therefore relative importance in maintaining streamflow. The intended goal of most IHS studies has been to gain a better understanding of hydrological flowpaths and catchment residence times (Reddy *et al.*, 2006; Rodgers *et al.*, 2005; Sklash & Farvolden, 1979). IHS studies seeking to define hydrologic end-member contributions generally require copious amounts of data, including measurement of catchment characteristics and parameters, timing and volume of runoff, isotopic analyses, rainfall measurement, and hydrometric data. Although valuable in shedding insight on hydrologic interaction, such studies are not practical for larger, watershed-scale studies. At the larger-scale, mixing model derived flow separations are being used to assess the relative contributions of various hydrologic flowpaths to total streamflow (Laudon & Slaymaker, 1997; Laudon *et al.*, 2002; Soulsby *et al.*, 2000; Tetzlaff *et al.*, 2007). Isotopic flow separations are also being used to develop more physically-based hydrological model calibrations, where isotopically-derived flows are compared with model-generated flows to assist in more accurate parameterizations (Bassett *et al.*, 2008; Vache & McDonnell, 2006; Lee *et al.*, 2007; Rodgers *et al.*, 2005; Stadnyk *et al.*, 2005). These studies have relied on measured isotope data to produce flow separations via mixing models, and have subsequently drawn comparisons between isotopically-derived flows and hydrologically modelled flows. There are however weaknesses with this approach to HS associated with the limiting assumptions and continuous application of the mixing models.

Perhaps due to problems with applying IHS over large domains, there has been an intensive focus to develop a detailed understanding of the physical relationship between various hydrologic end-members and sub-processes for the purposes of developing more robust, physically-based models. The problem however is one of scale: smaller, detailed processes are not applicable to the large domain and therefore *ad hoc* relationships with little physical basis are relied upon (Gunter, 2001). These conceptualizations of reality however are practical to apply and are the only means of representing hydrologic variability on the watershed-scale; the scale at which water resource management decisions are made. Therefore what seems to be required is a means to describe physical hydrologic interactions and predict hydrological variation with minimal field observations and across large domains while ensuring modelled predictions can be validated on the watershed-scale. Some mesoscale hydrological studies are therefore using stable water isotopes and IHS to study mesoscale hydrologic variation and contributions to streamflow (Blasch & Bryson, 2007; Gibson *et al.*, 2005; Stadnyk *et al.*, 2005). Model calibration may be enhanced by constraining both water and isotopic outputs to measured streamflow and isotopic data respectively, effectively reducing uncertainties in model parameterizations and validating the internal physical accuracy of the model (VanderHoven *et al.*, 2002).

Central to the successful use of isotope tracers in IHS studies however is the ability to spatially and temporally define $\delta^{18}O$ and $\delta^{2}H$ in precipitation (Genereux & Hooper, 1998). Since isotopes in precipitation are known to vary between and among events, the quantification of isotopes in precipitation becomes integral to hydrologic simulation of isotopes. Attention has therefore turned to the simulation of isotopes, both atmospherically and on the land surface with the anticipation of utilizing them to improve mesoscale modelling systems.

2.6 A Review of Stable Water Isotope Modelling

Isotopes are emerging as a useful tool for hydrologic model calibration and validation because they offer a means to validate not just streamflow, but also relative contributions by individual flowpaths over large watershed-scales. Using stable water isotopes for mesoscale hydrological model validation requires spatially distributed isotope data across large domains. Although isotopes have become widely used tracers of flowpaths and hydrological inputs, as with

hydrological modelling much of this work has previously been done on smaller, experimental watersheds (Carey & Quinton, 2005; Reddy *et al.*, 2006; Rodgers *et al.*, 2005; Tetzlaff *et al.*, 2007). Isotope tracers are practical for mesoscale applications because they capture and preserve information from the entire catchment area, but they can be relatively expensive to continuously monitor over large regions. Sporadic point-source measurements are inadequate as forcing data for land-surface-hydrology models that continuously simulate mesoscale hydrologic (and isotopic) response. Particularly sensitive are hydrological predictions reliant on well-defined climatic forcing data: without proper meteorological inputs, hydrological simulations inaccurately represent measured flows. It has previously been shown that in order to improve the accuracy of hydrological simulations, more accurate regional climate data that are distributed, continuous, and representative of actual meteorological conditions are required (Kouwen *et al.*, 2005; Pietroniro *et al.*, 2006; Pohl *et al.*, 2007; Toth *et al.*, 2006). There is a trend therefore towards simulating the movement and fractionation of stable water isotopes in both climatic and hydrologic cycles to supplement discontinuous sample sets and further enable the use of water isotopes in mesoscale water resource studies.

2.6.1 Isotope-enabled Circulation Models

Both GCM's and RCM's are becoming isotopically-enabled, modelling isotopic variation in precipitation and vapour transport over continental and regional scales (Hoffmann *et al.*, 2000; Schmidt *et al.*, 2006; Sturm *et al.*, 2005). The stable water isotope intercomparison group (SWING) was formed with the goal of comparing isotope-enabled GCMs to one-another and to relate observational data for the purposes of improving GCM isotopic simulations (Noone, 2008; Sturm *et al.*, 2007a). One of the outlined objectives of the project was to facilitate the production of reliable atmospheric and isotopic forcing data to be used for land-surface parameterization schemes (Schott, 2005).

REMOiso (REgionales MOdel with ISOtopes) was one model involved in the SWING project. Developed by the Max Planck Institute of Meteorology, Hamburg, Germany, it is nested into the European Centre Hamburg GCM (ECHAM) and runs with a spatial resolution of 0.5 degrees (~54 km) over a timestep of 5 minutes. REMOiso simulates the isotopic composition

of atmospheric-derived precipitation, accounting for continental, topographic and orographic effects, as well as kinetic and equilibrium fractionation. A simplified land-surface scheme is included within the model to simulate soil temperature, energy and water budgets and fluxes from the land-surface; but does not incorporate a runoff-routing scheme (Sturm, 2005). REMOiso simulations of $\delta^{18}O$ in precipitation over North America have been shown to match well with point measurements and spatial discretizations of isotopes in precipitation from the CNIP network (Sturm *et al.*, 2006). This has resulted in the application of REMOiso to produce forcing data for LSMs as part of the iPILPS project (Henderson-Sellers *et al.*, 2006), and to spatially discretize isotopic inputs of precipitation and soil moisture initializations in a number of large-scale studies (Fischer & Sturm, 2006; Sturm *et al.*, 2007b; Sturm *et al.*, 2007a).

2.6.2 Isotope-enabled Land-Surface Models

In an effort to understand the fundamental relationship between land and atmosphere, and how stable isotopes are transported at the land-atmosphere boundary, a coordinated Project for Intercomparison of Land-surface Parameterizations (iPILPS) was started in September 2004 to compare the simulation of stable water isotopes from several land-surface parameterization schemes (Henderson-Sellers, 2006). Involved in Phase I of the iPILPS study are the REMOiso ILSS (Sturm *et al.*, 2005), the GISS ILSS (Aleinov & Schmidt, 2006), Iso-MATSIRO (Yoshimura *et al.*, 2006), iCHASM (Fischer, 2006), and ISOLSM (Riley *et al.*, 2002). Each isotope-enabled land-surface scheme (ILSS) reportedly simulated energy, water and isotope balances at three locations over a four year period. Simulated output from the LSMs was compared to a host of climatic, meteorological and energy flux measurements taken under the iPILPS imitative (Henderson-Sellers *et al.*, 2004). The intended goal of iPILPS is to 1) develop a framework for the comparison of ILSS models, and to 2) improve current land surface schemes by additionally constraining mass transport, through comparison with stable water isotope data (Henderson-Sellers *et al.*, 2006). Results of phase I of the project have uncovered a number of potential problems with the ILSSs; have shed-light on isotopes, water and energy balance relationships; and have diagnosed isotopic sensitivities resulting from land-surface interactions. The iPILPS study is leading to the development of a series of functional LSMs, which can be used to study land-surface-atmosphere inter-relationships and water-energy cycling.

2.6.3 Modelling Isotopes in Surface Hydrology

Isotope mass transport in the hydrologic cycle has been studied on the smaller, experimental scale by incorporating isotope tracers into process-specific models to study the variation in oxygen-18 and deuterium over time. For example, Braud *et al.* (2005a) and Singleton *et al.* (2004) studied the evolution of the isotopic response surface in soils. A key focus in these studies was to define and model the transport of isotopes through soil columns resulting from the exchange of water and mass flux. Stable water isotopes are ideal tracers for such mass transport studies because they cannot be exchanged without the presence of a water flux; moreover, if there is a hydrologic exchange, there is an isotopic exchange. One of the limiting factors Braud, *et al.* (2005b) found was the required physical accuracy of the hydrologic processes in order to accurately transport isotope mass. Other limitations included the computational requirements of such simulations and the ability to validate model outcomes with measurable, observable changes in isotopic composition that are outside of experimental and analytic error (Braud *et al.*, 2005b). Bench-scale studies are useful in defining the expected behaviour of isotope mass fractionation and are therefore useful in the design of conceptual representations to be applied on larger scales.

Several studies have also sought to model the movement of stable water isotopes over larger catchment-scales. Wissmeier & Uhlenbrook (2007) enabled the TAC process-oriented catchment model with a mixing cell solute transport scheme for ^{18}O. The exchange of solute, or ^{18}O was simulated using a series of perfectly well-mixed reservoirs that included fractionation and diffusion processes but neglected kinematic effects. Runoff generated by the model is directed through a system of linear reservoir units along a single flow direction. Generally good agreement was found between simulated and measured concentrations of $\delta^{18}O$ in streamflow produced by the model in the Dreisam basin (258 km^2). It was reported that the initial objective of validating the TAC model could not however be achieved due to large uncertainties associated with the ^{18}O composition of precipitation, and the lack of data for model initialization over such a large region (Wissmeier & Uhlenbrook, 2007). The misfit of simulated to measured data could not be directly associated to weaknesses in modelled conceptualizations, and therefore equifinality could not be ruled out. This first attempt to model $\delta^{18}O$ at the catchment-scale was limited by the ability to calibrate and initialize the model; the regionalization of input

data including the composition of precipitation and the neglect of topographical effects; solute routing errors based on conceptual simplification; and the ability of TAC model to physically represent direct runoff and infiltration processes. This study highlights the need for physically-based representations of both routing and runoff generation processes when simulating $\delta^{18}O$, even on large-scales. Spatially distributed inputs of isotopes in precipitation, and representative hydrologic and isotopic initializations were also shown to be important for model calibration.

Fekete *et al.* (2006) were among the first to hydrologically simulate isotope tracers at the continental-scale. An isotope-enabled version of the water balance and transport model (iWBM/WTM: Vorosmarty *et al.*, 1991) was developed to simulate isotopic variation in runoff over large, continental-scales. Utilizing global monthly ^{2}H and ^{18}O inputs obtained from GNIP, Fekete *et al.* (2006) modelled the isotopic variation in several large rivers in the continental United States of America. The model was calibrated at five locations with varying characteristic climates and was then applied globally to test the sensitivity of streamflow isotopic composition in response to climate drivers (i.e., isotopic composition in precipitation) and landcover characteristics. Model validation was performed for the contiguous United States using the United States Geological Survey's (USGS) isotope dataset for streamflow, where it was found that iWBM/WTM overall generated representative volumes of runoff. Stable water isotopes were found to be useful tools for model validation and for examining the relationship between runoff and precipitation, both quantity and composition. At the global scale however, verification of internal hydrologic storage can not be performed owing to the coarse model resolution and limitations in the physical representation of these storages.

Iorgulescu *et al.* (2007) predicted $\delta^{18}O$ variation in catchment outflow and storage using a parametric hydrochemical model. The hydrochemical model uses parameterizations of direct precipitation, soilwater and groundwater to estimate catchment runoff. The model was applied to the well-instrumented Haute-Mentue research basin (12.5 km^2) where $\delta^{18}O$ was simulated for the purposes of inferring runoff timescales and mixing volumes of the catchment. The model developed by Iorgulescu *et al.* (2007) relied on long-term measurements of isotopes in precipitation, soilwater and discharge to describe the behaviour of the catchment isotopic response at the basin outlet. This study is the first to simulate sub-process isotopic variation

(i.e., soilwater) at the catchment-scale and found that the process of doing so resulted in model parameterizations becoming increasingly more meaningful. The authors concluded that the increased realism of model conceptualizations justifies the increased model complexity. Although able to improve knowledge of the interaction and cascade-like mixing of catchment-scale sub-processes, the approach taken by Iorgulescu *et al.* (2007) is limited in its applicability to remote, mesoscale catchments because of the multitude of parameters and measured data required to derive the behavioural model.

It was suggested by Fekete *et al.* (2006) that isotope simulations would be expected to improve should more detailed models with more realistic architectures be used to simulate isotope transport and fractionation within the hydrologic cycle. Furthermore Iorgulescu *et al.* (2007) commented on the strong linkage between catchment sub-processes generating runoff and a systematic change in streamflow isotopic signal. It seems that both studies reinforce the advantages in developing more advanced isotopically-enabled hydrological models. In keeping with the methodology for model improvement outlined by Kirchner (2006), isotopes in hydrological models seem to be promising, practical tools for mesoscale model validation and internal hydrologic verification of conceptually-based process representations. The previous studies outlined in this section served to indicate that modelling both hydrology and isotopes over large spatial and temporal scales requires computational efficiency of the modelling system; physically-representative conceptualizations of streamflow and runoff generation processes; and forcing of basin topography, meteorological inputs, and proper initializations.

2.7 Future Research Needs

There remains a gap in the current body of literature surrounding the development of an isotope-enabled, efficient hydrological model that can reproduce $\delta^{18}O$ in streamflow and hydrological storage at the watershed-scale. Difficulties encountered include the computational requirements of simulating, in detail, flow generation processes across large domains. It is for that reason that conceptualizations of reality are utilized in mesoscale hydrological models, where the loss of physical accuracy and detail then make mesoscale modelling a very 'black box'

and an uncertain process. There is a desire to improve estimation uncertainty in mesoscale hydrological models, and to design model parameterizations that have a physically realistic basis.

By incorporating isotope tracers into hydrological modelling systems variations in isotopic signals can be compared with measured isotope data to further constrain model predictions. The constraint of both water and isotope budget greatly minimizes the potential for equifinality and significantly increases the physical-basis for model parameterization. Perhaps the biggest challenge in using isotopes as a validation tool in hydrological modelling remains the accurate simulation of atmospheric isotope composition used for hydrological forcing. Kirchner (2006) proposed a shift in focus for mesoscale hydrological modelling that would see modellers:

1. Make use of the extensive data networks and field observations available to researchers;
2. Replace 'black-box' approaches to modelling with 'grey box' approaches that better capture the non-linear characteristics of hydrology;
3. Develop more physically-based representations of hydrologic behaviour at larger catchment scales;
4. Decrease the amount of parameterization in hydrologic models to ensure they are feasibly run at larger scales; and to
5. Develop new methods to incisively and comprehensively test these large-scale models

Therefore, a successful mesoscale isotopically-enabled hydrological model should make use of distributed meteorological inputs and remotely-sensed landcover and basin topographical data to describe basin and climatic variability. The model will need to utilize conceptualizations to improve computational efficiencies, but must maintain a strong physical basis for process representation at the watershed-scale. To be practical in use, additional parameterizations should be minimized, and should ideally have defined physical limitations for calibration. Research presented evaluates whether the hydrological simulation of isotopes can provide a feasible method to validate mesoscale models, and tests its applicability to remote, minimally gauged basins.

Chapter 3

Study Regions

One of the intended objectives of this thesis is to develop and test the isoWATFLOOD model for its ability to accurately reproduce streamflow and $\delta^{18}O$ variation in streamflow, as well as water volume and $\delta^{18}O$ in hydrological storage. To meet these objectives, it was necessary to have study sites with both hydrometric and isotopic records covering a spatial domain on the order of thousands of square kilometres. It was also desirable to have more than one study site; one for model calibration and verification, and another for independent model validation. In the interests of testing the model's applicability across a broad variety of hydrological and physiographic settings, it was advantageous to choose contrasting study sites: one urbanized, populated and with many hydrometric gauges; and one uninhabited, remote, and with few hydrometric gauges. Given the above criteria, two Canadian study sites were chosen: the Grand River Basin (GRB) in southern Ontario and five basins in the Fort Simpson region in Canada's Northwest Territories (NWT). The GRB (Section 3.1) lies in the centre of the Great Lakes drainage basin. Much of the drainage area is agricultural and forested, with densely populated regions in the central basin. Many of the rivers and creeks that drain the GRB are regulated with reservoirs. In contrast, the five watersheds in the Fort Simpson region (Section 3.2) lie in south-central NWT in the Canadian arctic and sub-arctic at the confluence of the Mackenzie and Liard Rivers. The Fort Simpson Basins (FSB) are predominantly covered by wetlands and dense forests, are sparsely inhabited, and have a largely unregulated drainage network.

The following sections describe each the climatology, geology, ecology, hydrology and the available measured data for both study sites. One year of data (1997) from the Fort Simpson site was used for model development, calibration and verification. Model validation was performed on subsequent years, 1998 and 1999 (presented in Chapter 8 of this thesis). The Grand River study site was utilized for mesoscale, model validation and hydrological variability assessment (presented in Chapter 9 of this thesis) from 2003 through to the end of 2005.

3.1 Grand River Basin, ON, Canada

The Grand River Basin (GRB) lies between Georgian Bay and Lake Erie [79° 30´ to 80° 57´ West; 42° 51´ to 44° 13´ North], stretching from Dundalk, ON in the north to Dunnville, ON in the south. The watershed is located approximately 100-km west of Toronto, ON, Canada (Figure 3.1). This watershed is southern Ontario's largest, with a drainage area of over 6,000 km^2.

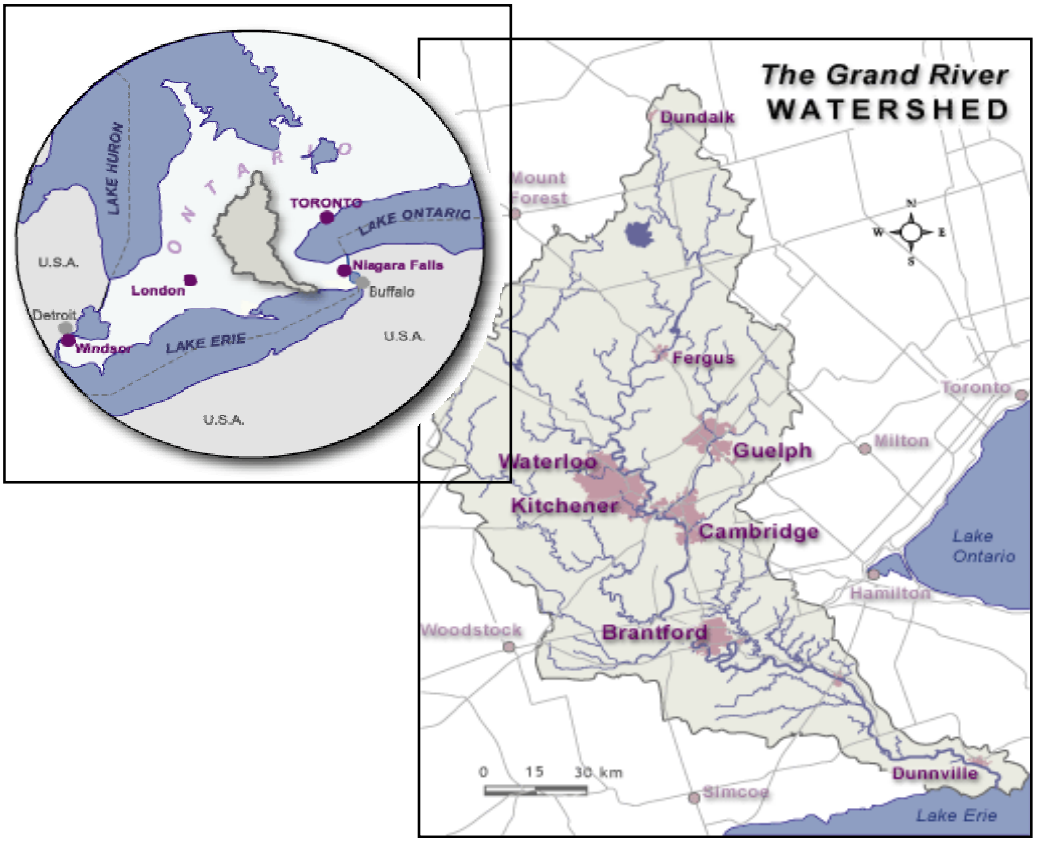

Figure 3.1 – Location of the GRB (GRCA, 2008a).

The GRB was chosen as a study site for this research due to the strong understanding of water resources and hydrology within the watershed resulting from years of extensive sampling programs, and because of a recent initiative to collect and analyze river isotope data across the watershed. The drainage area of the GRB includes rural lands in the north and south; and the central, heavily populated, cities of Kitchener, Waterloo, Cambridge, Guelph and Brantford. It is both variable in landcover characterization, but typical of southern Ontario watersheds with extensive forested areas and agricultural lands interspersed by major urban centres. The GRB is part of the Great Lakes Basin (GLB), draining on average more than 55 cubic meters per second (cms) of water annually into Lake Erie drainage basin (Water Survey of Canada (WSC), 2001). It is considered among one of the most biologically diverse river systems in the GLB, but in recent years its biological community has begun to show signs of stress due to declining water habitat and quality (Metcalfe-Smith *et al.*, 1997).

The Grand River has a unique heritage in southern Ontario. For many communities along the Grand River, the river has historically been a source of transportation, power generation, agricultural and drinking water supply. To protect these communities and the economic prosperity of the region, several dams were constructed to prevent the annual occurrence of flash flooding, and to supply flow augmentation for the dry summer months. Increased urbanization and deforestation of the GRB has led to a degradation of the natural watershed and water quality of the Grand River and its main tributaries (GRCA, 2008a). Today the watershed houses more than 787,000 people who rely on groundwater and surface water resources within the GRB for their water supply. Between 2001 and 2007 the population of the basin grew between 4-10% on average and between 10-20% in Waterloo Region (i.e., Kitchener, Cambridge and Waterloo) (Statistics Canada, 2007). The watershed's resources are in high demand among competing stakeholders including residential, commercial, and industrial users, as well as farmers.

The following sections describe the GRB's hydroclimate, geology, hydrology and ecology. Detailed information as to the collection of hydrometric, meteorological and isotopic data used in this research is presented.

3.1.1 Hydroclimate

The hydrology of southern Ontario is generally characterized as a humid climate (typical continental climate modified by the Great Lakes) with high amounts of precipitation, particularly in the northwest and annual runoff ranging from 200-600 mm (WSC, 2001). The GRB crosses four different climate zones, and two forest zones (GRCA, 2008a). The upper portion of the basin, the Dundalk Uplands, is typically cool with more precipitation falling as snow than rain. In the mid-basin, there is higher than average precipitation on the west side of the watershed. In Lake Erie County, the lower portion of the basin, the climate is typically milder and drier (Ivey, 2002).

Scattered throughout the GRB are several Environment Canada Class A Synoptic weather stations and a host of other weather stations that record hourly temperature, wind speed, rainfall, snowfall, and a variety of other meteorological variables. In southern Ontario, January and February are typically the coldest and driest months of the year; contrasted by July and August, which are typically among the warmest and wettest. The warmest air temperatures tend to occur in July and can reach average daily maximums of 27$^{\circ C}$ (Environment Canada, 2004). Average annual precipitation varies from 850 to over 1000 mm, with the highest amounts recorded to the north-west side of the basin; decreasing to the south-east. Rainfall accounts for 80 percent of the precipitation falling in the basin and typically occurs in late summer and early fall. Snow cover typically occurs from January to the end of April. Snowfalls can reach depths on average of 250 cm per year in the snow-belt region to the north-west (Environment Canada, 2004). Extreme rainfall events are most common in July and August and can result in flash flooding of the basin, as can the spring snowmelt in March and April. The average air temperature and total yearly precipitation over the study period (i.e., January 2004 to December 2005), recorded at the Brantford MOE station (i.e., south-central GRB), was 9$^{\circ C}$ and 790 mm, respectively (Environment Canada, 2004).

The climate of the GRB is affected by several types of air masses resulting in highly variable climate. The principle moisture source for this region is the warm, humid tropical air masses originating over the Gulf of Mexico. It has been estimated that these air masses provide somewhere around 75% of the GLB and GRBs precipitation (USGS, 2006). Re-evaporated

moisture from the Laurentian Great Lakes and other surface waters contribute less than 20% of the local moisture, but can occasionally generate lake-effect local precipitation (GRCA, 2008a). Cold, dry polar air masses from northern Canada contribute moisture to the Great Lakes region and the GRB during the winter months. Polar maritime air masses originating in the north Pacific and Atlantic Oceans can contribute moisture to the Great Lakes region, although typically these air masses lose most of their moisture before reaching the Great Lakes (USGS, 2006).

3.1.2 Geologic Setting

The headwaters of the Grand River (525 masl) originate in the Dundalk and the Grand Valley region. Basin elevation decreases in a south-easterly direction where the Grand River drains into Lake Erie (100 masl) at Port Maitland, approximately 128 km south of the headwater (straight-line distance). Dominating the northern landscape of the GRB are the Dundalk and Stratford till plains consisting of poorly drained sandy-silt clays and clayey tills. Natural wetlands and marshy areas are common in the north because of the poorly draining surficial geology. To the north east, soils become sandier and are well-drained promoting large forested areas and riparian zones, or channelized wetlands. The central Grand River is significantly steeper and has cut deep gorges through the outcropping dolostone bedrock (i.e., Elora Gorge). Instead of clayey till underlying the river in the north, the central Grand lies primarily on gravel beds (Chapman & Putnam, 1984). The lower portion of the Grand River is flat and low-lying, formed on an ancient glacial lake bed consisting silts and clays (Chapman & Putnam, 1984). To the west is the Oxford till plain and the Mount Elgin ridges; to the east, the Flamborough plain with shallow soils, wetlands, and bedrock outcrops; and to the south, the Norfolk sand plain and aquifer followed by the Haldmand clay plain and delta draining into Lake Erie (Ivey, 2002).

3.1.3 Ecology

The headwaters of the GRB provide natural habitats for many rare bird and plant species, particularly in the densely forested and open marshy regions. The central portion of the GRB is the most heavily populated region, home to three of the largest cities in the watershed

(Kitchener-Waterloo, Cambridge, and Guelph) and a significant transportation corridor, Highway 401, which cuts through the middle of the watershed affecting both hydrology and wildlife migration. The ecology of the central portion of the basin has been significantly stressed by increasing rural development. The eastern Guelph drumlin fields in this region are among the most heavily forested areas in the watershed and maintain productive wetlands and coldwater fisheries deemed Environmentally Significant Areas (Ivey, 2002). In the lower Grand, ecologically significant wetlands and cold water courses support a variety of provincially and regionally important species and coldwater fisheries.

LandSat satellite imagery shown on Figure 3.2 indicates the dominate landcover classifications in the GRB are urbanized (or impervious), bare soil, forested, agricultural, wetlands, and water.

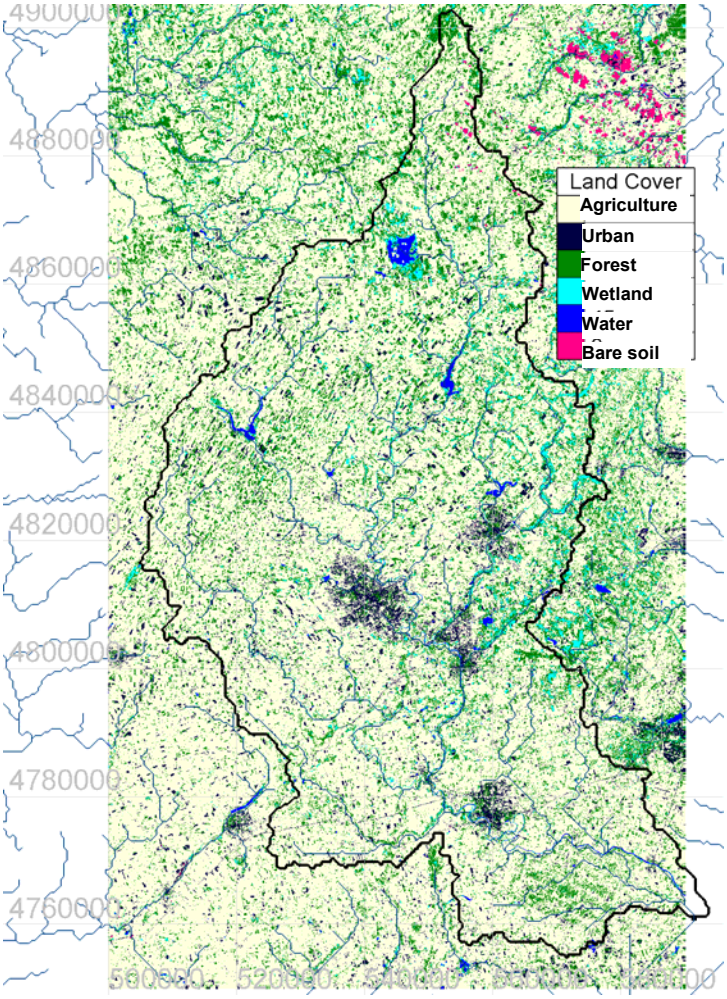

Figure 3.2 – Landcover classification map for the GRB.

3.1.4 Hydrology

In addition to the Grand River (6,245 km^2), the GRB houses four major tributaries: the Conestogo (~800 km^2), Speed (~750 km^2), Nith (1,030 km^2), and Eramosa (~230 km^2) Rivers. The watershed is a highly instrumented basin with 41 streamflow gauges (some maintained by the WSC, and some by the GRCA) and seven Ministry of the Environment (MOE) water quality gauges (pH, temperature, conductivity, and dissolved oxygen) currently monitoring main tributaries and other smaller streams and rivers. The basin includes seven controlled reservoirs: Lake Belwood, Conestogo Lake, Shades Mills, Luther Dam, Laurel Reservoir, Woolwich Reservoir, and Guelph Lake. There are more than 40 sub-basins identified within the watershed, ranging in drainage area from 20 km^2 to 5,170 km^2 (Figure 3.3).

The often flashy hydrologic response of southern Ontario watersheds is generally driven by the dense urban regions and associated deforestation and draining of wetlands. The hydrological regime is quite variable from north to south and is typically described by three regions: the upper Grand, central and lower Grand. The upper Grand is characterized by high elevation plateaus with low-relief marshy areas induced by poorly drained soils, leading to sustained streamflows interspersed by flashy runoff responses during large events. The central Grand has steeply sloping, incised channels and significant urban centers that produce high amplitude hydrographs. The lower Grand is dominated by clayey till, low gradient, agricultural lands that typically produce large volumes of runoff, but with more damped responses due to wetland storage retention in the lower Grand River region. Snowmelt hydrographs typically show more than one distinct freshet due to the temperate southern climate, and streamflow generally peaks in April as a result of the spring freshet. Annual minimum discharge generally occurs in the winter months when small tributaries are completely ice-covered, and main tributaries are at least partially ice-covered. Peak summer streamflows result from sudden storm events that produce large amounts of runoff throughout the basin.

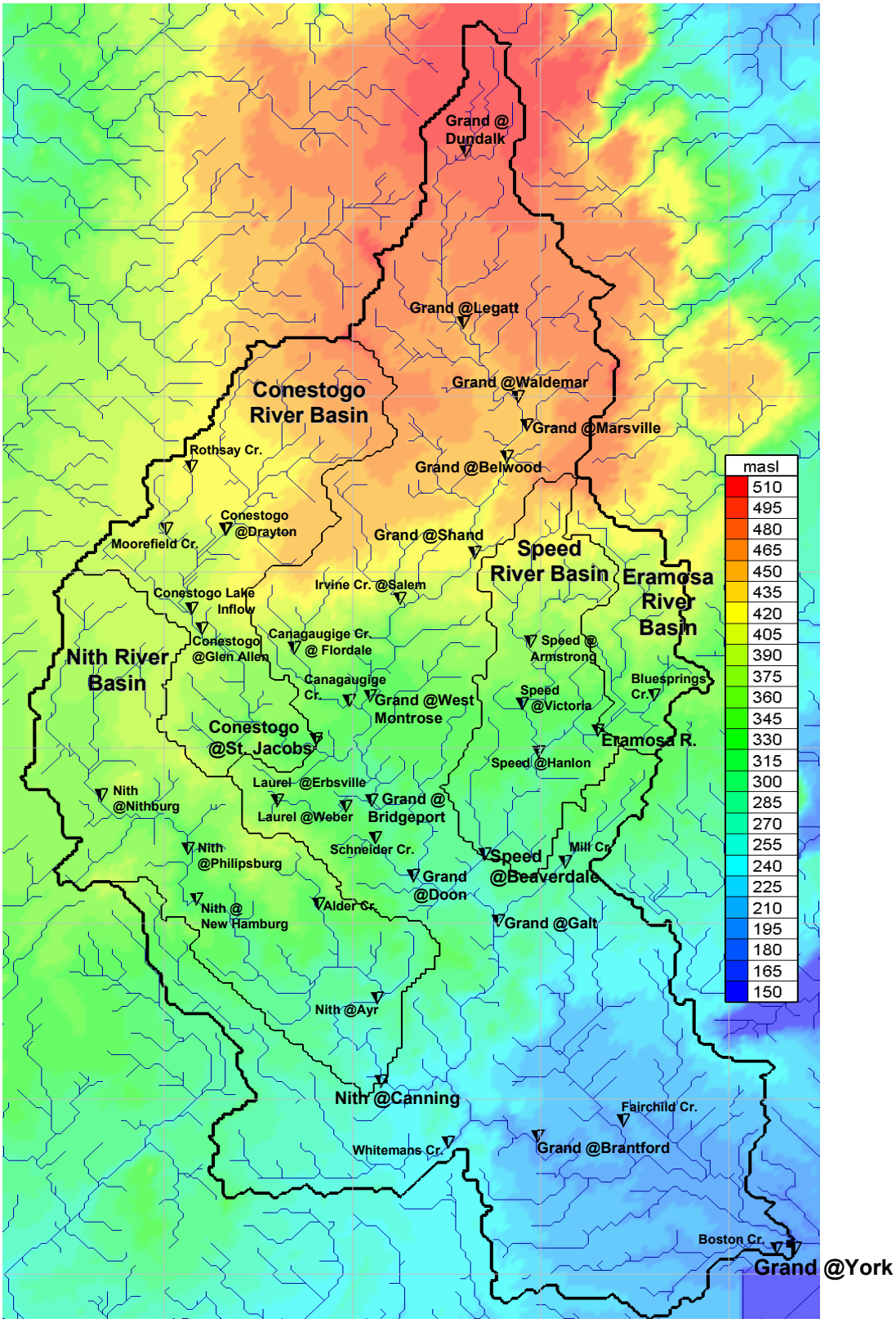

Figure 3.3 – Delineation of GRB indicating elevation, streamflow gauge locations, and main tributaries.

The climate, ecology, and geology of the GRB contribute to create a highly variable landscape with variable hydrologic responses. Dominant end-members contributing to streamflow are rainfall, snowmelt and wetland/riparian inflows. The presence of underlying silty and clayey tills coupled with yearly snowmelt and severe thunderstorm events contribute to flashy event hydrographs. In the low-lying bogs and wetlands lining the eastern edges of the GRB, sustained fluxes from baseflow and wetland storage are significant contributors to streamflow hydrographs.

3.1.5 Hydrometric and Meteorological data

The GRB has an excellent historical hydrometric data record with some records dating back to the early 1900s, and most records having approximately 30 years or more of data. Main tributary and sub-basin gauges have complete hydrometric data sets for the study period (2003-2005). Table 3.1 summarises the mean annual discharge for the upper Grand and each main tributary during the study period compared to the long-term average discharge. Two of the five tributaries indicate below average flow during the study period (i.e., Grand at West Montrose and Eramosa at Guelph). The Conestogo River recorded above average flows in 2003 and 2004, and the Speed and Nith Rivers both recorded above average flows in 2004. The study period was overall reasonably representative of long-term flow conditions.

Table 3.1 - Summary of average annual discharge for five main tributaries of the GRB as compared with long-term average over gauge lifespan (WSC, 2001).

Sub-basin	Drainage Area (km^2)	Mean discharge (cms)	Annual Average Discharge (cms)		
			2003	2004	2005
Grand River at West Montrose	1,170	9.49[1]	5.66	7.77	5.28
Conestogo River at St. Jacobs	789	8.81[2]	8.88	10.9	7.79
Eramosa River at Guelph	236	1.23[3]	0.631	0.920	0.949
Speed River at Cambridge	761	4.98[4]	4.66	5.51	4.76
Nith River at Canning	1,030	11.3[5]	11.9	12.7	11.7

[1]Averaged over gauge lifespan from 1968-2005; [2]Averaged over gauge lifespan from 1913-1916 & 2002-2005;
[3]Averaged over gauge lifespan from 1962-2005; [4]Averaged over gauge lifespan from 2002-2005;
[5]Averaged over gauge lifespan from 1913-2005, discontinuously.

The WSC and GRCA have intermittently maintained a total of 48 streamflow gauges within the GRB (GRCA, 2008b). Hydrometric gauges in the study area are float-based water level recorders that relate flow depth to volumetric flowrate via a manually determined rating curve.

Rivers are manually surveyed and periodically flows are measured to establish up-to-date rating curves that estimate hourly flow rates from water levels.

Precipitation data were recorded at 12 GRCA monitoring stations throughout the GRB (Figure 3.4). Air temperature, wind speed, barometric pressure, and relative humidity are also measured at these same locations. Daily reservoir release data for all seven reservoirs were obtained from the GRCA, along with air temperature, rainfall and snowfall data monitored at each reservoir location.

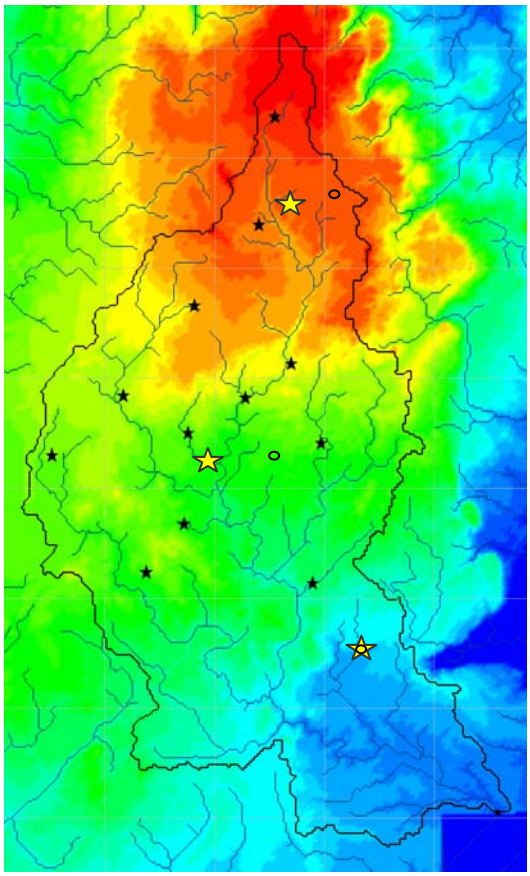

Figure 3.4 – GRCA precipitation and climate monitoring stations (stars), Environment Canada WMO Climate Normals comparison stations (circles), and GRCA climate stations compared to Climate Normals (yellow stars).

To characterize the climate during the study period (2003-2005) three Environment Canada monitoring stations were chosen to represent climate in the upper Grand, central-west, and the mid-lower GRB. Table 3.2 summarizes the Climate Normals (1971-2000) (Environment Canada, 2004) from the three GRB meteorological stations representing the upper Grand (Orangeville MOE), central-west (Waterloo Wellington Airport) and lower Grand (Brantford MOE).

Table 3.3 summarizes the average climate during the 2003-2005 study period for the same three locations.

Table 3.2 - Climate Normals from 1971-2000 (Environment Canada, 2004) for three GRB locations.

Climate Variable	**Climate Normals (1971-2000):**		
	Orangeville	**Waterloo**	**Brantford**
Mean daily air temperature (°C)	6	6.7	8
Relative humidity (%)	n/a	88	n/a
Total Precipitation (mm)	891.7	907.9	892.3
Total Rainfall (mm)	731.5	765	779.6

Table 3.3 – Average climate during the 2003-2005 study period for three GRB locations (Environment Canada, 2004).

Climate Variable	**Average over study period (2003–2005):**					
	Whole Year			**Ice-off Season (May-Oct)**		
	Orangeville	**Waterloo**	**Brantford**	**Orangeville**	**Waterloo**	**Brantford**
Mean daily air temperature (°C)	6.2	6.5	7.9	15.0	15.2	16.3
Relative humidity (%)	n/a	n/a	n/a	n/a	n/a	n/a
Total Precipitation (mm)	926.4	822.7	810.3	487.4	460.7	465.6
Total Rainfall (mm)	729	n/a	715.9	487.0	n/a	465.6

In addition to rain gauge data, weather radar in the form of a 1.5 km Constant Altitude Plan Position Indicator (CAPPI) image was used to represent the spatial distribution of precipitation throughout the GRB. Weather radar data were obtained from King City radar Station (43°51'N, 79°34'W, 360 masl). In the GRB there have historically been problems with false radar beam echoes from the escarpments located in the north-west and eastern portions of the basin that lead to inaccuracies in precipitation estimation. Therefore rain gauge data are used to ground-truth the radar-derived hourly precipitation estimates.

3.1.6 Isotope data

A comprehensive isotope sampling program in the GRB was launched in late 2003 for the purposes of assessing the utility of stable water isotopes in mesoscale hydrological research studies within the GLB (Gibson, 2005). A detailed sampling program began in January 2004 to monitor $\delta^{18}O$ and $\delta^{2}H$ in streamflow. Sampling was carried out on all 27 sub-watersheds at Provincial Water Quality Monitoring Network locations associated with the surface water quality monitoring program of the Grand River drainage network, as well as 16 additional locations

corresponding with GRCA gauge locations (Figure 3.5). Sampling was performed by the GRCA on behalf of the Ontario MOE (Day, 2005). Streamflow samples were collected and analysed for $\delta^{18}O$ and $\delta^{2}H$ at a frequency of eight samples per year during the ice-free months. Additional samples were periodically taken during ice-on months in order to assess whether streamflow isotopic compositions during the winter were representative of groundwater compositions, the dominant end-member assumed to contribute to streamflow during these periods. Additional streamflow samples were taken on Whiteman's Creek on a bi-weekly basis throughout the year as part of a more detailed baseflow study at this coldwater course, environmentally significant site (Day, 2005).

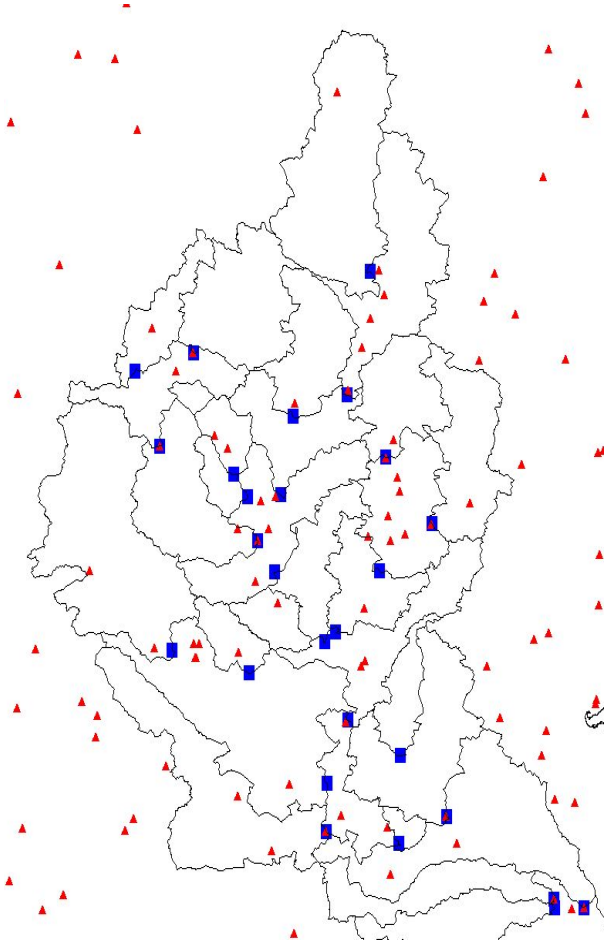

Figure 3.5 – Map of isotope sampling locations (blue squares) corresponding with GRCA gauges and PWQO water quality monitoring locations (red triangles).

Samples of groundwater were collected for isotopic analysis from Provincial Groundwater Monitoring Network wells located within the watershed and from Long Point by the GRCA during the study period (2003-2005). Samples were taken randomly to assess expected variations in the isotopic composition of the groundwater over a year. All samples collected and analysed

from the 2003-2005 isotope sampling program (including river water samples, groundwater, and precipitation) were used to produce a δ^2H-$\delta^{18}O$ plot for the GRB, the first of its kind for the Great Lakes region (Figure 3.6). The regression line through snow and local groundwater samples has a slope of ~7.4, which is lower than the slope of the GMWL (8). This slope reflects the composition of local precipitation preserved in local groundwater samples and in winter precipitation and is in good agreement with LMWL slope of ~7.7 (for 2000 and 2001) estimated by St. Amour (2008) at the University of Waterloo Weather Station located in the central GRB. Regression of surface water samples collected in the GRB yielded a slope of ~6.7 reflecting evaporative enrichment in these samples relative to meteoric waters.

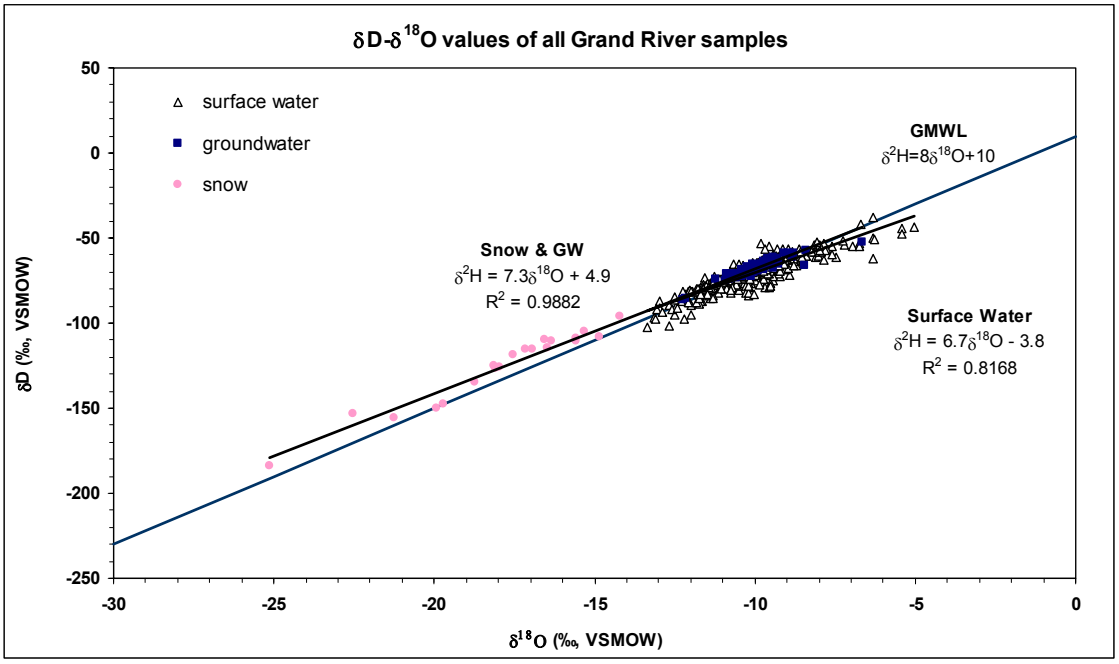

Figure 3.6 – δ^2H-$\delta^{18}O$ plot of Grand River Basin isotope data.

3.2 Fort Simpson Basins, NWT, Canada

The Fort Simpson Basin (FSB) study region lies within the Lower Liard River valley in close proximity to the community of Fort Simpson, Northwest Territories (61°45'N; 121°14'W) (Figure 3.7), located at the confluence of the Mackenzie and Liard Rivers (Figure 3.8).

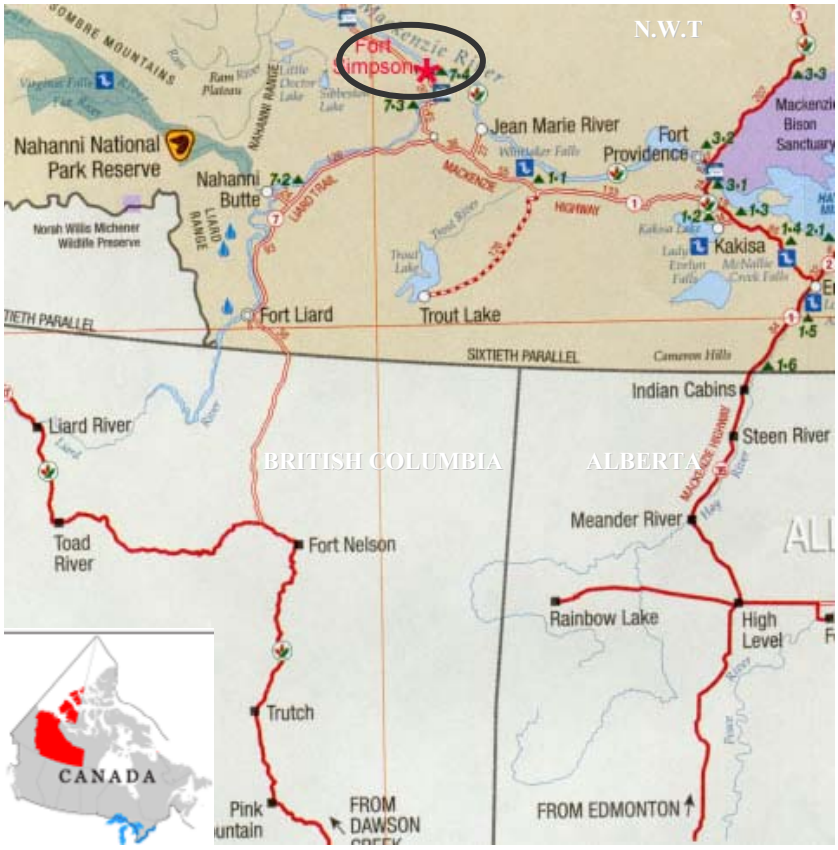

Figure 3.7 – Location of Fort Simpson, NWT in south-central NWT, Canada (Fort Simpson Historical Society, 2008; Government of Northwest Territories, 2000)

The lower Liard river valley is within the 400-km wide discontinuous permafrost zone corridor of Canada's interior plains and is characterized by a wetland-dominated regime. The FSB is part of the Mackenzie drainage basin, the 10th largest watershed in the world with peak flows frequently exceeding 25,000 cms, and is also part of the Mackenzie GEWEX study (Rouse, 2000; Stewart *et al.*, 1998). The Liard River (Figure 3.8), although considerably smaller than the Mackenzie, is the largest tributary of the Mackenzie north of the sixtieth parallel (Hamlin, 1996). Meltwater volume and timing from the Liard's wetland-dominated regime are generally known to trigger ice break-up on the lower Mackenzie River system causing the formation of ice-jams. The flooding from these ice-jams is typically the largest annual hydrologic event with flood levels exceeding those that would be produced under normal open water conditions with similar discharge rates (Prowse, 1986).

Figure 3.8 – Confluence of the Mackenzie and Liard Rivers near Fort Simpson, NWT (Fort Simpson Historical Society, 2008).

River basins in this region are characterized by extensive, flat headwater zones with large regions of open water and wetlands, contrasted by steeper regions in the lower part of the study region where channels are incised into mineral soils (Hayashi *et al.*, 2004).

The following sections describe the FSB climate, geology, hydrology and ecology. Detailed information as to the collection of hydrometric, meteorological and isotopic data are also presented.

3.2.1 Hydroclimate

The discontinuous permafrost in the central part of the Mackenzie basin is believed to be particularly sensitive to climatic warming because small changes in climate force large changes in hydrological behaviour, namely runoff pathways and water storage (Rouse, 2000).

In the FSB there is one Class A Synoptic weather station located at the Fort Simpson airport (61°45'N, 121°14'W, 169.2 masl). The long-term Climate Normals for air temperature at the Fort Simpson airport indicate an average temperature of -3.2°C, ranging from -25.4°C in January to 17.2°C in July on average (Burn *et al.*, 2004). Mean annual precipitation is 369 mm, with 59.2 mm falling in July on average. Snowfall accounts for an average of 170.3 mm (snow water equivalent, swe) of yearly precipitation from August to May, with October and November recording the highest snowfalls (29.4 and 27.3 cm, respectively) (Burn *et al.*, 2004). The average temperature and precipitation over the study period from 1997 to 1999 was -1.4°C and 438 mm, respectively, with 208 mm falling as snow (St Amour *et al.*, 2005). The difference between the study period average and long-term average is due to warm winters and wet summers associated with the El Niño Southern Oscillation (ENSO) effect in 1998 (Petrone *et al.*, 2000).

Environment Canada Climate Normals indicate wind directions from the northwest, and from the southwest during maximum hourly wind gusts (Burn *et al.*, 2004). Moisture sources for this study region are typically moisture-laiden maritime arctic moisture masses, where cold air descends southward across North America from the polar-regions. During the summer months, air masses are affected by moisture evaporating from the multitude of northern lakes dotting the landscape. During the winter months, air masses are typically cold and dry and are derived from continental arctic sources originating over snow- and ice-covered regions in the high arctic (Burn *et al.*, 2004).

3.2.2 Geologic Setting

Old sand dunes deposited when glacial lakes covered the area stretch northward in the Mackenzie valley from the winter road near the community of Jean-Marie. Underlying stratigraphy commonly consists of a thick accumulation of organic peat deposited over extensive

areas of poorly drained lacustrine (silt and sand) sediments, which overlie poorly drained glacial deposits (till), below which lie thick clay deposits with low permeability (Aylsworth *et al.*, 2000). Moving in a northwesterly direction across the study region, elevations increase and the terrain consists of large flat areas with rolling till deposits over Cretaceous shales. The topographic relief tends to increase towards the northwest-westerly region of the basin, with Martin River having the steepest gradient (6.7%) and highest elevation (730 masl) (Hamlin, 1996). Scotty Creek, characterized by peat plateaus and flat oligotrophic bogs (Hayashi *et al.*, 2004), is a low-lying basin (240 masl) with the shallowest relief (0.2%) (Hamlin, 1996). The Martin Hills are a prominent feature in the study region, visible throughout most of the area as the largest topographic relief between the western side of the Mackenzie River and the much higher Nahanni Mountain range 100 km west of Fort Simpson.

3.2.3 Ecology

The study area is characterized by meandering streams, discontinuous permafrost and extensive peatlands (bogs and fens) (Hamlin, 1996). Permafrost ranges from 10 percent in the lowlands near Fort Simpson, to 60 percent on the elevated plateaus near Trout Lake (Rennie *et al.*, 1981). Vegetation is dominated by large, homogeneous stands of deciduous and coniferous trees surrounding the rivers and wetlands, and within the wetlands. Wetlands dominate parts of the region, specifically Scotty Creek where up to 60% of the basin is covered with open or partially treed wetlands (Hamlin, 1996). The wetlands can be further classified by hydrological behaviour as channelized fens (~10-20%) and flat bogs with little to no channel interaction (Hayashi *et al.*, 2004). The dominant vegetation observed in the wetlands is a buoyant mat of *Sphagnum riparium*-dominated peat supporting sedges and other emergent aquatic vegetation (Hayashi *et al.*, 2004). Mature plateaus support a variety of shrubs and trees (*Picea mariana*) and groundcover consisting of lichens and mosses overlying sylvic peat (Hayashi *et al.*, 2004).

The Mackenzie and Liard valleys are prone to forest fires in the hot, dry summer months. In 1994 and 1995, forest fires destroyed significant amounts of forest and vegetation cover in the valleys. Re-growth areas from forest fires do make up a significant portion of the landcover classification in the FSBs, and therefore a transitional landcover designation was created for

hydrological modelling to mimic the increased runoff generation from these more sparsely vegetated areas. A LandSat image of the Fort Simpson region shown on Figure 3.9 indicates the various landcover classifications identified for FSB, including the abundance of wetland (light blue) and transitional reforestation recovery from forest fires (yellow) (Toyra, 1997).

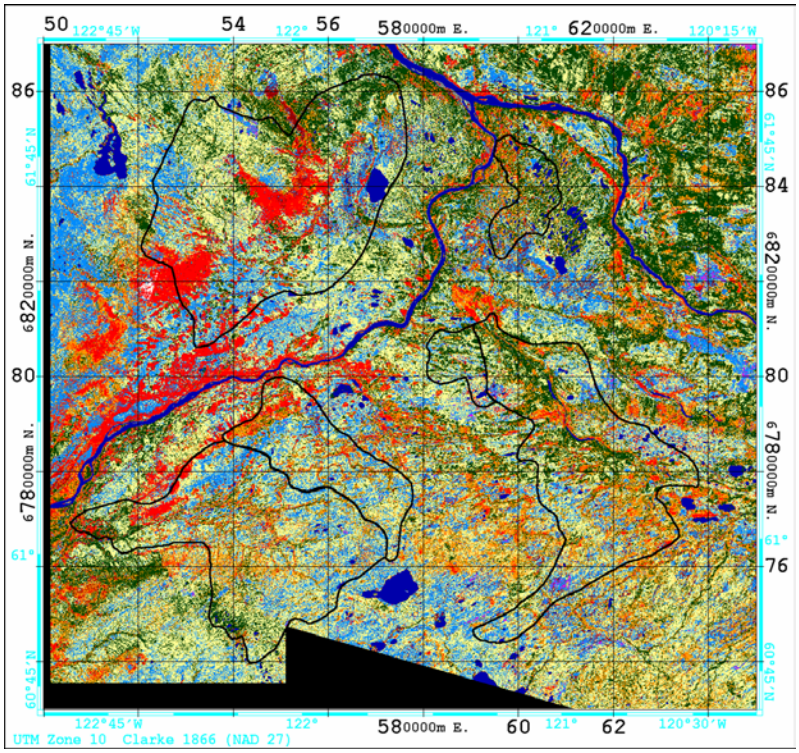

Figure 3.9 - Landcover map for the FSB (Toyra, 1997).

Red/**Orange**=mixed/deciduous
Green=conifer
Yellow=transitional
Light blue=wetland
Dark blue=water

3.2.4 Hydrology

The Fort Simpson study area is divided into five wetland-dominated mesoscale river basins: Jean-Marie (1,310 km^2), Martin (2,050 km^2), Birch (542 km^2), Blackstone (1,390 km^2), and Scotty Creek Rivers (202 km^2) (Figure 3.10).

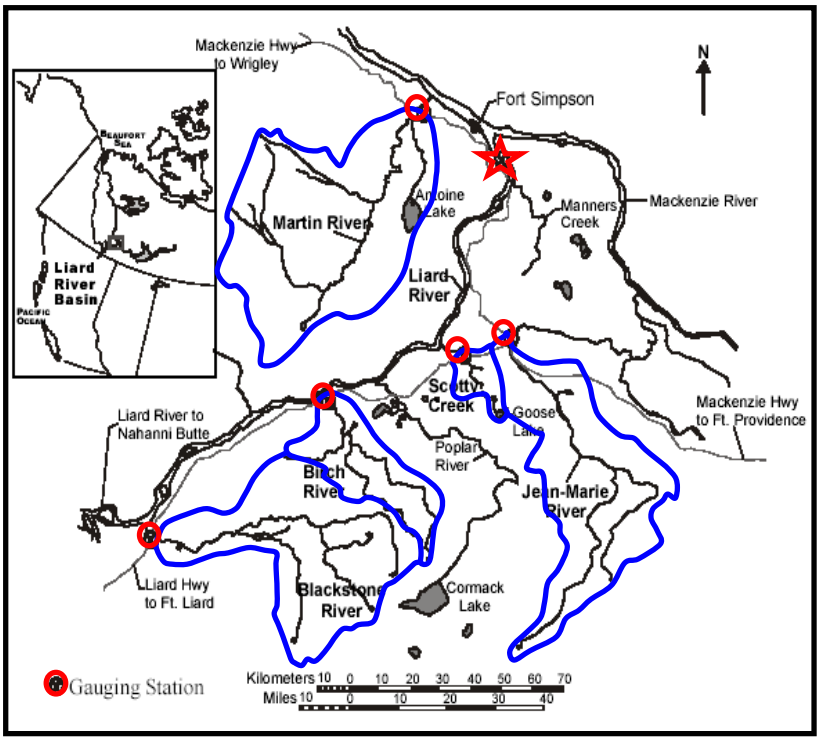

Figure 3.10 - Map of FSB and basin delineation (St Amour et al., 2005).

The hydrology of the Northwest Territories is generally characterized by low precipitation amounts and low annual runoff (~200 mm), with maximum runoff (>500 mm) occurring in the western Cordilleran region (Environment Canada, 2004). The hydrologic response of the dry, northern regions of the NWT is generally not well known or monitored. Generally speaking this northern Canadian region is sparsely populated and largely undeveloped. The Liard River drains the central portion of the Mackenzie River Basin (MRB) and has a total drainage area of 275,000 km^2, which comprises a substantial portion of the MRB (Burn *et al.*, 2004). The Liard basin contains several streamflow gauging stations and meteorological stations but has no significant or controlled lakes to moderate streamflow discharge. The hydrological regime is generally characterized by low-flows in the winter months when rivers are completely covered by ice and are assumed to be baseflow-dominated. Streamflow hydrographs begin to rise in late April to early May with the start of the spring freshet and are snowmelt-dominated until June when the hydrographs peak. From June until winter low-flow in December, there is a gradual decline in streamflow hydrographs, with annual minimum discharge occurring in late March or early April prior to the spring freshet (Burn *et al.*, 2004). Average annual discharge of the Liard River basin is 2,470 cms (WSC, 2001).

The Fort Simpson region lies within the lower Liard River valley and is sub-divided into five sub-basins contributing to the Liard or Mackenzie River basins. Jean-Marie River lies just outside of the Liard River basin but has similar physiographic and meteorological characteristics as ungauged areas of the Liard; Jean Marie River drains in an easterly direction into the Mackenzie River near the town of Jean-Marie.

The climate, ecology, and geology of the FSB all contribute to create a moisture laden landscape with large amounts of surface (wetland or bog) and subsurface storage (soil moisture and baseflow). Dominant hydrological end-members contributing to streamflow are snowmelt (spring freshet) and baseflow (ice-on and low-flow periods) (St Amour *et al.*, 2005; Stadnyk *et al.*, 2005). The presence of discontinuous permafrost, large snowmelt events, and warm, moist summers all contribute to rapidly peaking runoff followed by prolonged streamflow recession. In the low-lying bogs and flat plateaus (Scotty Creek and Birch River) sustained fluxes from baseflow and wetland storage have been estimated to be as high as 80% of the total streamflow hydrograph and serve to delay and lower peak hydrograph responses following runoff events (St Amour *et al.*, 2005).

The Jean-Marie River, Martin River and Scotty Creek catchments contain areas with extensive fen peatlands situated in low-lying regions and surrounding most channels. Both Birch and Blackstone River catchments tend to be bog-dominated peatlands with little or no fen peatlands present (Aylsworth & Kettles, 2000). The distinction between bog and fen is very important as each wetland classification has very different hydrological responses. Bog-dominated landscapes tend to retain water and release it slowly following large events, in comparison to fen-dominated landscapes that dampen peak runoff responses but retain less water in the landscape overall. To account for the distinction, two types of wetland classifications were created for WATFLOOD modelling: disconnected wetlands (bogs) and connected wetlands (fens, or riparian zones lining the channels).

3.2.5 Hydrometric and Meteorological data

Hydrometric data for three of the five basins have a good historical record (approximately 30 years); however two of the basins were only recently gauged: Scotty Creek and Blackstone River (early and mid 1990s, respectively). All sub-basin streamflow gauges had a complete hydrometric data set for the study period freshet and summer seasons: from April to August, 1997 to 1999. Table 3.4 shows the mean annual discharge for each of the five rivers comprising the FSB as compared to the long-term average discharge.

Table 3.4 – Summary of average annual discharge for five sub-basins of FSB as compared with long-term average over gauge lifespan (WSC, 2001).

Basin	Drainage Area (km^2)	Mean discharge (cms)	Annual Average Discharge (cms)		
			1997	1998	1999
Jean-Marie	1,310	4.55*	5.12	4.59	4.32
Martin	2,050	7.65*	10.4	7.74	6.58
Birch	542	2.54**	3.05	2.31	2.17
Blackstone	1,390	9.24^^	11.6	7.78	7.38
Scotty	202	0.544^	0.449	0.517	0.464

*Averaged over gauge lifespan from 1972-2005;**Averaged over gauge lifespan from 1974-2005;
^Averaged over gauge lifespan from 1995-2005; ^^Averaged over gauge lifespan from 1991-2005.

The WSC maintains daily discharge measurements of the Liard River and locations near the outlet of the five catchments. Hydrometric gauges in the study area are nitrogen-based manometer gauges measuring pressure head at the gauge line in deep water. Rivers are manually surveyed and flows are measured periodically to establish rating curves to estimate hourly flow levels. Hourly flow estimates are only available during the ice-free seasons (approximately from mid-May to mid-November); during the rest of the year, daily estimates of discharge are used. Since daily flows were the only flow measurements consistently available for the entire study period in all five basins, daily flows were used for comparison to simulated hourly flows.

Precipitation data were obtained from a single rain gauge servicing all five catchments, located at the Fort Simpson airport Class-A synoptic weather station (star on Figure 3.10). Air temperature data were collected from the weather station located at Fort Simpson Airport, and randomly throughout the basin when samples were collected. Both precipitation and air temperature data failed to accurately represent conditions within the five catchments several times throughout the study period due to the lack of proximity of the rain gauge (located outside of all five sub-basins) and coarsely-spaced temperature sampling locations. The rain gauge failed

to record several rainfall events that clearly passed through the study region as evidenced by a sharp rise in the observed streamflow hydrographs in all five basins. Due to the remote, unpopulated nature of this study region however, there was no better alternative to this single rain gauge during this study period, which serves to reinforce the need to produce reliable simulated forcing for such areas. Extensive snow course surveys, converted to snow water equivalent (SWE) in millimetres, were conducted, and a survey of landcover types was recorded for each of the five catchments from March 1997-1999 when snow thickness was at a maximum (Onclin *et al.*, 2000).

Table 3.5 summarises the Climate Normals (1971-2000) (Environment Canada, 2004) and the climate parameters monitored during the study period from 1997-1999 (St Amour *et al.*, 2005).

Table 3.5 – Climate Normals for 1971-2000 (Environment Canada, 2004) compared with climate summary for 1997-1999.

	Normals (1971-2000):		**Study Period:**					
	Annual	**Ice-off (May-Oct)**	**Whole Year**			**Ice-off Season**		
			1997	**1998**	**1999**	**1997**	**1998**	**1999**
Mean daily air temperature (°C)	-3.2	10.3	-1.9	-0.7	-1.7	9.8	12.1	9.7
Relative humidity* (%)	73	69	76	73	73	70	66	67
Total Precipitation (mm)	369	260	479	405	431	408	323	271
Total Rainfall (mm)	224	220	331	294	228	331	286	226
Average SWE^ (mm)	n/a	n/a	69±13	85±20	94±24	n/a	n/a	n/a

*Relative humidity Climate Normals from 1961-1990;
^SWE obtained during late March at maximum snow thickness.

3.2.6 Isotope data

During the study period streamflow and snow samples were taken periodically from the five catchments and analysed at the University of Waterloo Environmental Isotope Laboratory for $\delta^{18}O$ and $\delta^{2}H$ relative to the Vienna Standard Mean Ocean Water (VSMOW). Maximum analytical uncertainties of δ values are ±0.1‰ for $\delta^{18}O$ and ±2‰ for $\delta^{2}H$ (St Amour *et al.*, 2005). Snow samples were obtained in late March using a depth-integrated snow sampler at sites accessible by road and from a helicopter. Sampling of streamflow, rain, wetlands and lakes was conducted during the open-water season with a distinct focus on the spring freshet period

to ensure isotopic variation was accurately represented. Since sampling of streamflow could only occur periodically throughout the study period, isotopic values of streamflow were interpolated to daily values weighted according to the daily volumetric discharge. The result was a time-series partitioning of streamflow into snowmelt, surface water and groundwater components.

Streamflow isotopic partitioning was inferred from the natural cycle of seasonally active source waters. Streamflow samples collected in the late-fall, prior to ice-on conditions and without influence from event water were considered to be representative of a baseflow hydrograph and therefore the average isotopic composition of the interflow, or soilwater discharge. Streamflow samples obtained during ice-on periods throughout the winter were found to be the most depleted isotopic compositions representative of winter low-flows (groundwater discharge). The observed trend in isotopic composition of streamflow suggested a predominately groundwater-fed regime during late winter (St Amour *et al.*, 2005). St. Amour *et al.* (2005) produced the following δ^2H-$\delta^{18}O$ plot for the FSB (Figure 3.11), which indicates annual differences in isotopic composition attributed to the change in air mass circulations and shows the offset of local meteoric and evaporated waters from the GMWL.

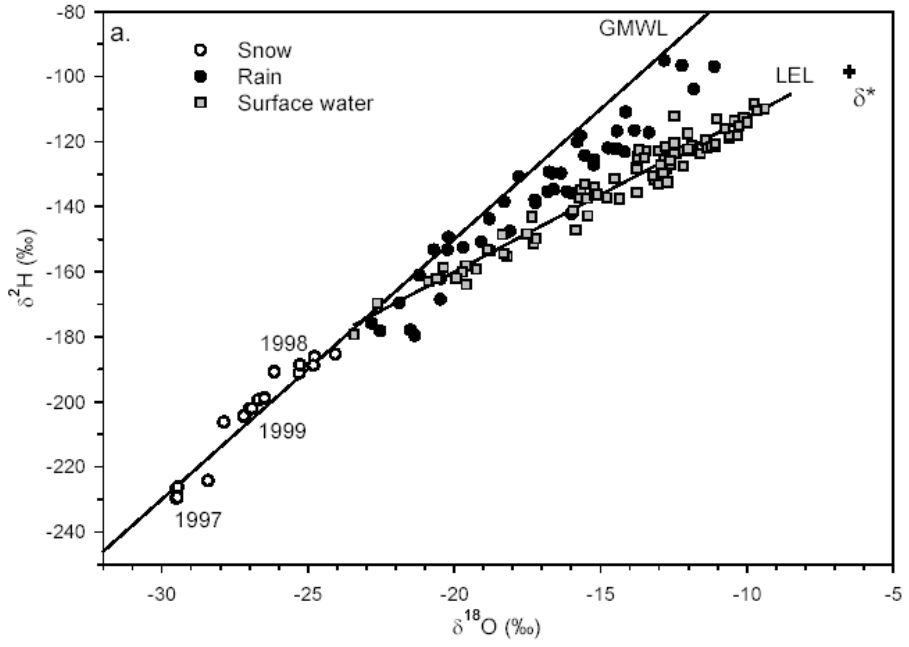

Figure 3.11 – δ^2H-$\delta^{18}O$ plot of isotope data collected in the FSB (St Amour et al., 2005).

Table 3.6 presents the average measured $\delta^{18}O$ composition of snowmelt, rainfall, and surface water during each of the study periods, as compiled by St. Amour *et al* (2005) and used for analysis in this thesis.

Table 3.6 – Average measured $\delta^{18}O$ of source waters for FSB (St Amour et al., 2005).

Source	**1997**		**1998**		**1999**	
	$\delta^{18}O$ (‰)	**n**	**$\delta^{18}O$ (‰)**	**n**	**$\delta^{18}O$ (‰)**	**n**
Snowpack	-32.8	35	-26.2	34	-29.2	52
Surface water*	-23.4	49	-17.4	19	-18.4	3
Rain	-19.1	13	-22.8	20	-25.9	12
Groundwater^	n/a		-19.7	9	n/a	

*Surface water comprised of lakes and fens; ^Groundwater seepage collected in Manners Creek.

3.3 Chapter Summary

The FSB is an uninhabited, wetland-dominated sub-arctic region with discontinuous permafrost. This study site is unregulated and is sparsely monitored, except for a snapshot of hydrometric and isotopic data in selected rivers. In contrast the GRB is a highly populated basin supporting several of Southern Ontario's largest cities. It is characterized by till plains, forests and agricultural lands and is both highly regulated and monitored hydrometrically and isotopically. Successful application of a hydrological model to both these study sites will generate confidence in the robustness of a model, allowing for accurate reproduction of distinct, landscape-driven hydrologic responses. This robustness helps to establish confidence in the accuracy and representativeness of the model, and allows for general model calibration rather than unique calibration of each sub-basin as is the case with other models. It is for these reasons that these two study sites were chosen for this modelling study and will be used to establish model robustness and representativeness across highly variable mesoscale watersheds with different hydrological controls.

Chapter 4

WATFLOOD Hydrological Modelling

Singh and Frevert (2002) derived helpful criteria to aid in model selection for watershed-scale hydrological modelling research, where (if possible), the model should be 1) representative over the watershed scale, 2) comprehensive in its treatment of the hydrologic cycle, 3) applicable to a wide array of problems (operational hydrology, water quality, agriculture and forest practices, etc.), 4) connective with GIS and remote sensing data, and 5) geographically representative of the regions being modelled. From Chapter 2, it was identified that the model chosen should also enable a future coupling with atmospheric modelling systems, and possess separable flowpaths that are not overly parameterized.

The WATFLOOD model was designed for use on large scales; it has been shown to reliably reproduce streamflows in the Mackenzie basin catchment, which is over 1,700,000 km^2 (Pietroniro *et al.*, 2006; Toth *et al.*, 2006), and routinely models watersheds in the thousands of square-kilometres (Benoit *et al.*, 2003; Dibike & Coulibaly, 2007). WATFLOOD is a partially physically-based model because of its use of conditional statements in the coding framework to keep modelling efficiencies high. The model utilizes physically-based equations to comprehensively simulate mesoscale hydrological processes, such as the Philip formula for infiltration, Manning equation for overland flow, and either Hargreaves or Priestley-Taylor (semi-physically-based) equations for estimating evapotranspiration (Kouwen, 2007). The WATFLOOD model and its internal hydrological processes have been validated in several studies over the years, each of which has shown that the model behaves in a realistic manner for operational use (Bingeman *et al.*, 2006; Stadnyk *et al.*, 2005). WATFLOOD has been adapted for

use with GIS data, such as DEMs and LandSat imagery, but has also been adapted to fully utilize and aid in assessing the reliability of radar data (Benoit *et al.*, 2003; Fassnacht *et al.*, 1999; Klyszejko, 2006). WATFLOOD's capability to incorporate remotely-sensed data sources, coupled with its ability to efficiently model large areas over long time-sequences with minimal field measurements, has facilitated the broad-application of the model. WATFLOOD has earned the reputation of being a robust and efficient hydrological modelling system for use in a wide variety of watersheds for a wide array of hydrological problems (Kouwen *et al.*, 2005). The WATFLOOD model was selected for this study because it meets all five of Singh and Frevert's (2002) criteria for model selection, because it was readily accessible, offered the opportunity to interact with the source code and model creator, and because it met the operational requirements for this study. The capability of WATFLOOD to model large regions with minimal field data made it ideal for the incorporation of an isotope mass balance routine, which in other model frameworks would be far too computationally expensive for practical mesoscale application.

The WATFLOOD hydrological model (Kouwen, 2007) is a semi-distributed, mesoscale model for watersheds having response times larger than one hour. The model was originally developed as an event-based model (Kouwen, 1988); however it has been adapted for use in continuous simulation of long time sequences, including climate change studies (Pietroniro *et al.*, 2003). Its basic computational structure is formed by grouped response units (GRUs) designed to provide a distributed approach to modelling while keeping the computational efficiency very high (Kouwen *et al.*, 1993). Grids are composed of GRUs: one for each hydrologically significant landcover type, where the hydrological responses from all GRUs in an element are summed to give a total hydrological response (Figure 4.1).

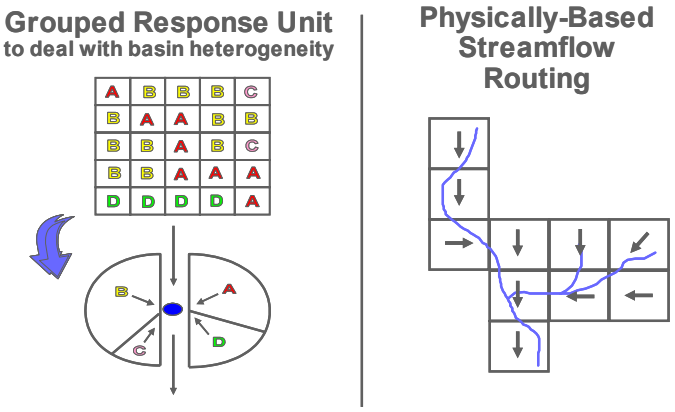

Figure 4.1 - WATFLOOD GRU concept.

Groups are formed based on hydrological similarity generally defined by landcover types derived from satellite imagery. Beven (1996; 2002) uses a similar method in TOPMODEL called an index of hydrological similarity determined from topographical data and knowledge of soil type that determines an effective transmissivity profile for various soil types. WATFLOOD instead relies on the assumption that similar landcovers exist in regions of similar soil types and topographic conditions, but cannot define unique soil transmissivities. The disadvantage therefore is that there is no means of defining soil-based parameters; with the GRU approach a grid is divided into a number of distinct hydrological classifications (i.e., GRUs) with similar combinations of landcover and soil type (Collischonn *et al.*, 2007). Location within the cell is inconsequential and instead a soilwater budget is computed for each GRU; runoff is generated from the GRUs, summed, and routed through the channel network (Kouwen *et al.*, 1993).

The model incorporates vertical and horizontal water budgets that include surface water, interflow and groundwater components, wetland hydrology, wetland-channel interaction, and soil moisture; all of which contribute to total streamflow (Figure 4.2).

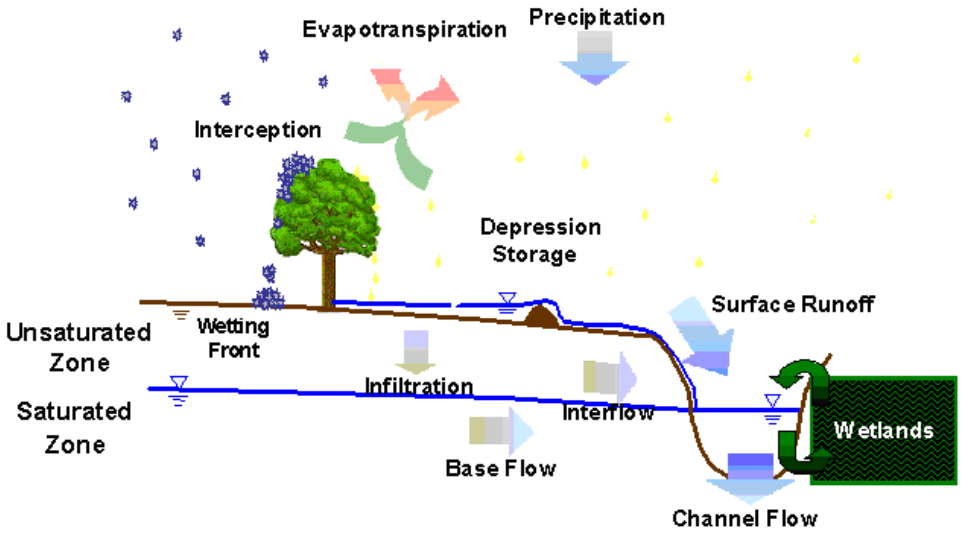

Figure 4.2 - Graphical representation of WATFLOOD's hydrology.

Conceptualization of a WATFLOOD watershed divides runoff generation into three fluxes: overland flow, interflow and baseflow. On the surface a limiting value of depression storage is controlled by an exponential function of accumulated rainfall excess (Section 4.1.1). Surface runoff, or overland flow is generated by an infiltration excess controlled by the Philip formula

(Philip, 1954); based on the Green-Ampt (Green & Ampt, 1911) formula only including head due to surface ponding and capillary potential (Section 4.1.2). Interflow is WATFLOOD's dominant storm flow mechanism simulated as a variable-depth, shallow aquifer response controlled by a linear relation with land surface slope and water content (Snelgrove, 2002) (Section 4.1.2). WATFLOOD's baseflow component is generated from a deep, lower zone storage (LZS) reservoir fed by soilwater drainage from the upper zone storage (UZS) above. Drainage from UZS to LZS is controlled by a function of the moisture content less the retention capacity of the soil layer. The outflow from LZS or baseflow is controlled by a two-parameter power law formulation (Section 4.1.3).

Contributions to streamflow can therefore be segregated as fast, medium or slow response, respectively depending on the originating compartment. Once in the channel drainage network, streamflows are routed from upstream to downstream using a storage routing technique (Section 4.3). The WATFLOOD model also includes wetlands hydrologically coupled to the channels (Section 4.4). Lateral flux components generated by the surface, UZS, and LZS contribute either directly to the wetland, or if no wetlands are present, then to the channel drainage system. WATFLOOD also incorporates lake routing (Section 4.5) and snowmelt (Section 4.6) modules into its framework. From each of the various storage compartments, evapotranspiration (ET) is computed and used to reduce storages that lose water to evaporation (Section 4.2). A new evaporation-transpiration separation methodology (Section 4.2.4) was developed to segregate total evaporation (E) from ET. At the end of this chapter, measures for assessing the model's efficacy in reproducing streamflows and in hydrograph separation are presented (Section 4.7), along with a summary of the model set-up for the Grand River Basin (GRB) and Fort Simpson Basins (FSB), respectively (Sections 4.8 and 4.9).

4.1 Hydrological Processes

4.1.1 Surface Storage & Overland Flow

The WATFLOOD model has the ability to hold and store water on the land surface in small topographical depressions. Depression storage is computed in the model where the limiting

threshold of depression storage on the surface (S_d in mm) is reached exponentially as a function of the amount of precipitation (P_e) reaching the ground, or excess precipitation not intercepted:

$$d_s = S_d(1 - e^{-kP_e}) \quad (4.1)$$

where k is a constant derived from comparison of WATFLOOD depression storages to values reported by the American Society of Civil Engineering (ASCE) for various landcovers (Kouwen, 2007).

Water on the surface in excess of depression storage will generate infiltration into the soil column. When the infiltration capacity of the soil is exceeded and minimum depression storage is satisfied then water is discharged directly to the channel drainage system or to adjacent wetlands lining the channel. This excess overland flow (Q_r in cms) is calculated based on the Manning formula:

$$Q_r = (d1 - d_s)^{1.67} * S_i^{0.5} * A / R3 \quad (4.2)$$

where d1 is the surface storage (mm); d_s is the depression storage (mm); A is the grid area (m^2); and R3 is an optimized parameter representing roughness and channel length.

4.1.2 Infiltration, Upper Zone Storage & Interflow

Infiltration of water into the soil zone or UZS is modelled by the Philips formula (Philip, 1954) to incorporate surface water detention, which the Green-Ampt equation (Green & Ampt, 1911) does not. The Philip formula in WATFLOOD expresses the depth of water infiltrated (F in mm) per hour (t) as:

$$\frac{dF}{dt} = K\left[1 + \frac{(m - m_0)(Pot + d1)}{F}\right] \quad (4.3)$$

where K is an optimized parameter representing the infiltration hydraulic conductivity; m is the average soil moisture content of the soil up to the wetting front; m_0 is the initial soil moisture content obtained from input data or the Antecedent Precipitation Index (API) modified on an hourly basis; Pot is the capillary potential at the wetting front (mm) updated as the wetting front descends and reduces the pressure gradient; and d1 is the depth of water on the soil surface. In WATFLOOD gravitational drainage occurs when UZS exceeds RETN, or field capacity. Volumes of water in UZS less than RETN can only be depleted by evapotranspiration.

Water in UZS can be removed via evapotranspiration (Section 4.2), lateral interflow, or vertical drainage into the Lower Zone (Section 4.1.3). The interflow component in WATFLOOD is a lateral exfiltration of UZS contributing directly to wetland riparian zones or streamflow. The depth of UZS released in a given time step (DUZ in mm) through interflow is represented by a storage-discharge function:

$$DUZ = REC * (UZS - RETN) * S_i \qquad (4.4)$$

where REC is a dimensionless conductivity parameter (typically ranging from 1 to 10); UZS is the depth of water in the upper zone (mm); RETN is the pore water retention capacity of the soil (mm); and S_i is the overland slope. RETN is the minimum storage that must remain in UZS and is analogous to the capillary fringe or field capacity of the soil. Water in the UZS that is not lost through evapotranspiration or interflow is vertically drained into the LZS compartment.

4.1.3 Recharge, Lower Zone Storage & Baseflow

Vertical drainage from UZS to LZS occurs if the depth of water in the UZ is greater than the minimum retention (RETN) depth. The depth of water vertically drained (DRNG in mm) from UZS to LZS is computed based on a storage-discharge relationship, where the vertical gradient is determined by the amount of water available for drainage from the UZS:

$$DRNG = AK2 * (UZS - RETN) \qquad (4.5)$$

where AK2 is a dimensionless parameter representing the recharge conductivity, multiplied by the total storage available for drainage.

Exfiltration of LZS can only occur through lateral baseflow discharge (qlz in cms) computed via a baseflow depletion function:

$$qlz = LZF * LZS^{PWR} \qquad (4.6)$$

where LZF is the lower zone function specific to a river classification (typically 10^{-4} to 10^{-6}); and PWR is the depletion rate of the baseflow for the river classification (typically 1.5 to 2.5). Values for LZF and PWR are optimized parameters based on baseflow discharges (i.e., recession curves) determined from measured streamflow hydrographs at the basin outlet during low-flow periods. The baseflow component contributes directly to wetland riparian zones or to streamflow (Section 4.4).

4.2 Evaporation and Transpiration

There are three distinctive types of evaporation in WATFLOOD: evaporation from open water bodies, interception evaporation, and combined evapotranspiration from soils and plants.

4.2.1 Lake Evaporation

Lake evaporation occurs as open water evaporation where the actual rate of evapotranspiration (AET) is set equal to the potential rate of evapotranspiration (PET) during open-water seasons (i.e., no ice-cover). Evapotranspiration over lakes and water classes is entirely evaporation given there are no transpiring plants. Given there is no ice-cover module in WATFLOOD, snow depletion curves (SDC) are used to accumulate snow on frozen lakes, which automatically simulates ice-cover and stops evaporation. There is no moisture feedback functionality in the WATFLOOD model therefore AET=PET is always assumed over open water bodies.

4.2.2 Interception Evaporation

WATFLOOD accumulates an interception storage based on the model developed by Linsley *et al.* (1949) where falling precipitation is accumulated on vegetation according to maximum canopy storage capacities (h) and amount of storage loss due to canopy evapotranspiration (IET). Canopy storage capacity is defined for each land classification to account for vegetation type and density. During dormant seasons the storage capacity is reduced to model the effect of leaf area loss (Kouwen, 2007). Interception storage is computed hourly during precipitation events and is defined as the fraction of precipitation captured by the vegetation times the maximum storage possible (Kouwen, 2007).

4.2.3 Combined Evapotranspiration

In WATFLOOD there are three methods to estimate the combined effect of soilwater evaporation and transpiration occurring through plants. Where radiation data are available, the semi-physically-based Priestly-Taylor model (Priestly & Taylor, 1972) can be used to estimate

PET; where only temperature data are available, the Hargreaves model (Hargreaves & Samani, 1982) can be used; and where neither temperature nor radiation data are available, the original method of estimating evapotranspiration from published values can be used (i.e., Class-A pan evaporation).

AET is computed from PET using up to three coefficients to reduce the calculated PET. If IET is occurring, then it is first assumed that PET will be reduced by IET since evaporation will preferentially occur from intercepted moisture than from the soil column. PET is reduced by accounting for PET likely to occur from different vegetation types, the soil moisture content available for evaporation above the permanent wilting point of vegetation, and the soil temperature based on the degree-day (Kouwen, 2007).

4.2.4 Evaporation-Transpiration Separation

Since isotopic fractionation is assumed to occur only with evaporation (Section 2.4.2), it is necessary to separate evapotranspiration into evaporation and transpiration components. In keeping with WATFLOOD's philosophy of being an efficient modelling system that relies on as few sources of forcing data as possible, empirical methods were used to segregate the evaporation component of evapotranspiration via water levels and land-use classification.

The upper zone storage indicator (UZSI) is a parameter defined in WATFLOOD that estimates the amount of ET occurring as a function of soil moisture availability. ET occurs at the potential rate (i.e., PET) if the soil is saturated (Kouwen, 2007), and the rate of ET is reduced when soil moisture is less than saturation down to zero at the permanent wilting point (PWP). The UZSI is computed as (Neff, 1996):

$$UZSI = \left[\frac{(UZS - PWP)}{(SAT - PWP)} \right]^{0.5} \qquad (4.7)$$

where SAT is the soil moisture saturation level.

Evaporation occurs when water is available from the soil column in excess of the PWP, where both evaporation and transpiration reduce to zero as the water available approaches the PWP.

Assuming that atmospheric resistance (i.e., relative humidity) to evaporating water is less than stomatal resistance, as soil saturation increases the proportion of ET that is evaporation (water lost from soil) increases at a greater rate than transpiration. The proportion of evaporation (E in mm) to ET (ERATIO) can be estimated as a power function of the UZSI for each land classification where evaporation occurs from a soil surface:

$$ERATIO = a * UZSI^{b} \qquad (4.8)$$

where *a* represents the maximum E to ET partitioning reported in the literature for the given land class (i.e., 1 for bare soil, 0.5 for sparsely-vegetated area or low-yield crops, 0.1 or less for dense, high-water demand vegetation); and b is the rate at which the evaporative component of ET increases with soil saturation, representing the threshold saturation level required to see significant increases in E (i.e., 2 indicates an immediate increase in E at low saturation, compared with 8 which requires more than 25% saturation before E increases substantially).

A literature survey of studies utilizing direct measurements of water loss due to evaporation, or based on the transpiration capacity of various plants was conducted to determine typical E to ET ratios for various landcover classifications under dry versus saturated conditions. The values of *a* and *b* for various landcover classifications were determined based on the threshold values of E/ET obtained from the literature for dry and saturated conditions by plotting each power function. Figure 4.3 is an example of one such power function (E/ET ratio) generated for an agricultural land class, which typically has a maximum E/ET ratio of 0.5 (a=0.5) and where E should not significantly increase prior to 50% saturation of soil moisture (b>=8).

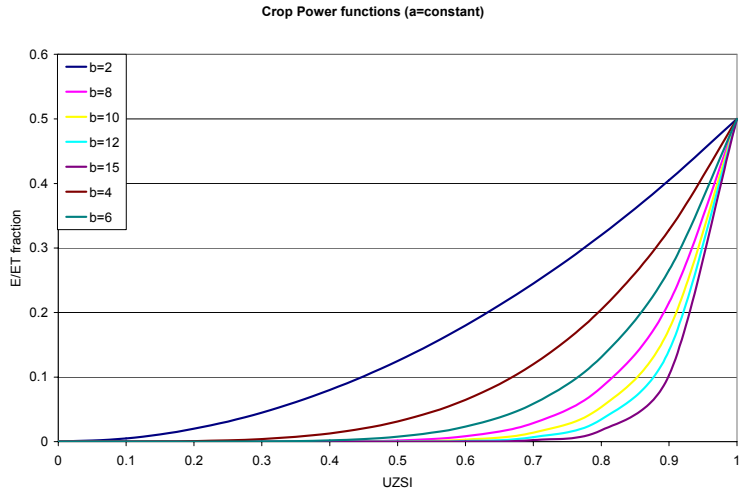

Figure 4.3 – Power function derived for the agricultural land classification, varying according to crop type.

Similar power functions with unique *a* and *b* coefficients to describe the E/ET ratio increase with soil wetting were developed for conifer forests, deciduous forests, mixed forests, burn re-growth (transitional), and wetland classifications. Table 4.1 summarises the coefficients determined from literature for each WATFLOOD land classification utilized in this study. Differences in the E/ET ratios reported can be attributed to the differences in landcover type within that classification (e.g., crop type), and the percent bare soil exposed for each landcover.

Table 4.1 – Power function coefficients determined for various land classifications based on literature-derived separations of E and ET.

Landcover	Literature	Maximum E/ET	Response of E to increasing soil moisture, m	Coefficients	
				a	b
Crop	(Kite, 2000)	0.075-0.30	Rapid increase with small m increase	0.5	2
	(Droogers, 2000)	0.16-0.54	E declines with crop growth and lack of m		
	(Kato *et al.*, 2004)	0.10-0.5	Rapid, 2x increases in E with increase in m		
	(Liu *et al.*, 2002)		Rapid increases in E observed as m increased		
Transitional	(Reynolds *et al.*, 2000)	0.42-0.90	E simulated for dry grasslands/shrubs; rapid response to m	0.75	2
	(Liu *et al.*, 2002)	~0.30	E reduced by increased ground cover and low m		
	(Yepez *et al.*, 2005)	0.57-0.78	Semi-dry, arid grasslands; E increased rapidly with irrigation		
Coniferous Forest (low LAI)	(Grelle *et al.*, 1997)	0.17	Generally low E and high T	0.5	6
	(Baldocchi & Vogel, 1996)	0.20-0.40	Emax determined by litter water content		
	(Kelliher *et al.*, 1998)	0.30-0.50			
Deciduous Forest (high LAI)	(Wilson *et al.*, 2000)	0.08-0.2	E low due to decreased radiation input	0.3	6
	(Moore *et al.*, 1996)	0.11	Litter water content determines Emax		
	(Ffolliott *et al.*, 2003)	0.20-0.55	Emax (Tmin) when foliage coverage high; high interception E		
Mixed Forest	(Komatsu, 2005)	0.10-0.55	High E with lower LAI	0.4	6
Thick Forest	(Komatsu, 2005)	0.10-0.55	High LAI (coverage) decreases E increase with m (lack of energy input)	0.10	10
Wetland	(Herbst & Kappen, 1999)	0.33-0.58	E decreases with height of reed stands; highly variable depending on size of wetland (radiation input)	1	2
	(Burian, 1973)	0.50	Open-water reed stand		
	(Sánchez-Carrillo *et al.*, 2004)	0.52-1.0	E driven by amount of inundation		

4.3 Routing Model

Contributing surface and subsurface water balances (i.e., from each GRU) are combined to produce a total runoff response for the grid. Runoff is added to the channel network and routed from upstream to downstream through the defined drainage order. The routing of water through the channel system is accomplished using a hydrologic storage routing technique, which involves a robust application of the continuity equation:

$$\frac{dS}{dt} = O - I \text{ or,}$$

$$\frac{S_1 + S_2}{\Delta t} = \frac{I_1 + I_2}{2} + \frac{O_1 + O_2}{2} \qquad (4.9)$$

where $I_{1,2}$ is the inflow to the reach (cms) at the beginning (i.e., I_1) and end (i.e., I_2) of the time step; $O_{1,2}$ is the outflow from the reach (cms) at the beginning and end of the time step; $S_{1,2}$ is the volumetric storage in the reach (m^3) at the beginning and end of the time step; and Δt is the routing time step (s). Flow is related to storage via the Manning or Chézy discharge equations. The complete form of the Chézy equation is expressed as:

$$Q = CA\sqrt{R\left(S_i - \frac{dy}{dx} - \frac{v}{g}\frac{dv}{dx} - \frac{1}{g}\frac{dv}{dt}\right)} \qquad (4.10)$$

where C is an empirically-based coefficient ($m^{1/2}/s$); A is the cross-sectional area (m^2); R is the hydraulic radius (m); S_i is the bed or internal grid slope (m/m); and g is the gravitational constant (m^2/s). For storage routing it is assumed that S_i is significantly greater than change in water surface (dy/dx), velocity (dv/dx), and acceleration (dv/dt). This assumption, although not always justified, is very close to reality for natural floods in steep rivers (S_i>0.002). However, when slopes are very flat (S_i<0.001) the dy/dx term can be of the same order of magnitude as S_i, leading to significant errors in the routing computations when the additional slope, velocity and acceleration terms are neglected (Henderson, 1966).

In WATFLOOD, a form of the Manning formula is used to relate flow to storage for Equation 4.9 when flow is maintained within the banks of the main channel using a representative river cross-section (shown on Figure 4.4):

$$Q = \frac{1}{nw^{2/3}} A^{3/2} S_i^{1/2} \qquad (4.11)$$

where n is Manning's roughness coefficient for the main channel ($m^{-1/3} \cdot s$); w is the channel width (m) A is the cross-sectional area of the main channel (m^2); and S_i is the bed slope (m/m). This form of the Manning formula assumes a wide (R~y), rectangular section (A=w*y) for the main channel. When water levels rise and exceed the main channel banks, then the Manning formula is modified to include the excess over-bank area and storage:

$$Q = \frac{1}{n * w^{2/3}} A^{3/2} S_i^{1/2} + \frac{0.17}{n_{ob}} (over - h * w)^{5/3} S_i^{1/2} \qquad (4.12)$$

where n_{ob} is the over-bank composite Manning's roughness; and h is over-bank depth of flow (m) for a triangular cross-sectional area (Figure 4.4).

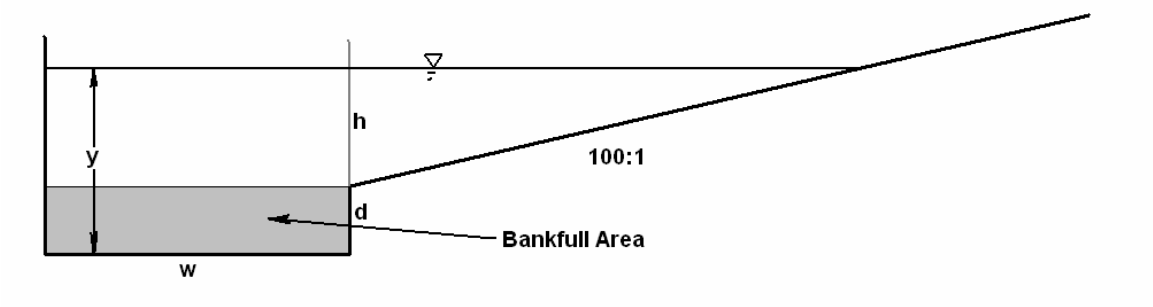

Figure 4.4 – WATFLOOD representative river cross-section (Kouwen, 2007).

Although many hydrological models use more complex methods of routing (i.e., hydrodynamic and diffusion-wave routing), on large watersheds the application of more complex techniques has yet to be proven more accurate and the differences are typically smaller than the noise in the data (Arora *et al.*, 2001; Kouwen, 2007). By using simplified storage routing, WATFLOOD keeps its computational efficiency high, enabling mesoscale modelling and sensitivity studies to be run over long time-periods. On low-relief watersheds where dynamic effects are large, or on smaller-scales (i.e., grids <1 km^2) where smaller hydrological errors are more meaningful, then the application of the WATFLOOD model would require routing to be performed offline using a dynamic wave model.

4.4 Wetland Routing

Wetlands in WATFLOOD represent channelized riparian zones acting as buffers to channel inflow or reservoirs for channel overflow. Wetland-channel interactions are reversible: under

normal flow conditions, wetlands provide channel inflows, however under channel flood conditions (high stage) the channels will overflow into the wetlands. Lateral interaction fluxes between the channel and wetland ($qo_{wet1,2}$ in cms) are governed by the Dupuis-Forchheimer discharge formula (Anderson, 1973):

$$qo_{wet_{1,2}} = \frac{K}{2}\left(h^2_{wet_{1,2}} - h^2_{cha_{1,2}}\right) \qquad (4.13)$$

where K represents the hydraulic conductivity of the wetland (m/s); $h_{wet1,2}$ is the height of standing water in the wetland (m) at the beginning (i.e., h_{wet1}) and end (i.e., h_{wet2}) of the timestep, respectively; and $h_{cha1,2}$ is the depth of flow in the main channel (m) at the beginning and end of the timestep. The hydrologic interaction between the wetland and channel is illustrated on Figure 4.5:

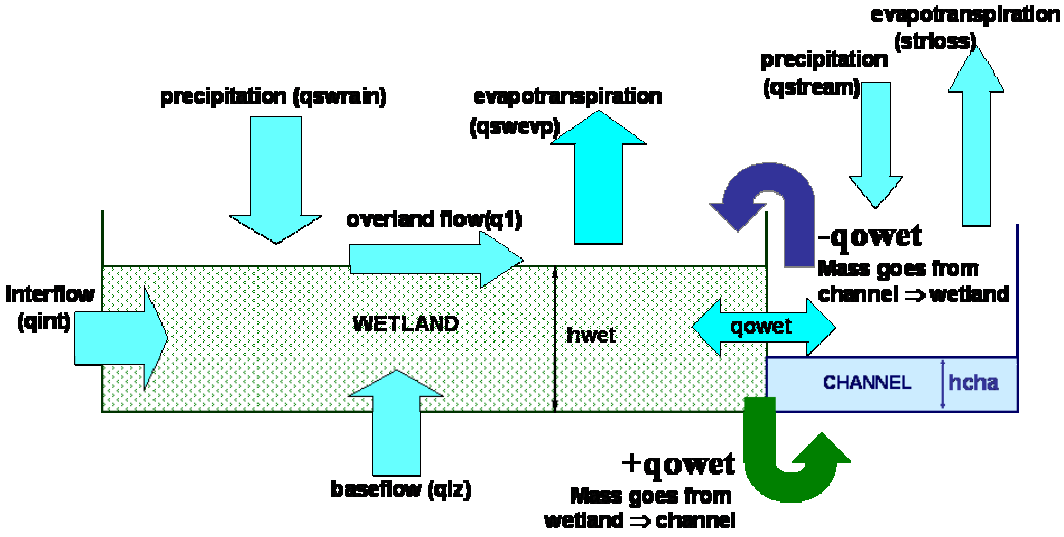

Figure 4.5 – Hydrologic interaction between WATFLOOD wetlands and channels.

Wetlands receive all lateral outflows from hydrologic storage (i.e., surface runoff, interflow, and baseflow), and direct meteorological inputs (i.e., snow and rain). Wetland storage is decreased by the lateral flux into the channel and by evapotranspiration loss. Since wetland areas are typically large, flows are routed through the wetland using hydrologic storage routing (Equation 4.9) and the relationship between storage and discharge from Equation 4.13.

4.5 Lake routing

For lakes within a watershed, reservoir grids are identified using distinct reach numbers, and the outlet to each lake identified as the last lake grid in the routing sequence. Flow can be routed through lakes via user-defined storage-discharge power functions:

$$O = b1 * S^{b2} \qquad (4.14)$$

or polynomial functions:

$$O = b1 * S + b2 * S^2 + b3 * S^3 + b4 * S^4 + b5 * S^5 \qquad (4.15)$$

where O is the lake discharge (cms); S is the total volumetric storage of the lake (m^3); b1 to b5 are optimized (or operationally defined) parameters. If reservoirs are controlled and regulated release data are available, then the releases are entered in a table and downstream discharge is based on the defined reservoir release data.

4.6 Snowmelt Model

WATFLOOD distinguishes between snow-covered and bare-ground areas, performing hydrologic storage and runoff calculations separately for both areas. The model tracks and updates the percentage change of snow-covered to bare-ground areas. Melting snow generates runoff from snow-covered area, which then infiltrates into UZS or produces overland flow.

WATFLOOD uses the temperature index model to compute depths of snowmelt (M in mm) using the well-known algorithm developed based on the National Weather Service River flow Forecast System (NWSRFS) model (Anderson, 1973):

$$M = MF\left(T_a - T_{base}\right) \qquad (4.16)$$

where MF is the melt factor or rate of melt per degree increase per time (mm/^{o}C/hr); T_a is the air temperature (^{o}C); and T_{base} is the base temperature beyond which melt begins to occur (user defined) (^{o}C). An hourly heat balance is calculated in the model for melt and non-melt periods. Equation 4.16 represents the maximum melt possible, given the snowpack is ripe and the air temperature is greater than the base temperature (i.e., a melt period).

During non-melt periods, the temperature of the snowpack warms and cools with the air temperature, but with a slight delay of snowpack temperature changes. A cumulative amount of heat is required to warm the snowpack to the 'ripe' phase, where it begins to melt; represented as the snow cover heat deficit (mm of water equivalent). The change in snowpack heat deficit (ΔH_s in mm of water equivalent) is driven by the difference between the antecedent temperature index (ATI) and T_a and is additionally decreased to account for freshly accumulated snow (S_f in mm of SWE):

$$\Delta H_s = NMF(ATI_1 - T_{a_2}) - \frac{S_f T_a}{160} \qquad (4.17)$$

where NMF is the negative melt factor, or rate of change in heat deficit by degree of air temperature increase optimized for each land class (mm/°C/day); ATI_1 is the ATI computed from the previous timestep (t-1); and T_{a2} is the air temperature during the current timestep (t). When T_a is greater than 0°C, then ΔH_s is assumed to equal zero and the total heat deficit is reduced by the maximum probable melt (M) from Equation 4.16.

The ATI is an indicator of the temperature at the surface of the snowpack that accounts for the delay in the warming or cooling of the pack driven by the air temperature, and is computed based on theory from the transient heat flow equation (Anderson, 1973):

$$ATI_2 = ATI_1 + tipm(T_a - ATI_1) \qquad (4.18)$$

where tipm is a rate parameter varying between 0 and 1, where the snowpack warms and cools at a faster rate for higher values of tipm (Anderson, 1973). Values ≤0.1 indicate a deeper 'surface layer' that inhibits heat transfer, therefore giving more weight to long-term air temperatures; compared with values of 0.5 that more heavily weight temperatures during the past day. Since it still cannot be conclusively stated what this parameter physically represents, values of tipm=0.2 are assumed in WATFLOOD (Kouwen, 2007), and have been shown to work well for southern Ontario (Donald, 1992).

4.7 Model Efficacy

The Nash-Sutcliffe goodness of fit (N_r) and percent deviation of runoff volumes (D_v) were the primary statistics used to determine model efficacy (i.e., how well modelled flows simulate the

measured streamflow), along with visual inspection of the catchments response to events from the shape and timing of the hydrographs.

Nash-Sutcliffe goodness-of-fit test is a common statistic used to assess the predictive power of hydrological models (McCuen *et al.*, 2006). It is a measure of the percentage of observed variance that is explained by the predictive data. Proposed by Nash and Sutcliffe (1970), N_r is estimated as (Nash & Sutcliffe, 1970):

$$N_r = 1 - \frac{\sum_{i=1}^{N}(Q_s - Q_i)^2}{\sum_{i=1}^{N}(Q_i - Q_i^*)^2} \qquad (4.19)$$

where Q_i^* is the average measured discharge, Q_i is the measured discharge, and Q_s is the simulated discharge. The second term in Equation 4.19 the mean square error (MSE) normalized by the natural variance in the observed data. A Nash-Sutcliffe coefficient (N_r) of one indicates perfect fit between simulated and measured streamflow; zero indicates the streamflow hydrograph is predicting no better than the average flow over the entire study period. Negative values are possible and indicate that simulations are worse than using the mean flow as an estimate of streamflow. Care should be used when interpreting the Nash-Sutcliffe coefficient, recognizing that it puts more emphasis on extreme events than on average flows.

The deviation of runoff volumes statistic (D_v), also known as predictive bias, is also a goodness-of-fit test that statistically compares measured and computed volumes of discharge during an event, providing information on how well the overall water balance is being modelled. It is calculated as follows:

$$D_V(\%) = \frac{\sum_{i=1}^{N}(Q_s - Q_i)}{\sum_{i=1}^{N} Q_i} \times 100 \qquad (4.20)$$

where Q_s and Q_i represent the simulated and observed streamflows, respectively; and N is the total number of values within the period of analysis. A value of zero indicates no difference between measured and simulated streamflow; a positive D_v indicates an under-estimation of simulated streamflow (i.e., missing source); and a negative D_v indicates an over-estimation of simulated streamflow (i.e., missing sink or excess source).

Model goodness-of-fit can also be assessed via proportionality plots that interpret how well modelled streamflows (or proportions of streamflow) match with measured streamflows (or verified contributions to streamflow). Proportionality plots are also indicators of model bias or error tendencies, showing patterns in how the model represents simulated flows over time. If modelled streamflows were 100% representative of measured flows, then points would plot along the 45-degree line (slope of one).

4.8 Model Set-up: Grand River Basin

The GRB (~6,000 km^2) was continuously modelled from October 2003 to December 2005 using the WATFLOOD hydrological model at a 2-km spatial resolution. Model calibration was performed on an existing 1993 data set (streamflow simulation only) so that the combined hydrometric-isotopic data set for the study period could be used for model validation.

Basin topography was derived from a 50-m digital elevation model (DEM) of southern Ontario using the EnSim pre-processor to generate WATFLOOD-compatible watershed files. Channels were identified by topographic lows in elevation, and by water land classifications. Four distinct river classifications and one default classification were defined for the GRB to account for changes in channel shape, roughness, and slope. The default river classification was utilized for the central portion of the basin, and for the majority of the Grand River main stem. Additional river classifications were created to describe the wetland-dominated regime of the Eramosa River; the flat, wide channels in the lower-Grand; the baseflow dominated, coldwater course of Whiteman's Creek; and the flashy, flood-susceptible Nith River.

Based on the LandSat imagery of the GRB (Figure 3.2), seven distinct land classifications were identified and used in the WATFLOOD model as shown in Table 4.2.

Table 4.2 – Percent landcover classification based on LandSat imagery for the GRB.

Land class	Urban	Bare Soil	Forest	Agriculture	Wetland (fen)	Wetland (bog)	Water
GRB	1.5%	3.1%	16.7%	75.6%	2.5%	0.01%	0.7%

The GRB houses some of southern Ontario's most productive farmlands and is largely utilized for agriculture, which is reflected in Table 4.2. Secondary to agriculture, over 16% of the

watershed remains forested with a large variety of tree species unique to each region of the basin. The expansive urbanization of the watershed has led to a significant decrease in forested area within the watershed since the late 1700s when over 95% of the watershed was forested (Ivey, 2002). Although not common throughout the basin, the northern and north-eastern regions of the watershed have prominent bare areas identified as drumlin fields. Many of the natural wetlands in the basin have been drained, however in the northern and eastern regions of the basin wetlands and marshy areas still exist and help to regulate high amounts of runoff from urbanized areas.

Initial soil moisture data were obtained for three locations within the GRB in October of 2003: Guelph (4820000N, 558000E), Waterloo Weather Station (4813494N, 535812E), and Shand Dam. Point soil moisture data (i.e., API-derived) were distributed across the domain using MOIST.EXE. Initial soil moisture was also estimated based on knowledge of antecedent conditions from the fall season previous to the spring freshet.

Hourly temperature data were measured at 12 locations throughout the watershed, seven of which corresponded to operational reservoirs. Temperatures were distributed using the WATFLOOD pre-processor program TMP.EXE (Kouwen, 2007) using a distance weighting method for each grid in the domain. Temperature data were representative of meteorological conditions within the watershed because of good spatial resolution of the data and coverage of the varying climatic zones in the basin.

Hourly precipitation was recorded at 12 GRCA climate stations using Environment Canada approved rain gauges. For such a large region however, spatially distributed rainfall data available from the King City RADAR (WKR) are more desireable and are used during the winter months. Raw CAPPI radar images received from WKR converted to a WATFLOOD-compatible format using RADMET.EXE. Point rainfall data from rain gauges were used to ground-truth radar by correcting anomalous precipitation estimates and filling in missing data using the CALMET.EXE program (Kouwen, 2007). Radar data for the 2003 to 2005 study period were representative of meteorological conditions; however due to beam attenuation and false echoes, anomalous precipitation estimates still exist in the data.

Hourly streamflow discharges were monitored continuously at GRCA and WSC gauges in the GRB. Measured hourly provisional streamflows for the study period were obtained from the GRCA for the 41 sub-basin outlets being modelled. Modelled streamflows were computed on an hourly basis to compare with measured streamflow.

There are seven controlled reservoirs located within the GRB. Water is routed through the lakes using GRCA-defined rule curves for each of the seven reservoirs (GRCA, 2008c). For the controlled reservoirs, hourly reservoir release discharge data were obtained from the GRCA and used to replace simulated streamflows in reservoir outlet grids to ensure downstream flows are accurately computed from reservoir discharge data.

A unique set of hydrological parameters was defined for each land classification in order to define a unique hydrologic response for each landcover type, and the various river types (Appendix A.1.1). Isotope initialization parameters were defined to describe ambient surface water and baseflow compositions and meteoric input waters (snow and rain) (Appendix A.1.2).

Model calibration was performed manually on a 1993 data set using streamflow data alone since isotope data were only available from 2003-2005. Model efficacy was assessed statistically using Nash-Sutcliffe and percent volumetric deviation statistics. For model validation isotope initialization parameters were derived based on field measurements from the isotope sampling campaign and from the CNIP database (Birks *et al.*, 2004). Since continuous simulation was performed from October 2003 to the end of 2005, re-initialization of isotope parameters was not necessary. Results and analysis from the model validation runs in the GRB are found in Chapter 9.

4.9 Model Set-up: Fort Simpson Basins

The FSB (~6,000 km^2) was modelled using WATFLOOD at a 10-km spatial resolution for three, four-month study periods: April-August 1997, 1998, and 1999 respectively. Model calibration was performed on the 1997 dataset; while model validation runs were conducted

using the 1998 and 1999 data. Following model calibration, the model was run continuously from December 1996 to December 1999 for analysis of streamflow and isotopic simulations.

Basin topography was derived from a 50-m DEM generated from NTDB digital data from the 1:250 000 NTS map sheets 95A, 95B, 95G, and 95G (Töyra, 1997). Data were imported into Arc/Info, converted into grids, and then exported into PCI for analysis and DEM generation. Channels were identified by topographic lows and by the water land classification. Each sub-basin was assigned its own distinct river classification for parameterization due to the distinct differences in channel roughness, slope, and stratigraphy in each of the five sub-basins.

Land classifications were identified from LandSat imagery shown in Chapter 3 (Figure 3.9). Derived from this image, Table 4.3 shows the percent distribution amongst the seven landcover types identified for the FSB and used in the WATFLOOD model.

Table 4.3 - Distribution of percent landcover for the FSB.

	Mixed / Deciduous	Conifer	Transitional	Wetland (fen)	Wetland (bog)	Water	Impervious
Jean-Marie River	28%	22%	32%	11%	4%	1%	1%
Martin River	24%	20%	36%	13%	4%	2%	1%
Birch River	29%	8%	36%	18%	6%	1%	1%
Blackstone River	27%	14%	37%	14%	5%	2%	0%
Scotty Creek	14%	29%	38%	9%	3%	6%	2%

Table 4.3 indicates that transitional (burn re-growth) landcover is dominant in all five catchments. The second most dominant landcover is mixed and deciduous tree cover in all except Scotty Creek, where conifer tree cover is the second most dominant. All five sub-basins have a substantial proportion of combined wetlandcoverage that is mostly connected to the channel network (i.e., fen classification). Birch and Blackstone Rivers have the highest percentage wetlands and also the highest percentage of bog, or disconnected drainage classification. Wetlands in the FSB are sub-divided into fen and bog classifications; bogs generally occur topographically higher than fens, which results in very little to poor drainage. They are therefore maintained only through direct precipitation or runoff from adjacent plateaus (Hayashi *et al.*, 2004; Woo, 1988; Zoltai *et al.*, 1988). Fens on the other hand receive drainage by subsurface seepage since the water table remains at surface level (Hayashi *et al.*, 2004; Quinton & Roulet, 1998; Woo, 1988; Zoltai *et al.*, 1988). Differences in hydrologic response become

apparent between bog-dominated (i.e., Birch and Blackstone rivers) and fen-dominated sub-basins (i.e., Jean-Marie River and Scotty Creek) (St Amour *et al.*, 2005). Fen areas are modelled using wetland hydrology in WATFLOOD (Section 4.4), whereas bog regions are modelled using the runoff-drainage storage relationships in WATFLOOD.

Initial soil moisture was estimated based on knowledge of antecedent conditions from the fall season previous to the spring freshet for each of the study periods.

Snow course surveys were randomly conducted at 12 locations throughout the study region during the winter months of each of the three study seasons (Hamlin, 1996). Snow course survey data were obtained at sites representative of six of the seven land classifications (i.e., combined wetland classification) to assist in snow cover distribution weighting. Point snow course data from the surveys were distributed using the WATFLOOD pre-processor program SNW.EXE (Kouwen, 2007) to obtain distributed snow cover data.

Daily total precipitation and hourly temperatures were recorded at the Fort Simpson Airport. Daily estimates of precipitation and hourly temperatures were distributed using the WATFLOOD pre-processor programs RAGMET.EXE and TMP.EXE, respectively (Kouwen, 2007), which use a distance weighting method for each grid in the domain. There were problems with the representativeness of the precipitation data because of the remoteness of the rain gauge from the study basins. Several significant rainfall events were missed in the summer months, but definately occurred as was evidenced by the observed rise in streamflow hydrographs. Since temperature data were also collected randomly at several locations throughout the study region, they were used to ground-truth the distributed temperature data and to verify their accuracy.

Daily streamflow discharges were continuously monitored during the ice-off seasons at the outlet of all five FSBs. Since rivers are unregulated in the FSB, no controlled reservoirs or reservoir releases were present in the model set up.

A unique set of hydrologic parameters was defined for each land classification to define unique hydrologic responses for each landcover, and the five distinct river types (Appendix A.2.1).

Isotope initialization parameters were also defined to describe measured background compositions in surface water, baseflow and meteoric water (snow and rain) obtained from field sampling campaigns in 1997 through to 1999 (Appendix A.2.2).

Model calibration was performed manually on the 1997 data set with both streamflow and isotope data. Model efficacy was assessed statistically for streamflow estimation using Nash-Sutcliffe and percent volumetric deviation statistics. Visual inspection was used to fit continuously simulated isotopic compositions to single point (in time) measurements. For model validation, only isotope initialization parameters were changed to physically represent measured isotope compositions of surface waters, baseflow and input waters specific to the study year. This re-initialization for isotopes was only necessary when continuous simulation was not being performed. The model was validated using the 1998 and 1999 study seasons to assess the accuracy of both streamflow and isotopic river composition continuously from April to August. Results from these simulations can be found in Chapter 8.

4.10 Model Limitations

As with any model, there are inherent assumptions and limitations implicit from the modelling framework. WATFLOOD uses kinematic wave routing, and therefore should not be applied to very flat sloping catchments where dynamic wave routing is more appropriate. WATFLOOD is however configured for linking with dynamic wave models such as DWOPER and Flow-1D for such situations where dynamic wave routing is required (Pietronio *et al.*, 2003). Soil structure and heterogeneity cannot be explicitly parameterized within the model framework, and therefore it is important that heterogeneities can be sufficiently represented by the landcover classification. For situations where there are significant heterogeneities of underlying soils however, additional GRUs can be used to represent these variations in the soil type. The parameterization scheme in WATFLOOD is based upon landcover and river type classifications. With any model, the results can only be as realistic as the inputs used for the modelling; WATFLOOD relies on spatially and temporally accurate estimates of precipitation for its water balances. Given the remote nature of some of the study sites, precipitation estimates are occasionally flawed. These input errors translate to errors in streamflow simulation, which would be the situation for any

model. The advantage WATFLOOD has over other models is the fewer number of parameters required to run the model, and the ease and accuracy with which these parameters can be derived through calibration, and transferred to and from other hydrologically similar watersheds.

Significant errors can also arise from the coarse spatial resolution of the model. WATFLOOD uses a mesoscale grid (up to ten-by-ten kilometres in this study). The advantage of using such large grid sizes is realized by a decrease in computational effort and input parameterization that is required to run the model. The inherent disadvantage of the grid size however is that local heterogeneity may be lost and can only be captured by landcover differentiation within a grid. It can be argued that local heterogeneities are "averaged-out" over larger scales, and that perhaps are not fully realized when predicting something as non-unique as discharge (Beven, 1997; 2002). Dominant hydrological processes may be captured and satisfactorily controlled by landcover variations and a simplified three layer conceptualization as is used in WATFLOOD.

4.11 Chapter Summary

The WATFLOOD hydrological modelling system is an efficient, mesoscale watershed model capable of accurately reproducing streamflow variation over long-time sequences for a variety of hydrologically-differing watersheds. Alternative hydrological and groundwater models require an array of forcing inputs that must be measured using detailed field studies. One of the goals of this research is to provide a practical means of validation for hydrological models without the requirement of a detailed field work investigation. The WATFLOOD model is both comprehensive in its inclusion of hydrologic interactions and compartments, and physically-based in the theories it employs to model these interactions. WATFLOOD is classified as a partially physically-based model that utilizes logical conditions to increase the computational efficiency of the model, making it viable for mesoscale climate change and sensitivity studies. As with all models, there are limitations to the application of the WATFLOOD model, specifically for flat, low-relief areas where dynamic forces are significant in the momentum equation for routing. The WATFLOOD model for most natural watersheds however is a robust model proven to accurately represent internal hydrological processes and modelled streamflows (Bingeman *et al.*, 2006). Finally, as described in Chapter 2, Environment Canada's development

of the MESH framework (Pietroniro *et al.*, 2007) could one day facilitate the incorporation of isoWATFLOOD into a larger coupled atmospheric-hydrologic modelling system. WATFLOOD therefore seems to be a logical choice for the implementation of an isotope-enabled hydrological modelling system given the detailed knowledge and access to the models framework. Prior to the development of isoWATFLOOD however, the WATFLOOD model must first be capable of identifying and separating individual flowpath contributions to streamflow.

In the next chapter the development of the WATFLOOD tracer module is described, where streamflow hydrographs are separated into their contributing end-member flowpaths. The tracer module has assisted in WATFLOOD parameter calibration and is the first step in the development of the isoWATFLOOD model. Results from two baseflow HS studies will show how the WATFLOOD model accurately computes the regional baseflow of the streamflow hydrograph for two distinctly different study basins: the Grand River, ON and Fort Simpson, NWT.

Chapter 5

WATFLOOD Hydrograph Separation

Hydrograph separation studies in hydrological modelling have helped to identify and constrain errors associated with equifinality in streamflow simulation. Researchers have identified the need to develop methods to test if models are getting the 'right answers' for the 'right reasons' (Kirchner, 2006). Kirchner (2006) proposed a methodology for improving the reliability and uncertainty estimation in hydrological modelling that outlines a new focus for modellers (Section 2.7). Consistent with that focus, the WATFLOOD model makes full use of existing data networks, including remotely-sensed data; it utilizes physically-based equations to describe hydrologic interactions; it incorporates a minimal amount of parameterization to make it feasible for mesoscale modelling; and it is efficiently designed such that it is practical to use over large domains. The WATFLOOD tracer module was created to sensibly and comprehensively test modelled results in mesoscale basins.

The tracer module was integrated into WATFLOOD as a stand-alone module that is transferable to other modelling systems. A flowchart of the WATFLOOD modelling system, highlighting the addition of the tracer module, is provided in Appendix B. Modelling the isotopic variation in streamflow requires the segregation of contributions to total flow from each hydrologic component, and rigorous verification of these compartmental flows.

The tracer module consists of a series of conservative tracers, or hydrograph segregation options as illustrated on Figure 5.1:

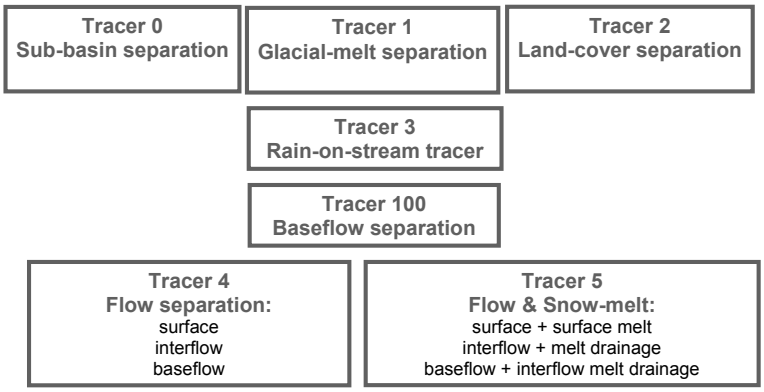

Figure 5.1 – WATFLOOD tracer module components for hydrograph separation.

Each tracer segregates one or more components contributing to streamflow. For example, Tracer 3 (rain-on-stream) generates a secondary hydrograph that shows the proportion of total streamflow originating from rainfall onto the stream. Tracer 0 apportions total streamflow into contributions from individual sub-basins, or gauges. The baseflow tracer (Tracer 100; Section 5.1) assists WATFLOOD modellers with watershed parameter calibration. Three-component hydrograph separation (Tracer 4; Section 5.2) is also used for parameter calibration but is particularly useful in verifying modelled streamflows are computed from physically-representative internal processes. WATFLOOD-derived baseflow is compared to two common baseflow separation models in Section 5.3 to assess the models accuracy in estimating baseflow response. For verification of the WATFLOOD baseflow response, WATFLOOD-derived baseflow is compared to isotopically-separated baseflow in Section 5.4 of this chapter.

5.1 Baseflow Hydrograph Separation

During flow separation, conservative tracers are added to the baseflow component at the time of generation and are used to track the volumetric contribution of the baseflow component through the WATFLOOD model using Tracer 100. The result is a streamflow hydrograph that is additionally segregated to show the contribution to that hydrograph from the baseflow component (Figure 5.2):

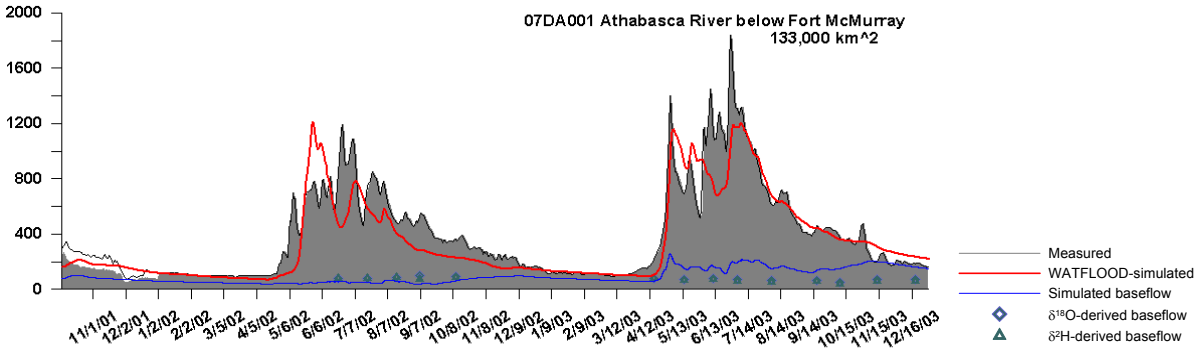

Figure 5.2 – Example of a baseflow hydrograph separation for the Athabasca River, Canada.

To apportion the baseflow component of streamflow, a slug of conservative tracer (MIN_{GW} in kg) is added to the stream determined by the mass concentration of tracer ($C_{IN,GW}$ in kg/m^3) and the volumetric flow of the baseflow component (qlz in m^3):

$$MIN_{GW} = C_{IN,GW} * qlz * t \qquad (5.1)$$

Tracer mass inflow (Equation 5.1) is assumed to be instantaneously and completely mixed throughout the stream element.

Once added to the stream, tracer mass is hydrologically routed with streamflow using a second, parallel application of the continuity equation to compute the total mass of tracer (i.e., baseflow) stored in the stream:

$$S_2 = S_1 + \frac{MIN_{GW_1} + MIN_{GW_2} - MOUT_{GW_1} - MOUT_{GW_2}}{2} \qquad (5.2)$$

where, S_1 and S_2 (kg) are the mass of tracer in storage at the beginning (S_1) and end (S_2) of the time step respectively; and $MOUT_{GW1,2}$ (kg) is the mass outflow of tracer at the beginning ($MOUT_{GW,1}$) and end ($MOUT_{GW,2}$) of the timestep, respectively. Therefore the mass concentration of baseflow in the stream (C_{GW} in kg/m^3) is the amount of tracer mass stored (S_2 in kg) over total water stored (store2 in m^3) in the channel in any given timestep:

$$C_{GW} = \frac{S_2}{store_2} \qquad (5.3)$$

where, $store_2$ is the total volume of water in the channel (m^3). This concentration physically represents the fraction of baseflow contribution to total streamflow, derived from a mass balance of the conservative tracer.

The mass of tracer leaving a stream element ($MOUT_{GW}$ in kg) is determined as the fraction of total streamflow that is baseflow, less a proportion of streamflow lost through evaporation over the timestep:

$$MOUT_{GW} = C_{GW} * qo_2 * t - C_{GW} * strloss * t \qquad (5.4)$$

where, qo_2 is the total stream outflow at the end of the timestep in m^3/s; and strloss is the total evaporative flux lost from the stream over the timestep in m^3/s. The evaporative flux is assumed to be proportioned equally with the contributions to streamflow, and once added to the stream, all components have an equal potential to evaporate.

The mass of tracer leaving an upstream grid cell (n) is routed and added to the next grid cell (n+1) in the routing sequence as a mass inflow ($MIN_{GW,t}$):

$$MOUT_{GW,t}(n) = MIN_{GW,t}(n+1) \qquad (5.5)$$

Equations 5.1 through 5.5 are repeated until a tracer mass outflow has been computed for each grid in the routing sequence.

Surface flow, interflow (Tracer 4; Section 5.2), and melt components (Tracer 5) can be segregated from total streamflow in the same manner. Although all tracers in the module have been coded, only Tracer 4, 5 and 100 have been verified and are considered ready for operational use. Since initial tracer concentration or mass storage in each compartment is not easily obtained, initialization is not feasible. Instead a sufficient model spin-up ensures that errors resulting from improper initialization are minimized.

Given the coarse grid resolution of WATFLOOD grids (i.e., 4 km^2 to 100 km^2), instantaneous and complete mixing of tracers is not entirely reasonable. Early breakthrough of segregated flow components has been observed when using the tracer model, with sub-components appearing before simulated streamflow in response to a runoff event. Mathematically this translates to end-member concentrations greater than one in a single timestep, or component contributions that are more than 100% of total flow (i.e., correct amount of mass, however it is not in sync with the correct volume of water). This mathematical error represents the level of incorrectness of the modelling assumptions and is not physically possible since tracer concentrations represent fractional contributions of end-members generating total flow. A solution was found by

adopting a retardation coefficient that is applied to tracer outflows to effectively constrain the mass transit of tracer, as is done for many numerical method solutions (Chapra, 1997a; Rutherford, 1994; Schnoor, 1996). The dimensionless retardation coefficient (*coeff*) is based on a dispersion factor, D^*:

$$coeff = \frac{D^*}{U^2 \cdot tt} \tag{5.6}$$

where D^* (m^2/s) is the Péclet number that is defined as (Rutherford, 1994):

$$D^* = \frac{U \cdot \Delta x}{2} \tag{5.7}$$

where U is the average channel velocity (m/s); tt is reach travel time in seconds; and Δx is the grid length in meters. Any excess tracer in a given time step is delayed until the next time step, at which point it is then added to the streamflow. The result of applying the coefficient was a damping of the tracer, delaying tracer appearance and prolonging the residual tail (Figure 5.3). A mass balance check during simulation is performed for each grid at every timestep to ensure that the change in storage of tracer is equal to the computed inflow minus the computed outflow (i.e., that mass is neither created nor destroyed).

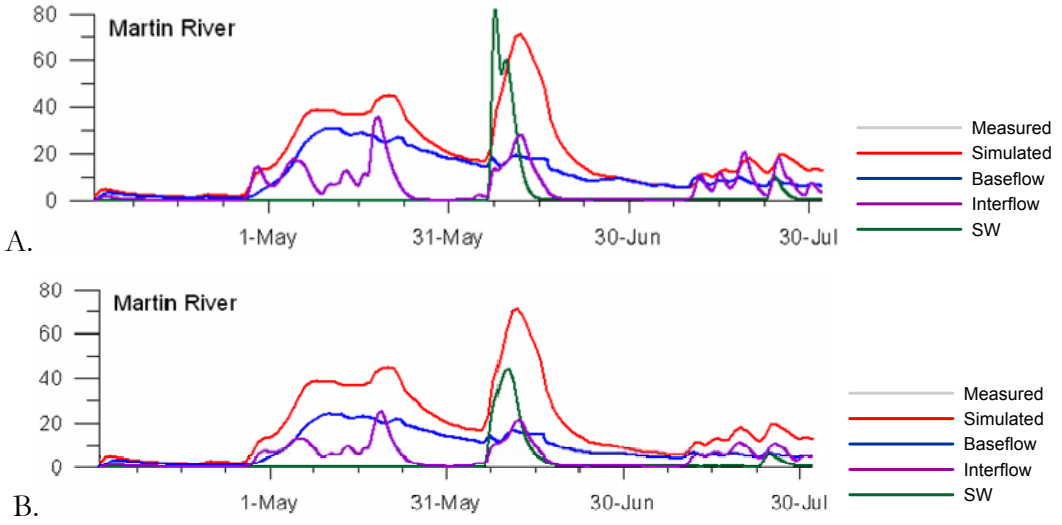

Figure 5.3 – Streamflow hydrograph separation for Martin River, FSB, A. without dispersion coefficient, B. with dispersion coefficient.

These results appear to be more realistic given that there is an expected lag period between a storm event and the effect of that storm on subsurface flows (e.g., baseflow). The lag time between a storm event and response of the subsurface hydrograph should increase with increasing depth from the surface due to the increased travel time of the storm flow.

5.1.1 Tracers and Wetlands

If wetlands are present, then tracer mass is routed twice for each hydrological component: once through the wetland, and again in streamflow. Since wetlands in WATFLOOD represent riparian zones (fens) lining the channel, the mathematics of tracer mass routing in wetlands do not significantly change from channel routing. A mass of tracer is added to the wetland associated with the inflow of each end-member (e.g., baseflow, or qlz in m^3/s):

$$MIN_{wet,GW} = C_{IN,wet} * qlz * t \qquad (5.8)$$

The mass inflow is then routed in parallel with wetland flows using storage routing and the same application of the continuity equation from channel routing (Equation 5.2). Once the mass of tracer in wetland storage ($Swet_{GW,2}$) is calculated, the mass concentration of tracer ($C_{WET,GW}$ in kg/m^3) in the wetland can be defined as

$$C_{wet,GW} = \frac{Swet_{GW_2}}{wstore_2} \qquad (5.9)$$

where $wstore_2$ is the total volume of water in the wetland (m^3). Equation 5.9 represents the fractional contribution to wetland flow from that particular hydrologic end-member (e.g., baseflow).

Tracer mass outflow from the wetland is calculated as a percentage of total wetland outflow associated with that end-member, less the mass of tracer lost with evaporation from the wetland:

$$MOUT_{wet,GW} = C_{wet,GW} * qo_{wet_2} * t - C_{wet,GW} * qsw_{evp} * t \qquad (5.10)$$

where $qo_{wet,2}$ is the wetland outflow at the end of the timestep in m^3/s; and qsw_{evp} (in cms) is the total evaporative flux out of the wetland over the timestep in m^3/s. Since the wetlands are defined as channelized fens lining the channels, the mass flux out of the wetland is defined as the mass flux into the adjacent channel:

$$MOUT_{wet,GW} = MIN_{GW} \qquad (5.11)$$

Equations 5.1 to 5.5 are applied to route wetland contributions in the channel to compute the proportion of streamflow associated with each component of wetland outflow.

If the head gradient in the channel is greater than that in the wetland, then the wetland outflow $qo_{wet,2}$ is negative (i.e., indicating a wetland inflow). When this reversal of gradient occurs, channel inflow is recomputed to account for the loss in tracer mass from the channel associated with the negative $qo_{wet,2}$ flux:

$$MIN_{GW} = MIN_{GW} + C_{wet,GW} * qo_{wet_2} * t \qquad (5.12)$$

And wetland inflow is modified to account for the gain in tracer mass from the channel compartment:

$$MIN_{wet,GW} = MIN_{wet,GW} C_{wet,GW} * qo_{wet,2} * t \qquad (5.13)$$

Recalling that $qo_{wet,2}$ is negative, the second term is added to $MIN_{WET,GW}$. With the modified inflows, tracer mass is then routed through the wetland (Equations 5.9 to 5.11), and in the channel (Equations 5.2 to 5.5).

5.2 Three-Component HS

The three-component HS in WATFLOOD is performed by Tracer 4 that partitions surface water runoff, interflow and baseflow contributions to streamflow. Three-component HS is the foundation of isoWATFLOOD, subsequently described in Chapter 6. Complete flowpath segregation is necessary so that isotope concentrations can be uniquely associated with end-member flowpaths to preserve discrete isotopic variations in the hydrologic storages.

The three-component HS tracks mass inflows, storages, concentrations, and outflows of three end-members (i.e., surface runoff, interflow, and baseflow) simultaneously. Parallel sets of equations for surface runoff and interflow components are generated in addition to Equations 5.1 to 5.5 to route tracer mass for each end-member. In addition to Equation 5.1 which defines the tracer mass inflow to the channel for the baseflow component, Equations 5.14 and 5.15 are added to simultaneously compute the tracer mass inflows for surface runoff and interflow:

$$MIN_{SW} = C_{IN,SW} * (q_1 + q_{1fs}) * t \qquad (5.14)$$

$$MIN_{IF} = C_{IN,IF} * (q_{\text{int}} + q_{\text{int}\,fs}) * t \qquad (5.15)$$

where q_1 is the surface runoff, or overland flow (m^3/s) from bare ground; q_{1fs} is the surface runoff produced from snowmelt (m^3/s); q_{int} is the lateral interflow, or soilwater component to the channel (or wetland) from UZS (m^3/s); and q_{intfs} is the interflow component derived from snowmelt infiltration into the UZS (m^3/s). An additional set of equations is generated for each step of the tracer routing process. If there are wetlands, parallel sets of Equations 5.8 through 5.11 are also derived for surface runoff and interflow components in wetland storage.

Tracer module verification of component separation is conducted by a series of two studies in this chapter. First a comparison between WATFLOOD baseflow and two other, well-known baseflow separation models: BFLOW (Arnold *et al.*, 1995) and HYSEP (Sloto & Crouse, 1996) is conducted (Section 5.3). The comparison of one model to another however does not fully constrain the uncertainty in baseflow prediction. WATFLOOD baseflow separations were therefore verified against isotopically-derived baseflow separations (St Amour *et al.*, 2005; Section 5.4).

5.3 WATFLOOD Baseflow Separation: Grand River Basin, ON

In conjunction with the Grand River Conservation Authority (GRCA), a study was performed that compared WATFLOOD-derived baseflow (i.e., Tracer 100) to alternative methods of baseflow separation typically used by conservation authorities: the HYSEP and BFLOW models. Each model is based on similar theory, which automates the separation of baseflow from measured streamflow data. BFLOW is a program developed for use with the SWAT hydrological model and is supported by the Soil and Water Research Laboratory, USDA Agricultural Research Service (Arnold *et al.*, 1995; Arnold & Allen, 1999; Nathan & McMahon, 1990). HYSEP is a baseflow separation program developed by the USGS (Sloto & Crouse, 1996).

The objectives of this study were to determine if WATFLOOD baseflow simulations are:

1. Representative of baseflow separation techniques currently used in practice; and
2. More physically realistic than these currently used baseflow separation techniques, as assessed by the baseflow response to storm events.

The study methodology is presented in Section 5.3.1. The BFLOW and HYSEP software packages and results from the application of each model to the streamflow dataset are presented in Sections 5.3.2 and 5.3.3, respectively. Results and implications of this study discussed in Section 5.3.4 conclude that WATFLOOD baseflow separations are representative of other baseflow separations performed by commonly used models. WATFLOOD simulations, however, incorporate specific basin characteristics, making hydrograph separations more physically representative of natural flowpath variations than conventional baseflow separation models.

5.3.1 Study Methodology

Hydrographs were generated for 23 of the 41 gauges in the Grand River Basin (GRB). Results from all twenty-three gauges were used in the analysis of the baseflow separation, however a few strategic locations were chosen for detailed comparison due to their hydrological contrast to one-another. Results are presented for two coldwater, baseflow-dominated watercourses of interest to the GRCA: the Eramosa River at Guelph (222 km^2), and Whiteman's Creek at Mount Vernon (379 km^2) near Brantford (Figure 3.3). Each watercourse is baseflow-dominated, but has significantly different physiographic features. The Eramosa River is fed largely from the Galt and Paris Moraines at the central-eastern edge of the GRB: a thick deposit of till, with large areas of disconnected drainage. In contrast Whiteman's Creek is an ecologically significant cold-water course located in the Norfolk Sand Plains in the south GRB: a relatively thin deposit of sand with flat topography. The different underlying geologies result in different basin drainage and hydrological storage mechanism, leading to differences in baseflow generation.

Measured streamflows are daily estimates of flow beginning in the early 1960's and continuous until 2001. Both the HYSEP and BFLOW models were run using the entire measured streamflow data set. The WATFLOOD model was run continuously from 1993 to 2000 using operational radar data for precipitation input that was obtained from King City Radar. Unfortunately simulations showed a large degree of inconsistency with measured precipitation due to changes that were made to the calibration of the radar products in 1994. Since 1993 was the most consistent year, simulation results are presented for 1993 alone. WATFLOOD

simulations produced hourly estimates of streamflow and baseflow, which were averaged on a daily basis for direct comparison to HYSEP and BFLOW simulations.

The HYSEP and BFLOW models were run using various baseflow separation options internal to each program. Visual analysis was used to select one option for each model that was most representative of 'natural' baseflow conditions. Natural baseflow components of streamflow are typically long-term discharges contributing to streamflow that do not immediately respond to meteorological events and sustain streamflows between events (Buttle, 1998; Commonwealth of Australia, 2006; Jones *et al.*, 2006). Once a desired option was selected for each model, results from the two baseflow models were compared with the WATFLOOD baseflow simulations.

5.3.2 BFLOW Modelling

The BFLOW or Base-Flow program segregates baseflow from streamflow by recursively passing a digital filter over the streamflow record. The digital filter, originally described by Nathan & McMahon (1990), has no physical basis in ground water flow theory but has been adopted because it is objective and reproducible (Arnold *et al.*, 1995). The baseflow filter is defined by Arnold *et al.* (1995) as:

$$q_t = \beta \cdot q_{t-1} + \frac{(1-\beta)}{2}(Q_t - Q_{t-1}) \qquad (5.16)$$

where, q_t and q_{t-1} are the quick response surface runoff in the current and previous timestep, respectively (m^3/s); Q_t and Q_{t-1} are total streamflow in the current and previous timestep, respectively (m^3/s); and β is the filter parameter. The filter was originally used in signal analysis and processing and separates low-frequency baseflow from higher frequencies of quick-flow (Nathan & McMahon, 1990). The filter parameter β affects the attenuation of baseflow and was determined by Nathan and McMahon (1990) and Arnold *et al.* (1995) to range from 0.9 to 0.95 (optimally β=0.925). The baseflow component (b_t in m^3/s) of the total streamflow hydrograph is therefore defined as:

$$b_t = Q_t - q_t \qquad (5.17)$$

The filter can be passed three consecutive times over the streamflow record: forwards, backwards and forwards again. The reverse pass nullifies any phase distortion created by the forward pass (Nathan & McMahon, 1990). The estimated baseflow is output with each consecutive pass of the filter, producing three time series estimates of baseflow. The user can then select the optimum pass based upon knowledge of the catchment and typical baseflow recession curves. The number of filter passes affects the degree of smoothing of the baseflow hydrograph, and generally leads to lower baseflow estimates with each increasing pass (Arnold *et al.*, 1995).

Results comparing the three filter options (i.e., one, two and three passes of the filter) are presented on Figure 5.4 and Figure 5.5 Eramosa River and Whiteman's Creek, respectively. The BFLOW-3 option in both Eramosa River and Whiteman's Creek basin appears to be more representative of a 'natural' baseflow profile relative to the BFLOW-1 and BFLOW-2 options, which produce physically unrealistic profiles. This is most apparent during the spring freshet from April to May where BFLOW-1 and BFLOW-2 simulations rise well into the event hydrograph, which is more typical of a snowmelt runoff increase. Future model comparisons will therefore use BFLOW-3 simulations.

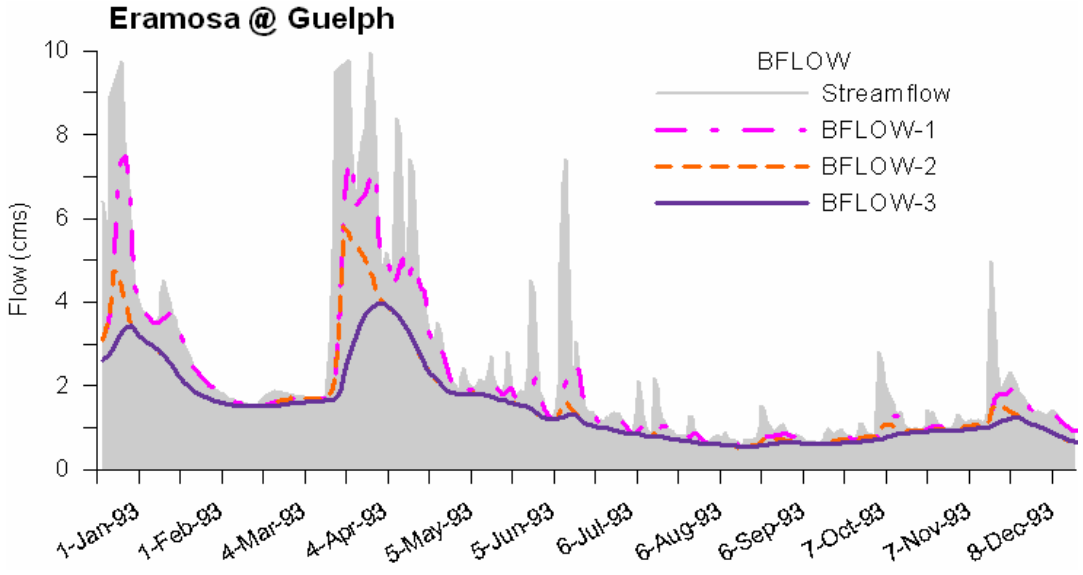

Figure 5.4 –BFLOW 1993 simulations for the Eramosa River.

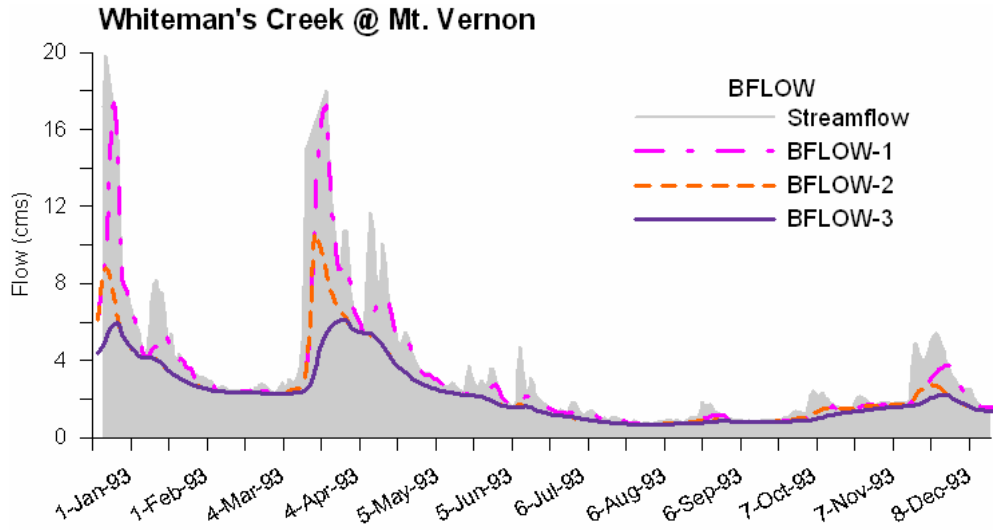

Figure 5.5 – BFLOW 1993 simulations for Whiteman's Creek.

5.3.3 HYSEP Modelling

HYSEP segregates baseflow from total streamflow by determining the lowest flow during a specified runoff period, or interval. The duration of surface runoff is based solely on the drainage area of the basin as defined from an empirical relationship (Linsley *et al.*, 1982):

$$N = Area^{0.2} \qquad (5.18)$$

where N is the number of days after which surface runoff ceases (the interval length); and Area is the drainage area in square miles. The interval 2N* used for baseflow hydrograph separations is the nearest odd integer between 3 and 11 nearest to 2N (Pettyjohn & Henning, 1979). If the streamflow record permits, baseflow separation begins one interval (2N* days) prior to the start of the simulation and proceeds for 2N* days after the end of the simulation to improve the accuracy of the separation. Otherwise, start and end dates coincide with the record or simulation period. HYSEP model options include:

Fixed Interval

The hydrograph is divided into sequential time blocks, each block equal to the duration one interval (2N* days). The lowest discharge is found within each interval, assumed to be baseflow, and is assigned as the baseflow discharge to all time steps in that interval. This is repeated for each interval of the hydrograph, as shown on Figure 5.6-A (Sloto & Crouse, 1996).

Sliding Interval

Each data point in a hydrograph is examined for the lowest discharge. A period equal to one half the interval less one day, or [0.5(2N*-1)] is considered before and after the data point (i.e., the discharge becomes centred on the data point). The lowest flow during the interval is then assigned to the data point in question as an estimation of baseflow, and the process is then repeated for the next low-flow in the hydrograph. This method replicates a moving minimum, as illustrated on Figure 5.6-B (Sloto & Crouse, 1996).

Local Minimum

This method determines if a data point in question is the lowest flow within a length of time equal to the interval. A period of one half the interval less one day, 0.5(2N*-1), is considered both before and after the data point; summing to a total interval of 2N* for each point. If the data point in question is the lowest point within the interval, the flow at that point is assumed to be baseflow. If the data point is not a local minimum, the program moves on the next data point. Once all data points have been considered, the program linearly interpolates between low-flows to estimate a continuous time series of baseflow as illustrated on Figure 5.6-C (Sloto & Crouse, 1996).

Based on the respective drainage areas of the Eramosa River (226 km^2, or 88 mi^2) and Whiteman's Creek (379 km^2, or 145 mi^2), calculated simulation intervals were 5 and 7 days, respectively. These intervals however were found to be too low as they produced high estimations of baseflow (i.e., reaching well into event hydrographs). Therefore additional simulations were run with an interval of 21 days chosen in an attempt to decrease baseflow profiles by increasing the low-flow period (Bellamy, 2004). Results are presented on Figure 5.7 and Figure 5.8 for the Eramosa River and Whiteman's Creek, respectively.

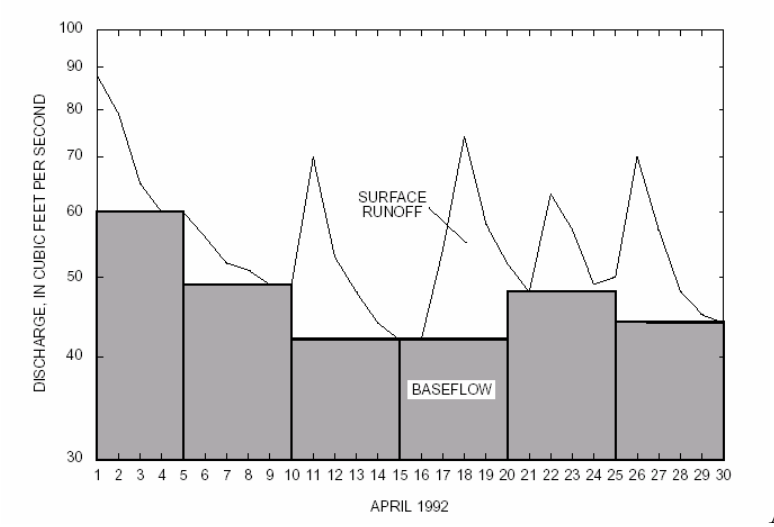

A.

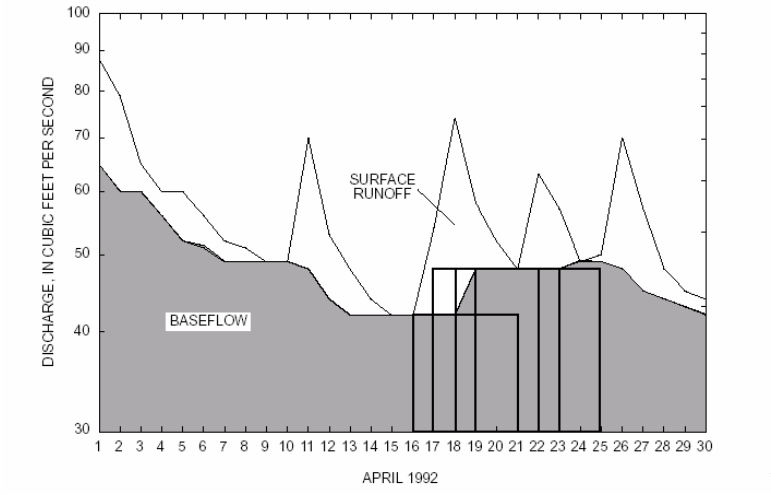

B.

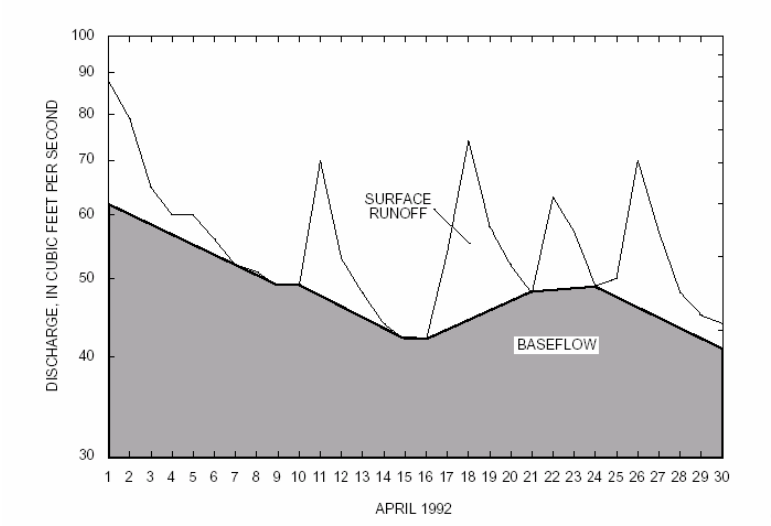

C.

Figure 5.6 – HYSEP model options A. fixed interval, B. sliding interval, and C. local minimum (Sloto & Crouse, 1996).

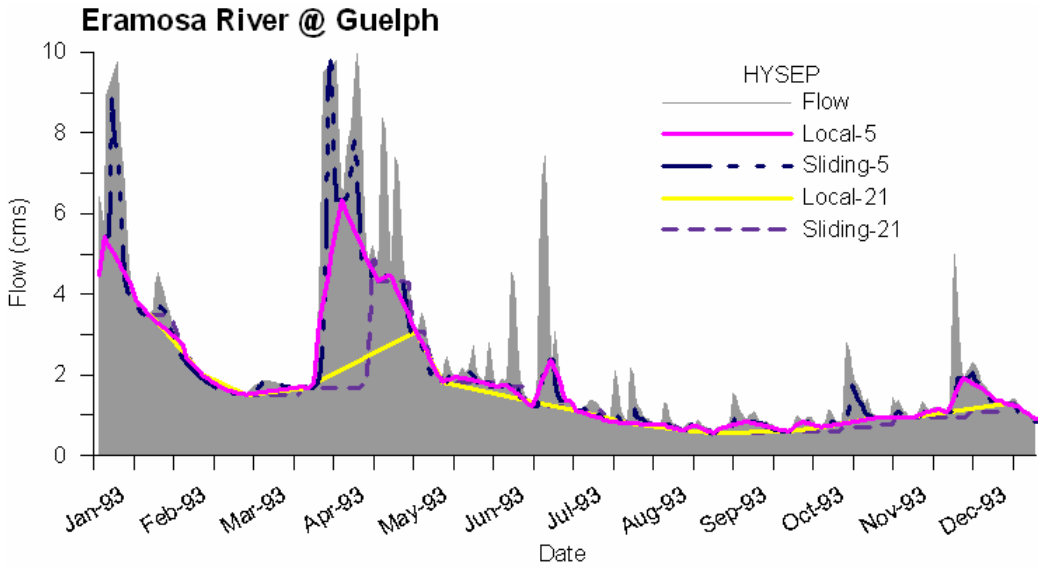

Figure 5.7 – HYSEP 1993 simulations for the Eramosa River.

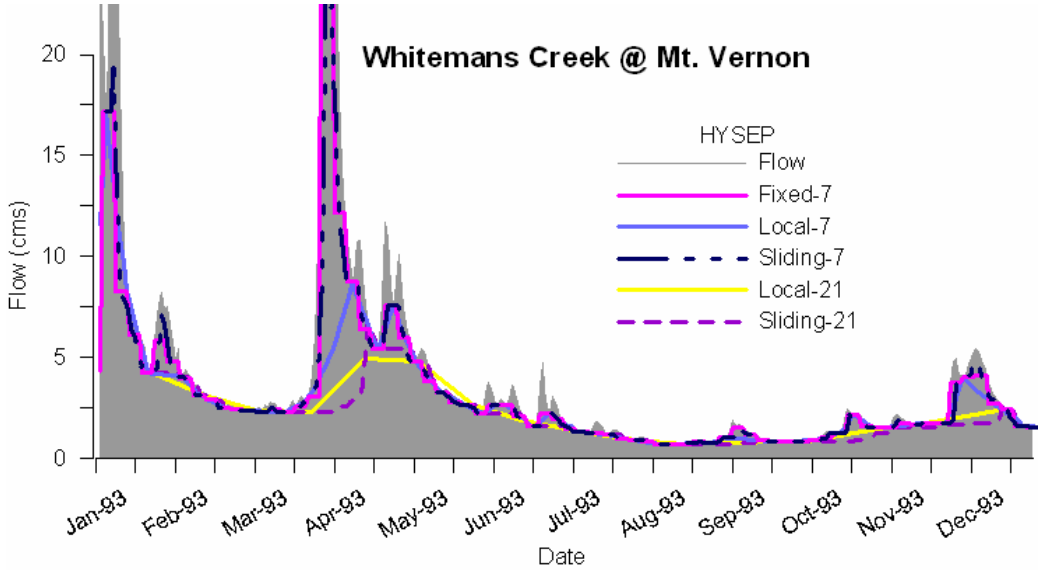

Figure 5.8 – HYSEP 1993 simulations for Whiteman's Creek.

The HYSEP simulations at the correct interval period correlating to drainage area were not physically realistic estimations of baseflow. At the higher interval (21 days) estimations of baseflow were lower and more reasonable; however, this was the result of increased averaging of the data by extending the interval to nearly one month (i.e., 21 days). Given the baseflow separation options used by the HYSEP model, using such a large interval period (i.e., in

exceedance of the recommended 11 day maximum interval) yields a monthly linear interpolation of baseflow. The most realistic estimate of baseflow from the HYSEP model was obtained the local 21-day minimum and sliding 21-day interval simulations.

5.3.4 Results & Implications

A direct comparison of WATFLOOD-simulated baseflow was made to the BFLOW model alone given that the BFLOW-3 results were found to be more physically realistic than HYSEP simulations. WATFLOOD baseflow is compared to BFLOW-3 simulations for Eramosa River and Whiteman's Creek during the 1993 study period, respectively (Figure 5.9 and Figure 5.10).

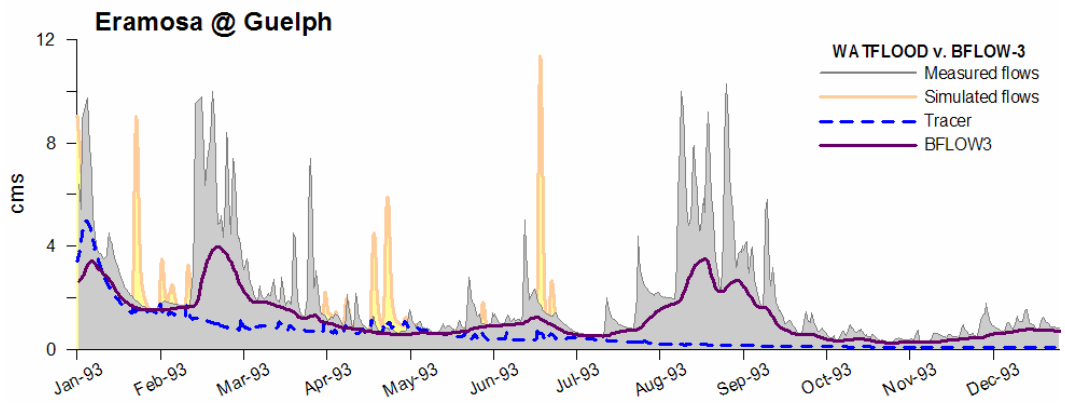

Figure 5.9 – WATFLOOD baseflow relative to simulated hourly streamflows, compared with the BFLOW-3 baseflow simulation relative to measured daily streamflows for the Eramosa River.

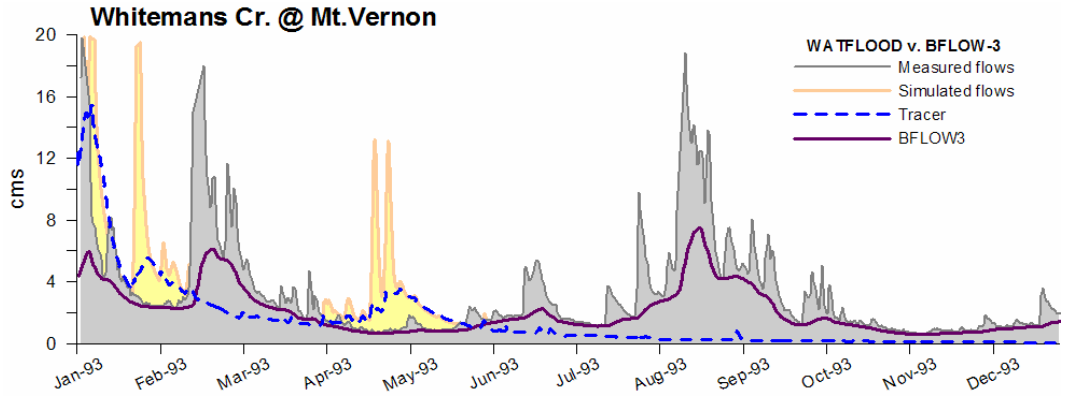

Figure 5.10 - WATFLOOD baseflow relative to simulated hourly streamflows, compared with the BFLOW-3 baseflow simulation relative to measured daily streamflows for Whiteman's Creek.

Figure 5.9 and Figure 5.10 also show WATFOOD-simulated flow relative to measured flow, indicating that there are discrepancies between measured (grey) and simulated flows (yellow). The lightly-shaded areas seen on the figures represent regions where WATFLOOD over-estimates total streamflow. Differences between simulated and measured streamflow create difficulties in directly comparing baseflow estimations from the two data sets: the BFLOW-3 model apportioned measured streamflow, but WATFLOOD baseflow is a proportion of the simulated flow. The result is that WATFLOOD-derived baseflow and BFLOW-3 simulated baseflow are often times in disagreement with each other because of errors in simulated flows (i.e., relative to measured flows). No conclusions can be drawn about which model is more physically representative of baseflow since each appears to generate a reasonable baseflow recession curve from its respective hydrograph.

In an attempt to resolve the dependence of the two baseflow simulations on different volumes of streamflow, each baseflow estimate was normalized by total streamflow (i.e., BFLOW-3 to measured streamflow, and WATFLOOD baseflow to simulated streamflow). Figure 5.11 presents baseflow proportionality plots for the Eramosa River and Whiteman's Creek simulations. If on average the models apportion the same baseflow then the slope of a linear regression through zero will be approximately one; as it is for Whiteman's Creek. In contrast, if WATFLOOD apportions less baseflow, then the slope of the linear regression will be less than one; as it is for Eramosa River.

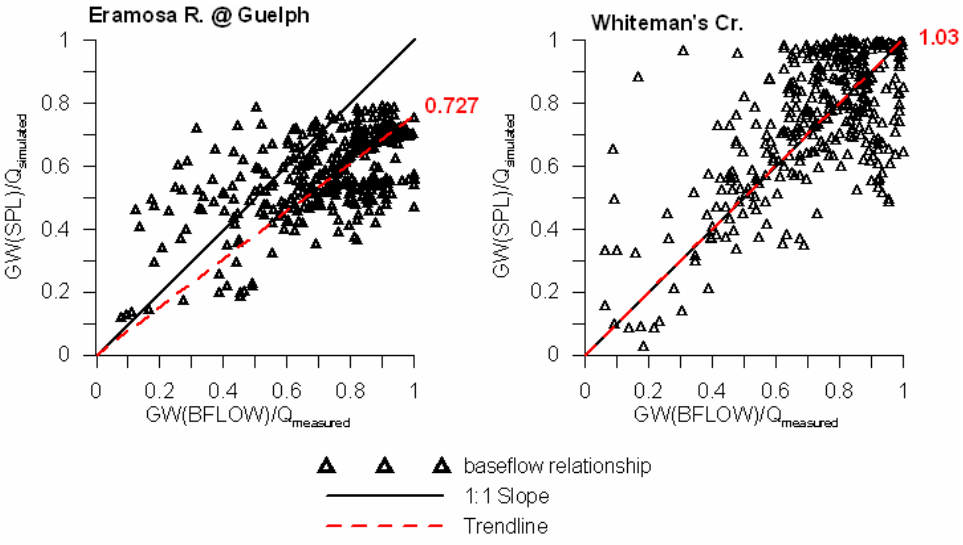

Figure 5.11 – Baseflow proportionality plots for Eramosa River and Whiteman's Creek comparing WATFLOOD baseflow to the BFLOW-3 simulated baseflow.

Figure 5.11 shows there are inter-basin differences in the relative performance of each model relating to the models' governing assumptions. In the Eramosa River WATFLOOD simulates less baseflow than BFLOW-3; for Whiteman's Creek, they model the same baseflow on average. Moreover the scatter on Figure 5.11 seems to indicate differences in baseflow estimation. The errors could be random in nature, or they could vary with hydrological condition (i.e., low versus high-flow periods).

To better understand the behaviour of each model under different conditions, and to eliminate inter-basin differences (i.e., landcover, runoff generation, etc.) histograms of baseflow fraction of total flow were generated and analysed for each basin (Figure 5.12 and Figure 5.13). The frequency of a particular fraction of baseflow is simulated and is compared between models to assess whether each model apportions baseflow similarly. The histograms implicitly distinguish between high-flow (i.e., low fraction of baseflow) and low-flow (i.e., high fraction of baseflow) periods based on fraction of baseflow.

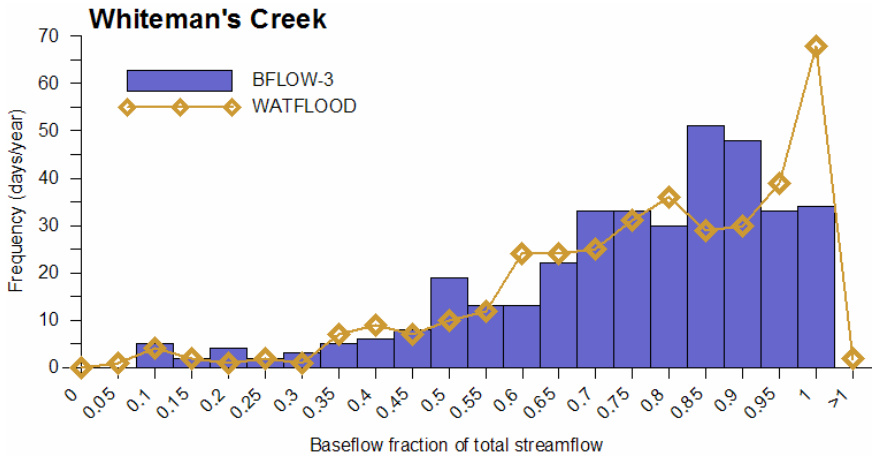

Figure 5.12 – Distribution of BFLOW-3 and WATFLOOD simulated baseflow for Whiteman's Creek.

Figure 5.12 indicates that BFLOW-3 and WATFLOOD produce very similar baseflow distributions during the 1993 study year. This is in agreement with the regression of baseflow proportionality for Whiteman's Creek (i.e., slope of 1.03; Figure 5.11). The models are comparable during high-flow periods (i.e., low baseflow fraction), but also exhibit similar trends and frequencies of simulation during low-flow periods (i.e., high baseflow fraction). This suggests that the two models apportion baseflow similarly during both high- and low-flow periods in Whiteman's Creek.

In complete contrast to the results from Whiteman's Creek, the distributions of baseflow for the Eramosa River are dissimilar (Figure 5.13). Although the models are in agreement during high runoff periods (i.e., low baseflow), they differ in their simulations of baseflow during average to low-flow conditions. WATFLOOD simulates a lower fraction of baseflow on average throughout 1993 than BFLOW-3, which is in agreement with the results of the regression (i.e., slope of 0.727; Figure 5.11). WATFLOOD baseflow simulations appear to indicate two common baseflow fractions ranging from 50-75%, compared with BFLOW-3 that exhibits one most frequent, higher baseflow fraction ranging from 85-95%.

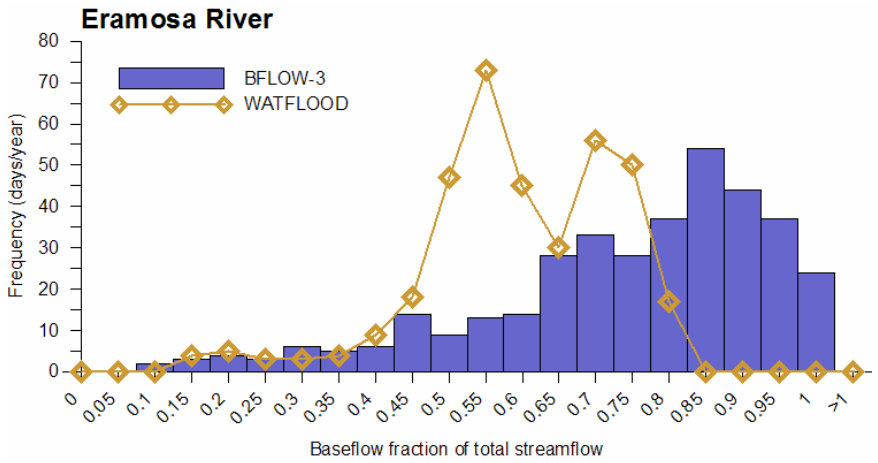

Figure 5.13 - Distribution of BFLOW-3 and WATFLOOD simulated baseflow for the Eramosa River.

The distributions of baseflow produced by the BFLOW-3 model appear similar in both basins (Figure 5.14), where as the distributions of baseflow generated by WATFLOOD show distinct inter-basin differences (Figure 5.15). On Figure 5.14 baseflows are apportioned exactly the same, *despite* known inter-basin differences in baseflow generation. WATFLOOD considers differences in characteristic basin hydrology through its internal parameterizations and accounts for differences in basin topography, resulting in the contrast shown on Figure 5.15.

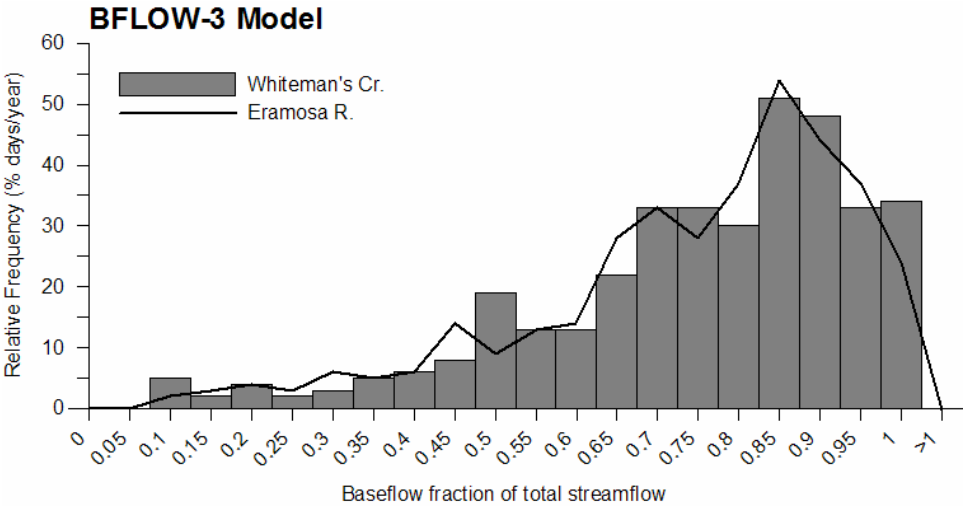

Figure 5.14 – Distribution of baseflow by the BFLOW-3 model.

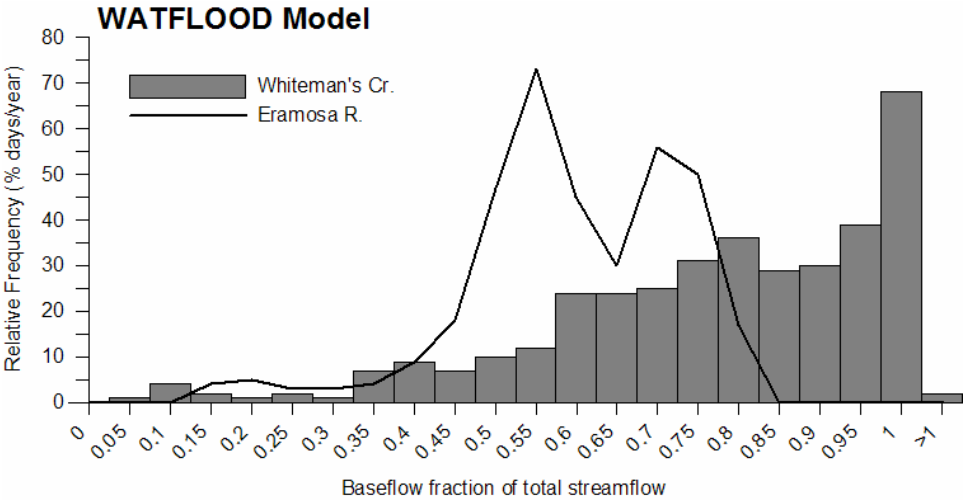

Figure 5.15 – Distribution of baseflow by the WATFLOOD model.

To assess which model most accurately interprets physical reality, it was necessary to determine if there were in fact significant differences in streamflow generation among the two basins. The distribution of measured flows was compared for Eramosa and Whiteman's Creek basins (Figure 5.16). In both basins between 93-97% of the streamflows were 10 cms or less for the 1993 study period. Since average to low-flow conditions are most common and not the extreme flow events (that indicated good model correlation on Figure 5.12 and Figure 5.13), flow distributions were generated for flows 10 cms or less, which did not distinguish extreme flow events greater than 10 cms. To remove the influence of drainage area on average runoff volume, all flows were normalized by drainage area of the basin.

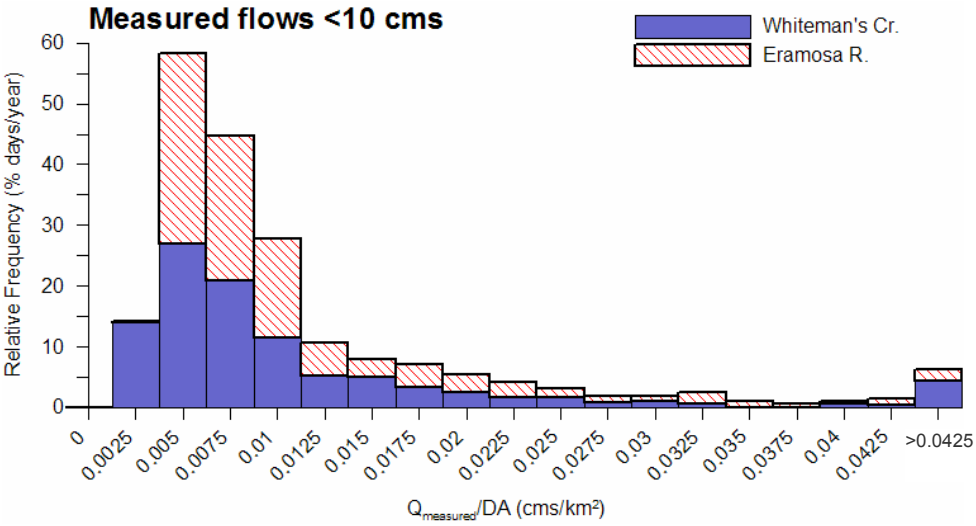

Figure 5.16 – Distribution of low-flow measured streamflows per unit area.

The lack of difference between measured flows in the Eramosa and Whiteman's Creek basins explains why the distribution of BFLOW-3 baseflow was the same: BFLOW-3 relies solely on streamflow to apportion baseflow. This does not however justify why WATFLOOD's baseflow simulations were different. In order to rule out a difference in simulated flows between the basins (i.e., geographical differences in meteorological forcing in the model), a distribution of simulated low-flows per unit area of basin was also generated (Figure 5.17).

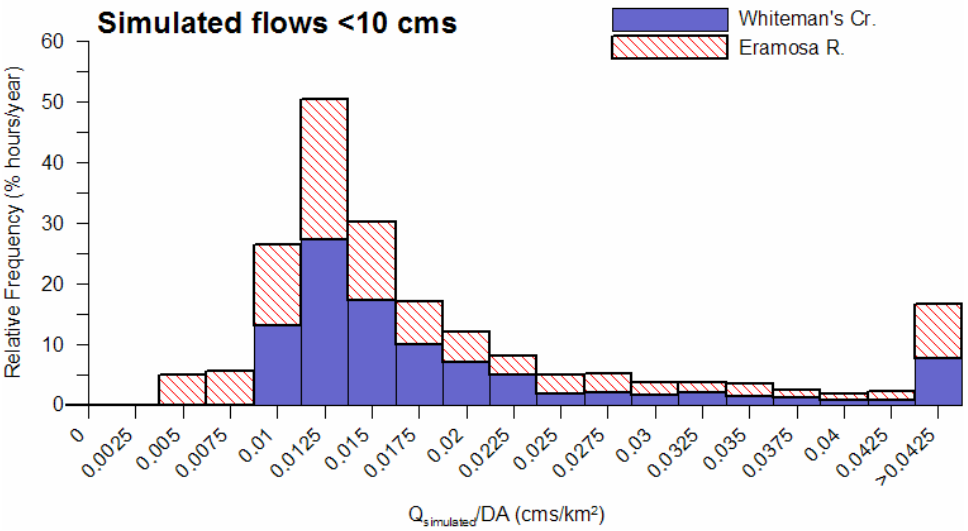

Figure 5.17 – Distribution of low-flow simulated streamflows per unit area.

Figure 5.17 shows that there are no significant differences in simulated streamflow to account for the inter-basin differences in baseflow estimation by WATFLOOD. With the difference in drainage area removed, it is the variability in the characteristic basin topography, landcover, and physiography that is driving the differences in baseflow distribution between the Eramosa River and Whiteman's Creek in WATFLOOD (shown on Figure 5.15).

It is found that variability in basin characteristics significantly influences baseflow generation in WATFLOOD, and that it should in fact be considered when simulating baseflow. BFLOW, HYSEP or any other offline baseflow generation model do not generate baseflow HSs that are as physically representative of basin characteristics from a hydrological model, which Eckhardt *et al.* (2008) also found in their analysis of the two baseflow indices. Longobardi and Villani (2008) recently worked to develop a baseflow separation algorithm that incorporated catchment physiographic features to capture true baseflow variation. Similarly, WATFLOOD incorporates remotely-sensed data to characterize topography, meteorological inputs, and landcover that help to define differences in internal hydrological responses. Although the WATFLOOD model is more physically representative than the BFLOW or HYSEP models in this sense, the uncertainty in its baseflow HS cannot be constrained due to a lack of measured data for comparison. Eckhardt *et al.* (2008), among many others, have recommended the use of tracer studies to verify baseflow contributions. Liu *et al.* (2008) successfully utilized stable isotope tracers to segregate and verify baseflow proportions of total streamflow.

5.4 WATFLOOD Baseflow Verification: Fort Simpson Basins, NWT

Integral to the scientific understanding of the water cycle and desegregation of flowpaths is the ability to accurately and precisely model the hydrologic cycle. As Section 5.3 has shown, the WATFLOOD model generates a representative baseflow component of streamflow in comparison with other commonly used techniques. The previous study however fell short of drawing conclusions about the predictive accuracy of the baseflow simulation. It has been recognized that the incorporation of 'soft' isotope data (i.e., comparison of simulated results to measured isotope data) into hydrological modelling studies can provide valuable insight on the inner workings of mesoscale watersheds, and a valuable tool for model verification (Vache &

McDonnell, 2006; Seibert & McDonnell, 2002; Kendall *et al.*, 2001; Soulsby *et al.*, 2000; Guntner *et al.*, 1999; Robson *et al.*, 1992).

The objective of the following study is to verify the accuracy of WATFLOOD baseflow discharge in the Fort Simpson Basins (FSB), Northwest Territories basin (~6,000 km^2) by comparing modelled hydrograph separations to isotopically partitioned streamflows. This section presents a comparison of baseflow contributions to streamflow derived using the WATFLOOD HS module with the results of conventional isotope hydrograph separation (St Amour *et al.*, 2005) for five wetland-dominated catchments along the lower Liard River. The comparison reveals highly promising agreement, verifying that the hydrological model is simulating baseflow contributions to total streamflow with reasonable fidelity, especially during the crucial snowmelt period. Sensitivity analyses of the WATFLOOD simulations reveals intriguing features about runoff generation from channelized fens, which has led to a modification of the model framework and has substantially improved subsequent simulations.

5.4.1 Methodology

A comparison of continuously-simulated WATFLOOD tracer-separated baseflow was made to point estimations of baseflow derived from measured $\delta^{18}O$ and $\delta^{2}H$ isotopic data for the FSB (St Amour *et al.*, 2005). WATFLOOD baseflow was simulated continuously in each of the five FSB from April to August 1997, 1998, and 1999, and was plotted and assessed based on its accuracy in replicating the 'measured' baseflow, as inferred by an isotope mixing model. The result of incorporating isotope data into the hydrological model was consistent with other hydrological studies in highlighting the importance of understanding the function of channelized fens in controlling the runoff response in this sub-arctic hydrological regime (Western *et al.*, 2001). Therefore, a modification of the WATFLOOD model to incorporate a percentage of connected-wetlandcoverage (i.e., channelized fen) was performed. The connected-wetland land classification was designed to account for low-relief, low-hydraulic gradient wetlands not directly and immediately interacting with streamflow.

Both streamflow and baseflow hydrographs were calibrated using 1997 measured streamflow and isotopic data. Quality and accuracy of the modelled results were assessed using goodness-of-fit statistics and proportionality plots (Section 4.7).

During calibration, it was found that the three parameters controlling wetland conductivity, porosity, and size were quite sensitive and significantly affected hydrograph attenuation and recession. Baseflow calibration occurred mostly by calibration of the lower zone function (lzf) and power function (pwr) controlling the flux of baseflow into the channel (qlz). Additionally, the rate of drainage from the UZS to the LZS was adjusted to account for much slower snow-covered drainages due to permafrost conditions.

Following calibration, the model was validated during the 1998 and 1999 April to August events. For validation simulations, no parameters were adjusted, and the WATFLOOD model was assessed on its ability to replicated 1998 and 1999 isotopically-inferred baseflows. It should be noted that the region experienced an abnormally warm and wet spring in 1998 in response to changes in atmospheric circulation during pronounced El Niño conditions, resulting in the early onset of the spring freshet by approximately one to two weeks.

5.4.2 Isotope Mixing Model

Groundwater has a relatively constant isotopic signature over time, reflecting the long-term precipitation average due to recharge and minimal evaporative influence (IAEA, 1981). Throughout the cold season in northern basins, streamflow isotopic composition is usually dominated by groundwater. During the spring, snowmelt mixes with groundwater-dominated streamflows, resulting in a depleted isotopic signal. As the freshet period ends, summer streamflows become isotopically-enriched due to higher rates of evaporation, and the resulting isotopic signal within the stream is also enriched. Variations in the isotopic composition of streamflow are therefore controlled by the balance between snowmelt and groundwater during the spring freshet period and by the balance between surface water and groundwater during late fall and winter. In northern environments, stable isotopes of oxygen and hydrogen in streamflow are seasonally influenced by the mixing of three inputs that are commonly

isotopically distinct; primarily snowmelt, surface water and groundwater. This allows for basin streamflow to be separated into its constituent components using a two-fold application of the classical two-component mixing model (Laudon *et al.*, 2002; Laudon *et al.*, 2004; St Amour *et al.*, 2005; Unnikrishna *et al.*, 2002).

The mixing ratio between source water components in streamflow can be determined using isotope mass and water balance calculations. Assuming instantaneous and complete mixing of all components in streamflow, total streamflow Q during the freshet period is the sum of direct snowmelt (D), baseflow (R) composed of a mixture of groundwater and surface water ($R=R_{SW}+R_{GW}$), and direct channel precipitation (P):

$$Q = D + R + P \qquad (5.19)$$

The simultaneous isotopic mass balance corresponding with the above water balance is:

$$\delta_Q Q = \delta_D D + \delta_R R + \delta_P P \qquad (5.20)$$

where, δ values refer to a change in isotopic composition of the component to streamflow with respect to the standard (VSMOW).

For long time sequences and smaller basins, the contribution to streamflow by direct precipitation can be assumed negligible as most precipitation recharges groundwater or becomes surface runoff. For the five Fort Simpson basins, this assumption can be considered reasonable given that the semi-permafrost, wetland-dominated regime would capture and feed precipitation to the channel network. The above equations can therefore be simplified to:

$$Q = D + R \qquad (5.21)$$

$$\delta_Q Q = \delta_D D + \delta_R R \qquad (5.22)$$

And specifically during the warm, post-freshet dry periods, the absence of snowmelt (D) further simplifies the above equations such that streamflow would be composed of baseflow.

The separation of total streamflow (Q) in the spring freshet period assumes total streamflow is comprised as a fraction of new, event based snowmelt (D) and old baseflow (R):

$$1 = \frac{D}{Q} + \frac{R}{Q} \qquad (5.23)$$

with isotopic contributions of snowmelt and baseflow during freshet recession derived by substituting Equation 5.22 into 5.21:

$$\frac{D}{Q} \approx \frac{\delta_Q - \delta_R}{\delta_D - \delta_R} \tag{5.24}$$

$$\frac{R}{Q} \approx \frac{\delta_Q - \delta_D}{\delta_R - \delta_D} \approx 1 - \frac{D}{Q} \tag{5.25}$$

The above equations represent the proportions of new and old water during the freshet period, respectively. During the spring freshet, the isotopic composition of streamflow would initially be characterized by the composition of snowmelt δ_D, and would gradually approach summer baseflow δ_R as the open-water part of the seasonal cycle progresses. During ice-free summer and fall periods, the isotopic composition of baseflow (δ_R) gradually enriches through the infiltration of evaporatively enriched water (i.e., $\delta_R \rightarrow \delta_{SW}$). During ice-on, low-flow periods, baseflow isotopic composition (δ_R) will approach the isotopic composition of groundwater (δ_{GW}) as surface water contributions, and evaporation wane (i.e., $\delta_R \rightarrow \delta_{GW}$). Therefore winter streamflow (i.e., when streams are ice-covered) is expected to have an isotopic composition close to that of groundwater.

Therefore, a second streamflow separation partitions the contributions of surface water inflow (R_{SW}) and old groundwater (R_{GW}) to baseflow (R):

$$R = R_{GW} + R_{SW} \tag{5.26}$$

$$\delta_R R = \delta_{GW} R_{GW} + \delta_{SW} R_{SW} \tag{5.27}$$

From the baseflow component separation during post-freshet periods (i.e., summer and fall), the isotopic compositions of the surface water (δ_{SW}) and groundwater (δ_{GW}) can be derived by substituting Equation 5.26 into 5.27:

$$\frac{R_{SW}}{R} = \frac{\delta_R - \delta_{GW}}{\delta_{SW} - \delta_{GW}} \tag{5.28}$$

$$\frac{R_{GW}}{R} = \frac{\delta_R - \delta_{SW}}{\delta_{GW} - \delta_{SW}} \approx 1 - \frac{R_{SW}}{R} \tag{5.29}$$

δ_{SW} is a combined isotopic composition of both surface water (lakes and wetlands) and rain given that the composition of these components are too close to differentiate. The isotopic

composition of groundwater (δ_{GW}) is representative of winter, low-flow periods where streamflow is being maintained by non-surface or soilwater fluxes. Figure 5.18 illustrates the isotopic partitioning of streamflow using the two-component mixing model approach (St Amour *et al.*, 2005).

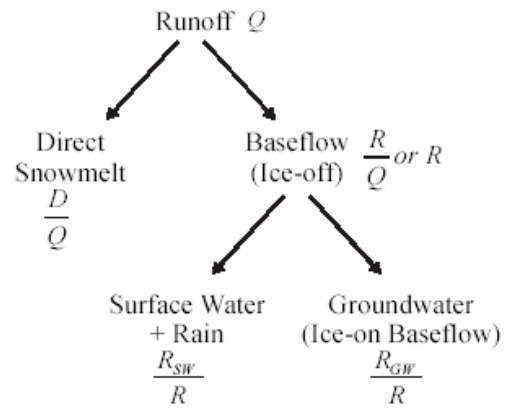

Figure 5.18 - Schematic representation of isotopic streamflow partitioning (St Amour et al., 2005).

It is the groundwater component of baseflow (R_{GW}) that is analogous to the WATFLOOD baseflow component. The isotope mixing model was applied by Natalie St. Amour, a Ph.D. student in Earth Sciences at the University of Waterloo, who was a co-collaborator for this study. Measured flows and isotopic compositions of streamflows were separated via the mixing model into old and new water contributions and compositions. 'Old' water or baseflow was then further separated to derive the groundwater portion of the total streamflow hydrograph for comparison to WATFLOOD-generated baseflow. Isotopically-inferred baseflow represents single point-in-time estimates as determined from measurements of $\delta^{18}O$ and $\delta^{2}H$ in streamflow, where slight differences exist between the baseflow estimation from each isotope.

5.4.3 WATFLOOD Modelling

The WATFLOOD hydrological model was run using the wetland hydrology option. During this study, it was discovered that use of percent wetlandcover as ascertained from LandSat imagery resulted in an over-estimation of wetlandcoverage. This finding has been supported by knowledge of the study site, landcover surveys and recent remote sensing studies in the FSB (Pietroniro & Prowse, 2002; Quinton *et al.*, 2003). It has substantiated that although extensive wetlandcoverage is apparent throughout the five catchments, not all of wetlands are hydraulically

connected to the channel via a direct flowpath. This was observed in simulated hydrographs and was corroborated by field site investigations showing that many of the wetlands nested in low-relief topography have no apparent connection to a channel (Hamlin, 1996; Quinton *et al.*, 2003). The treatment of wetlands in the WATFLOOD model was therefore altered to incorporate an additional landcover classification, "connected wetlands" representing channelized fens (Quinton *et al.*, 2003). This new land classification is a parameterized fraction of the existing wetland class, determined by model calibration. Results from this calibration indicated that approximately 25 percent of the FSB wetlands are hydraulically connected to a channel (i.e., channelized fens). This is inconsistent with reports that channel fens were shown to occupy about two-thirds of the overall wetland classes (Quinton *et al.*, 2003). Clearly, more information on the classification and understanding of the extent and function of these fens is required.

With the assumed 25 percent wetland hydraulic connectivity, streamflow simulations with baseflow separations for the five catchments from April to August 1997, 1998 and 1999 were completed. Results are presented on Figure 5.19, Figure 5.20 and Figure 5.21, comparing simulated streamflow (dashed red line) to measured flows (black line) and WATFLOOD baseflow (long dash blue line) to isotopically-derived point estimates of baseflow (symbols). Statistical results for these simulations are presented in Table 5.1, indicating baseflow proportionality slopes (from regression), Nash-Sutcliffe coefficients, and the deviation of runoff volumes. Groundwater proportionality plots for the 1997, 1998 and 1999 study periods have been provided in Appendix C: Figures C.1, C.2 and C.3, respectively.

It is important to note that coarse resolution of meteorological input data (i.e., the single point rain gauge at Fort Simpson airport) had a significant effect on the quality of the streamflow simulations for the FSB. Namely there were several significant summer rainfall events not recorded by the rain gauge during each simulation period. This is most notable in June of 1997: a significant rainfall event was observed by the rise in measured streamflow hydrographs in four of the five basins, but was not detected by the rain gauge and therefore did not result in a simulated event hydrograph. During these missed event periods, significant error in baseflow estimation is also observed since simulated flows become baseflow-dominated with the absence of event hydrographs. This phenomenon can be observed during the summer months of the three study years due to unrecorded precipitation events missed by the rain gauge.

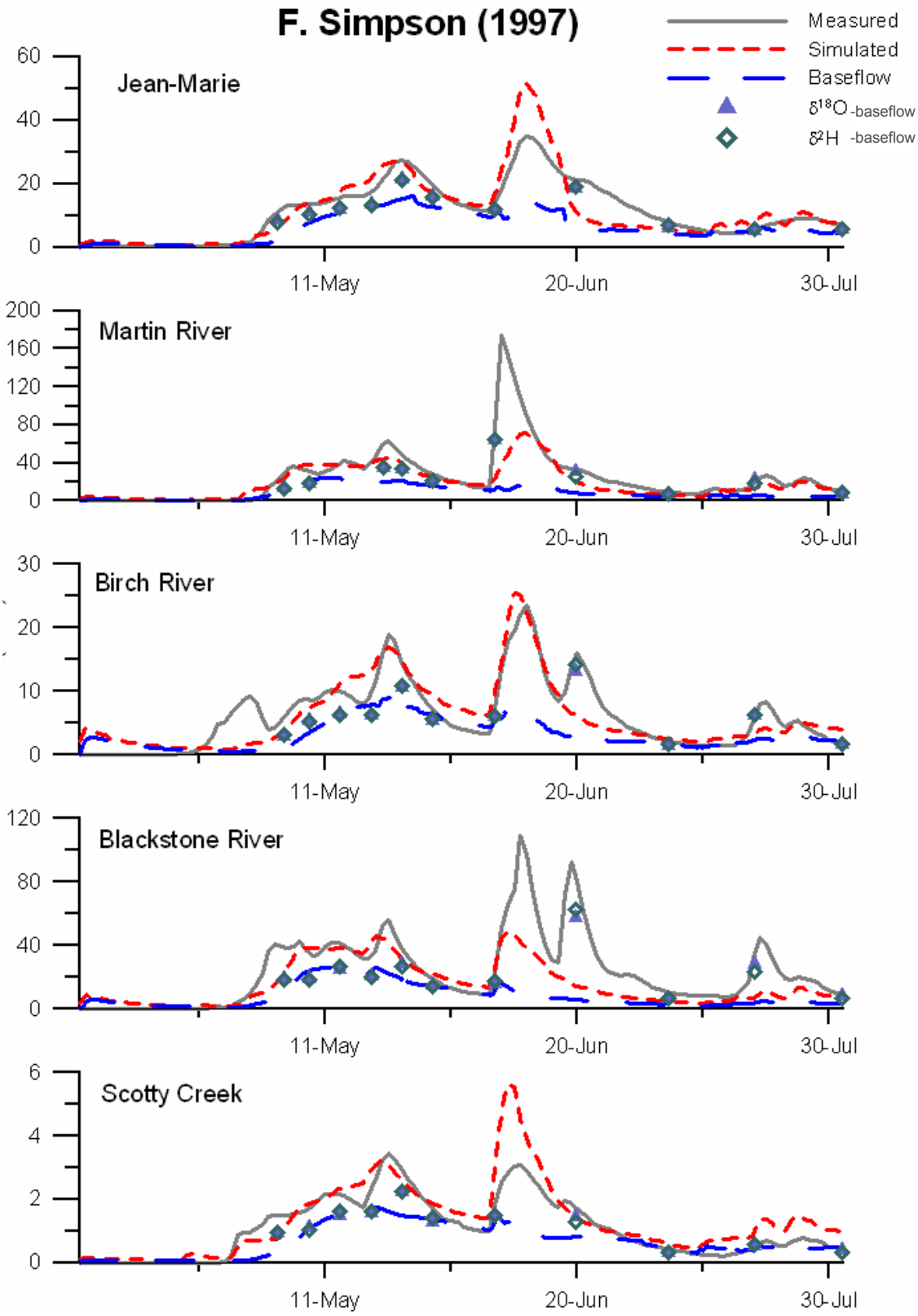

Figure 5.19 – Fort Simpson baseflow hydrograph separations for the 1997 calibration period.

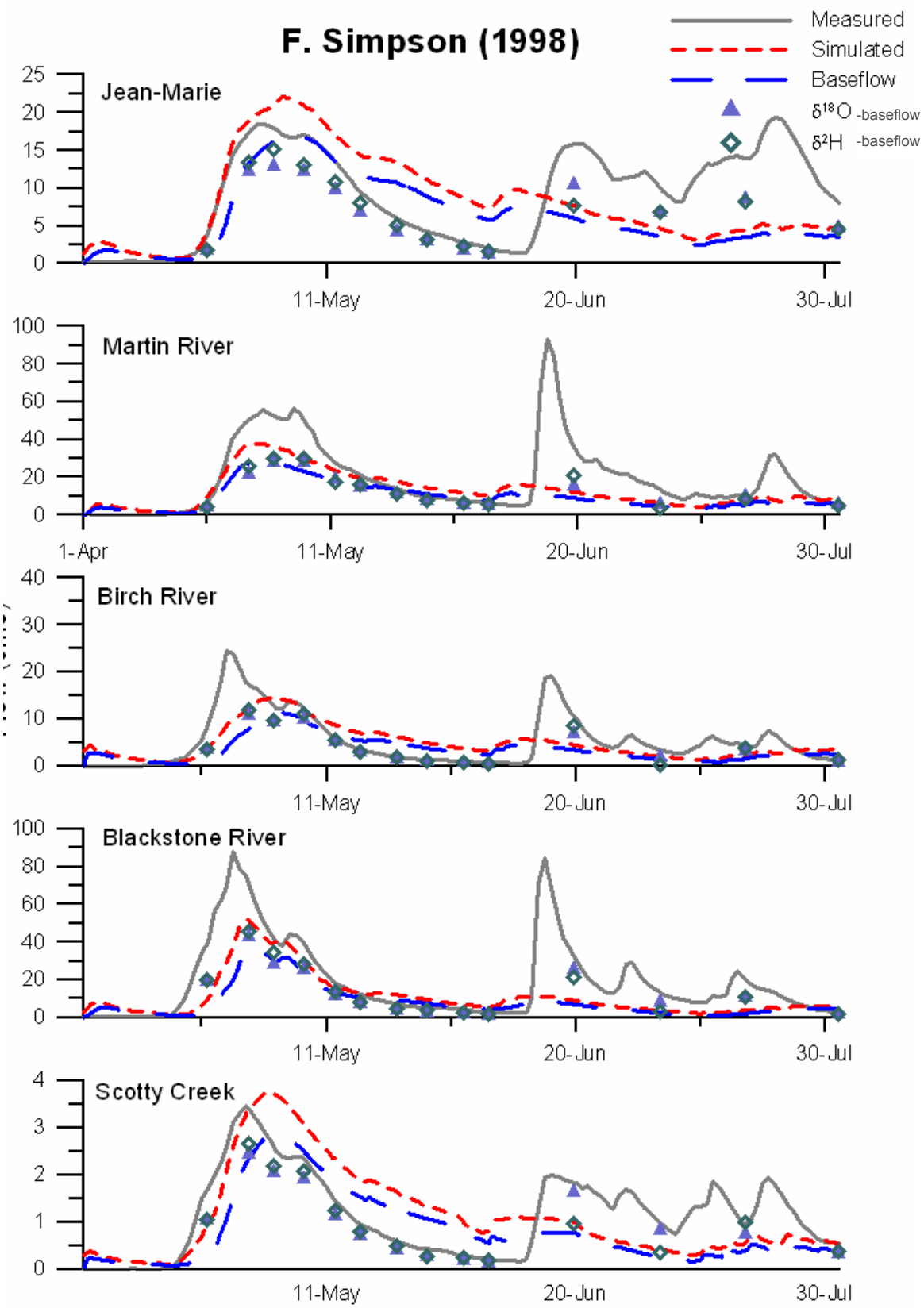

Figure 5.20 – Fort Simpson baseflow hydrograph separations for the 1998 event period.

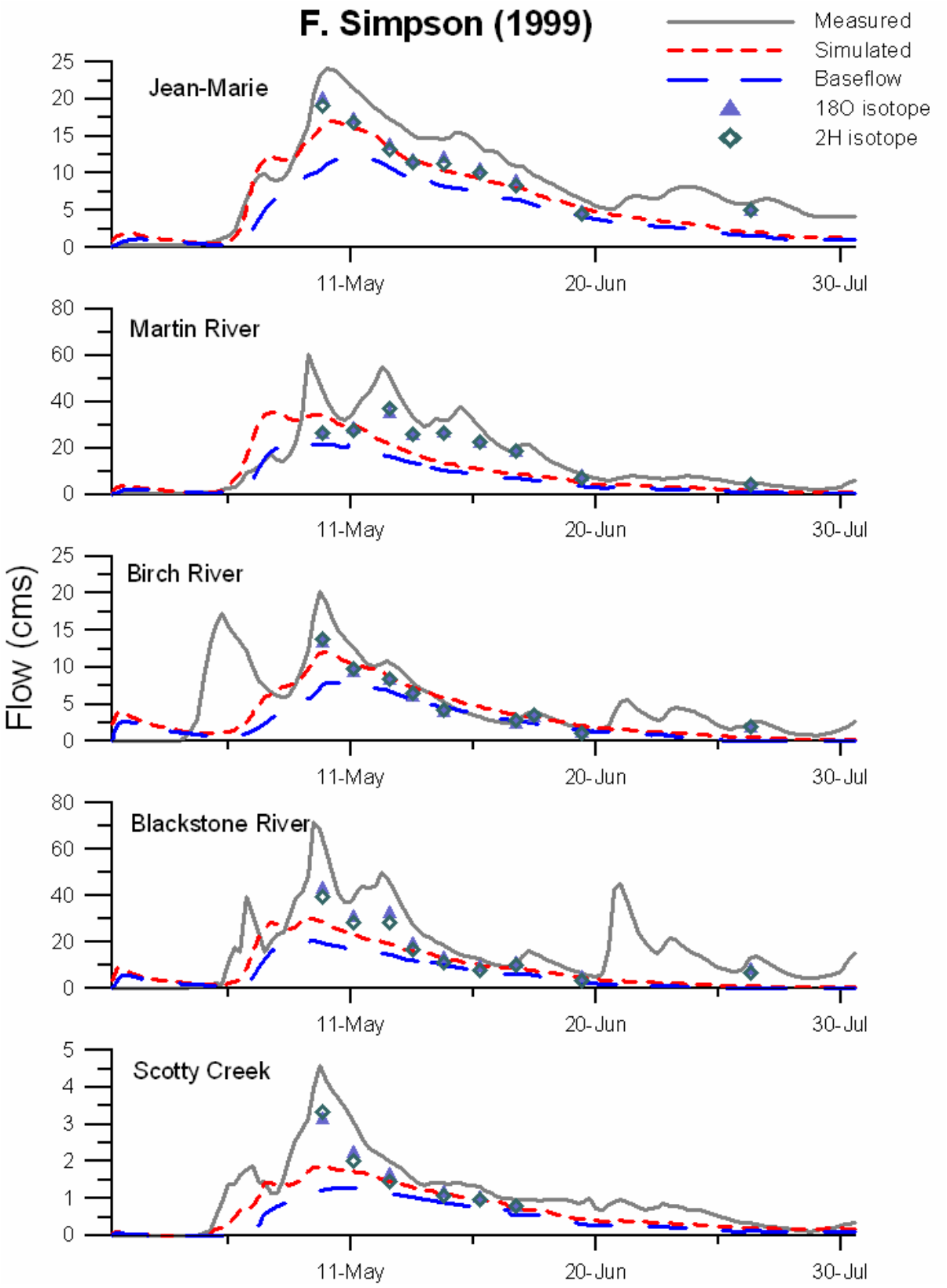

Figure 5.21 - Fort Simpson baseflow hydrograph separations for the 1999 event period.

Table 5.1 – Statistical summary of WATFLOOD simulation, including baseflow proportionality to isotopically-derived baseflow.

Year	Basin	Slope of proportionality plot	Nash	%Dv
1997	Jean-Marie	0.735	0.723	2.62
	Martin	0.653	0.569	-21.15
	Birch	0.739	0.702	-1.167
	Blackstone	0.798	0.387	-33.46
	Scotty	0.735	0.624	24.33
	Average	**0.73**	**0.60**	**-5.77**
1998	Jean-Marie	1.022	-0.074	-8.079
	Martin	0.982	0.32	-32.26
	Birch	0.935	0.389	-9.865
	Blackstone	1.157	0.339	-40.47
	Scotty	0.981	0.213	0.473
	Average	**1.02**	**0.24**	**-18.0**
1999	Jean-Marie	0.990	0.698	-28.79
	Martin	0.905	0.470	-33.06
	Birch	0.883	0.338	-29.92
	Blackstone	0.958	0.204	-50.05
	Scotty	1.010	0.549	-38.44
	Average	**0.95**	**0.45**	**-36.1**
Desired Outcome		1	1	0

5.4.4 Results & Implications

By visual inspection, the 1997 hydrographs (Figure 5.19) show reasonable fit of simulated to measured flows in each of the five catchments based on their hydrologic response to events (rising and falling of the hydrograph) and timing. In all catchments, WATFLOOD appears to over-estimate streamflow during the early freshet period, most notably for the Birch and Blackstone Rivers (wetland dominated catchments). Scotty Creek, Jean Marie and Martin river catchments all exhibited similar behaviour during calibration, indicating they have similar hydrologic responses. The Birch and Blackstone Rivers however indicated different hydrologic responses from the other catchments, most likely attributed to the responsive wetland hydrology dominating these catchments. Overall the 1997 freshet was well simulated exhibiting the representative runoff volume, timing, and recession trend of the snowmelt hydrographs. Post-freshet, simulated flows were less representative of measured flows overall due to the missed early June rainfall event. The Nash-Sutcliffe coefficient for the simulation varied from a worst-

fit simulation of 0.38 for Blackstone River to the best fit on Jean-Marie River at 0.72. The accuracy of fit for the catchments was also captured by the D_v, varying from 33% under-estimation of runoff volume for Blackstone River, to only a 2% deviation for Jean-Marie River. Baseflow proportionality plots (Figure C.1) indicate an overall under-estimation of baseflow by WATFLOOD in 1997 relative to isotopically-separated baseflow; varying from a slope of 0.65 (Martin River) to 0.8 (Blackstone River). It is interesting to note that despite difficulties simulating total streamflow in the Blackstone River catchment, baseflow was still well apportioned.

The 1998 validation simulation resulted in hydrographs (Figure 5.20) that exhibited a substantially worse fit of simulated to observed streamflow even by first inspection, noticeably during the snowmelt (freshet) period. In all catchments, WATFLOOD simulations prolonged the duration of the melt period, leading to high-volume, prolonged snowmelt hydrographs. This result is attributed to the onset of the 1998 El Niño event, which led to warmer and wetter conditions occurring earlier in the spring than normal, increasing the rate of snowpack depletion in comparison to the typical, calibrated melt conditions. Given that the same calibrated parameter set was used for all years, and that the simulations do not incorporate radiation data, the model could not accurately forecast the earlier and more rapid freshet. Previous work has shown that the addition of radiation data to the WATFLOOD model can largely correct these discrepancies; however radiation data were not available for this study. Resulting from the poorly modelled freshet period, Nash-Sutcliffe coefficients were generally low (indicating poor fit), varying from -0.07 (Jean-Marie River) to 0.38 (Blackstone River). The deviation of runoff volumes varies from 40% under-estimation of (Blackstone River), to a negligible over-estimation (0.5%) in Scotty Creek. Baseflow proportionality plots (Figure C.2) indicate that baseflow was over-estimated by WATFLOOD on the Blackstone River, with a slope of 1.16, whereas baseflow was most correctly apportioned on the Jean-Marie River (slope of 1.022); all other catchments under-estimated baseflow contributions to streamflow. The 1998 results illustrate that the Blackstone and Birch Rivers appear to model the El Niño freshet period more accurately than the other catchments (supported by their higher R^2 values), perhaps attributable to their wetland-dominated coverage, which would make streamflow hydrographs less responsive to early, flashier snowmelt events. Higher percentages of wetlandcoverage naturally dampen peak hydrographs and prolong recession curves. Some of the catchments, like Scotty

Creek, exhibit poor fit of simulated streamflow but overall, resulted in a good water balance. This is likely more because of the opportune cancellation of errors where the prolonged recession curve volume appears to have closely estimated the volume of the missed rain event.

By initial inspection, 1999 hydrograph simulations (Figure 5.21) exhibited improved fit over the 1998 simulations in each of the five catchments. The results correlate more closely with 1997 simulations, supporting evidence that the erroneous streamflow simulations in 1998 are in some way attributable to the El Niño event. In 1999 the freshet period once again occurred during the typical late spring season and occurred at a slower rate than in 1998. However some earlier, small precipitation events (likely a carryover of moisture from the El Niño event) occur in 1999 during the spring freshet and were once again missed by the rain gauge. These missed events, just as they did in the summer of 1997, lead to poorer fits (low R^2) of simulated to observed flows and an overall under-estimation of runoff volumes (negative D_v's). Nash-Sutcliffe coefficients varied from 0.2 for the Blackstone River to 0.55 for Scotty Creek. The D_v was consistently under-estimated due to the missed rain events, varying from 50% on the Blackstone River to –28% on the Jean-Marie River. Baseflow proportionality (Figure C.3) indicated, once again, a general under-estimation of baseflow contribution by WATFLOOD relative to isotopically-separated baseflow contributions. The Birch River simulation under-estimates groundwater contribution the most, with a proportionality slope of 0.88. Jean-Marie River and Scotty Creek correctly apportion groundwater with slopes of 0.99 and 1.01, respectively. The 1999 results again point to problems with the Blackstone River simulations, perhaps resulting from poorly estimated wetland connectivity (fen channelization).

Overall WATFLOOD baseflow was found to be reasonably representative of isotopically-derived baseflow separations despite some obvious discrepancies between simulated and measured flows (particularly missed summer events). The WATFLOOD model's estimation of baseflow was found to be physically representative of 'measured' baseflow hydrographs. Baseflow proportionality was generally less than one, indicating under-estimation relative to isotopically-separated baseflow; but in general, slopes were sufficiently close to one. An apparent trend from both the WATFLOOD and isotopic separations was that all five catchments are strongly baseflow-dominated, with groundwater contributions being in upwards of 60 to 95% of total streamflow. It is noted that the proportionality plots all indicate one or

two measurements where modelled groundwater from WATFLOOD is significantly lower than isotopically-separated groundwater. These points occurred in all catchments and correlate to the beginning of the freshet period on the rising limb of the melt hydrograph. These anomalous points can, at least in part, be explained by the numerical smoothing that results from the averaging of modelled hourly baseflow to obtain daily flows that correlate with the daily average isotope estimates. This smoothing results in a more gradual gradient on the rising limb of the hydrograph, resulting in a slower baseflow response to the freshet.

5.5 Chapter Summary

The addition of tracers into the WATFLOOD model has shown that it is possible to improve the understanding of the processes leading to streamflow generation through a combination of experiments, observations and models. HS has been recognized as a necessity in interpreting the physical reliability of model simulations (Beven, 2006), but is a tool that has been largely restricted to hillslope-scale studies. Stable water isotopes offer a practical validation of WATFLOOD's internal model dynamic and baseflow computations. Despite WATFLOOD's more conceptual approach to baseflow computation relative to full physically-based groundwater models, the model's estimation of baseflow contribution to streamflow verified against two other commonly utilized and accepted baseflow models, and by isotopically-separated baseflow contributions.

In the first study WATFLOOD-derived baseflow was compared to baseflow estimates from two other commonly used baseflow separation models. External baseflow separation models utilizing streamflow discharge alone do not physically represent geographical and physiographical differences in mesoscale watersheds. The two study basins in the GRB exhibited distinct differences in their landcover and wetland hydrological behaviours, producing distinct baseflow hydrograph responses using the WATFLOOD model. This sub-basin variability was not captured by the other baseflow separation models. The second study highlighted the application of water isotopes for mesoscale hydrological model calibration and verification of internal flowpaths.

Several published studies have sought to quantify runoff and baseflow components contributing to streamflow utilizing comprehensive field studies that used measured isotope soft data for comparison to modelled component (Vache & McDonnell, 2006; Brassard *et al.*, 2000; Wittenberg & Sivapalan, 1999). These methods, although accurate and informative, are not feasible for regional-scale watershed studies where flowpath verification is required to assist in defining large-scale conceptualizations of hydrological processes. The studies in this chapter however fell short of constraining modelled surface water and soilwater components. To fully verify and reduce uncertainty in a hydrological model, each flowpath should be validated against some form of 'measured' data. Section 5.4.2 pointed out that the components contributing to surface water and soilwater are difficult to distinguish isotopically and therefore the application of mixing models and measurement of field data are limited for these components. Internal flowpaths could instead be verified by constraining isotope inputs and streamflow compositions (i.e., output composition) and by continuously simulating mass mixing and transfer through each internal compartment in between using a series of physically-based equations. Reducing a model's degrees of freedom by constraining internal flowpaths to measured isotopic compositions of streamflow enables an analysis of the models conceptualization of flow processes during simulation. As with all modelling exercises, there will remain uncertainty in the outcome, but the incorporation of isotopes into hydrological models can help to constrain some of these uncertainties. The next chapter presents a description of the isoWATFLOOD isotopically-enabled hydrological model.

Chapter 6

The isoWATFLOOD Model

As with any tool there are limitations involving data availability, field investigations, mesoscale applicability, and costs associated with field work and analyses. For more than a decade there has been significant interest from the scientific community in developing isotope-enabled models capable of not replacing, but supplementing isotopic records in both paleo- and modern climatological and hydrological research (Turner & Barnes, 1998). The goal of such modelling projects has been to overcome observational deficits in isotope data. Several international initiatives currently share the objective of modelling stable water isotopes on large-scales. The Stable Water Isotope Intercomparison Group (SWING; Schott, 2005) provides a framework to compare isotope-enabled global circulation models (GCM) with observational data for the purposes of improving modelled simulations. Interests lie in the prediction and simulation of stable water isotope evolution through the meteorological cycle for the purposes of better understanding moisture and vapour cycling.

The Isotopes in Projects for Intercomparison of Land-surface Parameterization Schemes (iPILPS; Henderson-Sellers, 2006) is another project that was born from the longest running model intercomparison project that founded SWING. With stable water isotopes now being simulated in atmospheric moisture, the iPILPS project tests the ability of land surface schemes (LSS) to utilize varying atmospheric isotope inputs to simulate land surface responses to atmospheric variations. The objectives of iPILPS are to develop a suite of models capable of reproducing isotopic components of water and mass budgets on the land surface without adding

great complexity to the LSS's, and to improve the understanding of atmosphere/land-surface interactions.

Recently the British Columbia provincial government in Canada invested $94.5 million is developing the Pacific Institute for Climate Solutions (PICS) at the University of Victoria (Ommer, 2008). PICS's mandate is to bring together top researchers from across the world to develop innovative climate change solutions, and to disseminate new research and innovation directly to senior decision-makers within government and industry. Given the focus on climate change, proposals are being drafted that envision stable water isotopes as one of the foremost tools in assessing changes in modern-day climates and how those changes impact the hydrological cycle (Edwards, 2008). There is an emerging appeal for efficient, physically-based mesoscale hydrological simulation capabilities; and moreover, isotope-enabled hydrological models to assist in coupled hydrologic and isotopic mesoscale studies.

The development of the isoWATFLOOD model provides a means of internally verifying streamflow components *a priori* and offers the ability to continuously simulate hydrologic isotopic variation. The following chapter will describe the framework of isoWATFLOOD, and how it can be used to track $\delta^{18}O$ through the hydrologic cycle and within hydrologic compartments. Oxygen-18 was preferentially selected for this modelling study because its behaviour in the water cycle compared with hydrogen is better understood, especially fractionation during evaporation. The design of each of the model's modules will be discussed and reinforced with literature supporting the decisions and assumptions made within the modelling framework. Following this qualitative description of the model structure, the model is tested using four diagnostic tests developed to study the characteristic behaviour of the model (Chapter 7).

6.1 Overview of isoWATFLOOD

The isoWATFLOOD model externally couples an independent isotope simulation ($\delta^{18}O$) module to the WATFLOOD hydrological modelling system. This design allows the isotope module to be adapted for use in any hydrological modelling system, so long as the model has a

complete representation of the hydrologic cycle (i.e., surface water, soilwater and groundwater storages). isoWATFLOOD is controlled by a main module (isotope.f) that calls a series of subroutines to compute the mass of ^{18}O in hydrologic storage, transfering it between compartments. A schematic of the isoWATFLOOD subroutines in order of computation is presented on Figure 6.1.

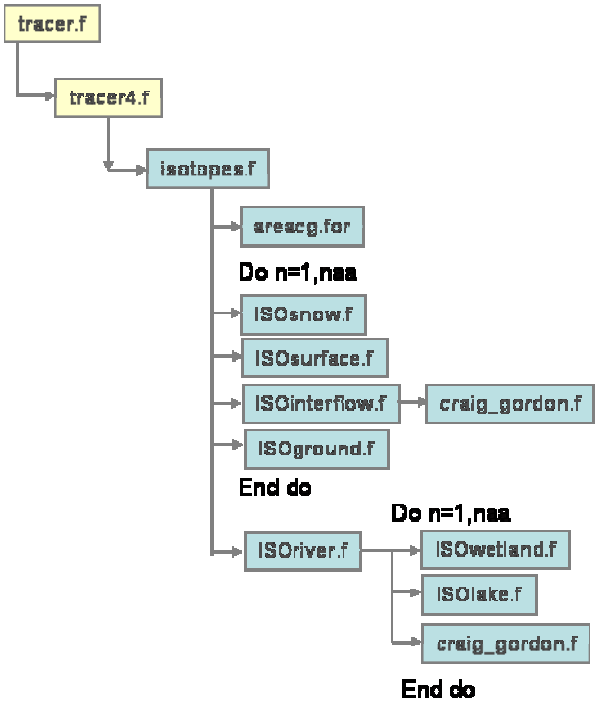

Figure 6.1 – Schematic representation of the isoWATFLOOD suite of programs.

In addition to WATFLOOD forcing data, isoWATFLOOD requires an input composition of precipitation and relative humidity data for atmospheric forcing (Section 6.2). Background concentrations of isotopes in storage are defined at the start of an event to initialize the model with antecedent isotopic conditions. Background concentrations (in ‰, VSMOW) are specified in the isotope input file 'isotope.par' (Appendix A.1.2 and Appendix A.2.2) and are obtained from measured data or previously obtained knowledge of average isotopic compositions in the region of interest.

Mass of ^{18}O in hydrologic storage (e.g., surface storage, UZS, LZS, etc.) is computed based on mass initially present, mass inflow, and mass outflow from a hydrologic storage. In channels, isotope mass is moved from upstream to downstream via streamflow advection (Section 6.4). Within each storage compartment, mixing and losses are uniquely computed based on the

hydrological behaviours typical of that storage compartment (Sections 6.5 to 6.8). Storage compartments are hydrologically connected via flowpaths defined and computed by WATFLOOD. With distinct isotopic compositions of hydrologic storages defined, isotope mass is advected into wetland storage (Section 6.9), or directly into the channel. Should there be a lake or reservoir in the routing sequence, isotope mass is budgeted within the lake and advected out of the lake with lake discharges (Section 6.10). A graphical representation of isoWATFLOOD's hydrology is provided on Figure 6.2, and will be explained in detail in the following sections in this Chapter.

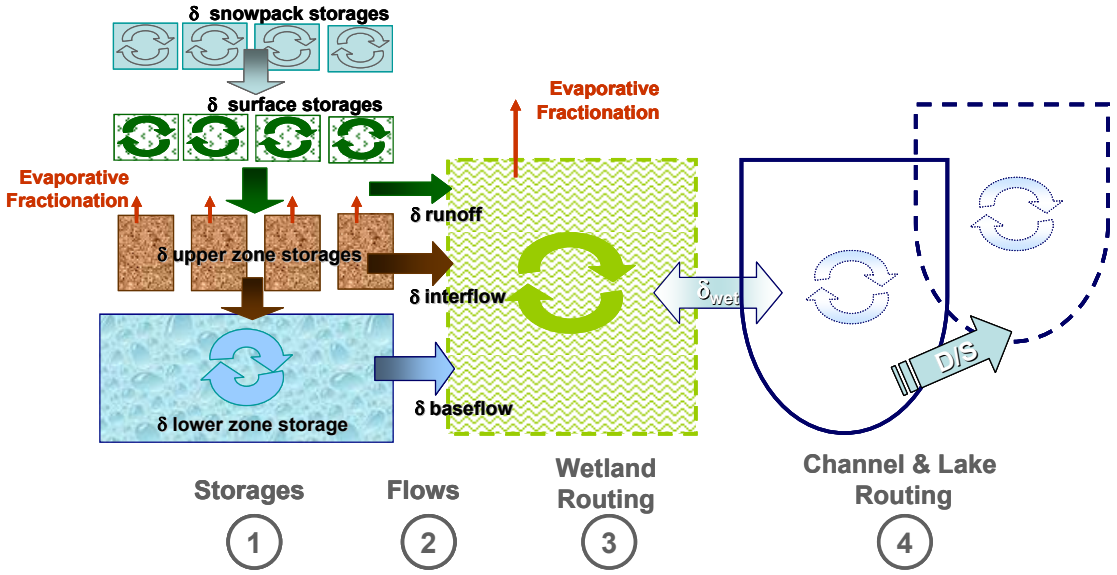

Figure 6.2 – Graphical representation of isoWATFLOOD hydrology.

At the expense of some computational efficiency, the benefit of simulating isotopes in parallel with water balance computations is the reduction in a model's degrees of freedom realized by the added constraint of simulated results to measured isotope data.

6.2 Atmospheric Forcing

All models require forcing. In the case of hydrological models, atmospheric forcing is a requirement as it is external to the scope of what is being simulated by the model. Predicting water budgets accurately on the land surface requires accurate precipitation and climate data; the incorporation of water isotopes means that in addition to water quantity, isotopic compositions

of the inputs (i.e., precipitation) are also necessary. Simulation of isotopic fractionation during evaporation also necessitated relative humidity data. There were two methods developed to atmospherically force isoWATFLOOD.

6.2.1 Modelled Atmospheric Forcing

The first method is to produce a representative time series of isotopes in precipitation and relative humidity data using an atmospheric model. Continuous measurements of isotopes in precipitation are typically not feasible due to prohibitive sampling and analysis costs; therefore isotope-enabled RCMs can be used to simulate spatially distributed meteorological inputs. The isoWATFLOOD can be interfaced with the REMOiso RCM (Sturm *et al.*, 2006; Sturm *et al.*, 2007a; Sturm *et al.*, 2005). REMOiso simulations of isotopes in precipitation and relative humidity data have been validated in a number of studies in Europe (Sturm, 2005), and South America (Sturm *et al.*, 2007b) (Section 2.6.1). Simulations produce gridded output data at a resolution of 0.5° (~54 km), which can be down-scaled to provide distributed inputs for isoWATFLOOD (Figure 6.3).

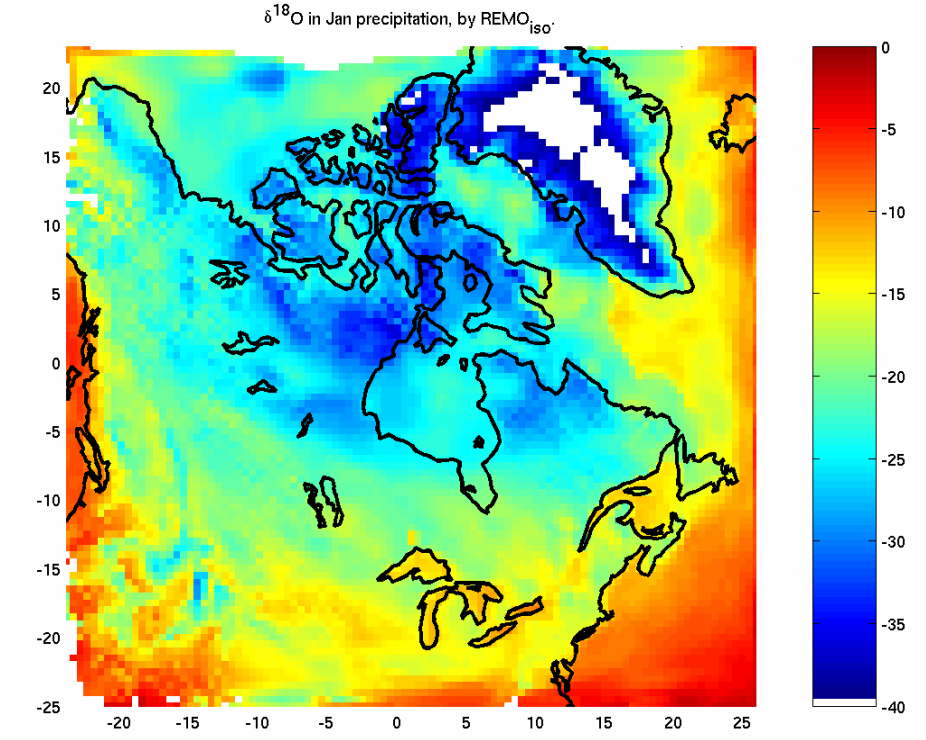

Figure 6.3 – REMOiso simulation of isotopes in precipitation over North America (Sturm et al., 2005).

Data from REMOiso output is transformed into a WATFLOOD compatible format and read by isoWATFLOOD during the isotopic simulation. Three variables can be read from REMOiso and used to force isoWATFLOOD: isotopic composition of rain ($\delta^{18}O_{rain}$), isotopic composition of snow ($\delta^{18}O_{snow}$), and specific humidity (q_s). $\delta^{18}O_{rain}$ and $\delta^{18}O_{snow}$ are used directly to define the isotopic compositions of surface inputs. Since it is relative humidity (h in %) that is required by isoWATFLOOD, specific humidity (q_a in g/kg) is transformed into relative humidity (h) based on the ratio of the vapour pressure in air to the saturation vapour pressure (Gill, 1982), assuming an open, evaporating water body:

$$h = \frac{e_a}{e_s} \qquad (6.1)$$

where the vapour pressure of air (e_a) is calculated using the specific humidity (q_a) and by assuming constant atmospheric pressure (p_a=101325 Pa) (Engineering ToolBox, 2005):

$$e_a = \frac{p_a}{\frac{0.622}{q_a} + 0.378} \qquad (6.2)$$

and where the saturation vapour pressure (e_s) is a function of the air temperature (T in ^oC) (Engineering ToolBox, 2005):

$$e_s = 10^{\frac{0.7859+0.03477T}{1+0.00412T}+2} \qquad (6.3)$$

The forcing of an isotope-enabled hydrological model by an isotope-enabled climate model enables detailed analyses of mesoscale variation in water resources (i.e., streamflow) that are more true to reality.

6.2.2 Specified Atmospheric Forcing

The second method of forcing was developed for study regions where isotopes in precipitation and climate data were not measured, and where distributed simulated output was not available. The composition of isotopes in precipitation can be specified in the isotope input file and is assumed to be constant over the study region for a particular event period. The constant compositions of isotopes in rain and snow can be obtained from the CNIP or GNIP data

repositories, which provide inferred maps of isotopes in precipitation on continental and global scales as was described in Section 2.4.1 (Figure 2.3).

Isotopes in precipitation vary both spatially and temporally, so the specification of constant compositions is not preferred but is unfortunately sometimes necessitated. For example, in the Fort Simpson Basin (FSB) isotopes in rainfall were measured and the yearly averages were found to vary substantially: -15.6‰ (1997), -20.1‰ (1998), -16.5‰ (1999) (St. Amour, 2008). In the Grand River Basin (GRB), samples from rainfall events were not collected but the long-term CNIP average composition for southern Ontario reflects the more enriched Gulf of Mexico moisture source (-10‰ to -7‰).

To compute relative humidity when only temperature data are known, temperature (T in ^{o}C) is used to compute saturation pressure (P_{sat} in Pa) based on the defined logarithmic relationship between the two variables (Engineering ToolBox, 2005):

$$p_{sat} = (3\times10^{-9}T^5 + 3\times10^{-7}T^4 + 3\times10^{-5}T^3 + 0.0015T^2 + 0.0441T + 0.6105)*10^3 \qquad (6.4)$$

The relative humidity, h is defined by the mass of water vapour in air (q_0 in g/kg) over the mass required to saturate the air volume (q_{sat} in g/kg):

$$h = \frac{q_0}{q_{sat}} \qquad (6.5)$$

where the mass concentration of water vapour in air (q_0 in g/kg) is assumed constant at 10 g/kg as defined by the Clausius-Clapeyron relationship (Sturm, 2007); and the mass of water to saturate the air volume (q_{sat} in g/kg) is computed based on the ratio of saturation vapour pressure (p_{sat}) to partial pressure (p_0) multiplied by the molar ratio of water to air (M_{H2O}/M_{air}=R=0.625), assuming air is 80% nitrogen and 20% oxygen:

$$q_{sat} = \frac{p_{sat}}{p_0} \times \frac{M_{H_2O}}{M_{air}} \qquad (6.6)$$

Given that temperature is a spatially discretized variable in WATFLOOD, relative humidity is computed for each grid in the watershed.

In natural environments humidity typically increases as evaporation proceeds on hot, dry days when there is ample moisture available for evaporation. If humidity increases substantially, the

rate of evaporation slows before moisture availability becomes a limiting condition. Modelling this process requires atmospheric feedback from surface hydrology, which is simulated by the Craig & Gordon model (Equation 2.5; Section 2.4.2) as described in the following section.

6.3 Modelling Evaporation

The isotopic mass balance of an evaporating water body is not preserved during evaporation; fractionation of heavy and light isotopes results in a build up of heavy isotopes in the evaporating water body. Described in Section 2.4.2, the Craig and Gordon model (Craig & Gordon, 1965) is used to compute the change in composition of the evaporating moisture (δ_E) when a surface water body of volume V is evaporating. Given that mass is conservative, if the evaporating moisture flux has fewer heavier isotopes, the isotopic composition of the water body (δ_L) will accumulate heavy isotopes and enrich in composition. This enrichment is both systematic and reasonably predictable (i.e., for ^{18}O). The water and mass balance for a shallow, well-mixed lake during an ice-free period represents the change in isotopic composition of the lake with a lake volume change:

$$V\frac{d\delta_L}{dt} + \delta_L\frac{dV}{dt} = I\delta_I - Q\delta_Q - E\delta_E \qquad (6.7)$$

where I and δ_I are the cumulative lake inflow (cms) and associated isotopic composition of the inflow (‰), respectively; Q and δ_Q are the lake outflow (cms) and isotopic composition of the outflow (‰); and E is the evaporative flux (cms) with composition δ_E (‰) determined by the Craig and Gordon model. isoWATFLOOD uses Equation 6.7 to alter the composition of an evaporating surface during ice-free periods. It is assumed that the water body is shallow and well-mixed, which is reasonable for the evaporating boundary layer at the top of the lake (i.e., wind-derived mixing).

Depending on the water body, there may be different configurations of the above mass balance: dams may or may not have an outflow component (i.e., high versus low-flow periods), there may or may not be significant changes in volume (i.e., the Great Lakes), or there may not be significant inflows (i.e., during dry periods). Research done by Gibson (2002a) describes the various configurations of mass and water balance equations used to describe the isotopic

composition of the water body following evaporation over a time step, Δt. There are two kinds of models used in isoWATFLOOD to describe the $\delta^{18}O$ of evaporating water, both of which were derived by Gibson (2002a): fraction-dependent and time-dependent models. The fraction-dependent model is applied to evaporating soils and wetlands given there can be a significant change in water volume, and the time-dependent model is applied to evaporating lakes where typically there is no appreciable change in water volume over the timestep.

The fraction-dependent model defines a fractional change in water volume, *f* and solves Equation 6.7 for the isotopic composition of the evaporating water body (δ_L) (Gibson, 2002b):

$$\delta_L = \delta_S - (\delta_S - \delta_0) f^{\left[\frac{-(1+mx)}{1-x-y}\right]} \qquad (6.8)$$

where δ_0 is the initial isotopic composition of the lake from the previous time step (per mille); δ_S is the steady-state isotopic composition of the water body (Equation 2.10); *x* is the evaporation to inflow ratio (E/I); and *y* is the outflow to inflow ratio (Q/I). Gibson (2002a) describes various forms of the water and isotope balance represented by Equation 6.8 that depend on the water and mass balance representing the evaporating water body. Each fraction-dependent model, however, represents a deviation from steady-state fractionation by a transient function. The transient function is proportional to the incremental isotopic enrichment of the varying lake volume at a rate proportional to a transient enrichment slope defined by the rate of heavy isotope build-up (*m*; Equation 2.11), *x* and *y*.

In contrast to fraction-dependent models, the time-dependent models instead evolve an isotopic composition over time when the volume does not change significantly (dV/dt=0). The water bodies' isotopic composition is described by (Gibson, 2002b):

$$\delta_L = \delta_S - (\delta_S - \delta_0) e^{-(1+mx)\left(\frac{I\Delta t}{V}\right)} \qquad (6.9)$$

where I is the sum of the inflows (m3/s). Time-dependent models represent a deviation from the steady-state isotopic composition by a transient exchange term that exponentially increases isotopic enrichment (δ_S-δ_0) by a transient enrichment slope proportional to *m*, Q/I, total inflow, and volume of the water body. As time evolves ($t \rightarrow \infty$) the isotopic composition of the lake (δ_L) tends towards the steady-state composition (δ_S).

Water evaporating from an open, large water body (i.e., lake or reservoir) is assumed to have little change in volume over the timestep. Open-water bodies are assumed to be dominated by turbulent mixing at the boundary layer (Figure 2.4) where winds carry away the evaporating moisture and reduce diffusive (or kinetic) fractionation effects. Wetlands on the other hand can significantly change in volume over the timestep as they drain water into a channel or flood during large events. In isoWATFLOOD wetlands are assumed to be partly affected by turbulent winds advecting moisture away from the boundary layer, but vapour exchange can also be diffusive because of vegetative cover at the wetland surface.

Evaporative controls from shallow soil layers are largely dependent on landcover type in isoWATFLOOD. The composition of the soil moisture is modelled in the same manner for each landcover, but has a different influence on soilwater composition depending on the amount of moisture evaporating from a given land class. Isotopic variation of soilwater is assumed to be fraction dependent since water in subsurface storage is significantly affected by evaporative loss (Section 6.7). An evaporating soil surface is assumed to be representative of a shallow, well-mixed water body. For one, evaporating water is reasonably well-mixed given it is entering the soil from surface storages that are shallow and have torturous flowpaths. When the soil layer becomes saturated, water evaporates from the soil column through both advection and diffusion since water is ponded at the surface of the soil column (Barnes & Turner, 1998). As the wetting front progresses downward and soil near-surface becomes unsaturated, evaporative fluxes are predominately diffusive in nature. Fraction-dependent models are used to describe the change in isotopic composition of soilwater; accounting for changing soil moisture conditions through the turbulent mixing (η) and vapour transport (Θ) parameters (Section 2.4.2).

Smaller scale studies have been conducted that seek to quantify isotopic fractionation during evaporation (Price *et al.*, In Preparation), however there is a gap in the research involving the ability to continuously model the isotopic change due to evaporation across regional and watershed scales. The characteristic behaviour of the oxygen-18 isotope during fractionation has been well developed and is becoming well understood (Gibson *et al.*, 1999; Gibson & Edwards, 2002; Gibson, 2002a; Gibson *et al.*, 2006). There are also many other researchers who have sampled large spatial domains periodically over several years, enabling a better understanding of the isotopic evolution of lakes and the role of evaporation (Brock *et al.*, 2007;

Clogg-Wright, 2007; Falcone, 2007; Sokal *et al.*, 2008; Wolfe *et al.*, 2007; Yi *et al.*, 2008). The isoWATFLOOD model provides the capability to continuously monitor changes in both lake and vapour compositions in response to atmospheric and hydrologic change.

6.4 River Routing: ISOriver

Isotope mass is advected with streamflow without concern for dispersion as stable water isotopes are naturally occurring constituents of water that do not require mixing. As flows are routed to the downstream cell, isotope mass is simultaneously moved to downstream grids. Isotopes are also moved from one storage compartment to the next with runoff and subsurface flows.

Simplified hydrologic storage routing is applied through a robust application of the continuity equation (Section 4.3) to route streamflow. A concentration of isotope mass is assigned to each storage and runoff component (isoS in m^3) to derive a coupled water and mass balance equation:

$$\delta_Q \frac{disoS}{dt} + isoS \frac{d\delta_Q}{dt} = \delta_I I + \delta_Q Q - \delta_E E \qquad (6.10)$$

where isoS (m^3) is volume of heavy isotopes in channel storage; I is the sum of all stream inflows over dt, having a flux-weighted average of δ_I; Q and E are the grid outflow and evaporative flux at the end of the timestep, dt (in seconds); δ_Q is the mass concentration of heavy isotopes in streamflow at the end of dt; and δ_E is the fractionated isotopic ratio of water evaporating from the stream over dt. Since the continuity balance in Equation 6.10 is used to describe the change in mass of heavy isotopes, δ-values in the model actually represent the relative mass of heavy oxygen (^{18}O) in water to total mass of oxygen (O) (or total volume of water), denoted from here-onwards as C^{18O}:

$$C^{18O} = \frac{^{18}O}{^{16}O + ^{18}O} = \frac{^{18}O}{O} \qquad (6.11)$$

It is assumed that other isotopes of oxygen can be neglected, and that the total mass of oxygen (O) is approximately equal to the sum of ^{18}O and ^{16}O.

During routing it is assumed that the river isotopes are non-fractionating along the flowpath since downstream advective forces dominate over boundary layer diffusive forces (IAEA, 1981). Therefore the loss of water from the stream due to evaporation is assigned the same isotopic composition as the streamflow ($\delta_E=\delta_Q$), and the $\delta_E E$ term is directly combined with $\delta_Q Q$ representing total outflow. By including $\delta_E E$ with the total mass outflow and assuming no fractionation along the flowpath ($d\delta_S/dt=0$), Equation 6.10 is further simplified:

$$\frac{disoS}{dt} = C_I^{18O} I + C_Q^{18O} Q \qquad (6.12)$$

The mass inflow at the end of a timestep ($C_{I,2}{}^{18O}I_2$) is computed based on a flux-weighted average of all inflow components contributing to streamflow, assuming that the inflows are instantaneously and completely mixed into the stream:

$$C_{I,2}^{18O} I_2 = C_P^{18O} P + C_{SM}^{18O} Q_{SM} + C_{SW}^{18O} I_{SW} + C_{IF}^{18O} I_{IF} + C_{GW}^{18O} I_{GW} \qquad (6.13)$$

where $C_{SW}{}^{18O}$, $C_{IF}{}^{18O}$, $C_{GW}{}^{18O}$ represent the concentrations of heavy isotope species (^{18}O) in surface runoff, interflow and groundwater components, respectively; and their associated inflows (I_{SW}, I_{IF}, I_{GW} in cms). If there are wetlands alongside the channel, then the component contributions are added to the wetlands instead of directly to the channel. Channel inflow is then alternatively computed as the sum of the meteorological inputs and wetland outflow:

$$C_{I,2}^{18O} I_2 = C_P^{18O} P + C_{SM}^{18O} Q_{SM} + C_{WET}^{18O} qo_{wet} \qquad (6.14)$$

Recalling from Section 4.4 that the wetland outflow (qo_{wet}) is reversible (i.e., negative when the channel overflows into the wetlands); wetland flux can either represent a channel inflow or a channel outflow according to Equation 6.14. Wetland hydrologic and isotopic routing is described in detail in Section 6.9.

Mass outflow of isotopes ($C_Q{}^{18O}Q_2$) is computed using the mass concentration of heavy isotopes in storage:

$$C_Q^{18O} = \frac{isoS_s}{store_2} \qquad (6.15)$$

where δ_S is the mass concentration of heavy isotopes in streamflow at the end of the timestep. Equation 6.15 represents an isotope R-value, or ratio of ^{18}O in storage to total storage volume ($^{16}O+^{18}O$). Changes in isotopic compositions of the streamflow and hydrologic storages are

reported based on comparing the simulated R-value to the R-value of Vienna Standard Mean Ocean Water (VSMOW), and multiplying by 1000 to get δ-values in per mille (‰):

$$\delta^{18}O_S = \left(\frac{R_S}{R_{VSMOW}} - 1 \right) \times 1000 \qquad (6.16)$$

Isotope mass storage in the channel at the end of the timestep is computed based on an isotopic storage continuity balance from the beginning to the end of the timestep:

$$isoS_2 = isoS_1 + \left(\frac{C_{I,1}^{18O} I_1 + C_{I,2}^{18O} I_2}{2} - \frac{C_{Q,1}^{18O} Q_1 + C_{Q,2}^{18O} Q_2}{2} \right) \Delta t \qquad (6.17)$$

Since C_Q^{18O} changes when the isotopic storage changes, which in turn alters the mass outflow, the advection of isotope mass requires an iterative solution. Convergence is based on a relaxation method where the new solution from each iteration is a function of both the old and the new "guess" from the previous and current iteration, respectively. A revised heavy isotope concentration is computed based on the mass change in storage, which yields a mass revised mass outflow to be computed. A new mass outflow ($C_{Q,2}^{18O} Q_2 \Delta t$) is computed, and is then relaxed by weighting the new outflow and the previous outflow:

$$C_{Q,2}^{18O} Q_2 = \theta (C_{Q,2}^{18O} Q_2)_{old} + (1 - \theta)(C_{Q,2}^{18O} Q_2)_{new} \qquad (6.18)$$

where θ is a relaxation parameter that increases after a specified minimum number of iterations, putting more emphasis on the old solution to force convergence. To reduce the numerical error inherent to the simulation based on truncation of computed values, double precision (64-bit) variables were used for all mass variables. With round-off error controlled, a convergence criterion was selected that would be two orders of magnitude less than the magnitude of the isotope mass being computed (i.e., on order of 10^{-3}) to reduce interference by numerical error:

$$(C_{Q,2}^{18O} Q_2)_{new} - (C_{Q,2}^{18O} Q_2)_{old} = 0.000\,01 \qquad (6.19)$$

Numerical error was controlled in all simulations to ensure the changes in simulated isotopic compositions were the result of hydrological change and not numerical errors introduced by the iterative sequence. Control over spatial error is described by the Péclet number (P_e in m^2/s), which computes numerical dispersion based on grid size (Δx in m), speed of flow (U in m/s), and dispersion of flow (E in m^2/s) (Chapra, 1997a):

$$P_e = \frac{U\Delta x}{E} < 2 \qquad (6.20)$$

The numerical dispersion of the simulation is determined as a combination of both spatial and temporal dispersion as described by (Chapra, 1997a):

$$E = \frac{\Delta x}{2}U - \frac{U^2\Delta t}{2} \qquad (6.21)$$

For large Δx the P_e number will increase leading to more error resulting from the coarse spatial domains and faster than actual velocities. If spatial error is significant, simulated solutions arrive before measured solutions (i.e., the isotopic response to an event artificially appears before streamflow). Average Péclet numbers of 0.45 (Grand River) and 66 (Fort Simpson) were computed from isoWATFLOOD simulations. This indicates that the 2-km GRB spatial resolution is stable, however dispersion errors will be generated in the FSB due to the coarser spatial resolution of 10-km. The dispersion coefficient (Section 5.1; *coeff*) in the Tracer module was designed to minimize this kind of numerical dispersion generated from coarse-resolution modelling.

Courant criteria define temporal error resulting from the choice of routing timestep (Δt in s) (Chapra, 1997a):

$$C_r = \frac{U\Delta t}{\Delta x} < 1 \qquad (6.22)$$

For stability and to achieve quick convergence in iterative solutions, the Courant criteria must be held true and is typically controlled via the timestep. In isoWATFLOOD simulations, the maximum routing timestep used was Δt=3600s. Maximum Courant numbers of 0.65 (Grand River) and 0.78 (Fort Simpson) were reported, indicating isoWATFLOOD solutions were temporally stable and the choice of routing timestep was appropriate for the scale of the basins; corroborated by the quick convergence of numerical solutions.

Dispersion error introduced by the assumption of instantaneous and complete mixing of inflows in isoWATFLOOD must also be checked. Although these assumptions are not physically realistic at the point of inflow, the spatial resolution of isoWATFLOOD permits these to be realistic assumptions since the grid cell length (i.e., the routing length) is far greater than the mixing length. Latitudinal dispersion, E_{lat} (m^2/s) was used to compute the inflow mixing length

(L_m in m) within WATFLOOD because it is slower acting (i.e., transverse to flow lines) and less dominant than longitudinal dispersion (Chapra, 1997a; Schnoor, 1996):

$$E_{lat} = 0.6 y u^* \qquad (6.23)$$

$$L_m = 0.1 U \frac{B^2}{y} \qquad (6.24)$$

where U is the average channel velocity (m/s); u^* is the critical channel velocity, or shear velocity equal to $\sqrt{gyS}$ (m/s); y is the depth of flow (m); and B is the channel width (m). Mixing length (L_m) was found to vary from 30 m (Scotty Creek, FSB) to 3.5 km (Martin River, FSB), and was consistently less than 1 km in the GRB. Given grid sizes used varied from 2-km to 10-km, the complete mixing assumption is justified. In natural channels, longitudinal dispersion is typically greater than lateral dispersion and therefore complete mixing is likely to occur in even shorter distances than what was predicted by Equation 6.24. Longitudinal dispersion (E_{lon} in m^3/s) was also computed using the approach derived by McQuivey and Keefer (1974) for large rivers with low Froude numbers (<0.5):

$$E_{lon} = 0.05937 \frac{Q}{S_i B} \qquad (6.25)$$

When the Froude number exceeded 0.5, the method by Fischer *et al.* (1979) was instead used:

$$E_{lon} = 0.011 \frac{U^2 B^2}{y u^*} \qquad (6.26)$$

Longitudinal dispersion was significantly greater than lateral dispersion; ranging from 1.5 times (Nith River) to 10 times greater (lower Grand River) indicating that complete mixing would likely be obtained in shorter mixing lengths.

Checking the stability of the numerical solution is a critical aspect of modelling isotopes in streamflow given changes in mass concentration simulated are on the same order of magnitude as typical numerical error. It is important to segregate actual isotopic variation from numerical drift inherent to the solution technique; and moreover to ensure that numerical dispersion is properly constrained.

These small changes in $\delta^{18}O$ within each hydrologic compartment contribute to the variability of $\delta^{18}O$ in streamflow. In the following sections, the approach to simulating isotopic variability in hydrologic storage compartments is explained in detail.

6.5 Snowmelt: ISOsnow

Snowfall generally has a more depleted signature than rainfall owing to shifts in continental air masses during winter months, and because of a phase change (i.e., freezing). Rainfall partially evaporates leading to fractionation of isotopes in the upper atmosphere or on the ground as was discussed in Section 6.3. When temperatures are at, near, or below freezing however, precipitation falls as snow and accumulates on the land surface until temperatures begin to rise. During pack ripening, it is necessary to model the isotopic fractionation resulting from phase change during thaw-freeze cycles.

In WATFLOOD snowfall or rain-on-snow is added directly to a snowpack. Each landcover classification has its own defined snowpack, and therefore there needs to be a separate isotope mass balance for each snowpack in each timestep to account for differences in depths, fractionations, and amounts of snowmelt runoff generated from each pack. Isotope mass balances are performed on a series of snowpacks; each receiving inputs, containing storage, and generating meltwater (Figure 6.4). When a snowpack ripens, it generates meltwater that has a different signature than the snow that originally fell and contributed to the pack formation. This alteration occurs because of a gradual ripening-freezing cycle that often occurs within the snowpack, which fractionates stable water isotopes due to phase changes (i.e., liquid to solid to liquid). The isotope mass balance for a fully-developed snowpack undergoing freeze-thaw cycles is illustrated on Figure 6.4.

Sublimation of a snowpack can lead to slight isotopic fractionation prior to pack ripening. Studies have found that fractionation resulting from sublimation can be up to 3‰ for $\delta^{18}O$ (Moser & Stichler, 1980), but more typically the reported effects of sublimation tend to be less than analytical uncertainties and are commonly neglected (St Amour *et al.*, 2005; Rodhe, 1998) and therefore have not been included in the isoWATFLOOD model.

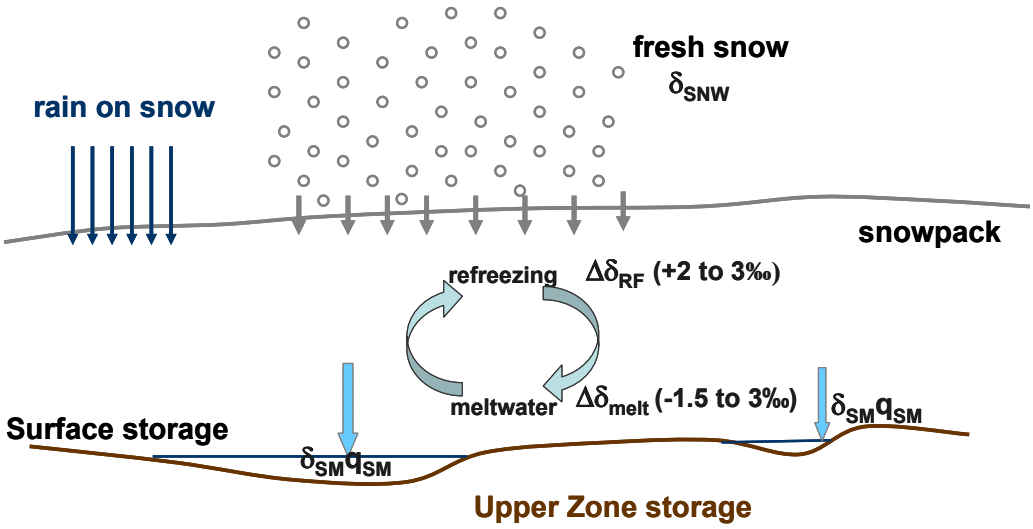

Figure 6.4 – Snowmelt isotope balance in isoWATFLOOD.

During the accumulation phase, fresh snowfall is added to a snowpack with a specified input composition from either the isotope.par input file (Appendix A.1.2 or Appendix A.2.2) or the spatially distributed input files (Section 6.2.1). If it rains on a snowpack (i.e., mixed precipitation or warm air-temperature precipitation), then the rainfall is assumed to freeze (lowering the heat deficit), and pack storage is increased. The isotopic composition of the precipitation during mixed events reflects either snow or rainfall and is determined based on the difference between the air temperature (T_a) and a calibrated base melt-freeze temperature (T_{base}) specified in the WATFLOOD parameter file. Both meteorological inputs increase the amount of potentially-available meltwater in the pack, however so long as there is a heat deficit the pack will remain frozen and no isotopic fractionation is simulated by isoWATFLOOD.

As the air temperature increases the temperature of the snowpack rises, decreasing the heat deficit of the pack. Once enough energy has been accumulated, the pack will ripen and begins to melt. Meltwater interaction with snow is minimized when melting occurs more slowly, and if there is no additional rain during the melt period, then the melt process will lead to an equilibrium fractionation between the solid ice and liquid meltwater phases (Stichler *et al.*, 1981). In reality however, there is additional kinetic fractionation as the snowmelt exchanges with the atmosphere, which not only affects meltwater but also the residual snowpack. Based on experimentally-derived ice to water fractionations for ^{18}O, a constant 1.4 to 3‰ enrichment

(determined by calibration) in snowpack heavy isotopes is assumed and used to increase the snowpack $\delta^{18}O$ composition (i.e., deplete meltwater) in isoWATFLOOD (Cooper, 1998; IAEA, 1981). If the pack continues to warm, then this is the only fractionation simulated within the snowpack. As the water content of the snowpack increases, meltwater is released and will either pond in depression storages on the land-surface or will infiltrate into the upper zone storage (UZS). The initial meltwater release is therefore the most isotopically depleted and, consequently, the residual snowpack becomes more enriched as melting progresses. This is an important natural variation to capture when modelling the isotopic composition of freshet runoff, which is why meltwater fractionation was added to isoWATFLOOD.

More frequently however there are periods of pack ripening during warm, sunny winter days; followed by refreezing when the temperature drops at night or because of a change in atmospheric circulation patterns. A number of studies have been conducted on Icelandic glacial ice, all of which have indicated that ice-water fractionation is an important factor governing the enrichment of heavier isotopes during firnification of a snowpack (IAEA, 1981; Jouzel & Souchez, 1982). Due to the absence of studies measuring the true ice-water fractionation separation, ice-water exchange is assumed to eventually reach equilibrium leaving the snowpack enriched in heavy isotopes and meltwater more depleted. Based on an equilibrium reaction assumption, a 2 to 3‰ enrichment factor (determined by calibration) is applied to simulated meltwater compositions as they refreeze back into the snowpack. During one seasonal cycle, the snowpack can undergo any number of thaw-refreeze cycles initiated by increases and decreases in air temperature. Despite the fact that the water-ice fractionation is typically ignored, studies done on Icelandic glaciers have indicated the importance of including the freeze-thaw fractionation effects when modelling the $\delta^{18}O$ variation in a snowpack (IAEA, 1981; Jouzel & Souchez, 1982).

In snowpacks, isotope mass is stored and accumulated when the pack is not ripe and the concentration of isotopes in storage (δ_{SP} in m^3/m^3) is determined based on a mass balance of heavy isotopes in storage ($isoS_{SP}$ in m^3). Inflows from precipitation (I in cms, δ_I in m^3/m^3), fractionations due to water refreezing (Q_{rf} in cms, ΔC_{rf} in m^3/m^3) and melting within the pack (Q_{melt} in cms, ΔC_{melt} in m^3/m^3) are all balanced to compute a change in pack storage:

$$\frac{disoS_{SP}}{dt} = C_I^{18O} I - (C_{SP}^{18O} + \Delta C_{melt}^{18O}) Q_{melt} + (C_{SM}^{18O} + \Delta C_{rf}^{18O}) Q_{rf} \quad (6.27)$$

where ΔC_{melt} and ΔC_{rf} are delta-value offsets (depletion of meltwater and enrichment during refreezing, respectively) converted to mass concentrations, or changes in heavy isotope storage relative to pack storage (m^3/m^3). Melting internal to the pack (Q_{melt}) reduces storage of snow, and water refreezing (Q_{rf}) back into the pack acts to increase snow storage. The concentration of heavy isotopes in storage (C_{SP}^{18O} in m^3/m^3) is derived from the ratio of heavy isotopes in storage to the total volume of snowpack storage (storeSNW in m^3):

$$C_{SP}^{18O} = \frac{isoS_{SP}}{storeSNW} \quad (6.28)$$

Once the pack has ripened and water begins to runoff of the pack (i.e., generate runoff), the water-mass balance is additionally affected by the outflow of isotopes leaving the pack (Q_{SM} in cms) and the isotopic fractionation occurring as water melts. It is assumed that if the pack is fully ripe that water within the pack does not refreeze, and therefore the refreeze term is removed from the mass balance equation:

$$\frac{disoS_{SP}}{dt} = C_I^{18O} I - C_{SM}^{18O} Q_{SM} - (C_{melt}^{18O} + \Delta C_{melt}^{18O}) Q_{melt} \quad (6.29)$$

where C_{SM}^{18O} is the isotopic composition of the snowmelt exiting the pack, which is equal to the concentration of heavy isotopes in storage at the time of melt. C_{SM}^{18O} is the isotopic composition assigned to meltwater entering surface depression storage, and to meltwater infiltrating into the UZS.

Ideally modelling isotopic fractionation within a snowpack would be done using fully-coupled heat and water balance equations. Although WATFLOOD simulates the melting of the snowpack using heat and water balance equations, isoWATFLOOD assumes constant fractionations during melting and refreezing within the pack. This assumption was made to simplify the model, and to test if a more complex heat-water balance was necessary. The literature supports that regions with lower seasonal isotopic amplitudes tend to have smaller δ-variations within snowpacks (and between summer and winter precipitation), and therefore the isotopic composition of snowpacks remain closer to the long-term average isotopic composition of streamflow (IAEA, 1981; Rodhe, 1998). The impact of snowmelt on the isotopic

composition of spring runoff would therefore lessen. In regions with high seasonal amplitudes however (i.e., high-latitude regions, including most of Canada), the ISOsnow module plays an important role in discerning the variability of freshet streamflow compositions. The ISOsnow module should be applied in regions with higher seasonal amplitudes and large snowmelt contributions to examine whether there is a need to simulate a more detailed water-isotope exchange within snowpacks.

Snowpack composition can vary substantially with depth of the pack, reportedly from 6-9‰ from top to bottom of the pack (Cooper, 1998). The amount to which compositions vary with depth largely depends on the consistency of the air masses delivering the snow to the catchment. The isoWATFLOOD model can simulate varied snowfall compositions when modelled forcing data are available (Section 6.2.1); however if constant inputs are assumed (Section 6.2.2), then simulated snowpack compositions remain constant with depth. Literature also supports that sublimation enriches the top layers of a snowpack by up to 10‰ (Cooper, 1998), where these studies have primarily been based on small-scale, localized measurements.

Given that the isotopic composition of the snowpack is primarily determined by the meteorological inputs of snow and rain, spatially distributed forcing is preferred for the model. If user-specified input is chosen, it should be noted that for catchments where large changes in elevation are inherent to the catchment topography, a fraction of snowfall should be applied to account for topographically-driven depletion in isotopes. As moisture is orographically lifted, the heavier isotopes precipitate preferentially and "rain-out" at lower-elevations. As elevation increases, precipitation therefore tends to be more depleted of the heavier isotopes at a rate of 0.15-0.5‰ per 100m of relief (IAEA, 1981). When isotopes in precipitation are derived from a climate model simulation, elevation effects are inherent within the distributed data. However, if a spatial interpolation is used to weight snow course survey data, then additional fractionation of the isotopes due to elevation effects should be considered within isoWATFLOOD.

When simulating the isotopic composition of streamflow in northern Canada, snowmelt is a dominant end-member and therefore needs to be simulated as a separate component of hydrologic storage. In addition to snowmelt, isoWATFLOOD also includes a constant, non-fractionating glacial meltwater contribution to surface storage. Despite the fact that isotopes

fractionate substantially within glacial ice (Rohde, 1998) meltwater runoff produced by the glaciers would be reasonably constant over short-term study periods (i.e., months or years). Both snowmelt and glacial meltwater are added directly to surface depression storages or infiltrated into subsurface UZS.

6.6 Surface Storage: ISOsurface

Although it is atypical that large quantities of water are seldom pooled and remain on the land-surface, this temporary hydrologic storage compartment is responsible for the transfer of meteoric waters and isotope mass into the subsurface. Water and isotope mass produced from melting snowpacks or glaciers is combined with freshly-falling precipitation and can fill small depression storages on the land surface that mimic a series of small puddles. Once in depression storage, surface water and isotopes will either be 1) transferred vertically into the soil layer, or UZS, or 2) if the maximum depression storage is exceeded, transferred laterally as overland runoff.

Water and isotope mass entering surface storage from snowpacks, glaciers or meteorological events can fill small depressions in the topography of the land-surface, if such depressions exist. In WATFLOOD, depression storage can be a calibrated parameter, or (more commonly), values from the ASCE Handbook (Task Committee on Hydrology Handbook of Management Group D, 1996) are specified for each land class designation. Some watersheds and land classifications are more likely than others to have depression storage. The surface storage zone in WATFLOOD can be considered as a transfer station more than a storage compartment, where there is a distinct mixing of source waters and a transfer of water to the next storage compartment. Figure 6.5 illustrates how water and isotope mass moves through the surface storage zone. The isotope mass balance described in this section, and represented on Figure 6.5, occurs for each land classification to account for differences in isotope mass transfer attributable to variable surface storage capacities and infiltration rates.

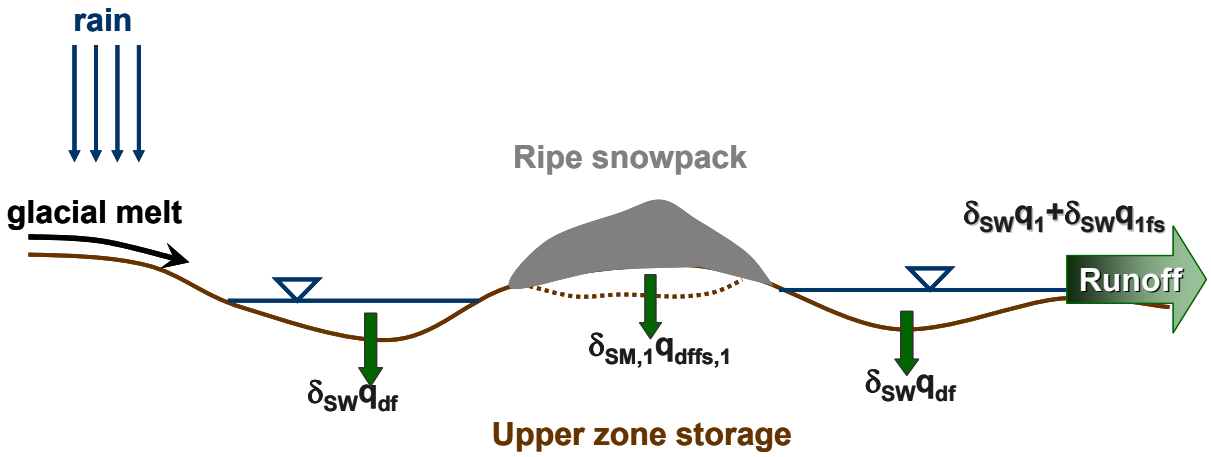

Figure 6.5 – Surface depression storage isotope balance in isoWATFLOOD.

Figure 6.5 shows isotope mass inflows from snowmelt (Q_{SM} with variable composition C_{SM}^{18O}, Section 6.5), glacial melt (Q_{gmelt} with constant composition C_{gmelt}^{18O}), and precipitation (P in mm/hr with forced composition C_P^{18O}). The surface storage compartment behaves as a conduit moving water and mass from the intake to the outflow, mixing isotope mass along the way. The following isotope mass balance equation describes the change in volume of heavy isotopes in surface depression storage ($isoS_{SW}$ in m^3):

$$\frac{disoS_{SW}}{dt} = C_{SM}^{18O} Q_{SM} + C_{gmelt}^{18O} Q_{gmelt} + C_P^{18O} P - C_{SW}^{18O} q_{df} - C_{SM}^{18O} q_{dffs} - C_{SW}^{18O} (q_1 + q_{1fs}) \qquad (6.30)$$

Since the mass and water balance is performed each hour, it is assumed that C_{SW}^{18O} is constant and non-fractionating over the timestep, dt. The outflow from surface storage retains the mixed source water composition derived from all inputs (C_{SW}^{18O}), where the mass is moved either into the soil column via infiltration flux (q_{df} and q_{dffs} in cms) or laterally into an adjacent wetland or channel via surface runoff (q_1 and q_{1fs} in cms). The infiltration flux, determined by Philip formula (Equation 4.3; Section 4.1.2) is apportioned into two fluxes, separating contributions to the UZS directly from bare ground infiltration (q_{df}), versus those directly from the snowpack (q_{dffs}). This is an important distinction given it allows for the use of the unique isotopic compositions of the different source waters. Similarly the runoff flux determined by Manning's equation (Equation 4.2; Section 4.1.1) is also apportioned into ponded surface water (q_1) versus direct snowmelt (q_{1fs}).

Using the same procedure as was used for channel routing (Section 6.4), isotope mass inflows and outflows are combined into summation terms, and Equation 6.30 is re-written to solve for the mass of isotopes in storage at the end of the timestep:

$$isoS_{SW,2} = isoS_{SW,1} + \left[\frac{\sum C_{I,1}^{18O} I_1 + \sum C_{I,2}^{18O} I_2}{2} - \frac{\sum C_{SW,1}^{18O} Q_1 + \sum C_{SW,2}^{18O} Q_2}{2} \right] \Delta t \qquad (6.31)$$

Where I_1, Q_1 represent the total inflow and outflow at the beginning of the timestep with mixed compositions $C_{I,1}{}^{18O}$ and $C_{SW,1}{}^{18O}$, respectively; and I_2, Q_2 represent the total inflow and outflow at the end of the timestep with mixed compositions $C_{I,2}{}^{18O}$ and $C_{SW,2}{}^{18O}$, respectively. The concentration of heavy isotopes in surface storage, $C_{SW}{}^{18O}$ (m^3/m^3) is therefore equal to the volume of heavy isotopes per total volume of water, $store_{SW}$ (m^3):

$$C_{SW}^{18O} = \frac{isoS_{SW}}{store_{SW}} \qquad (6.32)$$

which is computed and used to derive the outflows from the surface storage using an iterative application of the above two equations. As in channel routing, the computation of the outflow flux is relaxed within the iterative sequence by an evolving relaxation parameter, θ.

Should there be no surface retention, then the inflows are combined in surface storage and are transferred through the surface storage compartment into the UZS or overland. When there is no surface storage, the left-hand side of Equation 6.30 goes to zero and the mixed isotopic composition of the surface inflows is derived as follows:

$$C_{SW}^{18O} = \frac{\left(C_{SM}^{18O} Q_{SM} + C_{gmelt}^{18O} Q_{gmelt} + C_P^{18O} P - C_{SM}^{18O} q_{dffs} \right)}{(q_1 + q_{1fs} - q_{df})} = \frac{\sum \delta_I I}{Q} \qquad (6.33)$$

which assumes instantaneous and complete mixing. Given the relatively small size of the surface storage, and the knowledge that the runoff components contributing to surface storage are likely turbulent fluxes, this assumption is believed to be reasonable.

In isoWATFLOOD, it is assumed that there is no evaporation directly from the surface storage due to the turbulent mixing of inflows and relatively rapid infiltration, or generation of turbulent surface runoff (IAEA, 1981). Water in depression storage is seldom left in storage (unless on impervious landcover). On occasion when water remains in surface storage (i.e., during heavy rainfall events), evaporative potential is insignificant as a result of high humidities during rainfall.

6.7 Upper Zone Storage: ISOinter

The UZS is a direct link between infiltrating surface waters and the long-term hydrologic residence of water in lower zone storage (LZS). The UZS compartment in WATFLOOD is responsible for controlling the evaporative loss of infiltrated water, and for the mixing of multiple sources of water with varying compositions. In order to correctly constrain individual contributions to streamflow and isotope mass, correct simulation of mixing and evaporative processes within the UZS are necessary.

Once in the subsurface compartment, soil moisture is either 1) drained vertically into the LZS, 2) laterally conducted through the soil matrix as interflow, or 3) evaporated from a saturated, above field capacity, wetting front in the soil column. Figure 6.6 graphically illustrates how isotope mass enter, is stored, and leaves the UZS compartment in isoWATFLOOD. UZS isotope mass balances are performed for each land class: infiltration from each land class' surface storage is passed into the UZS of the same land class.

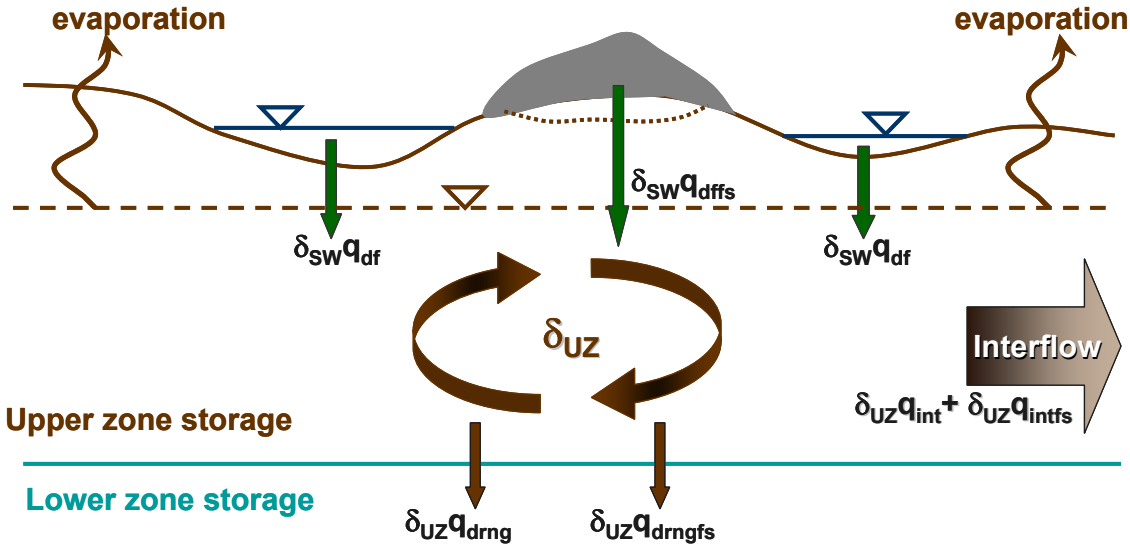

Figure 6.6 – UZS isotope balance in isoWATFLOOD.

In WATFLOOD the depth of water infiltrating into the soil column is controlled by the Philip formula (Equation 4.3; Section 4.1.2), which establishes a wetting front that descends vertically. Water in depression storage on the surface increases the pressure gradient driving the wetting front, increasing the rate of infiltration. The UZS compartment receives the infiltration flux and

the associated heavy isotope mass inputs (q_{df} with variable surface composition $C_{SW}{}^{18O}$, and q_{dffs} with variable snowmelt composition $C_{SM}{}^{18O}$). The isotope mass balance equation describing the change in volume of heavy isotopes in UZS ($isoS_{UZ}$ in m^3) is represented as follows:

$$\frac{disoS_{UZ}}{dt} = C_{SW}^{18O} q_{df} + C_{SM}^{18O} q_{dffs} - C_{UZ}^{18O}(q_{drng} + q_{drngfs}) - C_{UZ}^{18O}(q_{\text{int}} + q_{\text{int }fs}) \qquad (6.34)$$

Since the water-mass balance is performed on a maximum timestep of one hour, it is assumed that $C_{UZ}{}^{18O}$ is constant and non-fractionating between timesteps. The outflows from UZS are assigned the heavy isotope concentration of the UZS post-mixing. Exfiltration fluxes (i.e., q_{drng} and q_{int}) are partitioned to segregate the amount of water derived from snowmelt (i.e., q_{drngfs} and q_{intfs}). Once in the UZS however, there is no difference in heavy isotope concentration between these two fluxes and partitioning is performed only for sensitivity and mass balance purposes.

Using the same procedure methods for channel routing (Section 6.4) and mass transfer through surface storage (Section 6.6), isotope mass inflows and outflows are combined into summation terms and Equation 6.34 is re-written to solve for the mass of isotopes in UZS at the end of the timestep:

$$isoS_{UZ,2} = isoS_{UZ,1} + \left[\frac{\sum C_{I,1}^{18O} + \sum C_{I,2}^{18O} I_2}{2} - \frac{\sum C_{UZ,1}^{18O} Q_1 + \sum C_{UZ,2}^{18O} Q_2}{2} \right] \Delta t \qquad (6.35)$$

where I_1, Q_1 represent the total inflow and outflow at the beginning of the timestep with mixed compositions $C_{I,1}{}^{18O}$ and $C_{UZ,1}{}^{18O}$, respectively; and I_2, Q_2 represent the total inflow and outflow at the end of the timestep with mixed compositions $C_{I,2}{}^{18O}$ and $C_{UZ,2}{}^{18O}$, respectively. The concentration of heavy isotopes in the UZS, $C_{UZ}{}^{18O}$ (m^3/m^3) is represented by the ratio of heavy isotope volume to total water volume, $store_{UZ}$ (m^3):

$$C_{UZ}^{18O} = \frac{isoS_{UZ}}{store_{UZ}} \qquad (6.36)$$

where the solution is again iterative in nature since the outflow depends on the final isotope concentration of the UZS. As in channel routing and surface storage, a relaxed iterative solution technique is used to arrive at the final isotope concentration in the UZS. In isoWATFLOOD the concentration of the UZS is not explicitly a function of depth. A depth-dependent fractionation is indirectly simulated because of near-surface evaporative enrichment that does not affect the lower layers of the UZS (i.e., top of LZS) as was illustrated on Figure 2.5 in Section 2.4.2 (Barnes & Turner, 1998).

Isotope mass in subsurface storage is known to enrich over time from evaporative fractionation at the surface-soil interface (IAEA, 1981). In isoWATFLOOD evaporation is removed post-advective transport (i.e., which acts more quickly). Since turbulent vertical mixing is prevented because of soil porosity and tortuosity, during evaporation a steady-state isotopic profile will begin to form as upwards convective fluxes balance downwards diffusive fluxes (Barnes & Turner, 1998). Evaporation in isoWATFLOOD occurs from the surface-soil boundary when the soil is saturated, as is supported by several other researchers (Dincer *et al.*, 1974; Zimmermann *et al.*, 1967). When soil moisture at the surface becomes unsaturated, the rate of evaporation decreases due to lack of moisture availability and much higher downward diffusive gradients because plants are reserving moisture for consumption (i.e., soil field capacity). Evaporation from soil is considered negligible when water is ponded on the surface (i.e., there is surface storage) since the presence of the water prevents a moisture deficit gradient from being established. Changes in volume during soilwater evaporation are likely, therefore the fraction-dependent series of evaporation equations (Section 6.3) are applied to derive the enriched isotopic composition of the remaining UZS, C_{UZ}^{18O} after the loss of the isotopically depleted evaporative fluxes, C_E^{18O} (i.e., δ_E represented as a mass concentration). The outflow of isotopes from an evaporating UZS is re-defined to include the evaporative fractionation loss:

$$C_{Q,2}^{18O} Q_2 = C_{UZ}^{18O}(q_{drng} + q_{drngfs}) + C_{UZ}^{18O}(q_{\text{int}} + q_{\text{int}\,fs}) + C_E^{18O} q_{ev} \qquad (6.37)$$

To implicitly account for the change in isotopic composition with depth of the UZS, the concentration of heavy isotopes associated with vertical drainage to the LZS is assumed to be unaffected by the near-surface evaporative enrichment. Therefore for vertical drainage the composition of the mixed UZS, C_{UZ}^{18O} (i.e., prior to evaporative enrichment) is used instead (Barnes & Turner, 1998). Similarly the interflow component is typically removed from the UZS when pressure gradients are high and flow is not yet laminar (i.e., prior to evaporative enrichment of soilwater). By assigning variable concentrations to fluxes out of UZS, the model implicitly accounts for depth-dependent concentrations of heavy isotopes. Since the evaporative flux is depleted in heavy isotopes relative to the UZS, the remaining isotope mass in storage enriches during evaporation (Barnes & Turner, 1998).

The fraction-dependent models for evaporation derived by Gibson (2002a) are developed assuming open-water, well-mixed source water conditions. Although it can be assumed that the infiltrate at the surface-soil boundary is reasonably well-mixed given infiltration occurs across a narrow band of depth with a high mechanical gradient (Barnes & Turner, 1998), it cannot be assumed that evaporation from the soil column is analogous to open-water evaporation. The turbulent exchange parameter, η embedded in the kinetic fractionation coefficient (ε_K: Equation 2.8, Section 2.4.2) can be increased to one to account for the added hydraulic resistance when moisture escapes from a soil-atmosphere interface rather than open water-atmosphere interface (Barnes & Turner, 1998). The vapour transport parameter, Θ can also be increased to one to account for higher humidity gradients at the soil-atmosphere interface where vapour becomes trapped by vegetative cover at the boundary layer (Section 2.4.2). The adjustments to both parameters act to increase ε_K during soilwater evaporation to account for tortuosity in the soil column and increased resistance, and therefore increased mass differentiation (Barnes & Turner, 1998).

Implicitly imbedded in the computation of soil-water evaporative fractionation are landcover effects controlling the amount of transpiration from different landcover, or vegetation density. The rate of shallow groundwater recharge is dependent to some extent on vegetative cover (Gonfiantini *et al.*, 1998). Given the isotope mass balance and evaporative fractionation loss is computed uniquely for each landcover in WATFLOOD, there are several possible controls on soilwater fractionation: 1) different partition ratios of evapotranspiration for different landcover types (Section 4.2.4); 2) different evaporative losses from different landcovers (Kouwen, 2007); and 3) different ε_K turbulence and transport parameters (η and Θ).

Once evaporative flux is accounted for in the UZS outflow, the storage continuity balance is recalculated and the non-evaporative portion of isotope mass outflow is passed to the next hydrologic storage compartment.

6.8 Lower Zone Storage: ISOground

Perhaps the most consistent and persistent contributor to streamflow generation is that of the longer-term groundwater storage compartment. This compartment inevitably contributes to streamflow, and typically reflects lower amplitude isotopic and hydrologic signals reflecting highly mixed and homogenized meteoric input compositions from UZS. The LZS behaves as an infinite source, contributing compositions depleted in heavy isotope mass to streamflow and wetland compartments.

The LZS in WATFLOOD is not analogous to deep, regional groundwater, but instead represents a meteorologically-influenced (i.e., through UZS drainage) groundwater storage (Gonfiantini *et al.*, 1998; IAEA, 1981). Groundwater of meteoric origin is typically shallow, locally-derived water that bears the long-term mean composition of precipitation over the recharge area. This classification of groundwater is therefore expected to have a delayed and damped response to meteoric events (IAEA, 1981). Figure 6.7 illustrates the LZS compartment in isoWATFLOOD, including the transfer of mass into the compartment from all UZS land classes, and the baseflow flux (q_{LZ} in cms) removing mass from the compartment. Unlike the surface and UZS, LZS is one large reservoir receiving, mixing and transferring fluxes from one compartment.

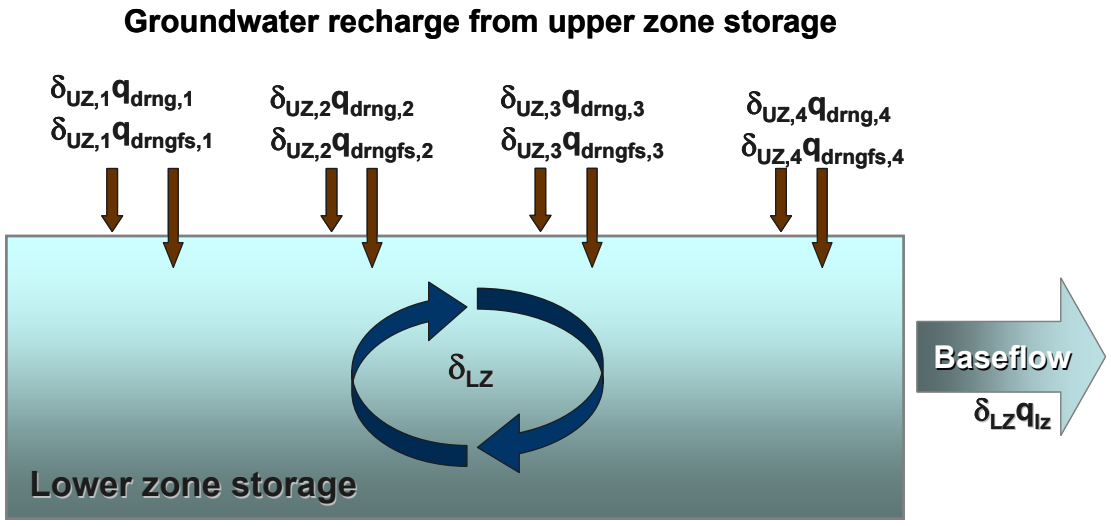

Figure 6.7 – LZS isotope balance in isoWATFLOOD.

The depth of water draining into the lower zone (LZ) is controlled by an empirical storage-discharge power function draining excess water in UZS (i.e., above capillary retention) into the longer-term groundwater storage (Equation 4.6; Section 4.1.3). LZS receives upper zone exfiltrate and an associated mass inflow of non-fractionated heavy isotopes leaving the bottom layer of the UZS (q_{drng} and q_{drngfs} with variable, pre-evaporative UZS composition C_{UZ}^{18O}). Figure 6.7 shows water and isotope mass in the LZ can then either reside in storage or exit laterally via the baseflow flux. The isotope mass balance equation describing the change in volume of heavy isotopes in LZS ($isoS_{LZ}$ in m^3) is represented as follows:

$$\frac{disoS_{LZ}}{dt} = C_{UZ}^{18O}(q_{drng} + q_{drngfs}) - C_{LZ}^{18O} q_{lz} \qquad (6.38)$$

Given there are no evaporative losses from LZS, it is assumed that C_{LZ}^{18O} is constant and non-fractionating between timesteps.

The same mass transfer equations apply to the LZS as were used in surface and UZS to quantify the volume of heavy isotopes in LZS at the end of a timestep ($isoS_{LZ,2}$ in m^3):

$$isoS_{LZ,2} = isoS_{LZ,1} + \left[\frac{\sum C_{UZ,1}^{18O} I_1 + \sum C_{UZ,2}^{18O} I_2}{2} - \frac{\sum C_{LZ,1}^{18O} Q_1 + \sum C_{LZ,2}^{18O} Q_2}{2} \right] \Delta t \qquad (6.39)$$

where I_1, Q_1 represent the total inflow and outflow at the beginning of the timestep with compositions $C_{UZ,1}^{18O}$ and $C_{LZ,1}^{18O}$, respectively; and I_2, Q_2 represent the total inflow and outflow at the end of the timestep with compositions $C_{UZ,2}^{18O}$ and $C_{LZ,2}^{18O}$, respectively. The concentration of heavy isotopes in the LZ, C_{LZ}^{18O} (m^3/m^3) is therefore defined:

$$C_{LZ}^{18O} = \frac{isoS_{LZ}}{store_{LZ}} \qquad (6.40)$$

where a relaxed-iterative solution is required given the outflow depends on the final isotope concentration of the LZS.

Instantaneous and complete mixing of the inflows in the LZ is assumed in isoWATFLOOD. Although physically mixing would not occur instantaneously in the LZS due to the size of the compartment, the effect on isotopic composition of the LZ is relatively minor. This is due to the mechanically-driven mixing in the UZS contributing well-mixed isotope mass inflows to shallow groundwater storage. A possible consequence of this mixing assumption would be the early arrival of event waters in streamflow via the baseflow flux, or a quicker isotopic response to evaporatively enriched recharge water draining into the LZ. Despite the above mixing

assumption being a stretch of physical reality, it is noted that currently accepted groundwater isotopic separations used on tritium for groundwater dating make the same instantaneous and complete mixing assumption (Gonfiantini *et al.*, 1998; Walker & Krabbenhoft, 1998). Furthermore hydrodynamic dispersion within the LZ aquifer is assumed negligible because isotopes are naturally occurring constituents of water. The LZ aquifer is also assumed to be isotropic with no distortion of flow lines (i.e., laminar, uniform flow) (Gonfiantini *et al.*, 1998). Post-routing the isotopic composition of the LZS is assumed to be the same everywhere and constant between timesteps, which is physically realistic. In saturated zones groundwater flow is typically laminar and behaves as flow in an ideal, isotropic porous media (Gonfiantini *et al.*, 1998).

6.9 Wetland Hydrology: ISOwetland

Wetlands are the sustenance of many hydrologic systems, at times sustaining a significant amount of streamflow and providing natural flood attenuation and sediment filtration of surface runoff. Resulting from their importance in the hydrological cycle, many researchers have examined wetland contributions to snowmelt runoff (Hayashi *et al.*, 2004; Falcone, 2007), connectivity and contribution to streamflow generation (Ocampo *et al.*, 2006; Quinton *et al.*, 2003), and their role in nutrient and tracer mixing (Brassard *et al.*, 2000). Owing to their characteristic hydrologic behaviour of prolonged water retention and gradual release, mixing and routing within wetlands is a key component of the isotope transport model.

Wetlands in WATFLOOD are sub-divided into two classifications: channelized fens and flat bogs (Section 4.9). The WATFLOOD wetland hydrology module represents the hydrology of channelized fens that interact directly with streamflow. Fens lining a channel receive all hydrologic storage discharges, including surface water runoff (q_1 and q_{1fs}), soilwater interflow (q_{int} and q_{intfs}) and groundwater discharge (q_{lz}). A mixed and routed wetland discharge (qo_{wet}) contributes to streamflow (under normal flow conditions). During high-flow periods (i.e., channel over-bank) there is a flow reversal where wetland discharge ceases and becomes an inflow of streamflow (i.e., qo_{wet} is a negative flowrate). Figure 6.8 illustrates wetland isotope hydrology in the isoWATFLOOD model.

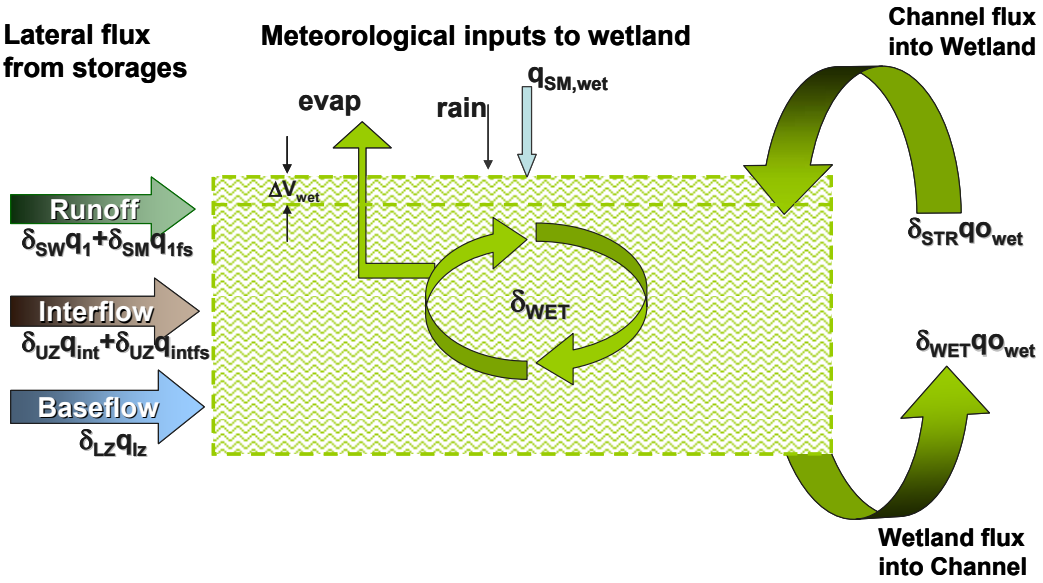

Figure 6.8 – Wetland storage balance coupled with channel interaction in isoWATFLOOD.

Wetlands in isoWATFLOOD receive variable water and mass inflows from rainfall and snowmelt, having isotopic mass compositions C_P^{18O} and C_{SM}^{18O}, respectively. Wetlands also capture and retain all lateral runoff components from surface and subsurface hydrologic storages: runoff, interflow and baseflow. As discussed in previous sections, each lateral flux has its own distinct and variable isotopic composition: C_{SW}^{18O}, C_{UZ}^{18O} and C_{LZ}^{18O}, respectively. Water exits the wetland via the reversible qo_{wet} flux controlled by the relative water level difference between the wetland and adjacent channel (Equation 4.13, Section 4.4). The isotope mass balance equation describing the change in volume of heavy isotopes in wetland storage ($isoS_{wet}$ in m^3) is represented as:

$$\frac{disoS_{wet}}{dt} = C_P^{18O}P + C_{SM,wet}^{18O}q_{SM,wet} + C_{SW}^{18O}q_1 + C_{SW}^{18O}q_{1fs} + C_{UZ}^{18O}(q_{int} + q_{int\,fs}) + C_{LZ}^{18O}q_{lz} - C_{wet}^{18O}qo_{wet} \quad (6.41)$$

where the wetland flux term ($C_{wet}^{18O}qo_{wet}$) is reversible and becomes an inflow when qo_{wet} becomes negative (i.e., representing a channel inflow to the wetland). Equation 6.41 is simplified to solve for the mass in storage at the end of the timestep ($isoS_{wet,2}$ in m^3):

$$isoS_{wet,2} = isoS_{wet,1} + \left[\frac{\sum C_{I,1}^{18O}I_1 + \sum C_{I,2}^{18O}I_2}{2} - \frac{\sum C_{wet,1}^{18O}qo_{wet,1} + \sum C_{wet,2}^{18O}qo_{wet,2}}{2}\right]\Delta t \quad (6.42)$$

The concentration of heavy isotopes in the wetland, C_{wet}^{18O} (m^3/m^3) prior to evaporative fractionation is obtained from the above isotope mass storage relative to total wetland storage (wstore in m^3):

$$C_{wet}^{18O} = \frac{isoS_{wet}}{Wstore} \qquad (6.43)$$

where a relaxed-iterative solution is used to obtain a convergence between the outflow and isotope mass in storage.

Wetlands in WATFLOOD represent large, laminar pools of water in highly saturated regions adjacent to faster-flowing, advection-dominated channels. When water levels are low, transpiration is more dominant than evaporation, acting to reduce water levels within the wetland but not fractionating isotope mass. Evaporation from wetlands however can be substantial when water levels are high (i.e., the wetland behaves more as a lake), and therefore isotopic fractionation must be accounted for in the model. In the water balance, evaporation is removed as a wetland outflow when the wetland storage (wstore) is greater than the natural wetland capacity (wcap), an indicator that the wetland is inundated. Wetland riparian zones are analogous to shallow, laminar, highly vegetated water bodies, where continuous evaporative loss can significantly change the wetland volume and isotopic composition. Therefore Gibson's (2002a) fraction-dependent models (Section 6.3) are used to model the heavy isotope enrichment within wetlands during evaporation (δ_E or C_E^{18O} in mass concentration of heavy isotope).

Similar to the UZS (Section 6.7), evaporative outflows are computed and removed post-routing given advection-dominated flow would occur much more quickly than diffusion-dominated evaporative enrichment. The wetland outflow is recomputed following routing to account for the isotopically depleted evaporative loss (qsw_{evp} in cms):

$$C_{Qwet}^{18O} qo_{wet,2} = C_{wet}^{18O} qo_{wet,2} + C_E^{18O} qsw_{evp} \qquad (6.44)$$

Wetland storage balances are re-computed following the removal of the evaporative flux to capture the resulting evaporative-enrichment effect in wetland storage. The more enriched wetland composition, C_{Qwet}^{18O} is computed from Equation 6.43. The lateral exchange flux between the wetland and the channel reflects the non-evaporated wetland concentration given advection processes are assumed to occur first. Some researchers have found up to a 2‰

enrichment in water in wetland storage post-evaporation (Rodhe & Myberg, 1996), which would largely depend on the water level, synoptic conditions, and amount of vegetative cover.

Wetlands do not always satisfy the open-water, well-mixed assumptions that Gibson's (2002a) fraction-dependent models are derived from. Inflows can be assumed to be well-mixed during normal flow conditions considering they are mixed prior to entering the wetland and along their flowpath, and that they are most typically slow, well dispersed, continuous loadings along the bank of the wetland. In the case of wetland reversal, channel inflows from contributing upstream reaches can also be considered well-mixed in isoWATFLOOD (Section 6.4). Wetlands during channel flooding are routed twice: once as the lateral inflows and meteorological inflows enter, and a second time to mix channel inflows with wetland storage. During evaporation, water near the surface of the wetland would become temporarily more enriched than the lower wetland storage, establishing a non-uniform wetland composition. At the start of the next timestep however, inflows contributing to the wetland (particularly during events) promote advective mixing prior to the computation of wetland discharge, helping to re-establish a more uniform composition. Wetlands with longer residence times and higher porosities can be considered to be generally well-mixed and representative of a single isotopic composition.

Wetland evaporation, and therefore isotopic fractionation, is predominately affected by the height of water in the wetland and the amount of vegetative cover over the wetland. If the water level is sufficiently high, the vegetation becomes submerged and the wetland behaves as an open-water body where approximately 100% of evapotranspiration is evaporative. This is important to distinguish within isoWATFLOOD since evaporation is fractionating, whereas transpiration is assumed to be non-fractionating. Although some of the literature suggests that transpiration can slightly fractionate isotopes, the amount of fractionation is substantially smaller than evaporative fractionation and therefore is relatively inconsequential on such large scales (Sturm *et al.*, 2007b).

During low-water stands (i.e., below wetland capacity), wetland evaporation behaves similar to that of soil-water evaporation. During sustained dry periods where water levels are very low, plant uptake and usage of water (i.e., transpiration) in the wetland matrix dominates over the

fractionating evaporative flux. Therefore evaporation is considered to be negligible and in comparison with transpiration and there is no isotopic fractionation simulated.

During normal water-levels where the wetland is not at capacity and vegetative cover is still very much visible, both evaporation and transpiration are considered significant, making the partitioning of the two processes important (Section 4.2.4). The evaporative component of wetland evapotranspiration is used to fractionate isotope mass, but not quite at the potential of open-water evaporation. The kinetic fractionation parameters are adjusted to account for partial resistance, but not as much as is encountered in saturated soils (Equation 2.9, Section 2.4.2). The turbulence (Θ) and transport (η) parameters are used to increase kinetic fractionation due to increased resistance from vegetative cover and higher humidity at the boundary layer.

Wetlands absorb, filter, and dampen pronounced streamflow fluctuations. Their hydrological function therefore is characterized as a large mixing tank that serves to delay and lessen significant hydrological change.

6.10 Reservoir Routing: ISOlake

Lakes and reservoirs hydrologically function as large storage tanks of water and as wetlands do, regulate downstream hydrologic and isotopic variability. Often lakes are reservoirs with controlled storage/release relationships designed to provide flood attenuation to urban settlements and sustenance of low-flow to sustain fisheries.

In WATFLOOD lakes receive meteoric water and inflows from upstream grids; storing and mixing these inflows with the existing volume of lake water. Open-water evaporation removes water from the lake surface (strloss with isotopic composition δ_E or C_E^{18O} in mass concentration). Figure 6.9 illustrates the isotope mass balance performed over a large area. Lakes are designated as part of the water land classification, and like wetlands, they receive inputs from surrounding grid outflows.

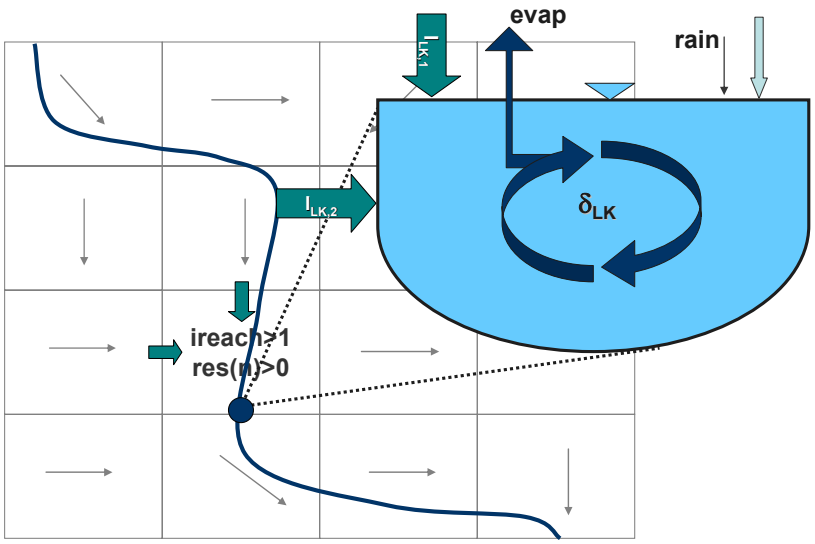

Figure 6.9 – Lake storage isotope balance in isoWATFLOOD.

Lake routing in WATFLOOD is based on a storage-continuity relationship that determines the lake discharge (qo_2 in cms with mass concentration C_{lake}^{18O}) based on the amount of storage (store2 in m^3) within the lake (Equation 4.14 or 4.15, Section 4.5). Mass inflows include meteorological inputs from rain (P with mass concentration C_P^{18O}), direct snowmelt (f_{excess} with mass concentration C_{SM}^{18O}), streamflow from upstream grids (qo_2 with concentrations C_{STR}^{18O} unique to each grid), and lateral inflows from adjacent hydrological storages (q_1 and q_{1fs} with concentrations C_{SW}^{18O} and C_{SM}^{18O}, respectively; q_{int} and q_{intfs} with concentration C_{UZ}^{18O}; q_{lz} with concentration C_{LZ}^{18O}; and qo_{wet} with concentration C_{wet}^{18O}). The inflows contributing to the lake are collected in ISOriver when the next grid in the drainage sequence is defined as a lake grid. Once at the lake outlet, ISOlake is used to route the accumulated mass inflow through the lake via the following isotopic mass balance equation:

$$\frac{disoS_{lake}}{dt} = C_P^{18O}P + C_{SM,water}^{18O}q_{SM,water} + C_{SW}^{18O}q_1 + C_{SM}^{18O}q_{1fs} + C_{UZ}^{18O}(q_{int} + q_{int\,fs}) + C_{LZ}^{18O}q_{lz} + C_{wet}^{18O}qo_{wet} - C_{lake}^{18O}qo_2 \quad (6.45)$$

which can be simplified to solve for the mass in storage at the end of the timestep ($isoS_{lake,2}$ in m^3), after inflows are combined:

$$isoS_{lake,2} = isoS_{lake,1} + \left[\frac{\sum C_{I,1}^{18O}I_1 + \sum C_{I,2}^{18O}I_2}{2} - \frac{\sum C_{lake,1}^{18O}qo_1 + \sum C_{lake,2}^{18O}qo_2}{2}\right]\Delta t \quad (6.46)$$

Lake seasonality is taken into account by adding meteorological inputs with variable isotopic compositions directly to the lake water body. Seasonal changes are reflected in the composition of surface runoff and subsequently subsurface lateral inflows because of continuous modelling and the interconnection between hydrologic storages. The concentration of heavy isotopes in the lake, C_{lake}^{18O} (m^3/m^3) is obtained by the ratio of heavy isotopes accumulated in the lake storage to total volume lake storage ($store_2$ in m^3):

$$C_{lake}^{18O} = \frac{isoS_{lake}}{store_2} \qquad (6.47)$$

The lake outflow is obtained once again using the relaxed-iterative approach given the new lake storage depends on the outflow, which is a function of the concentration of heavy isotopes in storage.

Open water bodies can lose significant amounts of water due to evaporation over extended periods of time; therefore lake water in residence can become characteristically enriched relative to source waters and inflows (IAEA, 1981). Equation 6.45 does not account for isotopic fractionation that occurs during evaporation. In WATFLOOD, lake evaporation is removed at the outlet of the lake (an assumption made by the model), and therefore evaporative fractionation occurs post-routing similar to the UZS and wetland compartments. The total mass outflow equation is defined as:

$$C_{Qlake}^{18O} qo_2 = C_{lake}^{18O} qo_2 + C_E^{18O} strloss \qquad (6.48)$$

where C_{Qlake}^{18O} represents the isotopically enriched surficial lake concentration post-evaporation, as determined by the time-dependent Gibson (2002a) models (Section 6.3). Each of Gibson's (2002a) lake balance models are integrated into the isoWATFLOOD framework to account for variations in the hydrologic behaviour of a lake in a given timestep, including desiccating lakes ($\Sigma I=0$, or no inflow), terminal lakes ($qo_2=0$, or no outflow), lakes where inflows balance outflows and evaporation ($I=Q+E$), and lakes that have a net change in volume ($dV/dt\neq0$).

The ISOlake module simulates a lake of constant isotopic composition, which may not be physically representative when considering lake mixing layers and the effect of the thermocline. Marked horizontal inhomogeneities in isotopic composition are reported for lakes that 'short-circuit', where river inflows do not fully and completely mix with the main lake volume and

instead flow more directly towards the lake outlet. Large lakes with substantial surface-areas and relatively consistent dimensions however tend to be well-mixed laterally due to wind action, and instead vertical inhomogeneities are more the issue. This would apply to the majority of the large Canadian lakes modelled by WATFLOOD. Vertical stratification in temperate-zones, such as Canada, is caused by the formation of thermoclines where warm and cold waters do not mix because of density differences. The isotopic mass composition of the warm epilimnion is reportedly more enriched than that of the deeper, colder hypolimnion because of surface evaporation (IAEA, 1981). Vertical stratification can be accounted for by altering the volume of the lake to simulate only the epilimnic region, or the upper layer where evaporative enrichment occurs. In isoWATFLOOD this is implied given that the lake storage volume is not initialized prior to the start of the simulation, and therefore only the active through-flow (i.e., height above the reservoir boards, or 'new' water contribution) is accounted for isotopically. It should be recognized however that when the epilimnic and hypolimnic layers turn-over, the resultant shift in isotopic composition of the lake water will not be captured by the isoWATFLOOD model.

Given that an average isotopic composition is assumed through the lake depth, but that evaporative enrichment physically occurs only at the upper layers of the lake, discharges are assumed to leave at or near the lake surface where evaporative enrichment has affected the mass concentration. This assumption is not unreasonable if lakes are in fact reservoirs or dams with overflow spillways controlling lake discharge. In the case of natural through-flow lakes, the assumption is still not entirely unreasonable when the hydraulics governing outflow are considered: there is less resistance at the air-water boundary than at the bed-water boundary, yielding higher velocities near the surface. A higher proportion of outflow would therefore be expected from the surface of the lake; the layers subjected to evaporative enrichment.

If a lake is sufficiently large, the isotopic composition of atmospheric vapour over the lake (δ_A) may deviate from the assumed equilibrium with meteoric precipitation (Equation 2.9, Section 2.4.2) because of vapour recycling and mixing with evaporated lake moisture. In order to simulate this process, an atmosphere-lake vapour feedback loop and vapour mixing model would be required in the ISOlake module. Without vapour mixing, large lakes with significant depleted vapour contributions from evaporation would use δ_A compositions (i.e., from

Equation 2.9) that are too enriched in heavy isotopes for δ_E simulations (Equation 2.5), resulting in an over-estimation of isotopic fractionation (i.e., overly-enriched lake water).

Despite its current limitations, isoWATFLOOD it is an improvement upon other isotopic models of lake basins that often neglect overland flow and subsurface leakage, or assume constant isotopic compositions associated with these inflows.

6.11 Chapter Summary

The distinct advantage of modelling isotope mass transfer within the context of a physically-representative hydrological framework is the ability to segregate and simulate changes in both flowpath quantity and composition. This facilitates detailed, mesoscale studies of groundwater and surface-water interactions. Although there has been a need to do so in a physically realistic sense, modelling such complex interactions efficiently across large domains has been a limiting factor. Walker & Krabbenhoft (1998) point out in the concluding remarks of their synopsis of groundwater and surface-water interactions that the idea of assigning one spatially and temporally constant value of groundwater is not sufficient. They emphasize the utility of isotope tracers, but also the need to have more detailed analyses of flowpaths in general. The idea that shallow aquifer systems are directly connected to meteorological inputs highlights even more the need to understand climate change and the sensitivity of modern water resources. The isoWATFLOOD model can support the idea that all hydrological end-members are connected.

Turner & Barnes (1998) point out the need to advance the work of solute transport modelling and the need to integrate catchment-scale isotopic data for model calibration. There is interest therefore in modelling time-varying hydrologic responses not only hydrologically, but also isotopically. The coupling of hydrological and isotopic modelling facilitates accurate source separations and provides a means to verify those contributions. Therefore there are distinct advantages to modelling both water and mass transport simultaneously, preserving spatial and temporal variances.

Before utilizing the model in hydrological studies however, it is necessary to first examine isoWATFLOOD's response to synthetic problems that are designed to diagnose if the model's behaviour is predictable and defensible. The next chapter reports the results of a series of diagnostic tests performed using isoWATFLOOD (Chapter 7). Once the model diagnostics are complete, isoWATFLOOD will be applied to the Fort Simpson Basins, NWT to assess the mesoscale behaviour of the model, and to assess its ability to predict isotopes in streamflow in mesoscale watersheds (Chapter 8). Once the model has been verified in the FSB, isoWATFLOOD will be applied to the Grand River Basin, ON for a second model validation and to perform the first mesoscale hydrological and isotopic variability study using simulated streamflow and isotope data (Chapter 9). In these subsequent chapters, the isoWATFLOOD model will be assessed on its ability to recreate measured streamflow and the isotopic composition of streamflow, as well as its simulation of isotopic changes in hydrologic storage.

Chapter 7

isoWATFLOOD Diagnostics & Performance Metrics

Model diagnostics and performance metrics are designed to inform modellers if engineered models perform in an expected manner, or if there are identifiable problems with the models performance. Performance metrics are engineered, controlled scenarios designed to test the models response against an expected outcome, testing the validity of logical constructs within a model's framework.

Before applying the isoWATFLOOD model to the Fort Simpson Basin (FSB) and Grand River Basin (GRB) datasets, four performance metrics were developed to rigorously and decisively test the models characteristic behaviours. The objective of this chapter is to demonstrate that the isoWATFLOOD behaves as expected under artificially generated scenarios that measure the models response to variable forcing and hydrologic characterizations. The first performance metric tests the model's response to evaporation (Section 7.1); the second tests the model's routing scheme (Section 7.2); the third tests the influence of wetlands (Section 7.3); and the fourth tests the model's routing through reservoirs (Section 7.4). The following performance metrics utilize FSB and GRB basin delineations, but were run using artificial forcings not representative of actual meteorological and hydrological observations.

7.1 Diagnostic 1: Evaporation

A diagnostic test of isoWATFLOOD's response to evaporation and evaporative fractionation was performed. Given that streamflow is the culmination of all the hydrologic storages, isotopes in streamflow were compared for a model simulation with 1) full evaporation (i.e., soil and bog, wetland and stream evaporation), 2) no in-stream evaporation (i.e., strloss=0), and 3) without any evaporation from the stream, wetlands or soil and bog storages (i.e., strloss=qsw_{evp}=ev=0).

The FSB Scotty Creek (~200 km^2) basin was selected for this metric because it is a low-relief (50m of elevation), mild sloping (S_i=0.0032) basin, and has a relatively large percentage of the basin covered by flat bogs with standing water (10% bog; 20% fen) (Hayashi *et al.*, 2004). Given these hydrological and topographical characteristics, the effect of evaporation within this basin is significant.

In the 1997 study period, the spring freshet was complete by early- to mid-June. Commencing shortly after the conclusion of the freshet was the onset of summer evaporation of surface waters. The isoWATFLOOD model was run for the 1997 study period (i.e., April to August); however results will focus on a period from the end of May to the end of July when evaporation was most influential in the basin. Evaporation was controlled (i.e., turned on or off) in the headwater grid of the basin, where the effect was measured at the outlet of the basin (i.e., one grid downstream).

Given that evaporation is a defined outflow, the model is expected to simulate an increase in streamflow from the 'with evaporation' to the 'without evaporation' scenario. Streamflow for the 'with evaporation' scenario should be isotopically more enriched than streamflow 'without evaporation' resulting from reduced mass fractionation. The work of Hayashi *et al* (2004) reported a 1-2‰ evaporative enrichment in Scotty Creek bogs and fens.

Figure 7.1 presents the Scotty Creek streamflow simulations, which indicate differences between the three scenarios during the evaporative season. The isoWATFLOOD model simulates a progressive increase in streamflow from the 'with evaporation' (case a) to 'without wetland evaporation' (case b) and finally to the 'without any evaporation' (case b) scenario, performing as

expected. Figure 7.1 shows that the baseline simulation (with evaporation) represents the lowest streamflow of all three simulations after mid-June, which coincides with the onset of the evaporative season in WATFLOOD. A greater influence of soil and bog evaporation is seen on Figure 7.1, indicating strong evaporative potential from these land classifications. Where no evaporation from soil surfaces or bogs was simulated, streamflow increased by ~11% or 0.14 cms on average. Although channel evaporation affects the water balance, this effect is minimal resulting in a negligible increase in streamflow when 'strloss' not simulated (0.017%).

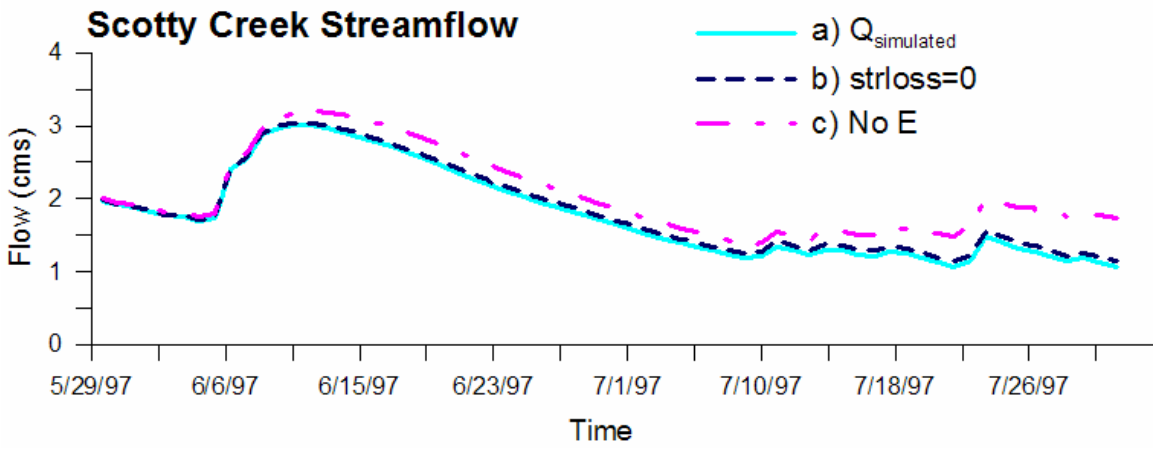

Figure 7.1 – Streamflow simulations for evaporation metric comparing scenarios with a) full evaporation ($Q_{simulated}$), b) no channel evaporation (strloss=0), and c) no evaporation.

Scotty Creek isotopic simulations also performed as expected, simulating a distinct depletion in streamflow isotope composition as evaporation was reduced. Figure 7.2 shows the baseline, full evaporation scenario (case a) where isotopic enrichment relative to the other lower-evaporation scenarios is simulated for Scotty Creek. Isotopic enrichment of streamflow is not considered to be significant (IAEA, 1981) and therefore is not simulated by the isoWATFLOOD model, resulting in no difference between 'case a' and 'case b' scenarios. When evaporation soil and bog storage is shut-off, a distinct depletion of streamflow is observed relative to the 'with evaporation' scenario (case a) (Figure 7.2, case c). Beginning on June 1st, a divergence in streamflow composition is simulated between case 'a' and case 'c'. As summer progresses and the effect of evaporation increases, the depletion of 'case b' relative to 'case a' also increases, approaching a 1.35‰ shift in the isotopic composition by the end of the summer. The isotopic enrichment offset attributable to evaporation is well within the summer enrichments reported by Hayahsi, *et al.* (2004) in Scotty Creek basin.

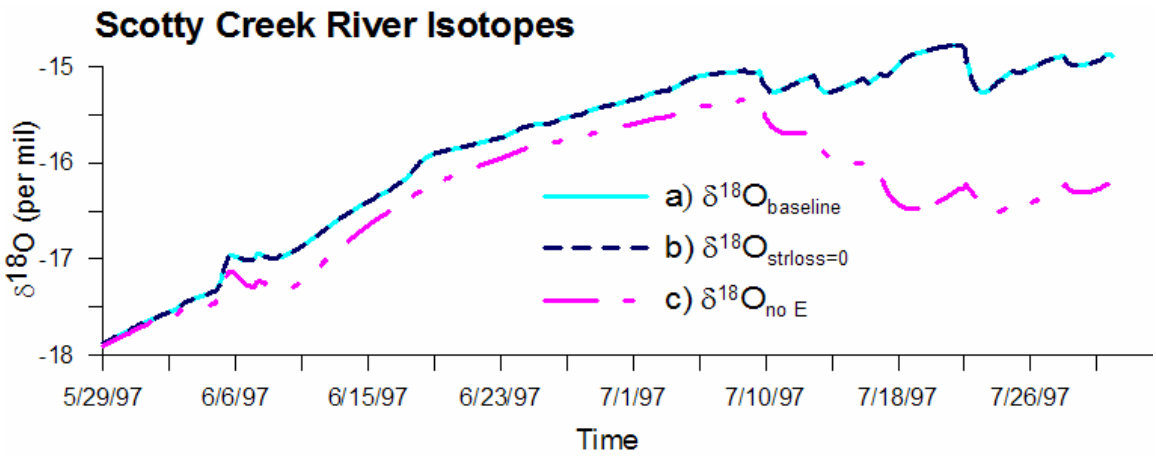

Figure 7.2 – Isotope simulations for evaporation metric comparing scenarios for a) full evaporation, b) no channel evaporation, and c) no evaporation.

The evaporation diagnostic on isoWATFLOOD indicates a predictable and rational model performance with respect to the effect of evaporation on streamflow generation, as well as isotopic enrichment resulting from evaporative loss.

7.2 Diagnostic 2: Precipitation

A diagnostic test of isoWATFLOOD's response to precipitation was performed. Simulated streamflow and $\delta^{18}O$ of streamflow were analysed at the source grid as well as downstream at the basin outlet for the following scenarios: 1) baseline conditions with variable 1997 precipitation with the average summer composition (-15.7‰); 2) continuous precipitation (1mm/hr) applied to the headwater grid at a constant composition of -15.7‰, and 3) continuous 1mm/hr of precipitation applied to the headwater grid with an enriched composition of -10‰.

The FSB's Jean-Marie River (~1,300 km^2) was selected for this diagnostic because it is characterized by average, mild sloping channels (S_i=0.002-0.003), and a total vertical drop of approximately 800 m from the basin headwaters to the basin outlet. Jean-Marie River's most prominent landcover types are transitional re-growth forests recovering from extensive forest fires (i.e., 32%). The basin has a significant amount of forested area (29% deciduous, 23% conifer), and connected-drainage wetland area (14%). It is considered representative of a larger northern Canadian river system and runoff basin.

The isoWATFLOOD model was run for the entire 1997 study period; results are analysed for the post-freshet period (beginning May 1, 1997) when precipitation falls as rain. Constant rainfall was artificially applied to an upland grid in the basin, where the models performance was measured at both the source grid and downstream at the basin outlet. The source grid (n=55) was chosen because it is representative of the average basin landcover distribution, it was an upland grid near the western headwaters of the basin, and because it contributed fully to the basin (100% of its drainage area was within the basin). The model's ability to route increased rainfall-runoff and isotope mass downstream was assessed by comparing seasonal, variable precipitation to two artificially applied continuous rainfall sources (1 mm/hr) with varied isotopic compositions (-15.7‰ and -10‰).

A satisfactory hydrological model performance is an increase in streamflow volume from the variable rainfall (case a) to continuous rainfall scenario. Seasonally variable rainfall will result in a variable streamflow composition, increasing and decreasing in response to the enriched rainfall events. It is expected that the model will simulate continuous rainfall isotopic compositions as a distributed loadings, where isotopic compositions will asymptotically approach the composition of rainfall; reaching a constant composition of streamflow should there be sufficient time in the simulation (Chapra, 1997b). The effect in moving from the headwater grid to the outlet is the same isotopic profile but with a less enriched composition due to mixing along the flowpath with other, more depleted source waters.

The effect of a continuous precipitation source on baseflow was also measured to ensure the correct streamflow response was predicted from correct internal hydrological behaviour. Little or no effect on the isotopic composition of baseflow is expected between 'case a' and 'case b' because there is no change in composition of vertical drainage, only increased volumes of drainage. From the first two scenarios however, an increase (enrichment) in baseflow composition is expected with 'case c' because of the enrichment in rainfall composition; baseflow is expected to asymptotically approach the composition of local precipitation (IAEA, 1981).

Streamflow simulations performed as expected (Figure 7.3), modelling a distinct increase in streamflow at the outlet of the basin with the artificial application of a continuous 1 mm/hr

upland rainfall source. The simulated increase in basin runoff at the outlet due to the excess rainfall was 8.86E+08 m^3 (84 cms) of water from the addition of 8.93E+08 m^3 of rainfall upstream of the outlet. This translates to a net deficit in runoff volume versus rainfall input of approximately 0.6 cms, which is attributed to rainfall on snow covered area.

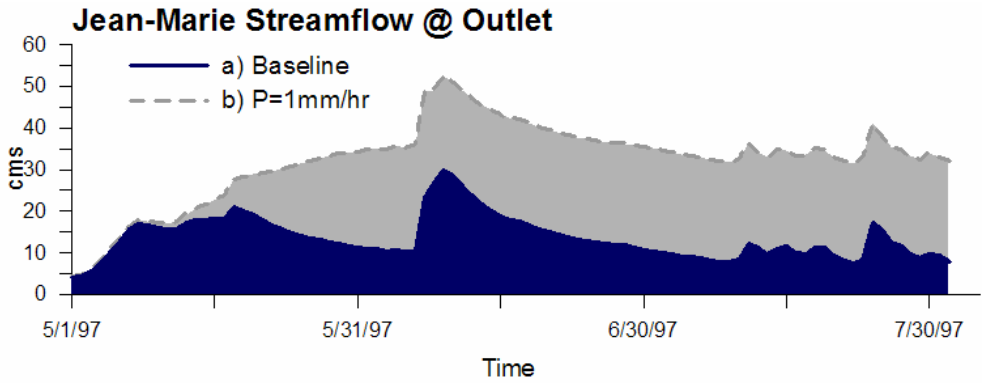

Figure 7.3 – Hydrological response for precipitation metric comparing a baseline simulation to a forced continuous rainfall source of 1 mm/hr rainfall applied to the upland portion of the basin.

The baseline isotopic profile (Figure 7.4) is more depleted and more variable (i.e., in response to rainfall events) than the continuous rainfall scenarios (cases b and c). A quantitative summary of the average isotopic compositions in the source grid, the standard deviation of streamflow composition and simulated minimum and maximum compositions is summarised in Table 7.1.

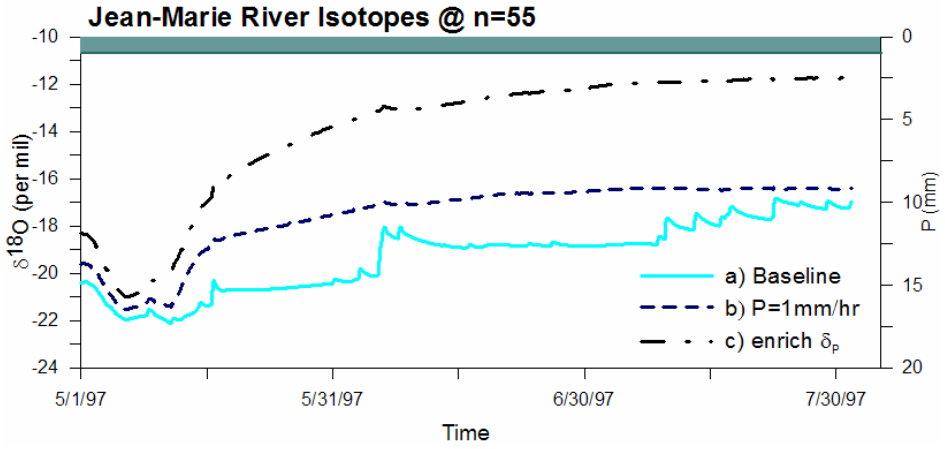

Figure 7.4 – Isotopic response for precipitation metric in source grid comparing a) 1997 measured precipitation, b) continuous rainfall source (1 mm/hr; -15.7‰), and c) continuous rainfall source with enriched isotopic composition (-10‰).

Table 7.1 – Statistical comparison of isotopic simulations for isoWATFLOOD precipitation metric in upland source grid.

	a) Baseline (‰, VSMOW)	**b) Constant P (1 mm/hr) (‰, VSMOW)**	**c) Enriched $\delta^{18}O_{rain}$ (‰, VSMOW)**
$\delta^{18}O_{rain}$	-15.7	-15.7	-10
Average $\delta^{18}O_{stream}$	-19.793	-18.368	-15.417
$\Delta\delta^{18}O_{stream}$*	+2.28	+2.83	+7.51
$\Delta(\delta^{18}O_{stream} - \delta^{18}O_{rain})$	-1.15	-0.69	-1.72

* Difference between April 1st, 1997 and August 1st, 1997 compositions of streamflow

The baseline scenario (case a) simulated a +2.28‰ enrichment in isotopic composition from April 1st to August 1st, and an offset of the most enriched streamflow composition relative to meteoric water of –1.15‰. The continuous rainfall with average meteoric composition (case b) is visibly more enriched than 'case a' and attains a constant isotopic composition that asymptotically approaches a composition close to meteoric rainfall (–0.69‰ difference). The depletion of this constant composition relative to meteoric water is most likely the influence of baseflow and fen discharge. A significantly more enriched constant composition is attained with the enriched rainfall source (case c) relative to both previous scenarios, however, the same isotopic profile as 'case b' is simulated, as expected. The isotopic composition of streamflow did not fully reach the enriched composition of rainfall (–1.72‰ difference), which is attributed to an increased depletion-potential of baseflow and fen discharge relative to enriched meteoric waters. It is apparent from Figure 7.4 that streamflow is highly responsive volumetrically and isotopically to meteoric water inputs. It should be noted however that enriched rainfall events analogous to 'case c' would in reality be much shorter in duration (and therefore smaller in volume), therefore having less impact on streamflow compositions.

Figure 7.5 verifies that there is no change in isotopic profile in response to an increase in runoff volume (but not composition) from 'case a' to 'case b'. When the isotopic composition of rainfall is enriched however, then baseflow compositions enrich, tending towards a constant composition closer to that of the meteoric water input composition (case c).

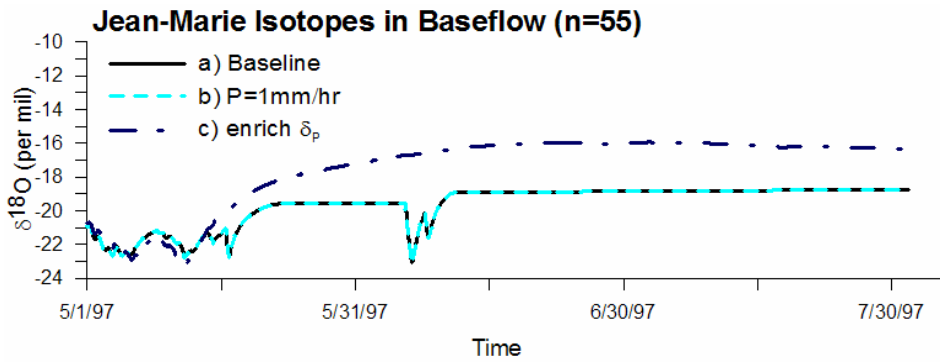

Figure 7.5 – Isotopic baseflow response for precipitation metric in the source grid for a) baseline scenario, b) continuous rainfall source of 1 mm/hr (-15.7‰), and c) more enriched continuous rainfall source of -10‰.

At the basin outlet, Figure 7.6 shows that the effect of the upland rainfall is in fact routed to downstream grids. The isoWATFLOOD model performs as expected by routing the excess rainfall mass contributions to streamflow in 'case b' and 'case c' to the basin outlet. The 'case b' isotope profile represents a distributed loading conveyed downstream from the continuous upland rainfall. The 'case c' isotope profile also exhibits the distributed loading behaviour, but also reflects the enriched meteoric composition of rainfall relative to 'case a' and 'case b' profiles.

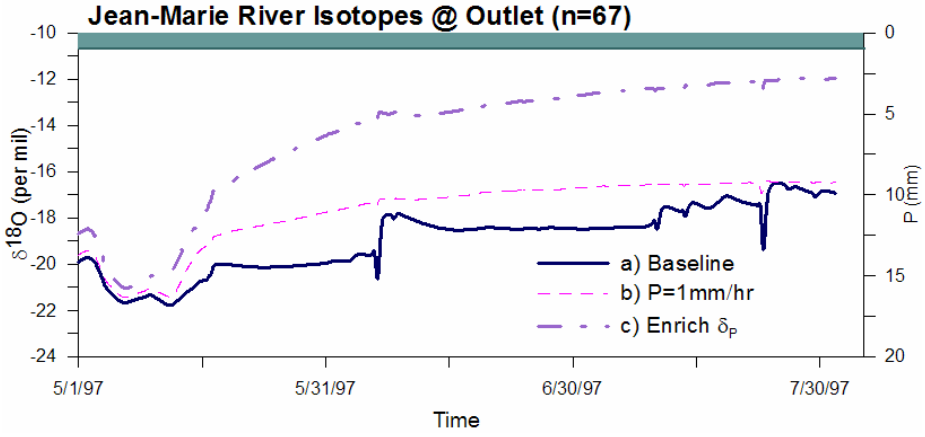

Figure 7.6 - Isotopic response to precipitation metric at the basin outlet to a) 1997 measured precipitation, b) continuous rainfall source (1 mm/hr; -15.7‰) in upland source grid, and c) continuous rainfall source with enriched isotopic composition (-10‰).

From upstream to downstream, the isotopic composition remains relatively consistent for all scenarios when Table 7.2 is compared to Table 7.1.

Table 7.2 – Statistical comparison of isotopic simulations for isoWATFLOOD precipitation metric at Jean-Marie outlet.

$\delta^{18}O$ (‰)	**a) Baseline**	**b) Constant P (1 mm/hr)**	**c) Enriched $\delta^{18}O_{rain}$**
$\delta^{18}O_{rain}$	-15.7	-15.7	-10.0
Average $\delta^{18}O_{stream}$	-19.511	-18.521	-15.893
$\Delta\delta^{18}O_{stream}$*	+2.20	+2.67	+7.19
$\Delta(\delta^{18}O_{SS} - \delta^{18}O_{rain})$	-0.77	-0.72	-1.94

* Difference between April 1st, 1997 and August 1st, 1997 compositions of streamflow

Figure 7.7 compares the evolution of the upstream isotopic profile in response to the continuous rainfall source (-15.7‰) with the isotopic profile seen at the outlet of the basin for the same source. The two profiles exhibit similar trends in response to the rainfall source The outlet profile (n=67; case b) however is delayed relative to the upstream (n=55; case a) profile, indicating that isotope mass is being advected downstream to the basin outlet with a slight delay in transit time, as is expected. Figure 7.7 also shows that the upland source grid (case a) is slightly more enriched than the outlet profile (case b) attributable to the basin outlet being the combination of isotopic profiles from all upstream grids.

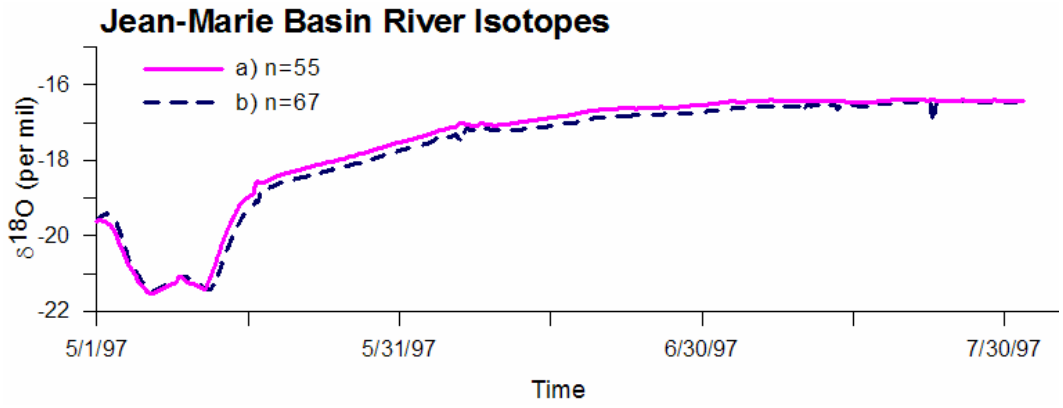

Figure 7.7 – Comparison of isotopic response to continuous rainfall source of -15.7‰ between the upland source grid and downstream basin outlet for the isoWATFLOOD precipitation metric.

The results of the precipitation diagnostics indicate a predictable and realistic model response to a continuous, constant volume rainfall, and to a significant enrichment in the composition of continuously falling rainfall.

7.3 Diagnostic 3: Wetlands

A diagnostic of isoWATFLOOD's response to wetland hydrology was performed. Isotopes in streamflow and baseflow were compared for two simulations, 1) with wetland routing to simulate channelized fens, and 2) with no wetland routing, where channelized fen land classes were functionally treated as flat bogs.

The Scotty Creek watershed was also used for this performance metric in part to further ensure the performance metrics from evaporation are verifiable with the wetland metrics. The Scotty Creek Basin was, however, primarily selected for this metric because of it's high percentage of wetlands and it's low-gradient channel network that encourages hydrologic interaction between channelized fens and the channel.

The isoWATFLOOD model was run for the 1997 study period; once with full wetland hydrologic routing to establish a baseline for the Scotty Creek Basin, and again without wetland routing. With wetland hydrology, total wetland area is segregated into flat bogs and channelized fens. As outlined in Section 4.9, the flat bog classification does not hydrologically interact with the channel, but instead transfers water vertically into upper and lower zone storage. In contrast, channelized fens directly interact with the channel by receiving all lateral surface and subsurface runoff components and releasing them more gradually into the channel via a reversible interaction flux. Results of each simulation were compared at the outlet of Scotty Creek basin to evaluate the basin-wide impact of the different wetland classifications.

It is expected that the elimination of channelized fens will produce 'flashier', quick response flows that result in higher amplitude streamflows. The isotopic profile however is expected to change seasonally: following the spring freshet, streamflow composition without fens should be more depleted relative to with fens because of increased direct snowmelt runoff. As summer progresses and evaporative fluxes increase, decreased enrichment without fens would be expected because of lower evaporative enrichment of the inflows contributing to streamflow.

A comparison of simulated streamflow shows that the model simulates a flashier, higher amplitude hydrograph without the presence of channelized fens (Figure 7.8). Without fens, a

60 mm increase in depth of runoff was simulated at the basin outlet due to the absent fen storage capacity. An average baseflow increase of 0.03 cms without fens was simulated and is attributed to a higher volume of drainage into lower zone storage. Whether wetlands are entirely responsible for the simulated increase in streamflow in reality can only be determined through the observation of measured streamflow responses to storm or freshet events. The 'with wetland' hydrograph shows not only a damping of streamflow response, but also a prolonged streamflow recession following event water contributions. As channel levels decrease during low-flow periods (i.e., the end of June), discharge from fen storage increases (Equation 4.13, Section 4.4), sustaining the hydrograph.

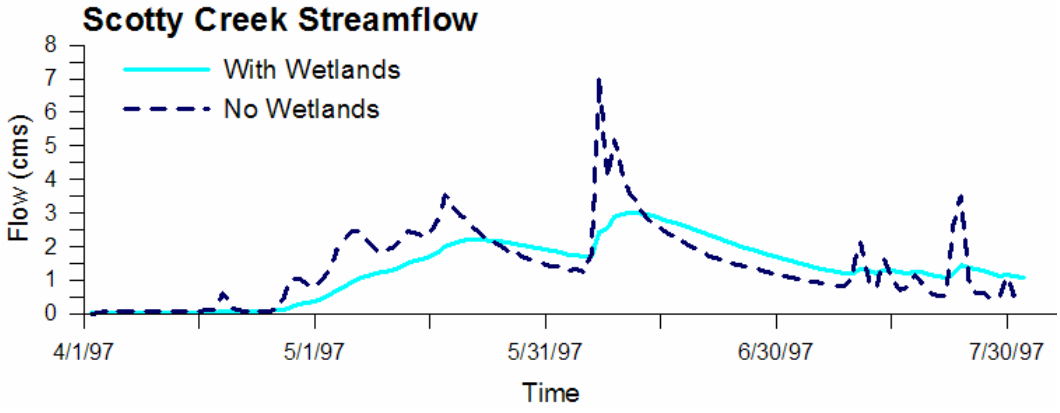

Figure 7.8 - Hydrological response to wetland metric comparing simulations 'with' and 'without' connected wetlands.

The freshet isotopic response shown on Figure 7.9 indicates streamflow isotopic enrichment (by ~8‰) from the 'with wetland' to 'without wetland' scenario, counter to the expected response. Without wetlands, snowmelt is released directly into the channel and is followed by a freshet rainfall event that directly enriches streamflow. With the influence of wetlands, streamflows remain depleted for a longer period of time, gradually releasing retained snowmelt contributions. The 'with wetland' simulation is observed to dampen streamflow response to direct meteoric precipitation (i.e., the early May freshet rainfall) by more gradually responding to source water composition changes.

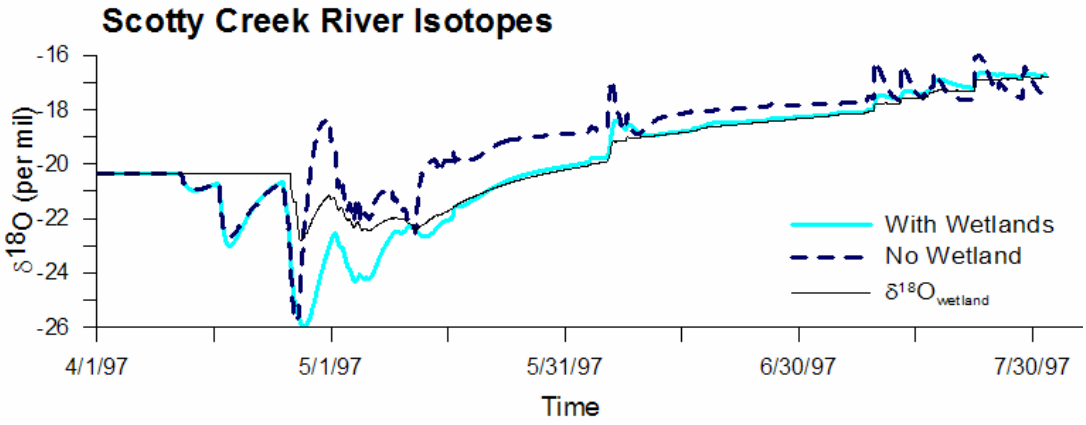

Figure 7.9 - Isotopic response for wetland metric comparing 'with' and 'without' connected wetland scenarios.

As summer progresses, streamflow compositions 'with' and 'without wetlands' begin to converge to the simulated wetland composition (Figure 7.9). The 'without wetlands' isotopic profile however is more responsive to meteoric events, and maintains a visibly more enriched profile than the 'with wetlands' composition because of the influence of enriched bog storage. The addition of wetland hydrology to the model results in a prolonged, indirect snowmelt contribution to streamflow through fen discharge, and a damped response to event water contribution in general. Interestingly, during the late summer between rainfall events, 'with wetland' compositions become more enriched than 'without wetland' (i.e., bog-dominant) compositions. This result is reflecting the reduction in bog evaporation from lack of water availability between event water contributions.

The isoWATFLOOD model simulates a prolonged, depleted meltwater contribution when channelized fens are present in the model. Although not initially expected, this result is supported by the literature that classifies fens as primarily baseflow dominant receiving inputs from subsurface drainage (Hayashi *et al.*, 2004; Quinton & Roulet, 1998; Woo, 1988; Zoltai *et al.*, 1988), whereas bogs are meteorically-driven with compositions reflecting short-term event water signatures (Hayashi *et al.*, 2004; Woo, 1988; Zoltai *et al.*, 1988). The 'with wetland' simulations were shown to lower both streamflow and isotopic amplitudes, damping responses to runoff events. Without the presence of channelized fens, both hydrograph and isograph responses were more reactive, with sudden and more pronounced changes to flow and isotopic composition.

7.4 Diagnostic 4: Reservoir Routing

A diagnostic test of isoWATFLOOD's ability to route flow and simultaneously transfer isotope mass through a controlled reservoir was performed. Since the FSB does not contain any controlled reservoirs, the GRB was used for this diagnostic test. Simulated streamflow and isotopes were compared at two gauges in a sub-basin of the GRB: Canagaguige Creek, which contains a controlled reservoir. The first gauge is located upstream of the reservoir, whereas the second gauge is downstream of the reservoir; the comparison between the two gauges enables the model's routing response to be evaluated.

The Canagaguige Creek sub-basin lies in the central portion of the GRB and contains the Woolwich reservoir, just north of the town of Elmira, ON (Figure 7.10).

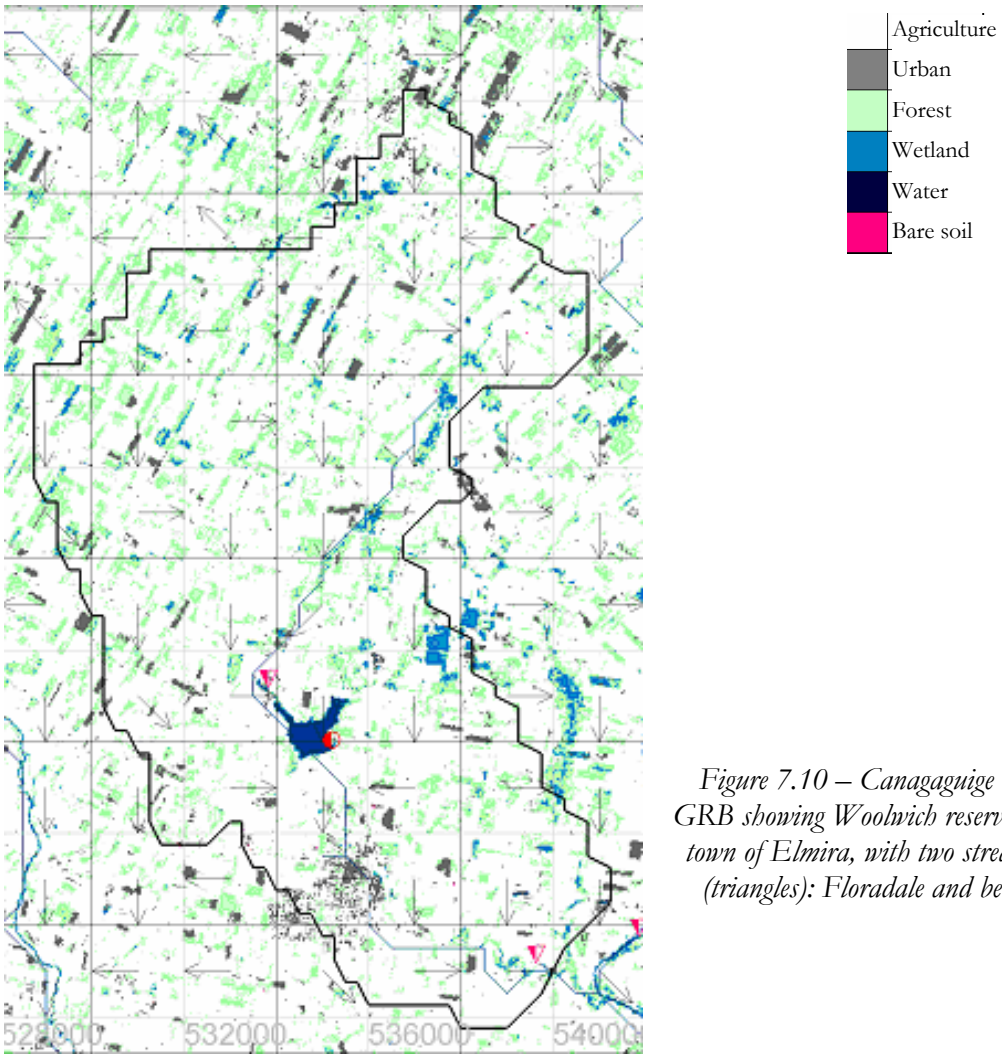

Figure 7.10 – Canagaguige Creek in the GRB showing Woolwich reservoir north of the town of Elmira, with two streamflow gauges (triangles): Floradale and below Elmira.

The Canagaguige Creek basin (116 km^2) is representative of the central GRB with the majority of the basin used for agriculture (~86%) and woodlot (~10%), and with only a small proportion of wetland (fen) (2%), bare soil (1%) and urban (1%) area. The headwaters of Canagaguige Creek are characterized by a steeply sloping (S_i=0.01-0.02 m/m), incised channel. In the central and lower portions of the basin, the relief shallows and the channel is mildly sloping (S_i=0.002-0.003 m/m) to the outlet. Elevation decreases from north to south in the sub-basin, with a total drop of 110 m in the short distance from the headwaters to the creek outlet (~16 km^2 straight-line).

The study period used for this diagnostic was the first full year of simulation, beginning in early January 2004 and ending late December 2004. The model was run continuously for the entire GRB from October 2003 (spin-up) until late December 2004.

Simulations are expected to show both a hydrologic and isotopic delay between the upstream and downstream reaches of Canagaguige basin. Given the relatively small drainage area of the sub-basin, streamflow show the same characteristic response to event flows at both gauges. The downstream flows, given the influence of reservoir regulation, should show a damped and delayed response in comparison to upstream event-based responses. Isotopically it is difficult to predict the expected outcome without first knowing whether the reservoir is gaining (increasing storage) or losing (decreasing storage), and what dominant end-members are contributing to lake storage. Given the substantial surface-area of the reservoir (Figure 7.10), the influence of isotopically-depleted snowmelt should dominate spring and early summer reservoir storages, resulting in a more depleted downstream isotopic composition of streamflow relative to upstream. In the late summer however, when reservoir storage is decreasing because of evaporative loss, there should be a slight enrichment in the isotopic composition of downstream streamflow relative to upstream flow.

Simulation of streamflow in Canagaguige Creek shows that streamflows below Elmira (1.797 cms) are greater than those upstream of Elmira (0.966 cms) (Figure 7.11); however, average flow per unit drainage area is actually less downstream of the Woolwich reservoir according to Table 7.3 (0.015 cms relative to 0.017 cms upstream).

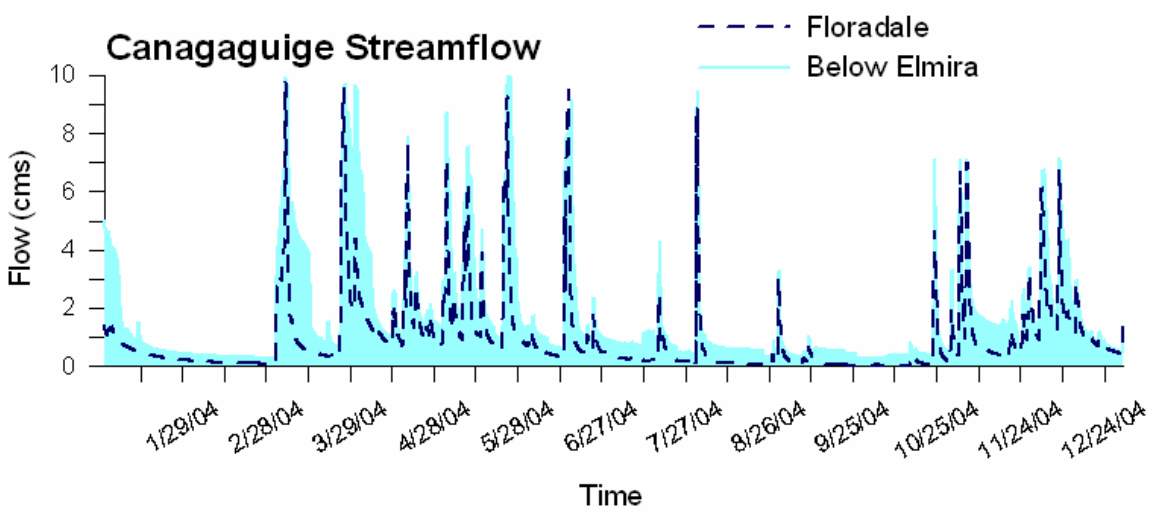

Figure 7.11 – Hydrologic response to reservoir routing metric, comparing flows upstream (Floradale) and downstream (below Elmira) of the Woolwich reservoir.

Table 7.3 – Statistical summary of hydrologic simulation during reservoir routing metric.

Flow (cms)	**Floradale**	**Woolwich Outflow**	**Below Elmira**
Drainage area (km^2)	56	n/a	116
Average (Average/km^2)	0.966 (0.017)	0.791	1.797 (0.015)
Standard deviation (σ)	1.608	1.483	2.564
Minimum	0.034	0.000	0.271
Maximum	26.09	25.22	32.476

The downstream hydrograph (Below Elmira) shows a prolonged recession curve in comparison with the quick-response, storm-flow response of the upstream flows at Floradale (Figure 7.11). The minimum simulated flow increases from upstream (0.034 cms) to downstream (0.271 cms), indicating higher low-flows at the downstream gauge. Downstream variability (i.e., standard deviation and maximum discharge) is shown to increase relative to upstream and reservoir outflows because peak flow (i.e., maximum flow) increases.

Analysis of simulated flow frequency confirms that average and peak flows are higher below Elmira and that lower flows are more frequent upstream of the reservoir at Floradale (Figure 7.12). Overall the spread in the distribution of downstream flows is less than the spread visible for upstream flows. The model provides an accurate physical representation of hydrological alteration resulting from a reservoir supplementing downstream flows in a channel.

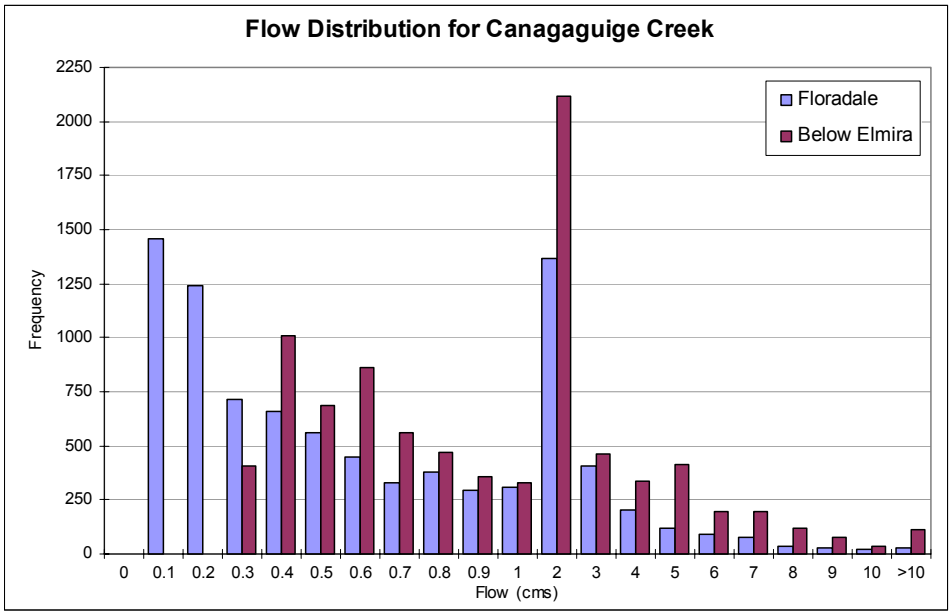

Figure 7.12 – Distribution of simulated streamflow before and after Woolwich reservoir for reservoir routing metric.

Canagaguige Creek flow isotopically enriches (on average) from upstream to downstream (Table 7.4). Perhaps counter-intuitively, Figure 7.13 shows streamflow below Elmira is more enriched during winter and late fall, and more depleted during the summer periods relative to upstream Floradale compositions. This is the result of the Woolwich reservoir supplying discharge to downstream reaches that is the mixture of current and previous season contributions (i.e., during the summer, predominately snowmelt; and predominately evaporatively enriched water during the fall and winter). Both Figure 7.13 and Table 7.4 show the reservoir has a smoothing effect on the downstream 'below Elmira' isograph, decreasing the amplitude and standard deviation of downstream isotopic variations. This damping effect was expected.

Table 7.4 – Summary of isotopic simulation for reservoir routing metric.

$\delta^{18}O$ (‰)	Floradale	Woolwich Reservoir	Below Elmira
Average	-9.264	-9.769	-9.094
Standard deviation (σ)	1.686	0.416	1.309
Minimum	-16.640	-10.960	-14.293
Maximum	-4.600	-9.183	-5.775
$\Delta\delta^{18}O$ (Jan 31 to Sep 1)	-1.10	+0.54	+1.00

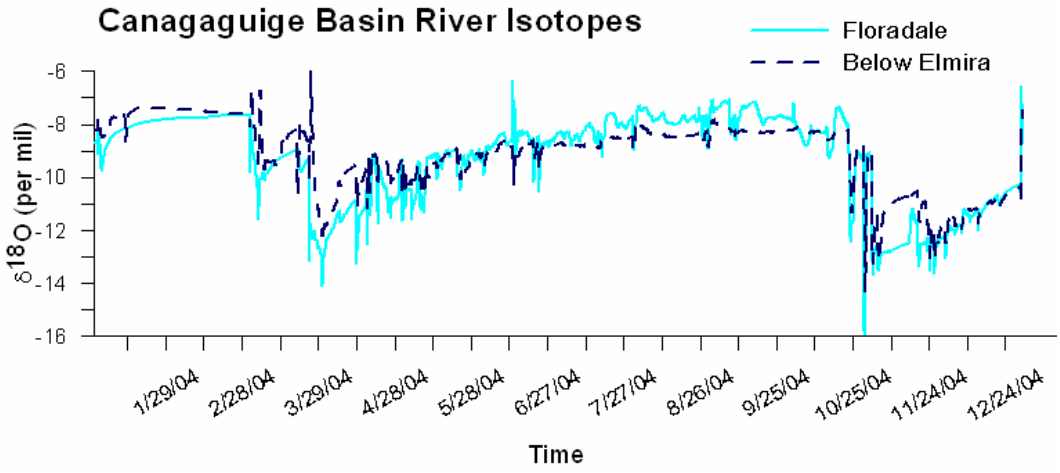

Figure 7.13 –Isotopic response before (Floradale) and after (below Elmira) Woolwich reservoir for reservoir routing metric.

Figure 7.14 illustrates that simulated Woolwich reservoir volumes increase during the spring and early summer of 2004, coinciding with the depletion in 'below Elmira' compositions relative to the upstream Floradale isotopic profile. This supports the notion that the depletion is the result of a gradual release of snowmelt-depleted water stored in the reservoir to the downstream reaches of Canagaguige Creek.

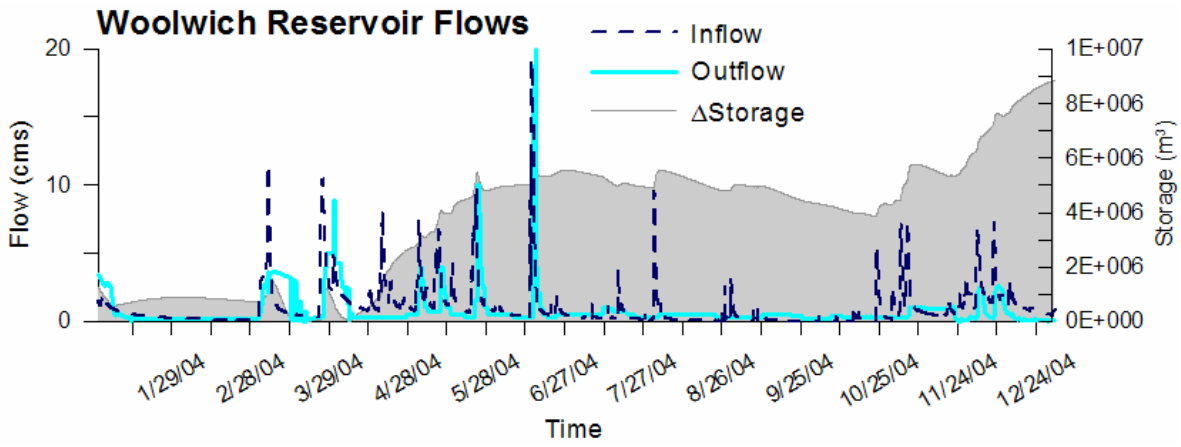

Figure 7.14 – Simulated reservoir hydrologic response for reservoir routing metric.

Figure 7.15 illustrates the distributions of $\delta^{18}O$ in streamflow between the upstream (Floradale) and downstream (below Elmira) gauges. The distribution supports previous results (Table 7.4; Figure 7.13) that found the downstream gauge (below Elmira) gauge to be more frequently enriched relative to upstream compositions. Figure 7.15, however, also shows that the most

frequently occurring composition at the downstream gauge is more depleted (-8‰) than the most frequently occurring composition upstream (-7.5‰), which is a reflection of the snowmelt contribution from Woolwich reservoir to the downstream gauge. The comparison of distributions highlights the smaller variation in composition in the downstream reach (i.e., narrower distribution) resulting from the regulatory effects of the reservoir.

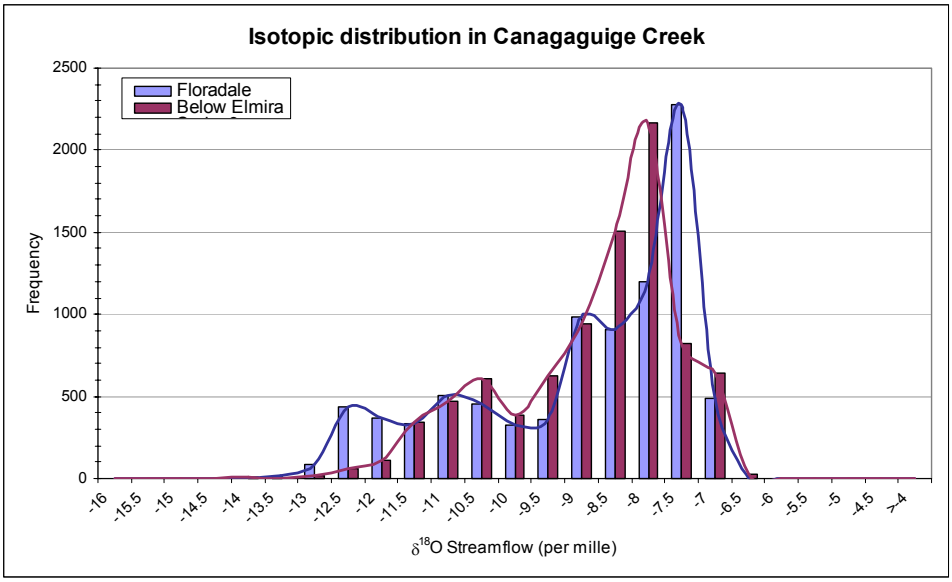

Figure 7.15 – Distribution of $\delta^{18}O$ upstream and downstream of Woolwich reservoir for reservoir routing metric.

The model responds in a physically realistic manner to the presence of a reservoir within the Canagaguige basin. The model simulated lower downstream hydrologic and isotopic variability because of the reservoirs influence. Isotopically, the reservoir enriched winter and fall downstream compositions, and depleted summer compositions because of seasonally-variant dominant end-members contributing to reservoir storage.

7.5 Chapter Summary

Performance metrics are a useful tool for modellers during model development. Utilizing a systematic and quantitative methodology, the modeller is able to diagnose problem areas with respect to the model's behaviour in response to controlled scenarios. By forcing a number of false scenarios with predictable outcomes, it is possible to assess the model's representativeness.

This chapter has shown that the isoWATFLOOD model performs in a predictable and rational manner in response to four diagnostic tests. The models performance during each metric was quantitatively evaluated both hydrologically and isotopically. For each diagnostic, only the models ability to simulate a physically realistic and expected response to a varied forcing was assessed, and not the models ability to accurately simulate measured streamflow and isotopic data.

Given the isoWATFLOOD model performed as expected in response to these four diagnostic tests, it will now be applied to the FSB (Chapter 8) and GRB (Chapter 9) for calibration, validation, and verification studies. The model's ability to reproduce measured streamflow and $\delta^{18}O$ of streamflow data will be assessed in the subsequent chapters of this thesis. Chapter 8 will focus on the FSB where the isoWATFLOOD model will be both calibrated (i.e., 1997 dataset) and validated (i.e., 1998 and 1999 data sets). Chapter 8 will also verify the isotopic variation within each hydrologic storage compartment, evaluating the model's physical representativeness of internal hydrological processes. Chapter 9 applies the model to the GRB without recalibration to validate the model's robustness in mesoscale isotopic simulation, and utilizes the model in a mesoscale variability assessment study. The intent is to design a model capable of reproducing the $\delta^{18}O$ of streamflow in mesoscale basins, and in the process of doing so, better constrain model parameterizations through the rigorous coupled hydrologic-isotopic approach to modelling.

Chapter 8

Validation & Verification of isoWATFLOOD

Reliable tools for modelling are required to offer insight into mesoscale hydrological processes, process interactions and water resource allocations. Traditional hydrological models are adequate when studying the magnitude of hydrologic variability, but they fall short of informing users about the reasons for variations in streamflow generation. In a recent study, Vázquez *et al.* (2008) suggested a multi-criteria protocol should be used to evaluate hydrological models, noting that the analysis of flow components in model calibration enhances the physical consistency of model predictions. Maneta *et al.* (2008) evaluated a hydrological simulation using separation of flow sub-components, and found that although hydrographs were well replicated; internal parameterizations were not well represented. In an attempt to *verify* runoff generation mechanisms, stable water isotopes have been utilized as natural environmental tracers because they preserve hydrologic information over expansive domains and time scales. Recent focus has been on developing models capable of simulating isotopic responses to atmospheric and hydrological change within existing model frameworks. Several atmospheric and coupled atmosphere-land surface models have successfully simulated stable water isotopes in meteorology and energy-water balance cycling for the purposes of better defining and diagnosing atmosphere-land-surface hydrologic cycling. A natural next step is to now shift the focus onto the cycling and storage of isotopes on the land surface to investigate their movement across landscapes.

The isoWATFLOOD model has been developed to progress mesoscale hydrological modelling calibration and validation capabilities by further constraining simulations using the isotopic composition of streamflow. Streamflow $\delta^{18}O$ is far more sensitive to hydrological change than flow data, and their accuracy depends entirely on the correct apportioning of sub-component contributions to streamflow.

In this chapter, isoWATFLOOD is calibrated using measured streamflow and isotope data and validated using two non-calibration period events. Rigorous verification of simulated sub-process contributions to streamflow from hydrologic storage is also undertaken. This chapter presents the results for the model calibration in the Fort Simpson Basin (FSB) for the 1997 event (Section 8.1). During model calibration, the issue of equifinality in streamflow simulation is addressed through the analysis of two equal streamflow simulations with contrasting internal parameterizations. Prior to the development of isoWATFLOOD, intuitive reasoning (using time series plots of state variables) was relied upon to evaluate simulation correctness. The application of isoWATFLOOD, however, is shown to indicate highly contrasting simulations of $\delta^{18}O$ (Section 8.1.1). The model is then validated with the 1998 and 1999 events for its ability to reproduce streamflow and $\delta^{18}O$ in streamflow in the FSB (Section 8.2). Following both calibration and validation of the model, a continuous simulation from October 1996 to December 1999 is used to analyse hydrologic and isotopic variability (Section 8.2.3). Verifications of $\delta^{18}O$ variations during evaporation and in hydrologic storage were conducted using the three-year continuous simulation (Sections 8.3 and 8.4).

The objectives of this chapter are therefore to ascertain if isoWATFLOOD can:

1. Accurately reproduce streamflow in remote, mesoscale watersheds using a partially physically-based, computationally efficient model;
2. Identify and constrain correct physical representations of internal hydrological processes that provide more physically-based representations of streamflow;
3. Accurately reproduce $\delta^{18}O$ variation in streamflow across mesoscale domains; and,
4. Identify external and internal hydrologic changes producing variations in both streamflow quantity and composition.

This chapter demonstrates that the coupling of isotopic and streamflow simulation is a practical and useful methodology for mesoscale hydrological model calibration, providing a new level of certainty in model validation.

8.1 Model Calibration

In keeping with WATFLOOD's efficiency philosophy, new parameterizations were minimized in the development of isoWATFLOOD; only isotopic initialization parameters were added. These parameters describe the isotopic composition of rainfall and snowmelt, the initial compositions of hydrologic storages (i.e., river water, soilwater and baseflow), and the offset due to fractionation occurring during melting and refreezing ('isotope.par'; Appendix A.2.2). Isotope initializations for the FSB were derived from measured data reported by St. Amour *et al.* (2005).

During the calibration study, isoWATFLOOD was run continuously from April 1997 to August 1997 to simulate streamflow, HS of streamflow (Tracer 4: surface runoff, interflow and groundwater flow), and corresponding $\delta^{18}O$ compositions. Initially, parameters from the FSB baseflow separation study (Section 5.4) were used with isoWATFLOOD, yielding the pre-calibration simulation. Modifications to the WATFLOOD model between the time when that study was published (i.e., 2005) and when isoWATFLOOD was fully developed (i.e., 2007) resulted in the isoWATFLOOD pre-calibration simulation exhibiting poorer fits to measured streamflow in the FSB (i.e., Figure 8.1 compared with Figure 5.19).

Although simulated flows did not replicate measured flows as well as they had previously (on Figure 5.19), they were reasonably representative of both the timing and volume of measured streamflows in each of the five FSBs. In all basins the timing of spring freshet contributions to streamflow was captured, as was the volume of streamflow generated from the melt events. Summer rainfalls however were generally poorly captured by the model. Jean-Marie and Scotty Creek River basins simulated the summer rainfall event in early June, whereas in the other three basins (i.e., Martin, Birch and Blackstone Rivers), summer flows were substantially under-predicted and the streamflow response to the early June rainfall event was not simulated. This phenomenon is also represented on Figure 5.19.

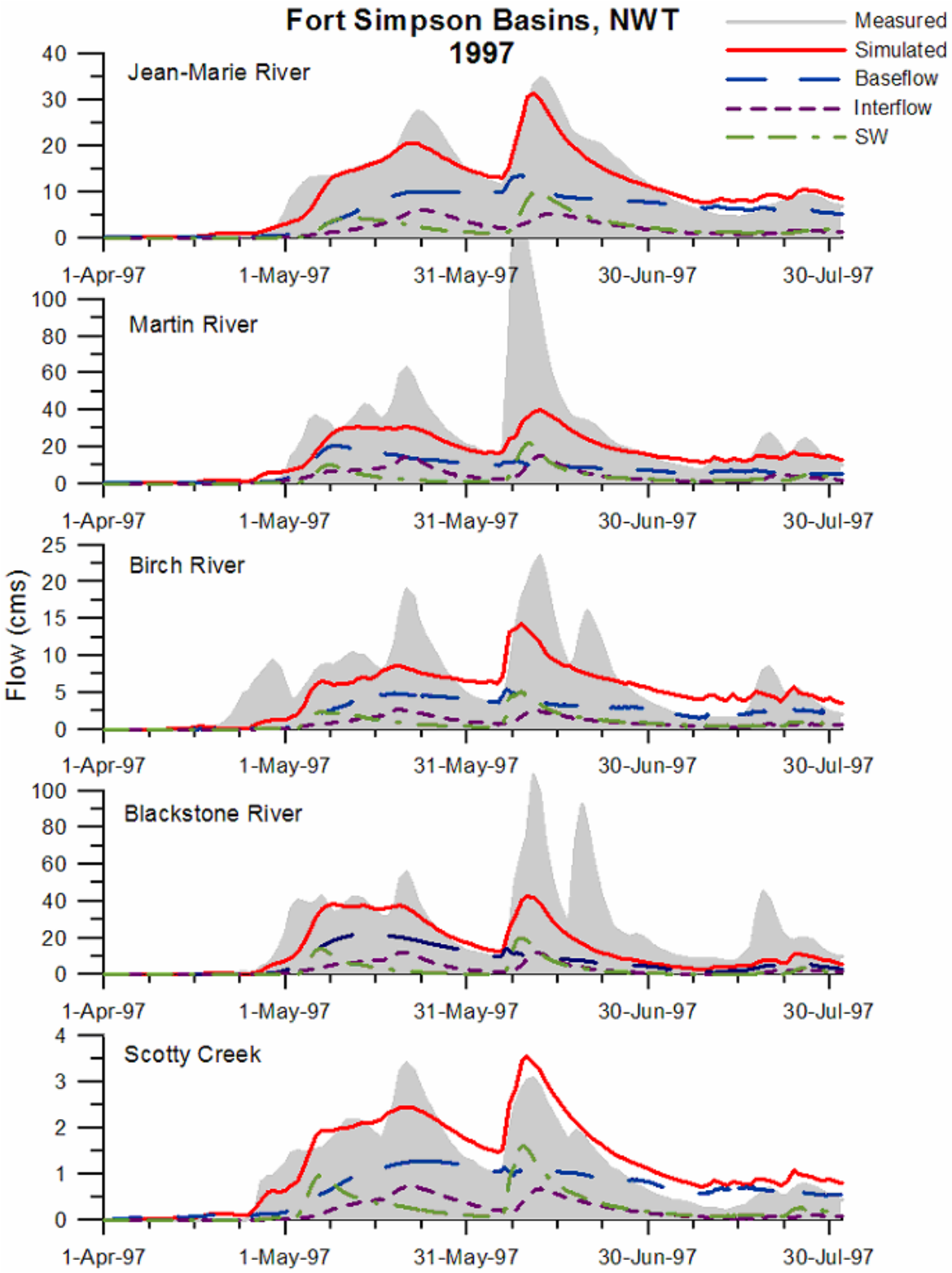

Figure 8.1 – 1997 isoWATFLOOD pre-calibration streamflow simulations for the FSB.

Most notable regarding this pre-calibration simulation was the hydrograph separation of surface runoff (i.e., SW), interflow and local groundwater (i.e., baseflow). Previously the FSB study in Section 5.4 had analysed only the baseflow contributions to streamflow and had neglected examining surface water and interflow contributions (i.e., because Tracer 4 was not yet verified). This pre-calibration simulation unexpectedly showed a lack of physical representativeness of surface runoff and interflow component separations despite both streamflow and baseflow simulations having been verified. The pre-calibration parameter set had been calibrated by fitting baseflow to isotopically-separated baseflow contributions from St. Amour *et al.* (2005). Assessing the other two components contributing to streamflow on Figure 8.1 reveals problems with the model's internal response and sub-process apportioning based on this pre-calibration parameterization. For example, in Jean-Marie River surface water and baseflow respond simultaneously and are lagged by a response from interflow. This response is physically impossible since the UZS drains into the LZS to generate baseflow response; more correctly, baseflow should lag interflow. Furthermore, the Martin River baseflow on Figure 8.1 is the first and earliest response to the snowmelt event, lagged by surface water and finally interflow. The internal model response is driven by model parameterizations; these unrealistic responses occurred because surface storages (ds and dsfs) were under-represented and infiltration conductivities were significantly larger than what is considered to be realistic (ak and akfs). This results in an early overland (runoff) response on the surface, and a conduit-like UZS that wicked water directly into LZS with little or no retention in UZS to generate interflow. These results clearly show the need for internal process calibration and verification regardless of how well streamflow is being simulated relative to measured flows.

Following the pre-calibration simulation, model calibration was performed manually on all five FSBs using the 1997 event time series (April to August 1997) and a manual split-sample approach. WATFLOOD parameters were altered for successive simulations using statistical output and visual inspection of both hydrographs and HSs to derive suitable parameter values. During this second model calibration, isoWATFLOOD was used to isotopically constrain simulated $\delta^{18}O$ to measured $\delta^{18}O$ of streamflow using a visual best-fit approach. The objective was to produce simulated streamflow from physically realistic internal responses, using isotopic simulations to assist in defining parameterizations. Although the fit of simulated to measured flows was monitored quantitatively, the physical representativeness of simulated internal

hydrological processes was measured qualitatively by visual inspection alone. Results of the model calibration are presented on Figure 8.2, indicating simulated and measured streamflows, as well as sub-component contributions to streamflow from surface runoff, interflow and baseflow.

Calibration results (Figure 8.2) show distinct differences from the pre-calibration simulation (Figure 8.1). From inspection of Figure 8.2, the simulated snowmelt response is accurately captured by the model; particularly in Martin River where both timing and volume of the snowmelt is well simulated. Simulated flows exhibit consistent summer rainfall response errors similar to those from the pre-calibration run indicating a lower-than-measured runoff volume response to the early-June rainfall event. It seems likely that this is the result of the rain gauge being approximately one hundred kilometres from the river basins, located at the Fort Simpson airport. Although there are some improvements in the calibrated simulations, new errors have been introduced such as the early runoff response to a June rainfall event in Jean-Marie River basin. Figure 8.3 directly compares simulated streamflows from the pre-calibration and calibrated simulations.

An increase in simulated runoff volume from pre- to post-calibration is observed on Figure 8.3. By visual inspection, the post-calibration simulations generally (except for Blackstone River) estimate more snowmelt runoff, and the same or greater summer rainfall-runoff. On Figure 8.3 Jean-Marie and Martin River post-calibration predict earlier and higher amplitude streamflow responses to snowmelt relative to their pre-calibration simulations. Similarly the timing of the early-June rainfall-runoff response in Jean-Marie and Martin Rivers appear to be more immediate. The two simulations were compared using proportionality plots to assess the accuracy of each simulation relative to measured flows (Figure D.1 in Appendix D). Measured and simulated flows were normalized by the average measured and simulated flow respectively to remove the effects of model predictive biases. If the modelled data were to exactly match the measured data, the data would fall along the 1:1 line. Linear regressions of the data were made to compare the average correlation between measured and simulated data.

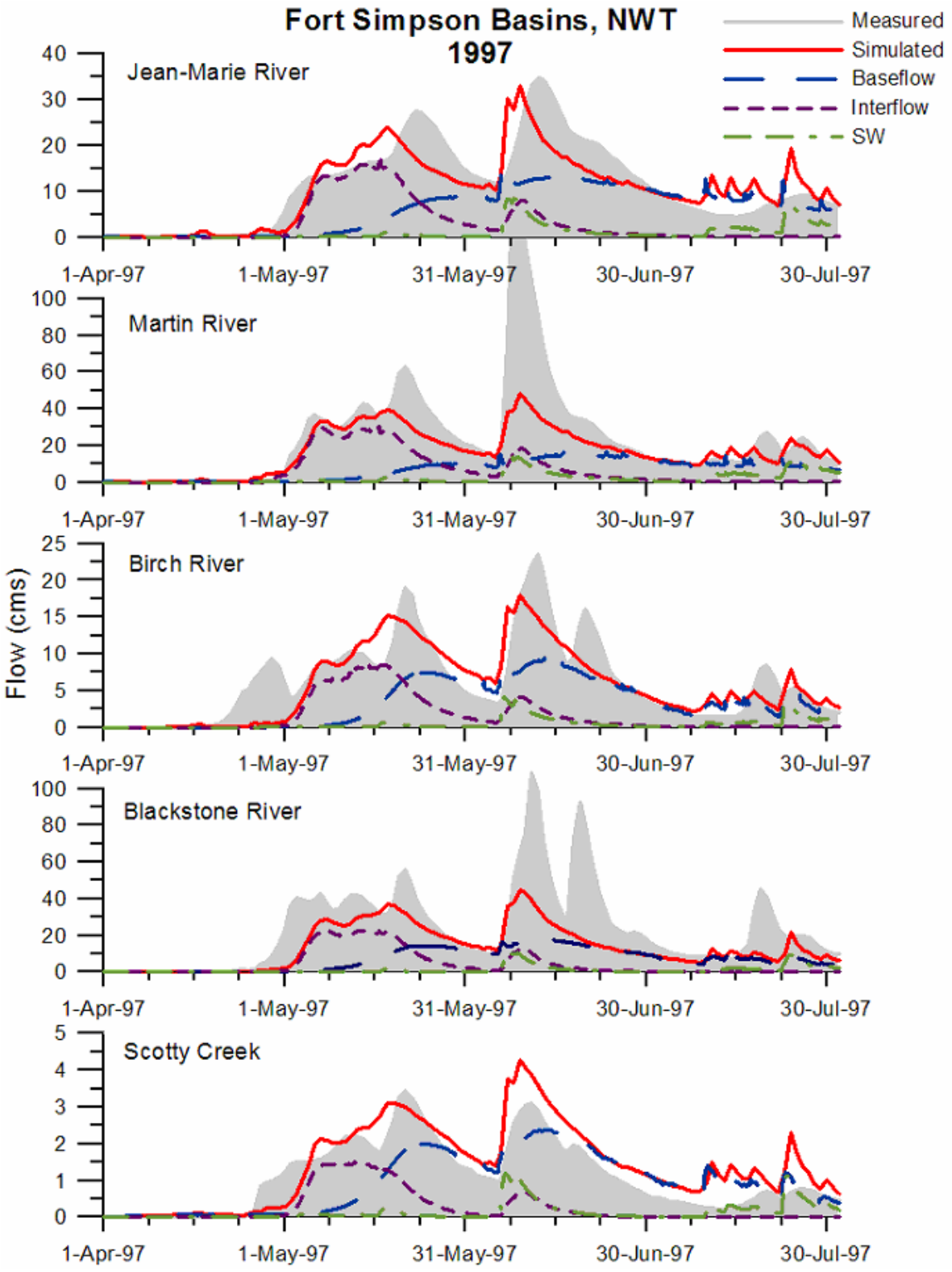

Figure 8.2 - 1997 isoWATFLOOD calibrated streamflow simulations for the FSB.

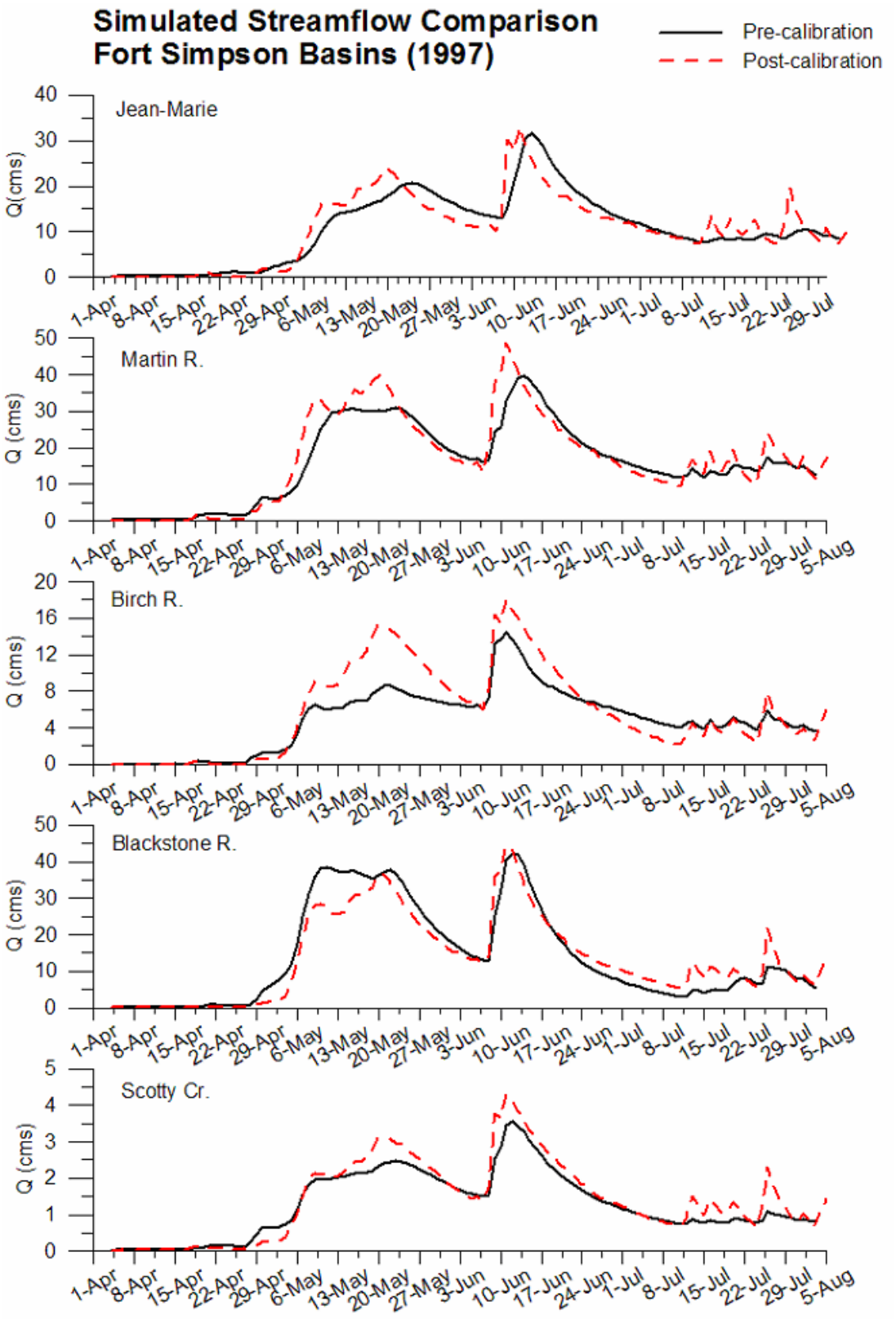

Figure 8.3 – Comparison of 1997 hydrographs for pre- and post- calibration simulations in the FSB.

To quantitatively contrast the two simulations, Table 8.1 summarises the statistical results from both simulations, as well as the regression slopes and R^2 values from Figure D.1.

Table 8.1 – Statistical comparison of the 1997 pre- and post-calibration simulations for the FSB.

Basin	DA (km^2)	Pre-calibration				Post-calibration			
		Nash	$\%D_v$	Slope	R^2	Nash	$\%D_v$	Slope	R^2
Jean-Marie R.	1313	0.7	-5	0.943	0.90	0.7	-5	0.899	0.63
Martin R.	2050	0.5	-30	0.671	0.15	0.5	-30	0.717	0.41
Birch R.	642	0.7	-6	0.834	0.46	0.7	-6	0.913	0.65
Blackstone R.	1405	0.3	-42	0.876	0.52	0.3	-42	0.849	0.51
Scotty Cr.	155	0.6	31	0.901	0.83	0.6	31	0.913	0.77
Average	**n/a**	**0.5**	**-10**	**0.845**	**0.57**	**0.5**	**-10**	**0.858**	**0.59**

From Table 8.1 the Nash-Sutcliffe coefficients on average represent a 50% better model estimation of measured streamflow over the average flow. The Jean-Marie, Birch and Scotty Creek Rivers have among the highest Nash-Sutcliffe statistics (i.e., closest to one) indicating the model is most representative of measured streamflows in these sub-basins relative to the other FSBs. The Nash-Sutcliffe coefficients and percent deviation of runoff volume statistics did not change from pre- to post-calibration indicating observed differences between the two simulations cancelled out over the entire simulation. Runoff volumes were under-estimated in four of the five FSBs; Scotty Creek being the only catchment having an over-estimation of runoff volume.

Examination of Figure D.1 (Appendix D) illustrates differences in the model's prediction of streamflow in pre- and post-calibration simulations, which is reflected in the regression slope and R^2 statistic for each simulation in Table 8.1. Both the fen-dominated Jean-Marie and Scotty Creek basins have slopes close to one, indicating the best fit between simulated and measured streamflows in the FSBs. Martin River significantly under-estimates measured flows in both simulations (although there is some improvement from pre- to post- calibration), and also indicates poor linearity between measured and simulated flows resulting in low R^2 values. Simulated high-flows are substantially under-estimated in Martin River relative to measured high-flows; likely the result of poor rainfall forcing data in early-June (Figure 8.1 and Figure 8.2). In all FSBs there appear to be only small changes in slope with improvements in fit (i.e., closer to one) in three of the five basins. Jean-Marie and Blackstone Rivers both showed an increased tendency to under-predict high measured flows in the post-calibration simulation (i.e., lower regression slopes). In Jean-Marie basin this is the result of timing errors, and in Blackstone

River, it is the result of under-predicting snowmelt contributions (Figure 8.2 and Figure 8.3). In the other three FSBs, the post-calibration simulation demonstrated an improved fit of simulated to measured streamflows.

Both pre- and post-calibration simulations appear to perform equally as represented by no change in Nash-Sutcliffe coefficients or $\%D_v$; and consistent regression slopes of ~0.85 confirming the general under-estimation of simulated relative to measured flow. By both visual and quantitative inspection of streamflow it is not possible to ascertain which simulation, and therefore parameter calibration, gives a more accurate prediction of streamflow for the FSBs: it appears that there is a trade-off in error.

More easily distinguishable, however, are the differences in sub-component flow separations contributing to streamflow. In the pre-calibration simulation (Figure 8.1), internal sub-component flows were not seen to be characteristic of expected surface runoff, interflow and baseflow hydrologic responses. In the post-calibration simulation (Figure 8.2), however, streamflow hydrographs were derived from physically realistic internal responses. During the spring freshet on Figure 8.2 for example there is a substantial response from the interflow component reflecting the direct infiltration of meltwater into the UZS, and only a small amount of excess surface runoff derived once the infiltration capacity is exceeded. Baseflow responds to the drainage of snowmelt into the LZS; however this response is lagged by the interflow response. In early-June during the rainfall event however, there is an immediate storm flow contribution from surface runoff that is slightly lagged by a response from interflow, and eventually baseflow. As summer progresses, baseflow contributions are seen to increase to nearly 100% of streamflow when there is no rainfall to produce surface runoff, and soil moisture is evaporated and used for plant uptake effectively decreasing interflow runoff. Although post-calibration, flow separations appear to be more physically realistic than those prior to calibration, it is not possible to verify from sub-component analysis alone that they are in fact correctly apportioned.

In Section 5.4, WATFLOOD-simulated baseflow was compared to isotopically-derived baseflow for the purposes of verifying WATFLOOD's baseflow separation. This still however remains a comparison of WATFLOOD to another model (i.e., a mixing model with limiting assumptions).

Surface runoff and interflow components cannot be as easily segregated using the mixing model approach as their isotopic compositions are not necessarily distinct from one another at all times. The continuous simulation of both streamflow and $\delta^{18}O$ of streamflow (and hydrologic storages contributing to streamflow) presents the opportunity to isotopically constrain contributions from hydrologic storages, and therefore aid in model parameterization. Given the sensitivity of isotopic change relative to streamflow (i.e., typically three orders of magnitude less), and that isotopic signatures of hydrologic end-members are continuously tracked and therefore do not need to be distinct; modelling isotope mass in conjunction with the water balance lowers the model's degrees of freedom. By calibrating not only to measured streamflow, but also to the isotopic composition of streamflow, it is possible to identify model parameterizations resulting in unrealistic contributions from hydrologic storages by errors in $\delta^{18}O$ compositions of streamflow. The next section will provide an example of how equifinality in streamflow is reduced through the use of isoWATFLOOD modelling.

8.1.1 Resolving Equifinality

Model calibration to both simulated streamflow and isotope mass constrains isoWATFLOOD in two dimensions, necessitating correct internal dynamics to enable accurate predictions of $\delta^{18}O$ in streamflow. Both pre- and post-calibration simulations exhibited differences in their estimations of runoff at different times; however Table 8.1 indicated that on average the simulations were the same. Equifinality is described by two equal simulations of total streamflow arrived at by different contributions from internal hydrological responses. Appendix E presents a statistical analysis of the difference between the pre- and post-calibration streamflow simulations for each of the five FSBs that shows they are statistically equal simulations of streamflow. Both streamflow simulations are equal, but were arrived at by different internal processes where one model parameterization will be "more correct" than the other. Simulation of $\delta^{18}O$ in streamflow indicates problems with the pre-calibration parameterization where simulated $\delta^{18}O$ clearly does not replicate measured $\delta^{18}O$ in streamflow (Figure 8.4). In comparison, post-calibration isographs shown on Figure 8.5 (note the differences in the y-axis scale relative to Figure 8.4) show improved fits of simulated to measured $\delta^{18}O$ because of a more representative internal model parameterization.

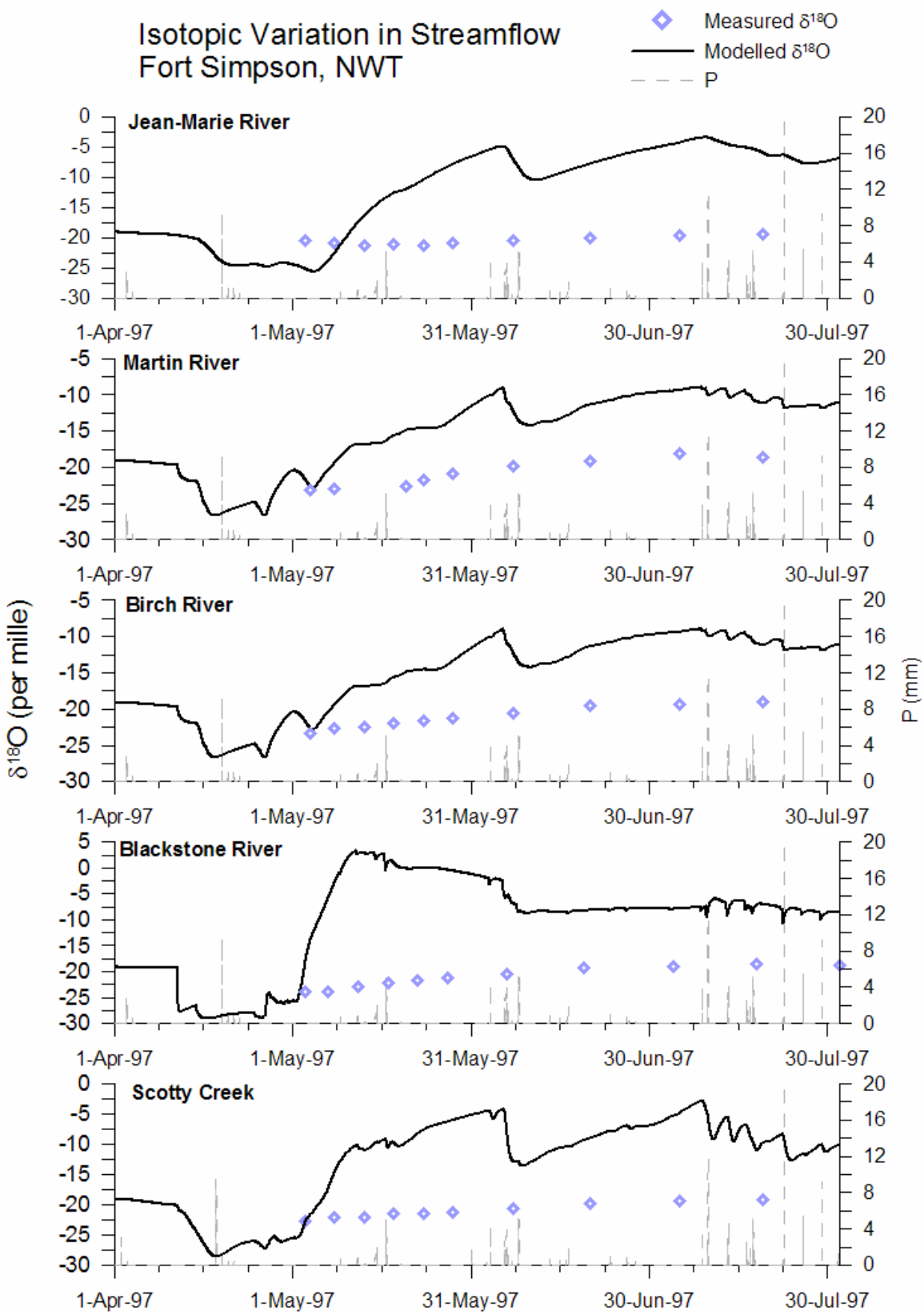

Figure 8.4 – isoWATFLOOD 1997 pre-calibration isographs in FSB.

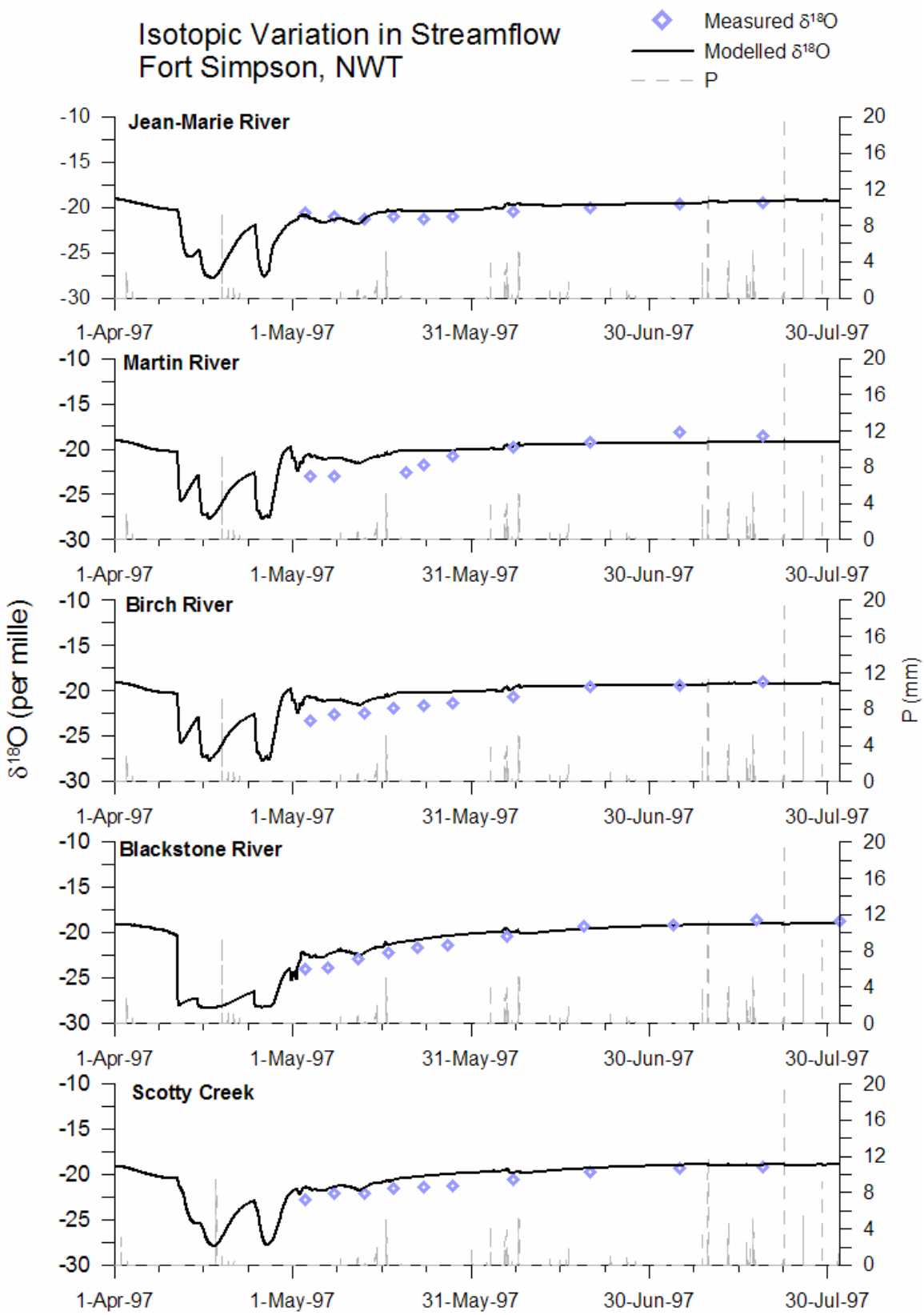

Figure 8.5 - isoWATFLOOD 1997 post-calibration isographs in FSB.

The pre-calibration simulation of $\delta^{18}O$ did not fit well with measured $\delta^{18}O$ in streamflow during the 1997 event. Simulated compositions are significantly more enriched in heavy isotopes than the measured compositions of streamflow (Figure 8.4). The initial freshet compositions deplete, which is expected due to snowmelt contributing to streamflow. Post-freshet, there is a sudden and rapid enrichment occurring at the beginning of May at the onset of evaporation in the FSB. These enrichments in streamflow coincide with increases in surface water runoff shown on Figure 8.1. In wetland-dominated regimes, surface runoff resides in depressions and wetland storages resulting in excess evaporative enrichment of the runoff before contributing to streamflow. Following the early-June rainfall event, isotopic compositions are pulled downwards towards the composition of meteoric water (-19.1‰) and then begin to slowly rebound (enrich) thereafter. The basins exhibiting the largest rainfall-runoff responses also exhibit the most depletion during this rainfall event (i.e., Jean-Marie and Scotty Creek River basins). From Figure 8.4, the effect of incorrectly apportioned sub-flows is far more apparent on streamflow isotopic composition than it is on streamflow volume and timing.

In contrast Figure 8.5 represents simulated $\delta^{18}O$ post-calibration. Noting the scale differences (i.e., y-axis) relative to Figure 8.4, simulated $\delta^{18}O$ post-calibration shows an improved fit to measured $\delta^{18}O$ compositions. Model parameterization for the post-calibration simulation was derived by fitting not only streamflow to measured flows, but simulated isotopes to measured isotopes in streamflow. By constraining simulated to measured isotopes, the post-calibration parameterization is more physically-based resulting in more physically realistic streamflow partitioning (Figure 8.2). The isotope simulation initially shows a series of two or three strong depletions during the freshet that are caused by the inflow of snowmelt into the channel as temperatures increase. The sudden increase in mid-April prior to a second melt event is caused by a rainfall event transporting more enriched meteoric water into the channel. Post-freshet (early May) the river composition steadies and is influenced only by intermittent rainfall events that very slightly increase streamflow composition (~May 15th). The large rainfall event in early-June shows a larger increase in isotopic composition (~0.5‰ enrichment) caused by rainfall onto the channel, and by the production of surface runoff as was noted on Figure 8.2. Throughout the summer, isotopic compositions continue to gradually enrich due to evaporative effects and enriched (relative to snowmelt) rainfall contributions. This 1997 post-calibration

simulation shows that the isotopic composition of streamflow can in fact be reproduced by a mesoscale hydrological model.

The end result is not necessarily a more accurate simulation of streamflow (although in some cases there may be), but a more physically-based model that better represents basin hydrology. Therefore a higher degree of confidence can be placed on model simulations that undergo more rigorous model calibrations, such as the one in this study. Following calibration of the model hydrologically and isotopically, streamflow simulations did not significantly improve (Table 8.1), which suggests that the quality of the input data should be questioned. The isoWATFLOOD model can therefore offer a starting point for continuous improvement of both the hydrological model and the quality of the forcing data.

8.2 Model Validation

To test isoWATFLOOD's robustness in reproducing streamflow and isotopes, the model was applied to 1998 and 1999 event seasons (April to August) without additional calibration. The two model validations serve to test isoWATFLOODs consistency in reproducing both streamflow and the $\delta^{18}O$ of streamflow.

8.2.1 1998 Simulation

The isoWATFLOOD model was run for the 1998 event season using the calibrated model parameterizations from Section 8.1 (post-calibration scenario). Isotopic initializations used for the 1998 event are provided in Appendix A.2.2, and were used to define antecedent isotopic conditions. The isoWATFLOOD model was run continuously from April 1998 to August 1998 to produce both hydrographs and isographs for each of the five FSBs.

Streamflow hydrographs shown on Figure 8.6 indicate general over-estimations of streamflow runoff during the 1998 event season, particularly following freshet. The timing of the freshet hydrograph was reproduced in Birch, Blackstone and Scotty Creek River basins, but was slightly early in Jean-Marie and Martin Rivers. The unusually warm and wet 1998 freshet period was

noted by other researchers studying the hydrology of the FSB region, and has been attributed to the onset of the El Niño southern oscillation (Hayashi *et al.*, 2004; St Amour *et al.*, 2005). The onset of early warming led to an earlier-than-normal spring freshet that was reproduced for Birch and Blackstone river basins, but was simulated too early in Jean-Marie and Martin River basins. In Jean-Marie, Birch and Scotty Creek River basins the freshet runoff volume was significantly over-estimated relative to measured flows. The prolonged hydrograph recessions appear to be sustained by large baseflow responses, indicating excessive infiltration of snowmelt into the LZS as opposed to the generation of a more substantial runoff response. Streamflow is interflow-dominated during the early freshet as snowmelt infiltrates into the UZS, causing a delayed baseflow response. Later in the summer months, the hydrographs are baseflow-dominated between rainfall events as surface and soilwaters evaporate, lowering runoff and interflow responses. In mid-June, a significant rainfall event caused a surface runoff response that was slightly under-captured relative to measured streamflows in all five basins. Jean-Marie and Scotty Creek basins simulated this event most successfully, likely due to their close proximity to the rain gauge. Substantial summer streamflow errors are inherent to FSB simulations and are attributable to poorly defined meteorological inputs.

A statistical summary of the 1998 isoWATFLOOD simulation confirms the poor fit of simulated to measured streamflow (i.e., low Nash coefficients) and the over-estimation of runoff volume (i.e., positive $\%D_v$) (Table 8.2).

Table 8.2 – Statistical summary of 1998 isoWATFLOOD streamflow simulation in the FSB.

Basin	**DA (km^2)**	**Nash**	**$\%D_v$**	**Slope**	**R^2**
Jean-Marie R.	1313	-0.5	29.7	1.091	0.06
Martin R.	2050	0.6	-1.49	0.800	0.41
Birch R.	642	0.4	25.2	1.009	0.46
Blackstone R.	1405	0.6	-16.3	0.688	0.61
Scotty Cr.	155	-0.3	44.1	1.298	0.49
Average	**n/a**	**0.2**	**16.8**	**0.977**	**0.41**

Proportionality plot slopes in 1998 (Figure D.2) reinforce the model's tendency to over-estimate streamflow. The poor linearity between measured and simulated streamflow in some FSBs (low R^2) is the result of systematically over-estimating freshet flows and under-estimating summer rainfall events (i.e., Jean-Marie River basin; Figure D.2). The near-one proportionality slope in Jean-Marie River basin represents a cancellation of over- and under-estimation error as opposed

to a well-fit simulation, reinforced by the negative Nash-Sutcliffe coefficient and low R^2 value. Visually apparent from Figure 8.6, and also shown in Table 8.2, Martin and Blackstone Rivers show the best fit of simulated to measured streamflow with good correlation in terms of both timing and volume of flow.

The isotopic composition of streamflow in 1998 was in general representative of measured $\delta^{18}O$ of streamflow (Figure 8.7). The variation of streamflow $\delta^{18}O$ throughout the summer months was reproduced by the model, including late summer enrichment slopes and depletion by summer rainfall in mid-June. The spring freshet period indicates error between simulated and measured isotopic compositions of streamflow; which can be the result of poorly defined initializations, antecedent conditions, or the use of constant composition precipitation during the 1998 study period (i.e., -20.8‰). Initializations used to start-up the model were averages over the 1998 season, and it is likely that the compositions of hydrologic storages and precipitation may have been more depleted (i.e., carried-over from 1997) than the longer-term 1998 seasonal values reflected. A more depleted snowpack and hydrologic storage would result in a more depleted streamflow composition during the 1998 freshet (end of April) as meltwater contributes to streamflow. This phenomenon was not simulated by the isoWATFLOOD model and is likely also in part attributable to the early freshet rainfall events that enriched simulated streamflow compositions in the model. Cold weather rainfall events are commonly more depleted than seasonal average rainfalls. The coincidence of an isotopic depletion with this early freshet rainfall suggests that the composition of precipitation was likely more depleted than the average composition used by the model. The reliance of simulated results on model initialization is commonly addressed by adding a longer model spin-up period to initialize hydrologic storages, or by using more representative distributed model inputs.

Given the sensitive nature of isotopic compositions due to the significance of small changes in mass concentration (i.e., on the order of 10^{-03}), it is unlikely (if not impossible) to successfully simulate $\delta^{18}O$ with non-representative internal hydrology. The 1998 FSB simulation therefore reinforces that the isoWATFLOOD model is representing internal responses in a physically-based manner. A second validation study (i.e., for the 1999 event) will be conducted to further test the model's ability to reproduce streamflow and $\delta^{18}O$ in the FSB.

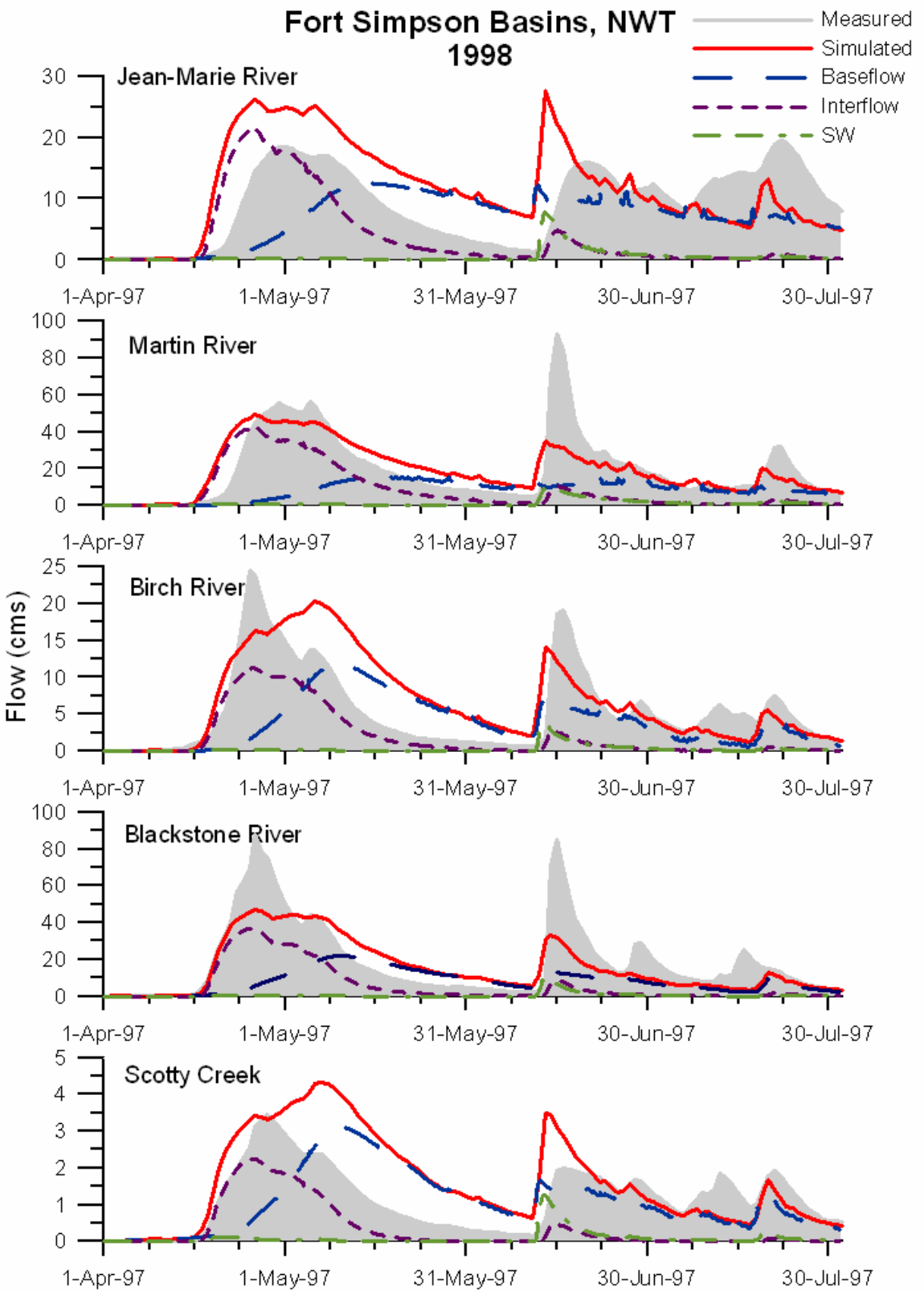

Figure 8.6 – 1998 isoWATFLOOD hydrographs for the FSB.

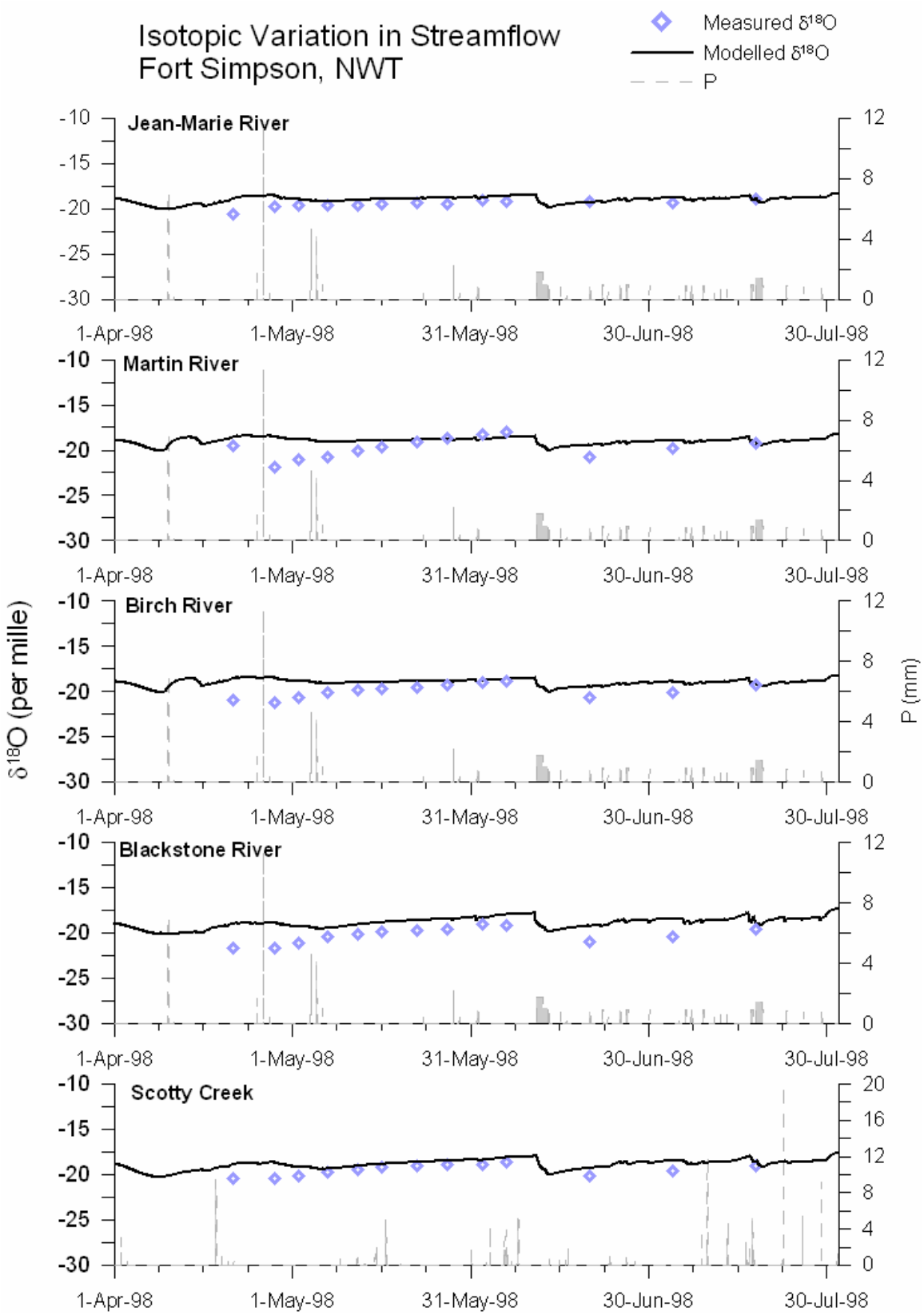

Figure 8.7 – 1998 isoWATFLOOD isographs for the five basins in the FSB.

8.2.2 1999 Simulation

The isoWATFLOOD model was run for the 1999 event season using the post-calibration model parameterizations (Section 8.1.1). Isotope initializations were defined for the 1999 event in the 'isotope.par' file (Appendix A.2.2) so that meteorological inputs and hydrologic storages were representative of the 1999 season. The isoWATFLOOD model was run continuously from April 1999 to August 1999 to produce both hydrographs and isographs for the FSBs.

Simulated streamflows in 1999 showed overall improved fits to measured flows as compared with the 1998 simulation, but still under-represented observed freshet hydrographs (Figure 8.8). Jean-Marie, Birch and Scotty Creek River basins again showed a more prolonged freshet streamflow recession than was measured, which was again sustained by the baseflow response in these basins. In the Birch River, the 1999 spring freshet occurred half a month earlier than in the other four catchments leading to a shift in the entire event season hydrograph. This was not captured by the isoWATFLOOD model since the model uses one set of meteorological data for the entire watershed, translating to a common freshet across all sub-basins. It is notable that the 1999 summer season was overall well modelled, particularly in comparison to the 1998 summer (i.e., very wet and rainy) season. During the summer of 1999 there is a distinct decrease in runoff throughout all five basins. The reduction in streamflow is overall well simulated by isoWATFLOOD, and although a few late summer rainfall events are once again missed, the streamflow recession curves from early June to late August are representative of measured streamflow.

The statistical summary of the 1999 simulation (Table 8.3) indicates an improvement in fit of simulated to measured flows by the higher (i.e., closer to one) Nash-Sutcliffe coefficients, particularly in the Jean-Marie and Martin River basins (0.7 in both). In 1999, streamflows were overall under-estimated, which was similar to 1997 streamflows and dissimilar to 1998 simulated streamflows.

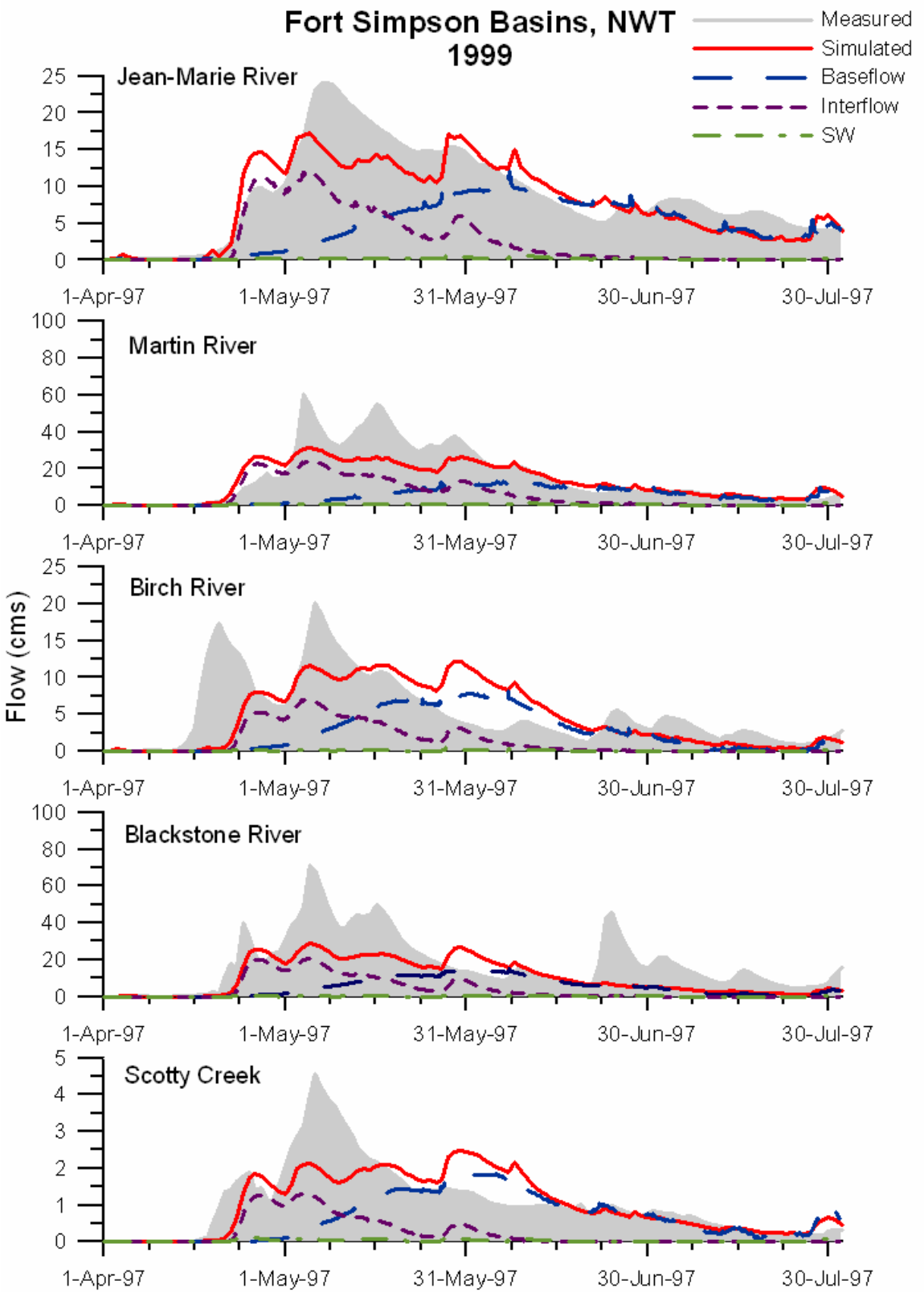

Figure 8.8 - 1999 isoWATFLOOD hydrographs for the five basins in the FSB.

Table 8.3 - Statistical summary of 1999 isoWATFLOOD streamflow simulation in the FSB.

Basin	DA (km²)	Nash	%D_v	Slope	R^2
Jean-Marie R.	1313	0.7	-8.83	0.853	0.71
Martin R.	2050	0.7	-12.5	0.714	0.64
Birch R.	642	0.1	-8.22	0.713	0.14
Blackstone R.	1405	0.3	-40.5	0.519	0.46
Scotty Cr.	155	0.5	-4.29	0.783	0.41
Average	**n/a**	**0.5**	**-14.8**	**0.977**	**0.41**

Generally simulated flows were improved in 1999 relative to 1998, as evidenced by the proportionality slopes (Figure D.3). Also note-worthy is the large under-estimation of runoff in the Blackstone River basin (D_v~-41%) that is the direct result of under-capturing two significant rainfall events: one in early May and one in late June. Consequently, simulated flows were considerably less than measured flows (Figure 8.8 and Figure D.3).

Despite errors in streamflow quantity, $\delta^{18}O$ of streamflow was shown to be well simulated relative to measured isotopic compositions (Figure 8.9). Simulations from 1997 through to 1999 demonstrate that what is most important to the accuracy of the $\delta^{18}O$ modelling exercise is the internal hydrological processes contributing to streamflow. In the 1999 event season, simulated $\delta^{18}O$ compositions were representative of measured compositions throughout the summer period, indicating that isoWATFLOOD is effectively simulating evaporative enrichment (Figure 8.9). During the freshet, there was again too little depletion of streamflow, which suggests that the isotopic composition of hydrologic storages at the start of simulation are being incorrectly initialized. Isographs on Figure 8.9 show an earlier isotopic depletion of streamflow in 1999 relative to 1997 and 1998.

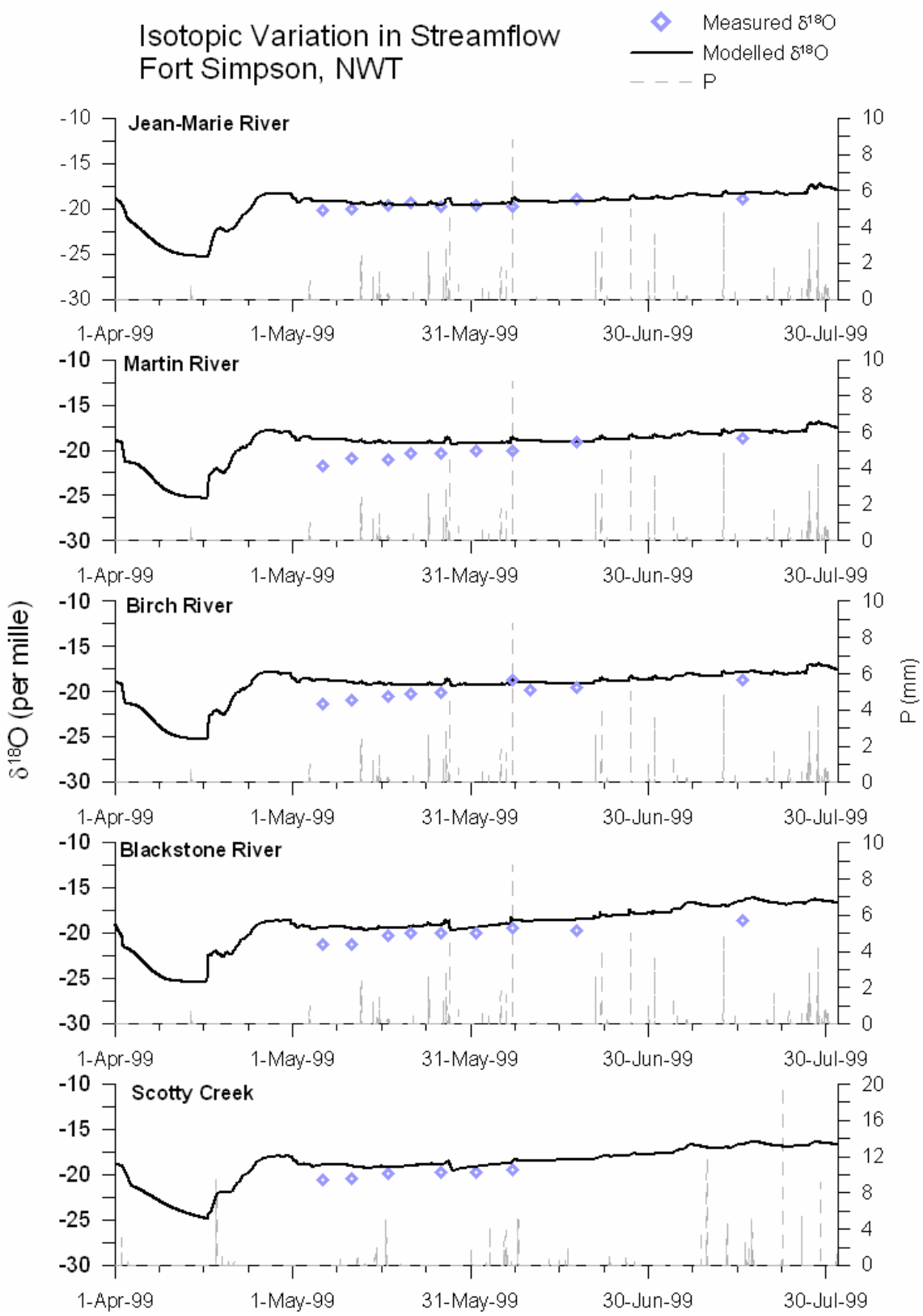

Figure 8.9 - 1999 isoWATFLOOD isographs for the five basins in the FSB.

An early snowmelt was noted by Hayashi *et al.* (2004) in 1999 and was attributed to a carry- over of warm moisture from the 1998 El Niño event. This finding is encouraging as the isotopic depletion derived from snowmelt appears well-timed, but unfortunately there were no measured data to validate whether the amount of river isotopic depletion was accurately simulated. The 1999 season was relatively dry and so the influence of meteoric precipitation on streamflow was minimal; increasing the proportion of streamflow contribution from hydrologic storage. Correct simulation of isotopes in streamflow during a drier season points to the models ability to representatively simulate isotopes in hydrologic storage. A more detailed examination of isotopes in storage follows in Section 8.4.

These simulations confirm that WATFLOOD's (and therefore isoWATFLOOD's) conceptualizations of mesoscale hydrology effectively represent the physical characteristics of the watershed and hydrological interactions between storage compartments. The errors in both the 1998 and 1999 isotopic simulations appear to have more to do with model initialization than with the model's physical representativeness of isotopic change in response to hydrologic change. A continuous simulation of the FSB, which includes a three month model spin-up, will be performed to reduce the simulations dependence on initial conditions.

8.2.3 Continuous Simulation

To reduce the models dependence on initial conditions a continuous simulation was developed for the FSB. Continuous simulations had not previously been considered because of the absence of measured hourly precipitation and flow data in the winter months. Daily values of precipitation were available however, and were considered adequate for the accumulation of snow. A simulation was performed beginning in October 1996 so that antecedent conditions would be initialized for the 1997 freshet. The model was run continuously through to December 1999. The 1997, 1998 and 1999 spring and summer event periods were the time frames of interest, however by running continuously, there was no need to reinitialize the model hydrologically or isotopically. Yearly values of isotopes in precipitation were still utilized (i.e., rainfall and snowfall) to reflect changing atmospheric conditions and the variability in the composition of local precipitation reported by St. Amour *et al.* (2005).

Streamflow hydrographs from continuous simulation of the FSB are presented on Figure 8.10. It should be noted that measured streamflows (i.e., grey shading) were only available during the ice-free, warmer months of 1997, 1998, and 1999 (April to August). Simulated streamflows (i.e., red lines) were generated beginning October 1996 and ending December 1999. For comparison to previous simulations, Table 8.4 shows the statistical summary of the FSB continuous simulation relative to the 1997, 1998, and 1999 combined seasonal averages.

Table 8.4 – Statistical summary of the Fort Simpson watershed continuous simulation.

Basin	**DA**	**Seasonal Avg.**		**Continuous**		**Seasonal Avg.**		**Continuous**	
	(km^2)	**Nash**	**$\%D_v$**	**Nash**	**$\%D_v$**	**Slope**	**R^2**	**Slope**	**R^2**
Jean-Marie R.	1313	0.3	5.42	0.5	-4.60	0.948	0.47	0.819	0.50
Martin R.	2050	0.6	-13.8	0.5	-21.4	0.744	0.49	0.55	0.38
Birch R.	642	0.4	3.53	0.4	-6.11	0.878	0.42	0.728	0.34
Blackstone R.	1405	0.4	-32.9	0.3	-41.3	0.685	0.53	0.457	0.40
Scotty Cr.	155	0.3	23.5	0.4	1.74	0.998	0.56	0.994	0.49
Average	**n/a**	**0.4**	**-2.84**	**0.4**	**-11.2**	**0.851**	**0.49**	**0.711**	**0.42**

From Table 8.4, the Nash-Sutcliffe coefficient on average did not change, however Jean-Marie and Scotty Creek showed slight improvement, and Martin and Blackstone Rivers slightly worsened. In 1997 (Table 8.1) the Nash-Sutcliffe coefficient was slightly higher at an average of 0.5 for the five basins; in 1998 it was lower (0.2); and in 1999 it was again higher (0.5). The continuous simulation naturally averages these inter-seasonal differences, but does generally improve modelled to measured data fits as is seen by the R^2 statistic from the proportionality plots. Although the slopes of the plots decreased on average and within each basin, the fit to the average slope was improved indicating fewer systematic model errors (Figure D.4). The fit of simulated to measured streamflow was not significantly improved visually or statistically. Continuously simulated runoff volume was under-estimated more than the average of simulated runoff volume from 1997, 1998 and 1999 seasons (-11.2% relative to -2.84%). However the seasonal average runoff volume is misleading because in 1998 there was a significant over-estimation, whereas 1997 and 1999 were under-estimated. Therefore the continuous simulation provides a more consistent model result with fewer errors in simulating inter-annually variability.

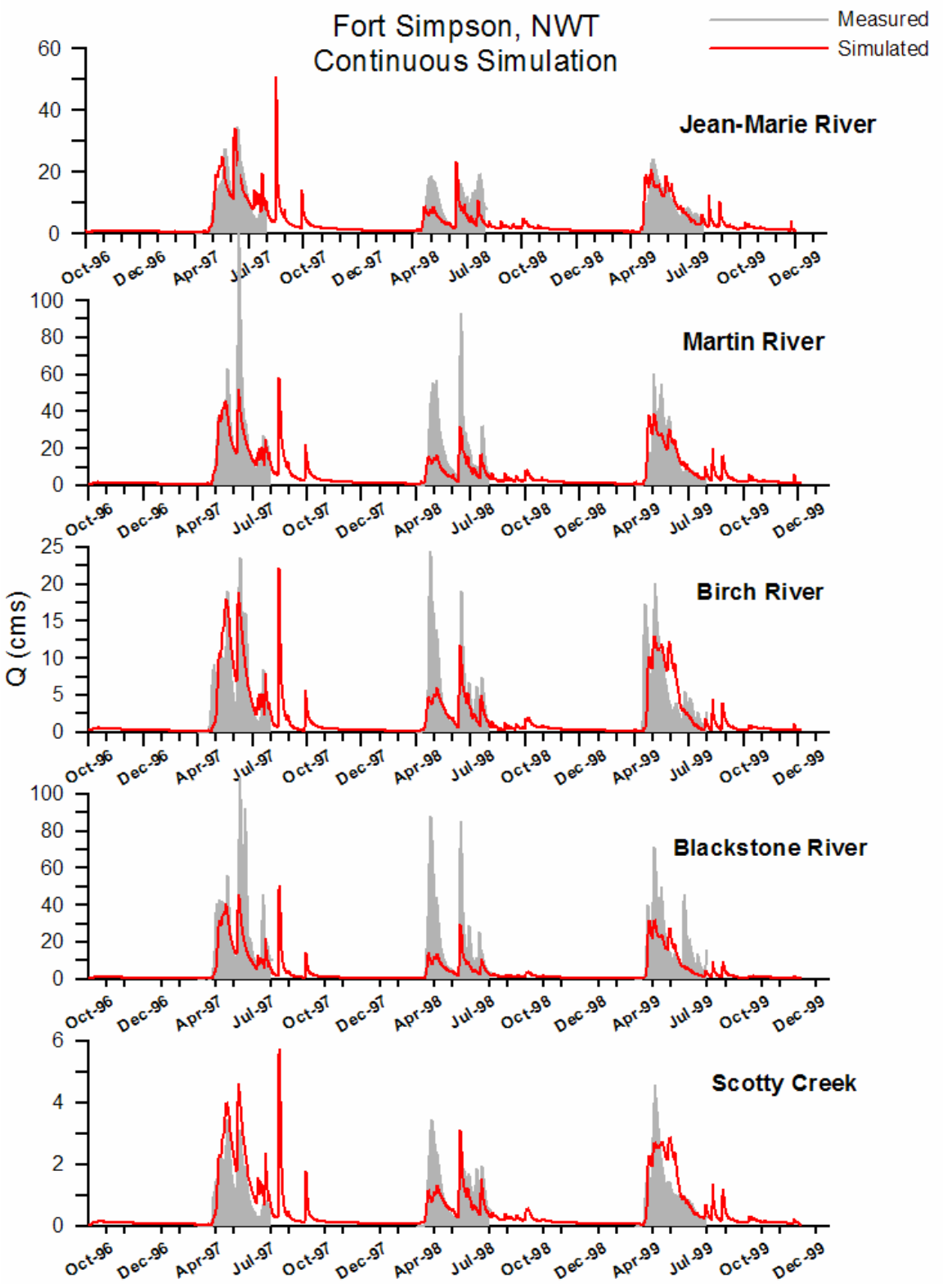

Figure 8.10 – isoWATFLOOD continuous streamflow simulation for the FSB.

Figure 8.11 presents the $\delta^{18}O$ variation of streamflow from October 1996 to December 1999 as simulated by isoWATFLOOD, and Table 8.5 presents a quantitative summary of the inter-basin isotopic variation.

Table 8.5 – Statistical summary of inter-basin isotopic variability for FSB continuous simulation.

Basin	**Average (‰, VSMOW)**	**$\sigma_{\delta 18O}$ (‰, VSMOW)**	**$\Delta\delta^{18}O$ (‰, VSMOW)**
Jean-Marie River	-19.416	0.890	9.90
Martin River	-19.389	0.921	10.63
Birch River	-19.233	1.231	11.34
Blackstone River	-19.196	1.159	10.53
Scotty Creek	-19.268	1.092	10.68
Average	**-19.30**	**1.06**	**10.6**

During the continuous simulation the trend of isotopic depletion during snowmelt influence and subsequent gradual summer enrichment from evaporation is captured by isoWATFLOOD. Visual inspection of the continuous simulation shows that the 1997 freshet resulted in more depleted streamflows than both 1998 and 1999. In 1998, simulated snowmelt depletions in Jean-Marie River and Scotty Creek were particularly close to measured freshet compositions, however in Birch and Blackstone Rivers late-winter compositions were more enriched relative to measured compositions, resulting in enriched freshet compositions.

Considering ecological (i.e., percentage land classifications) and geographical similarities and differences between the basins, it is not surprising that Jean-Marie and Scotty Creek behave similarly. Channelized fens in these basins likely help to offset the greater-than-average isotopic depletion from snowmelt and rainfall in the 1998 season, and therefore the model is better able to simulate measured $\delta^{18}O$ freshet compositions. This is represented in Table 8.5 where Jean-Marie River has the most depleted average composition and the lowest isotopic variability ($\Delta\delta^{18}O$) and standard deviation. During the winter months after fall freeze-up and before spring freshet (October to March), the model maintains a constant composition of isotopes in streamflow that is more enriched relative to measured compositions. During the winter months isotopes in streamflow naturally and very gradually deplete as the rivers become sustained by ice-on baseflow that has not undergone evaporative enrichment.

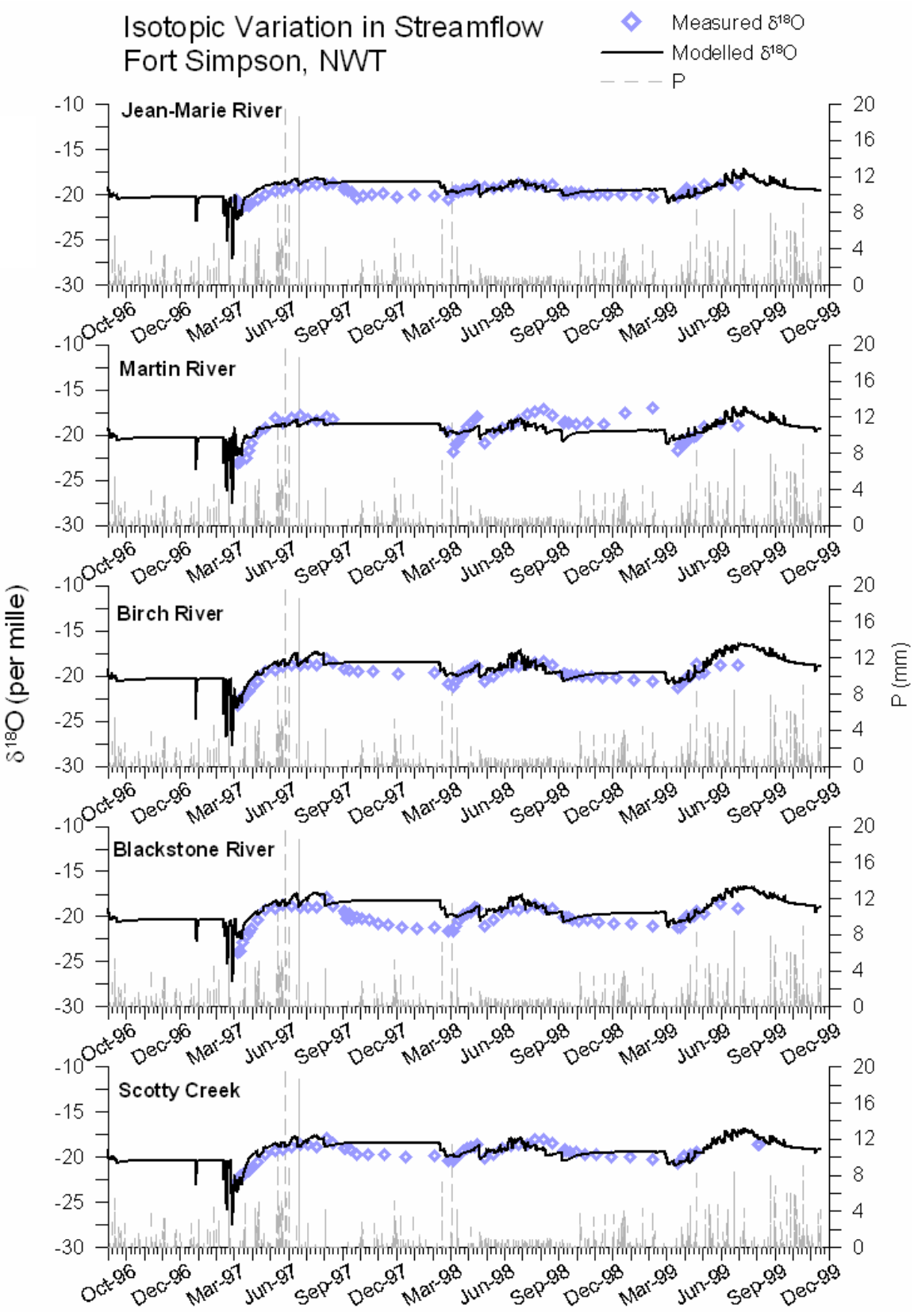

Figure 8.11 – isoWATFLOOD continuous simulation of isotopes in streamflow for the FSB.

Results of a more detailed examination of the snowmelt process representation in isoWATFLOOD are discussed in Section 8.4.1 to examine why the model is unable to reproduce the natural variation of ice-on winter streamflow. In the Martin River basin, isoWATFLOOD under-estimates summer evaporative enrichment of streamflow. Further investigation is required to determine whether the enrichment problem is caused by under-estimation of evaporation (Section 8.3); unrepresentative or overly-depleted rainfall contributions or compositions (Section 8.4.2); or because of mis-proportioned soilwater (Section 8.4.3), baseflow (Section 8.4.4) or wetland contributions (Section 8.4.5).

One of the main reasons for performing the continuous simulation was to improve the $\delta^{18}O$ fit during freshet by simulating fall antecedent conditions. Figure 8.12 compares the 1998 and 1999 freshets from seasonal simulations to continuous simulation freshets in the Martin River basin, which had among the worst results for the freshet period based on the seasonal simulations (Figure 8.7 and Figure 8.9). Figure 8.12 indicates an improvement from the seasonal to the continuous simulation. Although improved, simulated isotopic compositions in both 1998 and 1999 were still more enriched than measured compositions in the Martin River (and other FSBs) streamflows. Further investigation into the simulation of $\delta^{18}O$ in hydrologic storage is necessary to determine the cause of such errors.

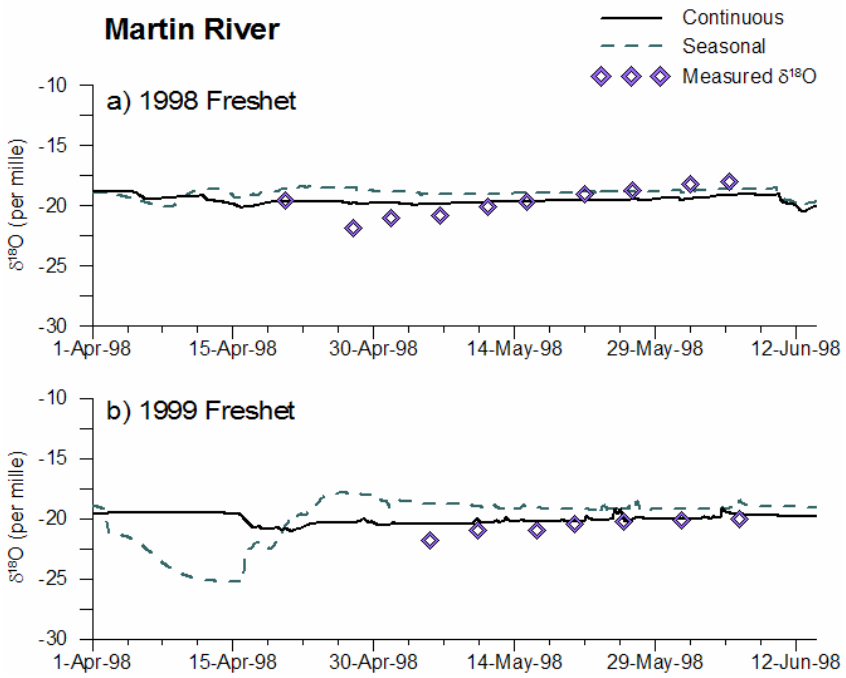

Figure 8.12 – a) 1998 and b) 1999 freshets from seasonal and continuous simulations of the Martin River

Errors in streamflow resulting from poor model forcing can now be distinguished from errors resulting from poor model internal dynamics. The ability of isoWATFLOOD to accurately reproduce the isotopic composition of streamflow continuously, despite errors in meteorological forcing, from 1996 to 1999 is promising. There remain questions however as to why the model simulates inadequate depletion during freshet periods, and why there are discrepancies with evaporative enrichment profiles. The isotopic response within each hydrological compartment will be the focus of the remainder of this chapter, and conclusions will be drawn as to the model's strengths, areas for improvement, and overall reliability in simulating isotopes in streamflow.

8.3 Modelling $\delta^{18}O$ in Evaporation

Evaporative enrichment is a significant control on the isotopic composition of hydrologic storages contributing to streamflow. In this section, the dynamics of evaporative fractionation and the ability of isoWATFLOOD to accurately simulate the isotopic composition of vapour are analysed. The $\delta^{18}O$ data for this analysis are derived from the continuous FSB simulation, however only 1997 late summer compositions are shown for clarity.

The composition of evaporating moisture (δ_E) is simulated in isoWATFLOOD using the Craig & Gordon model presented in Section 2.4.2, which describes the heavy isotope build-up in water remaining in storage after evaporation has occurred. Typically the composition of δ_E lies to the right of the meteoric water line along a backwards trajectory of the LEL in δ^2H-$\delta^{18}O$ space (Figure 2.1). The composition of vapour fluctuates based on the composition of input water (δ_I), atmospheric vapour (δ_A), and atmospheric conditions (i.e., relative humidity and temperature). Given that Equation 2.5 is quite sensitive to relative humidity, typically it is a dominant factor controlling the composition of vapour; δ_E is more depleted in arid environments and more enriched in humid environments. Figure 8.13 shows 1997 late summer variation in the composition of evaporating moisture (δ_E and δ^*), fluctuating with relative humidity (h; Equation 6.5) in the Scotty Creek River basin.

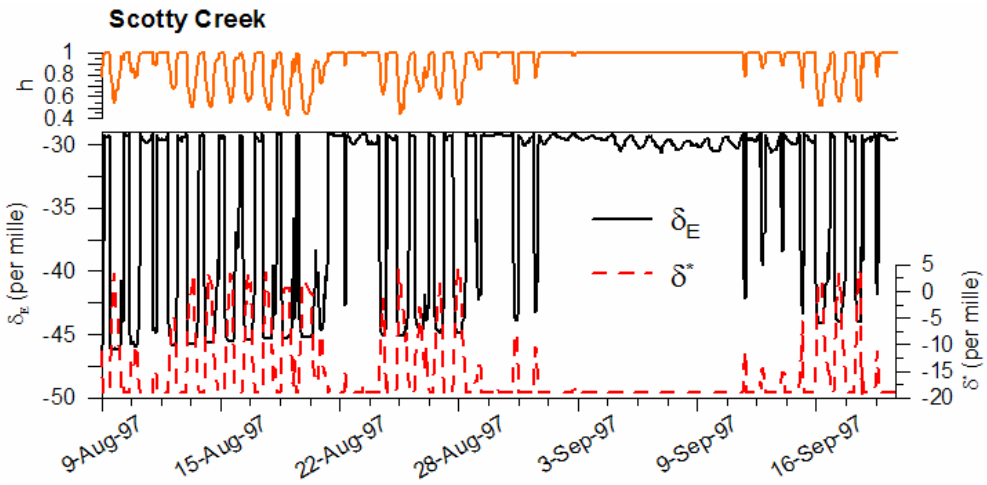

Figure 8.13 – isoWATFLOOD-simulated composition of evaporating moisture (δ_E).

δ_E is depleted in $\delta^{18}O$ relative to average input or source waters (soil and wetland storages). Given atmospheric vapour (δ_A) is assumed to be in approximate equilibrium with the composition of thaw-season precipitation (-19.1‰ for 1997), the average δ_A in 1997 is -25‰ for $\delta^{18}O$. The average composition of evaporated moisture simulated by the model was found to be significantly more depleted (-38‰) than both the input water and atmospheric moisture, as would be expected based on the theory of isotope-mass balance shown on Figure 2.1. Modelled δ_E is also proportional to the fluctuations in relative humidity. As relative humidity decreases, the humidity deficit (1-h) increases and the vapour further depletes in ^{18}O because of increased kinetic fractionation effects (Equation 2.8). Simulated fluctuations in relative humidity are highly pronounced, leading to short-term variability in δ_E. Given the strong dependence of δ_E on relative humidity, continuous atmospheric forcing for model simulations is preferable over the temperature-dependant computed relative humidity described in Section 6.2 and used in the FSB simulations.

From Figure 3.11 (the $\delta^{18}O$- $\delta^{2}H$ plot for the FSB), the expected composition of δ_E should lie to the left of the GMWL along the backwards trajectory of the LEL. The average isotopic composition of evaporating moisture in 1997 should therefore be less than -24‰, and should decrease along the same slope as the LEL predicted from long-term Climate Normals reported

in Chapter 3 (~4.2). The simulated average composition of -38‰ for $\delta^{18}O$ in 1997 therefore appears to be a reasonable estimation of evaporating moisture in the FSB.

Similarly, St. Amour *et al.* (2005) reported the limiting steady-state isotopic composition (δ^*) of surface water in the FSB during 1997 to be between -6 and -7‰. The isoWATFLOOD model computes an average δ^* for the 1997 season of -5.7‰, which is slightly more enriched than the reported value. The more enriched simulated δ^* composition could be accounted for by the averaged, constant composition of precipitation used in the model. St. Amour *et al.* (2005) used varying compositions of precipitation that were at times reported to be quite depleted relative to the seasonal average at times. This is an example of why it is preferable to model or directly measure time-varying inputs of isotopes in precipitation. Over the entire study period (1996 to 1999), the model simulates an average δ_E of -39‰ and average δ^* of -6.7‰, which fit with the isotopic framework derived by St. Amour *et al.* (2005). The simulation of isotopic fractionation of surface waters in isoWATFLOOD appears to be correctly simulated relative to observed isotopic conditions in the FSB.

When moisture evaporates, there is isotopic enrichment (i.e., an accumulation of heavy isotopes) in the remaining hydrologic storage. In isoWATFLOOD, this was simulated using the equations outlined in Section 6.3 (Equations 6.8 and 6.9) to describe evaporative enrichment in lakes modified to include wetland and soil moisture evaporative fractionation. To examine whether or not the isoWATFLOOD model simulates the subsequent isotopic enrichment of water remaining in storage, the soil moisture profile in Jean-Marie River basin was analysed (Figure 8.14). The 1997 soilwater $\delta^{18}O$ response surface was plotted for the UZS of one prevalent land classification: the mixed and deciduous tree classification. A second simulation was run where evaporation from the soil layers was turned off, allowing for an identification of the effect of evaporation on soil moisture composition similar to the model diagnostic performed in Section 7.1. Interpretation of the soil moisture profiles however is discussed in Section 8.4.3. Figure 8.14 compares the results of both simulations for 1997 in Jean-Marie River, where 'case a' is with soilwater evaporation and 'case b' is without evaporation.

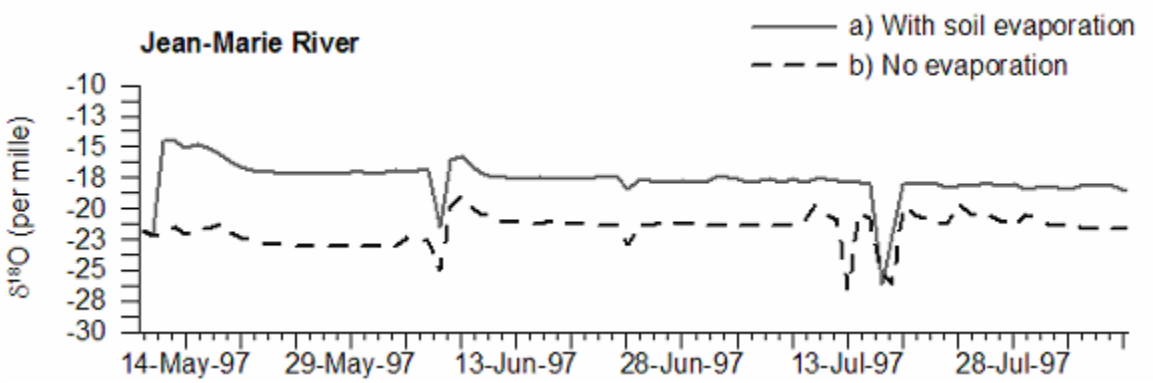

Figure 8.14 – Soil moisture $\delta^{18}O$ profile in upper zone storage simulated by isoWATFLOOD a) with soilwater evaporation, and b) without soilwater evaporation.

The first deviation between the two simulations occurs post-freshet (May 14th, 1997), once the snowpack melts and evaporation of soil and surface water begins. The 'case a' $\delta^{18}O$ profile remains more enriched (~2-3‰) than 'case b' throughout the 1997 summer season. According to Barnes & Turner (1998), an average 1‰ evaporative enrichment in soils is expected at humid soil surfaces; although there would be a great deal of variation about this average depending on specific meteorological and soil moisture conditions. isoWATFLOOD approximates an appropriate amount of soilwater enrichment considering 1997 was a wet summer with high soil moisture content. The 'case a' profile remains relatively constant throughout the summer and shows small fluctuations with evaporation and relative humidity, which would be expected as isotopic enrichment increases and decreases. The trend for 'case a' throughout the summer however, shows slight and gradual isotopic depletion that is not observed in 'case b'. This is the effect of precipitation on the evaporatively enriched profile (case a) as soilwater depletes with each rainfall event. In 'case b', soilwater is already more depleted than rainfall and instead experiences slight enrichments following some rainfall events (early- and late-July). This rainfall-driven response is particularly notable on Figure 8.14 for 'case b', where the composition of soil moisture enriches following each July rainfall event. Upon close inspection, the July 13-15th rainfall events cause a slight depletion of soil moisture in 'case a'. The isotopic depletion in evaporating moisture results in a gradual enrichment of soil moisture during periods of no rainfall relative to a case where there was no evaporation modelled.

8.4 Modelling $\delta^{18}O$ in Hydrologic storage

The application of isotope tracers as soft data in model calibration is not a new concept (Vache & McDonnell, 2006); however, the ability to implicitly model changes in $\delta^{18}O$ in mesoscale watersheds is just beginning to emerge. The isoWATFLOOD model has shown to improve model calibration (Section 8.1). The model has been validated hydrologically and isotopically for two events in the FSB, and the results have been realistic. It is also important however to also diagnose if the correct $\delta^{18}O$ of streamflow is simulated for the correct reasons. The following section will examine internal isotope profiles simulated by isoWATFLOOD, including snowmelt (Section 8.4.1), surface storage and overland flow (Section 8.4.2), soilwater storage and interflow (Section 8.4.3), LZS and baseflow (Section 8.4.4), and wetland storage (Section 8.4.5).

Data from two published FSB isotopic studies will be used for verification of isoWATFLOOD simulations. Hayashi *et al.* (2004) analysed isotopic variation and source water contributions in the Scotty Creek basin, performing a two-component isotopic separation of event and pre-event water to quantify snowmelt contributions to streamflow. St. Amour *et al.* (2005) also performed two-component isotopic mixing model separations; however applied the approach twice to segregate freshet and rainfall contributions as the season evolved. Using isoWATFLOOD, a more detailed analysis of the time-series isotopic evolution of these and other end-members is facilitated and compared with the results from the above studies.

The results presented in the following sections are derived from the continuous FSB simulation presented in Section 8.2.3. For analysis purposes, only one season of simulated results is shown at a time to enable a closer, more detailed examination of the model's behaviour. For each discussion the results from only one or two basins in the FSB have been shown; selected by their characterization of, and dependence upon on each hydrological process. The intent is to utilize the continuous simulation to determine both model strengths and areas for improvement identified by close examination of the processes contributing to streamflow generation and isotopic composition.

8.4.1 Snowmelt

Water frozen in a snowpack can undergo several cycles of melting and refreezing; each time undergoing isotopic fractionation. As the snowpack ripens and meltwater is initially produced, the early contributions to streamflow from meltwater are typically more depleted in heavy isotopes than the later stages of snowmelt contribution (IAEA, 1981).

The Martin River basin was selected for this analysis given that it has amongst the highest snow accumulation in the FSB. Isographs of the Martin River 1998 and 1999 freshet streamflow compositions were shown on Figure 8.12, whereas Figure 8.15 illustrates the step-wise isotopic variation of snowmelt simulated by isoWATFLOOD. The model simulates meltwater signatures only during melt events (i.e., when the snowpack is ripe, snow covered area is less than one but greater than zero, and meltwater is contributing to streamflow), causing a step-wise isograph to be produced.

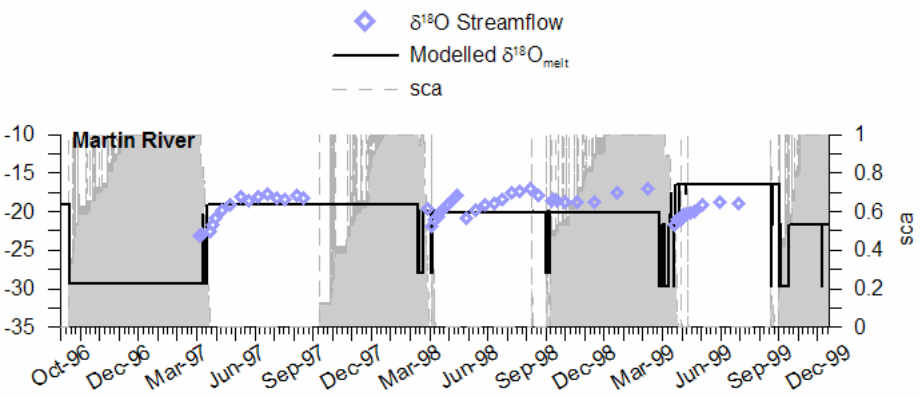

Figure 8.15 – Isotopic variation in snowmelt simulated by isoWATFLOOD for the Martin River basin.

The initiation of each snowmelt event visibly corresponds with the lowest isotopic composition of streamflow in March 1997, 1998, and 1999. A closer look at the 1999 freshet (Figure 8.16) shows even more clearly the early-melt depleted compositions from the ripe snowpack, (i.e., ~mid-April). Similar to findings of St. Amour *et al.* (2005), the most depleted isotopic signal of meltwater occurs simultaneously with the first peak in freshet streamflow. As the freshet progresses and the snowpack decreases, compositions of meltwater gradually enrich and approach summer meteoric water compositions. At the end of April (~April 29th), a more enriched composition of snowmelt is simulated by the model. During the 1999 freshet there

was a rainfall event (~April 28th) and water released from the pack was more enriched, reflecting the rainfall runoff signature.

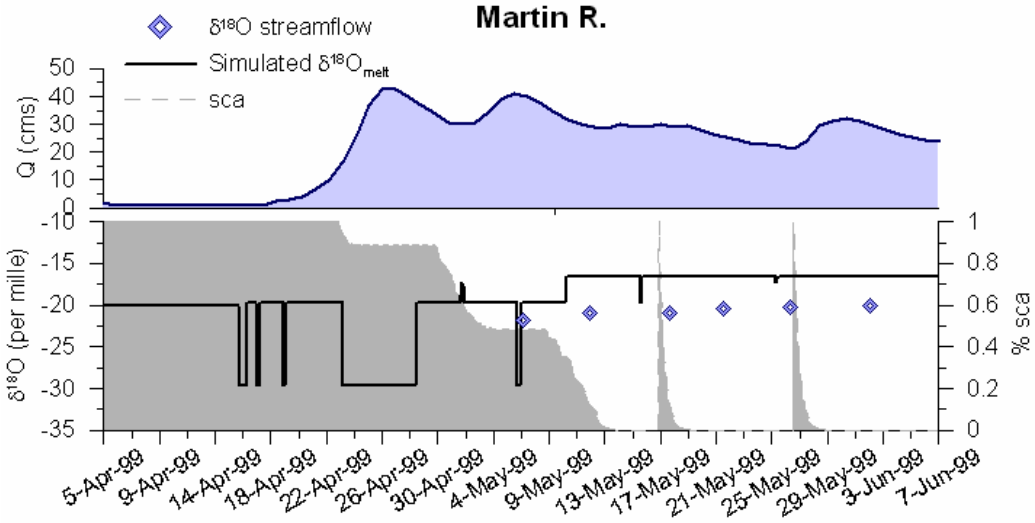

Figure 8.16 – isoWATFLOOD-simulated Martin River snowmelt for the 1999 freshet.

To examine the effect of snowmelt depletion on streamflow composition, a second simulation was run in isoWATFLOOD where variable snowmelt compositions were not simulated. Figure 8.17 compares the simulated $\delta^{18}O$ of streamflow in the Martin River basin when variable snowmelt composition is modelled (case a) to when it is not modelled (case b). The $\delta^{18}O$ of streamflow is more enriched when snowmelt composition is constant, offset above the variable snowmelt composition case. Particularly during the initial freshet where the snowpack begins to ripen and melt in mid-April, 'case a' and 'case b' are seen to diverge: the composition of streamflow in 'case a' depletes and the composition of streamflow in 'case b' enriches. Although there is no measured data for comparison, the literature supports streamflow depletion with the onset of snowmelt (Cooper, 1998; Hayashi *et al.*, 2004; IAEA, 1981; St Amour *et al.*, 2005).

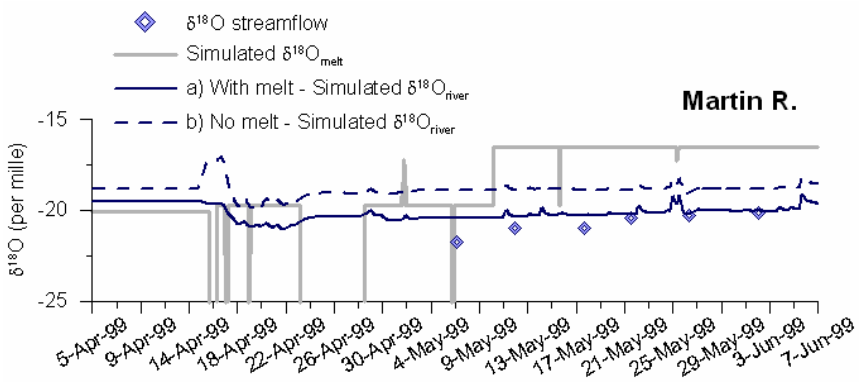

Figure 8.17 – isoWATFLOOD-simulated 1999 freshet in Martin River a) with snowmelt fractionation, and b) without snowmelt fractionation.

Figure 8.11 shows that the model deviates from measured winter ice-on isotopic compositions. Measured $\delta^{18}O$ compositions indicate a gradual depletion in streamflow as freeze-up is initiated and maintained, reflecting the influence of baseflow as the dominant end-member during ice-on periods. The isoWATFLOOD model simulates a gradual enrichment towards a constant, more enriched late fall composition that is maintained throughout the ice-on period. Simulated late fall enrichments are attributed to the increased contribution of enriched wetland water, likely indicating an over-estimation of wetland contributions or wetland enrichment. During the winter months the model does not simulate changes in ice or snowpack compositions, and when snow covered area is 100%, runoff processes contributing to streamflow are stagnated. The results of the continuous simulation show that the isotopic composition of snow cover and ice-on flows needs to be incorporated into the model.

Evaporation from the snowpack, or sublimation, would also result in additional isotopic fractionation of the snowpack and therefore enrichment of meltwater, but is not currently simulated by WATFLOOD or isoWATFLOOD.

Snowmelt generated from the pack typically contributes to streamflow after passing through sub-surface storages. The depleted isotopic signature of snowmelt during the spring freshet is seen in streamflow and within subsurface storages such as the UZS and LZS as surface water infiltrates. Surface storage and overland flow on bare ground area, however, carries a different signature derived than runoff from snow covered area.

8.4.2 Surface Storage & Overland Flow

Event water that is in excess of the infiltration capacity generates overland flow, or surface runoff. If the isotopic composition of meteoric water changes during a series of events, or if a mixed precipitation events occur, the $\delta^{18}O$ of surface storage and runoff is altered from the meteoric composition.

The Jean-Marie River basin was selected for this analysis at random since all basins exhibit the same overall response for surface water due to the assumed constant composition of meteoric inputs. Surface water storage varies with land classification, which alters the amount and frequency of surface storage but not the isotopic composition. Figure 8.18 illustrates the step-wise, discontinuous $\delta^{18}O$ variation of surface water simulated by isoWATFLOOD for the mixed-deciduous forest landcover classification in Jean-Marie River basin. The isotopic composition of surface water is simulated only when there is surface runoff generated during an event. The amount of surface water excess remaining in depression storage is represented on Figure 8.18 in grey, corresponding with the computation of an isotopic composition of the storage volume.

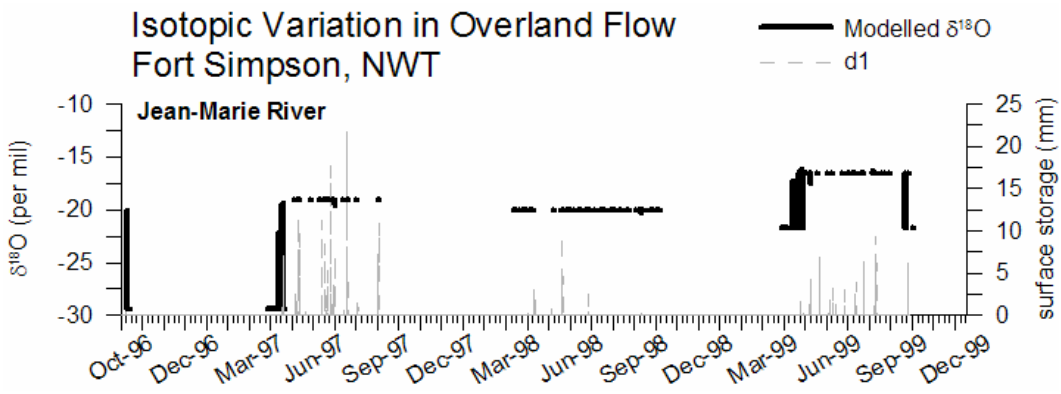

Figure 8.18 – isoWATFLOOD-simulated surface water storage for the Jean-Marie River.

Changes in composition are a reflection of seasonally varying compositions of precipitation defined in the 'isotope.par' file (Appendix A.2.2). Figure 8.19 enlarges a portion of the Figure 8.18 time-scale to show the surface water $\delta^{18}O$ variation for 1997; which was a wet, rainfall-dominated year relative to the other two study seasons (Table 3.5). The mixing of event waters during the freshet period (early May) is illustrated, where oscillating compositions are derived

from a series of rain-on-snow events. Overland flow and water infiltrating from surface storage carry a more depleted (i.e., relative to meteoric input) composition during freshet that gradually enriches towards the meteoric composition of rainfall (δ_P) as snow cover wanes. There is a strong correlation between the composition of meteoric water and the $\delta^{18}O$ of hydrologic storage (and therefore streamflow). If a constant meteoric composition is assumed (as it is here), then error is most certainly introduced into the simulation by not capturing the true variability of seasonal rainfall signatures.

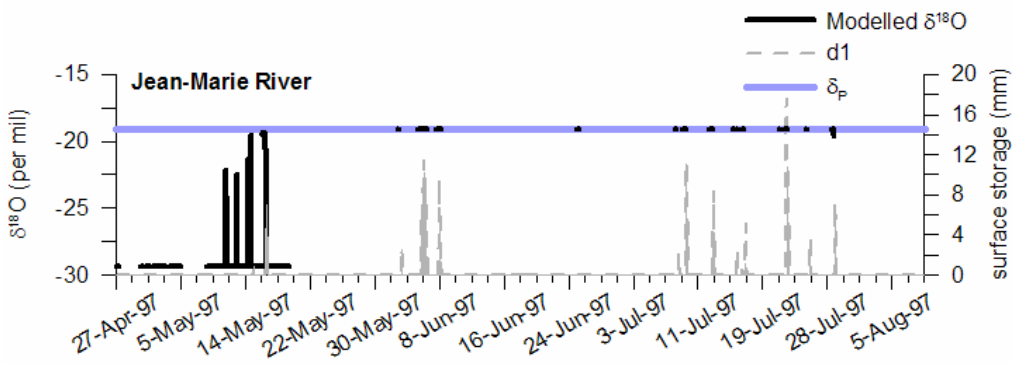

Figure 8.19 – 1997 isoWATFLOOD-simulated surface water storage for the Jean-Marie River basin.

St. Amour *et al.* (2005) reported that the spatial variability of rainfall was relatively low in the FSB, but that there was considerable temporal variability measured between rainfall events. An average variation of 11‰ in $\delta^{18}O$ of rainfall was reported in the FSB from 1997 to 1999. Given a variable rainfall composition is not used to force isoWATFLOOD, the model naturally simulates a more constant isotopic profile in surface storage that is affected only by the form of precipitation (i.e., rain or snow). In reality, the composition of precipitation is also affected by the amount of precipitation: more intense and larger events typically lead to more depleted precipitation. Errors derived from inaccurate forcing of isotopic simulations can be substantially reduced by using time variable meteorological inputs to represent the composition of rainfall and snowfall. Although it is preferable to measure compositions of rainfall, this is not feasible for mesoscale catchments simulated continuously over several years. To supplement measured data, an isotopically-enabled GCM or RCM could be feasibly used to derive variable atmospheric inputs (Section 6.2.1).

The majority of event water does not runoff, but generates infiltration into the subsurface (UZS) when the land classification is such that infiltration is possible (i.e., not impervious). Water contributing to UZS initially has the isotopic composition of the surface storage, which represents a signature close to (if not exactly equal to) the signature of meteoric water. Water infiltrating from snow-covered and bare-ground areas combine in the UZS to generate an isotopic composition unique to the soilwater in storage.

8.4.3 Upper Zone Storage & Interflow

Water infiltrating into the UZS combines with existing soil moisture or 'old' water that may have a similar signature, or be isotopically enriched from soilwater evaporation.

All five FSBs produced similar magnitude and variations in $\delta^{18}O$ of soilwater over the three year study period, therefore as an example Jean-Marie basin is shown on Figure 8.20 for the mixed-deciduous forest landcover classification. Figure 8.20 depicts both the change in volume (shown in grey, in mm of water) and composition of the UZS. isoWATFLOOD simulates variable soil moisture with frequent depletions during snow-free periods that are connected by constant compositions during frozen soil periods. During freeze-up, WATFLOOD does not infiltrate or evaporate water into or out of the UZS; therefore the isotopic composition during these periods remains constant at the composition at freeze-up. During snow-free periods however, considerable isotopic variation is simulated with an average $\Delta\delta^{18}O$ variation of 13.5‰ across all five basins over the three ice-free periods (April to September). The basins are all similar in their variation of soilwater composition, averaging between 6 to 7.7‰ change in $\delta^{18}O$ during the ice-free seasons. The 1997 season is the most variable as a result of the higher soil moisture and infiltration volumes due to heavy and frequent rainfalls. The Blackstone River was found to have the most variable soilwater composition, averaging a $\Delta\delta^{18}O$ of 7.7‰ from 1997 to 1999. In 1997 Scotty Creek was least variable ($\Delta\delta^{18}O$=4.5‰); and in 1999, Jean-Marie basin was least variable ($\Delta\delta^{18}O$=4.6‰).

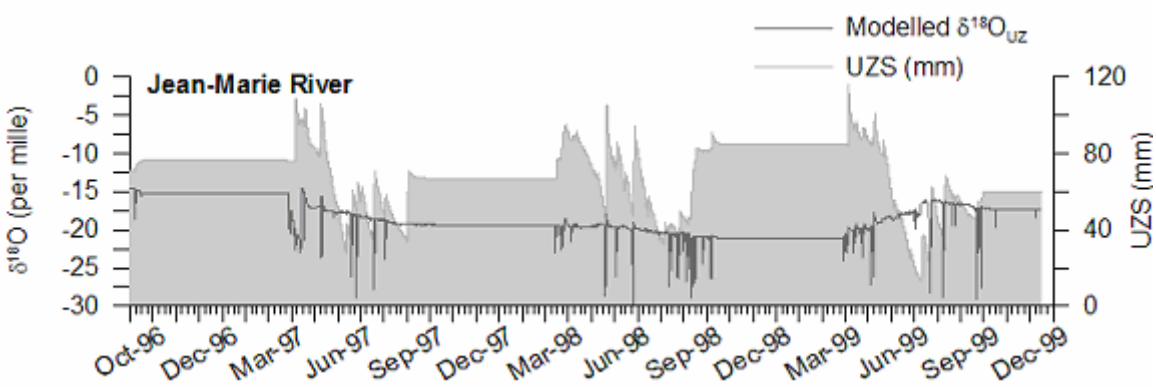

Figure 8.20 – Isotopic variation in soil moisture simulated by isoWATFLOOD in the FSB.

Land class distribution has a direct and distinct effect on the variability of soilwater $\delta^{18}O$ because of differences in infiltration, drainage and evaporation rates. To illustrate these land class induced variations of soilwater composition, the $\delta^{18}O$ of the UZS for each land class in the Jean-Marie River basin is shown on Figure 8.21 for one month in the summer of 1999 (June to July).

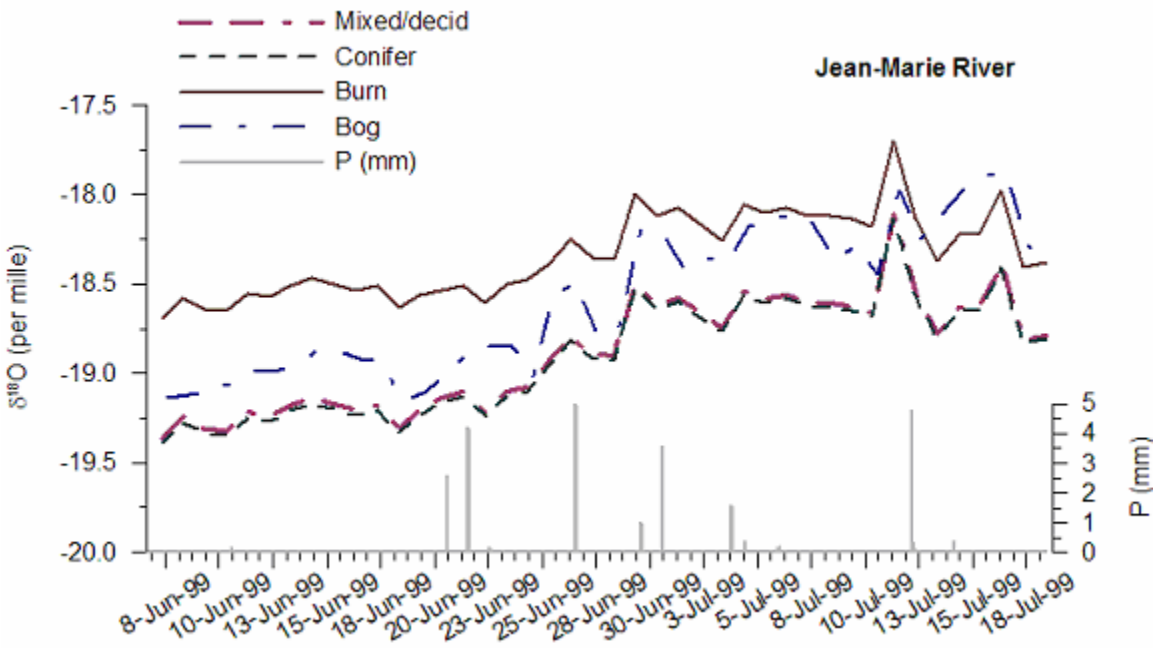

Figure 8.21 – Variation of 1999 soilwater composition by landcover classification for Jean-Marie River.

The soilwater composition of the transitional, or burn re-growth classification, is the most enriched because of increased soilwater evaporation due to a lack of ground cover. Vegetative

cover provides shade, therefore lowering heat input and acting to increase surface-soil boundary layer humidity gradients. With lower heat input and higher humidity, vegetated landcovers effectively reduce evaporation and therefore isotopic fractionation. The burn classification is analogous to bare ground or exposed soil, which is known to have higher rates of evaporation (Kite, 2000; Persaud & Khosla, 1999). The most depleted soilwater composition is simulated for the conifer land classification, which has extensive vegetative ground cover and shaded area. Little variation between the vegetatively covered land classifications is seen on Figure 8.21, indicating the differences in land class compositions are primarily influenced by evaporation of soilwater in storage. Interestingly the bog land classification is not as enriched as the transitional re-growth class, the result of low water levels decreasing the rate of evaporation (and therefore isotopic fractionation) because of increased vegetation and higher humidity at the bog-subsurface interface (Sánchez-Carrillo *et al.*, 2004). The 1999 season had the least amount of precipitation (and therefore runoff and infiltration) as compared with 1997 and 1998, resulting in the drying of surface hydrological storages. Figure 8.21 shows a 1‰ to 1.5‰ enrichment in the $\delta^{18}O$ of soilwater, which corresponds well with the 1‰ average soilwater enrichment (in humid environments) reported by Barnes & Turner (1998).

Figure 8.20 and Figure 8.21 show high variability in soilwater composition, and indicate occasional sudden depletions in the composition of soilwater. Figure 8.21 illustrates that the largest changes in soilwater $\delta^{18}O$ are often induced by rainfall events (e.g., July 10th, 1999), where the relative humidity (h) approaches one. As relative humidity approaches one, 'm' becomes large (i.e., kinetic fractionation increases the rate of heavy isotope build-up) and exponentially increases δ_L, which represents the isotopic composition of the soilwater. Although numerically this phenomenon is clear, it has been difficult to capture such isotopic variability in reality since continuous time series sampling is generally not feasible in field studies. There are studies however that reinforce the sudden and reactive nature of soil moisture isotopic composition in response to moisture content and event water infiltration (Iorgulescu *et al.*, 2007). Again, it is apparent that the quality of forcing data has a substantial role to play in accurately simulating the response of $\delta^{18}O$ in hydrologic storage. Both the composition of precipitation and the relative humidity have substantial effects on the variability of soilwater composition.

Combining with the water already in longer-term residence in the lower zone storage (LZS), soilwater drainage typically contributes a more enriched, event-derived source water signal to the LZS.

8.4.4 Lower Zone Storage & Baseflow

The LZS is characterized as shallow, event-responsive groundwater in isoWATFLOOD that receives water from the UZS, mixes it with existing water in LZS, and then drains laterally into channels or wetlands via baseflow.

The variation of $\delta^{18}O$ in LZS is shown on Figure 8.22 in comparison with mixing model derived baseflow compositions from Section 5.4. The simulated average composition of baseflow is more depleted than surface and soilwater at -19‰ on average over the three years. Baseflow (i.e., shallow groundwater) compositions should be representative of the long-term average composition of local meteoric water (IAEA, 1981), which considering both snow and rainfall is approximately -22‰ over the study period. This suggests insufficient simulated depletion of a source water component (Section 8.4.1 and Section 8.4.2), or the contribution of overly-enriched source water from ice-on periods (Section 8.4.1).

The simulated variation in LZS is shown to be responsive to the freshet and large rainfall events: periods where large volumes of water infiltrate into the LZS (Figure 8.22). During spring freshet, the composition of baseflow depletes to its lowest seasonal composition as the volume of water in LZS (i.e., shown in grey) rises with meltwater drainage. When there are multiple melt events, more than one isotopic depletion is observed in LZS composition (i.e., 1997 and 1998 freshets). Following spring freshet, LZS $\delta^{18}O$ enriches to a pseudo-constant summer composition influenced by drainage of enriched soilwater. Occasionally large rainfall events significantly depleted UZS compositions (discussed in Section 8.4.3) and result in summer baseflow depletions as observed in the wet 1998 season (i.e., May, June and September events).

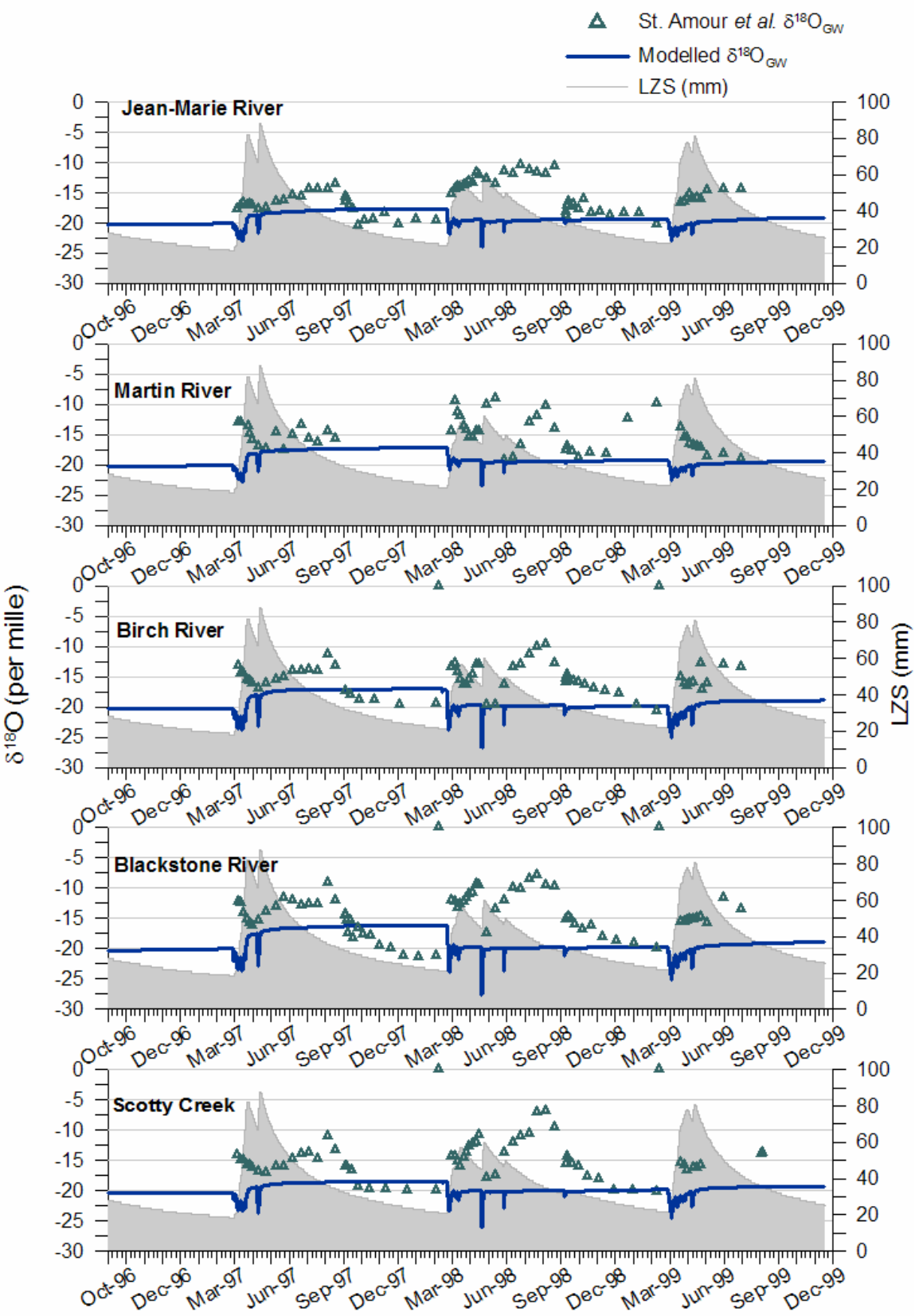

Figure 8.22 – Isotopic variation in baseflow simulated by isoWATFLOOD for the FSB.

Overall the LZS $\delta^{18}O$ response surface is steady due to the mixing of event-based soilwater inflows with existing water in residence, reducing isotopic variability. Maximum summer enrichments are limited by moisture availability and relative humidity (Section 2.4.2), resulting in an asymptotic approach to an enriched baseflow composition. Within the FSB, long-term average LZS compositions vary by only $\Delta\delta^{18}O$=0.76‰, representing muted inter-basin differences from soilwater.

'Measured' $\delta^{18}O$ compositions of baseflow shown on Figure 8.22 (i.e., triangles) are derived by St. Amour *et al.*'s (2005) mixing model approach (Section 5.4.2). Differences between the two simulations of baseflow composition are notable. Most similar are the simulations of late winter, ice-on compositions, where the two models appear to generally converge for all five basins (e.g., 1998). In 1997 however, the Birch and Blackstone River late-winter mixing model compositions were approximately 2‰ and 4‰ more depleted, respectively than the isoWATFLOOD simulation. Maximum enriched mixing model baseflow compositions (i.e., during summer) corresponded to percent baseflow contributions ranging from 55 to 98% of total streamflow (74% on average). Isotopically compositions seem too enriched, and hydrologically baseflow contributions seem high for the FSB regime (i.e., semi permafrost). The pre-calibration isoWATFLOOD simulation performed in Section 8.1 utilized a parameter set calibrated to reproduce St. Amour *et al.'s* (2005) estimates of baseflow (Section 5.4) and was shown to have unrealistic interflow and surface runoff responses. The lack of information available to quantifiably segregate soilwater from LZS components using the mixing model approach likely resulted in the mixing of these two components, leading to an over-estimation of the true baseflow component contributing to streamflow.

If St. Amour *et al.*'s (2005) baseflow compositions were in fact a mixture of soilwater and baseflow then late-winter ice-on compositions from the two models would be expected to converge given the lack of soilwater influence (shown on Figure 8.22). Similarly late summer evaporatively-enriched soilwater compositions should correlate with evaporatively-enriched summer compositions representing the dominant soilwater end-member. Figure 8.23 shows isoWATFLOOD-simulated soilwater compositions relative to mixing model derived baseflow, showing a convergence between the two models during summer periods.

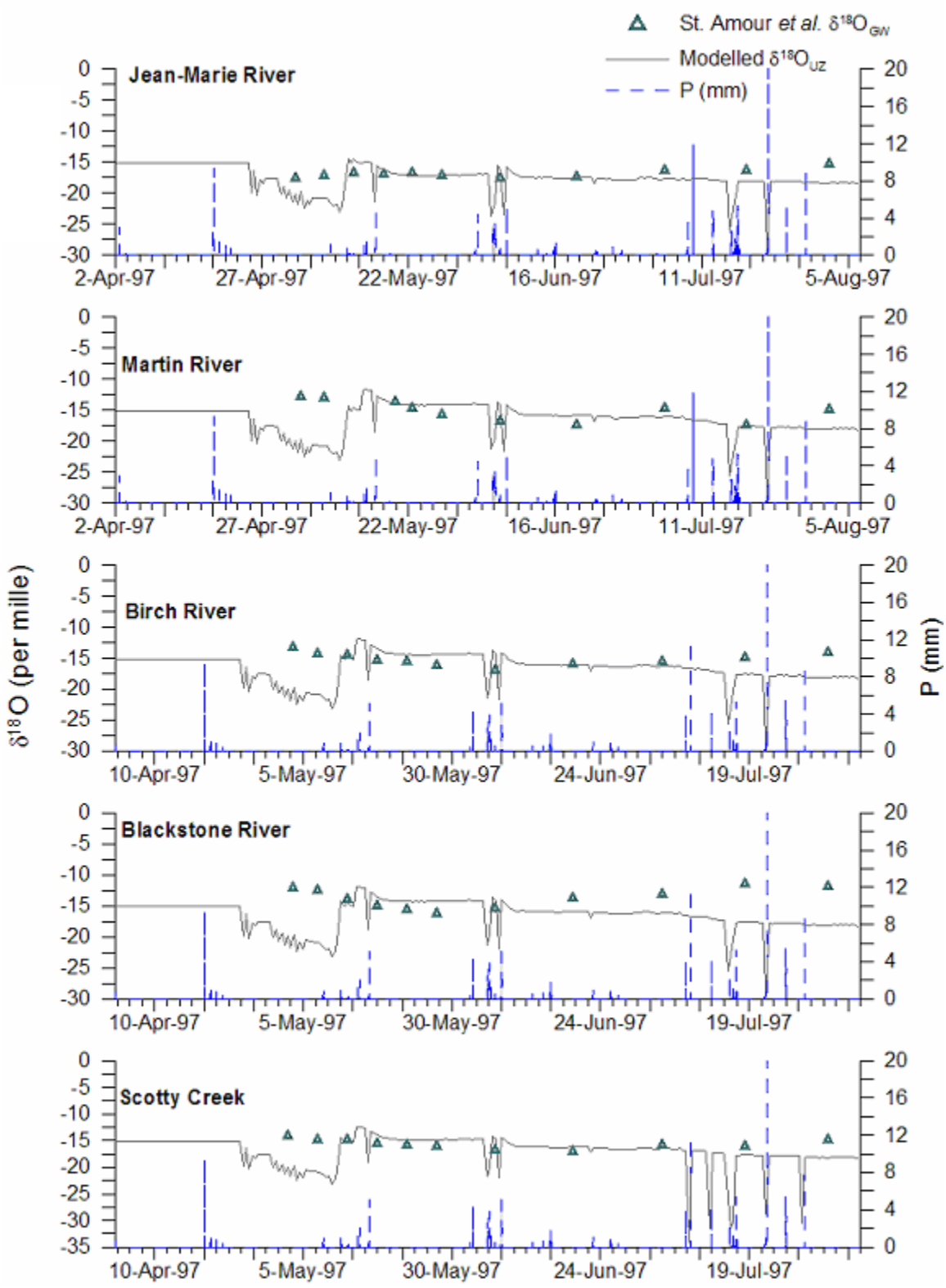

Figure 8.23 – isoWATFLOOD-simulated UZS composition relative to St. Amour et al.'s (2005) mixing model derived baseflow compositions for the FSB 1997 study season.

Post-freshet and summer mixing model baseflow compositions correspond to isoWATFLOOD-simulated UZS compositions better than they do with simulated LZS compositions (Figure 8.23). Late summer variations in mixing model compositions are shown to be well timed with sporadic rainfall events in 1997. Mixing model baseflow compositions (i.e., triangles) appear to be evaporatively influenced during late summer periods based on the general isotopic enrichment trend. They are also meteorically influenced based on small, intermittent depletions corresponding with rainfall events (Figure 8.23), as would be expected in soilwater. Figure 8.23 also illustrates that isoWATFLOOD soilwater compositions converge with mixing model compositions during summer periods, highlighting that sometimes rigorous separations between baseflow and soilwater components are in fact required for mixing model approaches. Model simulations in Blackstone and Birch Rivers however diverge during the late summer rainy period. Both basins have the highest percentage of bogs, which are highly responsive to meteoric water. The divergence between the models is likely the result of an under-estimation of bog evaporation by isoWATFLOOD, or the simulation of rainfall with a more depleted composition than what occurred in reality. isoWATFLOOD-simulated soilwater compositions appear to be slightly more depleted throughout the summer months, pointing to an under-representation of evaporative enrichment, or a more depleted (than in reality) rainfall signature.

The correlation between St. Amour *et al.*'s (2005) summer baseflow compositions with isoWATFLOOD soilwater, and the convergence of winter baseflow compositions, suggests the mixing model approach in fact combines these two sources of subsurface flow. This results in the over-estimation of summer baseflow quantity and composition by the mixing-model approach.

Based on reported theory and current literature (Barnes & Turner, 1998; Iorgulescu *et al.* 2007), near surface isotopic compositions should be temporally variable but should gradually converge with increasing depth. To illustrate isoWATFLOOD's simulation of $\delta^{18}O$ through depth of the subsurface, the isotopic composition of soilwater and LZS was plotted with time variant depth of the UZS (in mm of water) (Figure 8.24).

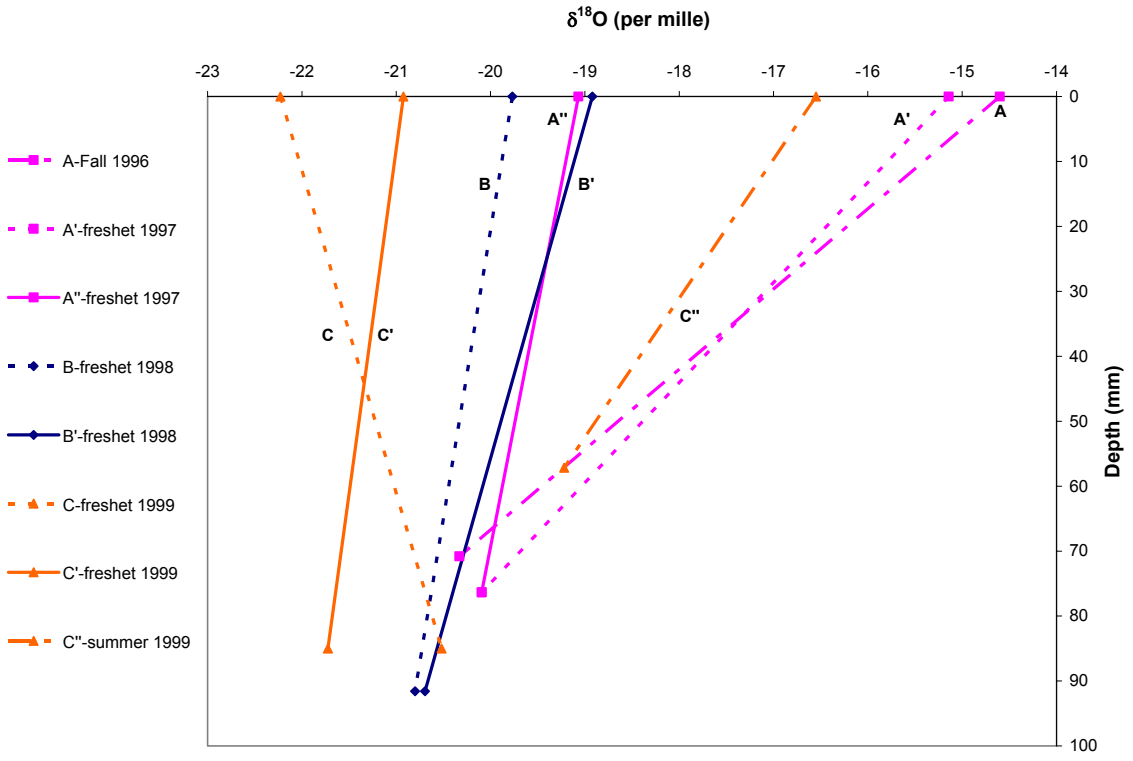

Figure 8.24 - Isotopic variation with depth simulated by isoWATFLOOD for the Jean-Marie basin.

Iorgulescu *et al.* (2007) reported convergence to baseflow compositions within approximately 140 cm of soil depth, which was also represented on Figure 2.5 (Section 2.4.2). The evolution of $\delta^{18}O$ simulated by isoWATFLOOD through the soil matrix on Figure 8.24 is presented for each study year (A-A"=1997, B-B'=1998, C-C"=1999). In late 1996 (A) $\delta^{18}O$ near-surface was isotopically enriched relative to the initial onset of the 1997 freshet (A'). As depleted snowmelt infiltrates into the subsurface, near-surface soilwater compositions deplete (A"), while LZS compositions remain relatively constant between 70 and 80 mm below the surface. In 1998, early freshet compositions (B) are initially depleted and evolve to more enriched near-surface compositions (B'). Lower zone compositions in 1998 were constant and more depleted than LZS compositions in 1997, and there is less difference between UZS and LZS compositions in general during 1998; likely a result of the heavy and frequent rainfall events. Near surface compositions at the onset of the freshet in 1999 (C) are the most isotopically depleted of the three years due to the influence of meteoric water in storage carried over from 1998. Baseflow isotopic compositions at the start of 1999 (C) are very close to those

in 1997 and 1998 resulting from 1998 water in LZS at the start of 1999. As 1999 freshet progresses (C'), near-surface compositions increase due to a series of enriched rainfall events, whereas LZS compositions deplete from the infiltration of depleted snowmelt. By late summer 1999 (C"), both the near surface compositions and LZS compositions become enriched relative to 1999 freshet $\delta^{18}O$ profiles resulting from the high evaporative losses from UZS and drainage of enriched soilwater into the LZS. In all years, convergence of the subsurface isotopic response is reached well within 100 mm depth into the subsurface.

All three years show a distinct mixing through depth of the soil column as is reported by other researchers (Iorgulescu *et al.*, 2007; Landon *et al.*, 2000). The evolution of the $\delta^{18}O$ profiles with depth of soil (from UZ to LZ) exhibit typical and explainable behaviours indicating a consistent and representative characteristic behaviour of both the soilwater and LZS profiling simulated by isoWATFLOOD.

The baseflow component is typically more depleted than the water it combines with (i.e., wetland or river water) given it is not directly evaporatively-enriched. Grid cells with fens capture the lateral baseflow component in the fen, along with interflow, overland runoff components prior to releasing these inflows to the channel.

8.4.5 Wetlands

Channel fens as summarised by Quinton *et al.* (2003) have the ability to act as streamflow buffers within hydrological regimes. Unlike the characteristic flat bog wetland classification, channelized fens connect lakes to streams and capture runoff from the surrounding landscapes. Fens receive runoff from surficial and subsurface storage, and hydrologically control runoff-release into adjacent channel networks.

The Jean-Marie River basin was selected to illustrate the isotopic variation in channelized fens because it is a fen-dominated catchment (Table 4.3). Figure 8.25 shows the isoWATFLOOD-simulated $\delta^{18}O$ composition from fens at Jean-Marie River outlet over the three year study period. Also shown on Figure 8.25 for reference is the variation in fen storage (i.e., wstore; right

axis) and the fen, or wetland outflow to the channel (i.e., qo_{wet}). The wetland outflow is shown to be negative in response to runoff from large events (e.g., late July 1997), indicating a wetland inflow from the channel. Given Figure 8.25 represents the basin outlet, or the sum of all upstream flows, wetland-channel flow reversal is more common than it would be in smaller drainage-area headwater grids. The isotopic composition of the Jean-Marie River fen indicates depleted freshet compositions (i.e., March 1997, 1998 and 1999) in response to the inflow of depleted meltwater into the wetland. Following the freshet, summer compositions enrich towards a pseudo-steady composition typically reached in early- to mid-June. The attainment of a constant summer composition in Fort Simpson fen sites was also reported by Hayashi *et al.* (2004) who found that the Main Fen site in Scotty Creek basin approached a relatively constant composition of -15.5‰ following spring freshet in 2000.

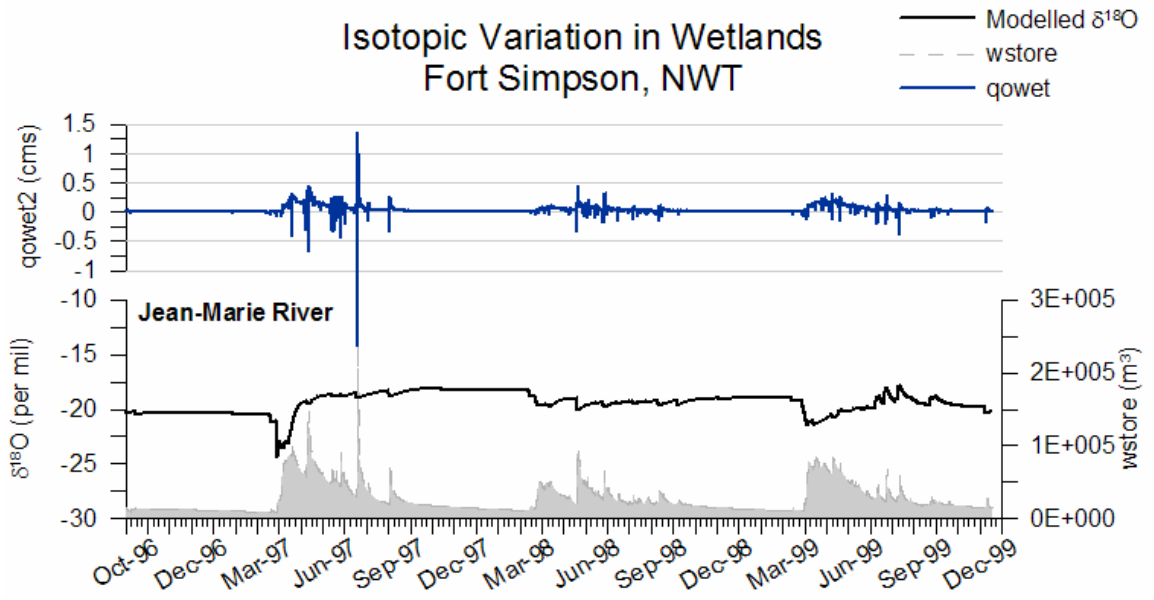

Figure 8.25 – Isotopic variation in fen-dominated Jean-Marie River basin as simulated by isoWATFLOOD.

On average summer fen compositions in Jean-Marie catchment were -18.4‰ ($\Delta\delta^{18}O$=3.0‰), 18.9‰ ($\Delta\delta^{18}O$=1.6‰), and -18.7‰ ($\Delta\delta^{18}O$=2.8‰) in 1997, 1998 and 1999, respectively (computed from June to October). The 1997 and 1998 seasons were more wet than 1999 with frequent and heavy rainfall events that inundate and saturate the fens, stabilizing their isotopic composition. In 1999 less frequent rainfall events result in a gradual drying of the basin and fens, therefore encouraging baseflow contributions to fens and rapid evaporative enrichment slopes (seen on Figure 8.25). Evaporation, and therefore evaporative fractionation,

sharply reduces during drying periods in isoWATFLOOD as a result of lower water levels in fens leading to more vegetative cover, higher humidity at the water surface, and higher non-fractionating transpiration rates (Section 4.2.4).

During winter ice-on periods, fen compositions tend to remain constant at late-fall, isotopically enriched values. This phenomenon is an artefact in the isoWATFLOOD model where ice-on (i.e., snow covered area greater than zero) means that fens freeze and hold their late-fall composition until spring freshet. In actual fact, larger fen sites likely do not entirely freeze-up, and isotopic compositions would gradually approach the baseflow composition.

In the FSB, fen $\delta^{18}O$ ranged from -18.8‰ (Blackstone River) to -19.3‰ (Scotty Creek) as shown in Table 8.6. The least depleted basins on average (Martin, Birch and Blackstone Rivers) were bog-dominated rather than fen-dominated, reflecting a larger influence of meteoric water rather than baseflow (Section 4.9). Both Jean-Marie and Scotty Creek basins (i.e., both fen-dominated) were the most depleted on average (-19.1‰ and -19.3‰, respectively). This reinforces St. Amour *et al.*'s (2005) observations that fen sites capture and slowly release significant amounts of depleted snowmelt and baseflow. The seasonal variation in fen composition ($\Delta\delta^{18}O$) ranged from 6.9‰ (Jean-Marie) to a 9.4‰ (Martin River), with higher percentages of fen leading to smaller fluctuations in $\delta^{18}O$ as a result of increased advective mixing and averaging of source waters. The average composition in fen sites was found to be similar to the three year average LZS compositions (Table 8.6); reinforcing that baseflow is a dominant contributing end-member to fens. Hayashi *et al.* (2004) reported that the isotopic composition in the Scotty Creek fen was comparable to measured baseflow compositions surrounding the fen. Table 8.6 shows that isoWATFLOOD also replicates this result.

Table 8.6 – Summary of Fort Simpson fen and baseflow $\delta^{18}O$ compositions simulated by isoWATFLOOD.

Basin	**$\delta^{18}O_{fen}$ (‰)**	**$\Delta\delta^{18}O_{fen}$ (‰)**	**$\delta^{18}O_{GW}$ (‰)**	**$\Delta\delta^{18}O_{GW}$ (‰)**
Jean-Marie R.	-19.1	6.9	-19.1	5.8
Martin R.	-18.9	9.4	-18.9	5.7
Birch R.	-18.9	8.6	-19.0	9.1
Blackstone R.	-18.8	7.8	-18.8	10.9
Scotty Cr.	-19.3	7.3	-19.5	7.0
Average	**-19.0**	**8.0**	**-19.1**	**7.7**

Fen sites, in addition to damping streamflow isotopic and hydrologic responses, also provide natural flood attenuation during significant runoff events. Two large rainfalls induced channel flooding in August and September of 1997, producing large amounts of runoff in all five basins and raising channel levels above top of bank. Wetland reversal was induced whereby channel water flowed into adjacent fens, altering the isotopic composition of the fen storages. Figure 8.26 shows the influence of enriched channel water on fen $\delta^{18}O$ compositions in Scotty Creek (fen-dominated) and Blackstone River (bog-dominated) basin fen sites (i.e., at gauge outlets).

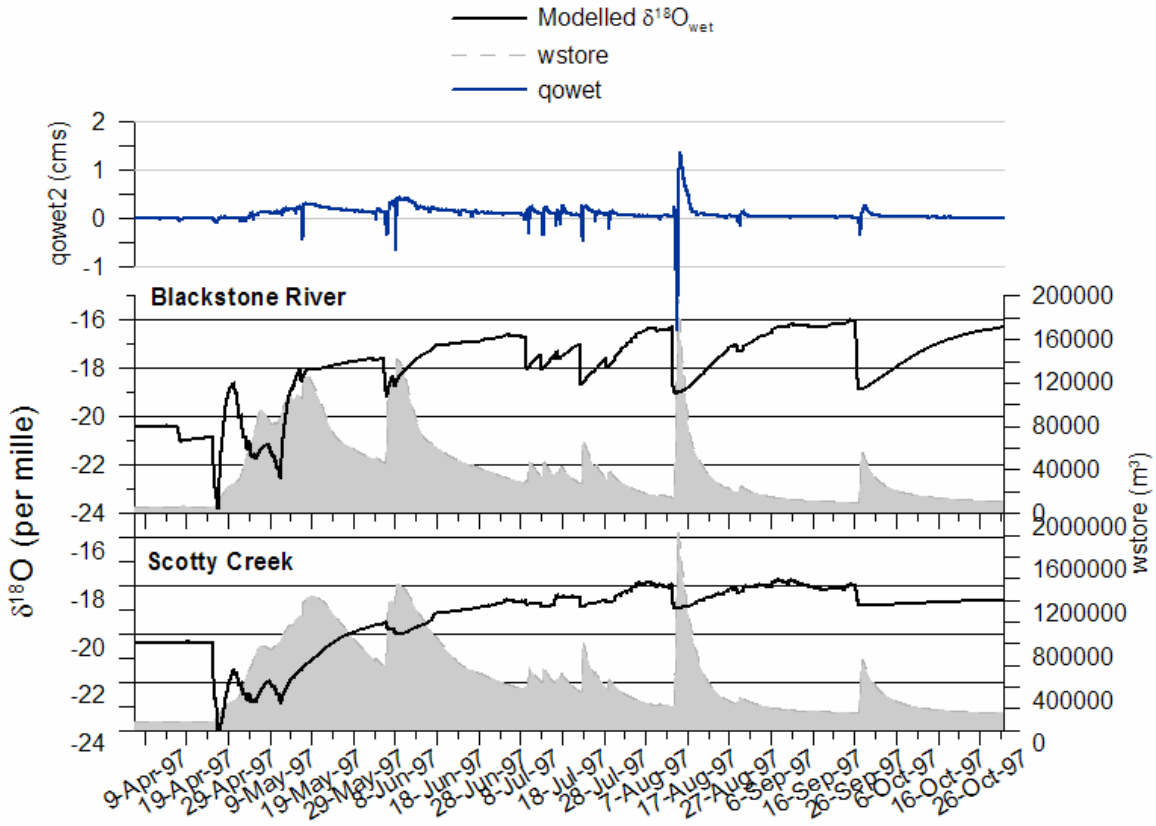

Figure 8.26 – Comparison of Scotty Creek (fen-dominated) and Blackstone River (bog-dominated) isotopic response to wetland flow reversal.

The reversal between the fen and channel causes an immediate increase in wetland storage and depletion in fen $\delta^{18}O$. The damping response of increased fen area is observed by comparing the response of bog-dominated Blackstone River and fen-dominated Scotty Creek to the August and September rainfall events. The Blackstone River fen site shows 3‰ enrichment in fen composition resulting from the inflow of enriched channel water into smaller fen sites (i.e., less volumetric damping) during both events. In contrast the Scotty Creek fen in response to the same rainfall events shows only 1‰ enrichment in fen composition for a similar volume

increase in fen storage (axis on the right). The simulated Scotty Creek fen composition is less variable than Blackstone River's fen composition, which is expected given the increased buffering capacity of the larger, more dominant fen site at Scotty Creek. During freshet, the Scotty Creek fen is also seen to reach and maintain a more depleted composition because of snowmelt retention. This is attributed to the influence of fen area, where more snowmelt is captured and retained for longer periods of time in larger fens. The fen-dominated catchments therefore tend to be more isotopically depleted, but less-variable on average as Table 8.6 shows.

The hydrologic response of channelized fens simulated by isoWATFLOOD appears to generate realistic trends and variability within FSB fen sites. Moreover, the capability of the model to reverse hydrologic gradients to receive channel inflow simulates the effect of over bank flooding of wetlands adjacent to channels, an important hydrological event in northern Canadian regimes (Falcone, 2007; Wolfe *et al.*, 2007).

8.5 Chapter Summary

In this chapter it was shown that although it is possible to reasonably simulate streamflow in remote, mesoscale catchments; the quality of the simulation is greatly dependant on the quality of forcing data. FSB streamflow simulations show how errors in rainfall data translate to errors in streamflow. Despite errors in model forcing however, the isoWATFLOOD model generates a more physically-based representation of streamflow by constraining internal model dynamics using both streamflow and the $\delta^{18}O$ of streamflow. When internal model dynamics are correctly constrained, the model accurately reproduces $\delta^{18}O$ in streamflow within the five FSBs. The model also facilitates a detailed examination of the variability in the processes contributing to streamflow $\delta^{18}O$. The ability to internally analyse streamflow generation processes in an efficient manner eliminates the necessity to utilize black-box modelling approaches. This approach to modelling enables a separation between errors derived from parameter uncertainty and error derived from model conceptualizations of hydrological processes.

The isoWATFLOOD model has been shown to reproduce isotopic variation in FSB streamflow. Despite the model's strengths, there are areas for improvement identified in this

chapter for the future versions of isoWATFLOOD, particularly during ice-on periods. The model has succeeded in reducing the likelihood of equifinality in streamflow simulation and has shown that it is possible to design a mesoscale modelling system that can reduce uncertainty in a feasible and efficient manner. With the incorporation of isotopes into WATFLOOD, and the presence of isotope data for model calibration, the use of a less parameterized model across large domains is justifiable. Operationally, such models are more desirable so long as they can produce simulations with provable certainty.

Using isoWATFLOOD, uncertainty in parameter estimation is highly constrained assisting with easier diagnosis of remaining causes of error between simulated and measured data. The reduction of parameter uncertainty is particularly difficult in remote, mesoscale catchments such as the FSB. Several researchers have recently developed statistical methods for simulation that help to address such issues under the Predictions in Ungauged Basins (PUB) initiative (Aronica & Candela, 2007; Chiang *et al.*, 2007; Feyen *et al.*, 2007; Feyen *et al.*, 2008). The isoWATFLOOD model is capable of assisting with parameter constraint in PUB basins, with the added advantage of constraining not only streamflow but also internal hydrological processes. Iorgulescu *et al.* (2007) calibrated a hydrochemical parametric model using ^{18}O isotopes to isolate individual hydrological processes. Their study highlighted the role of hydro-dynamic mixing processes in explaining ^{18}O tracer behaviour at the watershed scale; however they concluded that longer-term data sets and analyses would be necessary to increase parameter identifiability and relevance of hydrological process contributions (Iorgulescu *et al.*, 2007).

The next chapter presents the application of the isoWATFLOOD model to the Grand River Basin (GRB): a densely gauged, urban and agricultural basin. The model is not re-calibrated using isotopic simulation (i.e., hydrological calibration only) and is directly applied to the GRB using a previously existing parameter set. The goal of this second validation study is to determine the robustness of the isoWATFLOOD modelling system by evaluating whether less parameterized models can accurately capture hydrologic variability across a variety of contrasting hydrological regimes. The ability of the model to reproduce streamflows and the isotopic variation in streamflow in the GRB will be assessed using a more refined spatial grid (4 km^2), facilitating a discussion of simulated spatial and temporal variability.

Chapter 9

Stable Water Isotopes in Mesoscale Hydrological Modelling

In mesoscale hydrological studies, it is important to simulate representative streamflows from physically representative flowpaths. There is, however, a limited understanding of hydrological processes acting on the regional watershed-scale since flow processes cannot simply be scaled-up from smaller research-based catchment studies where such processes are well-defined (Kirchner, 2006). Particularly for prediction of streamflow in ungauged basins (PUB; Spence *et al.*, 2004) where measured streamflows are not readily available for model validation, internal model dynamics are relied upon for some degree of model calibration. Mesoscale hydrological variability and climate change impact studies also utilize hydrological models fed by variant climate forcing scenarios or other model inputs to predict potential impacts on streamflow generation. Model parameterizations of land-use are varied to infer the impacts of increasing urbanization on runoff generation (Barnett *et al.*, 2008; Dibike & Coulibaly, 2007; Pietroniro *et al.*, 2006; Pohl *et al.*, 2007; Quilbe *et al.*, 2008). Such simulations are made by models validated to modern-day streamflows, and typically with no validation of how internal hydrologic responses are changing. This is cause for concern given changes to precipitation or temperatures have an initial and direct impact on hydrological storages and process interactions that subsequently lead to changes in streamflow generation. In many modelling exercises, observing the effect of model parameters on internal flowpaths can help to define the physically realistic limits of the parameters themselves (Section 8.1.1).

Embedding water isotopes into a mesoscale hydrological model simulation enables the characterization of climate and hydrological change from both the hydrologic and isotopic perspective. Continuous simulation of hydrologic and isotopic variability connects changes in streamflow directly to the causes for those changes, which is validated by the isotopic response. In predictive climate change modelling, uncertainty in streamflow forecasting is typically constrained by subjecting the model to highly variable past climatic conditions to assess the models ability to recreate measured flows. The ability to derive inferred $\delta^{18}O$ records from sediments and other proxies (Danis, 2003; Wolfe *et al.*, 2005) establishes a much longer historical record than is available from streamflow, therefore also offering the potential to calibrate hydrological models on much longer historical records. By ensuring hydrological models accurately reproduce extended historical records, certainty in their future predictions can be enhanced.

In urbanized areas where streamflows *usually* are available for model calibration, the focus is on simulating mesoscale hydrologic behaviour and sensitivities to land-use change, urbanization, and operational water regulation. Quantifying with certainty the projected effects of anthropogenic alteration or the forecast of water storage and discharge requirements demands watershed-scale analyses. Power generators utilize mesoscale hydrological models to ascertain quantities of water needed for storage or release as flow stages vary from high to low-flow periods. The increase in climate variability in recent years has necessitated the utilization of hydrological models to predict possible variations in streamflow. Vicuna *et al.* (2008) reported one such study where several hydrological scenarios were established to inform power generators of the potential effects on reservoir storage, and to determine whether or not there was a sufficiently large storage capacity such that power supplies would not be interrupted. WATFLOOD is an attractive model for such studies because it is capable of efficiently modelling long time-series over large spatial domains; it facilitates alterations to reservoir locations and land classification; and it requires less parameterizations, and therefore rigorous calibration, than other similarly capable modelling systems. Canadian power generators such as Quebec Hydro, Ontario Power Generation and Manitoba Hydro are planning to use the WATFLOOD model for climate change studies and future operational applications (Kouwen, 2008).

In southern Ontario specifically there has been a focused effort to better understand the hydrology of the Laurentian Great Lakes system along the Canada-U.S. border. The necessity to understand this system is rooted in the need to realize changes to the water supply within the Great Lakes Basin (GLB). Both Canadian and U.S. governments rely on these waterways for transport of goods into and out of the countries, as well as for industry and domestic water use. Such a coordinated research effort involves regional hydrological modelling forced by meteorological simulations or ensemble forecasts of possible weather events. Environment Canada is currently developing such a modelling system (Modélisation Environmentale Communautaire: MEC) that is designed to produce operational hydrological forecasts from the coupling of land-surface-atmosphere and hydrological models (Pietroniro *et al.*, 2007). Their mandate is to improve water resource management in the Laurentian Great Lakes basin by using a coupled hydrometeorological modelling and ensemble forecasting approach. McBean & Motiee (2008) published a climate change impact study focused on the GLB that utilized traditional statistical analyses of long-term meteorological and hydrological data sets to determine if there were in fact statistically significant deviations of modern-day hydrologic conditions from those in the past. Results showed significant variability in predictions, with different results for different lakes that were attributable to lake size and location within the basin. Overall there is concern that some of the hydrologic changes observed in the basin may be the result of global warming and climate change (McBean & Motiee, 2008).

The isoWATFLOOD model is used in this chapter to produce a continuous simulation of GRB streamflow and isotopes, which is first validated against measured streamflow (Section 9.1.1) and isotopic time-series (Section 9.1.2) data. The simulation is then used to perform a qualitative assessment of the hydrologic and isotopic variability in the GRB. The variability assessment specifically examines how isotopes can facilitate the study of land-use alteration impacts (Section 9.2.1), and quantification of long-term lake water balances (Section 9.2.2). Lastly, the isoWATFLOOD model demonstrates its unique ability to visually portray both temporal and spatial variability in mesoscale hydrological research (Sections 9.2.4 and 9.2.3).

9.1 Modelling the Grand River Basin

The GRB is used for this study because of the availability of both hydrometric and isotopic data covering the spatial extent of the watershed for an extended time period. As was described in Section 4.8, the GRB is simulated in WATFLOOD at a resolution of 2 km by 2 km, covering a total area of over 6,000 km^2. There are four main tributaries within the watershed: Conestogo, Eramosa, Speed and Nith Rivers. From Chapter 3, Figure 3.3 shows the regional extent of the basin and the delineation of the main tributaries as it is in WATFLOOD. Landcover classifications are defined from the LandSat map presented previously on Figure 3.2.

The isoWATFLOOD model was run continuously for two full years (2004 to 2005) with a three-month model spin-up period from October to December 2003. Streamflow and isotopes were continuously simulated for all 41 GRB streamflow gauges, however results are presented for eight strategic locations: four points along the Grand River main-stem and four main tributary outflows (Table 9.1). The intent is to capture changes in hydrologic and isotopic response from the headwaters to the outlet of the basin, and to capture changes induced by tributary inflows. Analyses are performed on the stations presented in Table 9.1, each of which had complete hydrometric and isotopic data sets for 2004 and 2005.

Table 9.1 – Summary of stations included in analyses and rationale for station inclusion.

Gauge	DA (km^2)	Rationale
Grand @ Waldemar	620	Headwater basin; contains one controlled reservoir
Grand @ W. Montrose	1346	Characteristic of upper- to mid-Grand transition with steeper slopes; one reservoir between Waldemar and West Montrose; one tributary between (Irvine River), upstream of Conestogo tributaries
Conestogo @ St. Jacobs	820	Main tributary inflow to Grand River; one reservoir in sub-basin
Eramosa @ Guelph	226	Main tributary inflow to Speed River; wetland-dominated regime
Speed @ Beaverdale	710	Main tributary inflow to Grand River; one reservoir in sub-basin
Grand @ Galt	3494	Characteristic of mid- to lower-Grand with shallower slopes; last of controlled reservoir contributions; downstream of three of the four tributary inflows
Nith @ Canning	985	Main tributary inflow to Grand River; unregulated
Grand @ York	6245	Outflow of Grand River basin; culmination of all upstream hydrologic responses

Regional differences in the geology, ecology, and hydrology of the upper, middle and lower GRB were discussed in Section 3.1; however here Figure 9.1 illustrates the differences in basin landcover affecting sub-basin characteristic hydrologic responses in this study.

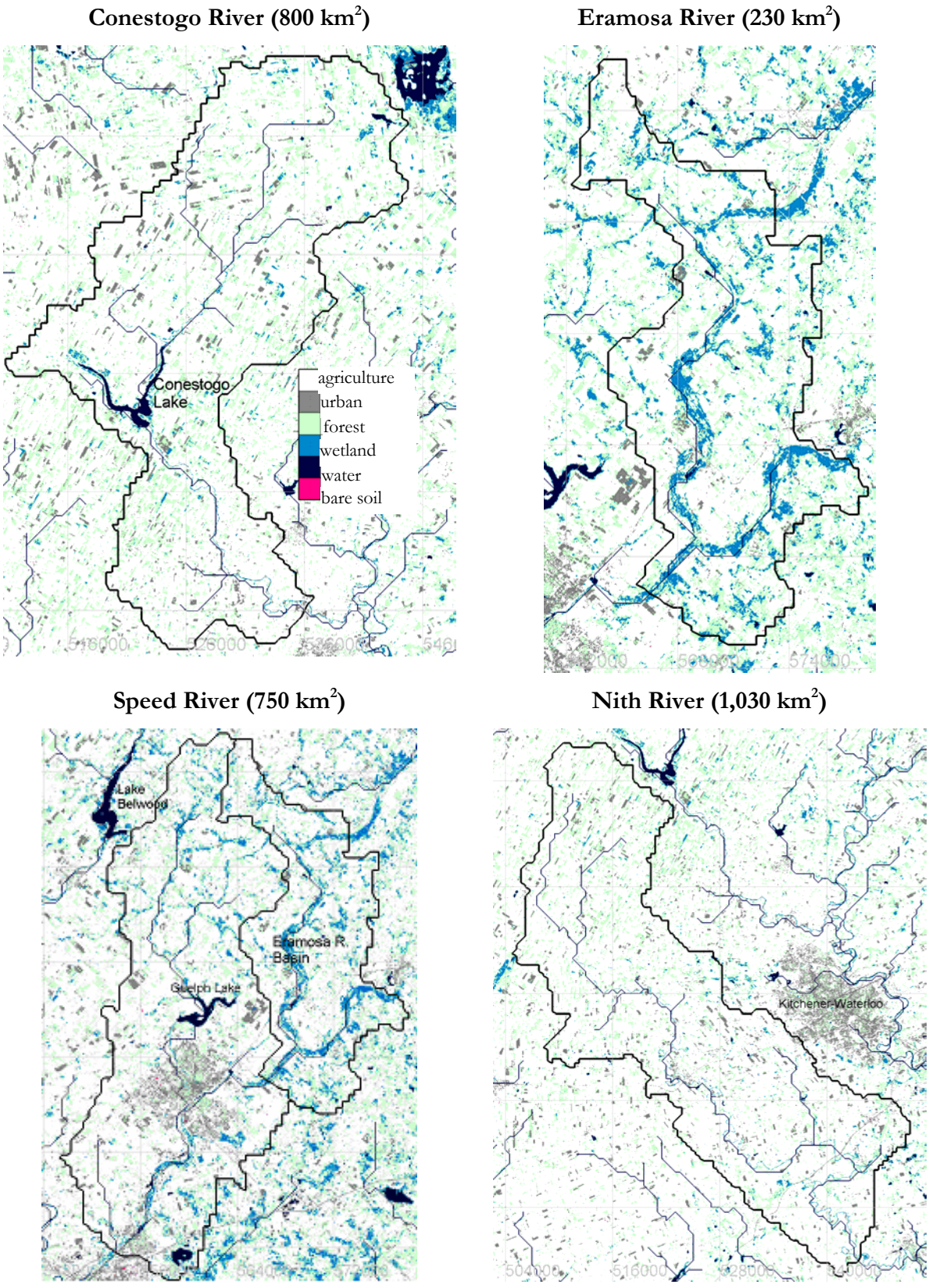

Figure 9.1 – Landcover classifications for the four main tributaries of the GRB.

On Figure 9.1 the progression from more forested, wetland-dominated terrain in the upper- (headwaters of the Conestogo River) and mid-Grand (Speed and Eramosa) to the flat, agricultural-based lands in the lower Grand (Nith River) is visible. Both the Eramosa and Speed River basins indicate a higher percentage of channelized fens lining the main river stems and tributaries. Several riparian zones line the inflow reaches of Lake Conestogo, visible in the middle of Conestogo River basin and to the north of the Nith River basin. Northeast of the Speed River basin is Lake Belwood, and contained within Speed River basin is Guelph Lake. The City of Guelph is within the Speed River basin and Kitchener-Waterloo lies to the east of the Nith River basin. The selection of these four tributaries in conjunction with the four gauges along the Grand River main stem is expected to capture GRB variability associated with characteristic land classifications and differences in geological and ecological regimes.

The isoWATFLOOD model was run continuously from October 2003 until December 2005 with no calibration to isotopic responses. The parameter set utilized for this simulation was optimized to streamflow and tracer-separated baseflow contributions alone (Appendix A.1.1). Isotope forcing data ($\delta^{18}O_{rain}$ and $\delta^{18}O_{snow}$) were defined based on long-term average compositions estimated by the CNIP database for southern Ontario, and from measured compositions from snowpacks during the sampling period (Appendix A.1.2). Hydrologic storage initializations defined in Appendix A.1.2 were derived from measured ice-on, low-flow and mid-summer isotopic compositions.

Simulated streamflow results from WATFLOOD are presented in Section 9.1.1, and Section 9.1.2 presents the results from the isoWATFLOOD GRB simulation. Section 9.2 utilizes the $\delta^{18}O$ simulation in conjunction with hydrological and meteorological data to assess the internal water balance of the GRB. The effects of wetland alteration on both hydrologic and isotopic variability are discussed in Section 9.2.1, and the water balances of lakes in the GRB are discussed in Section 9.2.2. A preliminary assessment of the inter-annual variability (Section 9.2.3) and spatial variability (Section 9.2.4) within the GRB is conducted using visualizations of $\delta^{18}O$ simulation data.

9.1.1 Hydrological Modelling

Since measured streamflows provided by the GRCA were provisional data, a quality control check was performed on the data via visual inspection. There were three anomalous peak flows identified and removed from the Waldemar gauge observed data set where streamflow during a low-flow period (i.e., 0 to 0.1 cms) instantaneously peaked to between 200 and 400 cms for one hour only, and then dropped back to low or no flow. These data are not considered realistic and were therefore removed prior to plotting and statistical analyses. Additionally, there are known problems with the winter observed streamflows at the West Montrose gauge due to ice-jam formations (Barlett, 2008); recorded observed flows are approximately one order of magnitude larger than expected flows. Precipitation data from uncalibrated radar were used during the winter months (January to March); tipping bucket data were measured at precipitation stations throughout the GRB (Figure 3.4) and used for summer precipitation data.

Hydrographs produced from the WATFLOOD simulation are presented on Figure 9.2 and Figure 9.3 (i.e., upper- to mid-Grand, and mid- to lower-Grand, respectively) for the eight gauges listed in Table 9.1. Table 9.2 summarises the statistical results from the two-year GRB hydrological simulation. The slope and R^2 statistics reported in the last two columns of Table 9.2 are derived from proportionality plots presented in Appendix F (Figures F.1 through F.8) that compare the fit of simulated to measured flows.

Table 9.2 - Statistical summary of WATFLOOD streamflow simulation for the GRB.

Basin	**DA (km^2)**	**Nash**	**$\%D_v$**	**Slope**	**R^2**
Grand @ Waldemar	620	0.191	11.38	0.415	0.293
Grand @ W. Montrose	1346	0.540	-10.01	0.722	0.497
Conestogo @ St. Jacobs	820	0.605	-7.552	0.734	0.576
Eramosa @ Guelph	226	-0.009	15.55	0.868	0.082
Speed @ Beaverdale	710	0.400	11.80	0.953	0.453
Grand @ Galt	3494	0.701	6.857	0.867	0.637
Nith @ Canning	985	0.198	-0.521	0.681	0.193
Grand @ York	6245	0.242	9.565	0.869	0.322

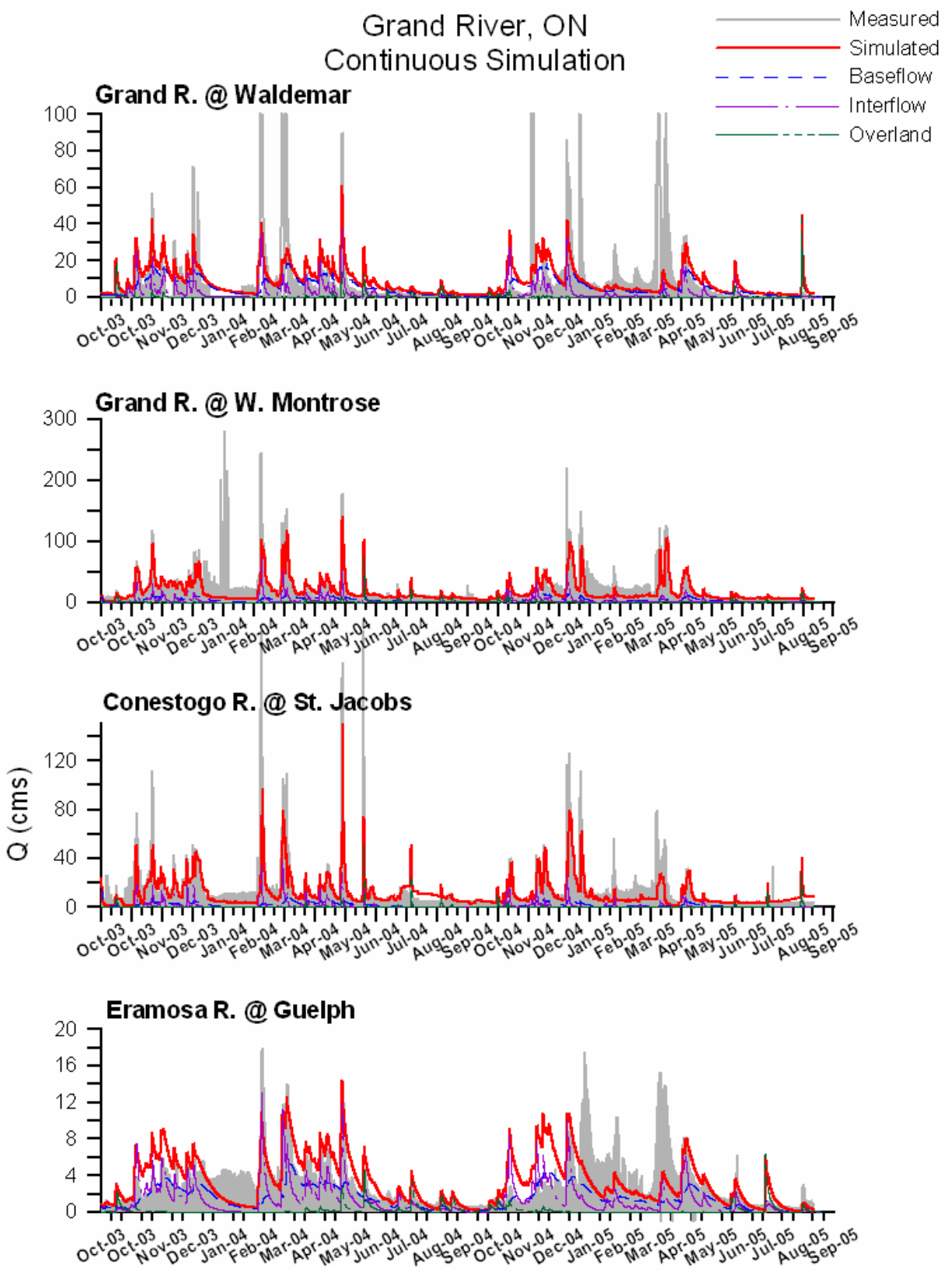

Figure 9.2 – Hydrographs from isoWATFLOOD simulation of the upper GRB.

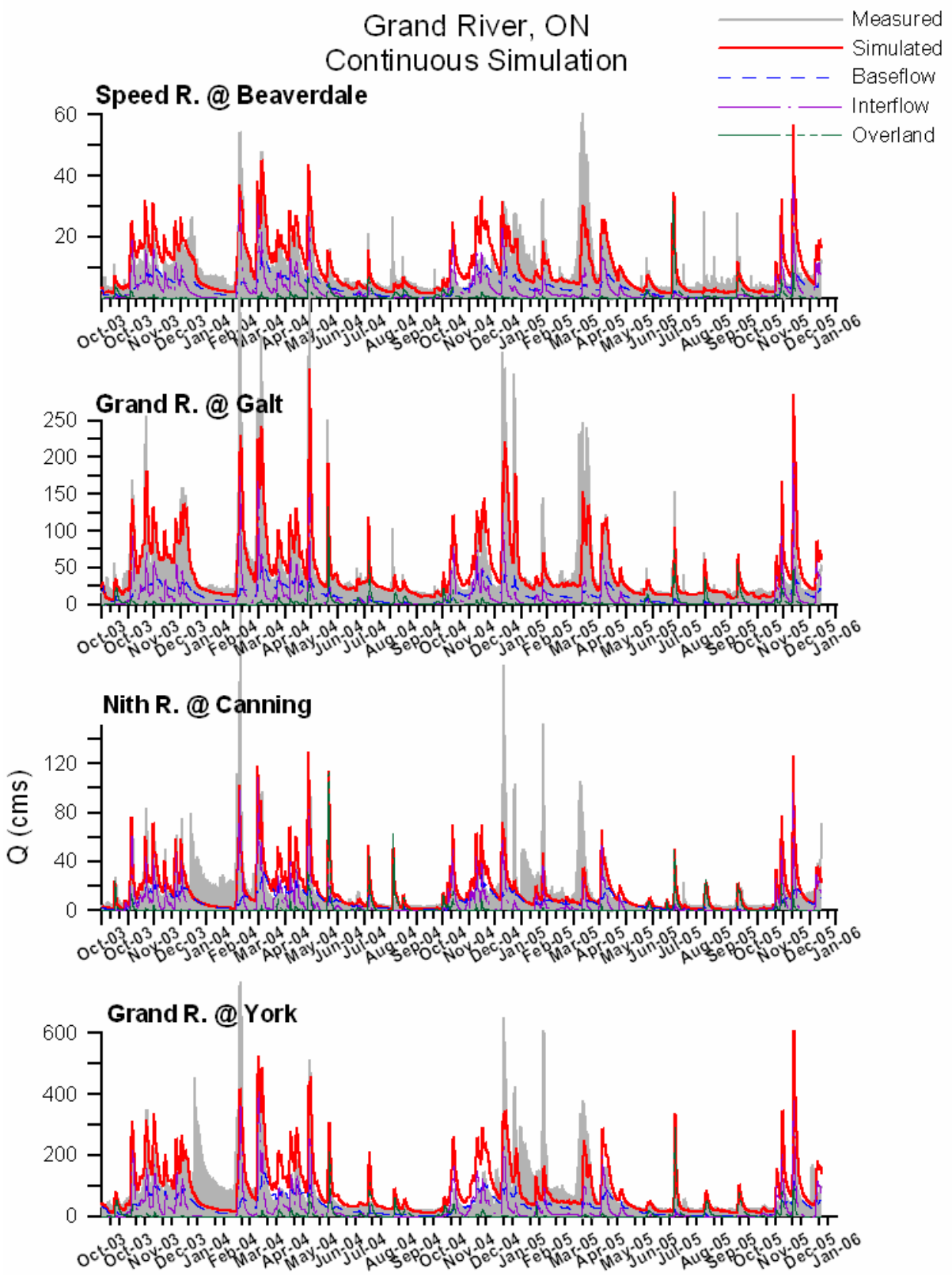

Figure 9.3 - Hydrographs from isoWATFLOOD simulation of the lower GRB.

From Figure 9.2 and Figure 9.3 it is apparent that WATFLOOD under-estimates peak flows during spring freshet in the GRB. This result is not surprising as there are known problems associated with the radar-derived estimates of snow fall throughout the winter months, which are not validated by rain gauge data. The deviation of runoff volume statistic in Table 9.2 indicates West Montrose, Conestogo, and Nith River gauges (i.e. negative numbers) under-estimate streamflow on average; where each of these basins has their headwaters in the Ontario snow belt region. The under-estimation of runoff volume is not directly caused by the model, but rather inherent to the simulation because of the under-estimated precipitation forcing data. The slopes of the proportionality plots at these gauges also indicate a simulated under-estimation and poor linearity of the simulation (Table 9.2). Figure 9.4 and Figure 9.5 more closely examine the three-month spin-up period used for model calibration (2003) and streamflow simulations for 2004 and 2005. The under-estimation of meltwater-derived runoff is apparent in 2004 and 2005 on Figure 9.4 and Figure 9.5.

The proportionality plot for the Waldemar gauge (Figure F.1) reflects the tendency of the model to under-estimate high streamflows (slope=0.415), and Figure 9.4 confirms that these under-estimations by the model most frequently occur during the winter. In the headwater region (Waldemar and West Montrose), considerable snow falls are expected due to higher elevations and proximity to regions where lake effect snowfall often occurs. Throughout the rest of 2004 and 2005, simulated flows match both the peak and timing of measured streamflows at the Waldemar gauge (Figure 9.4). Beginning in late fall of both 2004 and 2005, streamflows are over -estimated by the model, but not as significantly as winter under-estimations of streamflow. Late fall over-estimations of streamflow are attributed either to anomalous precipitation forcing within the headwater basin, or to a slow simulated release of water in wetland and bog storage. Under-estimation of spring flows and over-estimation of late fall flows results in a lower correlation between simulated and measured flow data (R^2=0.293), and a low Nash-Sutcliffe coefficient (0.191), reflecting the poor fit (on average) of simulated to measured flows. The model, however, reasonably reproduces both the timing and volume of observed streamflow between these two problem areas. The regression between simulated and measured flows would be greatly improved if the substantially under-estimated winter flows were removed from the regression analysis (Figure F.1).

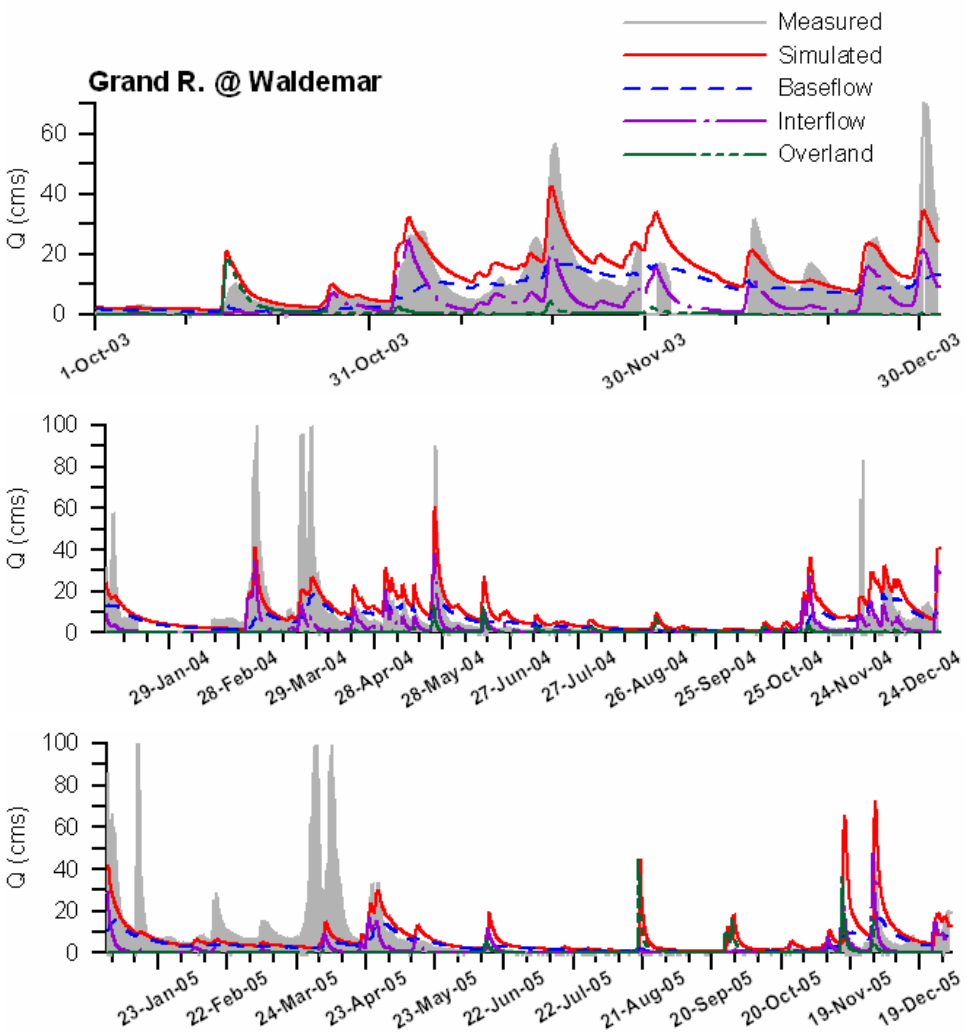

Figure 9.4 – Yearly hydrographs for the Grand River at Waldemar gauge as simulated by isoWATFLOOD.

The Grand River at West Montrose also shows a tendency to under-estimate spring melt events, which are typically the largest runoff events in a seasonal cycle and therefore have the most significant impact on the simulation (Figure 9.5; Figure F.2). The proportionality plot (Figure F.2) illustrates the large bias in under-representing these high freshet flow events, where the low simulated flows plot below the regression line (slope=0.722) and lower the fit of simulated to measured data (R^2=0.497). There is a higher degree of correlation between measured and simulated streamflow at the West Montrose gauge than Waldemar because high-flows are overall more accurately simulated relative to observed data.

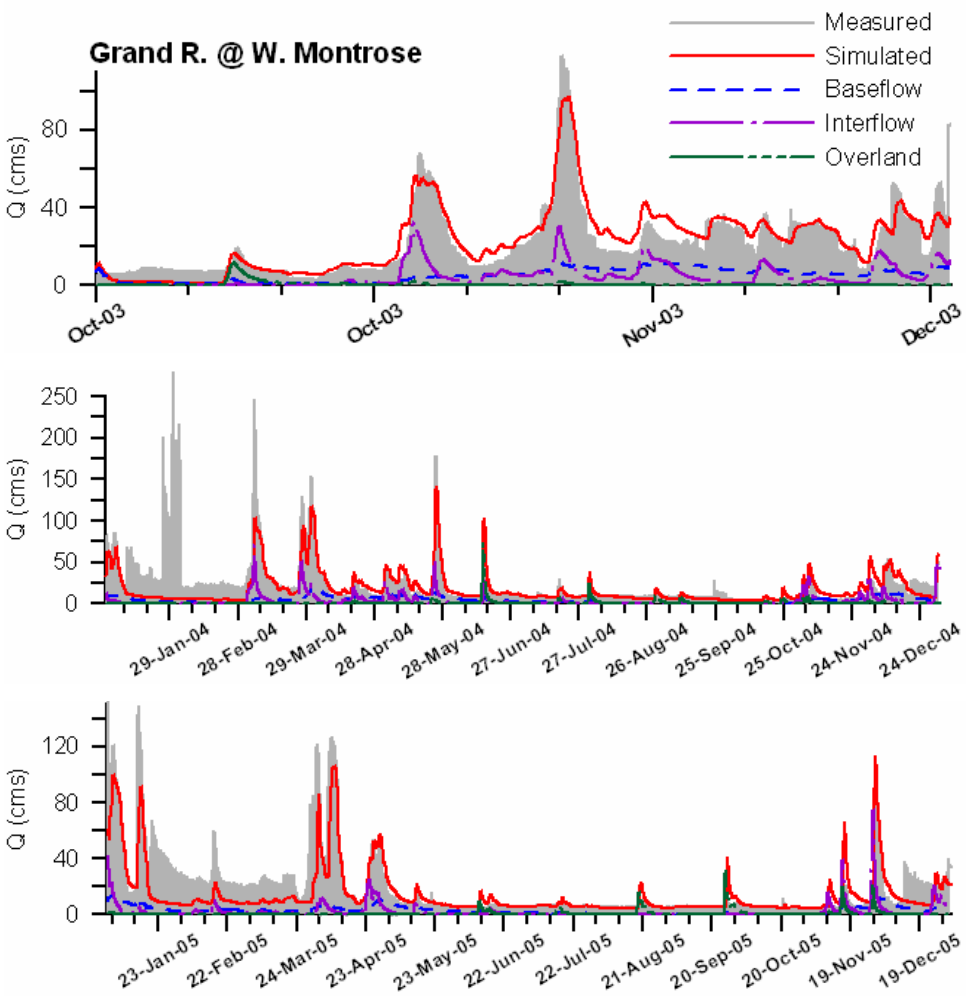

Figure 9.5 - Yearly hydrographs for the Grand River at West Montrose gauge as simulated by isoWATFLOOD.

The improved fit of simulated to measured flows throughout the rest of the 2004 and 2005 seasons is because West Montrose lies downstream of Lake Belwood, a controlled reservoir (via Shand Dam) with regulated release data. Reservoir outflows are assigned to the outlet grid of the reservoir, negating the propagation of errors from upstream reaches. Subsequently grids downstream of reservoirs exhibit improved fits of simulated to measured streamflows, such as the calibrated 2003 hydrographs show at West Montrose (Figure 9.5). Similarly both Conestogo River at St. Jacobs and Grand River at Galt exhibit improved fits of simulated to measured streamflows (Nash-Sutcliffe coefficients and proportionality slopes closer to one) than the other uncontrolled sub-basins.

The Conestogo River similarly shows problems with winter radar-derived precipitation in that peak winter flows were under-estimated by WATFLOOD (Figure 9.2; Figure F.3). Overall there was a good fit of simulated to measured flow data, with a Nash-Sutcliffe of 0.605 and proportionality slope of 0.734 (R^2=0.576). Figure F.3 shows the systematic under-estimation of winter flows, but otherwise indicates random model estimation error and no additional model bias. There was also a clear under-estimation of runoff volume by the model (%D_v=-7.5%).

The Eramosa and Speed Rivers (Figures F.4 and F.5, respectively) interestingly show an equal proportion of both over- and under-estimation of streamflow, leading to proportionality slopes relatively close to one (slope=0.868 and 0.953, respectively), with poor correlation between simulated and measured data (R^2=0.082 and 0.453, respectively). Figure 9.6 compares the Eramosa River 2003 calibrated streamflow hydrograph with the hydrograph just downstream of where the Speed River joins the Grand River (Grand at Galt).

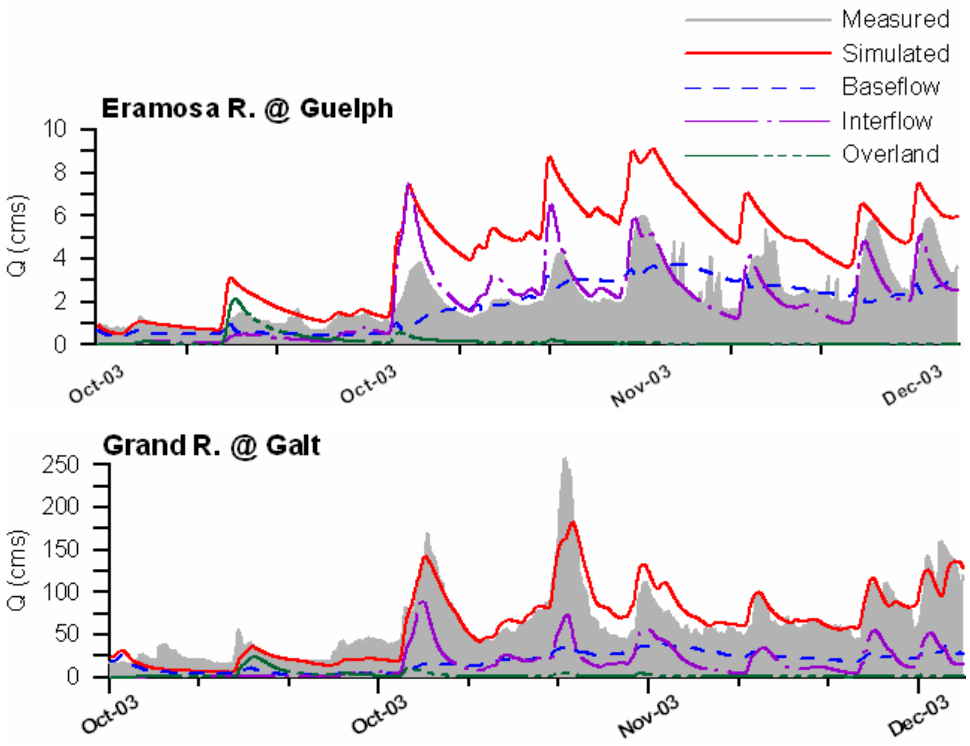

Figure 9.6 – 2003 isoWATFLOOD Eramosa River hydrograph in comparison with the downstream Grand at Galt hydrograph.

Eramosa River streamflows are over-estimated relative to measured flows (0.4 cms on average over the two-year period), where a portion of this excess streamflow drains downstream into the lower Speed River basin. Over-estimations of streamflow within Eramosa basin are suspected

to be derived from groundwater pumping that is known to occur within the basin for domestic, commercial, and industrial use; which the model does not currently simulate. Nestle, for example, currently holds a Certificate of Approval from the Ministry of the Environment to remove up to 47.4 million litres per day from the Eramosa River watershed. The excess 0.4 cms of simulated flow on average over the two-year period translates to an average over-estimation of 34.8 million litres per day that could easily be accounted for by water withdrawal permits removing water from the basin before it reaches the outlet.

Figure 9.6 shows that the over-estimation of Eramosa River streamflow is isolated to the Speed and Eramosa River basins, and that it is not a consistent model error. Where the Speed River drains into the Grand River the upstream over-estimation of Eramosa streamflow is visible in a slight over-estimation of Grand River low-flows, but the over-estimation (particularly during peak flow) does not persist in the main stem of the Grand River. Although the over-estimation is carried downstream, the Eramosa River tributary contributes only a small fraction of the total Grand River flow and therefore the error is essentially imperceptible. When pumping occurs and is not simulated by the model, over-estimations during simulation are expected.

The observed hydrologic variation of the lower Grand River is captured by WATFLOOD. The Grand River at Galt simulation was among the best of all gauges with a Nash-Sutcliffe coefficient (0.701) and proportionality slope (0.867) close to one, and a small 6.8% under-estimation of runoff volume over the two-year simulation. Both the yearly hydrographs (Figure 9.7) and proportionality plot (Figure F.6) show a good fit of simulated to observed streamflow, in part attributed to the controlled streamflow releases from the upstream reservoir system.

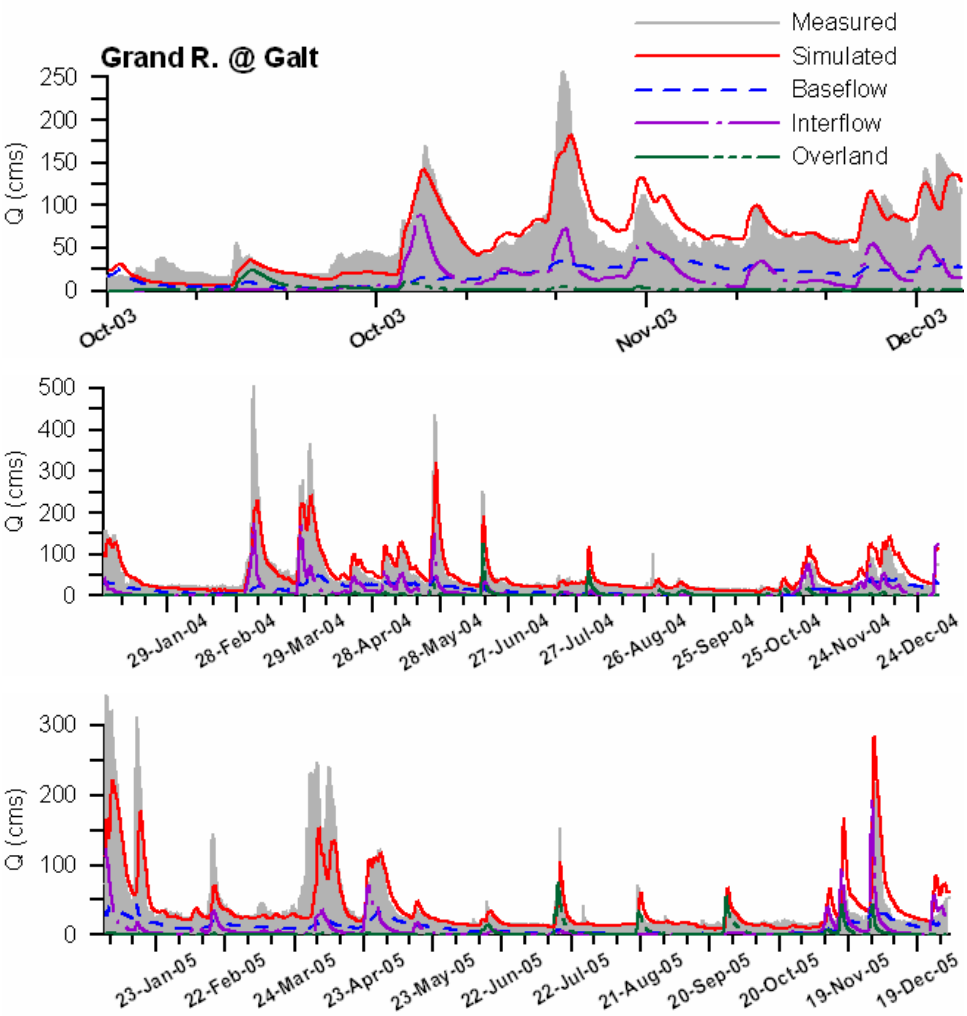

Figure 9.7 - Yearly hydrographs for the Grand River at Galt gauge as simulated by isoWATFLOOD.

The Nith River, an unregulated river in the lower portion of the GRB, very closely simulates runoff volume (-0.521%); however there is cancellation of error contributing to this success (Figure F.7). Both the low Nash-Sutcliffe coefficient (0.198) and proportionality slope (0.681) indicate correlation error between simulated and measured data. The proportionality plot (Figure F.7) shows distinct under-estimations of high-flows by the model, which is again the result of under-estimated winter, radar-derived precipitation (i.e., tracking to the right of the regression line). Given the Nith River's distance from the radar dome in King City coupled with the problems with radar-derived winter precipitation data, under-estimations of winter flows are inevitable by the model (Figure 9.3). Aside from the errors attributed to snowfall however, the scatter between simulated and measured flows appears to be randomly distributed about the 1:1

slope indicating the model does not have systematic simulation biases. In fact, the model shows good correlation to observed data when these under-estimated winter flows are neglected.

At the outlet of the GRB, there is a simulated 9.5% over-estimation of runoff that is close to the average over-estimation of 12% across the whole GRB. The Nash-Sutcliffe coefficient at the York gauge indicates a poor fit of simulated to measured streamflow that is also reflected in the correlation coefficient for the proportionality plots in Table 9.2 (R^2=0.322). From the proportionality plot (Figure F.8), the effect of under estimating spring peak runoff is observed in the data lying to the right of the regression line. There is an over-estimation of low-flow visible above the 1:1 line that is in part downstream propagation from the Eramosa and Speed River tributaries (and is also visible at the Grand at Galt gauge). Figure 9.8 shows that peak summer storm flows were captured by the model indicating there were appropriate amounts of precipitation measured by the rain gauges during these storm events. Figure 9.8 also indicates, however, an over-estimation of hydrograph recession curves that could be carried forward from slow hydrologic storage releases upstream of the York gauge. The result is that simulated streamflow in 2003 is over-estimated during low-flow and streamflow recession periods, which is also seen in 2004 and 2005. Given the basin outlet is the summation of all upstream runoff, it is difficult to isolate where the problem originates other than to note that upstream reaches of the Grand did not appear to have this problem. This discrepency appears to be the result of water retained and released in wetlands immediately upstream of the York gauge (Whiteman's Creek and Fairchild Creek sub-basins) that may in reality retain and release large volumes of water slower than what is currently simulated by the model.

Over the two-year simulation period the WATFLOOD model under-estimates winter flows as a result of poor snowfall measurements by radar. The under-estimation of spring runoff from snowmelt is most prevalent in the northern regions of the basin, which is expected due to higher snowfall in the north during the study period (Table 3.3). Outside of the freshet, the model replicates peak flow, runoff volume, and the timing of peak flows reasonably well over the two-year study period despite low Slope and R^2 statistics influenced by the under-estimation of winter flows. The model has a tendency to over-estimate low-flows and flow recession curves in the lower reaches of the Grand River, which is attributed to the wetlands in this region having over-estimated discharges and (or) under-predicted storage capacities.

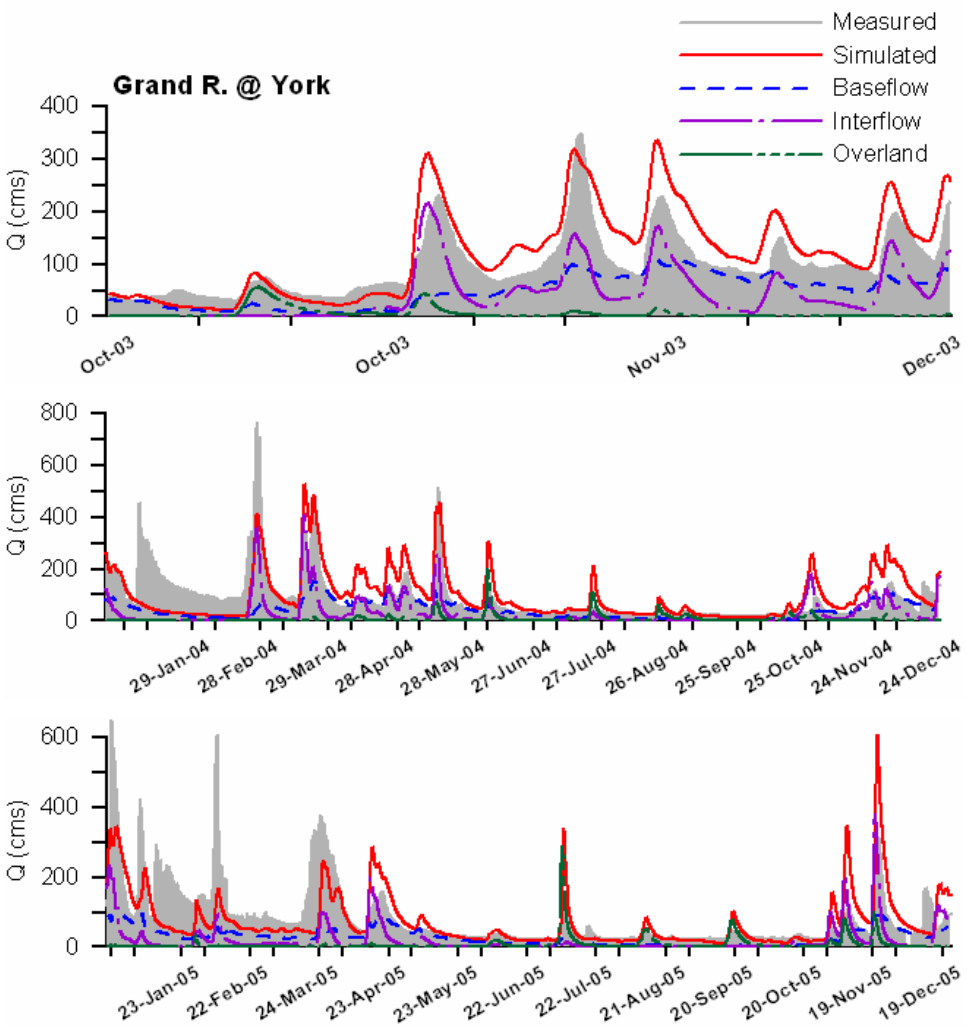

Figure 9.8 - Yearly hydrographs for the Grand River at York gauge as simulated by isoWATFLOOD.

Internal sub-flow contributions to total streamflow were also reasonably apportioned and showed variation from the headwater region to lower Grand River characteristic of the distinctive geology of the upper, middle and lower Grand River that was described in Section 3.1.2. Given the WATFLOOD model is calibrated for multiple watersheds (i.e., parameters are not associated for distinct sub-watersheds), the level of accuracy in simulating sub-watershed streamflow is sacrificed for model robustness and accurate representation of distinct landcover classes. Overall the WATFLOOD model produces a realistic simulation of GRB streamflow and of processes contributing to streamflow over the 2004 to 2005 study period. It should be noted that accurate GRB streamflow simulation (particularly data quality control) was not the focus of this study; the ability to simulate isotopic compositions of streamflow (with minimal

calibration) was the intended application. The next section presents the results of the $\delta^{18}O$ simulation, performed without further calibration of the existing GRB parameter set.

9.1.2 Isotopes in Streamflow

Figure 9.9 and Figure 9.10 show the isoWATFLOOD-simulated $\delta^{18}O$ for the upper and lower GRB gauges (i.e., from Table 9.1), respectively over the 2004 to 2005 study period. Table 9.3 presents a quantitative summary of the simulated variation in sub-basin isotopic composition.

Table 9.3 – Quantitative summary[1] of isoWATFLOOD-simulated variation in isotopes for the GRB.

Basin	DA (km^2)	Average[1] $\delta^{18}O$ (‰)	$\sigma_{\delta 18O}$[1] (‰)	$\Delta\delta^{18}O$[3] (‰)
Grand @ Waldemar	620	-9.271	1.621	13.55
Grand @ W. Montrose	1346	-9.707	1.141	8.07
Conestogo @ St. Jacobs	820	-9.835	1.644	10.00
Eramosa @ Guelph	226	-9.374	2.057	11.18
Speed @ Beaverdale	710	-9.736	1.467	10.18
Grand @ Galt	3494	-9.747	1.267	7.24
Nith @ Canning	985	-9.885	1.735	13.48
Grand @ York	6245	-9.867	1.443	7.76
Grand River Basin[2]	**6,245**	**-9.66**	**1.64**	**12.4**

[1]Based on n=19,725; [2]Average based on all 40 gauge locations, excluding Grand at York;
[3]Absolute difference between maximum and minimum $\delta^{18}O$ simulated.

Visual inspection of Figure 9.9 and Figure 9.10 show that the isoWATFLOOD model is able to replicate much of the observed variation in $\delta^{18}O$ composition of streamflow in the GRB. Particularly notable is that these results were obtained without re-calibration (using isotope data) of model parameterizations controlling internal model dynamics and apportioning of sub-flows. Therefore WATFLOOD was simulating GRB streamflows in a physically realistic manner, and analysis of the $\delta^{18}O$ simulation serves to reinforce this finding. The seasonal trend in observed $\delta^{18}O$ is captured by isoWATFLOOD; however some isotopic variations were missed by the model.

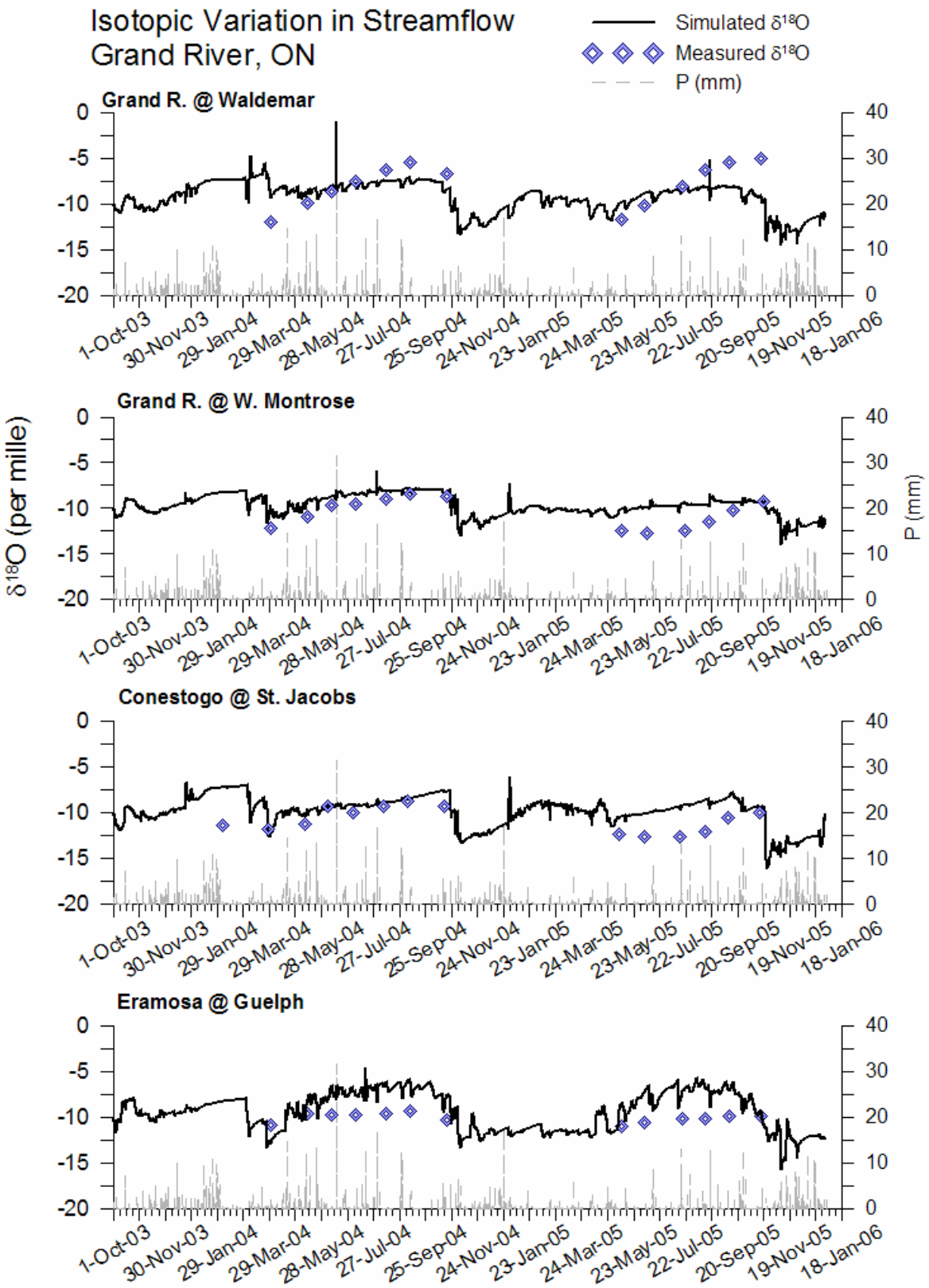

Figure 9.9 – Isotopic variation simulated by isoWATFLOOD for the upper GRB.

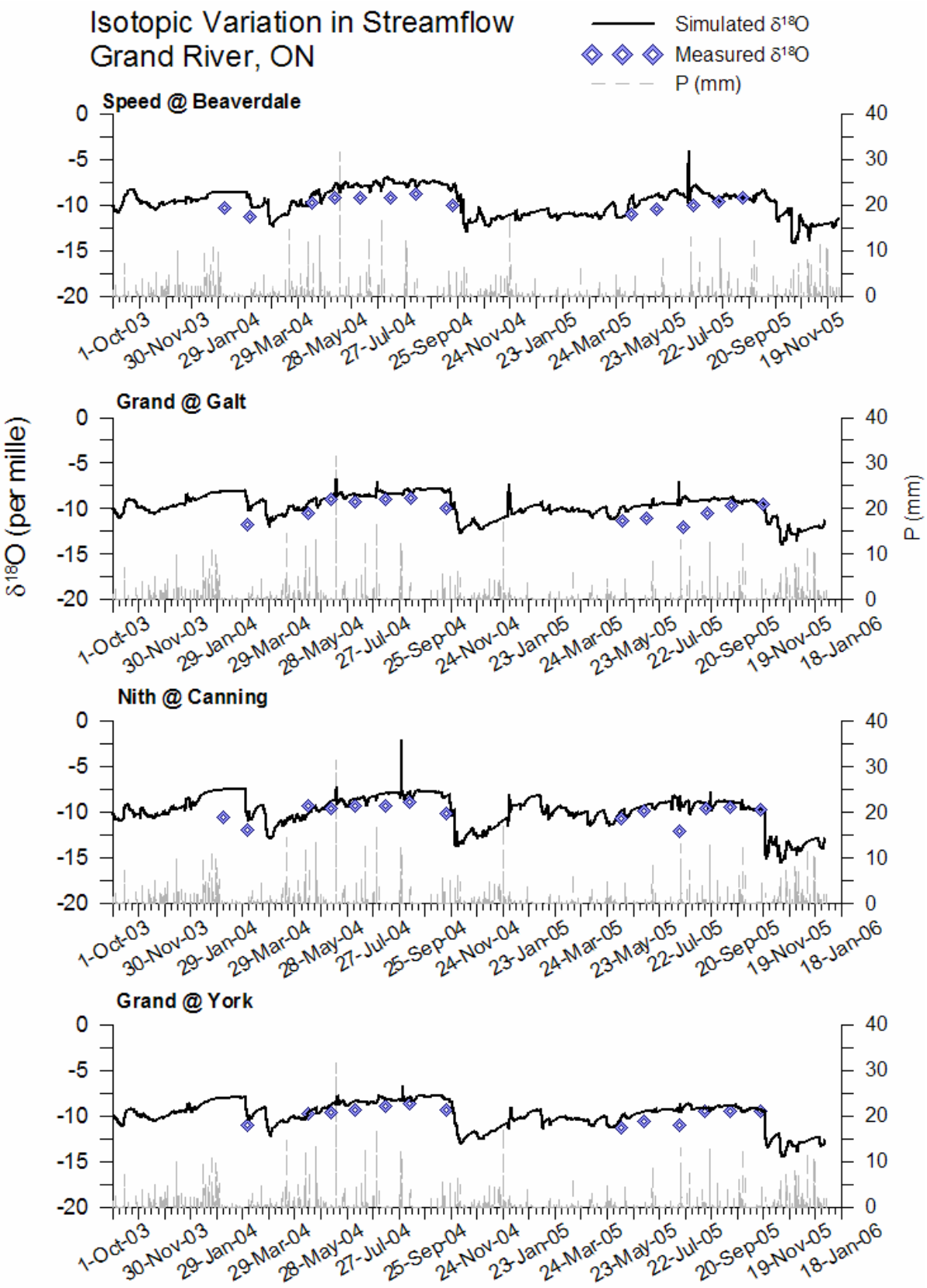

Figure 9.10 - Isotopic variation simulated by isoWATFLOOD for the lower GRB.

The upper GRB (Waldemar gauge) show markedly more pronounced changes in measured $\delta^{18}O$ than the mid and lower reaches of the GRB. These observed higher amplitude changes in isotopic composition are not well-replicated by the isoWATFLOOD model, which could be related to the over-estimation of runoff volumes in the headwater basins (Section 9.1.1). If in fact simulated wetland storages were larger than in reality, wetland discharges would be higher, promoting advective mixing and reducing the opportunity for evaporative enrichment. The lower amplitude of simulated $\delta^{18}O$ could also be related to the application of constant composition forcing data (i.e., rainfall and snowfall). Given that simulated $\delta^{18}O$ in 2004 was overall more representative of measured $\delta^{18}O$ than in 2005 (e.g., West Montrose and Conestogo at St. Jacobs), it is probable that the meteorological inputs ($\delta^{18}O_{rain}$ and $\delta^{18}O_{snow}$) were more depleted in 2005, lowering seasonal compositions. This same trend is also observed in mid-GRB gauges (e.g., Galt), but are damped in the lower-GRB due to mixing and upstream reservoir contributions. Defined isotopic temperature-rainfall and intensity-rainfall relationships show low-temperature, heavy continental rainfalls (and snowfalls) tend to be more depleted in heavy isotopes (Section 2.4.1). It is possible that these colder, heavier rainfalls are more common in the northern GRB, or that there is an influence of lake-derived moisture from the recycling of isotopically-depleted vapour from Lake Huron. Currently the effect of enriched precipitation on the $\delta^{18}O$ of streamflow is visible as several early spring and late fall rainfall events significantly enrich streamflow compositions (March 2004, November 2004, and May 2005), when in fact precipitation in these months would be slightly more depleted due to colder temperatures.

The input composition of meteoric precipitation (δ_P) was fractionated at temperatures less than or equal to four degrees Celsius by a constant liquid-ice separation of 3‰ (Feng *et al.*, 2002; Jouzel & Souchez, 1982; Stichler *et al.*, 1981). Figure 9.11 and Figure 9.12 contrast the previous $\delta^{18}O$ simulation for GRB gauges (case a) with simulated $\delta^{18}O$ of streamflow when low-temperature rainfalls are fractionated (case b).

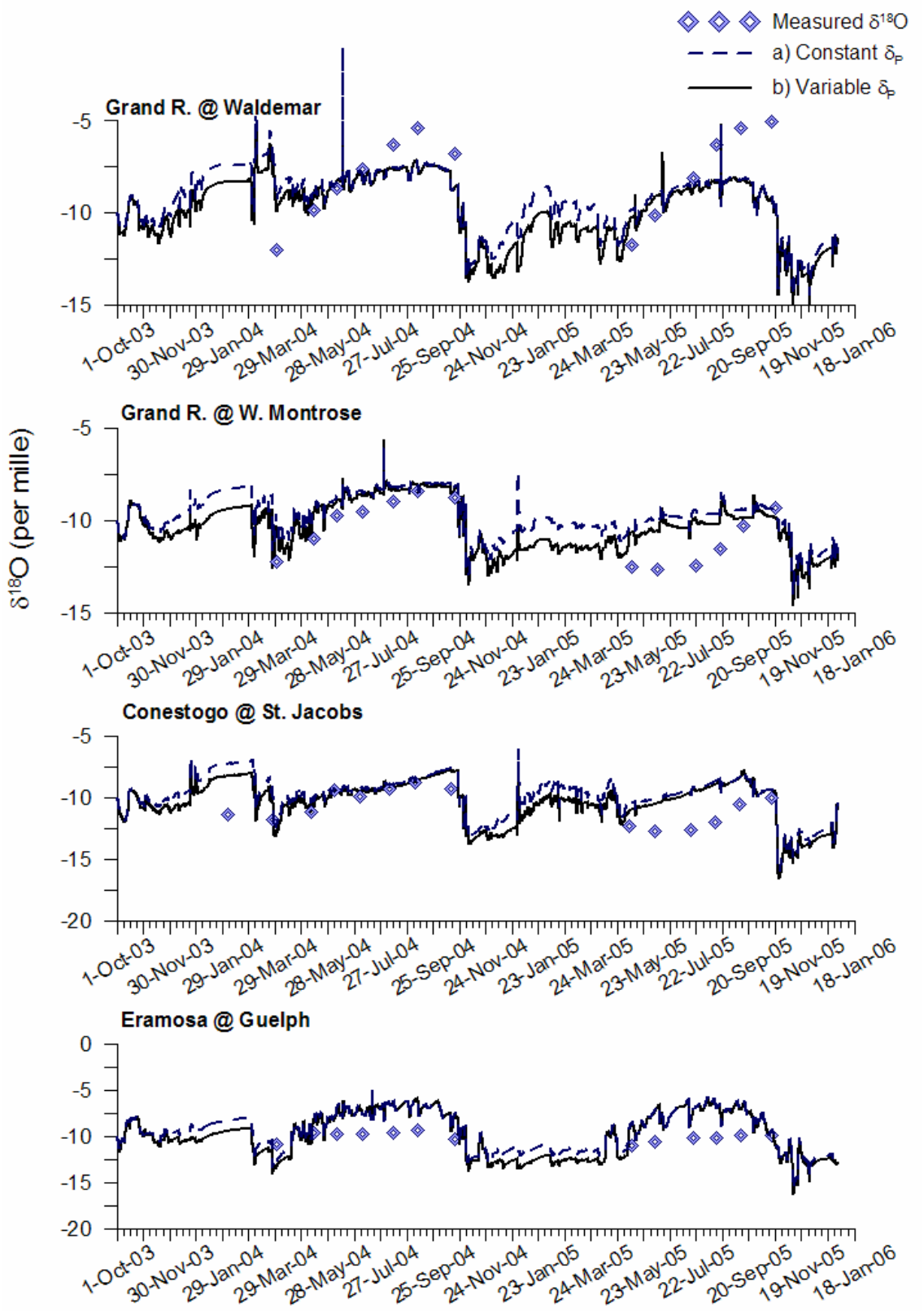

Figure 9.11 – Comparison of the isotopic composition of streamflow in the upper GRB simulated by isoWATFLOOD when low temperature rainfall is isotopically depleted.

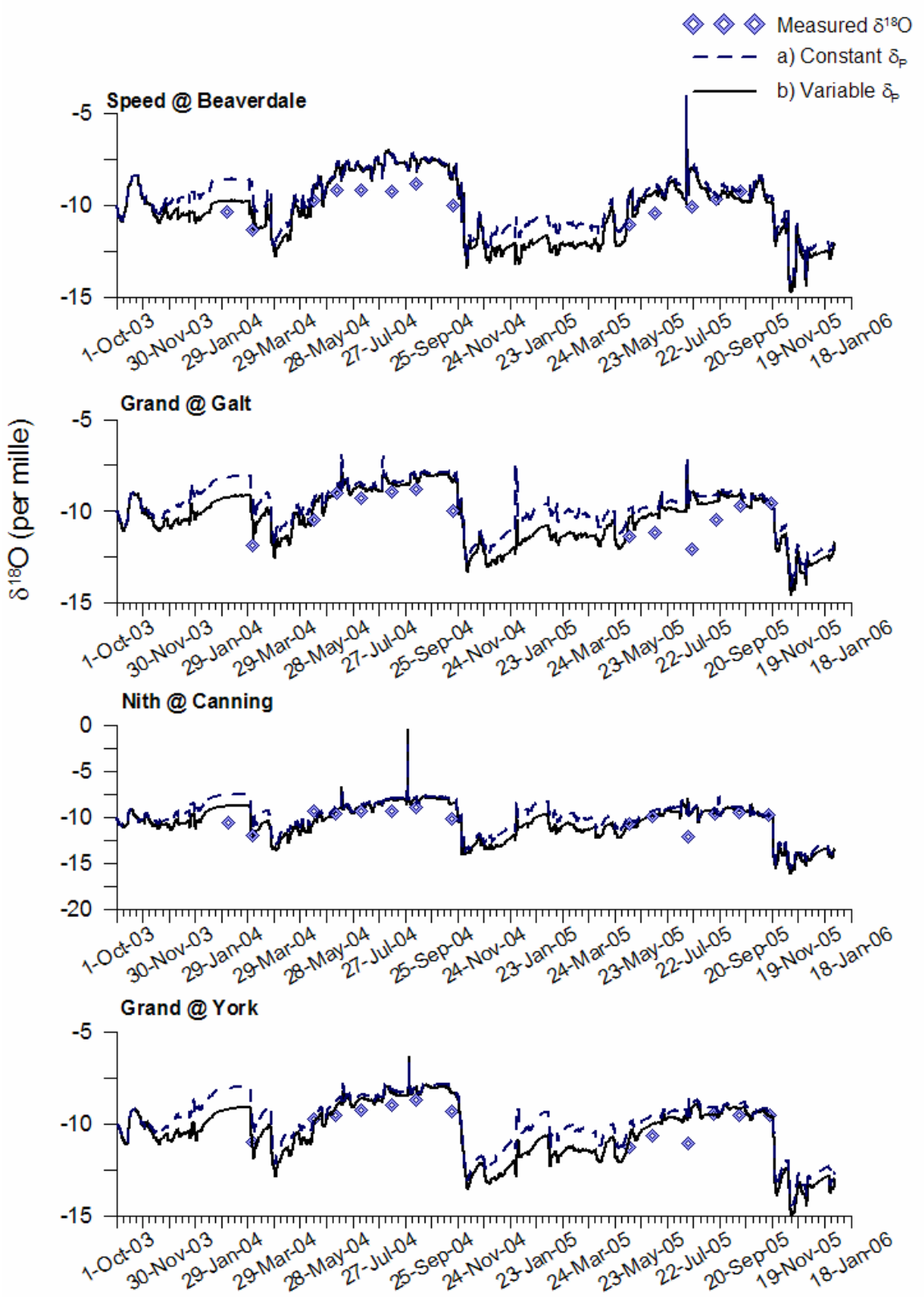

Figure 9.12 - Comparison of the isotopic composition of streamflow in the lower GRB simulated by isoWATFLOOD when low temperature rainfall is isotopically depleted.

Figure 9.11 and Figure 9.12, although valuable in their contribution to analysing the effect of meteoric composition on the $\delta^{18}O$ of streamflow, do not directly account for the inter-basin differences in enrichment and depletion slopes of $\delta^{18}O$. For the variable δ_p simulation (case b) isotopic compositions of streamflow are more depleted during the fall and winter months (e.g., November 2004 to March 2005) when temperatures are typically colder, and air masses originate more frequently from colder arctic regions (Section 3.1.1). During the warmer spring and summer periods, the simulations begin to converge as cold-temperature precipitation becomes less common. By late summer, the simulations are almost identical with only very slight depletions in the variable δ_p simulations (case b) relative to the constant δ_p simulations (case a) observed at the West Montrose and York gauges. In 2005 however a greater difference between the two simulations persists into the summer months from a lengthy spring melt in several of the basins. In fact, in the lower GRB the more depleted signature of streamflow induced by the variable δ_p simulation (case a) persisted well into the late summer months of 2005. This result was not observed to the same extent in the upper GRB reaches, indicating perhaps more natural buffering of variability and a higher tolerance to absorb meteorological variation in the headwater regions. More than likely this finding is related to the higher percentages of fen and bog in the headwater regions (Figure 9.1) that facilitate the mixing of source waters with 'old' water in storage, and encourage the evaporative enrichment of event waters residing in surface or near-surface storages. Regional variability in isotopic response to rainfall events, however, does appear to be captured by the isoWATFLOOD model. Although encouraging, this finding emphasizes the reliance of the isotopic streamflow simulation on the input composition of meteoric waters. Spatially and temporally variant compositions of precipitation are clearly an important factor in the ability of a model to accurately simulate streamflow isotopic variability.

Overall the amplitude of isotopic variation simulated in the GRB is reasonable, with an average change in $\delta^{18}O$ for the 41 gauges over the two-year study period of 9.663‰. This is a believable isotopic variation, but is conservative when compared with observed isotopes in snow relative to enriched surface water that resulted in a $\Delta\delta^{18}O$ of 20.11‰ from 2004 to 2005. On average the isotopic composition of streamflow is found to be very close to the long-term average composition of locally-derived precipitation (-9 to -10‰) reported by the CNIP database (Birks *et al.*, 2004), which is what would be expected in a strongly surface-water runoff-

dominated watershed like the GRB. The headwater basin (Waldemar) not surprisingly showed the most isotopic variation ($\Delta\delta^{18}O$ 13.55‰) resulting from the smaller drainage area and dominant influence of depleted meltwater contributions to streamflow, followed by high summer enrichments of water subsisting in bogs. The downstream reaches of the Grand River (Grand River at Galt and York) showed the least amount of isotopic variation (7.241‰ and 7.759‰, respectively) that is the result of enhanced mixing of various source water contributions as tributaries combine with the Grand River as it flows downstream. There is a decreasing trend in both the standard deviation of isotopic composition and the isotopic variance ($\Delta\delta^{18}O$) from the headwaters to the outlet of the Grand River that further supports this downstream mixing effect.

The Nith and Conestogo River basins had the lowest average $\delta^{18}O$ compositions over the two-year study period. Both basins have headwaters originating in the southern Ontario snow belt, which is located to the western edge of the GRB. From Figure 9.9 and Figure 9.10, both basins show considerable snowmelt depletions that would account for the low average compositions and higher isotopic variability (13.48‰ and 10.00‰ respectively). The Eramosa River basin also shows considerable variability in isotopic composition with high standard deviation (2.057‰) about the mean composition of streamflow over the two-year period, and a high variability in isotopic composition (11.18‰). However unlike the Nith and Conestogo Rivers, the Eramosa River had one of the most enriched isotopic compositions on average (-9.374‰). Upon inspection of the isograph (Figure 9.9), the influence of higher evaporation in the Eramosa and Speed Rivers is visible during summer months where evaporative enrichment occurs in the numerous wetlands characterizing these two basins (visible on Figure 9.1). Wetlands promote mixing of isotopically-distinct source waters during higher flow periods and retention of these waters throughout lower-flow and summer periods. There can be considerable evaporation from wetlands in runoff-dominated basins, resulting in characteristic enrichment signals in streamflow compositions. The response of the wetland-dominant Eramosa and Speed Rivers raises questions about the water holding capacity and stabilizing role such riparian zones play in the water cycle. Defining the role of wetlands in basin hydrology is integral to understanding the hydrological consequences inherent to anthropogenically altering or draining wetlands. The significance of wetlands and their environmental impact to the GRB, specifically within the

Eramosa and Speed River sub-basins, has been a recently debated topic (Bechtel, 2007; Outhit, 2008).

In the following section the role wetlands (Section 9.2.1) and lakes (Section 9.2.2) have on hydrologic variability will be analysed, as well as the impact that such controls have on downstream reaches of the Grand River. Furthermore, in the interest of establishing a baseline for hydrologic behaviour and variability in the GRB, both temporal (Section 9.2.3) and spatial (Section 9.2.4) variability will be assessed using climate data and hydrologic and isotopic data from the isoWATFLOOD simulation.

9.2 isoWATFLOOD Application to Mesoscale Hydrological Research

The GRB lies in close proximity to the rapidly expanding urban centre of Toronto, ON. With the demand for employees and the interest by many Canadians to live outside of major urban centres, greater demands are being placed on the suburb cities within a commuting distance of Toronto. Continual development within the GRB and transportation corridors in the GRB have necessitated the revision of the current watershed management plans to accommodate expanding populations, increased urbanization, and proposed highway expansions (Martin & van Vliet, 2008; Ministry of the Enviornment, 2007).

Section 9.2.1 will look at a preliminary assessment of the hydrologic value of the Eramosa River's wetlands, and the GRBs sensitivity to upstream land-use alteration. The economic value of wetlands is realized through the recognition that fresh, sustainable water supplies are increasingly scarce and in high demand. Quantification of the resultant changes to these supplies is directly translatable into a water supply loss to municipalities.

In the GRB there are a total of seven controlled reservoirs that provide flood attenuation and regulate Grand River streamflow discharge. Section 9.2.2 looks at the hydrologic and isotopic variability within GRB reservoirs, and verifies that lake isotopic variability is computed from physically realistic enrichment and depletion trends.

Lastly, inter-annual variability between the 2004 and 2005 study seasons (Section 9.2.3), and spatial variability (Section 9.2.4) inherent to the GRB will be qualitatively assessed using the isoWATFLOOD $\delta^{18}O$ simulation. The EnSim post-processor software package will be used to illustrate both temporal and spatial variations in isotopic compositions, which is an improvement over currently utilized interpolation techniques for point observations.

9.2.1 Assessing Impacts on Flow-Regimes

In southern Ontario, land for development of housing, roads, and commercial/industrial space is in high demand. Within the GRB, several large cities have been rapidly growing in recent years, resulting in increased demands on existing infrastructure (i.e., roads, housing and sewage). To meet these growing demands and to plan for future development, city officials have been looking to expand existing infrastructure; particularly roadways. For example proposals for a highway expansion (Ministry of the Environment, 2007) have been put forth to facilitate transportation between the Cities of Kitchener and Guelph and to connect them to the nearby metropolis of Toronto where many Kitchener and Guelph citizens work. Such infrastructure development is necessary, but has an ensuing impact on watersheds and their water resource allocations. The previous section (Section 9.1.2) discussed the distinct hydrological and isotopic behaviours of the Eramosa and Speed River basins and attributed some of these behaviours to the presence of wetlands, both bogs and fen, as dominant land classifications. In the interests of assessing the potential impacts of a transportation corridor development in the southern region of the Eramosa River watershed (i.e., in the proximity of the above proposed highway expansion, and expansion of highway 401), the isoWATFLOOD model was used to simulate hydrologic changes resulting from the land-use alteration. In isoWATFLOOD, wetland areas in the Eramosa River sub-basin were re-classified as impervious (i.e., paved or developed) area.

The model was run for the two-year simulation period with all other parameters kept the same to assess the difference between current and potential future hydrologic and isotopic variability. Figure 9.13 compares the hydrologic and isotopic responses from the current state of the basin (case a) to the potential future state of the basin (case b). Table 9.4 summarises the quantitative hydrologic and isotopic impacts to the Eramosa River, and downstream basins.

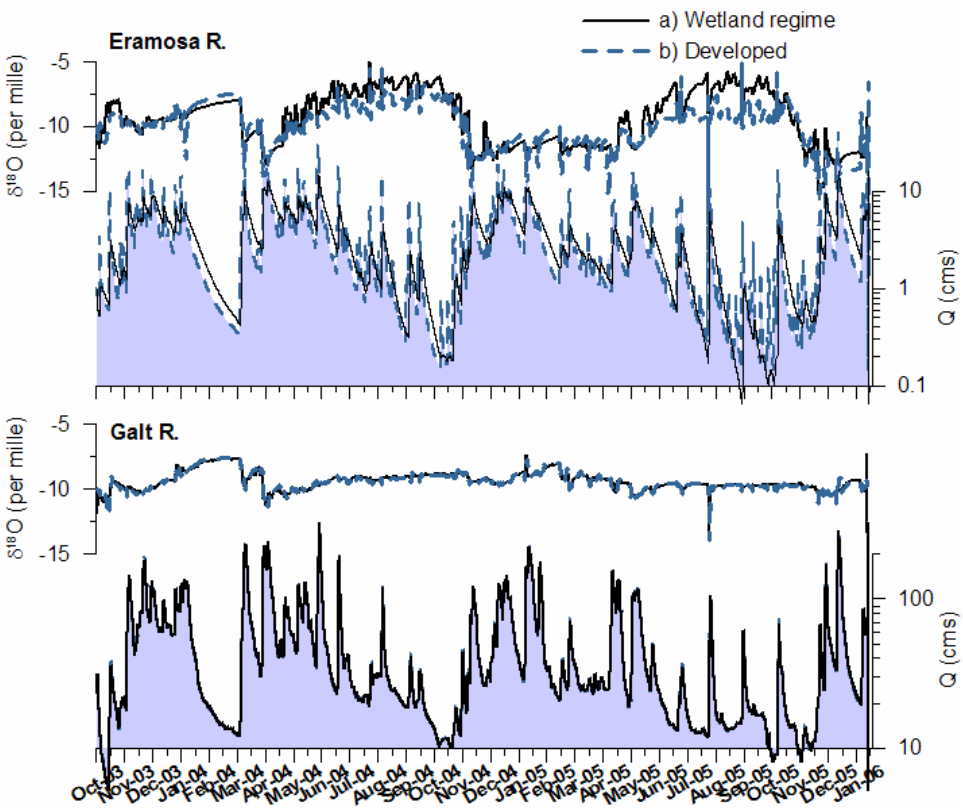

Figure 9.13 – Comparison of hydrologic and isotopic response to the draining and development of wetland area in Eramosa River basin and subsequent downstream impacts (Grand@Galt) as simulated by isoWATFLOOD.

Table 9.4 – Quantitative summary of the impacts of wetland development in the Eramosa River basin.

	Eramosa River			Grand River @ Galt		
	Wetland	**Developed**	**Δ**	**Wetland**	**Developed**	**Δ**
Average $\delta^{18}O$ (‰)[1]	-9.374	-9.898	-0.52	-9.401	-9.776	-0.38
$\Delta\delta^{18}O$ (‰)[2]	11.18	43.59	32.41	5.93	7.30	1.4
Average Q (cms)[1]	3.23	3.53	0.30	46.41	46.60	0.2
ΔQ (cms)[3]	15.8	40.7	25.9	315.8	322.4	6.6

[1]Based on n=19,725; [2]Absolute difference between maximum and minimum $\delta^{18}O$ simulated;
[3]Absolute difference between maximum and minimum simulated flow.

Figure 9.13 shows that the decrease in wetland area leads to an increase in the amplitude and frequency of runoff in the Eramosa River, a predictable response. Table 9.4 indicates that there is only a small increase in average streamflow when wetland areas are developed (0.30 cms), but a pronounced increase in peak versus low-flow runoff (25.9 cms) simulated at the Eramosa River outlet. Streamflow isotopic composition in the Eramosa River depletes by 0.52‰ on average due to the absence of evaporation from standing water stored in the wetlands and direct contribution of depleted snowmelt to streamflow. It should be noted, however, that this depletion is small and nearly insignificant when compared with ±0.2‰ analytical error for ^{18}O.

WATFLOOD tracer separations computed an average increase in surface runoff components contributing to streamflow of 0.5 cms, and an average decrease of 0.2 and 0.1 cms for interflow and baseflow components, respectively over the two-year simulation. The increase in variation of streamflow $\delta^{18}O$ is quite significant however (i.e., from ~11‰ to ~43‰), and is influenced by the reduction of source water mixing in wetlands that is instead replaced by an increase in direct runoff (Δq1+q1fs=224 mm, on average). The simulated change in runoff composition ($\Delta\delta^{18}O$=43.59‰) occurs because of the large difference between depleted snowmelt and enriched summer compositions, but is skewed by a sudden, not very realistic enrichment in runoff composition to +6.072‰ in December of 2005. The net increase in amplitude of runoff and runoff composition clearly shows the result of removing the natural buffering capacity wetlands provide to watersheds. It is generally believed that the anthropogenic alteration of wetlands increases streamflow amplitude and watershed hydrologic cycling (Brody *et al.*, 2008; Laudon *et al.*, 2007; McHugh *et al.*, 2007; White & Greer, 2006). This study helps to corroborate Gibson's (Gibson, 1996) hypothesis that a change in basin storage results in an associated change in evaporative enrichment of the discharge when water is hydrologically stored in wetlands.

The impact to the downstream reaches of the Grand River, although visually imperceptible are statistically significant. Approximately half of the average runoff increase realized in the Eramosa River is propagated downstream to the Grand River at Galt where a 0.2 cms average increase is simulated. Downstream streamflow variation did substantially increase, becoming more highly variable (ΔQ of 6.6 cms); although not as variable as the Eramosa River streamflows. The large Grand at Galt drainage area and contributions from upstream sources act to mute the more variable Eramosa River contributions to Grand River streamflow. Visually there are little to no changes to the Grand River main stem (isotopically and hydrologically), which is reinforced by the nearly insignificant decrease in isotopic composition (0.38‰). This highlights the importance of establishing a spatially distributed sampling program to evaluate isotopic responses to hydrological change. Had these results been obtained via measured isotopes in streamflow sampled only from the main stem of the Grand River, the extent of the hydrologic and isotopic variation would have likely been missed or greatly under-estimated.

Isotopic variation in the Grand River did increase ($\Delta\delta^{18}O$=1.38‰) clearly showing the propagation effect of increased upstream variability on the lower reaches of the Grand River.

This study emphasizes the important role wetlands have in the regulation of watershed hydrological response to runoff events.

9.2.2 Assessing Hydrologic Variability in Lakes

Controlled lakes and reservoirs in urban watersheds are designed to suppress high-flows and flash floods. Lakes act as watershed buffers by receiving the culmination of upstream inflows and overland runoff, storing a large percentage of this water, and decreasing the variation of streamflow in downstream reaches. Operationally, reservoirs need to be controlled so that there is storage space available in the spring to capture excess snowmelt runoff and prevent downstream flooding, versus the gradual release of storages throughout the summer to sustain streamflow and fish habitats. To assist regulators in designing appropriate reservoir controls it is important to understand each lake's regulatory requirement and upstream basin variability, including the hydrologic evolution from winter to summer. The objective of this section is to examine the hydrologic and isotopic variability of GRB controlled reservoirs, and to evaluate if simulated isotopic variations are physically representative of simulated hydrologic changes.

The simulated isoWATFLOOD $\delta^{18}O$ variation in the seven GRB controlled reservoirs is presented on Figure 9.14, along with simulated lake storages (m^3) for the two-year period. Table 9.5 presents a summary of simulated isotopic variation in the GRB reservoirs.

Table 9.5 – Summary of isotopic variation in GRB reservoirs from isoWATFLOOD simulation.

Lake	DA (km^2)	Surface Area (km^2)	Average $\delta^{18}O$[1] (‰)	$\sigma_{\delta 18O}$ (‰)[1]	$\Delta\delta^{18}O$[2] (‰)
Belwood	798.4	3.72	-9.513	0.940	5.03
Conestogo	592	3.2	-10.029	1.617	7.97
Shades Mills	105.3	0.24	-9.436	0.734	3.44
Luther	53.3	2	-9.655	1.424	5.44
Laurel	40	0.4	-10.387	0.821	4.68
Woolwich	60	0.6	-9.614	0.806	4.38
Guelph	224	2	-9.811	0.962	3.78

[1]Based on n=19,725; [2]Absolute difference between maximum and minimum $\delta^{18}O$ simulated.

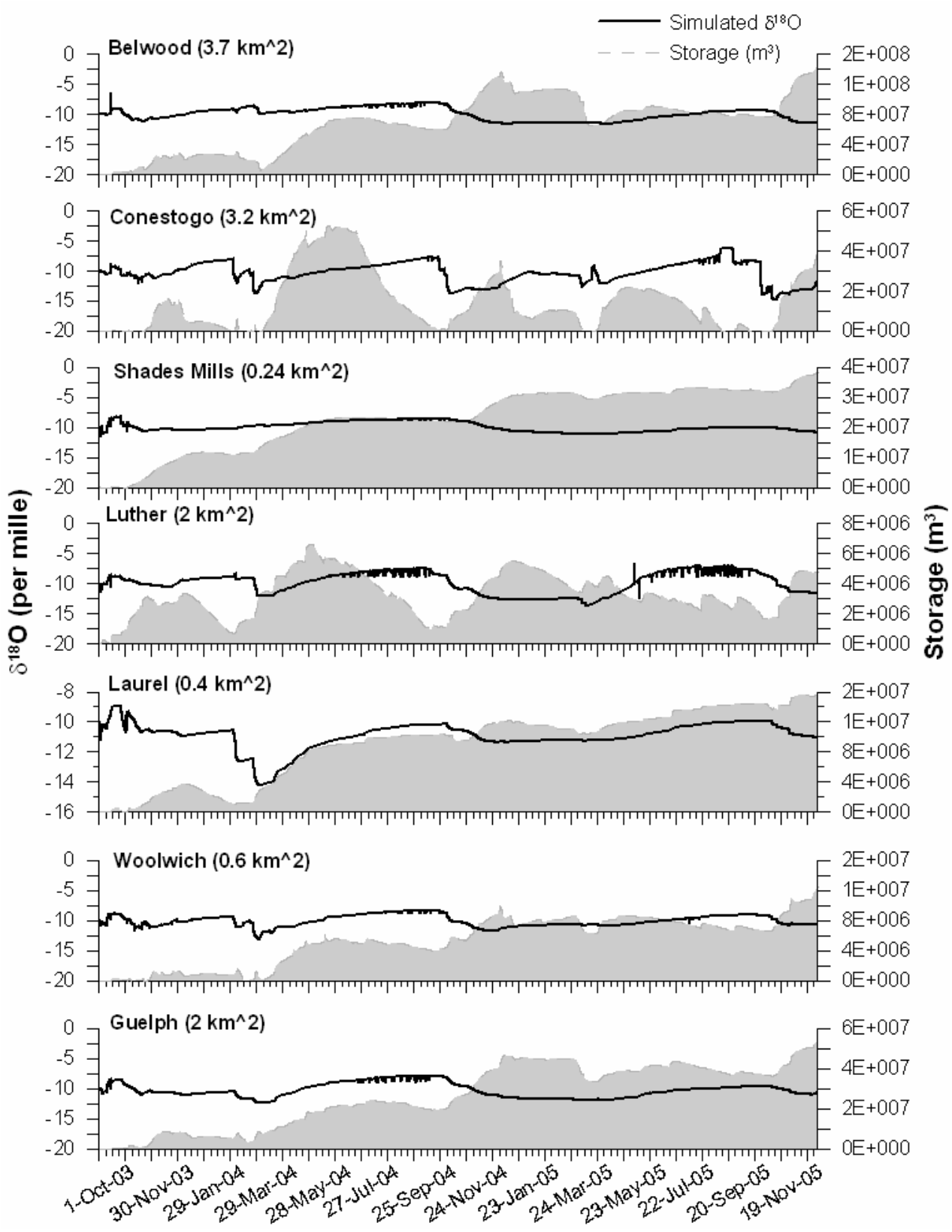

Figure 9.14 – isoWATFLOOD-simulated isotopic variation in GRB reservoirs.

In comparison to the simulated $\delta^{18}O$ of streamflow, Figure 9.14 shows more gradual and lower amplitude changes in composition of lake water (i.e., relative to streamflow). Lake storage plotted against lake isotopic response offers insight as to why changes occur in isotopic composition over time. Simulated lake storages in five of the seven reservoirs are seen to continually increase over the two-year simulation. Although not all reservoirs are annually lowered like Conestogo Lake and Luther Dam (according to the GRCA's operating rules: GRCA, 2008c), it is unlikely that storages continually increase in the other five reservoirs in reality. This instead occurs because lake storages are not initialized and inflows to the reservoirs are generally over-estimated (e.g., Grand at Waldemar) by the WATFLOOD model, however, releases are specified according to recorded data (Table 9.6). Proportionality plots at reservoir inflow gauges are provided in Appendix G (Figures G.1 to G.7).

Table 9.6 – Statistical summary of simulated inflow to GRB reservoirs.

Reservoir	Inflow Gauge	DA (km^2)	Nash	%Dv	Slope	R^2
Belwood	Grand @ UpBlwd	746	-0.026	-48.54	0.149	-0.594
Conestogo	Conestogo @ Glen Allen	612	0.768	-9.765	0.836	0.771
Shades Mills	Mill Creek	81	-0.591	26.83	1.195	0.438
Luther Dam	Grand @ Waldemar	620	0.191	11.38	0.414	-0.293
Laurel	Laurel @ Erbsville	20	-3.108	98.55	1.616	0.335
Woolwich	Canagaguige @ Floradale	56	0.177	48.85	0.494	0.108
Guelph Lake	Speed @ ArmstrongMills	160	0.168	20.043	0.466	-0.013

Table 9.6 shows that in all reservoirs but Lake Belwood and Conestogo Lake, inflows are over-estimated by the WATFLOOD model ($\%D_v$), where Conestogo Lake is shown on Figure 9.14 to be gaining and loosing throughout the simulation. Lake Belwood however shows significantly under-estimated inflows at the Grand River inflow, however, the large upstream drainage area means that there are several inflows contributing to the lake, some of which are being over-estimated by the model. Slopes of proportionality plots support the $\%D_v$ statistics at all reservoir inflow gauges except for Woolwich and Guelph Lake. Woolwich shows an over-estimation of volume, but a regression slope less than one because of significantly under-estimated peak, or event-based flows. The proportionality plot for Woolwich Dam however indicates a general over-estimation of inflow when these peak flows are removed (Appendix G; Figure G.3). Similarly, Guelph Lake inflows are also (on average) over-estimated, with the lower-than-one proportionality slope derived from one significant 2005 summer rainfall event that was under-estimated (Figure G.6). Isotopic simulations, however, are compared to simulated lake storages in order to evaluate their correlation to simulated hydrologic change.

During the summer of 2004, lake storages in all seven reservoirs show simulated volume decreases correlated with increases in isotopic composition; suggesting that lake evaporation is drawing down lake storage and resulting in the enrichment of heavy isotopes. This observation is reinforced by an increase in simulated lake evaporation from June through August 2004. During fall and spring snowmelt events (February 2004, November 2005, and March 2005), lake storage sharply increases and is marked by a strong isotopic depletion from snowmelt contributions to the lakes. Some lakes realize more or less enrichment and depletion, which is correlated to the upstream drainage area (i.e., volume of inflow) and storage capacity (i.e., surface area and volume) of the reservoir (Table 9.5). Generally speaking, the larger the lake and it's contributing area, the more moderated lake outflows will become.

Larger reservoirs moderate isotopic changes more effectively because 'new' inflows are mixed with 'old' water persisting in storage, resulting in seasonally averaged lake compositions. When lake storage fluctuates significantly (e.g., Conestogo Lake and Luther Dam), isotopic compositions are also more variable ($\Delta\delta^{18}O$=7.97‰ and 5.44‰, respectively) reflecting the distinct seasonality of different input sources. In Conestogo Lake, late fall and winter storages are very low since the lake is drained during the winter (GRCA, 2008c); resulting in dominant spring snowmelt contributions and significant isotopic depletions. Similarly, as depleted lake storages (i.e., meltwater dominated) begin to drain from the reservoir, remaining lake storages evaporate during the summer, enriching the isotopic composition of the lake. Both characteristic behaviours are simulated by isoWATFLOOD as is seen on Figure 9.14.

One clear advantage to isotopic analyses in hydrologic studies is the insight they provide on the specific components of the hydrologic cycle changing lake and streamflow water balances. The presence of a through-flow lake (i.e., Woolwich Dam) was shown to reduce both isotopic and hydrologic variability in the Canagaguige River basin (Section 7.4). Table 9.5 indicates that the average composition of Woolwich Dam tends to be more depleted than Canagaguige streamflows (Figure 7.13; -9.614‰ on average over the two-year period). Woolwich Dam is shown on Figure 9.15 to reduce both the $\delta^{18}O$ composition and variability of downstream flows throughout the two-year GRB simulation period.

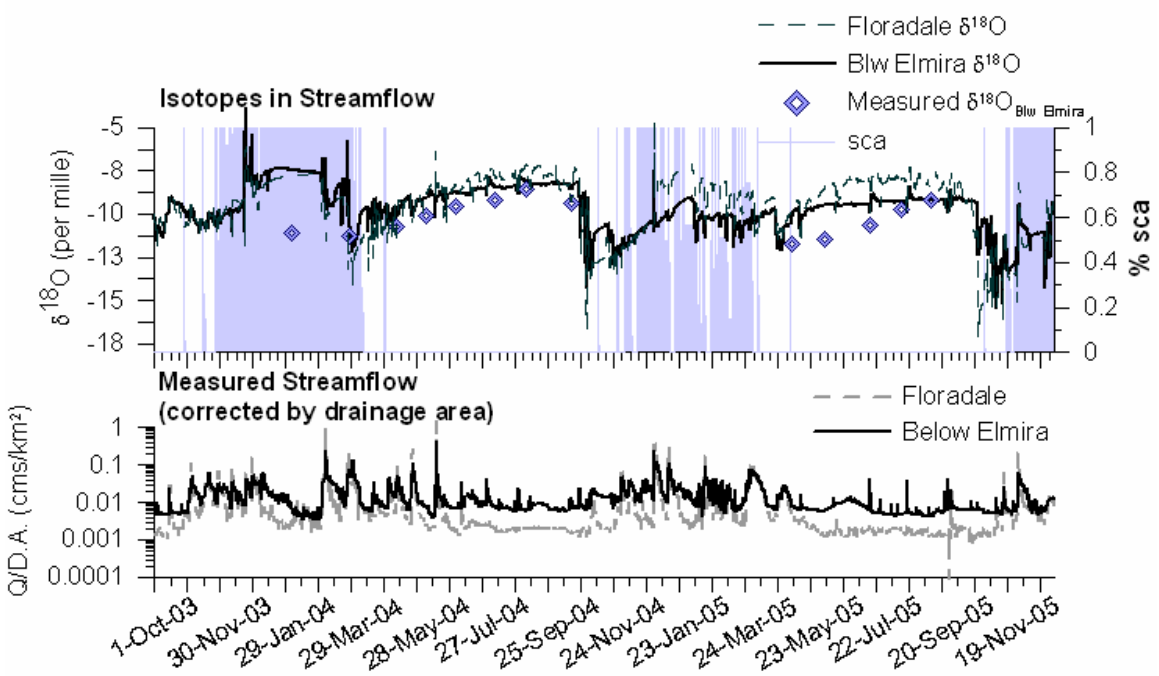

Figure 9.15 – Hydrologic and isotopic variability in Canagaguige Creek sub-basin.

The downstream depletion in isotopic response is attributed to the influence of snowmelt on Woolwich Dam storage (Figure 9.14) that results in the gradual, prolonged release of isotopically depleted water to the downstream reaches of Canagaguige Creek. Of the hydrological inputs contributing to Woolwich Dam, 48% of total simulated runoff into the lake is in the form of snowmelt. The contribution of snowmelt to the Woolwich reservoir is substantial because the reservoir is drawn-down during late fall and winter periods. This contribution seems reasonable given the seasonal distribution of precipitation and temperature in the GRB climate (Table 3.3).

Utilizing hydrological and isotopic data, detailed water balances can be performed on natural lakes to determine the percentage contributions by various end-members. This theory is applied to Woolwich Dam as an example, to illustrate that isotopically, the above mentioned 48% contribution by snowmelt can be computed. A two-component mixing model is applied from the onset of melting (i.e., April 1st) to the end of melting (i.e., May 1st, sca=0), where snowmelt is assumed to be the dominant contributing end-member and is isotopically distinct from the reservoir water in storage. The volume of snowmelt contributing to the lake can therefore be defined as

$$V_{snw} = \frac{\delta_{LK,2} V_{LK,2} - \delta_{LK,1} V_{LK,1}}{\delta_{snw}} \qquad (9.1)$$

where the change between the isotopic composition and storage volume of the lake prior to the onset of melt ($\delta_{LK,1}$ and $V_{LK,1}$) to after the melt period ($\delta_{LK,2}$ and $V_{LK,2}$) are assumed to be responsible for the increase in lake volume (V_{snw}). The above equation, using an assumed composition of snowmelt based on the long-term average for the GRB study period (-17.56‰), predicts a 47% contribution of snowmelt to Woolwich Dam in the 2004 freshet. This percentage contribution via the mixing model matches well with the simulated snowmelt contribution from WATFLOOD. Studies performed in northern Canadian deltas found that snowmelt replenished between 26 and 30% of total lake volume during freshet periods (Falcone, 2007). In these studies, lakes were not necessarily dry prior to freeze-up; decreasing percent meltwater contributions to total lake volume. Snowmelt composition is an important aspect of the above computation and therefore should be more accurately measured (i.e., temporally variant) for detailed water balance studies in natural lakes where inputs are not as easily quantified. In the above calculation, if snowmelt composition were to increase by 1‰ the contribution of snowmelt to the reservoir would instead be ~50%.

Lake isotopic composition varies with meteoric and end-member input compositions, but is also strongly affected by lake-specific characteristics. The amount of evaporation a lake undergoes is strongly correlated with lake surface area: the larger the open water surface, the more water volume is able to be lost to evaporation. For example, on Figure 9.14 Conestogo Lake (i.e., having one of the largest surface areas) shows the steepest summer isotopic enrichment profile. The lake with the largest surface area (i.e., Lake Belwood) was found to have a higher amount of isotopic variability ($\Delta\delta^{18}O$=5.03‰; Table 9.5), reflecting the larger difference between depleted freshet and enriched summer lake compositions. Changes in Lake Belwood's isotopic composition are not nearly as pronounced as the more sudden changes simulated in Conestogo Lake because they are buffered by the large volumes of water held in storage throughout the winter months (GRCA, 2008c).

It is important to ensure that the model is correctly simulating lake isotopic enrichment and that differences in enrichment rates are in fact correctly interpreted. Figure 9.16 plots the simulated $\delta^{18}O$ for Woolwich Dam lake water against the isotopic composition of the lake if it were in hydrologic steady-state (I=E+Q, δ_S), and the limiting steady-state isotopic composition

representing the $\delta^{18}O$ signature of the lake immediately before it desiccates (δ^*). The ability to assess $\delta^{18}O$ of the lake in relation to both δ_S (Equation 2.10, Section 2.4.2) and δ^* (Equation 2.12, Section 2.4.2) explains the lake enrichment profiles shown on Figure 9.14 as they tend towards constant late-summer compositions where no further enrichment is observed, despite the availability of water.

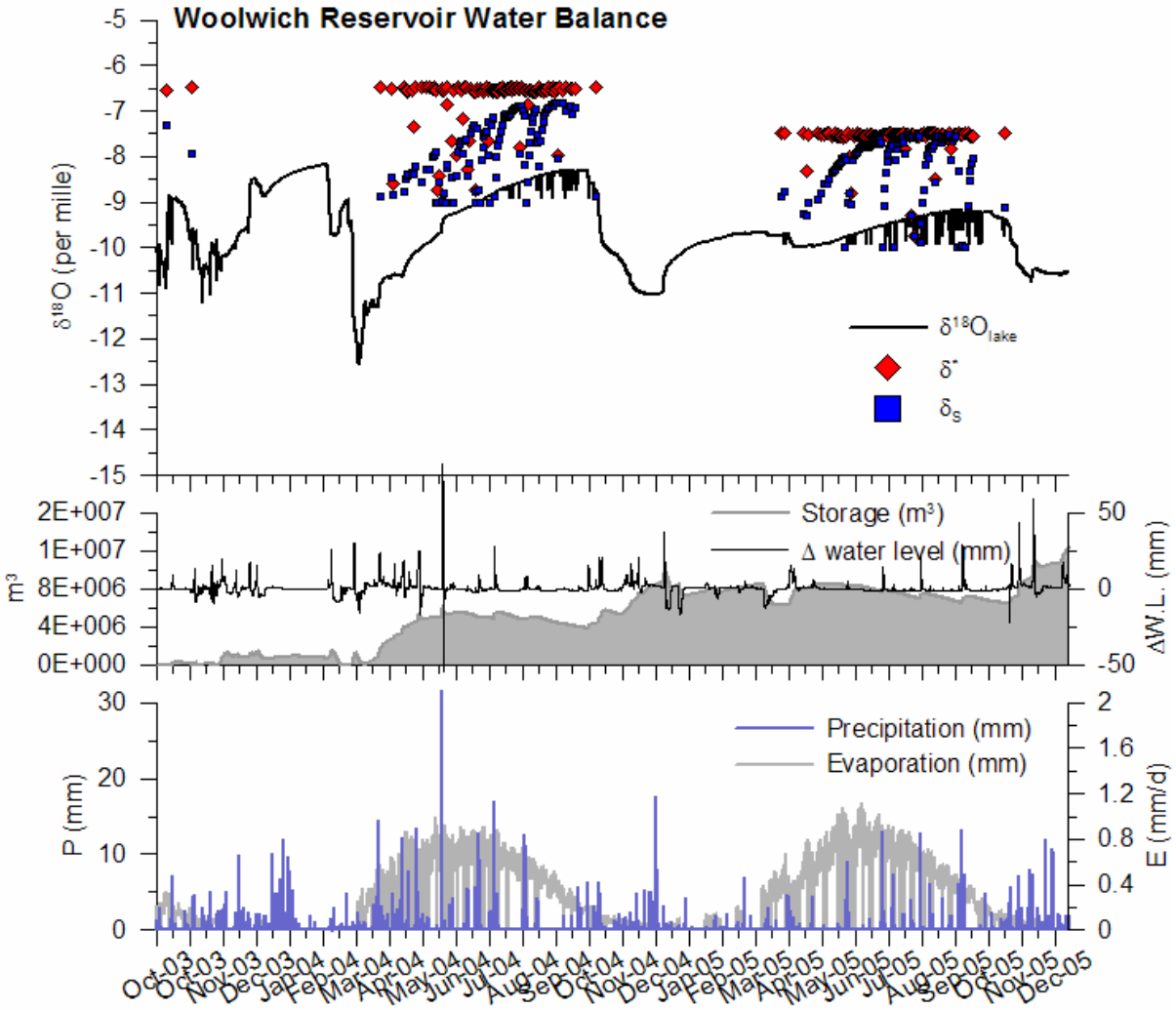

Figure 9.16 – Water balance for Woolwich Dam from isoWATFLOOD-simulated isotopes.

From spring to summer, simulated δ_S in Woolwich Dam gradually enriches towards the composition of δ^* as the lake composition enriches and relative humidity increases. Since the rate of heavy isotope build-up, *m* (Equation 2.11, Section 2.4.2) decreases as relative humidity increases, δ_S approaches (but is never equal to) the limiting δ^* composition as relative humidity approaches one. The limiting composition of the lake (i.e., if it were desiccating) remains

relatively constant given that it is a function of the high relative humidity gradient (i.e., 90-100%) assumed over lakes in the GRB during evaporative seasons when water is in storage. There is a slight depletion in δ^* seen as relative humidity increases even closer to one by late summer, significantly decreasing evaporation. Under high relative humidity, the physical basis of Equation 2.12 breaks-down given it is not physically possible to desiccate a lake under such atmospheric conditions. Instead a lakes most enriched isotopic composition attainable would be if it were in hydrologic steady-state (i.e., inflows equal to outflows). The isotopic composition of Woolwich Dam is therefore characterized as evolving towards isotopic steady state throughout the summer. By the end of summer and early fall, the composition of lake water reaches δ_S and the rate of enrichment slows. Lake compositions do not remain at steady state, but are seen to periodically deplete with summer rainfall and re-enrich back towards the composition of δ_S as evaporation commences following the rainfall event. Woolwich Dam is not simulated as a desiccating lake (Figure 9.14) and therefore the lakes most enriched isotopic composition remains far more depleted than δ^*.

Analysis of isoWATFLOOD-simulated $\delta^{18}O$ in GRB reservoirs has shown that the model simulates the isotopic enrichment and depletion of lake water in a physically realistic manner that is verifiable against simulated hydrological changes. The analysis of $\delta^{18}O$ data coupled with well-defined hydrologic variables enables lake water balances to be well-interpreted when control data are not available. The coupling of two isotope responses (i.e., δ^2H and $\delta^{18}O$), however, would enable the development of a δ^2H-$\delta^{18}O$ isotopic framework for a specific region, facilitating the diagnosis of short-term isotopic variability and changes in atmospheric moisture sources.

Continuously simulating $\delta^{18}O$ in parallel with hydrologic change produces a continuous time series of isotopic response: defining compositions at the start and end of an event of interest (i.e., which is difficult to capture in field studies). Using the isoWATFLOOD model and a few strategically timed samples, the isotopic variation between samples can be simulated. Rainfall-runoff models may provide information on the magnitude of variability in streamflow resulting from meteorological changes; however, they typically stop short of identifying why these changes to streamflow occur. The isoWATFLOOD model provides the added capability to simulate $\delta^{18}O$ in parallel with hydrological changes to water balances, and can therefore be used

in detailed hydrological studies to assess variability and attenuation of basin-scale changes. Variability assessment should be performed using both long time sequences and large domains in order to fully understand and characterize a watersheds behaviour and sensitivity to hydrologic change.

9.2.3 Inter-Annual Hydrological Variability

An advantage of the isoWATFLOOD model is the ability to conduct mesoscale variability assessments over long time sequences, generating continuous hydrologic and isotopic responses. Streamflow simulated by hydrological models is useful in understanding inherent inter-annual variabilities driven by meteorological changes, but it is also valuable in understanding how this inter-annual variability affects basin water balances and sub-process contributions. The examination of isotopic variability, coupled with changing meteorological and hydrological variables can offer significant insight as to how the GRBs water balance changes from the fall of 2003 to the end of 2005.

The focus of this section is to illustrate how isotopic analyses can shed light on internal hydrologic responses, and to show how isoWATFLOOD can facilitate evolving the isotopic signature of streamflow through time. Figures presented in this section represent streamflow and runoff $\delta^{18}O$ for the lower GRB region at single points in time (indicated on the corresponding Grand at York isograph). The evolution of the Grand at York isotopic response (i.e., presented below spatial plots, in $\delta^{18}O$ ‰, VSMOW) is qualitatively discussed and correlated to observed changes in both climate and hydrology recorded by the MOE Brantford Climate Station from 2003 to 2005. A description of the GRB's inter-annual variability in climate and streamflow at Brantford has been provided in Appendix G for reference.

Streamflows in southern Ontario are naturally lower in the summer months than in the wetter spring and fall months. A large factor in determining streamflow runoff is the precipitation recorded in the previous season. Continuous temporal analysis therefore plays a significant role in the ability to accurately simulate and characterize current hydrological events in a watershed. Beginning in the fall of 2003, high amounts of precipitation (Figure H.2) coupled with cool

temperatures (Figure H.1) acted to saturate local hydrological storages and reduce evaporation from soils in the late fall. In the following spring, significant snowmelt-induced runoff was both observed (Figure 9.8) and simulated (Figure H.3; $\Sigma fexcess_{Apr}$=151.5 mm) in 2004 (i.e., relative to 2005 where $\Sigma fexcess_{Apr}$=33.3 mm). The spring and early summer of 2004 were also wet, with high to average amounts of precipitation from May through July. Throughout the wetter early summer months, temperatures were lower than normal (i.e., relative to Climate Normals: Table 3.2) that acted to reduce evaporation in May through July of 2004 relative to other years ($\Sigma strloss(2004)_{May\text{-}Jul}$=20.4 mm; $\Sigma strloss(2005)_{May\text{-}Jul}$=22.5 mm). In August, however, temperatures increased and precipitation decreased below amounts seen in the 2003 and 2005 seasons. Due to a wet fall in 2003 and early, wet freshet in 2004 hydrological storages remained saturated post-freshet and throughout the summer. As late summer temperatures increased (Figure H.1), the evaporative potential of the saturated lower GRB also increased and resulted in high evaporative fluxes from soil and surface storages that resulted in significant late summer enrichment of streamflow and runoff components (Figure 9.9 and Figure 9.10). Table 9.7 contrasts the summer enrichment simulated in 2004 to streamflow enrichment during the summer of 2005, confirming more enriched minimum and maximum compositions and lower isotopic variability of streamflow in 2004.

Table 9.7 – Comparison of simulated $\delta^{18}O$ for 2004 and 2005, and 2004 and 2005 summer[1] periods for the Grand at York gauge.

$\delta^{18}O$ ‰, VSMOW	**Summer[1] 2004**	**2004**	**Summer[1] 2005**	**2005**
Average	-8.336	-9.351	-9.502	-10.371
Standard deviation	0.355	1.458	0.523	1.405
Minimum	-9.207	-13.091	-11.235	-14.448
Maximum	-6.690	-6.690	-8.604	-8.604
$\Delta\delta^{18}O$	2.52	6.401	2.63	5.845

[1]Summer was defined as May 1st through to August 31st

Figure 9.17 shows the isotopic response of the lower GRB basin in late summer (August 27th) of 2004.

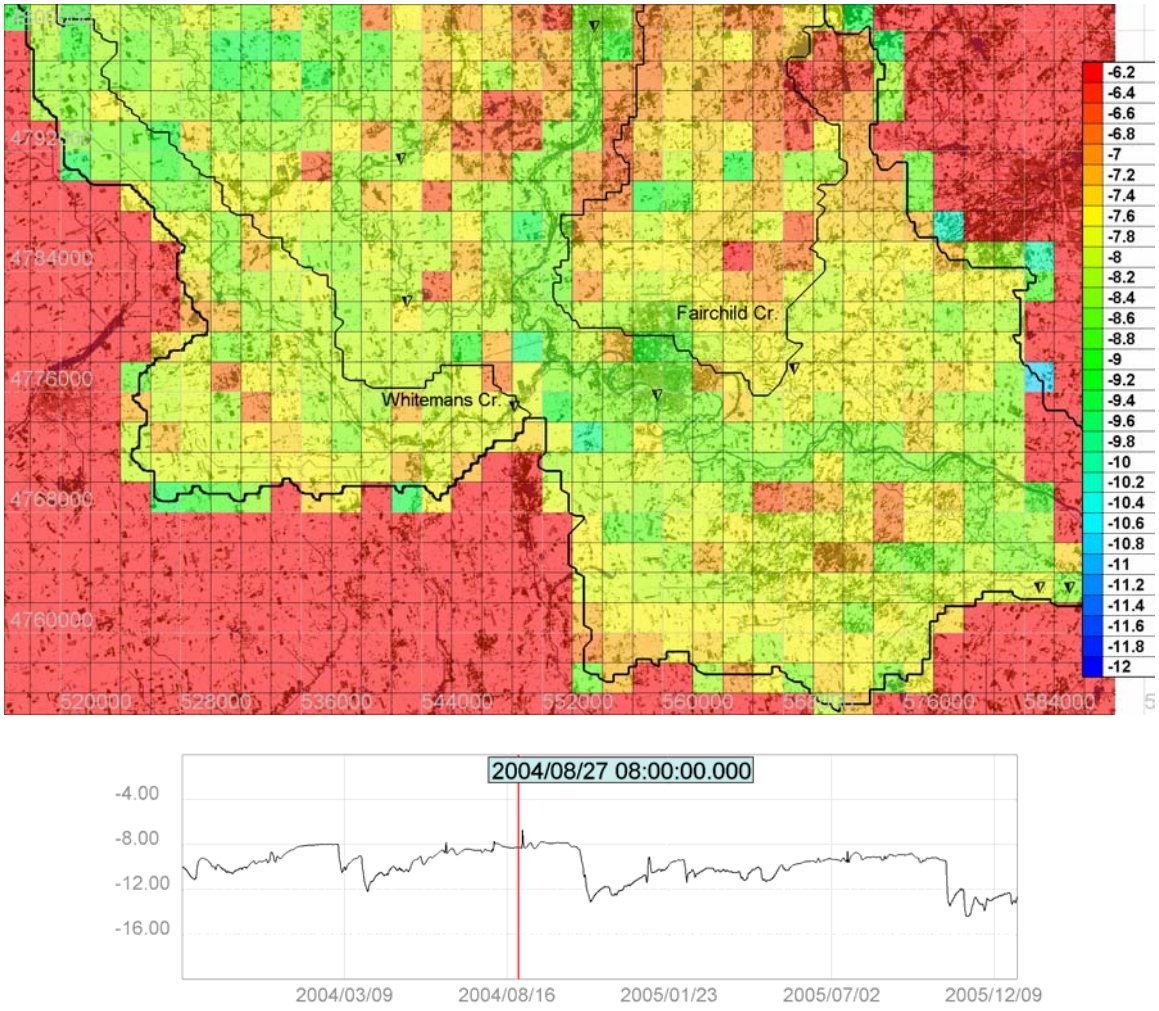

Figure 9.17 – Isotopic response of the lower GRB at York on August 27th, 2004.

Late in the summer of 2004 the Grand River and other tributaries (shown behind isoWATFLOOD outputs) are isotopically depleted (i.e., blue shades) relative to the surrounding catchment area (Figure 9.17), which is the result of the propagation of depleted rain and lake water (Section 9.2.2) from upstream reaches. Grid cells surrounding the main river stem are generally more enriched than the rivers (i.e., red shades) indicating that evaporative enrichment is occurring in these regions. Low precipitation (i.e., low humidity) and higher temperatures in August 2004 encourage evaporation of saturated soil and wetland storages and a higher rate of isotopic enrichment (*m*; Equation 2.11) of runoff components. Some wetlands (fens) surrounding the main river stem provide isotopically depleted inputs to river water because of their persistence in retaining and gradually releasing depleted baseflow, snowmelt, and rainfall

water in fen storage (e.g., Whiteman's Creek). Also notable is the boggy terrain of Fairchild Creek on the northeast side of Figure 9.17. These bogs tend to provide isotopically enriched source water to streamflow (i.e., the opposite of fens) because of their tendency to retain water in surface storage and undergo evaporation. These observations are consistent with the classical definitions of bogs versus fens described in Section 4.9, highlighting the need to differentiate these two distinct classifications of wetlands (Hayashi *et al.*, 2004). Following a rainfall event on August 28th, 2004, the bogs in the upper reaches of Fairchild Creek continue to supply more enriched source water to the lower reaches of the Grand River (i.e., at Fairchild gauge indicated by the triangle marker on Figure 9.18) as the depleted rainfall is mixed with the enriched surface water in bog storage. This particular rainfall event depletes the surrounding catchment area because the composition of rainfall is more depleted than the evaporatively enriched surface storages. The rainfall has a more immediate impact on the surrounding catchment area than the river, however; river water remains slightly more enriched than the catchment until the rainfall runoff eventually drains into the channels (Figure 9.18).

September and October of 2004 were warmer and drier than in 2003, and coupled with an overall drier summer period (Figure H.2). Streamflows in fall 2004 were low relative to 2003 and 2005 (Figure H.3). With higer temperatures and lower relative humidity, it would seem apparent that evaporation rates should increase in 2004, resulting in decreased streamflow runoff. At the onset of a late October (October 29th, 2004) rainfall event, however, isotopic compositions are shown to be generally more depleted than they were in August 2004. Even the boggy terrain of Fairchild Creek shows a relatively constant, more depleted isotopic composition, indicating that evaporative enrichment is not overly significant during this period of time. Reinforcing the isotopic results, simulated evaporation from soil storage in the fall of 2004 (September to November) was lower in 2004 ($evt(agri)_{avg}$=209 mm) than in 2005 ($evt(agri)_{avg}$=419 mm). Soil storages were also lower ($uzs(2004_{sep\text{-}nov})_{avg}$=45 mm; $uzs(2005_{sep\text{-}nov})_{avg}$=57 mm) and baseflows were higher ($lzs(2004_{sep\text{-}nov})_{avg}$=14.4 mm; $lzs(2005_{sep\text{-}nov})_{avg}$=12.7 mm) because of the drier 2004 summer (Figure H.2). Although not immediately intuitive, the lower evaporation rates are caused by reduced soilwater and surface storages.

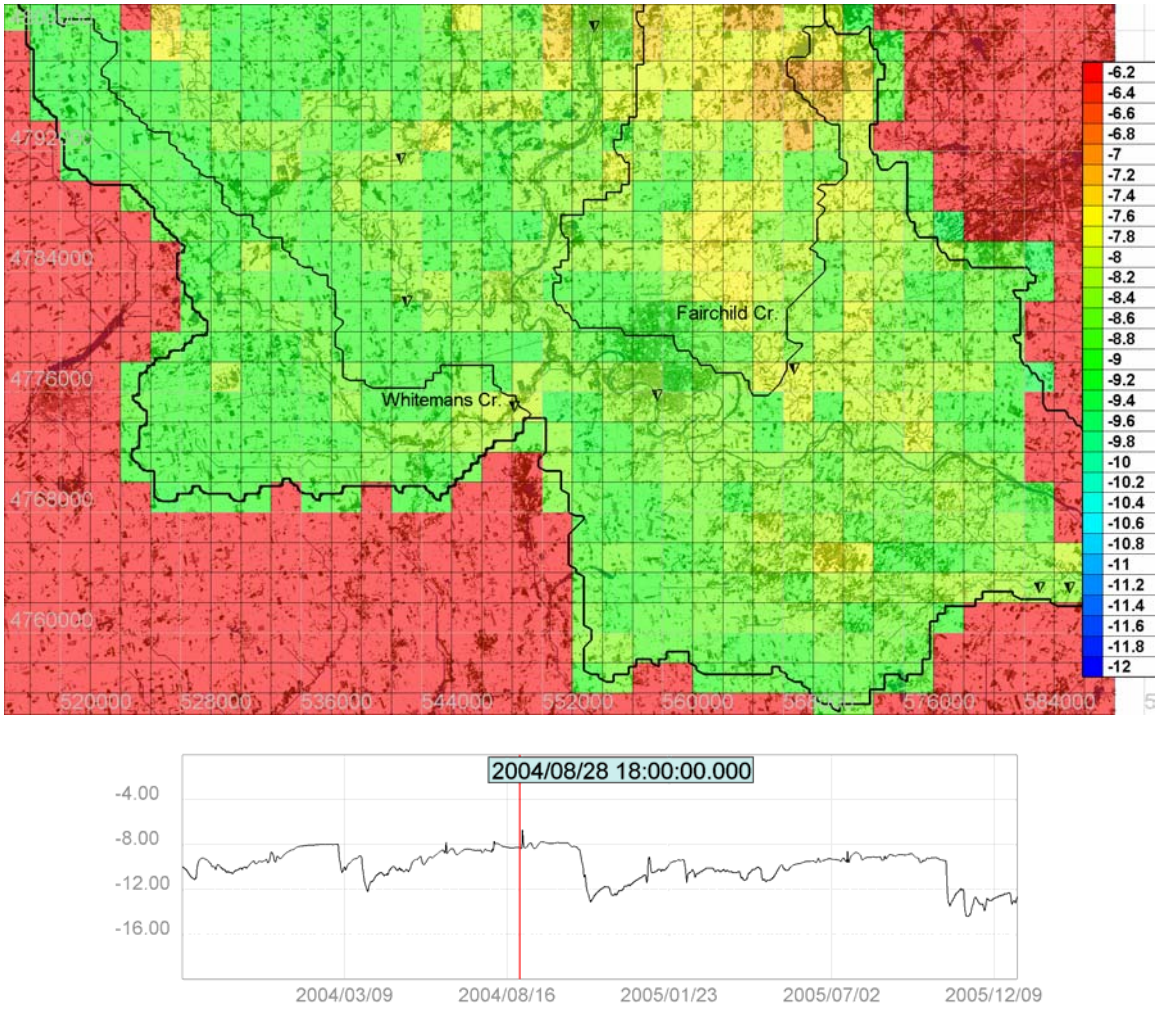

Figure 9.18 - Isotopic response of the lower GRB at York on August 28th, 2004.

Figure 9.19 illustrates the isotopic influence of a typical southwesterly rainfall event travelling across the lower GRB. The event represents a weather front bringing meteoric moisture to the GRB that is isotopically depleted relative to the surrounding storages, and clearly shows the differences in $\delta^{18}O$ derived from spatially distributed rainfall events (Section 9.2.4). The 2004 fall season corresponds with more depleted isotopic compositions relative to the rest of the study period. The influence of several late fall rainfall events isotopically depletes southern GRB storages and streamflows even further, rendering an isotopic response that is analogous to a freshet period (shown on Figure 9.19 isograph).

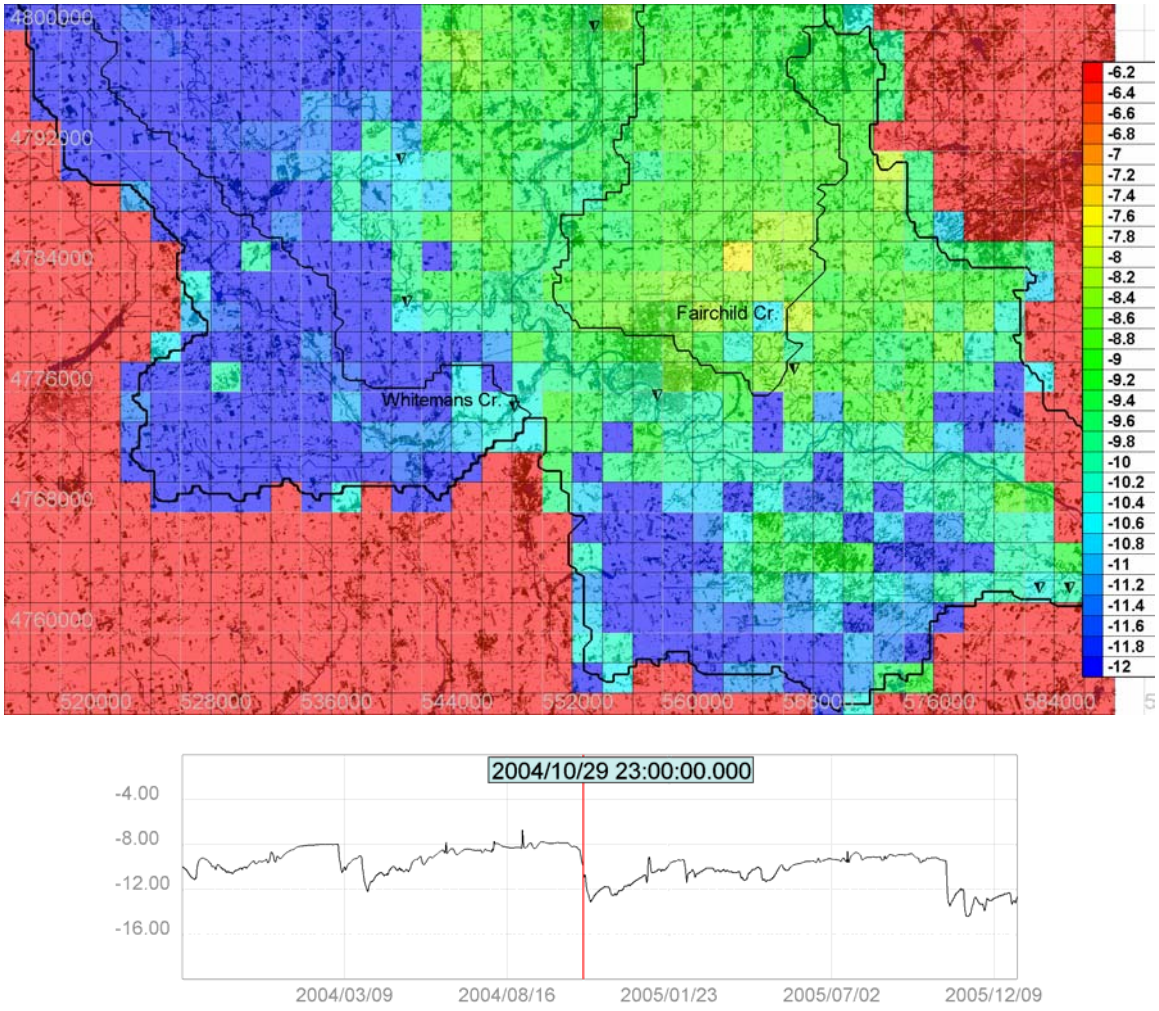

Figure 9.19 – Isotopic response of the lower GRB at York on October 29th, 2004.

Meteoric waters during the October 29th, 2004 event influence a larger portion of the lower GRB as the rainfall event evolves and runoff is induced. Figure 9.20 shows the isotopic distribution during the morning of October 30th, and Figure 9.21 illustrates the catchment and streamflow response by mid-day (nine hours later) once rainfall had ceased.

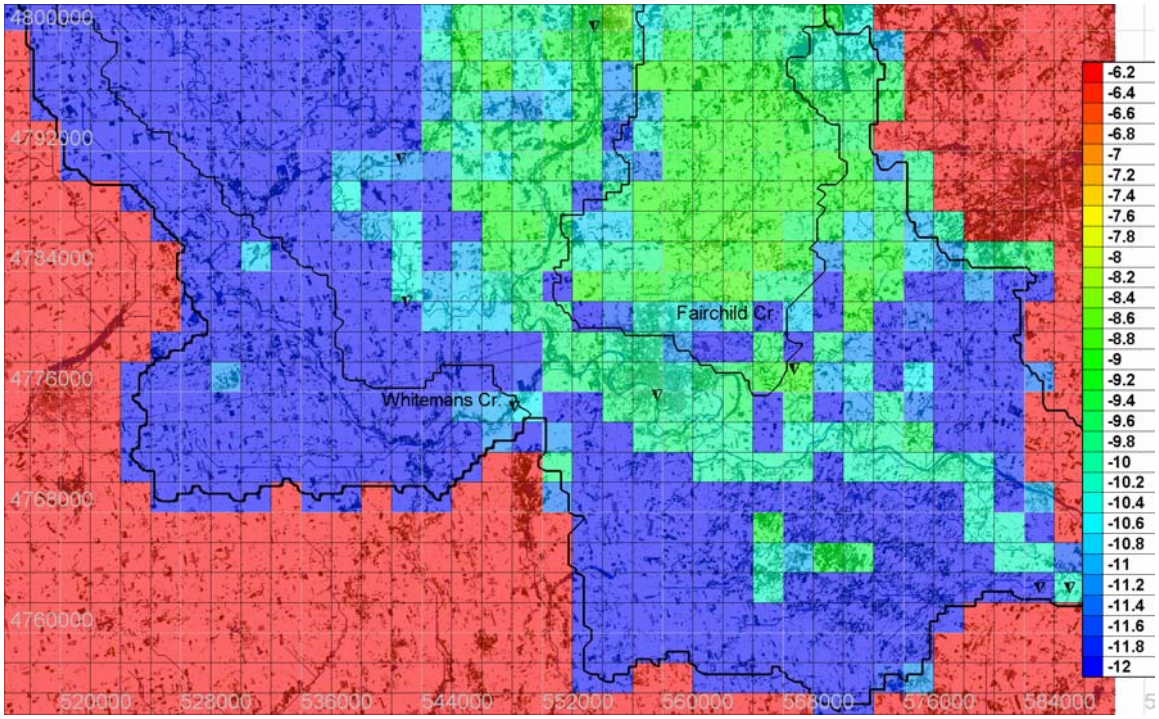

Figure 9.20 – Isotopic response of the lower GRB at York on October 30th, 2004.

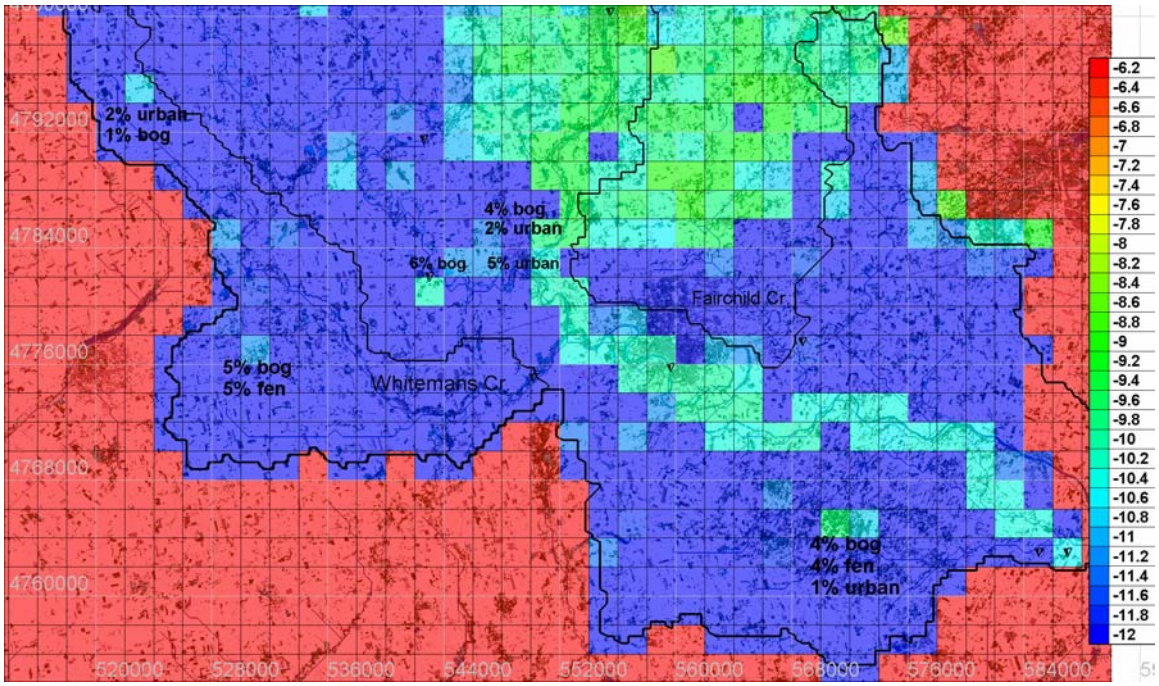

Figure 9.21 – Isotopic response of the lower GRB at York 9 hours later on October 30th, 2004.

The surrounding catchment area becomes more depleted because of meteoric source waters, but streamflows are seen to remain more enriched due to the influence of upland tributaries that did not receive the direct rainfall. Isotopic enrichment of the surrounding catchment begins

following the rainfall, and grids with higher percentages of urban and bog area begin to enrich more quickly than other grids (indicated on Figure 9.21). This particular event did not generate immediate, large volumes of runoff in the lower GRB (i.e., 30% of direct rainfall generated direct runoff) because soil and bog storages were low prior to the event. The lessened influence of this large rainfall event is because of runoff infiltration and bog retention. The water in hydrologic storage then progressively contributes to streamflow after being slightly enriched by evaporation from storage. Eleven hours after the start of the rainfall event, the effects of the evaporative enrichment are visible on the surrounding catchment area, along with the gradual contribution of depleted meteoric waters to channel flow (Figure 9.22).

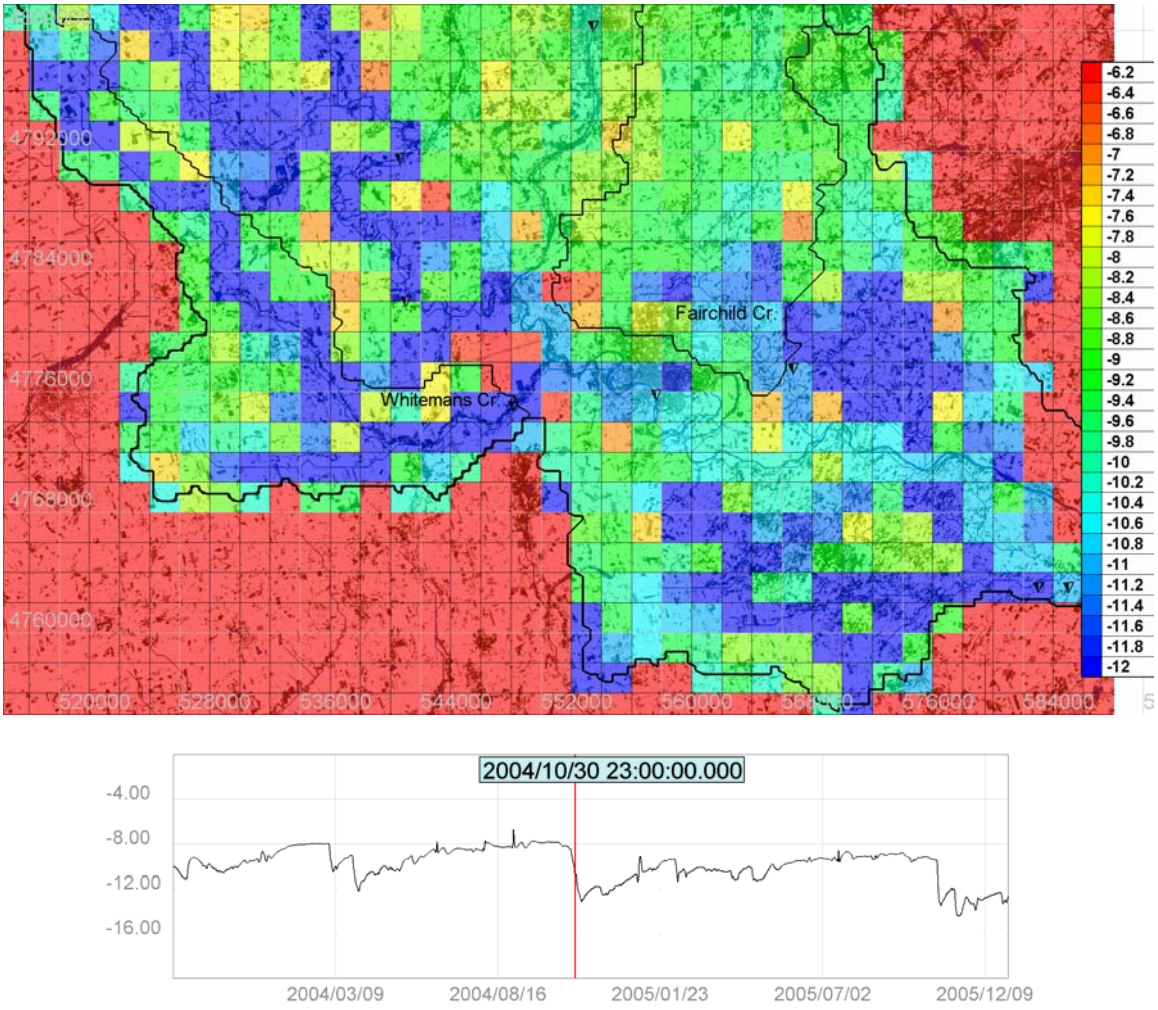

Figure 9.22 - Isotopic response of the lower GRB at York 20 hours later on October 30th, 2004.

Figure 9.22 shows the main stem river composition as remaining more enriched than the smaller surrounding tributaries draining upstream catchment areas influenced by the rainfall. Tributaries are clearly visible because they are now depleted relative to catchment areas on Figure 9.22; indicating isotopically depleted source water in catchment storage is being released into these smaller river networks. Although these tributaries drain directly into the Grand River, they do not significantly alter the lower Grand River $\delta^{18}O$ because their contributions are mixed with large volumes of upstream flow not influenced by the depleted rainfall event. The enrichment rate of the surrounding catchment area is also differential: the result of differences in land classification and thus evaporative fluxes (shown previously on Figure 8.21). Analysis of a regionally isolated event such as this one reinforces the need to perform strategically designed, spatially distributed analyses during hydrological investigations.

Winter 2005 brought warmer temperatures and wetter conditions than in 2003 and 2004 (Figures G.1 and G.2). Consequently streamflow runoff at the York gauge is highest in January, February, and April 2005 indicating a more gradual and persistent snowmelt period in 2005 whereby snow-cover persisted into early May ($\Sigma fexcess_{Apr\text{-}May}$=33.3 mm; sca=0.47). The initial peak flow in January was the result of a sudden and early warming (Figure H.1) that generated snowmelt runoff and subsequently high streamflows when soils and wetlands were still partially frozen. A late January depletion is observed on the York isograph (Figure 9.10) from influence of depleted meltwater. By the end of January 2005, snowpacks were smaller ($snowc_{2005}$=28 mm; $snowc_{2004}$=72 mm) and runoff was higher (Σrff_{2005}=383 mm; Σrff_{2004}=96 mm). The onset of an early melt period resulted in a more gradual freshet in 2005, reducing the snowmelt-derived isotopic depletion signal relative to the 2004 freshet. Isotopically depleted snowmelt is absorbed by fens lining the channel networks, and is then gradually released into streamflow throughout the spring and early summer seasons.

A large rainfall event on July 17th, 2005 is shown to deplete the lower GRB isotopic composition, establishing a constant composition across the region (Figure 9.23). Streamflow in the Grand River however remains more enriched than the surrounding catchment area from the influence of upstream runoff and displacement of evaporatively-enriched water from storage during the rainfall event.

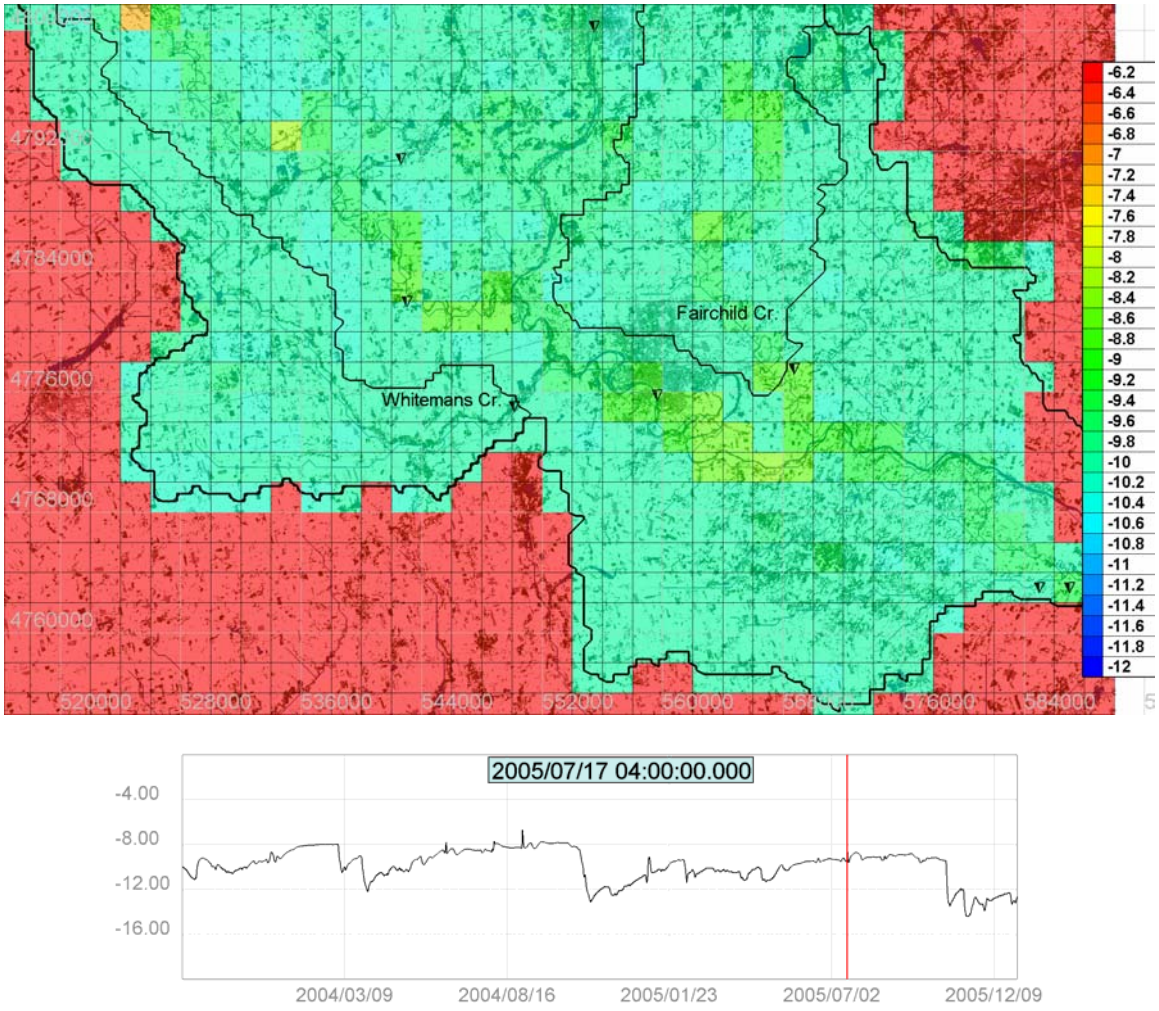

Figure 9.23 - Isotopic response of the lower GRB at York on July 17th, 2005.

The meteoric source water from the rainfall event gradually makes it way from the catchment area into small tributaries that eventually drain into the Grand River main stem. Twenty-four hours following the event, Figure 9.24 depicts a more enriched catchment area relative to the Grand River main stem and tributaries as the catchment areas drain and evaporate the event water, propagating the rainfall $\delta^{18}O$ signature downstream.

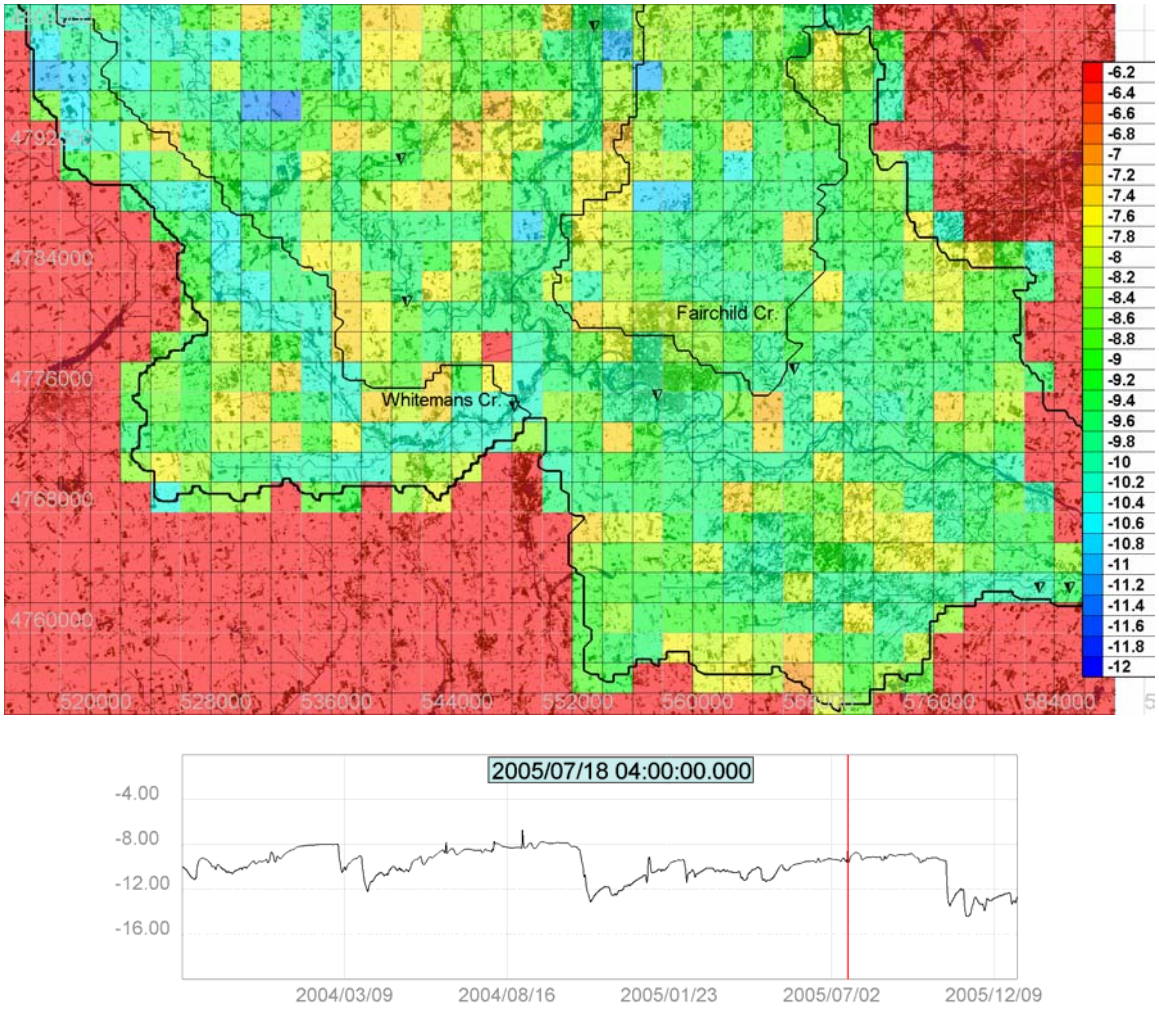

Figure 9.24 - Isotopic response of the lower GRB at York 24 hours later on July 17th, 2005.

Despite high temperatures and low streamflows in the summer of 2005, which might otherwise generate higher-than-normal evaporative enrichment, streamflow $\delta^{18}O$ in 2005 remained more depleted than average compositions in 2004 (Table 9.7). The prolonged snowmelt period in 2005 facilitated the filling of hydrologic storages with meltwater, enabling the longer-term residence of meltwater contributions in channel fens, bogs and soil storages. Snowmelt therefore had a prolonged effect on the 2005 seasonal water balance. The 2005 summer season (April to August) also underwent larger and more frequent rainfall events ($\Sigma P(2005)_{Apr\text{-}Aug}$=1626 mm; $\Sigma P(2004)_{Apr\text{-}Aug}$=900 mm) that contributed to more depleted (i.e., less evaporatively enriched) and more spatially constant isotopic compositions. The prolonged retention of snowmelt storage and consistent rainfalls also reduced isotopic variability ($\Delta\delta^{18}O$) of streamflow

in 2005 relative to 2004. Evaporation was significant in 2005 relative to 2004 ($ev(2005)_{avg}$=276 mm; $ev(2004)_{avg}$=56 mm), however it occurred immediately following rainfall events at an accelerated rate because of the higher summer temperatures (Figure 9.24). Following July 17th, 2005 isotopic compositions gradually rise as hydrologic storages enrich and depleted snowmelt compositions in storage are turned-over with summer precipitation.

Streamflows in the 2004 and 2005 seasons exhibit similar trends. Peak flows occur in the winter and fall, and low-flows occur during the summer. Despite initial differences in 2004 and 2005 winter flows, the remainder of the year (and in particular the summer seasons), are not notably different. The analyses of $\delta^{18}O$ of streamflow and runoff, however, has shown that the cooler summer of 2004 resulted in strong evaporative enrichment trends, and that despite strong evaporative fluxes in 2005, streamflows remained more isotopically depleted because of the prolonged influence of snowmelt and high volumes of rainfall. These results are not immediately intuitive, and therefore from strictly hydrologic and synoptic data, incorrect assessments of the seasonal controls on hydrologic water balances could easily be made. If model internal calibration were to occur based on such incorrect assessments, then the model would generate streamflows from incorrectly proportioned internal responses.

The above temporal analysis has shown that localized isotopic and hydrologic differences are often derived from spatially distributed meteorological inputs, land classifications, and differences in hydrologic storage retentions. This emphasises the importance of having properly defined and spatially distributed isotopic compositions of climate and landcover data. It was recognized that the temporal evolution of the Grand at York isotope response is derived from catchment runoff and the culmination of upland contributing source regions, lessening overall variability and generally depleting compositions. The hydrologic variability of the lower GRB is a function of all upstream variability and therefore it is important to understand the evolution of all upstream isotope responses.

9.2.4 Spatial Hydrological Variability

Basin hydrology is a series of connected storages, where typically the progression from one storage to the next reduces variability because of source water mixing. Different hydrologic storages and particular regions in a basin can have a more significant impact on river quantity and isotopic composition than other regions. This rationalization is particularly true in mesoscale hydrological research where differences in meteorological forcing and landcover evolve over time and space. Mesoscale hydrological modelling can help to identify regional hydrological differences, and also allows for changes to be made pre-emptively to facilitate the prediction of possible consequences resulting from hydrologic or climatic alteration.

This thesis has previously presented the geological (Section 3.1.2), ecological (Section 3.1.3), meteorological (Section 3.1.5), and hydrological (Section 3.1.4 and Section 9.1.1) characterizations of the GRB. This section presents a qualitative discussion of regional differences in isotopic response simulated for the Grand River and its main tributaries. Spatial analyses conducted over longer periods of time are traditionally performed using a series of data-derived interpolations formed independent of one another as a single snap-shot in time. This section illustrates how the isoWATFLOOD model and EnSim facilitate the spatial representation of isotopic simulations for mesoscale basins.

Section 9.2.3 described the evolution of the Grand at York isotopic response over the 2004 and 2005 study period. This section now evolves the isotopic response over the GRB domain along the main stem flowpath for a late July 2005 rainfall event. The simulated isotopic response for the GRB on July 27th, 2005 is illustrated on Figure 9.25.

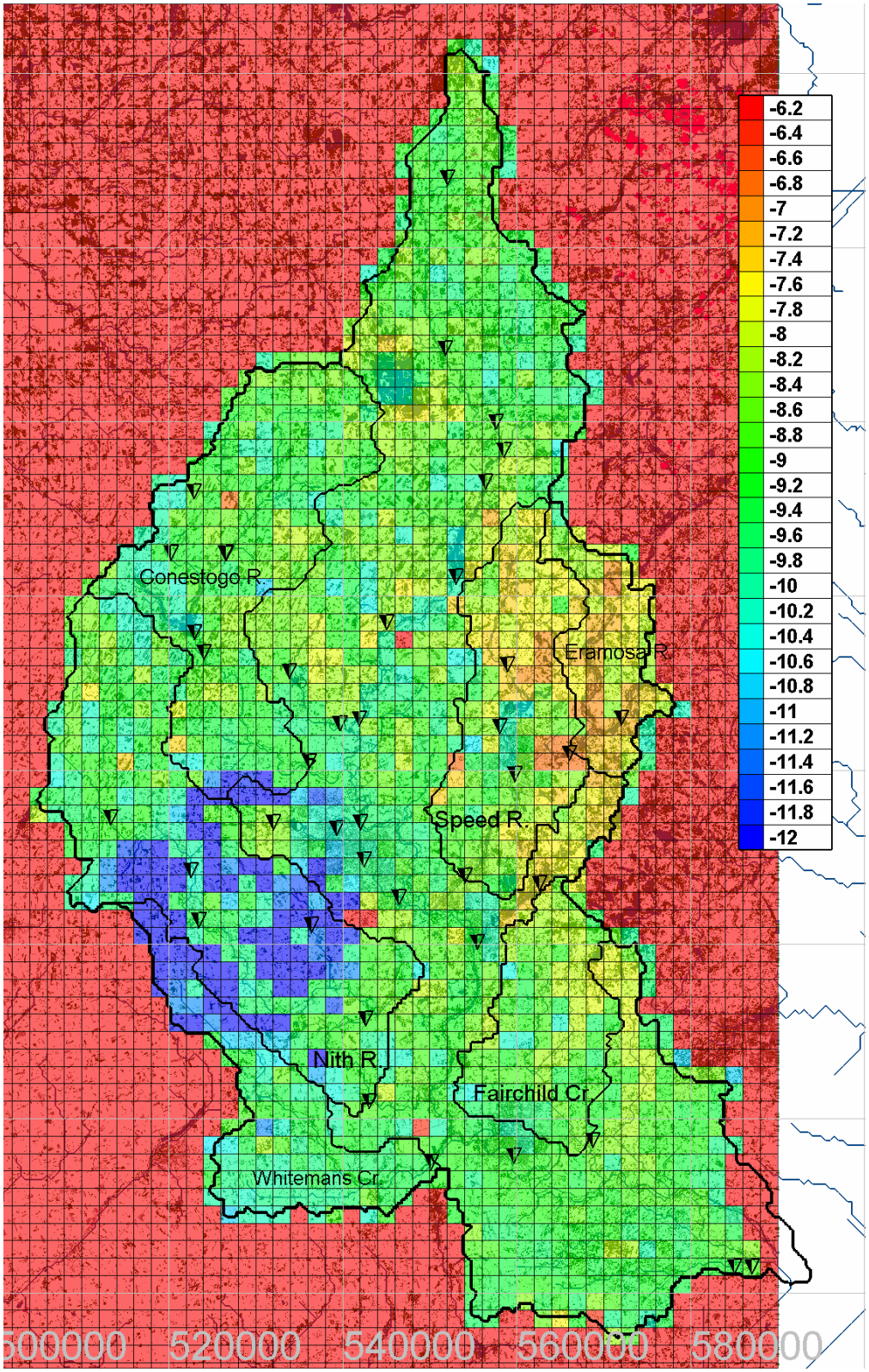

Figure 9.25 – Spatial variability in isotopic response for the GRB following a summer rainfall event (July 27th, 2005).

Apparent from this image are two isotopically-contrasting regions: the eastern edge of the GRB (Eramosa and Speed River basins), and the southwest region (Nith River basin). The rainfall event occurring on July 27th brings isotopically depleted meteoric water to the Nith River basin and other small tributaries in this region, including the headwaters of Whiteman's Creek. The cold water course of Whiteman's Creek is ecologically significant (i.e., coldwater trout fishery) and is known to be predominately baseflow sustained (Section 5.3.1). This sub-basin typically retains a more depleted average isotopic composition ($\delta^{18}O_{Whitemans}$=-9.969‰) than the rest of the GRB ($\delta^{18}O_{York}$=-9.867‰).

Figure 9.25 illustrates a successful application of isoWATFLOOD is reliant upon well-defined, spatially distributed meteorological data. In response to the rainfall event, Nith River and Whiteman's Creek basins become more isotopically depleted than the rest of the GRB, and the Grand River main stem. Although this is only one rainfall event of many occurring in the GRB between 2004 and 2005, it is typical of the origin of most GRB precipitation (Section 3.1.5), where the mid and southwest regions of the GRB generally receive the highest amounts of precipitation, particularly snowfall (Table 3.3). These regions of the GRB therefore tend to be more isotopically depleted than the eastern portion of the GRB as is represented on Figure 9.25.

In contrast to the more depleted western GRB, the Eramosa and Speed River basins show a more enriched $\delta^{18}O$ signal resulting from the abundance of open water and wetlands in this region compared to other regions in the GRB (Figure 9.1). The open water wetlands facilitate higher rates of evaporation, and therefore more isotopic enrichment throughout summer periods. The aerial influence of the wetland/bog terrain is visible as enriched streamflow and runoff compositions extend southward towards the Fairchild Creek basin, which is extensively characterized by bogs. In the eastern Eramosa and Speed River basins the influence of isotopically enriched Guelph Lake (Figure 9.1) on river compositions is also notable.

Using the EnSim post-processor software, isotope responses from the headwaters of the Grand River to the outlet and for significant tributaries are provided in Appendix I (Figures I.1 to I.11). The isotopic response at 11 gauges moving from the Grand River headwaters at Dundalk (Figure I.1) to the Grand River outlet at York (Figure I.11) were plotted from the

isoWATFLOOD simulation (Section 9.1.2). An increase in isotopic variability of streamflow towards the headwaters of the Grand River is simulated. The headwater basins (Figures I.1 and I.2) show more rapid and distinct evaporative enrichment signals than the mid- and lower-reaches of the GRB. This is a result of smaller drainage areas, shorter runoff transit times and therefore less source-mixing in the upland areas. Higher rates of evaporation are also promoted from extensive boggy terrain in the upper-west headwaters region (Figure 3.2).

In the mid-reaches of the Grand River (Figures I.3 to I.5), average compositions are not significantly different (Table 9.3) but the isotopic response and range of variability are. The steeply sloping West Montrose (Figure I.3) basin is more responsive to precipitation events, showing larger variability in response to rainfall and snowmelt events generating significant streamflow runoff and flashy isotopic responses. The Conestogo River (Figure I.4) also shows large, but less-flashy isotopic responses to seasonal events (i.e., particularly snowmelt). The damped isotopic response in the Conestogo River is influenced by the Conestogo Lake upstream of the gauge. The reservoir during and after the freshet period provides a persistent source of depleted streamflow (Figure 9.14); yet in the late-fall, provides significantly enriched compositions of streamflow to the Grand River because of high rates of evaporation (and decreasing water volumes) throughout the summer months. Downstream of the Conestogo River inflow is the Bridgeport gauge on the Grand River (reference Figure 3.3 for gauge locations) that reflects the evaporatively enriched Conestogo River inflows, but is more variable and responsive to smaller events indicating significant contributions from direct surface water runoff (Figure I.5).

The isotope responses of the Eramosa and Speed River tributaries (Figure I.6 and I.7) show significant amounts of summer enrichment as a result of evaporation in wetlands and bogs (Figure 9.1). Downstream of their inflows to the Grand River, the effects of these enriched summer flow contributions are observed at the Galt gauge (Figure I.8). The Grand at Galt gauge however shows less isotopic variability (Table 9.3) and response to runoff events because of the accumulation of streamflow from upstream source areas damping smaller hydrologic contributions. The lower reaches of the Grand River (Figures I.10 and I.11) are also less variable than upstream, headwater reaches because of this accumulation and mixing effect (Table 9.3). Although a sizeable contribution to the lower Grand, the more isotopically varied Nith

River compositions (Figure I.9) have only a slight effect on downstream Grand River compositions. Nith River isotopic variability is associated with increased runoff generation from largely agricultural and small urban settlements characterizing the basin (Figure 9.1).

Figure 9.26 presents the upstream to downstream evolution of isotopic composition along the Grand River main stem from October 2003 to December 2005, indicating the highly variable and enriched headwater basin compositions (red and magenta) relative to the mid- and lower-reaches of the Grand River. In the middle reaches (blue shades) the Grand River depletes relative to upstream reaches. West Montrose shows a large range of isotopic variability with more depleted freshet compositions than Bridgeport and Galt, with higher summer enrichments. The Bridgeport and Galt stations are downstream of the Conestogo and Speed River influences where regulated flows from upstream reservoirs moderate isotopic and hydrologic variability, and generally deplete isotopic compositions because of the prolonged retention of snowmelt in the reservoirs. In the lower reaches of the Grand River (green shades, dashed lines), compositions at Brantford and York become slightly more depleted and less variable than upstream reaches. These downstream gauges are the combination of tributaries added to the Grand River and are influenced by upstream reservoirs acting to dampen downstream variability (Section 9.2.2).

Figure 9.26 illustrates that there is a general depletion in isotopic composition accompanied by a decrease in variability moving downstream along the Grand River. The visible enrichment in the eastern portion of the basin (Figure 9.25) supports the findings from Section 9.2.1 that found these wetland-dominant regions provide hydrologic attenuation, resulting in high rates of evaporation and therefore moisture recycling. Without these environments, downstream runoff was shown to increase, with streamflows becoming more variable (Table 9.4). Similarly Section 9.2.2 showed that reservoirs act as moderators of both streamflow and isotopic composition, decreasing variability downstream of the reservoir. The spatial variability assessment presented in this section also detected this trend where gauges downstream of reservoirs introduced lower-amplitude isotopic responses to the Grand River (Figure 9.26).

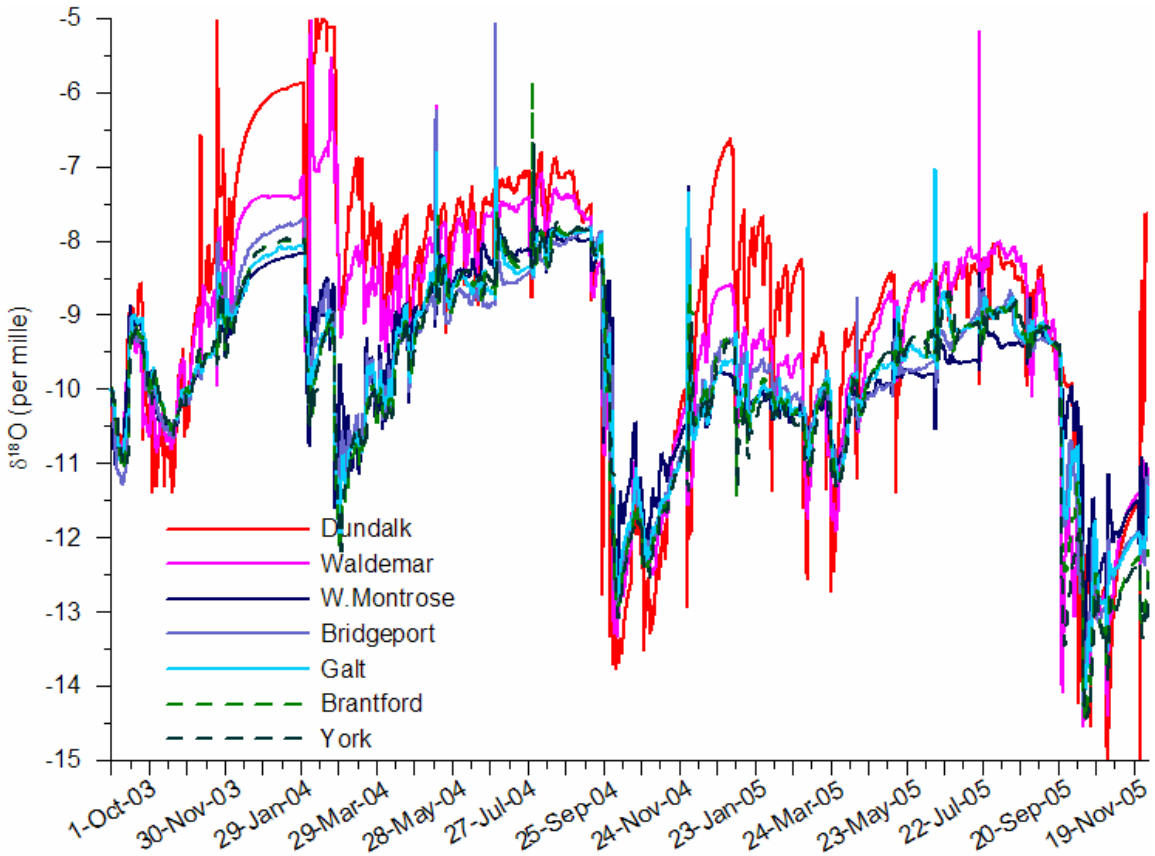

Figure 9.26 – Evolution of the Grand Rivers isotopic response from upstream to downstream.

Sustainable watershed management planning begins with the identification of key hydrologic features serving to offset and moderate hydrologic and meteorological change. Using an isotope-enabled hydrological model, in-depth studies can be conducted to identify traditionally more sensitive regions of a watershed, as well as the limits of a watershed's ability to buffer or moderate significant change. Mesoscale simulations of $\delta^{18}O$ facilitate the identification of regional hydrological differences in mesoscale watershed research, and offer an objective means of quantifying changes to lake, stream and hydrologic storage water balances.

9.3 Chapter Summary

This chapter demonstrates that the isoWATFLOOD model can replicate measured $\delta^{18}O$ data in streamflow without further model calibration for the isotopic simulation. This result highlights the robustness of the WATFLOOD model and demonstrates that the model, when properly

calibrated, generates streamflow simulations from physically representative conceptualizations of mesoscale hydrology.

Aside from the application of isoWATFLOOD to model calibration, this chapter demonstrates the usefulness of simulated $\delta^{18}O$ in assessing the hydrologic variability in mesoscale watersheds. The utility of performing both hydrologic and isotopic analyses allows for a more in-depth assessment of inter- and intra-basin changes affecting streamflow variability. More insight on the internal hydrologic changes controlling runoff-response when land-use is altered is offered through isotopic response analysis. Increased runoff generation results in a more depleted $\delta^{18}O$ signature of streamflow with much higher variance than when wetlands are present in the watershed. There was a more rapid transit of runoff directly into the stream (i.e., event water) that results from decreased event water retention within the watershed. Decreased intra-watershed retention can lead to significant impacts (over time) on groundwater recharge rates and ultimately water resource sustainability. Further investigation is required to support this hypothesis, but nevertheless the model provides some direction for the set-up of a field sampling and water resource monitoring program. Simulated isotopic compositions in GRB reservoirs were also verified using modelled $\delta^{18}O$ data to estimate simulated snowmelt contributions, and to provide context to the evolution of summer lake compositions. The importance of conducting mesoscale hydrologic investigations to evaluate the impacts of smaller-scale changes is emphasized in the evaluation of downstream variability. Environmental impact assessments, as a result, should extend beyond locally influenced areas and should consider the hydrologic changes beyond local watershed boundaries.

This chapter also demonstrates that the continuous simulation of $\delta^{18}O$ by isoWATFLOOD promotes the use of stable water isotopes in mesoscale hydrological research. Spatial plotting software (EnSim) enabled the visualization of simulated $\delta^{18}O$ data in a spatially and temporally continuous manner, without the need for mathematical interpolations. Interpolation methods are useful for spatially distributing a network of measured data; however they are mathematical functions that distribute points based on their separation distances. Mesoscale hydrology has been shown to be very much connected to antecedent conditions from previous seasons, as well as regional differences in landcover and hydrological response. The isoWATFLOOD model

coupled with the EnSim presents a viable alternative to traditionally used measured data spatial interpolations.

The role of stable water isotopes in hydrological modelling studies has been shown to extend beyond their advantage in deriving physically realistic model calibrations. Simulations of $\delta^{18}O$ offer insight as to the reasons behind observed (or simulated) variability in streamflow and runoff storage. This research facilitates the use of stable water isotopes in mesoscale hydrological research because of the ability to now predict isotopic response between measured data points with a physical basis. Traditionally engineers and modellers have sought to reproduce the variability of streamflow, whereas scientists instead have focused on identifying the reasons for such changes. The isoWATFLOOD model provides a tool that can be used to simultaneously evaluate the magnitude of hydrologic variation as well as the reasons (and long-term consequences) of such hydrologic changes.

Chapter 10

Conclusions and Recommendations

10.1 Summary of Conclusions

This dissertation presented the evolution of the isoWATFLOOD model, an isotope-enabled mesoscale hydrological model. The design of the model began with the implementation of a tracer module capable of segregating contributions to streamflow at their point of generation in WATFLOOD. Following the successful application of the tracer module to two baseflow generation studies, sub-component flows simulated by the tracer module were used as the foundation for isotopic modelling. Sub-component flows and hydrological storages having distinct isotopic signatures are combined and transferred in parallel with routed streamflow. The completed model passed four artificially derived diagnostic tests to evaluate model performance and characteristic behaviour. Once operational, a parameter calibration was performed in five remote, northern Canadian basins near Fort Simpson, NWT and a physically-based, unique parameter set was derived for the model based on hydrological and isotopic constraining. The model was subsequently able to reproduce the isotopic variation in streamflow and hydrologic storage within five Fort Simpson watersheds over a three year study period. Streamflow isotopic compositions were also successfully simulated for the Grand River watershed in southern Ontario without additional model calibration, demonstrating the model's robustness and versatility in mesoscale watershed modelling. The following summarizes the pertinent conclusions derived from the development of the isoWATFLOOD model, and its application to simulate the variation of $\delta^{18}O$ in mesoscale watersheds.

Hydrograph separation was found to be an important feature derived for the WATFLOOD model that enables the internal visualization of hydrological responses contributing to streamflow generation. Various methods of baseflow separation exist and are generally accepted for operational use; yet are currently used in practice without verification. Considerable differences among these various methods of baseflow separation were observed, where verification was facilitated by drawing comparisons with isotopically-separated baseflow contributions to streamflow. Of particular interest to modellers is that other components contributing to streamflow can similarly be validated (so long as they are isotopically-distinct), thereby assisting with parameter estimation and the constraint of internal model responses. Numerical tracers used to track internal flows for coarse grid resolutions were found to require dispersion coefficients to maintain Courant and Péclet modelling criteria, and to prevent the early appearance of flow components (i.e., prior to simulated streamflow). These dispersion coefficients were used for Fort Simpson Basin (FSB) simulations, but were not required for the Grand River Basin (GRB) due to the smaller grid resolution used.

The significant role that wetlands play in controlling basin hydrology was shown in the FSB. Considerable differences in watershed hydrological response were observed when wetlands were additionally classified into bogs and channelized fens. The dual wetland classification should be accounted for in hydrological simulations where wetland terrain is a prominent landcover designation in order to successfully reproduce both runoff volume and streamflow recession. Incorporating remotely-sensed landcover data into a hydrologic model parameterization facilitates the distinction between bog and fen hydrological response.

The WATFLOOD model was shown to reliably reproduce mesoscale streamflows in hydrologically dissimilar catchments: five Fort Simpson, NWT area watersheds and the Grand River, southern Ontario watershed. The model was shown to represent internal hydrological processes in a physically realistic way using a minimally parameterized, conceptually based framework. Given the use of constrained model parameterizations in these simulations, significant errors in the representation of freshet and rainfall events in both watersheds suggest that a substantial amount of error was introduced from poorly measured meteorological forcing data. So long as errors in forcing data persist, there is little else that can be done to improve hydrological simulations. Obtaining a good fit of simulated to measured streamflow is always

possible; however, it is not an accurate simulation unless the correct fit is obtained for the correct reasons. Overall, the WATFLOOD model was shown to reliably reproduce mesoscale streamflow with few required parameterizations, making it a practical and desirable tool for operational use.

The simulation of $\delta^{18}O$ in streamflow was able to constrain parameter calibrations in the FSB. Different parameterizations of internal processes were shown to generate equal simulations of streamflow; but only one parameterization accurately simulated the isotopic composition of streamflow. The fitting of simulated $\delta^{18}O$ to measured $\delta^{18}O$ tightly constrained model parameterizations and produced physically realistic internal sub-component contributions to streamflow. By constraining parameter uncertainty, residual simulation error is more easily diagnosed as either error in model conceptualizations or in forcing data.

The isoWATFLOOD model captured both the composition of, and variation in streamflow $\delta^{18}O$ for two mesoscale watersheds. The model was run without isotopic recalibration or the need for additional field investigations or data collection for parameterization. The model was shown to produce physically realistic isotopic evolutions of internal, smaller-scale sub-processes such as vapour and lake water compositions. It was shown that a change to upland landcover (i.e., increasing urbanization) results in changes to downstream water balances and runoff ratios. Particularly through retention and prolonged release from lake storage, the role of snowmelt was shown to have significant impacts on isotopic water balances in the GRB, highlighting the need for more winter sampling programs to better constrain snowmelt contributions and isotopic signatures. The isoWATFLOOD and EnSim software offer the ability to visualize the spatial variability in continuous isotopic responses, which facilitates assessment of mesoscale hydrological sensitivity.

Localized changes to land-use and subsequently sub-catchment water balances were found to alter larger-scale runoff and water storage balances. Understanding and defining watershed characteristic hydrological response, and pre-emptively conducting mesoscale, continuous time-series hydrological impact assessments are seen to be necessary measures required for the design of sustainable watershed planning and management policies.

10.2 Significance of Research

This research culminates in the introduction of the first isotope-enabled mesoscale hydrological model capable of continuously simulating $\delta^{18}O$ in streamflow and hydrological storages contributing to streamflow. The isoWATFLOOD model is an innovative tool that offers a practical means of providing a continuous $\delta^{18}O$ record in both remote and urban mesoscale watersheds. The isoWATFLOOD model addresses a gap in hydrological modelling research identified by Kirchner (2006), Beven (2006), and many others that calls for practical, physically-based methods that can be utilized for mesoscale model calibration and verification. At the same time, Gibson (1996) previously acknowledged the value in developing cost-effective methods that were less reliant on field instrumentation as a necessity for the advancement of mesoscale hydrological research. The investigative potential in continuously simulating both streamflow and $\delta^{18}O$ in streamflow has been revealed, and proves to be highly promising for climate change studies and mesoscale hydrological research.

The model significantly advances the capability of modellers to calibrate physically meaningful parameter sets; ensuring streamflows are generated from correctly apportioned, physically realistic internal dynamics. The methodology put forth by this research can be considered an effective and practical tool for model calibration in ungauged, mesoscale basins, which have recently become a focal-point in hydrological research (Weerakoon & Smakhtin, 2008; Spence *et al.*, 2004; Sivapalan *et al.*, 2003). The development of a minimally parameterized, computationally efficient hydrological model that is rigorously validatable in remote, ungauged basins is an important step forward in the ability to research climate change impacts.

The model is a significant advancement for hydrological research utilizing stable water isotopes by offering the ability to capture isotopic variation between long time sequences of measured data in a more cost-effective and less field intensive way. Simulated records of $\delta^{18}O$ in streamflow are generated from modelling the $\delta^{18}O$ in smaller-scale hydrological processes that combine to generate a single, mixed source runoff signature. Lake water balances affected by upstream runoff components and by evaporative enrichment can be analysed in detail, along with the isotopic evolution of soilwater, baseflow, and wetland storages. By adding the

capability of continuous simulation, current $\delta^{18}O$ records can be extended or supplemented with the modelled data. Drawing connections between short-term, smaller-scale hydrological processes and longer-term mesoscale hydrological variability enables a more holistic assessment of isotopic variability.

This research has demonstrated that stable water isotopes assist in defining the sources of variability in regional hydrological water balances and runoff responses. Although utilized in this study on gauged basins, this research is similarly applicable to predictions in ungauged basins (PUB) research (Spence *et al.*, 2004). Where hydrological modelling traditionally focuses on quantifying changes in hydrological response, stable water isotopes facilitate the quantification of internal catchment water balances controlling the response. In the assessment of climate change variability, it is important to quantify and predict how modifications to water cycling and storage result in hydrological variability. Stable water isotopes coupled with continuous hydrological modelling of large domains therefore offer the ability to connect small-scale alterations to longer-term watershed resource allocations. The conservative nature, long-term preservation, natural abundance, and practical field sampling methods of stable water isotopes appear to make them ideal tracers for mesoscale watershed research.

10.3 Future Initiatives

The culmination of this work has defined several initiatives that are central to the success of hydrological, and now isotopic, simulation in mesoscale basins. First, it was shown that despite the advancements in measurement of precipitation, there is still considerable work to be done to refine radar products and improve the density of monitoring networks to reduce systematic over- and under-estimation of precipitation. Hydrological models can assist with these efforts by ground-truthing radar-derived or alternative precipitation inputs by comparing simulated to measured streamflow. In addition to precipitation quantity, well defined compositions of precipitation are integral to replicating inter-seasonal variations in the $\delta^{18}O$ of streamflow. The Canadian Network for Isotopes in Precipitation therefore is an important initiative that needs to continue. The availability of time series evolutions of isotopes in precipitation enables the long-term simulation of $\delta^{18}O$ in streamflow without extensive field campaigns. Mesoscale stable

water isotope sampling programs are furthermore encouraged to collect data to define $\delta^{18}O$ variation in large river systems. The management of a data repository for isotopes in large rivers would be a useful initiative for modellers in the same way that the CNIP database is, but would require careful consideration of fair and equitable management rights and terms of use for the data.

This research has facilitated the identification of some key research objectives for future work, which include:

1. Continued development of the isoWATFLOOD model to advance the current modelling capabilities, including propositions to:

- Review the approach to evaporation-evapotranspiration partitioning to see if improvements can be made by incorporating humidity and temperature data. The proper allocation of evaporative fractions of evapotranspiration is important in the estimation of isotopic enrichments.
- Incorporate high resolution spatially distributed forcing data to describe changes in relative humidity and the composition of precipitation. Surficial hydrological storages are generally found to be isotopically distinct largely because of differential evaporative enrichment pre-dominantly controlled by humidity deficit. The $\delta^{18}O$ of streamflow was shown to be highly sensitive to variable compositions of precipitation.
- Develop a snowpack fractionation module to track and evolve the isotopic composition of the snowpack throughout the winter, including fractionation from sublimation. The fractionation of ^{18}O during melting and refreezing in snowmelt was found to be necessary but not adequate in describing ice-on and freshet isotopic responses, particularly in snowmelt-dominant regions.
- Utilize water quality transport theory (Jenkinson, In Progress) to improve the numerical computation of $\delta^{18}O$ in streamflow during impulse events where concentrations rapidly change, particularly in the upper zone storages. This includes refining the ISOsurface and ISOinter module to handle impulse loadings during high event water contributions.
- Include atmospheric feedback of evaporated moisture from lakes to refine δ_A. The effect of significant amounts of re-evaporated moisture on δ_A can be substantial in lake-

dominated regimes or basins with large lakes (Brock *et al.*, 2007; Clogg-Wright, 2007; Brock *et al.*, In Preparation).

- Add pumping capabilities to isoWATFLOOD so known and defined water extractions can be accounted for both hydrologically and isotopically.
- Integrate the δ^2H isotope into isoWATFLOOD to facilitate the coupled isotope approach of Yi *et al.* (2008) that will assist in hydrological variability assessment and the identification of climate variability.
- Add isotope model error to DDS option objective function in WATFLOOD optimization scheme.

2. Integrate meteorological forcing data from an isotope-enabled regional climate model (REMOiso; Sturm, 2005) into isoWATFLOOD. Spatially distributed fields of relative humidity and $\delta^{18}O$ in precipitation can be provided by the REMOiso model to improve the uncertainty associated with the current temperature-dependant relative humidity relationship and assumption of constant composition of precipitation.

3. Utilize the coupling of REMOiso and isoWATFLOOD to potentially assist with validation of REMOiso by providing a means to ground-truth meteorological forcing data through quantification of runoff generation.

4. Couple isoWATFLOOD with a lake isotope-hydrology model that fractionates isotopes in lake storage (Danis, 2003). Isotopic compositions of runoff can be fed to the lake model, an external lake water balance would be performed, and the composition of lake discharge can in turn be supplied back to the hydrological model. This coupling would improve the hydrological connection between surficial runoff and lake storages.

5. Apply the model to study climate change impacts in large, remote and scarcely gauged headwater watersheds (e.g., Mackenzie basin). It is proposed that sensitivity assessments be performed on runoff and isotopic variability using synthetic data from climate models by generating a range of hydrological predictions. The simulation of $\delta^{18}O$ provides the unique

opportunity to calibrate and validate long-term hydrological simulations based on longer historical records of isotopes (than streamflow).

6. Imbed the isoWATFLOOD model into the WATROUTE routing scheme used by Environment Canada in the MEC modelling system (Pietroniro *et al.*, 2007). The simulation of $\delta^{18}O$ of streamflow can feasibly assist with the PUB initiatives to derive more physically-based parameterizations of mesoscale hydrological models without streamflows (Spence *et al.*, 2004).

7. Initiate a field study program similar to that of Jenkinson (In Progress) to continuously sample streamflow and components contributing to streamflow. By measuring variability in runoff generation and sub-component contributions to runoff over time, rigorous model verification of internal processes can be performed both hydrologically and isotopically.

References

Abbott, M. B., Bathurst, J. C., Cunge, J. A., O'Connell, P. E., & Rasmussen, J. (1986a). An introduction to the European hydrological system — Systeme Hydrologique Europeen, "SHE", 2: Structure of a physically-based, distributed modelling system. *Journal of Hydrology, 87*(1-2), 61-77.

Abbott, M. B., Bathurst, J. C., Cunge, J. A., O'Connell, P. E., & Rasmussen, J. (1986b). An introduction to the European hydrological system SHE 1: History and philosophy of a physically-based, distributed modelling system. *Journal of Hydrology, 87*(1-2), 45-59.

Akintug, B., & Rasmussen, P. (2005). A Markov switching model for annual hydrologic time series. *Water Resources Research, 41*, W09424.

Aleinov, I., & Schmidt, G. A. (2006). Water isotopes in the GISS ModelE Land Surface Scheme. *Global and Planetary Change, 51*(1-2), 108-120.

Allison, G. B., & Leaney, F. W. (1982). Estimation of isotopic exchange parameters, using constant feed pans. *Journal of Hydrology, 55*, 151-161.

Allison, G. B., Barnes, C. J., & Hughes, M. W. (1983). The distribution of deuterium and ^{18}O in dry soils 2. *Journal of Hydrology, 64*(1-4), 377-397.

Anderson, E. A. (1973). *National Weather Service River Forecast System: Snow accumulation and ablation model.* (Memo No. NWS_HYDRO-17). Silver Springs, MD.: National Oceanographic and Atmospheric Administration.

Arnold, J. G., & Allen, P. M. (1999). Automated methods for estimating baseflow and ground water recharge from streamflow records. *Journal of the American Water Resource Association, 35*(2), 411-424.

Arnold, J. G., Allen, P. M., Muttiah, R., & Bernhardt, G. (1995). Automated base-flow separation and recession analysis techniques. *Ground Water, 33*(6), 1010-1018.

Aronica, G. T., & Candela, A. (2007). Derivation of flood frequency curves in poorly gauged Mediterranean catchments using a simple stochastic hydrological rainfall-runoff model. *Journal of Hydrology, 347*(1-2), 132.

Arora, V., Seglenieks, F., Kouwen, N., & Soulis, E. D. (2001). Scaling aspects of river flow routing. Hydrological Processes, 15(3), 461-477.

Aylsworth, J. M., & Kettles, I. M. (2000). Distribution of peatlands. In L. D. Dyke, & G. R. Brooks (Eds.), Physical environment of the Mackenzie valley, Northwest Territories: A baseline for the assessment of environmental change (pp. 49-55). Ottawa: Geological Survey of Canada.

Aylsworth, J. M., Burgess, M. M., Desrochers, D. T., Duk-Rodkin, A., Robertson, T., & Traynor, J. A. (2000). Surficial geology, subsurface materials and thaw sensitivity of sediments. In L. D. Dyke, & G. R. Brooks (Eds.), The physical environment of the Mackenzie valley, northwest territories: A base line for the assessment of environmental change (pp. 41-48). Ottawa, ON: Geologic Survey of Canada.

Baldocchi, D. D., & Vogel, C. A. (1996). Energy and CO_2 flux densities above and below a temperate broad-leaved forest and a boreal pine forest. *Tree Physiology, 16*(1-2), 5-16.

Barlett, J. (2008). *Observed winter flows at West Montrose gauge: 2004-2005 streamflow data*. Personal Communication with Kouwen N., Stadnyk T., Cambridge, ON: GRCA.

Barnes, C. J., & Allison, G. B. (1988). Tracing of water movement in the unsaturated zone using stable isotopes of hydrogen and oxygen. *Journal of Hydrology, 100*(1-3), 143-176.

Barnes, C. J., & Turner, J. V. (1998). Isotopic exchange in soilwater. In C. Kendall, & J. J. McDonnell (Eds.), *Isotope tracers in catchment hydrology*. First ed.: pp. 137-163. Amsterdam, The Netherlands: Elsevier.

Barnett, T. P., Pierce, D. W., Hidalgo, H. G., Bonfils, C., Santer, B. D., Das, T., *et al.* (2008). Human-induced changes in the hydrology of the western united states. *Science, 319*(5866), 1080.

Bassett, R. L., Steinward, A., Jorat, S., Petersen, C., & Jackson, R. (2008). Forensic isotope analysis to refine a hydrologic conceptual model. *Ground Water, 46*(3), 372.

Bechtel, G. (2007). Widening highway 7 makes a lot more sense. [Electronic version]. *Guelph Mercury*.

Bellamy, S. (2004). Communications regarding BFLOW and HYSEP modelling for WATFLOOD baseflow comparison study. Personal Communication with Stadnyk, T., Cambridge, ON: GRCA.

Benoit, R., Kouwen, N., Yu, W., Chamberland, S., & Pellerin, P. (2003). Hydrometeorological aspects of the real-time ultrafinescale forecast support during the special observing period of the MAP. *Hydrology and Earth System Sciences, 7*(6), 877-889.

Beven, K. (1997). TOPMODEL: A critique. *Hydrological Processes, 11*(9), 1069-1085.

Beven, K. (2002). Towards an alternative blueprint for a physically based digitally simulated hydrologic response modelling system. *Hydrological Processes, 16*(2), 189-206.

Beven, K. (2006). A manifesto for the equifinality thesis. *Journal of Hydrology, 320*(1-2), 18-36.

Bingeman, A. K., Kouwen, N., & Soulis, E. D. (2006). Validation of the hydrological processes in a hydrological model. *Journal of Hydrologic Engineering, 11*(5), 451-463.

Birks, S. J., Edwards, T. W. D., Gibson, J. J., Drimmie, R. J. & Michel, F. A. (2004). *Canadian Network for Isotopes in Precipitation (CNIP).* Retrieved 03/17, 2008, from http://www.science.uwaterloo.ca/~twdedwar/cnip/cniphome.html

Blasch, K. W., & Bryson, J. R. (2007). Distinguishing sources of ground water recharge by using delta ^{2}H and delta ^{18}O. *Ground Water, 45*(3), 294-308.

Blöschl, G. (2001). Scaling in hydrology. *Hydrological Processes, 15*(4), 709-711.

Brassard, P., Waddington, J. M., Hill, A. R., & Roulet, N. T. (2000). Modelling groundwater and surface water mixing in a headwater wetland: Implications for hydrograph separation. *Hydrological Processes, 14*(15), 2697-2710.

Braud, I., Bariac, T., Gaudet, J. P., & Vauclin, M. (2005a). SiSPAT-isotope, a coupled heat, water and stable isotope (HDO and $H_2{}^{18}O$) transport model for bare soil. Part I. Model description and first verifications. *Journal of Hydrology, 309*(1-4), 277-300.

Braud, I., Bariac, T., Vauclin, M., Boujamlaoui, Z., Gaudet, J. P., Biron, P., *et al.* (2005b). SiSPAT-isotope, a coupled heat, water and stable isotope (HDO and $H_2$18O) transport model for bare soil. Part II. Evaluation and sensitivity tests using two laboratory data sets. *Journal of Hydrology, 309*(1-4), 301-320.

Brock, B. E., Wolfe, B. B., & Edwards, T. W. D. (2007). Characterizing the hydrology of shallow floodplain lakes in the Slave River Delta, NWT using water isotope tracers. *Arctic and Antarctic Alpine Research, 39*(3), 388-401.

Brock, B. E., Yi, Y., Clogg-Wright, K. P., Edwards, T. W. D., & Wolfe, B. B. (In Preparation). Multi-year landscape-scale assessment of lakewater balances in the Slave River Delta, NWT, using water isotope tracers. Prepared for *Journal of Hydrology.*

Brody, S. D., Zahran, S., Highfield, W. E., Grover, H., & Vedlitz, A. (2008). Identifying the impact of the built environment on flood damage in Texas. *Disasters, 32*(1), 1-18.

Brown, V. A., McDonnell, J. J., Burns, D. A., & Kendall, C. (1999). The role of event water, a rapid shallow-flow component, and catchment size in summer stormflow. *Journal of Hydrology, 217*(3-4), 171-190.

Burian, K. (1973). Das schilfgurtel-okosystem eines steppensees. In H. Ellenberg (Ed.), *Okosystemforschuung.* (pp. 61-78). Berlin, Germany: Springer.

Burn, D. H., Cunderlik, J. M., & Pietroniro, A. (2004). Hydrological trends and variability in the Liard River Basin. *Hydrological Sciences, 49*(1), 53-67.

Burns, D. A. (2002). Stormflow hydrograph separation based on isotopes: The thrill is gone, what's next?. *Hydrological Processes, 16*(7), 1515-1517.

Buttle, J. (1998). Fundamentals of small catchment hydrology. In C. Kendall, & J. J. McDonnell (Eds.), *Isotope tracers in catchment hydrology* (first ed., pp. 1-49). Amsterdam, The Netherlands: Elsevier.

Cameron, D., Beven, K., & Naden, P. (2000). Flood frequency estimation by continuous simulation under climate change. *Hydrology and Earth System Sciences, 4*(3), 393-405.

Carey, S. K., & Quinton, W. L. (2005). Evaluating runoff generation during summer using hydrometric, stable isotope and hydrochemical methods in a discontinuous permafrost alpine catchment. *Hydrological Processes, 19*(1), 95-114.

Chapman, L. J., & Putnam, D. F. (1984). In Stuart M. L. T. (Ed.), *The physiography of Southern Ontario*. Toronto, ON: Ontario Geological Survey.

Chapra, S. C. (1997a). *Surface water-quality modeling*. New York: McGraw-Hill.

Chapra, S. C. (1997b). Distributed Sources. In G. Tchobanoglous (Ed.), *Surface water quality modelling*. First ed., pp. 170-171: WBC/McGraw-Hill.

Chen, R. S., Lu, S. H., Kang, E. S., Ji, X. B., Zhang, Z., Yang, Y., *et al.* (2008). A distributed water-heat coupled model for mountainous watershed of an inland river basin of northwest china (I) model structure and equations. *Environmental Geology, 53*(6), 1299-1309.

Chiang, S., Tachikawa, Y., & Takara, K. (2007). Hydrological model performance comparison through uncertainty recognition and quantification. *Hydrological Processes, 21*(9), 1179.

Choi, H. T., & Beven, K. (2007). Multi-period and multi-criteria model conditioning to reduce prediction uncertainty in an application of TOPMODEL within the GLUE framework. *Journal of Hydrology, 332*(3-4), 316-336.

Clark, C. O. (1945). Storage and the unit hydrograph. *Trans. ASCE, 110*, 1419-1488.

Clogg-Wright, K. P. (2007). Isotope-inferred water balances of Slave River Delta lakes, NWT Canada. M.Sc., Department of Earth Sciences, University of Waterloo: Waterloo, ON.

Collischonn, W., Allasia, D., Da Silva, B. C., & Tucci, C. E. M. (2007). The MGB-IPH model for large-scale rainfall-runoff modelling. *Hydrological Sciences Journal, 52*(5), 878.

Commonwealth of Australia. (2006). *Connected water: Baseflow component of streamflow*. Retrieved 05/07, 2008, from http://www.connectedwater.gov.au/processes/baseflow.html

Cooper, L. W. (1998). Isotopic fractionation in snow cover. In C. Kendall, & J. J. McDonnell (Eds.), *Isotope tracers in catchment hydrology*. First ed.: pp. 119-136. Amsterdam, The Netherlands: Elsevier.

Craig, H. (1961). Standard for reporting concentrations of deuterium and oxygen-18 in natural waters. *Science, 133*, 1833.

Craig, H., & Gordon, L. I. (1965). Deuterium and oxygen 18 variations in the ocean and the marine atmosphere. *Stable Isotopes in Oceanographic Studies and Paleotemperatures,* Spoleto, Italy. 9-130.

Crawford, N. H., & Linsley, R. K. (1966). *Digital simulation in hydrology: Stanford watershed model 4*.Stanford University, Dept. of Civil Engineering.

Danis, P. (2003). Modélisation du fonctionnement thermique, hydrologique et isotopique de systèmes lacustres: Sensibilité aux changement climatiques et amélioration des reconstructions paléoclimatiques. Doctorat, l'université de savoie, Paris, France.

Danish Hydraulic Institute (DHI). (1993). *MIKE SHE (*Technical Report. Netherlands: Danish Hydraulic Institute.

Dankers, R., Christensen, O. B., Feyen, L., Kalas, M., & de Roo, A. (2007). Evaluation of very high-resolution climate model data for simulating flood hazards in the upper Danube basin. *Journal of Hydrology, 347*(3-4), 319-331.

Dansgaard, W. (1964). Stable isotopes in precipiation. *Tellus, 16*(4), 436-468.

Dawson, T. E., & Ehleringer, J. R. (1998). Plants, isotopes and water use: A catchment-scale perspective. In C. Kendall, & J. J. McDonnell (Eds.), (First ed., pp. 165-202). Amesterdam, The Netherlands: Elsevier.

Day, S. (2005). *Status report of isotope project*. Burlington, ON: Environment Canada.

Dibike, Y. B., & Coulibaly, P. (2007). Validation of hydrological models for climate scenario simulation: The case of Saguenay Watershed in Quebec. *Hydrological Processes, 21*(23), 3123-3135.

Diefendorf, A. F., & Patterson, W. P. (2005). Survey of stable isotope values in Irish surface waters. *Journal of Paleolimnology, 34*(2), 257-269.

Dincer, T., & Davis, G. H. (1984). Application of environmental isotope tracers to modeling in hydrology. *Journal of Hydrology, 68*(1-4), 95-113.

Dincer, T., Al-Mugrin, A., & Zimmermann, U. (1974). Study of the infiltration and recharge through the sand dunes in arid zones with special reference to stable isotopes and thermonuclear tritium. *Journal of Hydrology, 23*, 79.

Donald, J. R. (1992). *Snowcover depletion curves and satellite snowcover-estimates for snowmelt runoff modelling*. Ph.D. Thesis, Department of Civil Engineering, University of Waterloo: Waterloo, ON.

Droogers, P. (2000). Estimating actual evapotranspiration using a detailed agro-hydrological model. *Journal of Hydrology, 229*(1-2), 50-58.

Dunn, S. M., Vinogradoff, S. I., Thornton, G. J. P., Bacon, J. R., Graham, M. C., & Farmer, J. G. (2006). Quantifying hydrological budgets and pathways in a small upland catchment using a combined modelling and tracer approach. *Hydrological Processes, 20*(14), 3049-3068.

Ebel, B. A., Loague, K., VanderKwaak, J. E., Dietrich, W. E., Montgomery, D. R., Torres, R., *et al.* (2007). Near-surface hydrologic response for a steep unchanneled catchment near Coos Bay, Oregon: 2 physics-based simulations. *American Journal of Science, 307*, 709-748.

Eckhardt, K. (2008). A comparison of baseflow indices, which were calculated with seven different baseflow separation methods. *Journal of Hydrology, 352*(1-2), 168.

Edwards, T. W. D. (2008). *Tentative PICS project proposal for isotope-enabled hydrological modelling.* Personal Communication with T. Stadnyk, University of Waterloo: Waterloo, ON

Edwards, T. W. D., Wolfe, B. B., Gibson, J. J., & Hammarlund, D. (2004). Use of water isotope tracers in high-latitude hydrology and paleohydrology. In R. Pienitz, M. S. V. Douglas & J. P. Smol (Eds.), *Long-term environmental change in Arctic and Antarctic lakes: Developments in Paleoenvironmental Research.* Dordrecht, The Netherlands: Kluwer Academic Publishers.

Engineering ToolBox. (2005). *The engineering toolbox: Water saturation pressure.* Retrieved 10/2007, 2008, from http://www.engineeringtoolbox.com/water-vapor-saturation-pressure-d_599.html

Environment Canada. (2004). *Canadian Climate Normals (1971-2000).* Retrieved 04/15, 2008, from http://www.climate.weatheroffice.ec.gc.ca/climate_normals/results_e.html

Falcone, M. D. (2007). Assessing hydrological processes controlling the water balance of lakes in the Peace-Athabasca Delta, Alberta, Canada using water isotope tracers. M.Sc. Thesis, Department of Earth Sciences, University of Waterloo: Waterloo, ON.

Famiglietti, J. S., & Wood, E. F. (1994). Multiscale modeling of spatially-variable water and energy-balance processes. *Water Resources Research, 30*(11), 3061.

Fassnacht, S. R., Soulis, E. D., & Kouwen, N. (1999). Algorithm application to improve weather radar snowfall estimates for winter hydrologic modelling. *Hydrological Processes, 13*(18), 3017-3039.

Fekete, B. M., Gibson, J. J., Aggarwal, P., & Vorosmarty, C. J. (2006). Application of isotope tracers in continental scale hydrological modeling. *Journal of Hydrology, 330*(3-4), 444-456.

Feng, X., Taylor, S., & Renshaw, C. E. (2002). Isotopic evolution of snowmelt: 1. A physically-based one-dimensional model. *Water Resources Research, 38*(10), 1217.

Feyen, L., Kalas, M., & Vrugt, J. A. (2008). Semi-distributed parameter optimization and uncertainty assessment for large-scale streamflow simulation using global optimization. *Hydrological Sciences Journal, 53*(2), 293.

Feyen, L., Vrugt, J. A., Nuallain, B. O., van der Knijff, J., & De Roo, A. (2007). Parameter optimisation and uncertainty assessment for large-scale streamflow simulation with the LISFLOOD model. *Journal of Hydrology, 332*(3-4), 276-289.

Ffolliott, P. F., Gottfried, G. J., Cohen, Y., & Schiller, G. (2003). Transpiration by dryland oaks: Studies in the south-western United States and northern Israel. *Journal of Arid Environments, 55*, 595-605.

Fischer, H. B., List, E. J., Koh, R. C. Y., Imberger, J., & Brooks, N. H. (1979). *Mixing in inland and coastal waters*. New York: Academic Press.

Fischer, M. J. (2006). iCHASM, a flexible land-surface model that incorporates stable water isotopes. *Global and Planetary Change, 51*(1-2), 121-130.

Fischer, M. J., & Sturm, K. (2006). REMOiso forcing for the iPILPS phase 1 experiments and the performance of REMOiso in three domains. *Global and Planetary Change, 51*(1-2), 73-89.

Fort Simpson Historical Society. (2008). *Village of Fort Simpson, NWT, Canada.* Retrieved 04/15, 2008, from http://www.fortsimpson.com/

Fritz, P., Cherry, J. A., Weyer, K. V., & Sklash, M. G. (1976). Runoff analyses using environmental isotope and major ions. *Interpretation of Environmental Isotope and Hydrogeochemical Data in Groundwater Hydrology,* Vienna, Austria. 111-130.

Gallart, F., Latron, J., Llorens, P., & Beven, K. (2007). Using internal catchment information to reduce the uncertainty of discharge and baseflow predictions. *Advances in Water Resources, 30*(4), 808-823.

Gat, J. R. (1981). *Lakes* (Technical Report No. Series 210). Vienna, AU: International Atomic Energy Agency.

Gat, J. R. (1996). Oxygen and hydrogen isotopes in the hydrologic cycle. *Annual Review of Earth and Planetary Sciences, 24*(1), 225-262.

Gat, J. R., & Levy, Y. (1978). Isotope hydrology of inland Sabkhas in the Bardawil area, Sinai. *Limnology and Oceanography, 23*, 841-850.

Gat, J. R., Yakir, D., Goodfriend, G., Fritz, P., Trimborn, P., Lipp, J., *et al.* (2007). Stable isotope composition of water in desert plants. *Plant and Soil, 298*(1-2), 31-45.

Genereux, D. P., & Hooper, R. P. (1998). Oxygen and hydrogen isotopes in rainfall-runoff studies. In C. Kendall, & J. J. McDonnell (Eds.), *Isotope tracers in catchment hydrology* (first ed., pp. 319-346). Amsterdam, The Netherlands: Elsevier.

Gibson, J. J. (1996). *Non-steady isotopic methods for estimating lake evaporation: Development and validation in arctic Canada*. Ph.D. Thesis, Department of Earth Sciences, University of Waterloo: Waterloo, ON.

Gibson, J. J. (2002a). Short-term evaporation and water budget comparisons in shallow arctic lakes using non-steady isotope mass balance. *Journal of Hydrology, 264*(1-4), 242-261.

Gibson, J. J. (2002b). A new conceptual model for predicting isotopic enrichment of lakes in seasonal climates. [Electronic version]. *PAGES News, 10*(2) 10-11.

Gibson, J. J. (2005). *Grand River basin isotopes in streamflow field study*. Personal Communication with T. Stadnyk; Waterloo, ON.

Gibson, J. J., & Edwards, T. W. D. (2002). Regional water balance trends and evaporation-transpiration partitioning from a stable isotope survey of lakes in northern Canada. *Global Biogeochemical Cycles, 16*(2), 1026.

Gibson, J. J., Birks, S. J., & Edwards, T. W. D. (2008). Global prediction of δ_A and δ^2H-$\delta^{18}O$ evaporation slopes for lakes and soil water accounting for seasonality. *Global Biogeochemical Cycles, 22(2)*, GB2031, doi: 10.1029/2007GB002997.

Gibson, J. J., Edwards, T. W. D., & Prowse, T. D. (1999). Pan-derived isotopic composition of atmospheric water vapour and its variability in northern Canada. *Journal of Hydrology, 217*(1-2), 55-74.

Gibson, J. J., Edwards, T. W. D., Birks, S. J., St Amour, N. A., Buhay, W. M., McEachern, P., *et al.* (2005). Progress in isotope tracer hydrology in Canada. *Hydrological Processes, 19*(1), 303-327.

Gibson, J. J., Prowse, T., & Edwards, T. W. D. (1996). Evaporation from a small lake in the Continental Arctic using multiple methods. *Nordic Hydrol., 27*, 1-24.

Gibson, J.J., Edwards, T.W.D., & Prowse, T.D. (1996). Development and validation of an isotopic method for estimating lake evaporation. *Hydrological Processes, 10*(10), 1369-1382.

Gill, A. E. (1982). *Atmosphere-ocean dynamics*. New York ; Toronto: Academic Press.

Glasstone, S., Laidler, K. J., & Eyring, H. (1941). *The theory of rate processes*. New York: McGraw-Hill.

Gonfiantini, R. (1986). Environmental isotopes in lake studies. In P. Fritz, & J. -. Fontes (Eds.), *Handbook of environmental isotope geochemistry, the terrestrial environment* (Vol 2. ed., pp. 113-168). NY: Elsevier.

Gonfiantini, R., Fröhlich, K., Araguás-Araguás, L., & Rozanski, K. (1998). Isotopes in groundwater hydrology. In C. Kendall, & J. J. McDonnell (Eds.), *Isotope tracers in catchment hydrology*. First ed.: pp. 203-246. Amsterdam, The Netherlands: Elsevier.

Gotzinger, J., & Bardossy, A. (2007). Comparison of four regionalisation methods for a distributed hydrological model. *Journal of Hydrology, 333*(2-4), 374-384.

Government of Northwest Territories. (2000). *GNWT - environment and natural resources maps*. Retrieved 06/9, 2008, from http://www.enr.gov.nt.ca/maps/nwt_territories.htm

GRCA. (2008a). *The Grand River Conservation Authority (GRCA) - about the GRCA*. Retrieved 04/2008, 2008, from http://www.grandriver.ca

GRCA. (2008b). *River data: GRCA monitoring network (provisional data)*. Retrieved 06/10, 2008, from http://www.grandriver.ca/index/document.cfm?sec=2&sub1=9&sub2=2

GRCA. (2008c). *GRCA River Data - Reservoir Rules.* Retrieved 06/19, 2008, from http://www.grandriver.ca/index/document.cfm?sec=2&sub1=9&sub2=2

Green, W. H., & Ampt, G. A. (1911). Studies in soil physics 1: Flow of air and water through soils. *Agricultural Research, 4*, 1-24.

Grelle, A., Lundberg, A., Lindroth, A., Morén, A.-., & Cienciala, E. (1997). Evaporation components of a boreal forest: Variations during the growing season. *Journal of Hydrology, 197*(1-4), 70-87.

Gremillion, P., Gonyeau, A., & Wanielista, M. (2000). Application of alternative hydrograph separation models to detect changes in flowpaths in a watershed undergoing urban development. *Hydrological Processes, 14*(8), 1485-1501.

Gunter, B. (2001). Scaling in hydrology. *Hydrological Processes, 15*, 709-711.

Guntner, A., Uhlenbrook, S., Siebert, J., & Leibundgut, C. (1999). Multi-criterial validation of TOPMODEL in a mountainous catchment. *Hydrological Processes, 13*(11), 1085-1099.

Hamlin, L. P. B. (1996). *Snowmelt hydrologic modelling of northern wetland dominated river basins*: M.A.Sc. Thesis, Department of Civil Engineering, University of Waterloo: Waterloo, ON.

Hargreaves, G. H., & Samani, Z. A. (1982). Estimating potential evapotranspiration. *Journal of Irrigation and Drainage Division, 108*(3), 225-230.

Harris, D. M., McDonnell, J. J., & Rodhe, A. (1995). Hydrograph separation using continuous open system isotope mixing. *Water Res. Resear., 31*(1), 157-230.

Hayashi, M., Quinton, W. L., Pietroniro, A., & Gibson, J. J. (2004). Hydrologic functions of wetlands in a discontinuous permafrost basin indicated by isotopic and chemical signatures. *Journal of Hydrology, 296*(1-4), 81-97.

Henderson, F. M. (1966). Flood routing. *Open channel flow* (pp. 355-404). Upper Saddle River, NJ: Prentice-Hall, Inc.

Henderson-Sellers, A. (2006). Improving land-surface parameterization schemes using stable water isotopes: Introducing the iPILPS initiative. *Global and Planetary Change, 51*(1-2), 3-24.

Henderson-Sellers, A., Farquhar, G., McGuffie, K., Irannejad, P., Sturm, K., Noone, D., *et al.* (2004). *iPILPS: Isotopes in project for intercomparison of land-surface parameterization schemes*. Australia:

Henderson-Sellers, A., Fischer, M., Aleinov, I., McGuffie, K., Riley, W. J., Schmidt, G. A., *et al.* (2006). Stable water isotope simulation by current land-surface schemes: Results of iPILPS phase 1. *Global and Planetary Change, 51*(1-2), 34-58.

Henderson-Sellers, A., McGuffie, K., & Pitman, A. J. (1996). The project for intercomparison of land-surface parametrization schemes (PILPS): 1992 to 1995. *Climate Dynamics, 12*(12), 849-859.

Herbst, M., & Kappen, L. (1999). The ratio of transpiration versus evaporation in a reed belt as influenced by weather conditions. *Aquatic Botany, 63*(2), 113-125.

Hoeg, S., Uhlenbrook, S., & Leibundgut, C. (2000). Hydrograph separation in a mountainous catchment; combining hydrochemical and isotopic tracers. *Hydrological Processes, 14*(7), 1199-1216.

Hoffmann, G., Jouzel, J., & Masson, V. (2000). Stable water isotopes in atmospheric general circulation models. *Hydrological Processes, 14*(8), 1385.

Horita, J., & Wesolowski, D. J. (1994). Liquid-vapor fractionation of oxygen and hydrogen isotopes of water from the freezing to the critical temperature. *Geochimica Et Cosmochimica Acta, 58*(16), 3425-3437.

Hurkmans, R. T. W. L., de Moel, H., Aerts, J. C. J. H., & Troch, P. A. (2008). Water balance versus land surface model in the simulation of the Rhine river discharges. *Water Resources Research, 44*

IAEA & WMO (2006). *Global Network for Isotopes in Precipitation.* Retrieved 10/2008, 2008, from http://isohis.iaea.org

IAEA (2003). *Water and environment newsletter* No. 17. Vienna, Austria.

IAEA. (1981). *Stable isotope hydrology: Deuterium and oxygen-18 in the water cycle.* Technical Report No. 210. Vienna, AU: International Atomic Energy Agency.

Iorgulescu, I., Beven, K. J., & Musy, A. (2007). Flow, mixing, and displacement in using a data-based hydrochemical model to predict conservative tracer data. *Water Resources Research, 43*(3)

Ivey, J. (2002). *Grand River watershed characterisation report.* University of Guelph, Guelph, ON: Guelph Water Management Group.

Jenkinson, R. W. (In Progress). Macro-scale Surface Water Quality Modelling Considering Riparian Wetlands. Unpublished Ph.D. Thesis, Department of Civil and Environmental Engineering, University of Waterloo: Waterloo, ON.

Joerin, C., Beven, K. J., Iorgulescu, I., & Musy, A. (2002). Uncertainty in hydrograph separations based on geochemical mixing models. *Journal of Hydrology, 255*(1-4), 90-106.

Jones, J. P., Sudicky, E. A., Brookfield, A. E., & Park, Y. (2006). An assessment of the tracer-based approach to quantifying groundwater contributions to streamflow. *Water Resources Research, 42*(W02407)

Jouzel, J., & Souchez, R. A. (1982). Melting-freezing at the glacier sole and isotopic composition of the ice. *Journal of Glaciology, 28*, 35-42.

Kato, T., Kimura, R., & Kamichika, M. (2004). Estimation of evapotranspiration, transpiration ratio and water-use efficiency from a sparse canopy using a compartment model. *Agricultural Water Management, 65*(3), 173-191.

Kazezyilmaz-Alhan, C. M., & Medina, M. A. (2007). Kinematic and diffusion waves: Analytical and numerical solutions to overland and channel flow. *Journal of Hydraulic Engineering, 133*(2), 217-228.

Kelliher, F. M., Lloyd, J., Arneth, A., Byers, J. N., McSeveny, T. M., Milukova, I., *et al.* (1998). Evaporation from a central Siberian pine forest. *Journal of Hydrology, 205*(3-4), 279-296.

Kendall, C., & Coplen, T. B. (2001). Distribution of oxygen-18 and deuterium in river waters across the United States. *Hydrological Processes, 15*(7), 1363-1393.

Kendall, C., McDonnell, J. J., & Gu, W. (2001). A look inside black box hydrograph separation models: A study at the Hydrohill catchment. *Hydrological Processes, 15*(10), 1877-1902.

Kendall, C., Sklash, M. G., & Bullen, T. D. (1995). In Trudgill S. T. (Ed.), *Isotope tracers of water and solute sources in catchments*. Chichester, England: John Wiley & Sons, Ltd.

Kennedy, V. C., Kendall, C., Zellweger, G. W., Wyerman, T. A., & Avanzino, R. J. (1986). Determination of the components of stormflow using water chemistry and environmental isotopes, Mattole River basin, California. *Journal of Hydrology, 84*(1-2), 107-140.

Kienzler, P. M., & Naef, F. (2008). Subsurface storm flow formation at different hillslopes and implications for the 'old water paradox'. *Hydrological Processes, 22*(1), 104-116.

Kirchner, J. W. (2006). Getting the right answers for the right reasons: Linking measurements, analyses, and models to advance the science of hydrology. *Water Resources Research, 42*

Kite, G. (2000). Using a basin-scale hydrological model to estimate crop transpiration and soil evaporation. *Journal of Hydrology, 229*(1-2), 59-69.

Kite, G. W. (2002). *Manual for the SLURP hydrological model* (Manual No. Vol 12.2). Colombo, Sri Lanka: International Water Management Institute.

Klyszejko, E. S. (2006). *Hydrologic validation of real-time weather radar VPR correction methods*. M.A.Sc. Thesis, Department of Environmental and Civil Engineering, University of Waterloo: Waterloo, ON.

Komatsu, H. (2005). Forest categorization according to dry-canopy evaporation rates in the growing season: Comparison of the Priestley–Taylor coefficient values from various observation sites. *Hydrological Processes, 19*(19), 3873-3896.

Kouwen, N. (1988). WATFLOOD: A micro-computer based flood forecasting system based on real-time weather data. *Canadian Water Resources Journal, 13*(1), 62-77.

Kouwen, N. (2007). WATFLOOD/WATROUTE Hydrological Model routing & flood forecasting system. Unpublished manuscript [model user's manual].

Kouwen, N. (2008). *Future WATFLOOD initiatives and contracts*. Personal Communication with Stadnyk T., Waterloo, ON: University of Waterloo.

Kouwen, N., Danard, M., Bingeman, A. K., Luo, W., Seglenicks, F. R., & Soulis, E. D. (2005). Case study: Watershed modeling with distributed weather model data. *Journal of Hydrologic Engineering, 10*(1), 23-38.

Kouwen, N., Soulis, E. D., Bingeman, A., & Davison, B. (2003). *An introduction to WATFLOOD and WATCLASS MAGS Workshop*. Retrieved 05/24/2008, 2008, from www.usask.ca/geography/MAGS/Events/Workshops/Model/WATFLOOD-WATCLASS.pdf

Kouwen, N., Soulis, E. D., Pietroniro, A., Donald, J., & Harrington, R. A. (1993). Grouped response units for distributed hydrological modeling. *Journal of Water Resources Planning and Management, 119*(3), 289-305.

Krzysztofowicz, R. (2001). The case for probabilistic forecasting in hydrology. *Journal of Hydrology, 249*(1-4), 2-9.

Kunstmann, H., Schneider, K., Forkel, R., & Knoche, R. (2004). Impact analysis of climate change for an alpine catchment using high resolution dynamic downscaling of ECHAM4 time slices. *Hydrology and Earth System Sciences, 8*(6), 1030-1044.

Landon, M., Delin, G. N., Komor, S. C., & Regan, C. P. (2000). Relation of pathways and transit times of recharge water to nitrate concentrations using stable isotopes. *Groundwater, 38*(3), 381. doi:10.1111/j.1745-6584.2000.tb00224.x

Langmuir, I., & Langmuir, D. B. (1927). *J. Phys. Chem., 31*, 1719.

Laudon, H., & Slaymaker, O. (1997). Hydrograph separation using stable isotopes, silica and electrical conductivity: An alpine example. *Journal of Hydrology, 201*(1-4), 82-101.

Laudon, H., Hemond, H. F., Krouse, R., & Bishop, K. (2002). Oxygen 18 fractionation during snowmelt: Implications for spring flood hydrograph separation. *Water Resources Research, 38*(11)

Laudon, H., Seibert, J., Kohler, S., & Bishop, K. (2004). Hydrological flowpaths during snowmelt: Congruence between hydrometric measurements and oxygen 18 in meltwater, soil water, and runoff. *Water Resources Research, 40*

Laudon, H., Sjoblom, V., Buffam, I., Seibert, J., & Morth, M. (2007). The role of catchment scale and landscape characteristics for runoff generation of boreal streams. *Journal of Hydrology, 344*(3-4), 198-209.

Lee, K. S., Kim, J. M., Lee, D. R., Kim, Y., & Lee, D. (2007). Analysis of water movement through an unsaturated soil zone in Jeju Island, Korea using stable oxygen and hydrogen isotopes. *Journal of Hydrology, 345*(3-4), 199-211.

Leng, M. J., & Anderson, N. J. (2003). Isotopic variation in modern lake waters from western Greenland. *The Holocene, 13*(4), 605-611.

Liang, X., & Lettenmaier, D. P. (1994). A simple hydrologically based model of land surface water and energy fluxes for general circulation models. *Journal of Geophysical Research, 99*(D7), 415-428.

Liang, X., Lettenmaier, D. P., & Wood, E. F. (1996). One-dimensional statistical dynamic representation of sub-grid spatial variability of precipitation in the two-layer variable infiltration capacity model. *Journal of Geophysical Research, 101*(D16), 403-422.

Linsley, R. K., Kohler, M. A., & Paulhus, J. L. (1982). *Hydrology for Engineers.* (3rd ed.). New York, NY: McGraw-Hill.

Linsley, R. K., Kohler, M. A., & Paulhus, J. L. H. (1949). Applied hydrology. New York: Mcgraw-Hill.

Liu, C., Zhang, X., & Zhang, Y. (2002). Determination of daily evaporation and evapotranspiration of winter wheat and maize by large-scale weighing lysimeter and micro-lysimeter. *Agricultural and Forest Meteorology, 111*(2), 109-120.

Liu, Y., Fan, N., An, S., Bai, X., Liu, F., Xu, Z., et al. (2008). Characteristics of water isotopes and hydrograph separation during the wet season in the heishui river, china. *Journal of Hydrology, 353*, 314-321.

Lohmann, D., Raschke, E., Nijssen, B., & Lettenmaier, D. P. (1994a). Regional scale hydrology: I. formulation of the VIC-2L model coupled to a routing model. *Hydrological Sciences Journal, 43*(1), 131.

Lohmann, D., Raschke, E., Nijssen, B., & Lettenmaier, D. P. (1994b). Regional scale hydrology: II. application of the VIC-2L model to the Weser River, Germany. *Hydrological Sciences Journal, 43*(1), 143.

Longobardi, A., & Villani, P. (2008). Baseflow index regionalization analysis in a mediterranean area and data scarcity context: Role of the catchment permeability index. *Journal of Hydrology, 355*(1-4), 63.

MacKay, M. D., Seglenieks, F., Verseghy, D., Soulis, E. D., Snelgrove, K. R., Walker, A., *et al.* (2003). Modeling Mackenzie basin surface water balance during CAGES with the Canadian regional climate model. *Journal of Hydrometeorology, 4*(4), 748-767.

Maneta, M., Schnabel, S., & Jetten, V. (2008). Continuous spatially distributed simulation of surface and subsurface hydrological processes in a small semiarid catchment. *Hydrological Processes, 22*(13), 2196.

Martin, P., & van Vliet, D. (2008). *Ministry fo natural resources proposal for water-use planning and management in southern ontario (phase I and II).* Personal Communication with Stadnyk T., New Hamburg, ON: Aqua Resource, Inc.

Martinec, J., Siegenthaler, H., Oeschger, H., & Tongiorgi, E. (1974). New insight into the runoff mechanism by environmental isotopes. *Isotope Techniques in Groundwater Hydrology,* Vienna, Austria. *, 1* 129-143.

McBean, E., & Motiee, H. (2008). Assessment of impact of climate change on water resources: A long term analysis of the great lakes of North America. *Hydrology and Earth System Sciences, 12*(1), 239.

McCuen, R. H., Knight, Z., & Cutter, A. G. (2006). Evaluation of the Nash-Sutcliffe efficiency index. *Journal of Hydrologic Engineering, 11*(6), 597.

McDonnell, J. J., Stewart, M. K., & Owens, I. F. (1991). Effect of catchment-scale subsurface mixing on stream isotopic response. *Water Resources Research, 27*(12), 3065-3073.

McHugh, O. V., McHugh, A. N., Eloundou-Enyegue, P. M., & Steenhuis, T. S. (2007). Integrated qualitative assessment of wetland hydrological and landcover changes in a data scarce dry Ethiopian highland watershed. *Land Degradation & Development, 18*, 643-658.

McQuivey, R. S., & Keefer, T. N. (1974). Simple methods for predicting dispersion in streams. *Proceedings of the American Society of Civil Engineers., 100*(NEE4), 997-1011.

Metcalfe-Smith, J. L., Staton, S. K., Mackie, G. L., & Lane, N. M. (1997). Biodiversity of freshwater mussels in the lower Great Lakes drainage basin. *Plenary Presentation at the 3rd National EMAN Meeting,* Saskatoon, SK*., No. 97-90*

Migliaccio, K. W., & Chaubey, I. (2008). Spatial distributions and stochastic parameter influences on SWAT flow and sediment predictions. *Journal of Hydrologic Engineering, 13*(4), 258.

Ministry of the Environment. (2007). *Project: Highway 7 Kitchener to Guelph environmental assessment.* Retrieved 05/24/2008, 2008, from http://www.ene.gov.on.ca/envision/env_reg/ea/english/EAs/hwy7_amend.HTM

Mockus, V. (1957). *Use of storm and watershed characteristics in synthetic hydrograph analysis and application.* Washington, D.C.: U.S. Department of Agriculture, Soil Conservation Service.

Moore, K. E., Fitzgerald, D. R., Sakai, R. K., Goulden, M. L., Munger, J. W., & Wofsy, S. C. (1996). Season variation in radiative and turbulent exchange at a deciduous forest in central Massachusetts. *Journal of Applied Meteorology, 35*(122), 134.

Moser, H., & Stichler, W. (1980). Environmental isotopes in ice and snow. In P. Fritz, & J. C. Fontes (Eds.), *Handbook of environmental isotope geochemistry.* Vol. 1, pp. 141-178. New York: Elsevier.

Nash, J. E. (1957). The form of the instantaneous unit hydrograph. *Comptes Rendus Et Rapports, IASH General Assembly Toronto, International Association of Science and Hydrology (Gentbrugge),* Toronto, ON. *, 45*(3) 114-121.

Nash, J. E., & Sutcliffe, J. V. (1970). River flow forecasting through conceptual models part I: A discussion of principles. *Journal of Hydrology, 10*(3), 282-290.

Nathan, R. J., & McMahon, T. A. (1990). Evaluation of automated techniques for base flow and recession analysis. *Water Resources Research, 26*(7), 1465-1473.

Neff, T. A. M. (1996). Mesoscale water balance of the boreal forest using operational evapotranspiration approaches in a distributed hydrologic model. M.A.Sc Thesis, University of Waterloo: Waterloo, ON.

Noone, D. (2008). The influence of midlatitude and tropical overturning circulation on the isotopic composition of atmospheric water vapor and Antarctic precipitation. *Journal of Geophysical Research, 113*(D4)

Nourani, V., & Mano, A. (2007). Distributed flood runoff model at the subcontinental scale for southwestern Iran. *Hydrological Processes, 21*(23), 3173-3180.

Ocampo, C. J., Sivapalan, M., & Oldham, C. (2006). Hydrological connectivity of upland-riparian zones in agricultural catchments: Implications for runoff generation and nitrate transport. *Journal of Hydrology, 331*(3-4), 643-658.

Ogée, J., Cuntz, M., Peylin, P., & Bariac, T. (2007). Non-steady-state, non-uniform transpiration rate and leaf anatomy effects on the progressive stable isotope enrichment of leaf water along monocot leaves. *Plant, Cell and Environment, 30*(4), 367-387.

Ommer, R. (2008). *Pacific Institute for Climate Solutions.* Retrieved 04/28, 2008, from http://www.pics.uvic.ca/

Onclin, C., Carter, T., & Best, K. (2000). *Fort Simpson area snow surveys 1996-2002.*

Outhit, J. (2008, October 01, 2007). Wetlands, farms paved over. [Electronic version]. *The Record.*

Persaud, N., & Khosla, R. (1999). Partitioning soil-water losses in different plant populations of dry-land corn. Agricultural Water Management, 42(2), 157.

Petrone, R. M., Griffis, T. J., & Rouse, W. J. (2000). Synoptic and surface climatology interactions in the central Canadian sub-arctic: Normal and El Niño seasons. *Physical Geography, 21*, 368-383.

Pettyjohn, W. A., & Henning, R. (1979). *Preliminary estimate of ground-water recharge rates, related streamflow and water quality in Ohio* (Project Completion No. 552). Ohio: Ohio State University, Water Resources Center.

Philip, J. R. (1954). An infiltration equation with physical significance. *Soil Science, 77*(1), 153-157.

Pietroniro, A., & Prowse, T. D. (2002). Applications of remote sensing in hydrology. *Hydrological Processes, 16*(8), 1537-1541.

Pietroniro, A., Conly, M., Toth, B., Leconte, R., Kouwen, N., Peters, D., *et al.* (2003). Modeling climate change impacts on water availability in the peace and Athabasca Delta and catchment: Northern river basins initiative. (Final draft report, NREI contribution). NHRI, Saskatoon: Environment Canada.

Pietroniro, A., Fortin, V., Kouwen, N., Neal, C., Turcotte, R., Davison, B., *et al.* (2007). Development of the MESH modelling system for hydrological ensemble forecasting of the Laurentian Great Lakes at the regional scale. *Hydrology and Earth System Sciences, 11*(4), 1279.

Pietroniro, A., Leconte, R., Toth, B., Peters, D. L., Kouwen, N., Conly, F. M., *et al.* (2006). Modelling climate change impacts in the Peace and Athabasca catchment and delta: III—integrated model assessment. *Hydrological Processes, 20*(19), 4231-4245.

Pinder, G. F., & Jones, J. F. (1969). Determination of the groundwater component of peak discharge from the chemistry of total runoff. *Water Resources Research, 5*, 438-445.

Pohl, S., Marsh, P., & Bonsal, B. R. (2007). Modeling the impact of climate change on runoff and annual water balance of an arctic headwater basin. *Arctic, 60*(2), 173.

Price, J. S., Yi, Y., Whittington, P. N., & Edwards, T. W. D. (In preparation). *Physical and isotopic characterization of evaporation from Sphagnum moss.* Submitted to *Journal of Hydrology*.

Priestly, C. H. B., & Taylor , R. J. (1972). On the assessment of surface heat flux and evaporation using large-scale parameters. *Monthly Weather Review, 100*(2), 81-92.

Prowse, T. D. (1986). Ice-jam characteristics, Liard-Mackenzie River confluence. *Canadian Journal of Civil Engineering, 13*(6), 653-665.

Quilbe, R., Rosseau, A. N., Moquet, J. S., Savary, S., Ricard, S., & Garbouj, M. S. (2008). Hydrological responses of a watershed to historical land-use evolution and future land-use scenarios under climate change conditions. *Hydrology and Earth System Sciences, 12*(1), 101.

Quinton, W. L., & Roulet, N. T. (1998). Spring and summer hydrology of a subarctic patterned wetland. *Arctic and Alpine Research, 30*, 285-294.

Quinton, W. L., Hayashi, M., & Pietroniro, A. (2003). Connectivity and storage functions of channel fens and flat bogs in northern basins. *Hydrological Processes, 17*(18), 3665-3684.

Reddy, M. M., Schuster, P., Kendall, C., & Reddy, M. B. (2006). Characterization of surface and ground water $\delta^{18}O$ seasonal variation and its use for estimating groundwater residence times. *Hydrological Processes, 20*(8), 1753-1772.

Refsgaard, J. C., & Knudsen, J. (1996). Operational validation and intercomparison of different types of hydrological models. *Water Resources Research, 32*(7), 2189-2202.

Rennie, J. A., Reid, D. E., & Henderson, J. D. (1981). Permafrost extent in the southern fringe of the discontinuous permafrost zone, Fort Simpson, NWT. *Permafrost: Third International Conference,* Edmonton. *, 1* 439-444.

Reynolds, J. F., Kemp, P. R., & Tenhunen, J. D. (2000). Effects of long-term rainfall variability on evapotranspiration and soil water distribution in the Chihuahuan Desert: A modeling analysis. *Plant Ecology, 150*(1-2), 145-159.

Ribolzi, O., Andrieux, P., Valles, V., Bouzigues, R., Bariac, T., & Voltz, M. (2000). Contribution of groundwater and overland flows to storm flow generation in a cultivated Mediterranean catchment. quantification by natural chemical tracing. *Journal of Hydrology, 233*(1-4), 241-257.

Rideal, E. K. (1925). *J. Phys. Chem., 29*, 1585.

Riley, W. J., Still, C. J., Torn, M. S., & Berry, J. A. (2002). A mechanistic model of $H_2{}^{18}O$ and $C^{18}OO$ fluxes between ecosystems and the atmosphere: Model description and sensitivity analyses. *Global Biogeochemical Cycles, 16*(4), 1095.

Robson, A., Beven, K., & Neal, C. (1992). Towards identifying sources of subsurface flow – A comparison of components identified by a physically based runoff model and those determined by chemical mixing techniques. *Hydrological Processes, 6*(2), 199-214.

Rodgers, P., Soulsby, C., Waldron, S., & Tetzlaff, D. (2005). Using stable isotope tracers to assess hydrological flowpaths, residence times and landscape influences in a nested mesoscale catchment. *Hydrology and Earth System Sciences, 9*(3), 139-155.

Rodhe, A. (1998). Snowmelt-dominated systems. In C. Kendall, & J. J. McDonnell (Eds.), *Isotope tracers in catchment hydrology*. First ed.: pp. 391-433. Amsterdam, The Netherlands: Elsevier.

Rodhe, A., & Myberg, L. (1996). Transit times for water in a small till catchment from a step shift in the oxygen-18 content of the water input. *Water Resources Research, 32*(12), 3497-3511.

Rosenzweig, C., & Abramopoulos, F. (1997). Land-surface model development for the GISS GCM. *Journal of Climate, 10*(8), 2040.

Rouse, W. R. (2000). Progress in hydrological research in the Mackenzie GEWEX study. *Hydrological Processes, 14*(9), 1667-1685.

Rozanski, K., Araguas-Araguas, L., & Gonfiantini, R. (1993). In Swart P. K., McKenzie J., Lohmann K. C. & Savin S.(Eds.), *Isotopic patterns in modern global precipitation*. Washington, DC: American Geophysical Union.

Rozanski, K., Froelich, K., & Mook, W. G. (2001). *Surface water* (Technical document No. No. 39, Vol. III). UNESCO, Paris: International Atomic Energy Agency.

Rutherford, J. C. (1994). *River mixing*. New York, NY: John Wiley & Sons Ltd.

SAHRA. (2005). *Isotopes & hydrology*. Retrieved 03/2008, 2008, from http://www.sahra.arizona.edu/programs/isotopes/oxygen.html

Sánchez-Carrillo, S., Angeler, D. G., Sánchez-Andrés, R., Alvarez-Cobelas, M., & Garatuza-Payán, J. (2004). Evapotranspiration in semi-arid wetlands: Relationships between inundation and the macrophyte-cover: Open-water ratio. *Advances in Water Resources, 27*(6), 643-655.

Schmidt, G. A., Ruedy, R., Hansen, J. E., Aleinov, I., Bell, N., Bauer, M., *et al.* (2006). Present-day atmospheric simulations using GISS ModelE: Comparison to in situ, satellite, and reanalysis data. *Journal of Climate, 19*(2), 153.

Schnoor, J. L. (1996). Environmental modeling : Fate and transport of pollutants in water, air, and soil. New York: J. Wiley.

Schott, S. (2005). *SWING: Stable water isotope intercomparison group*. Retrieved 04/2008, 2008, from http://www.bgc-jena.mpg.de/bgc-synthesis/projects/SWING/index.shtml

Schotterer, U., Oldfield, F., & Frohlich, K. (1996). In Grassl H. (Ed.), *GNIP: Global network for isotopes in precipitation*. Bern, Switzerland: IAEA; PAGES; WMO; IAHS.

Seibert, J., & McDonnell, J. J. (2002). On the dialog between experimentalist and modeler in catchment hydrology: Use of soft data for multi-criteria model calibration. *Water Resources Research, 38*(11)

Seibert, J., Bishop, K. H., & Nyberg, L. (1997). A test of TOPMODEL's ability to predict spatially distributed groundwater levels. *Hydrological Processes, 11*(9), 1131-1144.

Seuffert, G., Gross, P., Simmer, C., & Wood, E. F. (2002). The influence of hydrologic modeling on the predicted local weather: Two-way coupling of a mesoscale weather prediction model and a land surface hydrologic model. *Journal of Hydrometeorology, 3*(5), 505.

Sikka, D. R., & Sanjeeva Rao, P. (2008). The use and performance of mesoscale models over the Indian region for two high-impact events. *Natural Hazards, 44*(3), 353-372.

Singh, R., Subramanian, K., & Refsgaard, J. C. (1999). Hydrological modelling of a small watershed using MIKE SHE for irrigation planning. *Agricultural Water Management, 41*(3), 149-166.

Singh, V. P., & Frevert, D. K. (2002). *Mathematical models of large watershed hydrology*. Highlands Ranch, Colorado: Water Resources Publications.

Singh, V. P., & Frevert, D. K. (2006). *Watershed models*. Boca Raton: CRC Taylor & Francis.

Singleton, M. J., Sonnenthal, E. L., Conrad, M. E., DePaolo, D. J., & Gee, G. W. (2004). Multiphase reactive transport modeling of stable isotope fractionation of infiltrating unsaturated zone pore water and vapour using TOUGHREACT. *VADOSE ZONE JOURNAL, 3*(3), 775-785.

Sivapalan, M., Takeuchi, K., Franks, S. W., Gupta, V. K., Karambiri, H., Laskshmi, V., *et al.* (2003). IAHS decade on predictions in ungauged basins (PUB), 2003-2012: Shaping an exciting future for the hydrological sciences. *Hydrological Sciences Journal, 48*(6), 857.

Sklash, M. G., & Farvolden, R. N. (1979). The role of groundwater in storm runoff. *Journal of Hydrology, 43*(1-4), 45-65.

Sklash, M. G., & Farvolden, R. N. (1982). The use of environmental isotopes in the study of high-runoff episodes in streams. In E. C. Perry Jr., & C. W. Montgomery (Eds.), *Isotope studies of hydrological processes* (pp. 65-73). DKalb, IL: North Illinois University Press.

Sloto, R. A., & Crouse, M. Y. (1996). *HYSEP: A computer program for streamflow hydrograph separation and analysis* (Water Resource Investigations No. 96-4040). Lemoyne, Pennsylvania: United States Geological Survey.

Snelgrove, K. R. (2002). *Implications of lateral flow generation on land-surface scheme fluxes*. Ph.D. Thesis, Department of Civil Engineering, University of Waterloo: Waterloo, ON.

Sokal, M. A., Hall, R. I., & Wolfe, B. B. (2008). Relationships between hydrological and limnological conditions in lakes of the Slave. *Journal of Paleolimnology, 39*, 533-550.

Soulsby, C., Malcolm, R., Helliwell, R., Ferrier, R. C., & Jenkins, A. (2000). Isotope hydrology of the Allt a' Mharcaidh catchment, Cairngorms, Scotland: Implications for hydrological pathways and residence times. *Hydrological Processes, 14*(4), 747-762.

Soulsby, C., Rodgers, P., Smart, R., Dawson, J., & Dunn, S. (2003). A tracer-based assessment of hydrological pathways at different spatial scales in a mesoscale Scottish catchment. *Hydrological Processes, 17*(4), 759-777.

Soulsby, C., Tetzlaff, D., Dunn, S. M., & Waldron, S. (2006). Scaling up and out in runoff process understanding: Insights from nested experimental catchment studies. *Hydrological Processes, 20*(11), 2461-2465.

Spence, C., Pomeroy, J. W., & Pietroniro, A. (Eds.). (2004). *Prediction in Ungauged Basins: Approaches for Canada's cold regions*. Ottawa, ON: Environment Canada.

Srinivasin, R., & Arnold, J. G. (1994). Integration of a basin-scale water-quality model with GIS. *Water Resources Bulletin, 30*(3), 453.

St Amour, N. A., Gibson, J. J., Edwards, T. W. D., Prowse, T. D., & Pietroniro, A. (2005). Isotopic time-series partitioning of streamflow components in wetland-dominated catchments, lower Liard river basin, Northwest Territories, Canada. *Hydrological Processes, 19*(17), 3357-3381.

St. Amour, N. A. (2008). *2000-2001 UW weather station isotope data (unpublished)*. Personal Communication with Stadnyk, T., Waterloo, ON: University of Waterloo.

St. Amour, N.A. (2008). *2000-2001 UW Weather Station Isotope Data.* Personal Communication with T. Stadnyk; University of Waterloo, Waterloo, ON.

Stadnyk, T., St Amour, N., Kouwen, N., Edwards, T. W. D., Pietroniro, A., & Gibson, J. J. (2005). A groundwater separation study in boreal wetland terrain: The WATFLOOD hydrological model compared with stable isotope tracers. *Isotopes in Environmental and Health Studies, 41*(1), 49-68.

Statistics Canada. (2007). *Greater golden horseshoe: Population change, 2001 to 2006 by 2006 census subdivision*. Ottawa, ON: Geography Division, Statistics Canada. Retrieved from 2001 and 2006 Censuses of Canada database.

Stewart, R. E., Leighton, H. G., Marsh, P., Moore, G. W. K., Ritchie, H., Rouse, W. R., *et al.* (1998). The Mackenzie GEWEX study: The water and energy cycles of a major North American river basin. *Bulletin of the American Meteorological Society, 79*(12)

Stichler, W., Rauert, W., & Martinec, J. (1981). Environmental isotope studies of an alpine snowpack. *Nordic Hydrology, 12*, 297-308.

Sturm, C., Hoffmann, G., & Langmann, B. (2007a). Simulation of the stable water isotopes in precipitation over South America: Comparing regional to global circulation models. *Journal of Climate, 20*(15), 3730-3750.

Sturm, C., Vimeaux, F., & Krinner, G. (2007b). Intraseasonal variability in South America recorded in stable water isotopes. *Journal of Geophysical Research, 112*, 1-14.

Sturm, K. (2005). *Regional atmospheric modelling of the stable water isotope cycle*. Doctorat, Sciences de la Terre et de l'Univers, l'Université Joseph Fourier (Grenoble 1).

Sturm, K. (2007). *Computing relative humidity*. Personal Communication [email] with Stadnyk, T.: Stockholm, Sweden.

Sturm, K., Birks, J., & Kelley, M. (2006). *Comparison of REMOiso $\delta^{18}O$ and $\delta^{2}H$ signals across North America with CNIP-generated fields*. Personal Communications with Stadnyk, T.: Pisa, Italy.

Sturm, K., Hoffmann, G., Langmann, B., & Stichler, W. (2005). Simulation of $\delta^{18}O$ in precipitation by the regional circulation model REMOiso. *Hydrological Processes, 19*(17), 3425-3444.

Tao, T., & Kouwen, N. (1989). Remote-sensing and fully distributed modeling for flood forecasting. *Journal of Water Resources Planning and Management, 115*(6), 809-823.

Task Committee on Hydrology Handbook of Management Group D. (1996). *Hydrology handbook*. (Second Ed.). New York: American Society of Civil Engineers.

Tetzlaff, D., Soulsby, C., Waldron, S., Malcolm, I. A., Bacon, P. J., Dunn, S. M., *et al.* (2007). Conceptualization of runoff processes using a geographical information system and tracers in a nested mesoscale catchment. *Hydrological Processes, 21*(10), 1289-1307.

Thorne, R., & Woo, M. k. (2006). Efficacy of a hydrologic model in simulating discharge from a large mountainous catchment. *Journal of Hydrology, 330*(1-2), 301-312.

Toth, B., Pietroniro, A., Conly, F. M., & Kouwen, N. (2006). Modelling climate change impacts in the peace and Athabasca catchment and delta: I—hydrological model application. *Hydrological Processes, 20*(19), 4197-4214.

Töyra, J. (1997). Generation of a digital elevation model and establishment of a database for the Fort Simpson study area (No. KW504-7-0074). Saskatoon, SK: National Hydrology Research Institute.

Turner, J. V., & Barnes, C. J. (1998). Modeling of isotope and hydrogeochemical responses in catchment hydrology. In C. Kendall, & J. J. McDonnell (Eds.), *Isotope tracers in catchment hydrology*. First ed.: pp. 723-760. Amsterdam, The Netherlands: Elsevier.

Uhlenbrook, S., & Hoeg, S. (2003). Quantifying uncertainties in tracer-based hydrograph separations: A case study for two-, three- and five-component hydrograph separations in a mountainous catchment. *Hydrological Processes, 17*(2), 431-453.

Uhlenbrook, S., & Leibundgut, C. (2000). Development and validation of a process oriented catchment model based on dominating runoff generation processes. *Physics and Chemistry of the Earth, Part B: Hydrology, Oceans and Atmosphere, 25*(7-8), 653-657.

Uhlenbrook, S., Frey, M., Leibundgut, C., & Maloszewski, P. (2002). Hydrograph separations in a mesoscale mountainous basin at event and seasonal timescales. *Water Resources Research, 38*(6), 31-1-31-14.

Unnikrishna, P. V., McDonnell, J. J., & Kendall, C. (2002). Isotope variations in a Sierra Nevada snowpack and their relation to meltwater. *Journal of Hydrology, 260*(1-4), 38-57.

USGS. (2006). *USGS water resources of Michigan: General climatology*. Retrieved 04/15, 2008, from http://mi.water.usgs.gov/fdgenclim.php

Vache, K. B., & McDonnell, J. J. (2006). A process-based rejectionist framework for evaluating catchment runoff model structure. *Water Resources Research, 42*(2).

Vandenschrick, G., van Wesemael, B., Frot, E., Pulido-Bosch, A., Molina, L., Stiévenard, M., *et al.* (2002). Using stable isotope analysis (delta-D & delta-^{18}O) to characterise the regional hydrology of the Sierra de Gador, southeast Spain. *Journal of Hydrology, 265*(1-4), 43-55.

VanderHoven, S. J., Solomon, D. K., & Moline, G. R. (2002). Numerical simulation of unsaturated flow along preferential pathways: Implications for the use of mass balance calculations for isotope storm hydrograph separation. *Journal of Hydrology, 268*(1-4), 214-233.

VanderKwaak, J. E. (1999). *Numerical simulation of flow and chemical transport in integrated surface-subsurface hydrologic systems*. Ph.D. Thesis, Department of Earth Sciences, University of Waterloo: Waterloo, ON.

VanderKwaak, J. E., K. Loague,. (2001). Hydrologic-response simulations for the R-5 catchment with a comprehensive physics-based model. *Water Resources Research, 37*(4), 999-1014.

Vázquez, R. F., Willems, P., & Feyen, J. (2008). Improving the predictions of a MIKE SHE catchment-scale application by using a multi-criteria approach. *Hydrological Processes, 22*(13), 2159.

Verseghy, D. (1991). CLASS: A Canadian land surface scheme for GCMs, part I: Soil model. *International Journal of Climatology, 11*(2), 111-133.

Verseghy, D., McFarlane, N. A., & Lazare, M. (1993). CLASS - A Canadian land surface scheme for GCMs, part II: Vegetation model and coupled runs. *International Journal of Climatology, 13*, 347-370.

Vicuna, S., Leonardson, R., Hanemann, M. W., Dale, L. L., & Dracup, J. A. (2008). Climate change impacts on high elevation hydropower generation in California's Sierra Nevada: A case study in the upper American river. *Climatic Change, 87*, S123.

Viessman, J. W., & Lewis, G. L. (1996). Unit hydrographs. In M. T. Slaughter (Ed.), *Introduction to hydrology* (fourth ed., pp. 188-233). New York, NY: Harper Collins College Publishers.

Vogt, H. J. (1976). Isotopentrennung bei der verdampfung von wasser. (Staatsexamensarbeit, Universitat Heidleberg). , 78.

von Bertalanffy, L. (1968). *General system theory: Foundations, development, applications*. New York: George Braziller.

Vorosmarty, C. J., Moore, I. B., Grace, A., Peterson, B. J., Ratetter, E. B., & Melillo, D. J. (1991). Distributed parameter models to analyze the impact of human disturbance of the surface hydrology of a large tropical drainage basin in Southern Africain. In van de Ven, F.H.M, D. Gutnecht, D. P. Loucks & K. A. Salewicz (Eds.), *Hydrology for the water management of large river basins* (). Yarmouth, Great Britain: International Association of Hydrologic Sciences (IAHS).

Wagnon, P., Ribstein, P., Schuler, T., & Francou, B. (1998). Flow separation on Zongo glacier, Cordillera Real, Bolivia. *Hydrological Processes, 12*(12), 1911-1926.

Walker, J. F., & Krabbenhoft, D. P. (1998). Groundwater and surface-water interactions in riparian and lake-dominated systems. In C. Kendall, & J. J. McDonnell (Eds.), *Isotope tracers in catchment hydrology*. First ed.: pp. 467-488. Amsterdam, The Netherlands: Elsevier.

Water Survey of Canada (WSC). (2001). *Hydat CD-ROM: Surface water and sediment data*. Ottawa, ON.

Weerakoon, S., & Smakhtin, V. (2008). *Predictions in ungauged basins (PUB)*. Retrieved 05/2008, 2008, from http://www.pub.iwmi.org/UI/Content/Default.aspx?PGID=0

Welhan, J. A., & Fritz, P. (1977). Evaporation pan isotopic behaviour as an index of isotopic evaporation conditions. *Geochemica et Cosmochimica Acta, 41*, 682-686.

Western, A. W., Blöschl, G., & Grayson, R. B. (2001). Toward capturing hydrologically significant connectivity in spatial patterns. *Water Resources Research, 37*(1), 83-97.

White, M. D., & Greer, K. A. (2006). The effects of watershed urbanization ont he stream hydrology and riparian vegetation of Los Penasquitos Creek, California. *Landscape and Urban Planning, 74*, 125-138.

Wilson, K. B., Hanson, P. J., & Baldocchi, D. D. (2000). Factors controlling evaporation and energy partitioning beneath a deciduous forest over an annual cycle. *Agricultural and Forest Meteorology, 102*(2-3), 83-103.

Wissmeier, L., & Uhlenbrook, S. (2007). Distributed, high-resolution modelling of ^{18}O signals in a mesoscale catchment. *Journal of Hydrology, 332*(3-4), 497-510.

Wittenberg, H., & Sivapalan, M. (1999). Watershed groundwater balance estimation using streamflow recession analysis and baseflow separation. *Journal of Hydrology, 219*(1-2), 20-33.

Wolfe, B. B., Hall, R. I., Last, W. M., Edwards, T. W. D., English, M. C., Karst-Riddoch, T. L., *et al.* (2006). Reconstruction of multi-century flood histories from oxbow lake sediments, Peace-Athabasca Delta, Canada. *Hydrological Processes, 20*, 4131-4153.

Wolfe, B. B., Karst-Riddoch, T. L., Hall, R. I., Edwards, T. W. D., English, M. C., Palmini, R., *et al.* (2007). Classification of hydrological regimes of northern floodplain basins (Peace-Athabasca Delta, Canada) from analysis of stable isotopes ($\delta^{18}O$, $\delta^{2}H$) and water chemistry. *Hydrological Processes, 21*, 151-168.

Wolfe, B. B., Karst-Riddoch, T. L., Vardy, S. R., Falcone, M. D., Hall, R. I., & Edwards, T. W. D. (2005). Impacts of climate and river flooding on the hydro-ecology of a floodplain basin, peace-athabasca delta, canada since AD 1700. *Quaternary Research, 64*(2), 147.

Woo, M. K. (1988). In Senneset K. (Ed.), *Wetland runoff regime in northern Canada*. Washington, D.C.: National Academy of Science.

Wood, E. F., Lettenmaier, D. P., & Zartarian, V. G. (1992). A land-surface hydrology parameterization with subgrid variability for general-circulation models. *Journal of Geophysical Research, 97*(D3), 2717.

WSC (2001). Hydat CD-ROM: Surface water and sediment data. Ottawa, ON.

Yadav, M., Wagener, T., & Gupta, H. (2007). Regionalization of constraints on expected watershed response behavior for improved predictions in ungauged basins. *Advances in Water Resources, 30*(8), 1756.

Yang, D., Herath, S., & Musiake, K. (2000). Comparison of different distributed hydrological models for characterization of catchment spatial variability. *Hydrological Processes, 14*(3), 403-416.

Yepez, E. A., Huxman, T. E., Ignace, D. D., English, N. B., Weltzin, J. F., Castellanos, A. E., *et al.* (2005). Dynamics of transpiration and evaporation following a moisture pulse in a semiarid grassland: A chamber-based isotope method for partitioning flux components. *Agricultural and Forest Meteorology, 132*, 359-376.

Yi, Y., Brock, B. E., Falcone, M. D., Wolfe, B. B., & Edwards, T. W. D. (2008). A coupled isotope tracer method to characterize input water to lakes. *Journal of Hydrology, 350*, 1-13.

Yoshimura, K., Miyazaki, S., Kanae, S., & Oki, T. (2006). Iso-MATSIRO, a land surface model that incorporates stable water isotopes. *Global and Planetary Change, 51*(1-2), 90-107.

Zeng, N., Yoon, J., Mariotti, A., & Swenson, S. (2008). Variability of basin-scale terrestrial water storage from a PER water budget method: The Amazon and Mississippi. *Journal of Climate, 21*, 248-267.

Zimmerman, U., Ehhalt, D., & Munnich, K. O. (1967). Soil water movement and evaporation: Changes in the isotopic composition of the water. *Isotopes in Hydrology,* Vienna, AU. 567-584.

Zoltai, S. C., Tarnocai, C., Mills, G. F., & Johnson, J. F. (1988). Wetlands of boreal Canada. In National Wetlands Working Group (Ed.), *Wetlands in Canada* (pp. 97-154). Ottawa: Sustainable development branch, Canadian Wildlife Service, Conservation and Protection, Environment Canada.

Glossary

$\%D_v$	Deviation of runoff volume statistic comparing measured and computed runoff volumes.
η	Turbulence parameter in kinetic isotope separation equation
Θ	Transport parameter in kinetic isotope separation equation
A	Channel reach cross-sectional area (m^2)
AET	Actual amount of evapotranspiration, typically reduced from the potential amount (PET).
ak2	Dimensionless conductivity parameter used to compute recharge of the LZS from bare ground infiltration
ak2fs	Dimensionless conductivity parameter used to compute recharge of the LZS from snow-covered area infiltration
ATI	Antecedent temperature index
ATI	Antecedent temperature index
B	Channel width (m) in dispersion computations
C_{GW}	Mass concentration of baseflow in lower zone storage compartment (kg/m^3) in WATFLOOD tracer module
$C_{IN,GW}$	Mass concentration of inflow (kg/m^3) to lower zone storage compartment
$C_{IN,IF}$	Mass concentration of inflow (kg/m^3) to upper zone storage compartment
$C_{IN,SW}$	Mass concentration of inflow (kg/m^3) to surface storage compartment
$C_{IN,wet}$	Mass concentration of inflow (kg/m^3) to wetland compartment
C_i^{18O}	Concentration of heavy isotopes in hydrologic reservoir *i* (kg ^{18}O/kg O)
C_k^0	Ratio of mass diffusivities of heavy to light isotope species for oxygen-18 (i.e., 28.6‰)
coeff	Retardation coefficient applied to tracer routing for large grid sizes (i.e., 10-km) to control numerical dispersion (dimensionless)
C_r	Courant numerical criteria used to constrain timestep
$C_{wet,GW}$	Mass concentration of baseflow in wetland compartment (kg/m^3) in WATFLOOD tracer module
D	Snowmelt runoff into channel in isotope mixing model (m^3/s)
D*	Numerical dispersion (m^2/s)
drng	Vertical drainage from upper zone to lower zone storage (m^3/s) from bare ground infiltration
DRNG	Depth of water draining from UZS to LZS (mm)
$drng_{fs}$	Vertical drainage from upper zone to lower zone storage (m^3/s) from snow melt infiltration
ds	Surface depression storage from bare ground (mm of water).
dsfs	Surface depression storage from snowmelt (mm of water).
DUZ	Depth of water in UZS (mm)
e_a	Vapour pressure of air (Pa)
e_S	Saturation vapour pressure of air (Pa)

ev	Evaporation from subsurface storage (mm)
ET	Evapotranspiration (mm of water)
f	Fraction of water lost due to evaporation of total volume of water in storage
fexcess	WATFLOOD generated snowmelt contributing to runoff (mm)
FSB	Fort Simpson Basins
GCM	Global circulation model
GLB	Great Lakes Basin
GMWL	Global meteoric water line: long-term average, flux-weighted composition of global precipitation in δ^2H-$\delta^{18}O$ space
GRB	Grand River Basin
GRCA	Grand River Conservation Authority
h	Relative humidity (in percent)
h_{cha}	Height of water in the channel (m)
HS	Hydrograph separation
h_{wet}	Height of water in the wetland (m)
IET	Interception evapotranspiration
$isoS_{x,1,2}$	Mass storage of heavy isotope species (kg) in storage compartment 'x' at beginning (i.e., $isoS_1$) and end (i.e., $isoS_2$) of timestep.
isotope.par	Input parameter file defining ^{18}O initialization compositions and ^{18}O meteorological isotope inputs.
isoWATFLOOD	Isotope-enabled version of WATFLOOD where $\delta^{18}O$ is modelled in parallel with runoff, hydrological storage and streamflow.
LEL	Local evaporation water line: long-term average, flux-weighted composition of local evaporating water bodies in δ^2H-$\delta^{18}O$ space
LMWL	Local meteoric water line: long-term average, flux-weighted composition of local precipitation in δ^2H-$\delta^{18}O$ space
LSS	Land Surface Scheme; models that simulate both water and energy fluxes between the atmosphere and land surface
lzf	Conductivity of LZS outflow based on river classification (optimized)
LZS	Lower zone storage, or shallow ground water (mm of water)
M	Depth of snow melt (mm)
m	Rate of heavy isotope accumulation resulting from evaporative fractionation (dimensionless)
MF	Melt factor describing the rate of melt per degree Celsius increase per unit time
MF	Melt factor or rate of snowpack melting per degree per unit time
$MIN_{GW1,2}$	Mass of inflow (kg) of baseflow entering channel storage at beginning (i.e., $MIN_{GW,1}$) and end (i.e., $MIN_{GW,2}$) of timestep in WATFLOOD tracer module
MIN_{IF}	Mass of inflow (kg) of interflow entering the channel storage (i.e., MIN_{IF}) in WATFLOOD tracer module
MIN_{SW}	Mass of inflow (kg) of surface water entering the channel storage (i.e., MIN_{SW}) in WATFLOOD tracer module
$MIN_{wet,GW}$	Mass of inflow (kg) of baseflow entering wetland storage (i.e., $MIN_{wet,GW}$) in WATFLOOD tracer module

MOE	Ministry of the Environment
$MOUT_{GW1,2}$	Mass outflow (kg) of baseflow in channel reach at beginning (i.e., 1) and end (i.e., 2) of timestep in WATFLOOD tracer module.
$MOUT_{wet,GW}$	Mass of outflow (kg) of baseflow leaving wetland storage (i.e., $MOUT_{wet,GW}$) in WATFLOOD tracer module
MRB	Mackenzie River Basin
naa	Number of WATFLOOD grids in basin routing sequence
Nash	Nash-Sutcliffe goodness-of-fit statistic measuring percent observed variance explained by the predictive data.
NMF	Negative melt factor or rate of change in heat deficit by degree of air temperature increase (optimized)
O	Lake discharge (m^3/s)
O	Lake outflow (m^3/s) defined by a discharge formula, or operating rule
P	Rainfall-runoff into channel in isotope mixing model (m^3/s)
p_a	Atmospheric pressure (101 325 Pa)
P_e	Pechlet numerical criteria used to constrain grid size
PET	Potential amount of evapotranspiration of moisture.
pH	Potential hydrogen, or a measure of the acidity of the water
PUB	Predictions in Ungauged Basins, referring to the prediction of streamflow by a hydrological model
PWP	Permanent wilting point, or minimum depth of water in UZS (mm)
pwr	Depletion rate of LZS based on river classification (optimized)
Q	Total runoff into channel in isotope mixing model (m^3/s)
q_1	Overland (surface) runoff (m^3/s) from bare ground area
q_{1fs}	Overland (surface) runoff (m^3/s) from snow covered area
q_a	Specific humidity
q_{ev}	Evaporative loss from storage during the timestep (m^3/s)
q_f	Infiltration from surface into upper zone storage (m^3/s) from bare ground
q_{ffs}	Infiltration from surface into upper zone storage (m^3/s) from snow covered area
Q_{gmelt}	Volumetric flow of glacial meltwater (m^3/s)
q_{int}	Soilwater runoff (m^3/s)
q_{intfs}	Soilwater runoff (m^3/s) from infiltrated snow melt
qlz	Lower zone, or baseflow (m^3/s)
Q_{melt}	Water melting inside the snowpack, contained within the snowpack (m^3/s)
q_o	Mass concentration of water in an air mass (kg/m^3)
qo_2	Channel outflow at the end of the timestep (m^3/s)
qo_{wet}	Wetland outflow (m^3/s)
Q_r	Overland flow in WATFLOOD, computed via the Manning equation (m^3/s)
q_{sat}	Mass concentration of water required to saturate an air mass (kg/m^3)
Q_{SM}	Snowmelt flux from snow-covered area in isoWATFLOOD (m^3/s)
qsw_{evp}	Evapotranspiration loss from wetland (m^3/s)
R	Baseflow runoff into channel in isotope mixing model (m^3/s)
R^2	Correlation coefficient defining the strength and direction of a linear relationship between two variables.

R3	Combined roughness and channel length parameter (optimized)
RCM	Regional circulation model
REC	Dimensionless conductivity parameter used to compute interflow
RETN	Depth of pore water retention in soil (mm)
R_{GW}	Baseflow contribution from groundwater in isotope mixing model (m^3/s)
R_S	Ratio of the heavy isotope species in the sample to total species in sample
R_{SW}	Baseflow contribution from surface water infiltration in isotope mixing model (m^3/s)
R_{VSMOW}	Ratio of heavy isotopes to total volume of sample of Vienna Standard Mean Ocean Water (VSMOW), the reference standard
S	Storage volume of water (m^3)
S_1, S_2	Mass storage (kg) of baseflow component in channel at beginning (i.e., S_1) and end (i.e., S_2)of timestep
SAT	Depth of water required for soilwater saturation (mm)
SDC	Snow depletion curves
S_i	Internal slope of a grid, or channel slope (m/m)
snowc	Total depth of snow in snowpack (mm)
$store_{1,2}$	Volume of water (m^3) in channel reach at beginning (i.e., $store_1$) and end of timestep (i.e., $store_2$)
strloss	Evapotranspiration loss from channel reach (m^3/s)
$Swet_{GW1,2}$	Mass storage (kg) of baseflow component in wetland at beginning (i.e., $Swet_{GW,1}$) and end (i.e., $Swet_{GW,2}$)of timestep
t	WATFLOOD routing timestep (s); ranges from 3600 seconds (1 hour) to 300 seconds (5 minutes)
T_a	Air temperature (^oC)
T_{base}	Base melt temperature, or temperature required for melt to initiate (^oC)
tipm	Rate parameter in ATI computation for snowmelt in WATFLOOD
tt	Travel time through reach (seconds)
U	Average channel velocity (m/s)
u^*	Shear, or critical channel velocity (m/s)
UZS	Upper zone storage, or soil moisture storage (mm of water)
UZSI	Upper zone storage indicator describing amount of soil moisture avaiulabel for evapotranspiration
V	Total water volume of storage (m^3)
w	Channel width (m) in WATFLOOD model
wcap	Wetland natural storage capacity (m^3), defined by the calibrated width to depth ratio and computed wetland water level, h_{wet}
WSC	Water Survey of Canada
$wstore_{1,2}$	Volume of water (m^3) in wetland storage at beginning (i.e., $wstore_1$) and end of timestep (i.e., $wstore_2$)
x	Evaporation to inflow (E/I) ratio (dimensionless)
y	Outflow to inflow (E/I) ratio (dimensionless)
ΔH_s	Change in heat deficit in a snow pack (mm of water)
Δx	Grid size (m)
$\Delta\delta_{melt}$	Change in isotopic composition when water melts in a snowpack (‰, VSMOW)

$\Delta\delta_{rf}$	Change in isotopic composition when water refreezes in a snowpack (‰, VSMOW)
E	Total evaporative loss over the time step in isotope mass balance equation (m^3/s)
I	Total inflow over the time step in isotope mass balance equation (m^3/s)
α^*	Equilibrium fractionation factor representing equilibrium exchange reaction kinetics
δ^*	Limiting isotopic composition of a desiccating water body
$\delta^{18}O$	The change in heavy isotope (^{18}O) build-up relative to the standard (VSMOW), defined by convention as negative numbers in ‰
δ^2H	The change in heavy isotope (^2H) build-up relative to the standard (VSMOW), defined by convention as negative numbers in ‰
δ_A	Isotopic composition of atmospheric moisture
δ_D	Isotopic composition of snowmelt (‰, VSMOW)
δ_E, C_E^{18O}	Isotopic composition of evaporating moisture (in ‰, VSMOW and mass concentration, respectively)
δ_{gmelt}, C_{gmelt}^{18O}	Isotopic composition of glacial meltwater (in ‰, VSMOW and mass concentration, respectively)
δ_{GW}	Isotopic composition of baseflow from 'old' groundwater (in ‰, VSMOW)
δ_I, C_I^{18O}	Isotopic composition of input water (in ‰, VSMOW and mass concentration, respectively)
δ_L, C_L^{18O}	Isotopic composition of body of water (in ‰, VSMOW and mass concentration, respectively)
δ_{lake}, C_{lake}^{18O}	Isotopic composition of lake water storage in isoWATFLOOD (in ‰, VSMOW and mass concentration, respectively)
δ_{LZ}, C_{LZ}^{18O}	Isotopic composition of the lower zone storage, or baseflow compartment in isoWATFLOOD (in ‰, VSMOW and mass concentration, respectively)
δ_P, C_P^{18O}	Isotopic composition of precipitation (in ‰, VSMOW and mass concentration, respectively)
δ_Q	Isotopic composition of mixed total runoff (in ‰, VSMOW)
δ_R	Isotopic composition of baseflow (in ‰, VSMOW)
δ_S	Isotopic composition of a water body in hydrologic steady-state where inflow is equal to outflow and evaporation (I=Q+E)
δ_{SM}, C_{SM}^{18O}	Isotopic composition of snowmelt in isoWATFLOOD (in ‰, VSMOW and mass concentration, respectively)
δ_{SNW}, C_{SNW}^{18O}	Isotopic composition of snow fall (in ‰, VSMOW and mass concentration, respectively)
δ_{SP}, C_{SP}^{18O}	Isotopic composition of the snowpack (in ‰, VSMOW and mass concentration, respectively)
δ_{SW}, C_{SW}^{18O}	Isotopic composition of baseflow from surface water infiltration (in ‰, VSMOW and mass concentration, respectively)
δ_{UZ}, C_{UZ}^{18O}	Isotopic composition of the upper zone storage, or soilwater compartment in isoWATFLOOD (in ‰, VSMOW and mass concentration, respectively)
δ_{wet}, C_{wet}^{18O}	Isotopic composition of the wetland storage compartment in isoWATFLOOD (in ‰, VSMOW and mass concentration, respectively)

δ_0	Initial isotopic composition of an evaporating water body (‰, VSMOW)
ε^*	Equilibrium isotopic separation representing fractionation due to equilibrium reaction kinetics
ε_k	Kinetic isotopic separation representing fractionation from mass diffusion and phase change processes
θ	Relaxation parameter used to converge routing

Appendix A

This Appendix presents the WATFLOOD parameter sets used for the Grand River Basin (GRB) and Fort Simpson Basin (FSB) modelling studies. It also presents the isoWATFLOOD isotope initialization inputs used for modelling both study sites.

Appendix A.1.1 – GRB WATFLOOD Parameter Set

```
# runtime    20:36:21
# rundate  2008-01-13
ver       9.300     parameter file version number
iopt          1     debug level
itype         0
numa          0     optimization 0=no 1=yes
nper          1     opt delta if = 0  -> absolute
kc            5     no of times delta halved
maxn      99999     max no of trials
iw            0
trce          4
iiout         4     landcover class for debug
typeo         4     no of land classes optimized(part 2)
nbsn          5     no of river classes optimized (part 2)
a1        0.250
a2     -999.999
a3     -999.999
a3     -999.999
a5        0.985     API coefficient
a6     3600.000     Minimum routing time step in seconds
a7        0.500     weighting factor - old vs. new sca value
a8        0.100     min temperature time offset
a9        0.333     max heat deficit to swe ratio
a10       2.000     uz discharge function exponent
a11       0.010     min h() for bare ground
a12       0.000     min precip rate for smearing
     default   eramosa   lwr_grand whitemans nith
lzf   0.100E-05 0.100E-05 0.100E-05 0.100E-05 0.100E-05
pwr   0.300E+01 0.300E+01 0.300E+01 0.300E+01 0.299E+01
R1n   0.100E-00 0.100E-00 0.500E-01 0.100E-00 0.100E-00
R2n   0.100E-00 0.100E-00 0.500E-01 0.100E+00 0.100E-00
mndr  0.100E+01 0.100E+01 0.100E+01 0.100E+01 0.150E+01
aa2   0.110E+01 0.110E+01 0.110E+01 0.110E+01 0.110E+01
aa3   0.430E-01 0.430E-01 0.430E-01 0.430E-01 0.430E-01
aa4   0.100E+01 0.100E+01 0.100E+01 0.100E+01 0.100E+01
theta 0.500E+00 0.300E+00 0.500E+00 0.500E+00 0.500E+00
widep 0.300E+02 0.100E+02 0.300E+02 0.200E+02 0.200E+02
kcond 0.224E+00 0.200E+00 0.255E+00 0.215E+00 0.250E+00
     bare_soil forest    crops     wetland   wetland   water     imperveous
ds    0.100E+01 0.100E+02 0.200E+01 0.100E+10 0.100E+10 0.000E+00 0.100E+01
dsfs  0.100E+01 0.100E+02 0.200E+01 0.100E+10 0.100E+10 0.000E+00 0.100E+01
Re    0.300E+01 0.400E+01 0.300E+01 0.100E+01 0.100E+01 0.100E+00 0.800E+00
AK    0.300E+01 0.120E+02 0.100E+01 0.400E+01 0.400E+03-0.100E+00 0.300E-10
AKfs  0.200E+01 0.120E+01 0.200E+01 0.400E+01 0.400E+03-0.100E+00 0.200E-10
retn  0.750E+02 0.750E+02 0.750E+02 0.400E+00 0.400E+00 0.100E+00 0.100E-10
ak2   1.320E-01 0.960E-00 0.660E-01 0.200E-01 0.200E+00 0.100E-02 0.100E-10
ak2fs 0.660E-01 0.960E-00 0.660E-01 0.150E-01 0.750E-10 0.100E-02 0.100E-10
R3    0.197E+02 0.848E+01 0.197E+02 0.898E-01 0.898E-01 0.400E-01 0.400E-02
```

```
R3fs  0.100E+02 0.100E+02 0.200E+02 0.100E+00 0.100E+00 0.400E-01 0.400E-02
r4    0.100E+01 0.100E+02 0.100E+02 0.100E+02 0.100E+02 0.100E+02 0.100E+02
ch    0.100E+01 0.900E+00 0.700E+00 0.700E+00 0.700E+00 0.600E+00
MF    0.120E+00 0.160E+00 0.110E+00 0.120E+00 0.120E+00 0.150E+00 0.150E+00
BASE -0.210E+01 0.322E+00-0.284E+01-0.121E+01-0.250E+01 0.000E+00 0.000E+00
NMF   0.100E+00 0.100E+00 0.100E+00 0.100E+00 0.100E+00 0.100E+00 0.100E+00
UADJ  0.000E+00 0.000E+00 0.000E+00 0.000E+00 0.000E+00 0.000E+00 0.000E+00
TIPM  0.100E+00 0.100E+00 0.100E+00 0.100E+00 0.100E+00 0.100E+00 0.100E+00
RHO   0.333E+00 0.333E+00 0.333E+00 0.333E+00 0.333E+00 0.333E+00 0.333E+00
WHCL  0.350E-01 0.350E-01 0.350E-01 0.350E-01 0.350E-01 0.350E-01 0.350E-01
fmadj     0.000
fmlow     0.000
fmhgh     0.000
gladj     0.000
rlaps     0.000
elvrf     0.000
flgev      2.00 1 = pan; 2 = Hargreaves; 3 = Priestley-Taylor
albed      0.11
aw-a       0.18      0.11      0.11      0.11      0.11      0.11      0.11
fpet       1.00      3.00      1.00      5.00      5.00      1.00      1.00
ftal       1.00      0.70      0.70      1.00      1.00      0.00      1.00
flint        1.        1.        1.        1.        1.        1.        1.
fcap       0.15      0.15      0.15      0.15      0.15      0.15      1.00
ffcap      0.10      0.10      0.10      0.10      0.10      0.10      1.00
spore      0.30      0.30      0.30      0.30      0.30      0.30      1.00
sublm        0.        0.        0.        0.        0.        0.        0.
tempa       50.
temp3       50.
tton         0.
lat.        50.
mxmn  10.2 12.3 12.1 12.3 14.3 14.2 13.8 14.0 13.1 10.6  8.2  9.3
humid 59.5 60.5 62.5 55.5 50.0 54.5 59.0 58.5 63.5 58.0 64.5 62.5
pres  95.1 95.1 95.1 95.1 95.1 95.1 95.1 95.1 95.1 95.1 95.1 95.1
ti2    jan  feb  mar  apr  may  jun  jul  aug  sep  oct  nov  dec
h1    0.11 0.11 0.11 0.11 0.60 0.60 0.60 0.60 0.60 0.35 0.11 0.11
h2    1.50 1.50 1.50 1.50 3.00 4.00 4.00 4.00 4.00 2.00 1.50 1.50
h3    0.04 0.04 0.04 0.04 0.53 1.00 2.00 2.50 2.50 1.00 0.04 0.04
h4    1.30 1.30 1.30 1.30 2.00 3.00 3.00 3.00 3.00 1.50 1.30 1.30
h5    1.30 1.30 1.30 1.30 2.00 3.00 3.00 3.00 3.00 1.50 1.30 1.30
h6    0.11 0.11 0.11 0.11 0.11 0.11 0.11 0.11 0.11 0.11 0.11 0.11
h7    0.01 0.01 0.01 0.01 0.01 0.01 0.01 0.01 0.01 0.01 0.01 0.01
```

Appendix A.1.2 – GRB Isotope Initialization Parameters

```
deltar          -9.5
deltas         -17.56
delta1         -10.0
delta2          -9.5
delta3         -15.0
delta4         -15.0
offset1          3.0
offset2          5.0
```

Appendix A.2.1 – FSB WATFLOOD Parameter Set

```
# runtime    13:04:06
# rundate  2007-05-15
ver       9.300     parameter file version number
iopt          1     debug level
itype         0
numa          0     optimization 0=no 1=yes
nper          1     opt delta 0=absolute
kc            5     no of times delta halved
maxn       2001     max no of trials
iw            0
itrc          4     tracer no GW=100,3-comp=4,6-comp=5
iiout         4
typeo         5     no of land classes optimized(part 2)
nbsn          5     no of river classes optimized (part 2)
mndr   -999.999
aa2    -999.999
aa3    -999.999
aa4    -999.999
a5        0.984     API coefficient
a6       900.000     Minimum routing time step in seconds
a7        0.900     weighting factor - old vs. new sca value
a8        0.135     min temperature time offset
a9        0.300     max heat deficit to swe ratio
a10       1.000     uz discharge function exponent
a11       0.010
a12       0.500     min precip rate for smearing
     jean-mariemartin    birch     backstone scotty
lzf   0.698E-06 0.327E-05 0.150E-05 0.750E-05 0.100E-05
pwr   0.255E+01 0.245E+01 0.269E+01 0.230E+01 0.269E+01
R1n   0.120E+00 0.800E-01 0.600E-00 0.400E-00 0.600E-01
R2n   0.080E-00 0.080E-00 0.080E-00 0.080E-00 0.080E-00
mndr  0.100E+01 0.100E+01 0.100E+01 0.100E+01 0.100E+01
aa2   0.110E+01 0.110E+01 0.110E+01 0.110E+01 0.110E+01
aa3   0.100E-01 0.100E-01 0.100E-01 0.100E-01 0.100E-01
aa4   0.100E+01 0.100E+01 0.100E+01 0.100E+01 0.100E+01
theta 0.405E+00 0.475E-01 0.476E+00 0.397E+00 0.446E+00
widep 0.300E+02 0.100E+02 0.300E+02 0.300E+02 0.300E+02
kcond 0.100E+01 0.300E+00 0.500E+01 0.300E+01 0.550E+01
     mix/dec   conifer   transit   wetland   wetland   water     impervious
ds    0.100E+01 0.100E+01 0.100E+01 0.100E+10 0.100E+10 0.000E+00 0.100E+01
dsfs  0.200E+01 0.200E+01 0.200E+01 0.100E+10 0.100E+10 0.000E+00 0.100E+01
rec   0.400E+00 0.400E+00 0.400E+00 0.100E+01 0.100E+01 0.100E+00 0.900E+00
ak    0.130E+01 0.130E+01 0.130E+01 0.110E+01 0.110E+01-0.100E+00 0.100E-10
akfs  0.130E+01 0.130E+01 0.130E+01 0.110E+01 0.110E+01-0.100E+00 0.100E-10
retn  0.850E+02 0.850E+02 0.850E+02 0.850E+02 0.850E+02 0.100E+00 0.100E+00
ak2   0.200E-01 0.200E-01 0.200E-01 0.550E-01 0.550E-01 0.140E-01 0.200E-01
ak2fs 0.050E-01 0.050E-01 0.050E-01 0.550E-01 0.550E-01 0.840E+00 0.200E-01
r3    0.394E+02 0.381E+02 0.381E+02 0.898E+01 0.898E+01 0.400E+01 0.400E+01
R3fs  0.394E+02 0.381E+02 0.381E+02 0.898E+01 0.898E+01 0.400E+01 0.400E+01
r4    0.100E+02 0.100E+02 0.100E+02 0.100E+02 0.100E+02 0.100E+02 0.100E+02
ch    0.900E+00 0.900E+00 0.900E+00 0.700E+00 0.700E+00
mf    0.600E-01 0.600E-01 0.600E-01 0.600E-01 0.600E-01 0.600E-01 0.600E-01
base -0.500E+00-0.500E+00-0.500E+00-0.100E+00-0.100E+00-0.400E+00-0.400E+00
nmf   0.100E+00 0.100E+00 0.100E+00 0.100E+00 0.100E+00 0.100E+01 0.100E+00
UADJ  0.000E+00 0.000E+00 0.000E+00 0.000E+00 0.000E+00 0.000E+00 0.000E+00
TIPM  0.200E+00 0.200E+00 0.200E+00 0.100E+00 0.100E+00 0.200E+00 0.200E+00
RHO   0.333E+00 0.333E+00 0.333E+00 0.333E+00 0.333E+00 0.333E+00 0.333E+00
WHCL  0.350E-01 0.350E-01 0.350E-01 0.350E-01 0.350E-01 0.350E-01 0.350E-01
fmadj     0.300
fmlow     0.600
fmhgh     1.000
gladj     0.000
rlaps     0.000
elvrf     0.000
flgev      2.00 1 = pan; 2 = Hargreaves; 3 = Priestley-Taylor
albed      0.11
```

```
aw-a       0.11      0.11      0.11      0.15      0.18      0.15      0.18
fpet       2.00      2.00      1.00      2.00      3.00      1.00      1.00
ftal       0.70      0.70      0.70      0.70      0.70      0.65      0.65
flint       1.        1.        1.        1.        1.        0.        1.
fcap       0.20      0.20      0.20      0.20      0.20      0.20      0.20
ffcap      0.10      0.10      0.10      0.10      0.10      0.10      0.10
spore      0.30      0.30      0.30      0.30      0.30      0.30      0.30
temp1       0.        0.        0.        0.        0.        0.        0.
temp2       0.
temp3      500.
tton       500.
lat.        60.
mxmn  10.2 12.3 12.1 12.3 14.3 14.2 13.8 14.0 13.1 10.6  8.2  9.3
humid 59.5 60.5 62.5 55.5 50.0 54.5 59.0 58.5 63.5 58.0 64.5 62.5
pres  95.1 95.1 95.1 95.1 95.1 95.1 95.1 95.1 95.1 95.1 95.1 95.1
ti2    jan  feb  mar  apr  may  jun  jul  aug  sep  oct  nov  dec
h1    0.01 0.01 0.01 0.21 0.21 0.41 0.51 0.51 0.51 0.51 0.01 0.01
h2    0.01 0.01 0.01 0.21 0.21 0.41 0.51 0.51 0.51 0.51 0.01 0.01
h3    0.01 0.01 0.01 0.21 0.21 0.21 0.31 0.31 0.31 0.31 0.01 0.01
h4    0.01 0.01 0.01 0.21 0.21 0.41 0.51 0.51 0.51 0.51 0.01 0.01
h5    0.01 0.01 0.01 0.21 0.21 0.41 0.51 0.51 0.51 0.51 0.01 0.01
h6    0.01 0.01 0.01 0.01 0.01 0.01 0.01 0.01 0.01 0.01 0.01 0.01
h7    0.01 0.01 0.01 0.01 0.01 0.01 0.01 0.01 0.01 0.01 0.01 0.01
```

Appendix A.2.2 – FSB Isotope Initialization Parameters

1997

```
deltar          -19.10
deltas          -29.35
delta1          -13.52
delta2          -14.6
delta3          -19.12
delta4          -20.27
offset1           0.0
offset2           0.0
```

1998

```
deltar          -20.10
deltas          -25.03
delta1          -13.90
delta2          -17.0
delta3          -18.95
delta4          -20.27
offset1           1.0
offset2           5.0
```

1999

```
deltar          -16.52
deltas          -26.79
delta1          -12.53
delta2          -14.52
delta3          -18.92
delta4          -25.27
offset1           3.0
offset2           5.0
```

Appendix B

This Appendix presents a flow chart illustrating the WATFLOOD modelling system, including the tracer module and isoWATFLOOD code components.

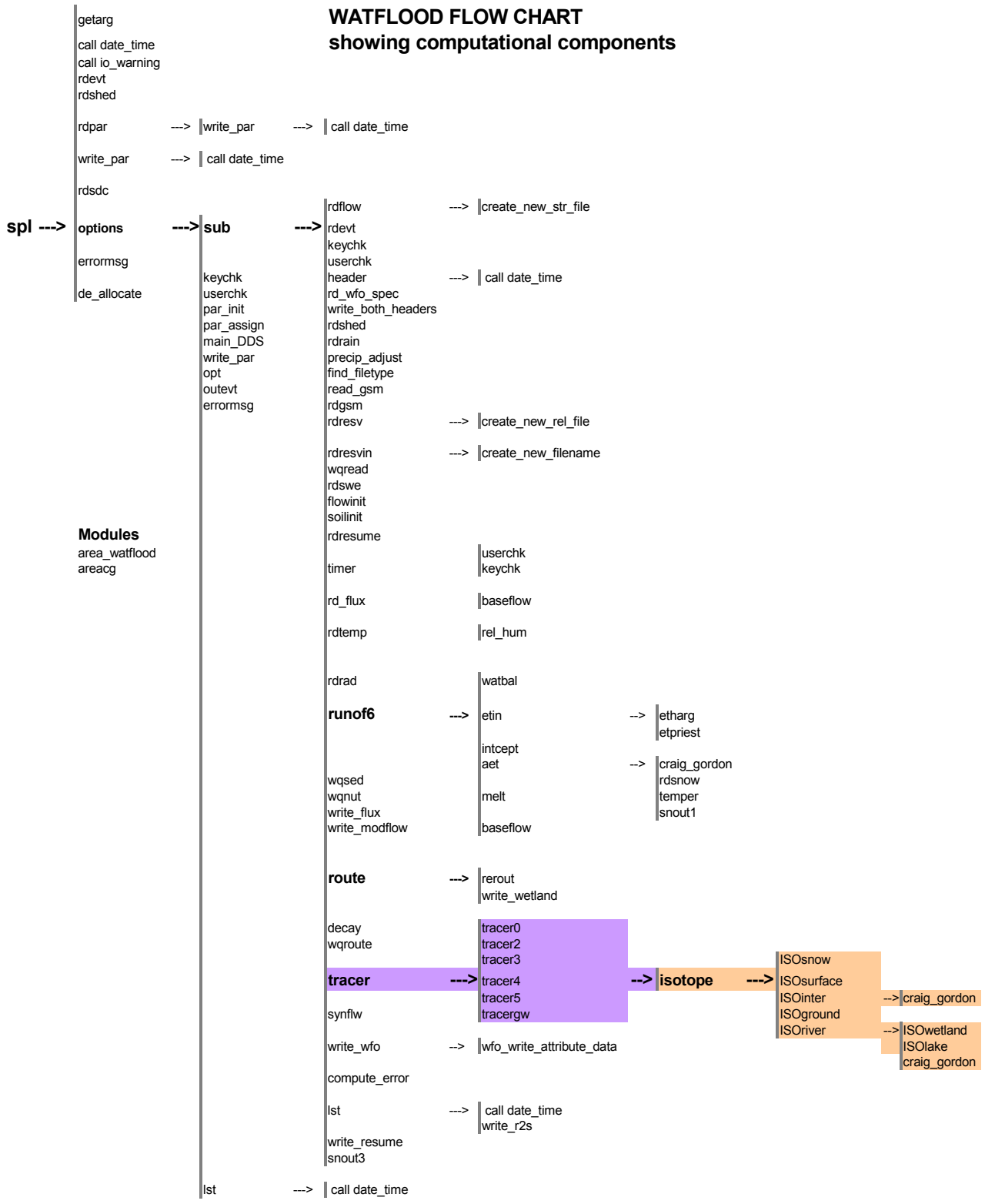
WATFLOOD FLOW CHART
showing computational components
spl
options
getarg
call date_time
call io_warning
rdevt
rdshed
rdpar
write_par
call date_time
write_par
call date_time
rdsdc
errormsg
de_allocate
sub
keychk
userchk
par_init
par_assign
main_DDS
write_par
opt
outevt
errormsg
lst
call date_time
Modules
area_watflood
areacg
rdflow
create_new_str_file
rdevt
keychk
userchk
header
call date_time
rd_wfo_spec
write_both_headers
rdshed
rdrain
precip_adjust
find_filetype
read_gsm
rdgsm
rdresv
create_new_rel_file
rdresvin
create_new_filename
wqread
rdswe
flowinit
soilinit
rdresume
userchk
keychk
timer
rd_flux
baseflow
rdtemp
rel_hum
rdrad
watbal
runof6
etin
etharg
etpriest
intcept
aet
craig_gordon
rdsnow
temper
snout1
wqsed
wqnut
melt
write_flux
write_modflow
baseflow
route
rerout
write_wetland
decay
wqroute
tracer
tracer0
tracer2
tracer3
tracer4
tracer5
tracergw
isotope
ISOsnow
ISOsurface
ISOinter
craig_gordon
ISOground
ISOriver
ISOwetland
ISOlake
craig_gordon
synflw
write_wfo
wfo_write_attribute_data
compute_error
lst
call date_time
write_r2s
write_resume
snout3

Appendix C

This Appendix presents baseflow proportionality plots for the FSB baseflow separation verification study presented in Section 5.4 of this thesis.

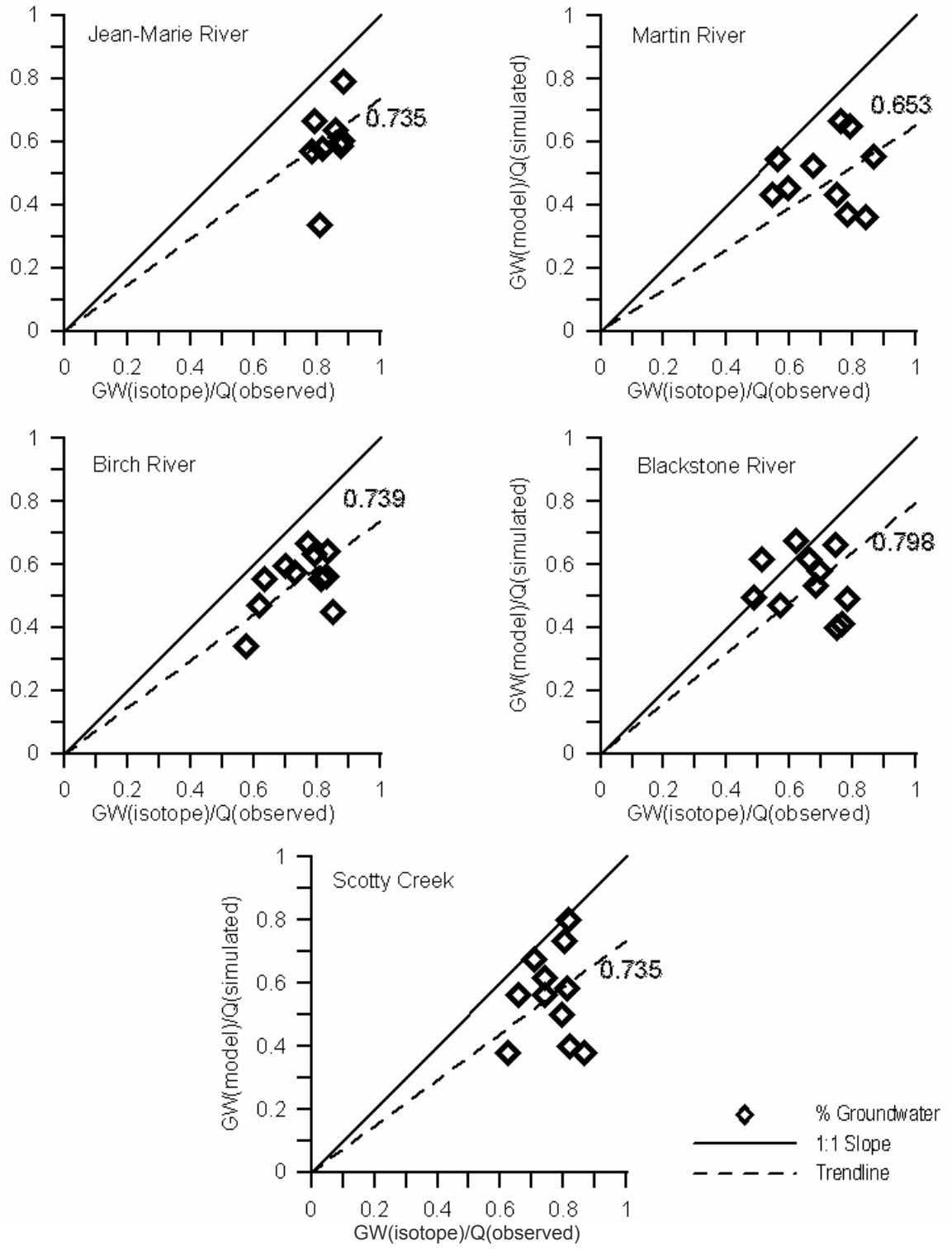

Figure C.1 – Baseflow proportionality plots from 1997 FSB simulation

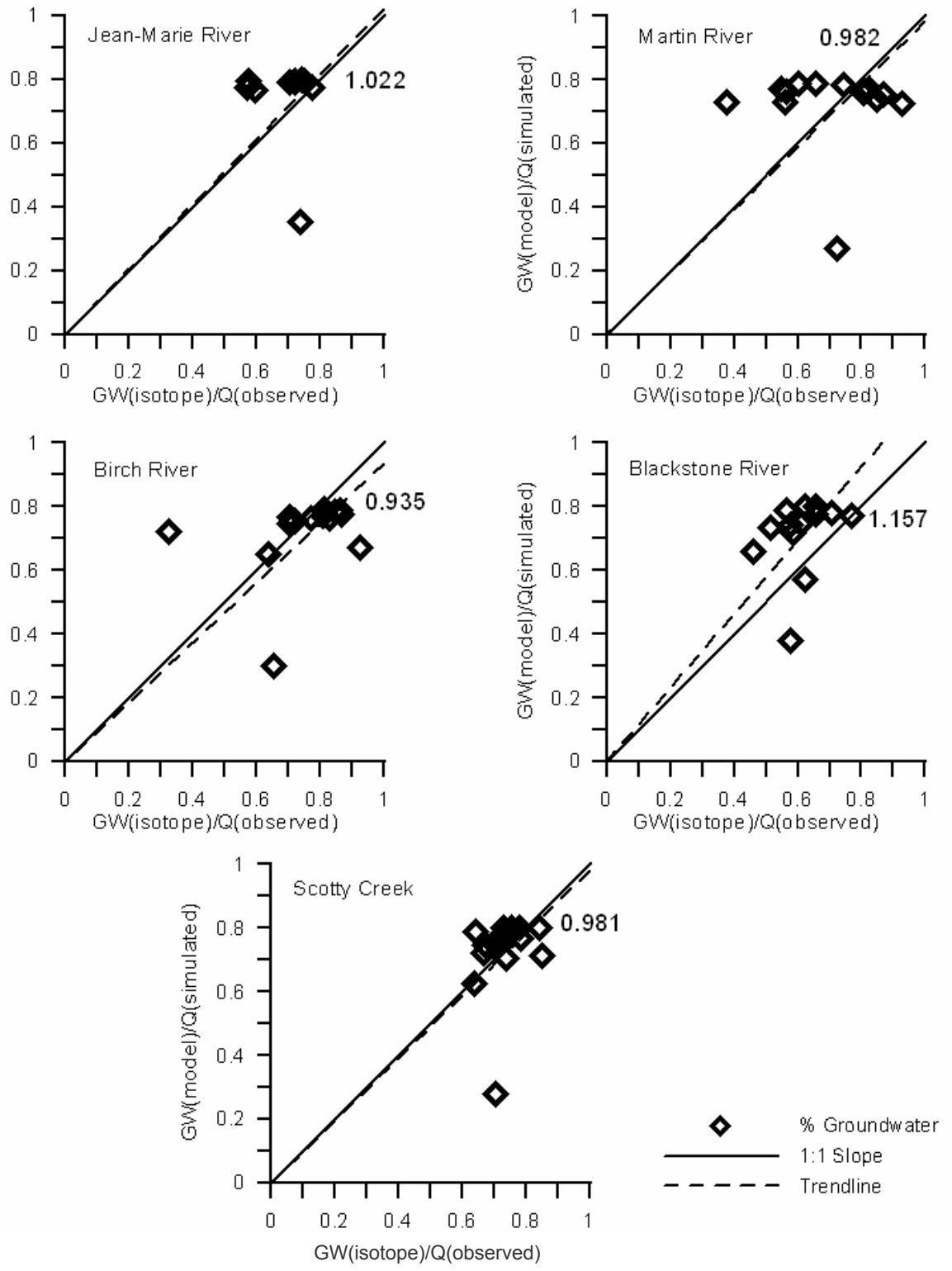

Figure C.2 – Baseflow proportionality plots from 1998 FSB simulation

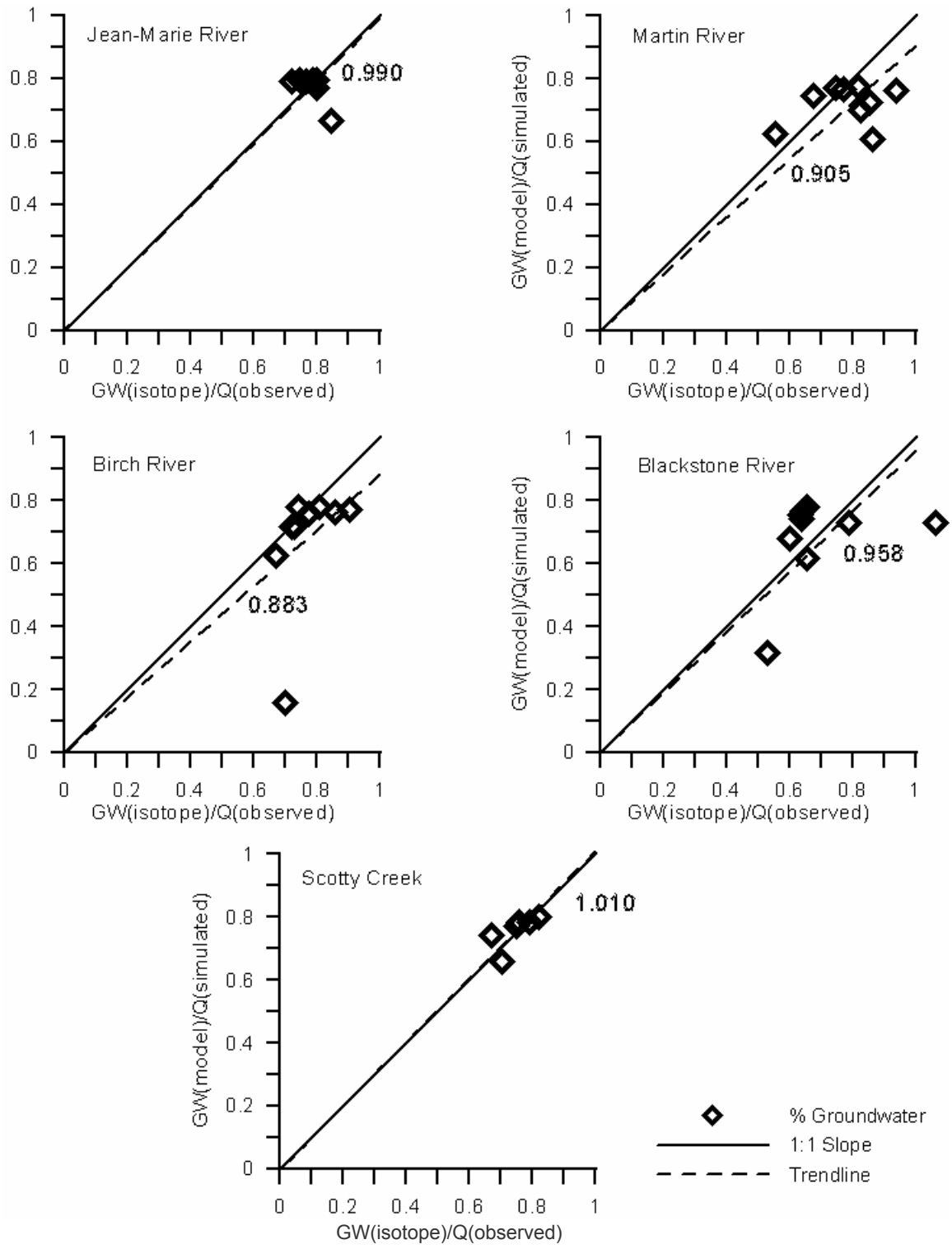

Figure C.3 – Baseflow proportionality plots from 1999 FSB simulation

Appendix D

This Appendix presents the streamflow proportionality plots for the FSB calibration simulations from Section 8.1 of this thesis. Dashed lines represented linear regressions through zero, providing a measure of model reproducibility of measured data. Streamflow generated from the pre- and post-calibration simulations are compared on proportionality plots (Figure D.1). Validation simulations for 1998 and 1999 are presented on Figures D.2 and D.3 respectively. Figure D.4 illustrates model proportionality to measured flows for the continuous simulation used in Chapter 8 model verification studies.

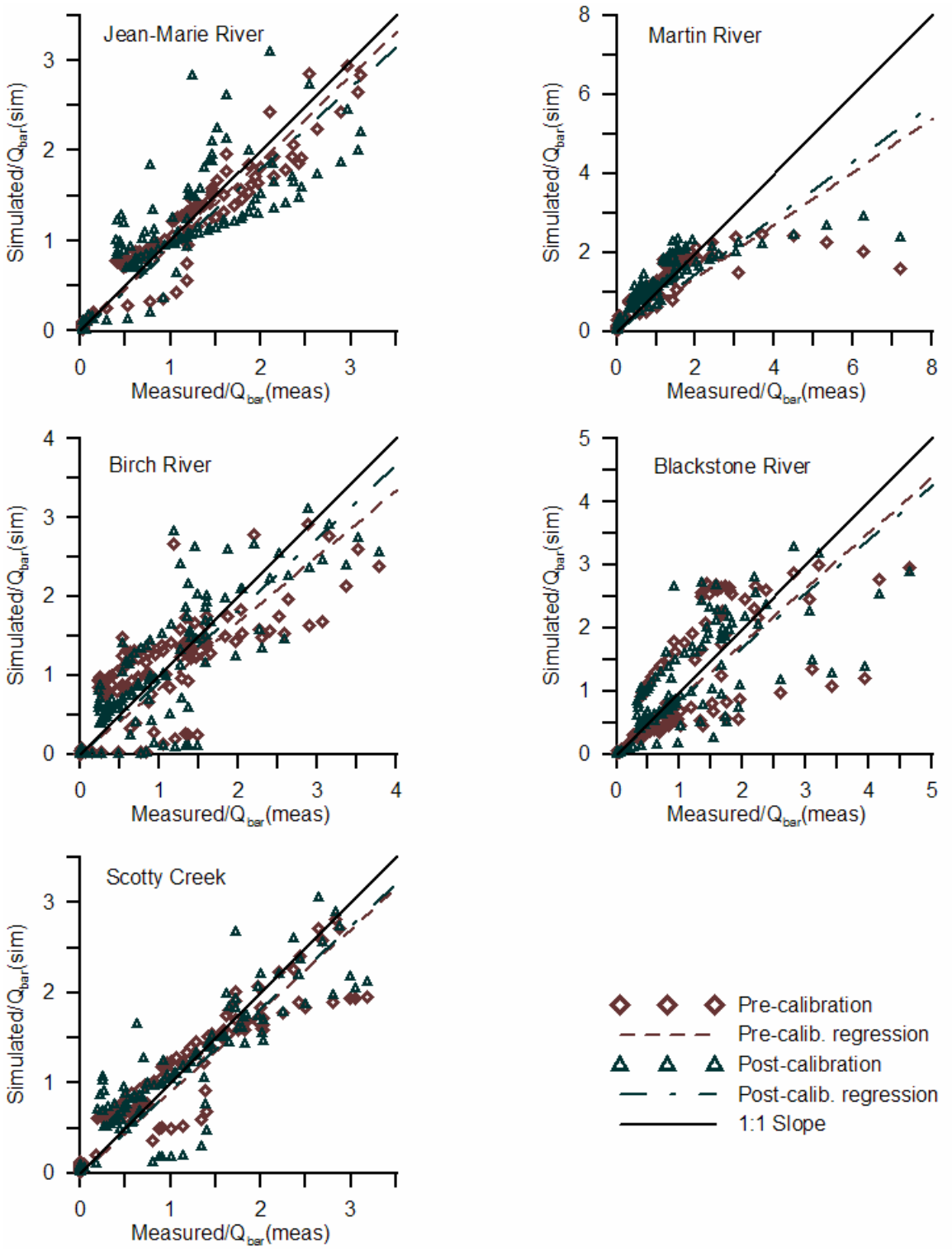

Figure D.1 – Proportionality plots for pre- and post-calibration 1997 FSB simulations

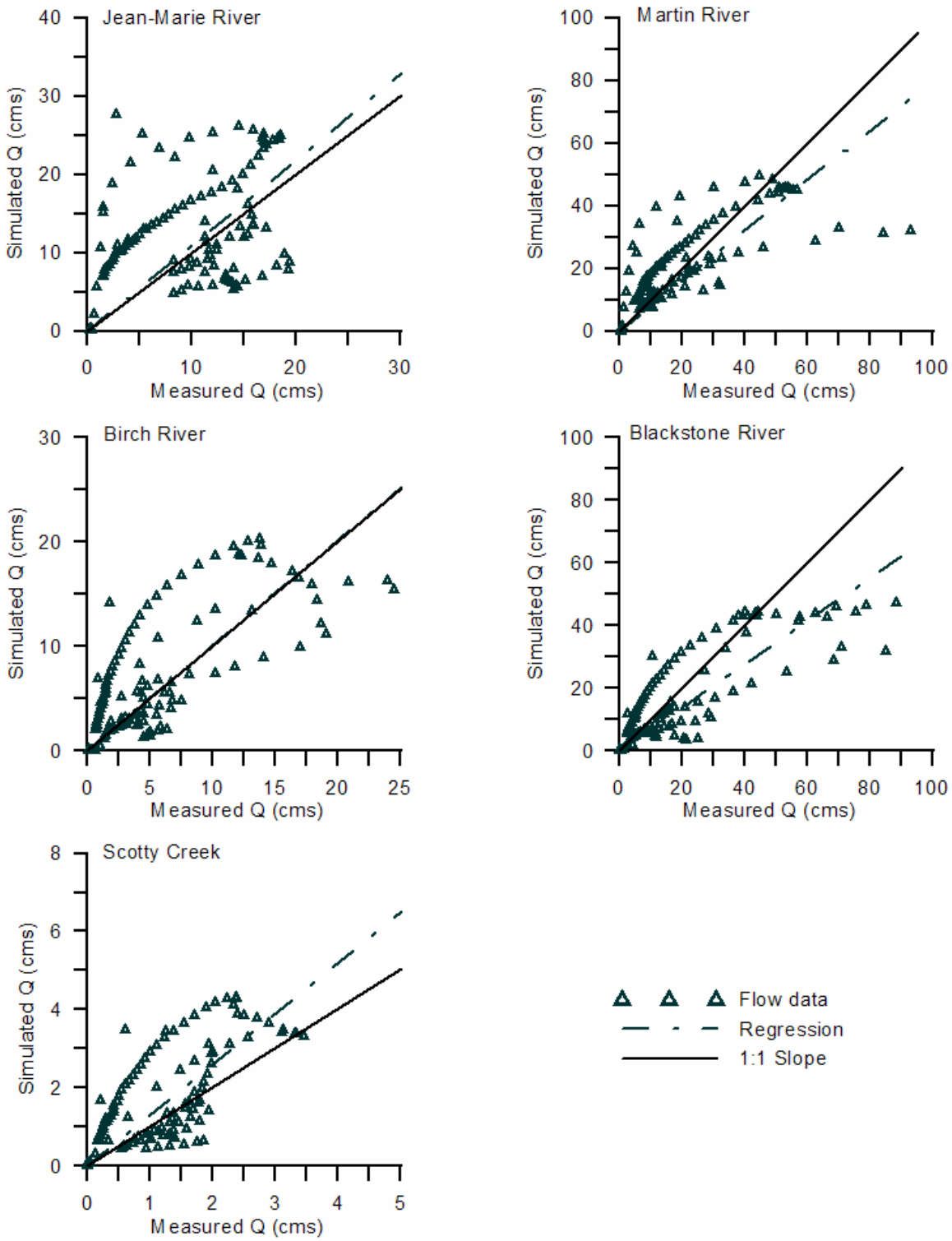

Figure D.2 –Proportionality plots for 1998 FSB simulations

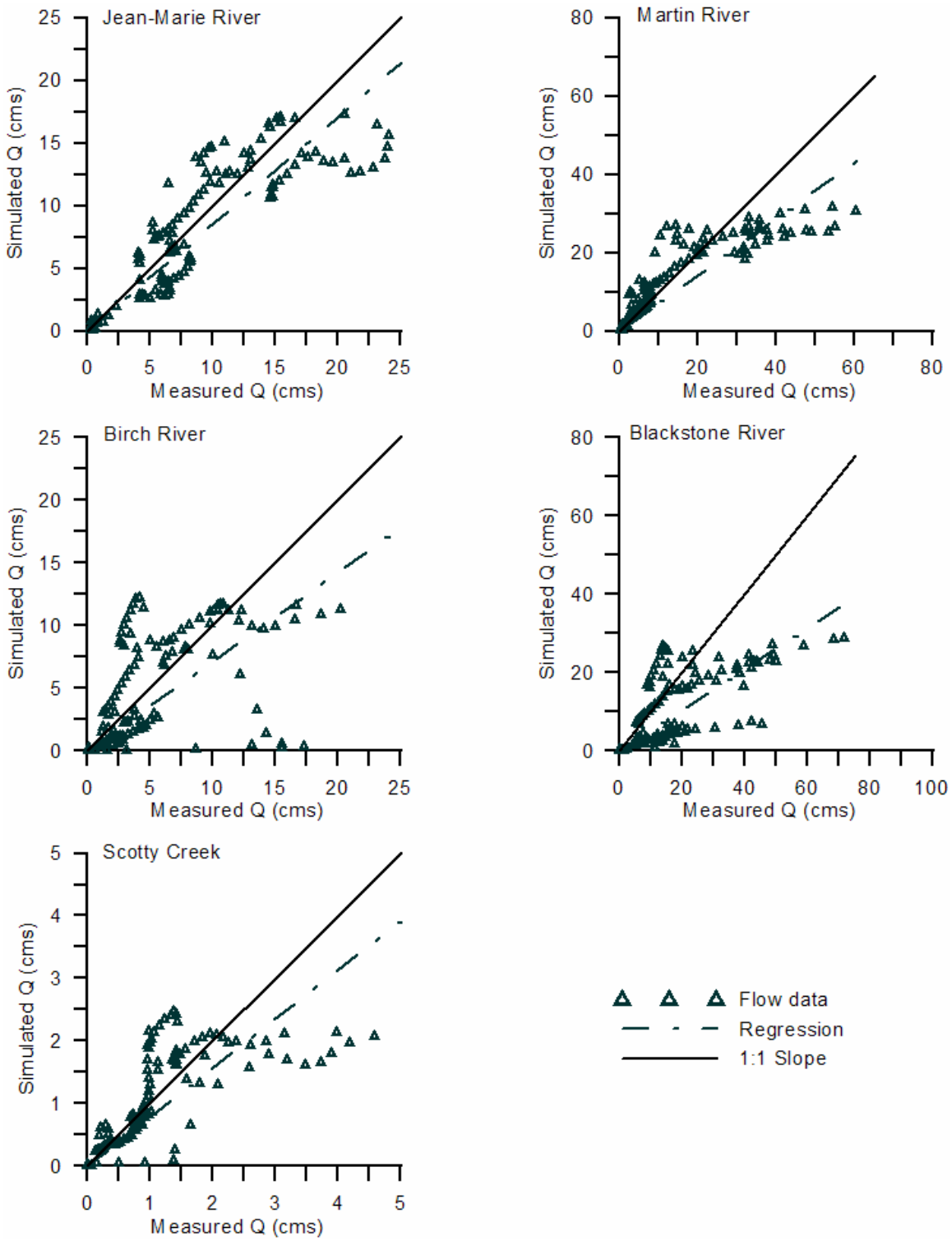

Figure D.3 –Proportionality plots for 1999 FSB simulations

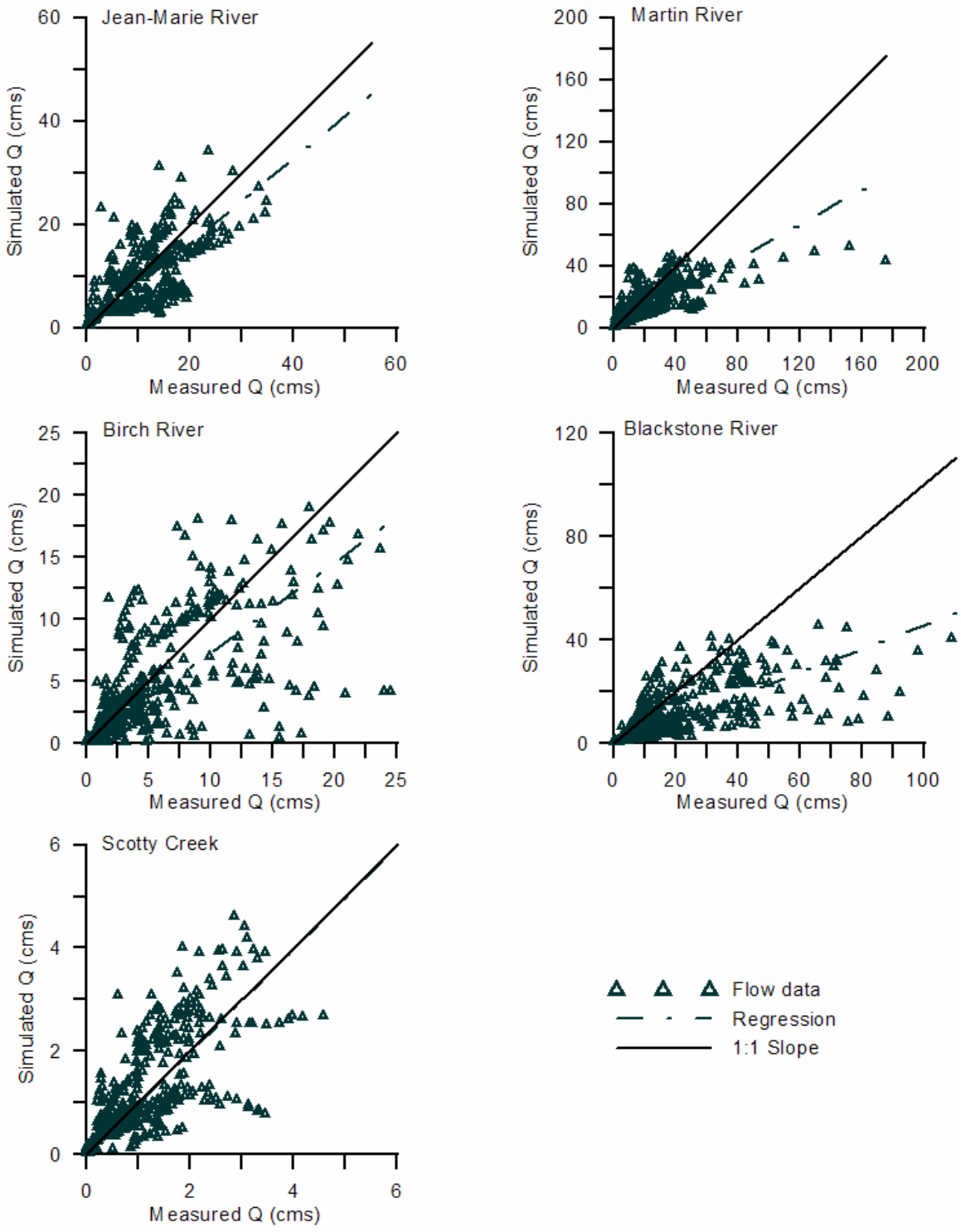

Figure D.4 –Proportionality plots for 1996-1999 continuous FSB simulations

Appendix E

This Appendix presents the results of the FSB pre- and post-calibration paired comparison t-tests to prove similarity between the streamflow simulations for Section 8.1.1 of this thesis. Equifinality is proved by showing there are statistically no differences between the streamflow simulations when each simulation is derived from a contrasting set of internal parameterizations.

Differences between the pre- and post-calibration simulations of streamflow were statistically compared using a paired comparison t-test. Such an analysis assumes the data normally distributed and uncorrelated therefore it was first necessary to apply a transformation to the streamflow data. Normal scores and correlation plots for each FSB (Appendix E; Figures E.1 through E.5) were prepared and used to find an appropriate transformation for the data using a trial and error approach. Jean-Marie River for example (Figure E.1) shows a linear relationship between the rank and the ranked difference in streamflows indicating the data are normally distributed following the transformation (case b), but that they were not prior to the transformation (case a). There is a distinct correlation between flow rate (i.e., Q) and the absolute difference in flow rate (i.e., $|Q_{pre\text{-}cal}\text{-}Q_{post\text{-}cal}|$) initially present in the data (case a), but following transformation (i.e., using $\sqrt{Q}$ and $\left|\sqrt{Q_{pre-cal} - Q_{post-cal}}\right|$) the data are uncorrelated. By trial and error a best transformation was selected for each basin (Figures E.1 through E.5) to approximate normally distributed differences (i.e., not all basins required the same transformation). A paired comparison t-test was then performed at the 95% confidence level such that:

$$t = \frac{\left|\overline{\Delta Q}_{transf}\right| - \mu}{\sigma_{\overline{\Delta Q}_{transf}} / \sqrt{n-1}} \qquad (E.2)$$

where $\overline{\Delta Q}_{transf}$ is the average of the absolute differences between transformed flows; μ is the null hypothesis equal to zero, or no difference between the two simulations; $\sigma_{\overline{\Delta Q}_{transf}}$ is the standard deviation of the differences; and n was 123 days of streamflow data. A p-value was

then computed for each basin from the t-distribution to verify whether the null hypothesis could be accepted with 95% confidence (p-value>0.05) (Table E.1).

Table E.1 – Summary of paired comparison t-tests for the Fort Simpson basins.

Basin	$\overline{\Delta Q}_{transf}$	$\sigma_{\overline{\Delta Q}_{transf}}$	**t**	**p-value**
Jean-Marie R.	0.044	0.44	1.105	0.27
Martin R.	-0.007	0.45	0.169	0.87
Birch R.	0.056	1.68	0.370	0.71
Blackstone R.	0.032	0.54	0.652	0.52
Scotty Cr.	0.001	46.74	0.0003	0.99

The p-values for each basin in Table E.1 exceed 0.05 indicating that there is likely no statistical difference between the pre- and post-calibration streamflow simulations. These two simulations therefore demonstrate statistical equifinality.

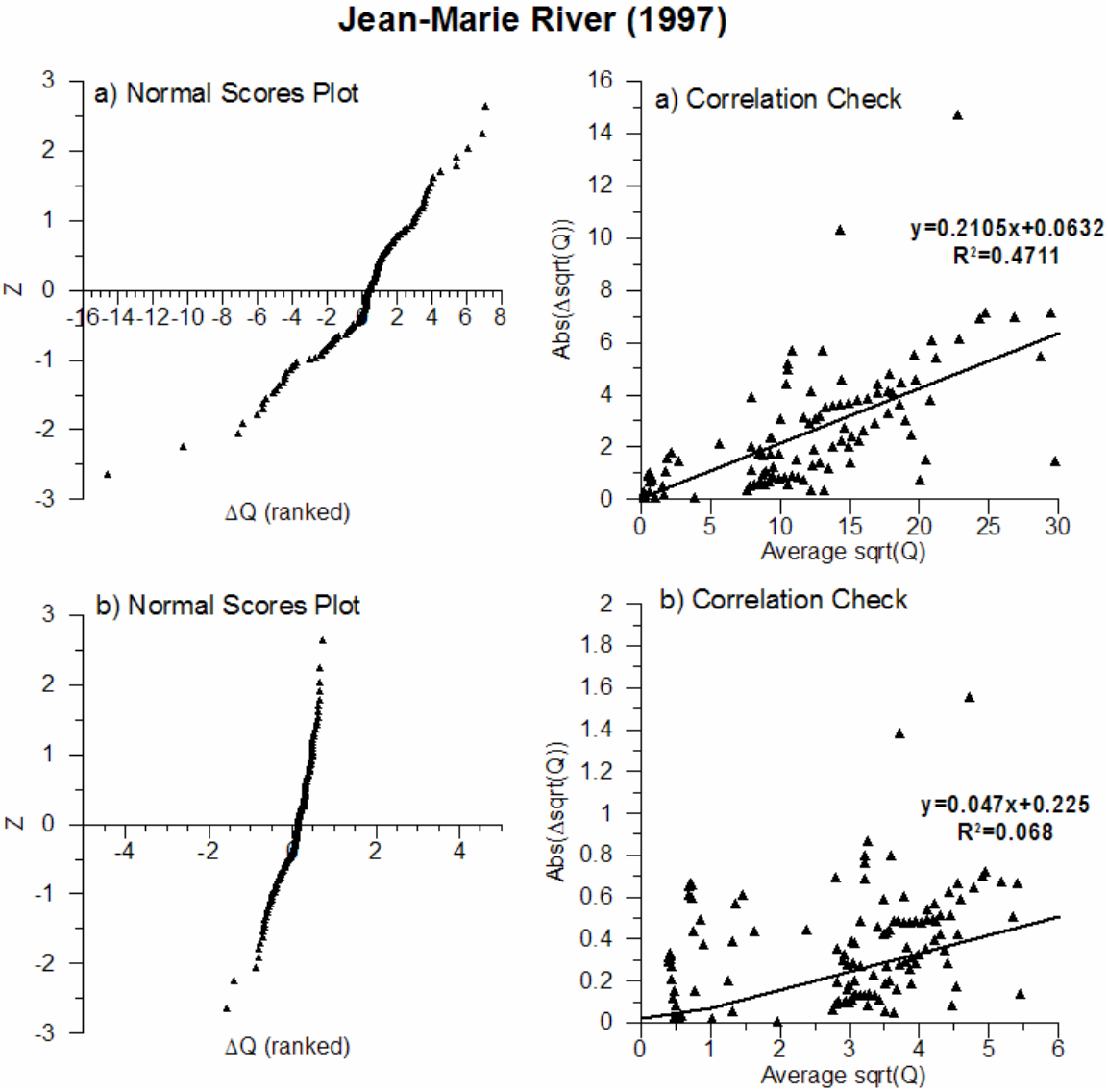

Figure E.1 – Analysis of differences in streamflow simulated pre- and post-calibration in Jean-Marie River basin a) without transformation, and b) with an appropriate transformation.

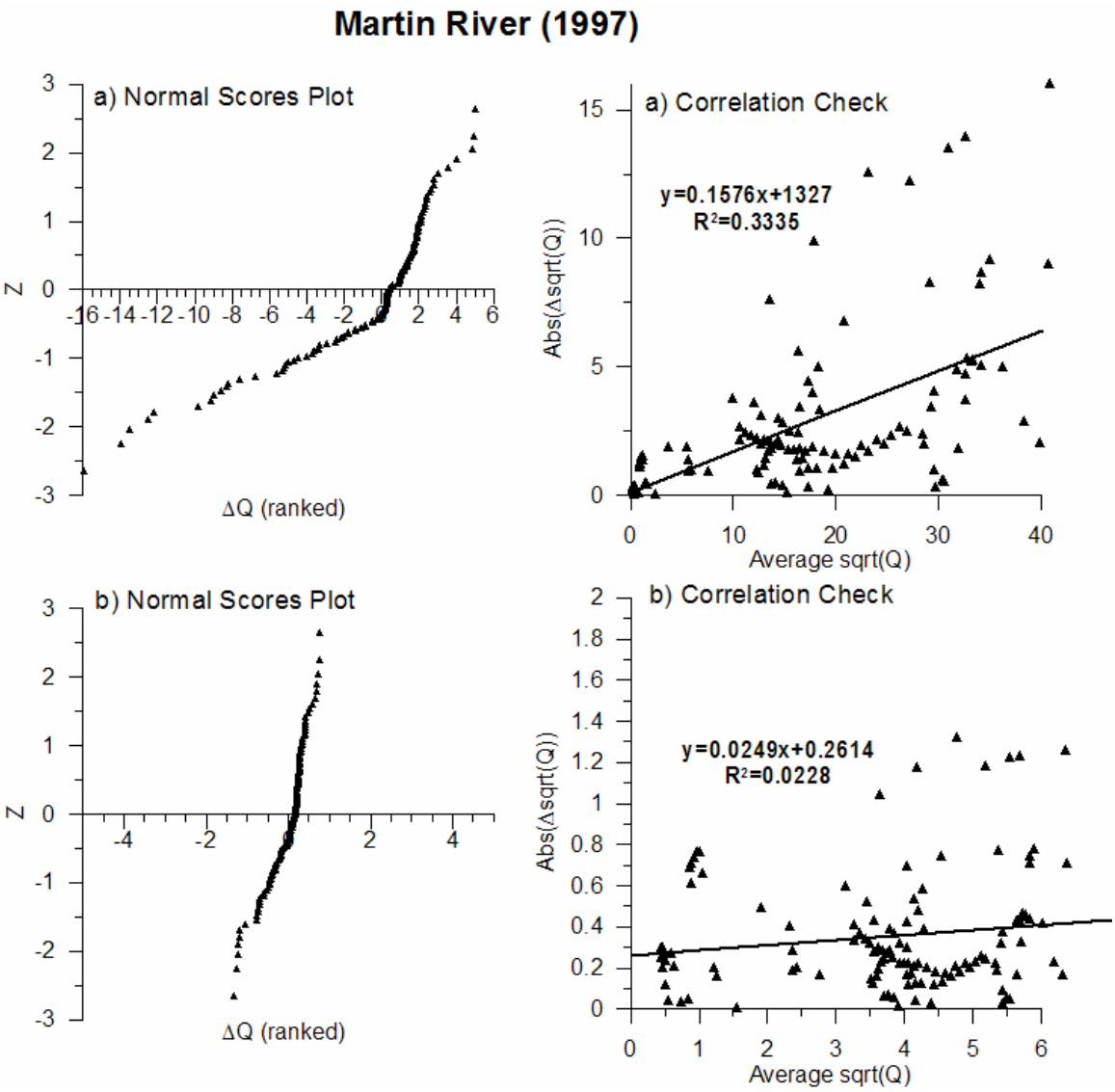

Figure E.2 – Analysis of differences in streamflow simulated pre- and post-calibration in Martin River basin a) without transformation, and b) with an appropriate transformation.

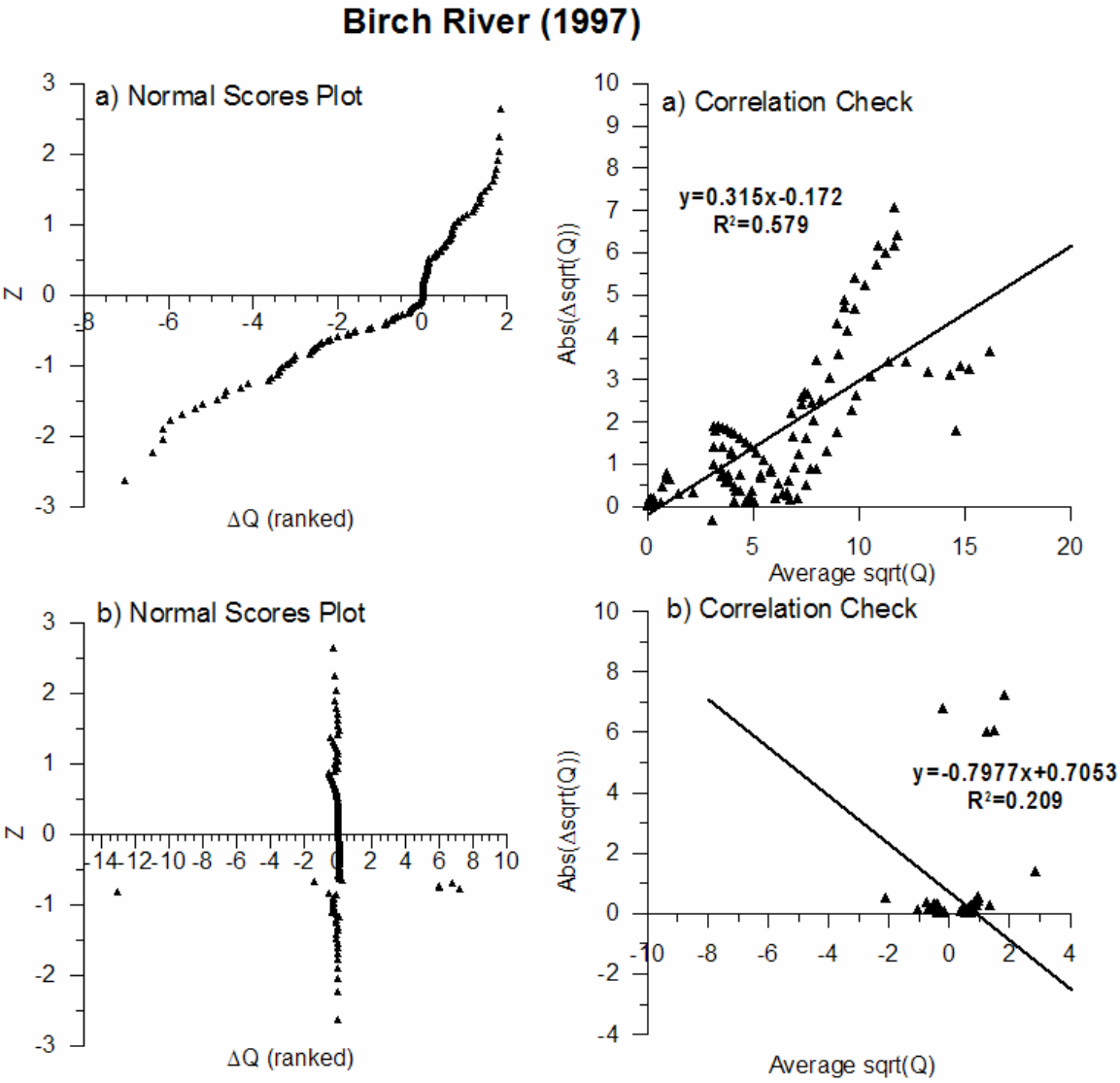

Figure E.3 – Analysis of differences in streamflow simulated pre- and post-calibration in Birch River basin a) without transformation, and b) with an appropriate transformation.

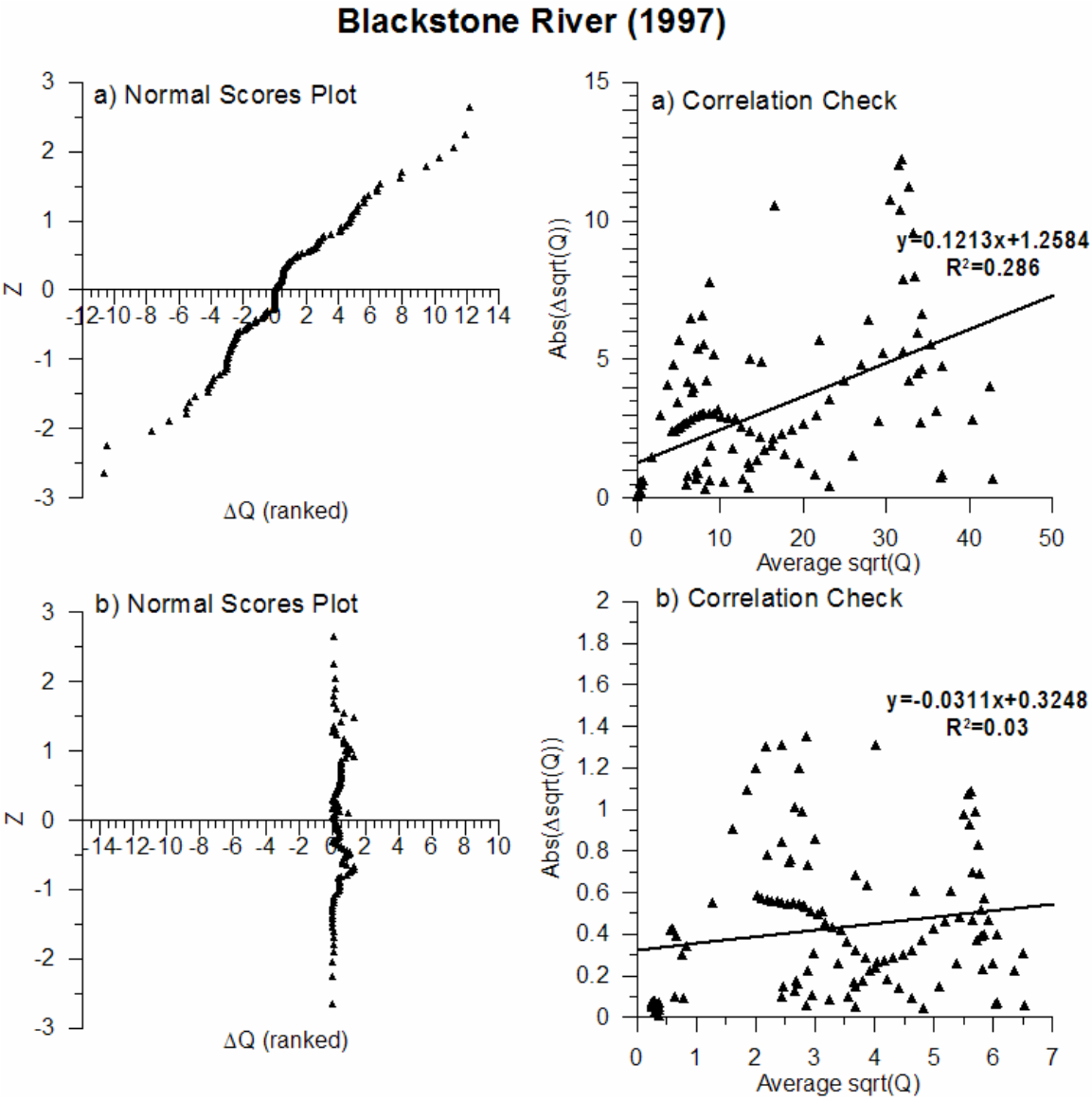

Figure E.4 – Analysis of differences in streamflow simulated pre- and post-calibration in Blackstone River basin a) without transformation, and b) with an appropriate transformation.

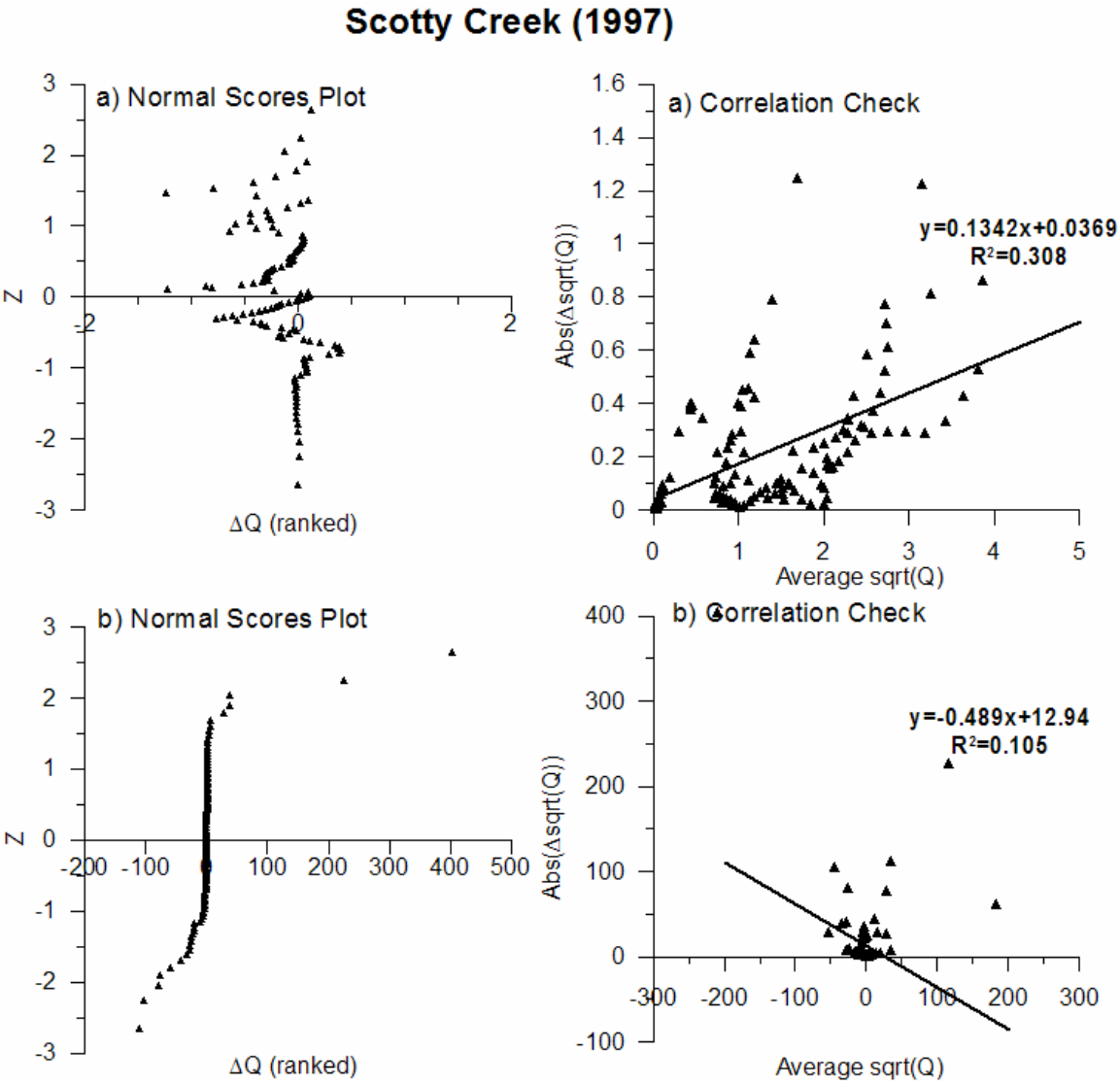

Figure E.5 – Analysis of differences in streamflow simulated pre- and post-calibration in Scotty Creek basin a) without transformation, and b) with an appropriate transformation.

Appendix F

This Appendix presents the streamflow proportionality plots for the eight GRB gauges from the validation simulation presented in Section 9.1 of this thesis. Dashed lines represent linear regressions through zero, providing a measure of model reproducibility of measured data. Figures F.1 through F.8 represent proportionality plots for streamflow simulations at the Grand River at Waldemar, Grand River at West Montrose, Conestogo River at St. Jacobs, Eramosa River at Guelph, Speed River at Beaverdale, Grand River at Galt, Nith River at Canning, and Grand River at York gauges, respectively.

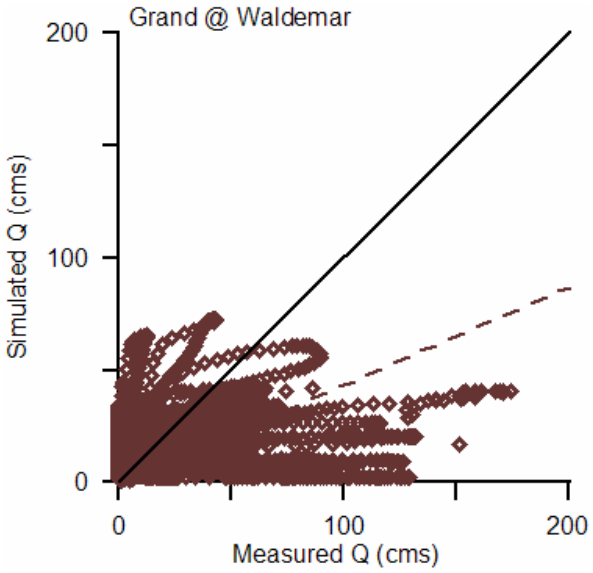

Figure F.1 – Grand River at Waldemar streamflows.

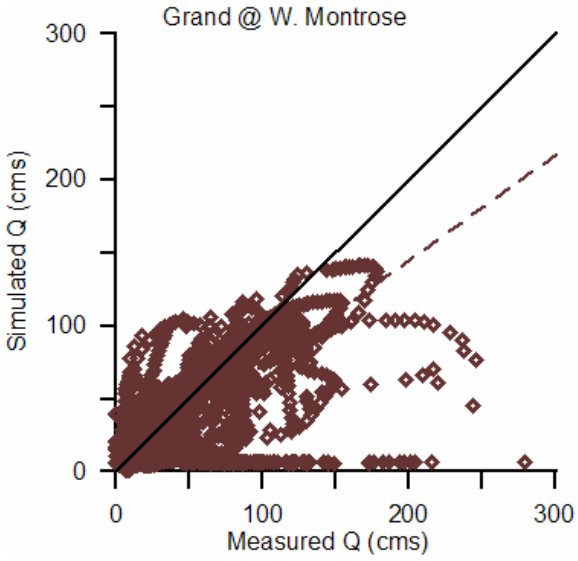

Figure F.2 – Grand River at West Montrose streamflows.

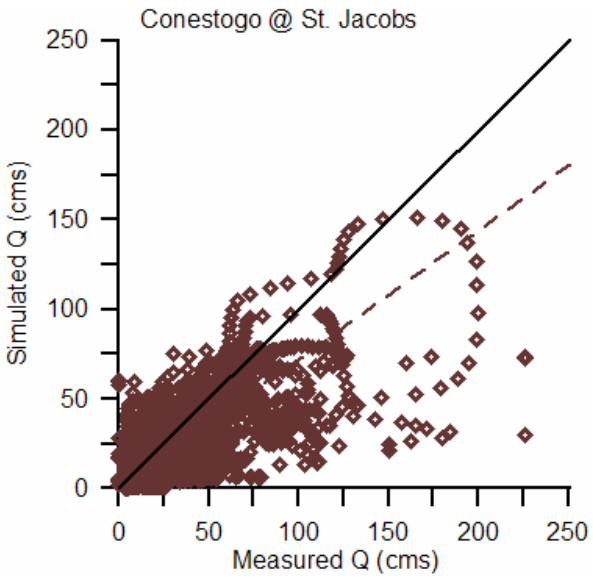

Figure F.3 – Conestogo River at St. Jacobs streamflows.

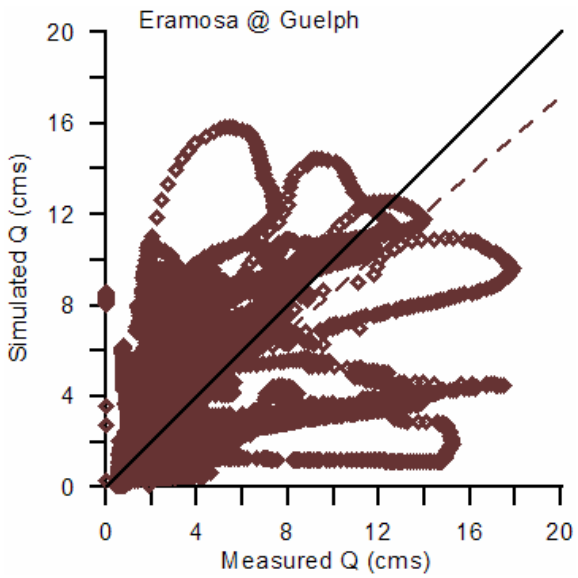

Figure F.4 – Eramosa River at Guelph streamflows.

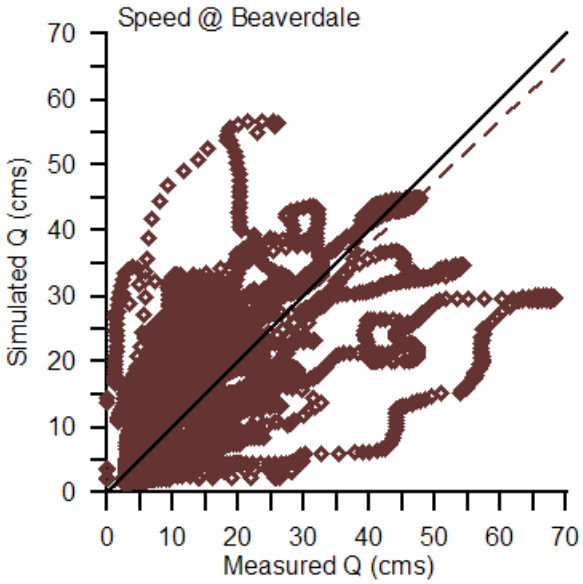

Figure F.5 – Speed River at Beaverdale streamflows.

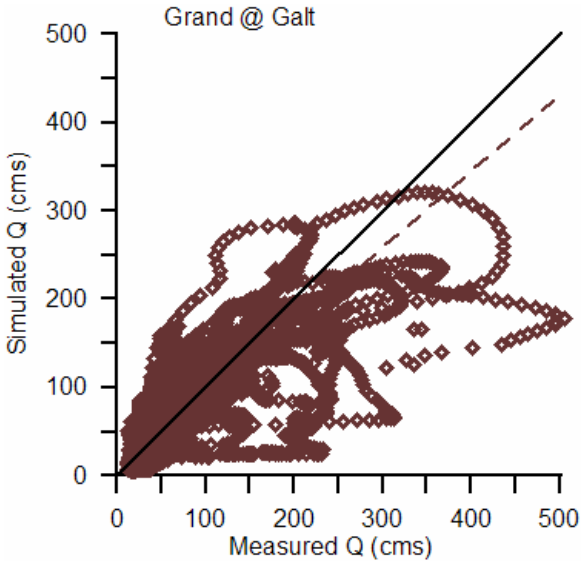

Figure F.6 – Grand River at Galt streamflows.

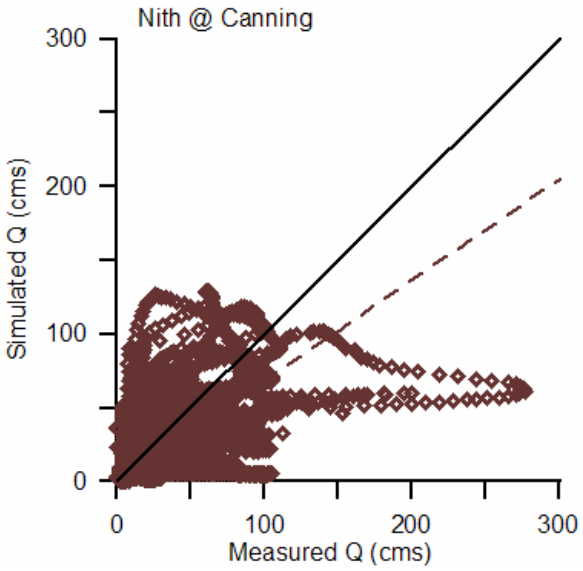

Figure F.7 – Nith River at Canning streamflows.

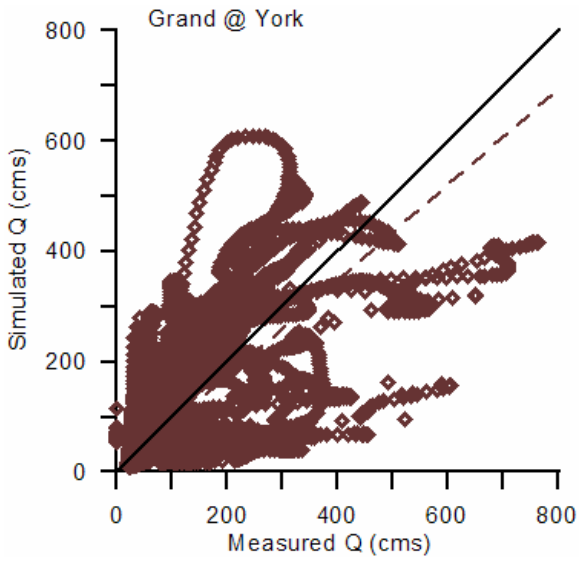

Figure F.8 – Grand River at York (outlet) streamflows.

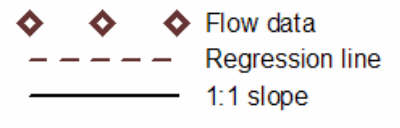

Appendix G

This Appendix presents the proportionality plots for the seven inflow gauge points to the GRB reservoirs. Dashed lines represent linear regressions through zero, providing a measure of model reproducibility of measured data. Figures G.1 through G.7 represent proportionality plots for streamflow simulations at the Grand River at Waldemar, Grand River at Upper Belwood, Canagaguige Creek at Floradale, Conestogo at Glen Allen, Laurel Creek at Erbsville, Speed River at Armstrong Mills, and Mill Creek, respectively.

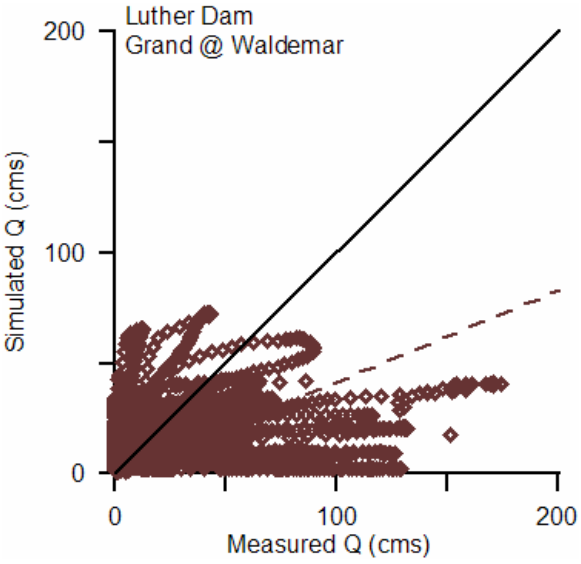

Figure G.1 – Luther Dam inflows.

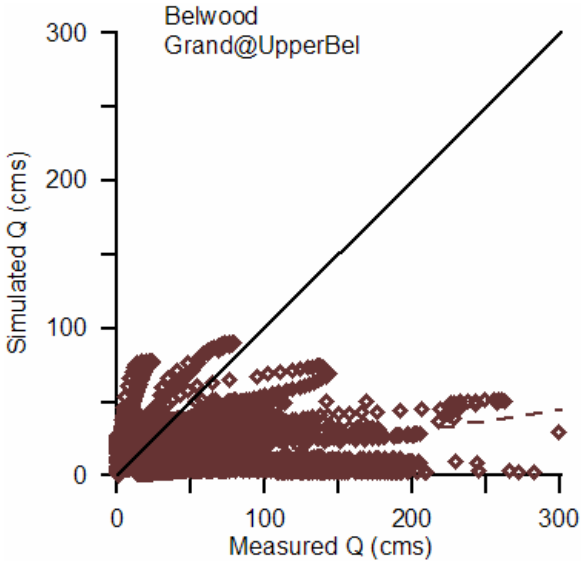

Figure G.2 – Lake Belwood inflows.

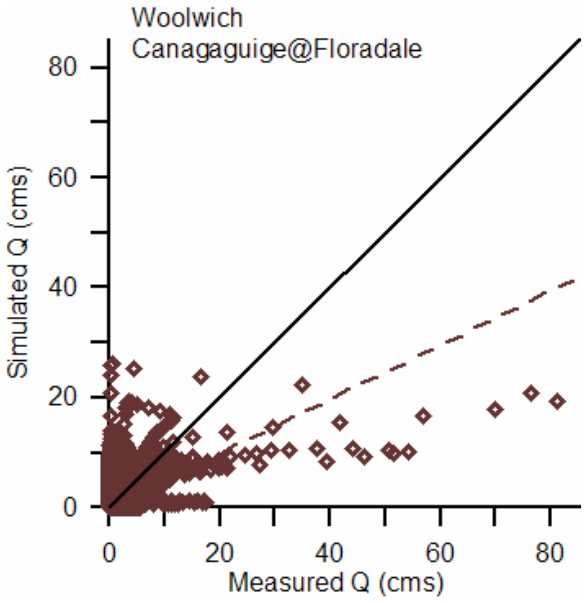

Figure G.3 – Woolwich reservoir inflows.

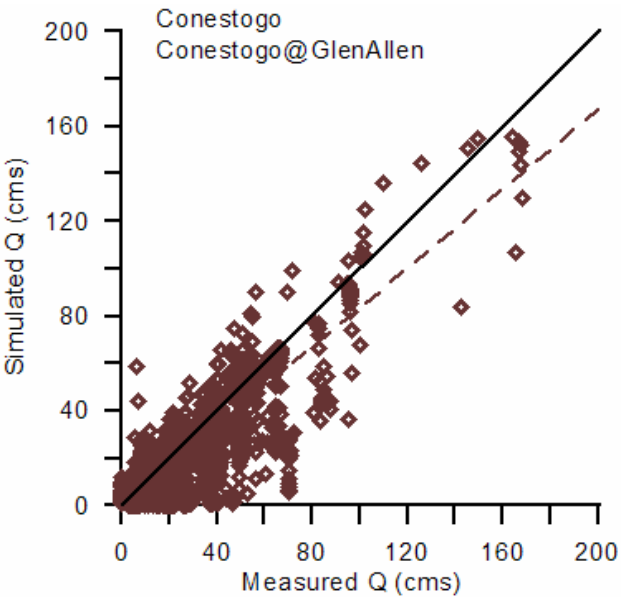

Figure G.4 – Lake Conestogo inflows.

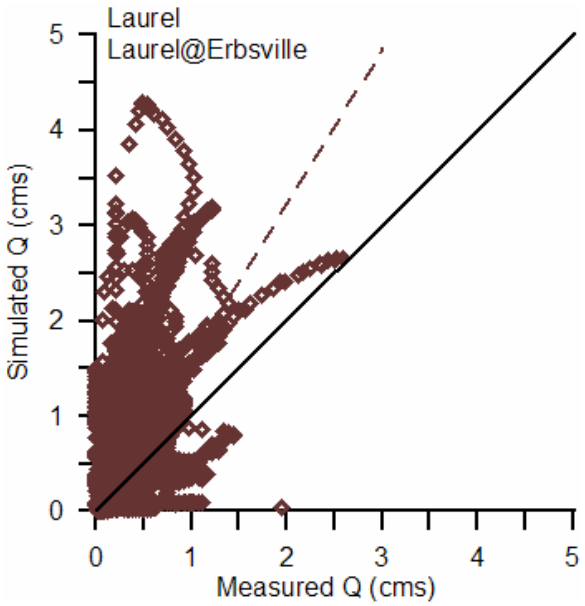

Figure G.5 – Laurel reservoir inflows.

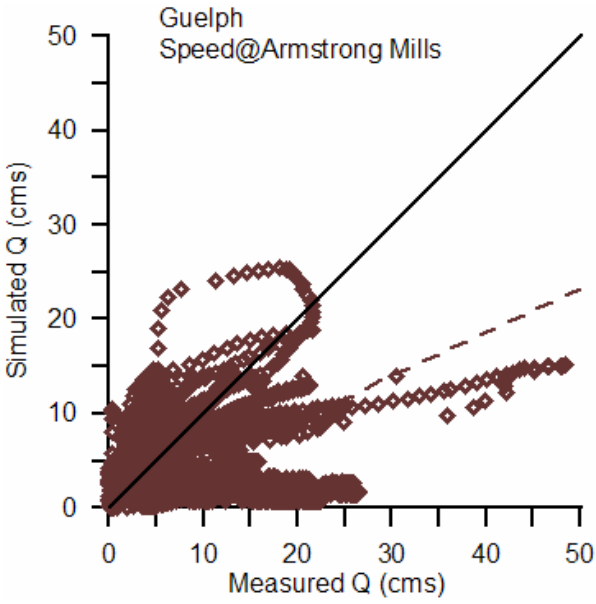

Figure G.6 – Guelph Lake inflows.

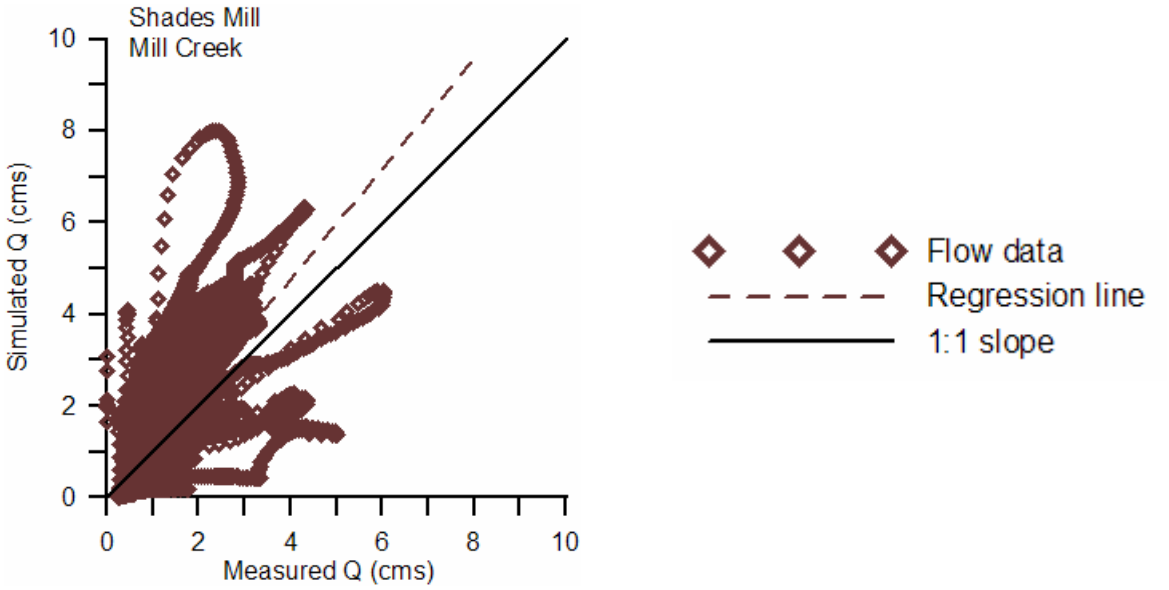

Figure G.7 – Shades Mills reservoir inflows.

Appendix H

This Appendix briefly summarises the changes in synoptic weather and hydrology (i.e., streamflow) during the 2003 to 2005 study period in the lower GRB. This Appendix compliments the analysis performed in Section 9.2.3 of this thesis.

Monthly temperature (Figure H.1) and precipitation (Figure H.2) from the MOE Brantford climate station (i.e., lower GRB) is plotted to contrast the changes in climate from 2003 to 2005. From the climate data the lower GRB in 2003 was overall cooler throughout the year than 2004 and 2005. In the fall of 2003 there were considerable amounts of precipitation that would generate wet antecedent conditions for the start of the simulation period. January of 2004 was cooler than in 2003 and 2005, but the 2004 freshet was warmer with high amounts of precipitation presumably derived from the El Niño southern oscillation (ENSO). Starting in spring however, precipitation in 2004 was low relative to 2003 and 2005 (but still above the long-term Climate Normals; Table 3.2), and the summer was uncharacteristically cool for this region of southern Ontario with a below normal average ice-off temperature of 13.3°C. Both average temperature (8.3°C) and total precipitation (886 mm) in 2005 were greater than in 2003 and 2004, but yet were at and below the long-term Climate Normals of the Brantford MOE station, respectively. This indicates a relatively cooler and drier climate than normal across the analysis period.

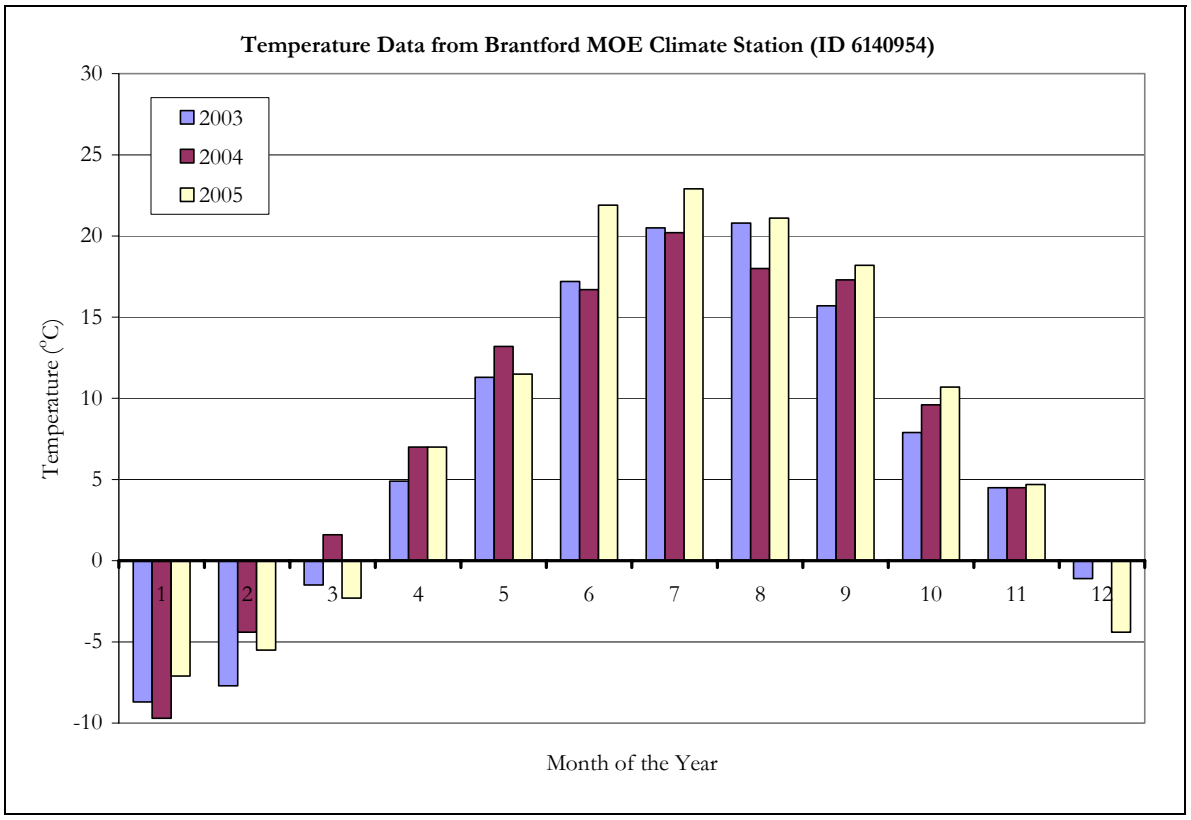

Figure H.1 – Brantford MOE climate station monthly temperatures for 2003, 2004, and 2005

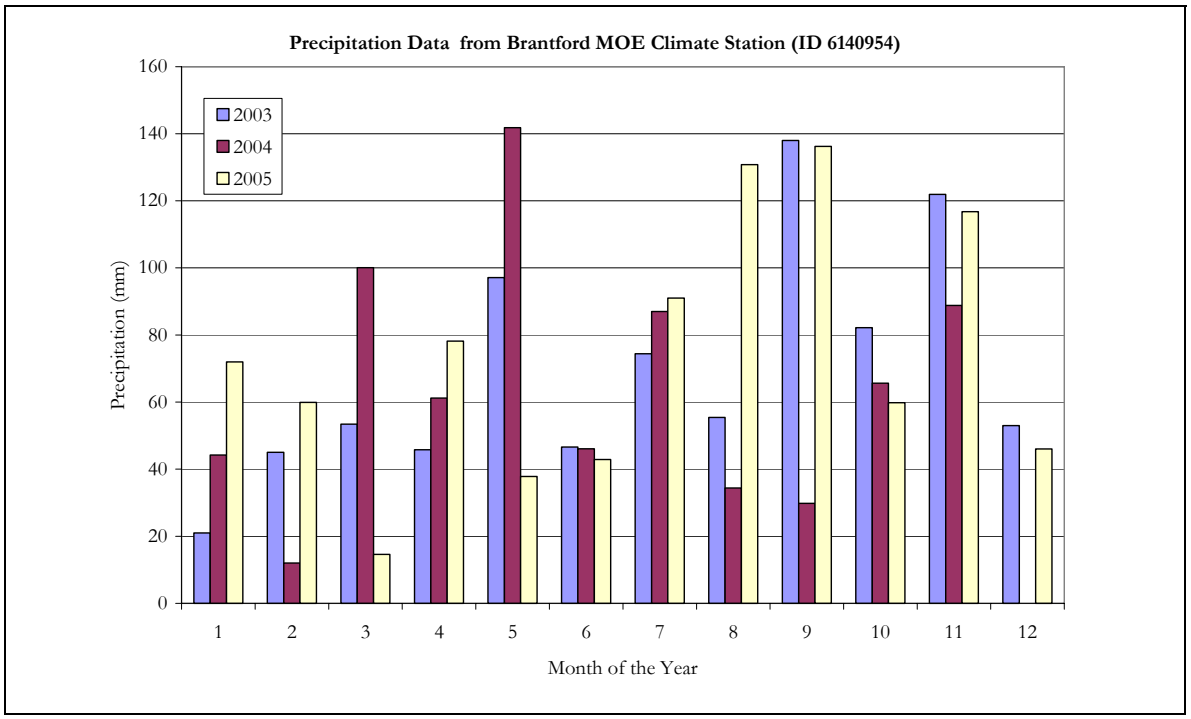

Figure H.2 - Brantford MOE climate station monthly precipitation for 2003, 2004, and 2005

Measured monthly average streamflows for the Grand at York streamflow gauge are shown on Figure H.3. In response to the climate characterization, flows were highest during the 2004 and 2005 freshet periods where winter and spring were both warm and moist. Streamflow during the summer of 2005, when precipitation was significantly higher, showed lower or similar streamflow runoff on average as compared with the much drier 2004 summer period. This indicates that precipitation in 2005 did not directly generate an increase in runoff, but instead was hydrologically stored on the surface (i.e., wetlands and bogs) or in subsurface storage.

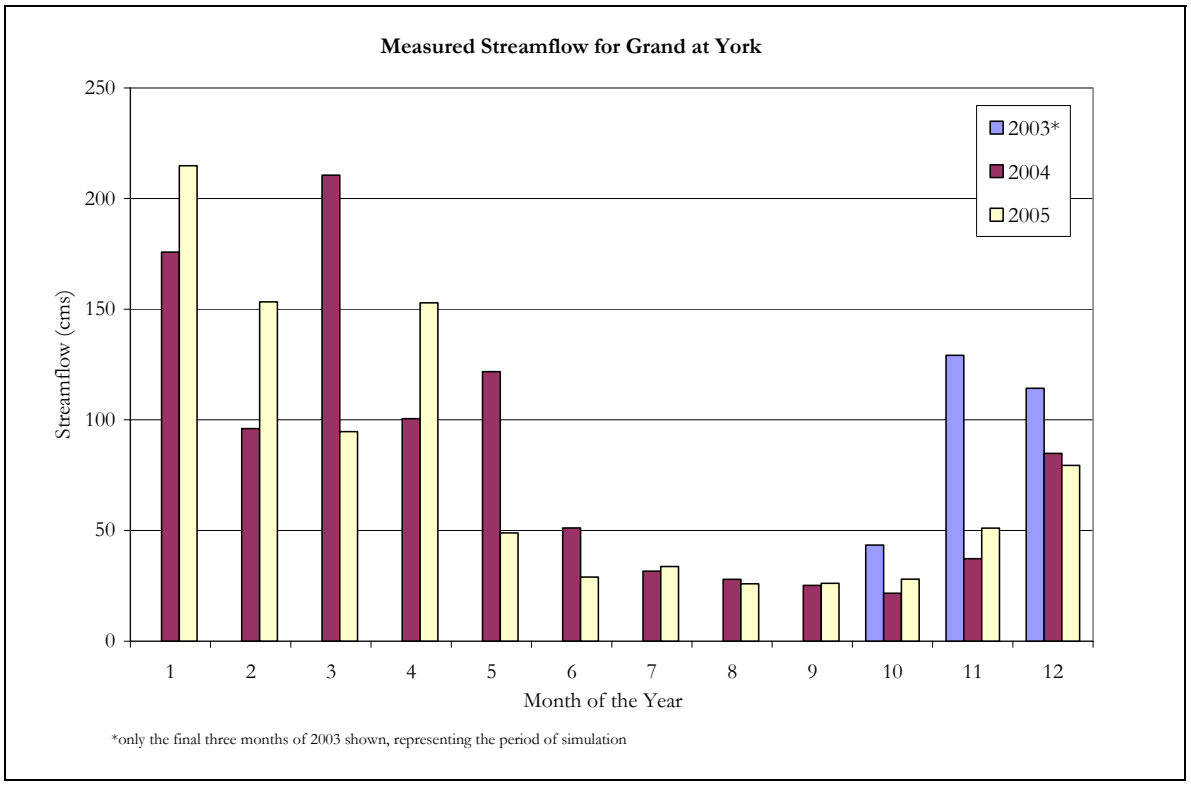

Figure H.3 – Monthly average streamflow measured at Grand at York for 2003, 2004, and 2005

Appendix I

This Appendix presents Figures I.1 through I.11, showing the isotopic response surfaces for the GRB from 2003 to 2005 from the headwaters of the basin to the outlet. This Appendix compliments the analysis performed in Section 9.2.4 of this thesis.

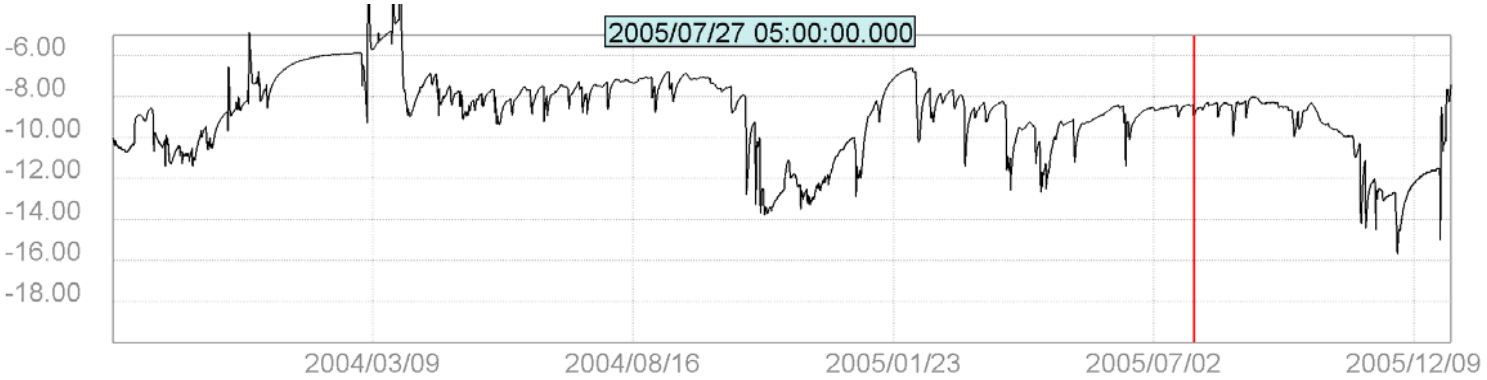

Figure I.1 - Grand @ Dundalk isoWATFLOOD-simulated response

Figure I.2 - Grand @ Waldemar isoWATFLOOD-simulated response

Figure I.3 - Grand @ W. Montrose isoWATFLOOD-simulated response

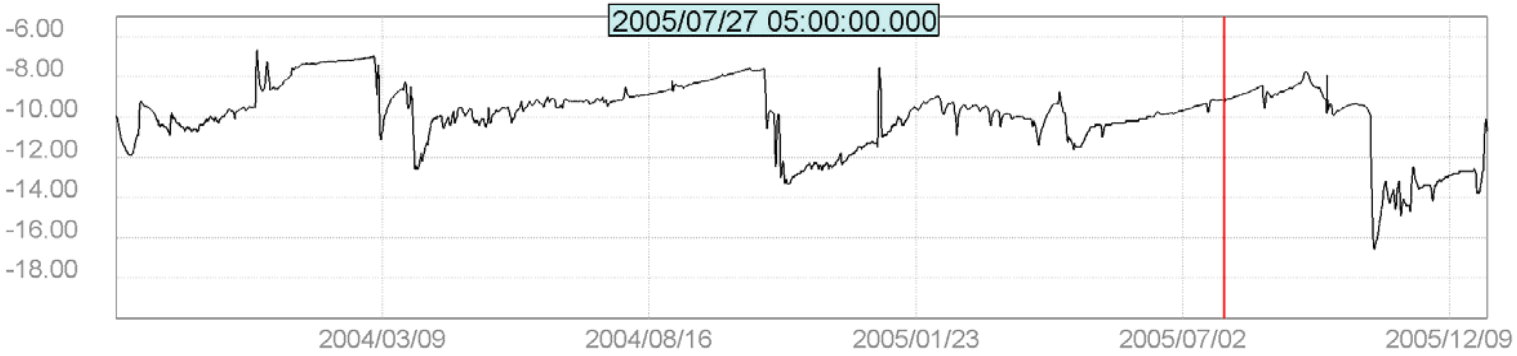

Figure I.4 - Conestogo @ St. Jacobs isoWATFLOOD-simulated response

Figure I.5 - Grand @ Bridgeport isoWATFLOOD-simulated response

Figure I.6 - Eramosa @ Guelph isoWATFLOOD-simulated response

Figure I.7 - Speed @ Beaverdale isoWATFLOOD-simulated response

Figure I.8 - Grand @ Galt isoWATFLOOD-simulated response

Figure I.9 - Nith @ Canning isoWATFLOOD-simulated response

Figure I.10 - Grand @ Brantford isoWATFLOOD-simulated response

Figure I.11 - Grand @ York isoWATFLOOD-simulated response